University of Southampton

Faculty of Medicine

Cancer Sciences

Generation and characterisation of anti-LILR antibodies for immunotherapy

Volume 1 of 1

By

Muchaala Jennett Swana

Thesis for the degree of Doctor of Philosophy

September 2016

UNIVERSITY OF SOUTHAMPTON

ABSTRACT

THE FACULTY OF MEDICINE

Cancer Sciences

Thesis for the degree of Doctor of Philosophy

GENERATION AND CHARACTERISATION OF ANTI-LILR ANTIBODIES FOR IMMUNOTHERAPY

By Muchaala Jennett Swana

Leukocyte Immunoglobulin (Ig)-Like Receptors (LILRs) (LIRs/ILT/CD85) are a family of cell surface receptors involved in innate and adaptive immunity. There are six activatory (LILRA) and five inhibitory (LILRB) LILRs, with imbalances associated with the progression of autoimmune diseases such as rheumatoid arthritis. The inhibitory LILRs are up-regulated in anti-inflammatory environments and have been implicated in tumour progression. LILRs could therefore be potential immunotherapeutic targets to treat both cancer and autoimmunity.

LILRB3 (ILT5/CD85a) is an inhibitory receptor belonging to this family. Although LILRB1 and LILRB2 have been extensively studied, LILRB3 has been less so. Its function is unclear but its restricted expression profile on myeloid cells makes it an attractive target. To help establish the potential of this family of receptors as targets for immunotherapy, a panel of LILRB1-, LILRB2- and LILRB3-specific monoclonal antibodies (mAbs) were generated by propriety phage display technology. To confirm specificity the mAbs were assessed for binding to LILRB-transfectants compared to mock-transfectants, as well as cells expressing other related LILRs. Two, six and sixteen antibodies displayed specific binding to LILRB1, LILRB2 and LILRB3, respectively in these assays. Antibody binding to LILRBs on myeloid cells including monocytes, macrophages and neutrophils were confirmed. Fine specificity and epitope mapping was performed using cross-blocking assays and HEK 293F-transfectants expressing mutated molecules of LILRB3, displaying varying numbers of extracellular domains. Using reporter cells capable of detecting receptor cross-linking, the antibodies were then screened for their ability to activate or inhibit cellular activation. The antibodies were assessed for their ability to regulate certain aspects of myeloid cell biology, including regulation of T-cell proliferation and macrophage phagocytosis. Finally, the antibodies were

tested *in vivo* to assess their ability to act as direct targeting antibodies. These reagents allowed us to assess the function and immunotherapeutic potential of LILR mAbs.

CONTENTS

LIST OF FIGURES

LIST OF TABLES

DECLARATION OF AUTHORSHIP

I, **Muchaala Jennett Swana**, declare that this thesis and the work presented in it are my own and has been generated by me as the result of my own original research.

Generation and characterisation of anti-LILR antibodies for immunotherapy.

I confirm that:

1. This work was done wholly or mainly while in candidature for a research degree at this University;

2. Where any part of this thesis has previously been submitted for a degree or any other qualification at this University or any other institution, this has been clearly stated;

3. Where I have consulted the published work of others, this is always clearly attributed;

4. Where I have quoted from the work of others, the source is always given. With the exception of such quotations, this thesis is entirely my own work;

5. I have acknowledged all main sources of help;

6. Where the thesis is based on work done by myself jointly with others, I have made clear exactly what was done by others and what I have contributed myself;

7. None of this work has been published before submission.

Signed: ……

Date: ……

ACKNOWLEDGMENTS

I would firstly like to thank my supervisors, Prof Mark Cragg and Dr Ali Roghanian, for giving me the opportunity to work on a great PhD project for 4 years, and their support and guidance throughout.

I would like to thank Dr Björn Frendéus and our collaborators at BioInvent for helping me produce some amazing antibodies. In particular, I would like to thank Dr Torbjörn Schiött and Ulrika Matson for their constant support, especially for enduring my constant barrage of emails during my write-up! Also a huge thank you to everyone at BioInvent who helped in some way with this project: Dr Ulla-Carin Tornberg, Björn Hambe, Anne Ljungars, Dr Mikael Mattsson and Dr Ingrid Teige. I would also like to thank our collaborators at the University of Cambridge – Prof John Trowsdale and Dr Des Jones for their input in this project, and all the BRF staff in Southampton for their support with my *in vivo* work.

A special thank you to RMRK aka Ruth Briton, Robert Oldham and Kirstie Cleary, for their help in and out of the lab during these past 4 years - your friendship and our regular trips to Santos and Shirley's upmarket Chinese buffets was always very much appreciated!

Finally I would like to thank my family: my parents for always supporting me and encouraging me both emotionally and financially in my education; making me always strive for better and being wonderful role models; most importantly putting up with me staying in school for this long! My sisters, Belinda, Matimba and Kasongo for always being my best friends and emotional support system. Last but not least, I would like to thank my husband Billy, for always pushing me to keep going when things were hard (I'm a lion!), and listening to me talk about nothing but science for 4 years! I appreciate you all, and I dedicate my thesis to my amazing family.

ABBREVIATIONS

Abbreviation	Definition
ACT	Adoptive cell transfer
AD	Alzheimer's disease
ADC	Antibody-drug conjugates
ADCC	Antibody-dependent cell cytotoxicity
ADCP	Antibody-dependent cell phagocytosis
AID	Activation-induced cytidine deaminase
ALL	Acute lymphoblastic leukaemia
AML	Acute myeloid leukaemia
APC	Antigen presenting cell
ARG1	Arginase 1
BCR	B cell receptor
BSA	Bovine serum albumin
CAR	Chimeric antigen receptor
CDC	Complement-dependent cytotoxicity
CDR	Complementarity determining region
CFSE	Carboxyfluorescein succinimidyl ester
CLL	Chronic lymphocytic leukaemia
DC	Dendritic cell
DENV	Dengue virus
ELA2	Neutrophil elastase
ELISA	Enzyme-linked immunosorbent assay

ER	Endoplasmic reticulum
FcR	Fc receptor
FMAT	Flourometric microvolume assay technology
GFP	Green fluorescent protein
GM-CSF	Granulocyte-macrophage colony-stimulating factor
GPI	Glycosylphosphatidylinositol
GVHD	Graft-versus-host disease
HAMA	Human-anti-mouse-antibody response
hCMV	human cytomegalovirus
HL	Hodgkin lymphoma
HLA	Human leukocyte antigen
HSC	Haematopoietic stem cells
IF	Immunofluorescence
IFN	Interferon
Ig	Immunoglobulin
IHC	Immunohistochemistry
IL	Interleukin
iNOS	Induced nitrous oxide
ITAM	Immunoreceptor tyrosine-based activating motif
ITIM	Immunoreceptor tyrosine-based inhibitory motif
KIR	Killer immunoglobulin-like receptor
KC	Kupffer cells
LILR	Leukocyte immunoglobulin-like receptors

LPS	Lipopolysaccharides
mAb	Monoclonal antibody
MAC	Membrane attack complex
M-CSF	Macrophage colony-stimulating factor
MDDC	Monocyte-derived dendritic cell
MDM	Monocyte-derived macrophage
MDSC	Myeloid-derived suppressor cells
MHC	Major histocompatibility complex
MS	Multiple sclerosis
NK cell	Natural killer cell
NHL	Non-Hodgkin's lymphoma
PCD	Programmed cell death
PCR	Polymerase chain reaction
PTK	Protein tyrosine kinase
RA	Rheumatoid arthritis
ROS	Reactive oxygen species
sALCL	Systemic anaplastic large cell lymphoma
scFv	Single chain variable fragment
SDS-PAGE	Sodium dodecyl sulphate-polyacrylamide gel electrophoresis
SEC	Size exclusion chromatography
SH2	Src homology 2
SLC	Surrogate light chain
SLE	Systemic lupus erythematosus

TAMS	Tumour-associated macrophages
TAP	Transporter associated with antigen presentation
TCR	T cell receptor
TGF	Transforming growth factor
TIL	Tumour infiltrating lymphocyte
TLR	Toll-like receptor
TNF	Tumour necrosis factor
β_2m	β_2-microglobulin

1 INTRODUCTION

1.1 The Immune System

The immune system is a collection of cells, tissues and organs that work together to fight off invading pathogens. There are four main functions of the immune system: recognition, elimination, tolerance and memory[1]. The immune system must recognise foreign cells through cell surface receptors, eliminate them with humoral and cellular responses, whilst also regulating the response carefully to ensure the body's own cells are not harmed, and finally prevent future attack through immunological memory[1].

1.1.1 Cells of the immune system

Cells of the immune system derive from pluripotent hematopoietic stem cells (HSCs) in the bone marrow, from which lymphoid and myeloid lineages arise (*Table 1.1*)[1].

Table 1.1 Myeloid and Lymphoid lineages

Cell		Lineage	Function
	Macrophage	Myeloid	• Phagocytosis • Anti-bacterial • Antigen presentation
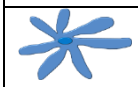	Dendritic Cell (DC)	Myeloid	• Phagocytosis and macropinocytosis • Antigen presentation
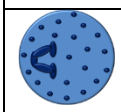	Neutrophil	Myeloid	• Phagocytosis • Anti-bacterial
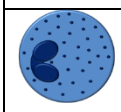	Eosinophil	Myeloid	• Killing of antibody-opsonised parasites • Allergic inflammation
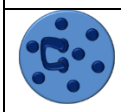	Basophil	Myeloid	• Killing of antibody-opsonised parasites • Allergic inflammation
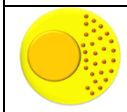	Natural Killer (NK) Cell	Lymphoid	• Recognise and kill non-self cells "(missing self") • Destroy intracellular pathogens, tumours and viruses
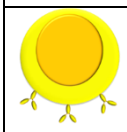	B cell	Lymphoid	• Produce antibodies
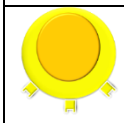	T cell	Lymphoid	• Killing, activation and regulation

Table compiled of data taken from Janeway 7th Edition[1].

1.1.2 Generating an immune response

1.1.2.1 The innate immune response

When microorganisms breach our first line of defence – skin (a physical barrier), and the mucosal epithelial lining around the airways and gut (chemical barriers) – the innate immune response is activated[1]. Cells of the innate immune system express receptors that allow them to recognise invading pathogens[1]. The first cells to respond to infectious agents are usually

phagocytic leukocytes (phagocytes)[1]. There are three types of phagocytic cells: collectively monocytes and macrophages, granulocytes and dendritic cells (DCs)[1]. The first cells to migrate from the blood to the site of infection are neutrophils[2].

Neutrophils, basophils and eosinophils are all granulocytes, named because of their granulated cytoplasm and identified by their staining properties[3]. Ehrlich discovered that eosinophils reacted to acidic dyes, basophils to basic dyes and neutrophils to neutral dyes, and they were named accordingly[3]. Basophils and eosinophils are relatively understudied and their function is less clear[1]. However, neutrophils are the most abundant granulocytes and these ingest and digest micro-organisms[1]. Neutrophils express Toll-like Receptors (TLRs), which allow them to recognise pathogens[2]. These cells are phagocytic, and with the help of reactive oxygen species (ROS) and enzymes, e.g., neutrophil elastase (ELA2) can destroy infectious agents[2].

Monocytes circulate in the blood continuously, but during infection they can enter tissues and differentiate into macrophages[1]. Macrophages are also part of the innate immune response, and express pathogen recognition receptors such as TLRs that recognise bacteria[1]. Bacteria are engulfed by phagocytosis and this triggers the release of cytokines and chemokines that result in the recruitment of other immune cells, causing inflammation, whereby cells flood to infected tissues from the blood[1]. Macrophages also act as scavenger cells, ridding the body of the host's dead cells and cellular debris[1]. Macrophages are highly plastic cells[4]. They can be categorised by their different phenotypes. Various different phenotypes have been proposed, but the simplest defines macrophages as either M1 or M2. M1 (classically activated) macrophages, which are polarised by bacterial Lipopolysaccharides (LPS) or tumour necrosis factor (TNF)-α and interferon (IFN)-γ, induce pro-inflammatory cytokine secretion such as interleukin (IL)-12 and IL-23[5, 6]. M1 macrophages are associated with so -called T_H1 responses (see later), are more efficient at antigen presentation and destroying intracellular pathogens, and are involved in eliminating tumours and preventing tissue damage[4]. M2 (alternatively activated) macrophages are associated with T_H2 responses (see later)[4]. These macrophages can be further sub-divided into three classifications: M2a, M2b and M2c[6]. M2a (alternative) macrophages are induced by IL-4 and IL-13, and are involved in inflammation, allergy, and the killing and encapsulation of parasites[6]. M2b (Type II) macrophages are induced by immune complexes (ICs), TLRs or IL-1R ligands[6]. They are involved in T_H2 activation and immunoregulation[6]. M2c (deactivated) macrophages are induced by IL-10 and glucocorticoid hormones, and are involved in immunoregulation, matrix deposition and tissue remodelling[6]. M2 macrophage subsets produce anti-inflammatory cytokines such as IL-10[4, 6].

DCs are also phagocytic and perform macropinocytosis, whereby they ingest extracellular fluid and its content[1]. Whilst they do engulf pathogens by phagocytosis, their main function however, is to act as antigen presenting cells (APCs); presenting fragments of pathogens to T lymphocytes (T cells) and thus being a crucial bridge between innate and adaptive responses[1]. DCs are described as Human Leukocyte Antigen (HLA)-DR^+ and $lineage^-$ cells[7]. Cytokines secreted by DCs regulate transcription factors that modulate T_H1, T_H2, T_H17 and regulatory T cell (T_{reg}) expression and differentiation[8] (see later). DCs, like macrophages are also highly plastic. There are at least three subsets of DCs: myeloid type 1 (mDC1) which are Blood Dendritic Cell Antigen (BDCA)-1^+, myeloid type 2 (mDC2) that are BDCA-3^+, and plasmacytoid DCs (pDCs) that are BDCA-2^{+}[8, 9]. Myeloid DCs express myeloid antigens such as CD11b and CD11c, whilst pDCs do not, but can be identified by their expression of CD123, CD303 and CD304[9]. DCs recognise antigens through TLRs, by recognising pathogen associated molecular patterns (PAMP), leading to secretion of pro-inflammatory cytokines that can initiate an immune response against the pathogens[10]. Whilst mDCs express TLR1-4, TLR6 and TLR8; pDCs express TLR7 and TLR9[10]. T cell proliferation has been shown to predominantly be induced by mDC1 cells, indicating that they are involved in T cell responses[10]. pDCs make up 0.4% of human peripheral blood mononuclear cells (PBMCs), and are involved in allergic responses, producing high levels of type I interferons[11]. They express high levels of FcεRI, which upon stimulation results in the secretion of pro-inflammatory cytokines IL-6 and TNF-α that lead to T_H1 responses, regulated by TLR9[11]. Therefore, the different populations of DCs may vary in the way they recognise pathogens and elicit immunity[10]. Another type of DC worth mentioning are follicular DCs (fDCs). These cells are found in follicles of secondary lymphoid organs[12]. The origins of fDCs are conflicting, with mouse studies suggesting mesenchymal origins, whilst other reports suggesting they are fibroblast-like cells, and pre-cursors for these cells are yet to be identified[12]. Regardless, these cells do not originate from haematopoietic cells like the DCs previously mentioned, and although they function as APCs, they do not internalise, process and present these antigens to HLA molecules, but instead to complement receptors CR1 and CR2[12]. These differences have led to the contention that despite their similar morphology to DCs, these cells may not actually be DCs[12].

Whilst neutrophils, macrophages and DCs deal with extracellular pathogens, Natural Killer (NK) cells respond to intracellular pathogens and tumours, and are the first cells to respond to viruses[2]. These cells help regulate the immune system through production of IFN-γ and TNF-α and they mediate killing by releasing perforin and granzymes that mediate apoptosis within the target cells[2]. One way in which, NK cells distinguish between healthy and infected cells,

is through Major Histocompatibility Complex (MHC) I expression, found on healthy cells but typically down-regulated on infected cells; this is referred to as the "missing self" hypothesis[2, 13].

1.1.2.2 The adaptive immune response

Lymphocytes are also important cells that make up the immune system and can be defined as either B lymphocytes (B cells) or T cells[1]. During the innate immune response, DCs act as phagocytes and ingest invading pathogens, which they subsequently present to naïve T cells that differentiate into effector cells, thus activating the cell-mediated immunity and adaptive immune responses[1]. Helper T cells help to fully activate B cells (which can also act as APCs), leading to the generation of antibody secretory plasma cells that lead to the humoral response[2]. All lymphocytes - T cells and B cells - have pre-determined antigen specificity through gene rearrangement, which occurs when they mature in the thymus or bone marrow, respectively[2]. Once a pathogen invades, mature lymphocytes that can specifically recognise the antigens expressed on them become activated and divide, replicating into clones with identical specificity: This is called clonal expansion[2]. A primary response is the first time these cells recognise an antigen; if an antigen reinvades, a faster and more substantial secondary response occurs[2]. The secondary response is due to memory cells produced during the primary response, which are primed to ensure the immune system can react more quickly and efficiently to any reoccurring infection[2].

1.1.2.2.1 Humoral Immunity

1.1.2.2.1.1 B cell Development

When the B cell receptor (BCR) is activated by an antigen, B cells differentiate into plasma cells which produce and secrete antibodies[1]. Antibodies are an important part of the adaptive immune response and have identical specificity to the B cell that produced it, as the antibody is effectively a secreted form of the BCR[1]. B cells arise from HSC and develop and mature in the bone marrow[2] (*Figure 1.1*).

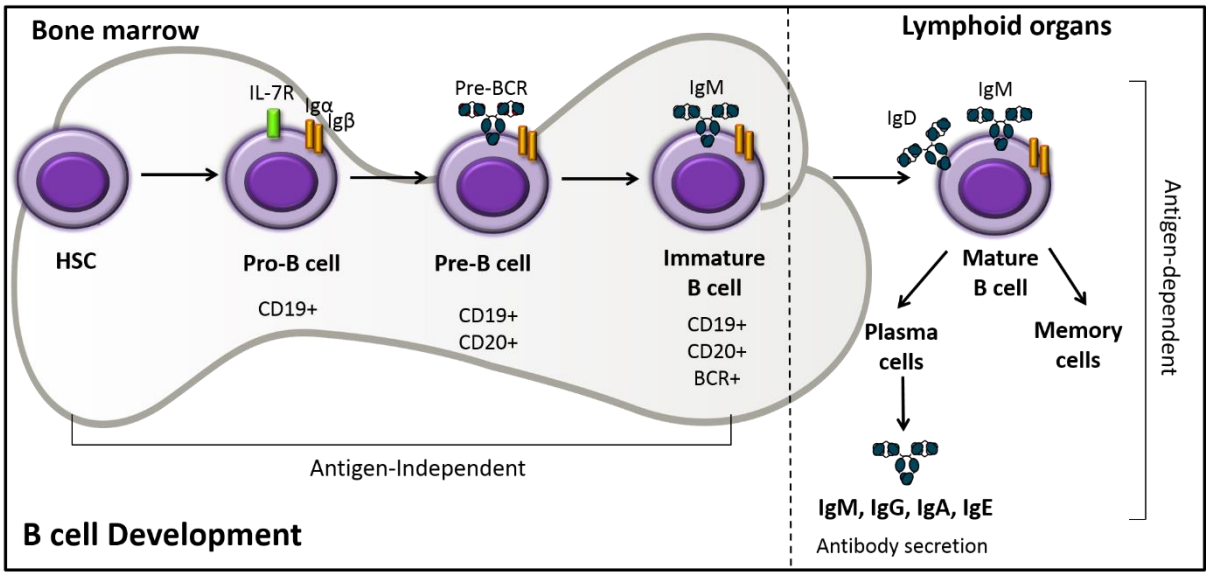

Figure 1.1 B cell development. B cells derive from HSCs in the bone marrow. These cells then differentiate into pro-B cells, expressing IL-7 receptors (IL-7R) that undergo heavy chain gene rearrangement. Pro-B cells differentiate into Pre-B cells, which express IgαIgβ heterodimer (CD79a/b) and a pre-BCR consisting of a heavy chain and surrogate light chain (SLC) on its surface. The pre-B cell undergoes light chain gene rearrangement and then differentiate into an immature B cell. Immature B cells express IgM on their surface and enter peripheral secondary lymphoid organs where they become naïve B cells that express both IgM and IgD that act as BCRs. Once activated by an antigen these naïve B cells can mature and differentiate into plasma cells that secrete IgM or IgG, IgA, IgE through class switching. Alternatively these cells can become memory cells. Figure sourced from[2, 14, 15, 16].

In the bone marrow, HSCs begin to differentiate into pro-B cells, which undergo heavy chain (μ) rearrangement, and express IL-7 receptors[2]. This rearrangement involves VDJC gene rearrangement (see later). The pro-B cell interacts with stromal cells that secrete IL-7[16]. IL-7 is thought to drive further maturation of the pro-B cell into a pre-B cell[2]. The pre-B cell expresses Igα (CD79a) Igβ (CD79b) heterodimer, and a pre-BCR that consists of a heavy chain, and a SLC[2, 15, 16]. During B cell development, the pre-BCR has two roles, in order to prevent autoreactivity. The first is to shut down the catalytic activity of enzymes involved in heavy chain gene segment rearrangement[15]. This prevents two heavy chain gene segments on the same cell from having two different specificities[15]. This process is known as allelic exclusion. The second role of the pre-BCR is to initiate light chain gene rearrangement[15]. The pre-B cell subsequently undergoes Igκ and Igλ light chain VJC rearrangement (see later) and differentiates into an immature B cell that expresses both the heavy and light chains, which come together to form soluble IgM[2]. Until this point, each stage of B cell development is antigen independent, however, an immature B cell will leave and enter the lymph nodes, spleen and other secondary lymphoid organs and become a naïve B cell that expresses both IgM and IgD, which act as antigen receptors[2, 17]. IgD expression on the surface of B cells occurs once the B cell leaves the bone marrow. Although both IgM and IgD are capable of

binding to the same ligands, the function of IgD is unclear[18]. Some reports have suggested it has no role in B cell development, whilst other studies have shown it can function as a BCR in replace of IgM[18, 19]. Upon antigen stimulation, B cells differentiate into either plasma cells that secrete antibodies or memory cells[17].

The invariant chain (Ii), an MHC II chaperone, has been shown to be important in the development of immature B cells into a mature cells[20]. Matza *et al* showed that mice lacking the Ii produced immature B cells that were arrested at this stage of development and unable to mature[20]. It is less clear which cytokines are important in human B cell development, although IL-7 is important in mice and has shown some importance in survival of pro-B cells in humans, it has not shown similar significance in human B cell development *in vitro* or *in vivo*[21].

To ensure Igs are able to recognise different foreign pathogens, diversity is essential[2]. However, there are not enough genes to encode each antibody that would be required to recognise the many pathogens that can invade. Therefore, the immune system creates diversity through a number of different mechanisms to ensure the largest possible antigen-specific repertoire of antibodies are produced[17]. They achieve this diversity in many ways, one of which is by having multiple germline segments that can be recombined to produce different antibodies[17]. The heavy chain has VDJC gene segments that undergo VDJ rearrangement to make the variable region of the antibody, whilst the light chain has VJC segments that perform VJ rearrangement to make the variable region of the light chain[2, 17]. These functional gene segments randomly combine to generate Ig diversity by site-specific recombination[2, 17]. The antibodies that are secreted from plasma cells are mono-specific (identical antigen specificity), but are bivalent, allowing the antibodies to cross-link antigens and ensuring their elimination[17].

Junctional flexibility, whereby alternative amino acids are added to "coding joints" also adds to variability[2]. Complementary nucleotides added to make a palindromic sequence at the "coding joint" is referred to as P-addition, whilst N-addition refers to when variable-region coding joints are encoded by nucleotide addition during gene segment rearrangement[2]. Addition of both of these nucleotides adds to the diversity of Igs. Due to gene segment rearrangement it is possible to generate various light and heavy chain genes, therefore when the two associate, many different combinations can arise, thus creating further diversity[2].

Somatic hypermutation is another way in which antibody diversity is achieved. Once a mature B cell leaves the bone marrow and enters peripheral lymphoid organs, antigen-dependent B

cell development occurs[22]. Mutations in the v-region of the antigen binding site are introduced through nucleotide substitutions, in "hot spots" that are susceptible to this kind of mutation[2, 22]. If this results in higher antigen-binding affinity of the BCR, the mutated B cells will survive and differentiate, whilst continuing to produce antibody-secreting plasma cells with the new specificity[22].

Mature B cells produce plasma cells that secrete IgM, however, when the relevant antigen binds to its specific BCR, the activated B cell can undergo class switching in the Ig heavy chain to produce different classes of Ig[2]. Subsequently, IgG, IgE or IgA antibodies are generated, each class dealing with invading pathogens in different ways (as described later). This involves the VDJ gene segments of the heavy chain combining with different constant heavy chain regions[2]. Switch regions (DNA flanking sequences), a switch recombinase enzyme that recognises and exercises recombination, and cytokines such as IL-4 that determine the class of Ig to be produced, all aid in class switching[2]. Another important contributing factor is the enzyme activation-induced cytidine deaminase (AID), which is important in both somatic hypermutation and in class switching[2]. This enzyme works by conversion of cytosine to uracil nucleotides[2]. As uracil is not one of the nucleotides found in DNA, it must be replaced with an alternative nucleotide, thus creating mutations in the sequence and therefore changing the transcript/messenger RNA (mRNA) and subsequent protein produced[2].

1.1.2.2.1.2 Antibodies

Antibodies are Igs that are secreted by B cells. The general structure of a typical antibody is the same: two heavy and two light chains that consist of two Fab arms with complementarity determining regions (CDRs), and an Fc stalk[1]. Antibodies can be subdivided into five different classes: IgG, IgM, IgA, IgD and IgE, distinguished by their different Fc regions (*Figure 1.2*)[1].

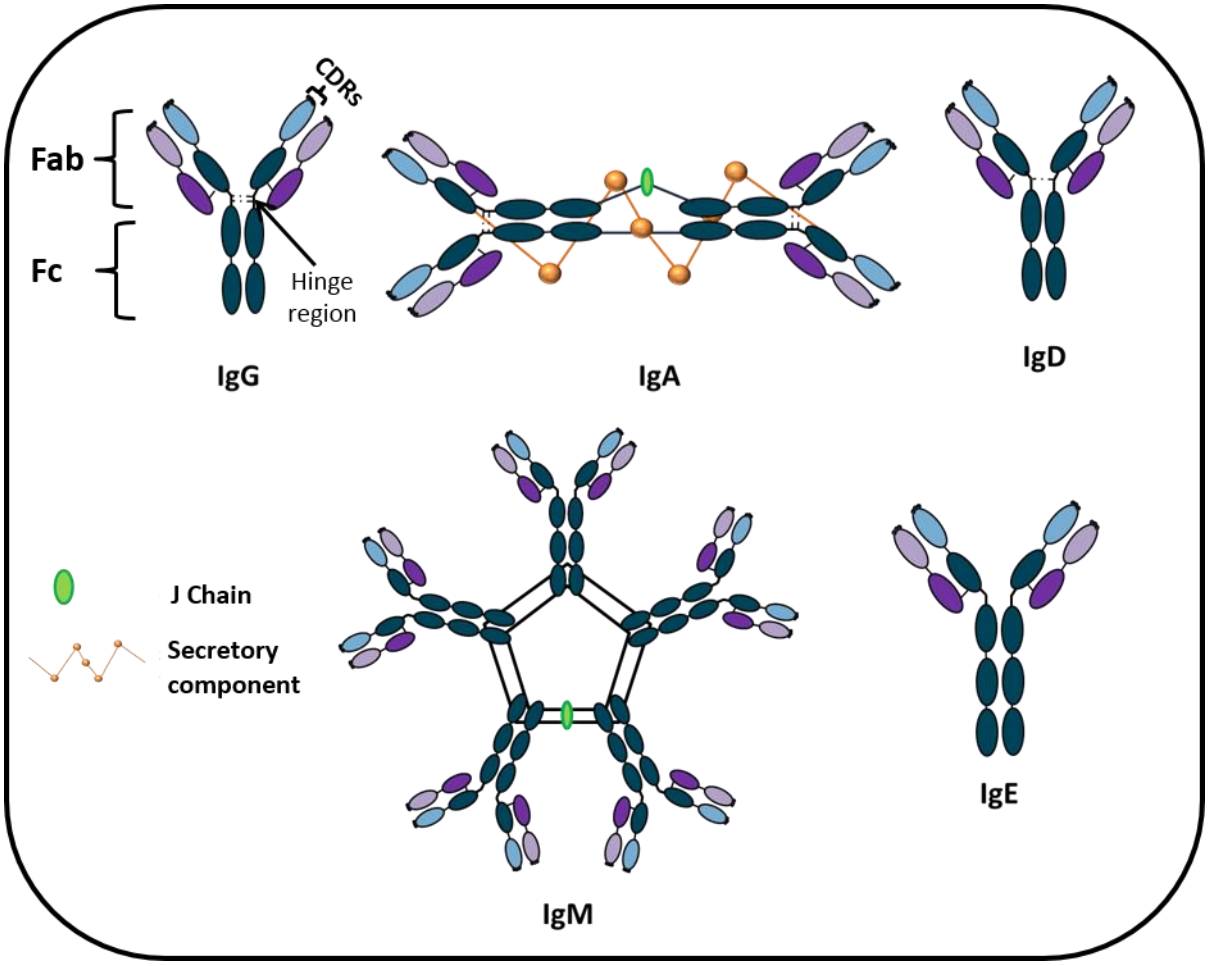

Figure 1.2 Five classes of immunoglobulins. IgG, IgA, IgD, IgM and IgE are all immunoglobulins secreted by B cells. Their basic structure is the same, each containing Fab arms with CDRs, hinge regions and heavy (blue) and light (purple) chains. However, they differ in their Fc region. IgG, IgA and IgD all contain 4 heavy chain domains with a hinge region whilst, IgM and IgE have 5 heavy chain domains and no hinge regions. IgM can also be in its surface bound form (not displayed here). IgD is similar in structure to IgG but is coated by more carbohydrates (more glycosylated). Dimeric IgA has a J chain polypeptide and a polypeptide chain known as a "secretory component". This J chain is also found in secreted IgM.

IgG, IgA and IgD all contain four heavy chain domains with a hinge region, whilst IgM and IgE have five heavy chain domains and no hinge[2] (*Figure 1.2*). IgG is the most abundant Ig found in serum[2]. There are four subclasses of human IgG: IgG1, IgG2, IgG3 and IgG4, which differ in their γ chain constant region[2]. All IgG sub-classes are important in foetal development by providing immune protection for the foetus, which is yet to develop humoral immunity[23]. IgG3 is the most effective activator of complement, and IgG1 and IgG3 mediate opsonisation as they bind more strongly to Fcγ Receptors (FcγRs) found on phagocytic cells (see later)[2]. IgA is found mainly in its monomeric form in serum, but its dimeric form in secretions (*Figure 1.2*)[2]. Dimeric IgA has a J chain polypeptide involved in polymerisation and a polypeptide chain known as a "secretory component" that is involved in membrane transport[2]. It is found at mucous membranes and plays a role in protection against bacteria and other infections[2]. IgM is found on the cell surface of B cells but can also be secreted by

plasma cells in its pentameric form (shown in *Figure 1.2*)[2]. Like dimeric IgA, IgM also has a J chain involved in polymerisation of IgM from a monomer to a pentamer[2]. IgM is the most efficient Ig at activating complement, and alongside IgG is involved in neutralising viral infections[2]. IgD is similar in structure to IgG, although it makes up only 0.2% of serum Ig, and its function is still unknown[2]. Its low quantity suggests that it may not play a major role in immunity, however, BCR signalling is important for B cell maturation and both IgD and IgM are expressed on mature B cells, and therefore IgD may play an important role in B cell development[24]. IgE is found in low levels in serum but is involved in allergic reactions such as hay fever and asthma[2]. IgE binds to FcεR on basophils and mast cells that release substances that aid in inflammation, such as histamine, which mediates allergic responses[2]. The function and serum concentrations of these Ig subclasses in healthy individuals are summarised in *Table 1.2*.

Table 1.2 Human Ig serum concentrations and functions

Immunoglobulin (Ig) subclass	Serum proportion	Function
IgG	80%	Phagocytosis Activation of complement Provides foetus with humoral immunity
IgA	10-15%	Involved in mucosal immunity
IgM	5-10%	Activating complement Neutralising viral infections
IgD	0.2%	Unknown
IgE	Very low	Allergic responses

Table compiled from Kuby's Immunology[2].

1.1.2.2.2 Cell-mediated Immunity

1.1.2.2.2.1 T cell development and T cell subsets

Like the BCR, the TCR defines T cells, and undergoes similar V(D)J rearrangement: the α chain has VJC gene segments that undergo VJ joining; whilst the β chain contains VDJC

segments that undergo VDJ joining[1]. The TCR also completes allelic exclusion and somatic hypermutation (*see earlier 1.1.2.2.1.1*)[1].

T cells arise from HSCs that have migrated into the thymus[25]. Cytokines such as IL-7 are crucial to their development, alongside NOTCH receptors required for differentiation and proliferation[21]. As they are produced, T cells are assessed for self-reactivity, and only those T cells that have a non-self-reactive TCR will be able to mature, leave the thymus and pass into the circulation[25]. When T cells first develop in the thymus they are classed as double negative (DN)[25]. DN cells have no CD4 or CD8 protein, and express the pre-TCR[26]. There are four stages of DN: $CD44^+$ $CD25^-$ C^{kit} (CD117), $CD44^+$ $CD25^+$ C^{kit}, $CD44^-$ $CD25^+$ and $CD44^-$ $CD25^-$ pre-TCR[25, 26, 27] (*Figure 1.3*). Once these DN cells express the mature TCR successfully, the cells proliferate and become double positive (DP) thymocytes that now express the complete αβ TCR and CD4 and CD8 proteins[26]. The DP thymocytes interact with cortical epithelial cells that express MHC I and MHC II molecules, which are associated with self-peptides[26]. The ability of thymocytes to recognise self-peptides is then tested. When this signal is too low or too high (self-peptides recognised weakly or too strongly, respectively), they are removed by apoptosis during a process known as negative selection[1, 26]. An ideal intermediate signal results in the cells maturing by positive selection[1, 26]. Thymocytes that express TCRs that can recognise self-peptides associated with MHC I molecules, become $CD8^+$ T cells, whilst those binding to MHC II molecules become $CD4^+$ T cells[26]. These single-positive cells then leave the thymus to populate lymphoid organs, where they can become activated by infectious agents[1].

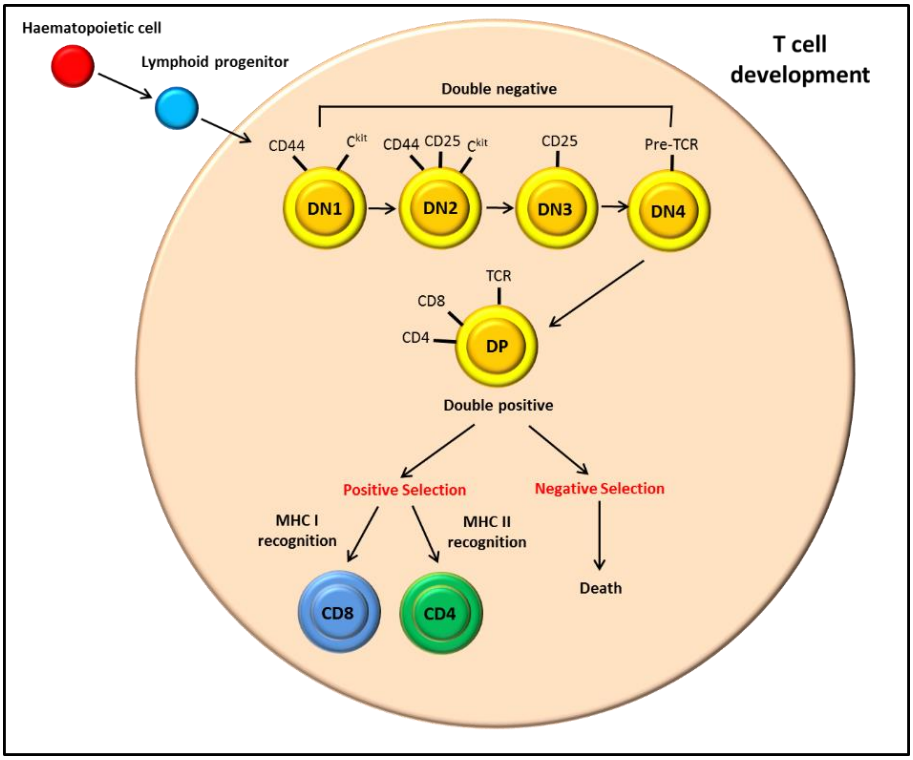

Figure 1.3 T cell development. Haematopoietic cells in the bone marrow that become committed lymphoid progenitors migrate to the thymus and become DN thymocytes, which are TCR negative and $CD8^{-}CD4^{-}$. These cells become DP. DP cells can mature into $CD8^{+}$ or $CD4^{+}$ cells by positive selection, depending on whether they recognise MHC I or MHC II self-peptides respectively. Conversely, self-reactive cells are removed by negative selection.

$CD8^{+}$ T cells are cytotoxic and kill infected cells, whilst $CD4^{+}$ T cells are more variable in their function and mechanism of action[1]. There are different $CD4^{+}$ T cells subsets, that are characterised by the cytokines they produce[1] (*Figure 1.4*).

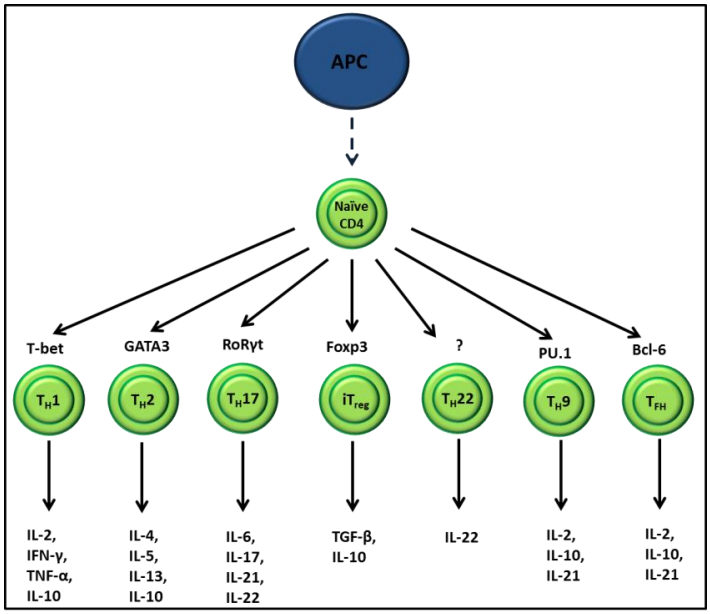

Figure 1.4 CD4+ T cell subsets. Naive CD4+ T cells can differentiate into different subsets, characterised by their cytokine profiles. Transcription factors are described as being "master regulators" of their differentiation. Their differentiation is driven by cytokines and the cells themselves also secrete different cytokines[1, 28, 29, 30, 31, 32].

When activated by APCs such as a DC (detailed earlier), $CD4^+$ T cells differentiate into different subsets. T_H1, T_H2, T_H17 and T_{reg} are the most well characterised of these[1]. T_H1 cells differentiate from naïve $CD4^+$ T cells following stimulation with IL-12 and IFN-γ; once polarised these cells secrete cytokines such as IL-2 and IFN-γ[1]. Transcription factors such as STAT4 and T-bet are important in their differentiation[1, 33]. T_H1 cells promote macrophage activation required for clearing bacterial infections, and aid in eliminating extracellular pathogens[1]. T_H1 cells are also involved in IgG antibody secretion through the activation of B cells[1]. T_H2 cells are polarised by IL-4 and they secrete cytokines such as IL-4 and IL-5[1]. Transcription factors such as GATA3 and STAT6 aid in their differentiation[1, 33]. GATA3 is involved in both inducing and maintainingT_H2 expression[1]. T_H2 cells drive B cell differentiation and the production of other Igs, in particular IgE[1]. T_H17 cells are polarised by transforming growth factor (TGF)-β and IL-6 with the help of transcription factor RoRγT; they secrete cytokines such as IL-2 and IL-17 and are involved in neutrophil recruitment in the first stages of infection[1]. T_{reg} cells are involved in controlling inflammation, maintaining tolerance by helping to eliminate self-reactive cells to prevent the development of autoimmunity[1]. Foxp3 is an important transcription factor in T_{reg} cell differentiation along with TGF-β[1, 28].

Other less characterised helper T cell subsets also exist. Follicular helper T (T_{FH}) cells were discovered in tonsils in the early 2000s through their unique high expression of CXCR5[34]. The discovery of Bcl-6 as the master regulator for T_{FH} cell differentiation along with

cytokines such as IL-21 established these cells as a distinct T_H subset[34]. T_{FH} cells maintain germinal centres and play an important role in B cell differentiation into memory cells or antibody-secreting plasma cells[34]. New T cell subsets such as T_H9 and T_H22 have also been described[31, 32]. T_H9 differentiation is driven by the transcription factor PU.1 and IL-9[32]. Gerlach *et al* showed that this new helper T cell subset has a role in ulcerative colitis and could be a therapeutic target in the treatment of chronic intestinal inflammation[32]. Although associated with T_H17, the cytokine IL-22 has also been implicated in being part of the T_H22 cytokine profile; a new subset that has therapeutic implications in inflammatory skin disorders and chronic inflammation[31]. T_H22 cells are thought to be polarised by IL-6 and TNF-α[35].

Characterisation and the role of these helper T cell subsets is far from straight forward. Although, these $CD4^+$ T cell subsets are characterised by their cytokine profile, the same cytokine can be involved in the differentiation of more than one subset e.g. IL-10 is believed to be important for T_H1, T_H2, T_H17 and T_{reg}[33]. Furthermore, these subsets are very plastic, and their profiles can change, making them very difficult to identify and study[33].

1.1.2.2.2.2 Tolerance

Successful B and T cell development are important to ensure that cells can recognise foreign pathogens and generate an immune response to eliminate these pathogens. However, the immune system must also ensure immune responses do not get out of control and start attacking the body's own cells. This is a process known as tolerance[1]. Tolerance can be divided into two categories: central tolerance and peripheral tolerance[1]. During development, self-reactive lymphocytes are eliminated by central tolerance in the bone marrow and by cross-presentation (see later) in the thymus[1]. Self-reactive lymphocytes that manage to mature and migrate to the periphery due to the absence of their self-antigens, are subsequently eliminated by peripheral tolerance[1]. Peripheral tolerance can occur in three different ways: peripheral anergy (weak signalling making them non-responsive to antigen stimulation), suppression (by regulatory cells such as T_{regs}) and deletion (by apoptosis)[1]. These 'checkpoint' mechanisms ensure that immune responses against self-cells and subsequent destruction of these cells is avoided, thus preventing the development of autoimmunity[1]. Sometimes foreign pathogens can disguise themselves as 'self' by "molecular mimicry", whereby they express antigens that resemble host antigens to avoid detection[1].

1.1.2.2.2.3 Antigen processing and presentation

MHC molecules or HLA molecules, as they are referred to in humans, play an important part in the adaptive cellular immune response. They are polymorphic cell membrane glycoproteins

that can be divided into two classes: MHC I and MHC II[1, 2, 36]. Classical MHC class I molecules are formed from a heterodimer consisting of a polymorphic α heavy chain and a non-polymorphic β2-microglobulin (β_2m) light chain; whilst MHC II is also a heterodimer formed of two homogenous peptide domains, made up of two α and two β domains[36](*Figure 1.5*).

MHC II molecules have expression restricted to APCs i.e., macrophages, DCs and B cells[36]. MHC II molecules bind to peptides that have been processed by endocytic pathways and therefore can present peptides from ingested extracellular proteins to $CD4^+$ T helper cells[36]. When these T helper cells become activated they release cytokines that in turn can activate cytotoxic T cells, as well as B cells and macrophages, thus also activating the humoral immune response[2]. These helper cells can also become memory cells[2].

MHC I molecules are ubiquitously expressed on all nucleated cells[36]. Proteasomes degrade intracellular peptides found in the nucleus and cytosol, which are then translocated to the endoplasmic reticulum (ER) with the help of transporter associated with antigen presentation (TAP)[36]. It is in the ER that MHC I molecules are assembled and the processed peptides are loaded on to the MHC I molecules, before they are sent to the cell surface for presentation to $CD8^+$ cytotoxic T cells[36]. This process allows monitoring of intracellular components of the cell. As all cells express MHC I molecules, and self-peptides are loaded onto them, the TCR will recognise these peptides as self and will not attack the cell[37]. This therefore provides the cells with a way of not being attacked by the immune system[37]. However, virally infected cells will present viral peptides onto MHC I, which $CD8^+$ T cells will recognise as non-self and attack[37].

NK cells operate in a different manner to T cells, as they express receptors that can recognise self MHC I on cells[37]. NK cell receptors include human killer cell immunoglobulin-like receptors (KIRs) (*see later*) and killer lectin-like receptors (KLRs)[37, 38]. Stimulation of activatory receptors activates NK cells to kill by granzymes and perforin, whilst inhibitory receptors prevent NK cells from killing[37, 38]. LILRA2 and LILRB1 belonging to the LILR family, are also expressed on NK cells[37, 38, 39]. Cells that express self MHC I remain unharmed by the NK cells, whilst cells that express foreign MHC I or do not express MHC I at all (e.g., during transplantation or down-regulated in disease) are lysed by NK cells[37, 38]. Cells often down-regulate MHC I once infected or they become malignantly transformed, therefore NK cells are able to kill these infected cells by recognising them in this way[37, 38].

A third class of MHC molecules also exists: non-classical MHC. Although some may play a role in regulating immunity and have APC function, others are not involved in immune responses at all, for example HFE (a non-classical MHC I molecule), which is involved in iron metabolism[40]. Non-classical MHC molecules are typically less polymorphic and are expressed to a lesser extent on cells than the classical MHC molecules[40, 41]. HLA-G is a non-classical MHC I molecule that has been implicated in interacting with KIRs and LILRs[40]. However, this remains a relatively understudied group of molecules[40].

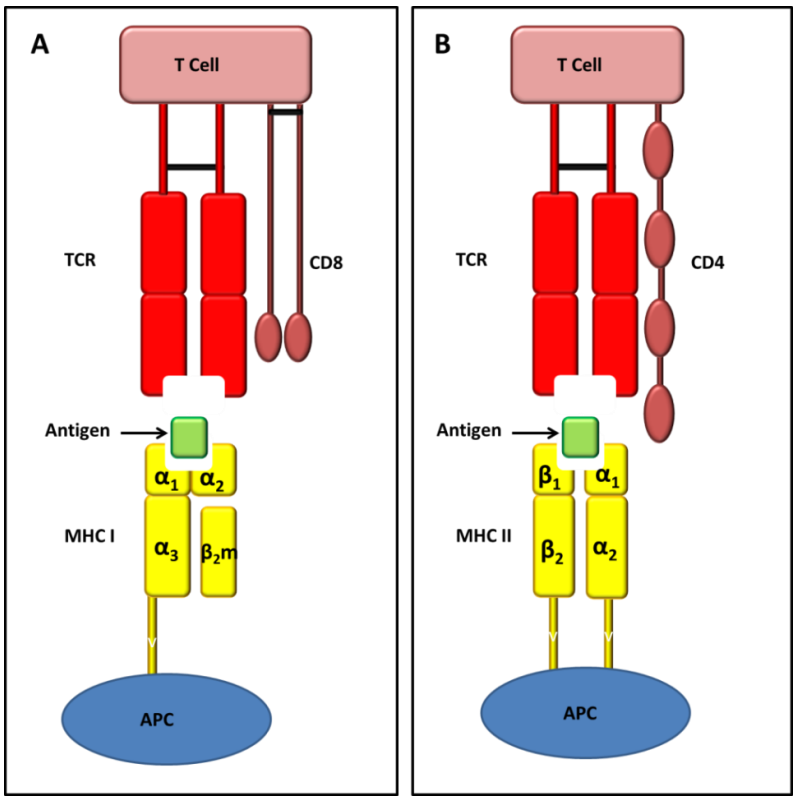

Figure 1.5 MHC antigen presentation to T cells. MHC I and MHC II molecules differ in their structures. A) Intracellular antigens are presented by MHC I molecules to CD8+ T cells. MHC class I molecules consist of a polymorphic heavy α chain and a non-polymorphic β2m light chain. B) MHC II molecules present extracellular peptides to CD4+ T cells. MHC II is a heterodimer formed of two homogenous α and β peptide domains.

1.1.2.2.2.4 Cross Presentation

An alternative pathway to the antigen presentation is cross-presentation. The MHC II pathway presents external peptides from the environment to $CD4^+$ T cells, whilst the MHC I pathway presents peptides synthesised internally to $CD8^+$ T cells[42]. However, $CD8^+$ T cells cannot become cytotoxic and eliminate transformed or infected cells without firstly being activated by APCs[42]. It has been shown experimentally that to overcome this, APCs that have not been directly infected can present extracellular antigens found on these cells through the MHC I pathway by cross presentation[42]. This occurs mainly through DCs, although the subsets

involved are unclear[42]. Cross-presentation was first described in 1976 by Michael J. Bevan, who found that upon injection of alloantigens into mice, $CD8^+$ T cell responses were primed[43]. This suggested that the recipients APCs induced $CD8^+$ T cell responses to extracellular antigens (normally presented to $CD4^+$ T cells). Impaired APCs can cause tumour cells and viruses, to go unnoticed[42]. During infection, cytotoxic $CD8^+$ T cells (CTLs) can be primed either directly, when DCs are infected with antigens derived from infectious pathogens or through cross-presentation[42]. Although, not fully elucidated, it has been shown that DCs are often impaired in tumours, and this dampens CTL responses[42]. It is then, when cross-priming of DCs are essential in activating CTLs to ensure anti-tumour responses[42].

1.2 Cell surface receptors of the immune system

Cell surface receptors are an integral part of the immune response, as they respond to external stimuli and transmit this information to the cell interior through signal transduction[1]. Receptors that are involved in cellular activation typically associate with protein kinases that result in cellular activation, whilst inhibitory receptors typically associate with phosphatases that cause inhibition of activation[44].

1.2.1 ITAMs and ITIMs

Activating receptors typically have, or associate with molecules that have, immunoreceptor tyrosine-based activating motifs (ITAMs) in their intracellular domains[44]. ITAMs have tyrosine residues in a consensus sequence of YxxI/Lx or YxxI/L[44]. When an activatory receptor is ligated by its ligand, these tyrosine residues are typically phosphorylated by Src family protein tyrosine kinases (PTK), which create docking sites for Syk family kinases such as Syk or ZAP70 that bind to Src homology 2 (SH2) domains (*Figure 1.6 below*)[44]. This recruits effector molecules such as phospholipase C-γ (PLCγ), which results in downstream cellular activation[44].

Inhibitory immune receptors typically have immunoreceptor tyrosine-based inhibitory motifs (ITIMs) in their intracellular domain[44]. They also have tyrosine residues in the consensus sequence: S/I/V/LxYxxI/V/L[44]. When inhibitory receptors are activated by their ligand, Src family PTK phosphorylate tyrosine residues in the receptor ITIM domains, which recruits phosphotyrosine phosphatases such as Src homology region 2 domain-containing phosphatase (SHP)-1 and SHP-2 or inositol phosphatases like phosphatidylinositol-3,4,5-trisphosphate 5-phosphatase (SHIP)[44]. Recruitment of these phosphatases results in dephosphorylation of

phosphorylated molecules from activation pathways such as Syk, which subsequently results in downstream inhibition of cell signalling pathways[44].

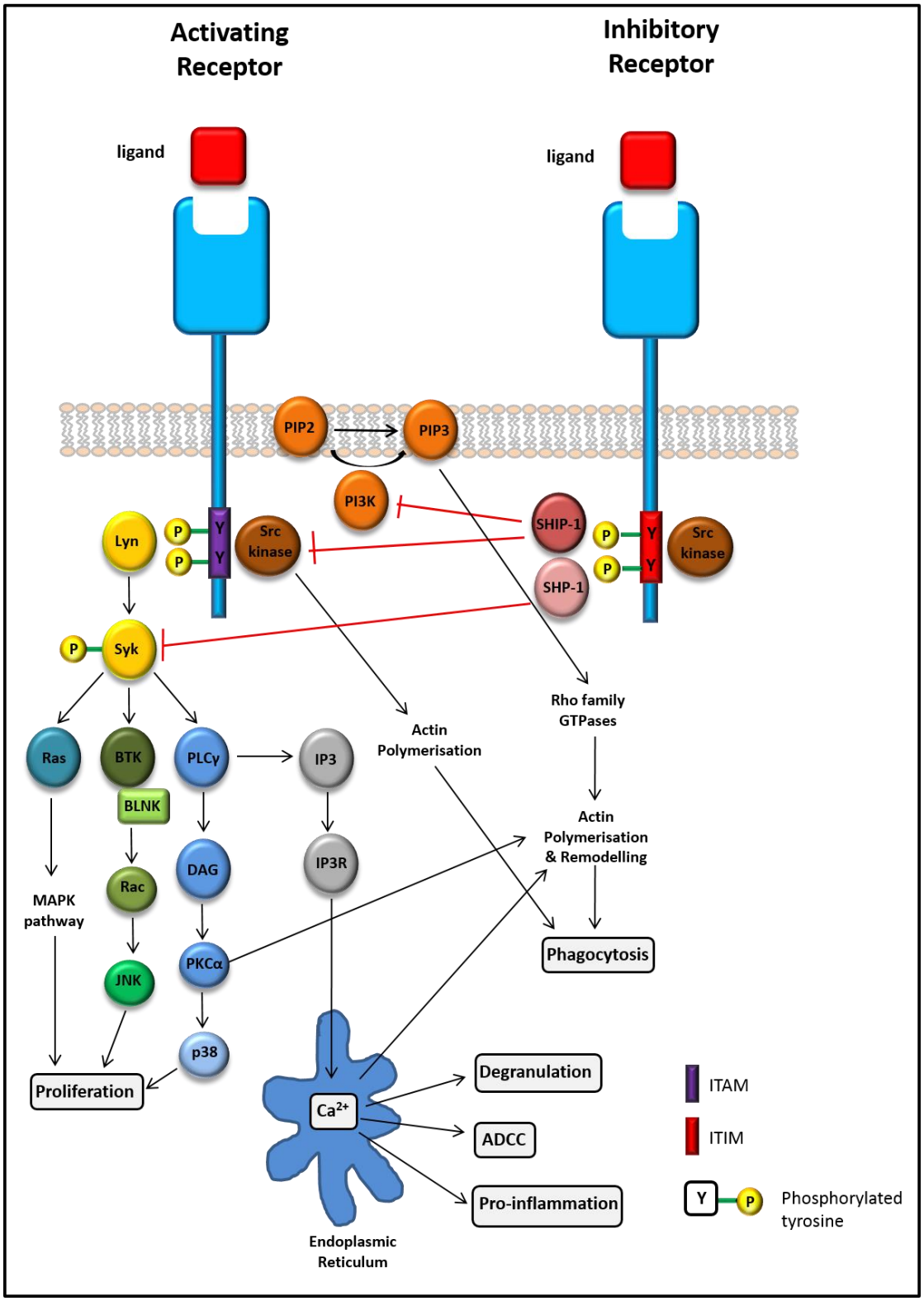

Figure 1.6 Activating and inhibitory receptor signalling through ITAMs and ITIMs. Upon ligation ITAMs in activating receptors are phosphorylated by Src family kinases. This recruits Syk family kinases such as Lyn and Syk, and leads to downstream activatory cell signalling. When inhibitory receptors are ligated, Src family kinases phosphorylate ITIMs, which recruit phosphatases such as SHP-1 and SHIP-1 that cause dephosphorylation and inhibition of cell signalling by inhibited activatory cell signalling pathways. SHIP-1 blocks the conversion of PIP2 to PIP3, which leads to downstream activation.

1.2.2 Fc receptors (FcRs)

FcRs are membrane glycoproteins and Ig receptors that are important for antibody function[2, 45]. There are a number of different FcRs expressed on different immune cells and each FcR binds to different classes of Ig. For example, FcαR binds to IgA, FcεRs binds to IgE and the different FcγRs bind to IgG[2]. Most FcRs can be found on the human chromosome 1q32.3[46]. However, FcαRI, is found on chromosome 19q13.4, along with human Ig-like cell surface receptors: KIRS and LILRs, sharing homology with these receptors[46]. The most prevent Ig in serum is IgG, and most therapeutic also mAbs are IgG[2, 47]. This indicates that FcγRs are particularly important.

Most FcRs have two extracellular Ig domains, with the exception of FcγRI, which has three domains (*Figure 1.7 below*) that are thought to provide the receptor with higher affinity for IgG[45]. All FcRs have transmembrane and intracellular domains; FcγRIIIB however, is attached to the cell membrane through a glycosylphosphatidylinositol (GPI) anchor and its expression is limited to neutrophils[48]. FcR expression is predominantly found on haematopoietic cells, although some have suggested they are expressed on certain T cell populations[46]. It is generally believed however, that T cells do not express FcRs[48].

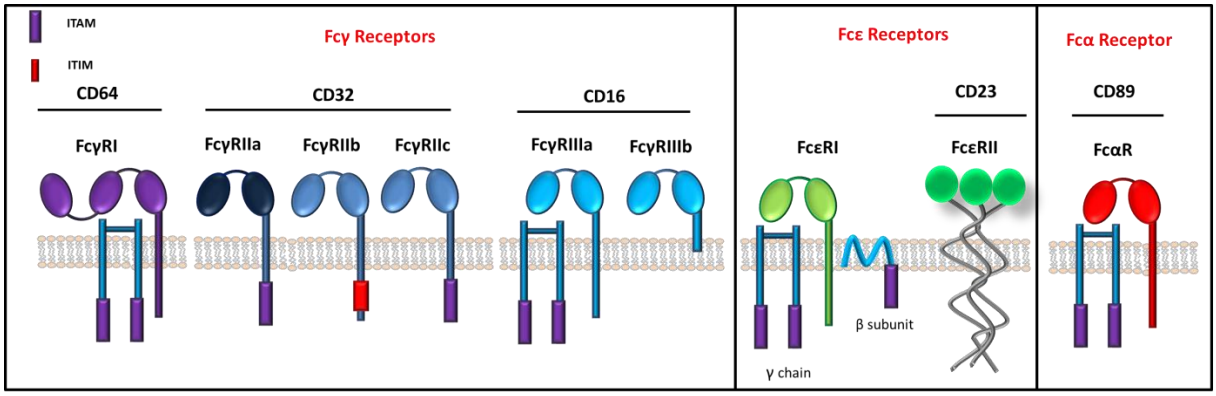

Figure 1.7 Human Fc Receptors. All FcRs have two extracellular domains with the exception of FcγRI, which has three. FcγRs bind to IgG antibodies, Fcα bind to IgA and FcεR bind to IgE. FcγRIIB is the only inhibitory receptor, and has extracellular ITIM domains involved in inhibitory signalling. The other FcRs have ITAMs or have accessory polypeptide chains that aid in activatory signalling. FcγRIIIB is attached to the cell membrane through a GPI anchor. FcεRII has a coiled stalk. Figure adapted from Jönsson & Daëron (2012)[49].

FcRs link the adaptive and innate immune responses by recruiting innate effector cells such as mast cells, neutrophils, monocytes and macrophages to initiate inflammation[45]. It is crucial that immune responses are regulated so as to avoid the destruction of healthy cells. This relies on a balance between activating and inhibitory FcRs, which control immune signalling by creating a threshold of activation through their expression on the same cell[45]. An imbalance

between the two types of FcRs can result in autoimmunity[45]. FcRs also regulate B cell and DC activation, through which they can also effect humoral and cellular immunity[48]. Uptake of ICs into DCs will determine the resultant T cell response[45]. The inhibitory FcγRIIB, has an important role in controlling self-reactivity, and deletion of this receptor has been found to result in loss of tolerance and development of autoimmune diseases[45].

Certain polymorphisms of FcγRIIA and FcγRIII indicate susceptibility to certain infections, and FcRs also have implicated propensity to parasitic infections by mediating endocytosis and phagocytosis[46, 50]. FcγRIIB has been associated with autoimmune diseases such as systemic lupus erythematosus (SLE), where even the slightest increase in the inhibitory receptor is thought to delay disease progression[51]. The receptor has been implicated in current mAb therapies, where anti-FcγRIIB mAbs can either directly affect therapy by targeting FcγRIIB, stimulating inhibitory signalling and reducing effector efficacy[51]. Alternatively, this effect can be indirect, for example with Infliximab (a TNF-α blocker), which has been shown to not only block the increase in FcγRIIA (associated with increased TNF-α) but also increase FcγRIIB expression; consequently decreasing disease severity in Rheumatoid Arthritis (RA)[51]. In the case of direct targeting mAbs such as anti-CD20 antibody Rituximab, FcγRIIB has been shown to hinder mAb therapy[52, 53, 54]. However, for immunomodulatory mAbs, the opposite is true, as FcγRIIB aids in the agonistic function of anti-CD40 mAbs through cross-linking more surface receptor[55]. This highlights the importance of balancing activatory and inhibitory FcγRs. High activatory/inhibitory (A/I) ratios are therefore important for direct targeting antibodies, but the opposite may be true for immunomodulatory mAbs[55, 56]. Thus, FcRs are an attractive target for immunotherapy[48, 57]. The expression pattern of these receptors and affinity for Ig is described in *Table 1.3* below.

Table 1.3 Expression and Function of Human FcRs

FcR	FcγRs						FcεRs		FcαRs
	CD64	CD32			CD16			CD23	CD89
	FcγRI	FcγRIIa	FcγRIIb	FcγRIIc	FcγRIIIa	FcγRIIIb	FcεRI	FcεRII	
Antibody ligand	IgG						IgE		IgA
Affinity	High	Low	Low	Low	Medium	Low	High	Low	Low
Expression	Monocytes Macrophages DCs Neutrophils Mast cells	Monocytes Macrophages DCs Neutrophils	Monocytes Macrophages DCs Neutrophils Basophils B cells	Monocytes Macrophages DCs NK cells	Monocytes Macrophages DCs NK cells	Neutrophils Basophils	Mast cells Basophils Monocytes Langerhans cells Allergic neutrophils	B cells T cells NK cells DCs Eosinophils macrophages	Macrophages Eosinophils Neutrophils
Effect of ligation	Activation	Activation	Inhibition	Activation	Activation	Neutral	Activation	Activation	Activation

Table compiled from data in[46, 48, 58].

There are other, less studied FcRs also. The neonatal Fc receptor (FcRn) is involved in transferring IgG from mother to foetus during gestation, and also plays a role in regulating levels of IgG in serum[59]. Interestingly, FcRn is more closely related to MHC I molecules than other FcRs, and is an MHC I homolog that is involved in IgG-mediated bacterial phagocytosis[59]. Another FcR known as polymeric immunoglobulin receptor (Poly IgR) is involved in the transport of polymeric IgA and pentameric IgM across epithelial surfaces[2, 60]. Fcα/μ is a receptor that can also bind to both IgA and IgM[61]. Unlike with Poly IgR, the J chain is not needed for IgM to bind to Fcα/μ[61]. The receptor binds to IgM ICs and internalises it by endocytosis, but little is known about its role in IgA internalisation[61].

1.2.3 Ig-like cell surface receptors (IgLRs)

Other regulatory receptors include IgLRs - a collection of cell surface receptors known to play a role in regulating the immune system and include LILRs[1].

1.2.3.1 Leukocyte Immunoglobulin-like Receptors (LILRs)

In 1997, whilst searching for NK cell inhibitory receptors distinct from KIRs, Marco Colonna discovered a group of IgLRs, which they called Immunoglobulin-like Transcripts (ILTs)[62]. At the same time, in Seattle, USA, David Cosman's group discovered a group of receptors they called Leukocyte Ig-like Receptors (LIRs)[63]. We now know these receptors belonged to the same family, and the standardised nomenclature is LILRs[39].

LILRs are IgLRs found on the human chromosome 19q13.4[64]. They are polygenic in nature; demonstrating allelic variation[64]. These receptors are also known as CD85 receptors and myeloid inhibitory receptors (MIRs)[65, 66]. LILRs comprise of an extracellular, a transmembrane and an intracellular domain involved in signalling[63]. There are two types of LILRs: activating and inhibitory. There are six known activating LILRs, which have truncated cytoplasmic domains; whilst the five inhibitory LILRs contain long cytoplasmic domains and possess two to four ITIMs[63] (*Figure 1.8*). With the exception of LILRA3, all of these receptors are thought to be membrane-bound[63]. Inhibitory and activating LILRs are expressed on both myeloid and lymphoid lineages[66] (*Table 1.4*).

1.2.3.1.1 LILR expression

LILRs are primarily expressed on myeloid cells. However, LILRB1 has been found on lymphocytes, with high expression on B cells but low levels on $CD3^+$ cells[67]. LILRB1 has also been found on memory $CD8^+$ T cells, and may contribute to memory inflation in

cytomegalovirus (CMV)[68]. Both LILRB1 and LILRA2 are found on NK cells[39]. However, antibody staining of LILRB1 on $CD56^+$ NK cells can range from low to undetectable on different donors[67, 69]. The variability in expression of LILRB1 on NK cells has been found to correlate with polymorphisms in the LILRB1 locus, with 3 SNPs in particular resulting in high expression on NK cells[69]. Other receptors have also displayed polymorphisms, which affect their expression. LILRA3 is high in Japanese populations, whilst LILRB2 is low in north-east Asian populations[70]. This suggests that LILR expression is influenced by environmental factors also, likely due to the fact that different populations are exposed to different pathogens. Both LILRB3 and LILRB4 are highly polymorphic receptors, and these polymorphism are often associated with diseases[71]. For example, LILRB4 SNPs affecting expression on mDCs, has been found to correlate with SLE[72].

Table 1.4 LILR expression profiles on immune cells

Receptor Name			Expression profile
LILRA1	-	CD85i	Macrophages
LILRA2	ILT1	CD85h	Monocytes, Macrophages, DCs, NK cells, Basophils, Eosinophils, Neutrophils
LILRA3	ILT6	CD85e	Produced by monocytes & only expressed in soluble form
LILRA4	ILT7	CD85g	pDCs
LILRA5	ILT11	CD85f	$CD14^-$ monocytes, Neutrophils
LILRA6	ILT8	CD85b	Unknown
LILRB1	ILT2	CD85j	Monocytes, Macrophages, DCs, Osteoclasts, Eosinophils, B cells, T cells, NK cells, Placental stromal cells
LILRB2	ILT4	CD85d	Monocytes, Macrophages, DCs, Osteoclasts, Basophils, Eosinophils, Placental vascular smooth muscle, Neural cells*
LILRB3	ILT5	CD85a	Monocytes, Macrophages, DCs, Osteoclasts, Basophils, Eosinophils, Neutrophils
LILRB4	ILT3	CD85k	Monocytes, Macrophages, DCs, Osteoclasts
LILRB5	-	CD85c	Unknown

Table adapted from Anderson *et al* (2009)[39] and various sources[62, 73, 74, 75, 76]

LILRs are expressed ubiquitously on myeloid cells[39]. Inhibitory LILRs are on most DCs, except pDCs. The only activatory LILR found on DCs is LILRA2 (and LILRA4 on pDCs) [39]. LILRs are also found on granulocytes. Neutrophils express LILRA2, LILRA5 and LILRB3[74, 75, 76]. LILRB1 and LILRB2 are also expressed on neutrophils but this was not seen with all donors[75]. Eosinophils express LILRA2, LILRB1, LILRB2 and LILRB3[39, 75]. The expression pattern of LILRA6 and LILRB5 are unknown, although LILRA6 has been found on monocytes at an mRNA level[39 77, 78]. LILRs are also expressed on osteoblasts (cells required for bone formation), and osteoclasts (derived from myeloid cells, and required for bone absorption)[79]. Although LILR expression has been mainly documented on immune cells, they have also been found on non-immune cells, such as neural cells, which express LILRB2[73].

1.2.3.1.2 LILR Structure

LILRA3 is the only LILR found to be expressed only in a soluble form with no transmembrane or cytoplasmic domain, and has been found to be absent in some individuals, and low in Caucasian populations[63, 80]. However, it has been speculated that more, if not all, LILRs may also be expressed in a soluble form[63, 64, 81]. This was illustrated by Borges *et al* who found four forms of LILRA5 by RT-PCR: two that were membrane-bound, and two that lacked transmembrane and cytoplasmic domains suggesting they were soluble, as they could be secreted when transfected into cell lines[74]. Soluble LILRs could be the result of alternative splicing, and may block their membrane-bound counterparts from interacting with their ligands. This is believed to be the case for soluble LILRB1, which was found to block membrane LILRB1 from binding to HLA-I molecules, therefore possibly acting as a negative regulator[81]. Whether these soluble LILRs are functional is unclear, but both membrane-bound and soluble LILRB4 have been shown to decrease T cell proliferation, whilst only membrane-bound LILRB2 could[82]. This indicates that LILRB2 relies on its intracellular signalling domains to function but LILRB4 does not, or that the ligands for LILRB2 may only be able to bind to the membrane-bound receptor. Soluble LILRs may also contribute to disease, for example, soluble LILRB4 protein has been found in melanoma, colon, rectum, and pancreatic carcinomas, leading to the induction of $CD8^+$ T suppressor cells (TS) and T_{reg} cell differentiation that cause suppression of immune responses against tumours[83]. Deletion of LILRA3 has also been implicated in non-Hodgkin's lymphoma (NHL) malignancy[84]. Therefore, tumours may exploit these soluble LILRs for immune evasion. Soluble LILRs have also been implicated in autoimmunity. Soluble LILRA3, although constitutively expressed in normal serum, was significantly upregulated in RA patients and correlated with disease severity, indicating soluble LILRs may also play a role in inflammatory conditions[85].

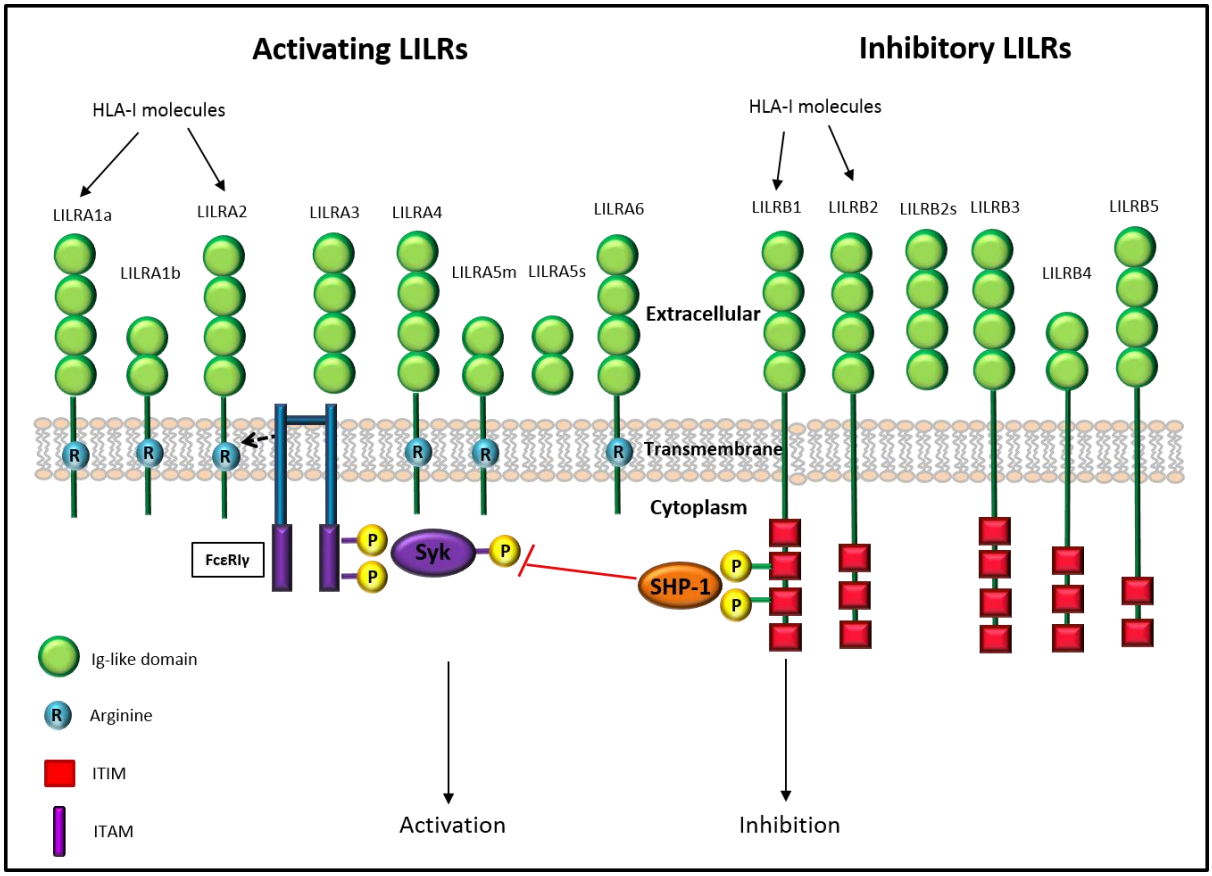

Figure 1.8 Structure and signalling of LILRs. LILRs regulate the immune response through activation or inhibition. The extracellular domains of these LILR receptors bind to their ligands. In the case of LILRB1 and LILRB2 these ligands are HLA-I molecules. Ligands for other LILR receptors are less studied and therefore still largely unknown, although it is thought that LILRA1, LILRA2 and LILRA3 also bind to HLA-I molecules. Due to alternative splicing, some receptors can be found in either of two forms: membrane (m) or soluble (s), as in the case of LILRA5, LILRB1, LILRB2 and LILRB4. Both activating and inhibitory LILR isoforms are defined by their cytoplasmic and transmembrane domain residues. Activating LILRs have short cytoplasmic tails and a charged arginine residue in their transmembrane domain through which they associate with ITAM-bearing gamma chains of activating Fc receptors. Phosphorylation of these ITAM domains by Src homology 2 domain-containing tyrosine kinases results in downstream activatory signalling. In comparison, inhibitory LILRs have 2-4 ITIMs in their cytoplasmic domains that negatively influence intracellular signalling by recruiting tyrosine phosphatases such as SHP-1 thus leading to downstream inhibitory signalling. Figure adapted from Brown *et al*, 2004[66].

LILRs can be categorised into two groups, which are based on their ability to bind or not bind to HLA-1 molecules; group 1 LILRs bind to these molecules, whilst group 2 do not. LILRA1, LILRA2, LILRA3, LILRB1 and LILRB2 belong to group 1. LILRA4, LILRA5, LILRA6, LILRB3, LILRB4 and LILRB5 belong to group 2[86]. This difference in ligand binding is based on their differences in structures. All group 1 LILRs share ~70% sequence homology with LILRB1/LILRB2[87]. The second group of LILRs have been less studied, and their structure, function and ligands less characterised, sharing <60% sequence identity with LILRB1/LILRB2, and more than 85% of changes in these residues are accounted for by

substitutions or deletions, which could explain why these LILRs do not bind to HLA-1 molecules[86,87].

Chapman *et al* resolved the crystal structure of the first two domains (D) of LILRB1 (D1 and D2) at 2.1 Å resolution, and showed that each domain has an Ig-like structure[88]. They showed LILRB1 has a structure of β-strands in two anti-parallel β-sheets, with helical regions mixed in, and the folding topology is similar to homologous KIRs[89]. Based on their sequences they predicted the last two domains (D3 and D4) would be similar in structure[89]. The structure of LILRB2 was solved at 1.8 Å resolution by Willcox *et al*, through model replacement, using LILRB1 as a first order model[90]. LILRB2 was found to also have a structure made up of two anti-parallel β-sheets, a similar folding topology to KIRs, but less α-helical structures compared to that seen with LILRB1[90].

LILRA2 is also a group 1 LILR. The crystal structure of LILRA2 D1/D2, have also been solved at 2.6 Å resolution[91]. Although, similar to LILRB1/LILRB2 in topology, displaying β-strands in two anti-parallel β-sheets with α-helixes entwined, LILRA2 was also found to have changes in residues in known HLA-I binding sites of D1, as a result of 2 α-helixes replacing a β-strand in the domain[91]. LILRA2 also displayed 3D-domain swapping in D2, whereby identical β-strands were swapped, allowing two LILRA2 molecules to form dimers of its D1/D2 domains [91]. Dimerization can be advantageous as it provides a larger surface area for ligands to bind[91].

The first three-dimensional structure for a group 2 LILR was solved at 1.85 Å resolution by Shiroishi *et al*, who solved the crystal structure for the D1/D2 domains of LILRA5 by molecular replacement, using LILRB1 or LILRB2 as a search probes[87]. The D1/D2 domains were found to be different from LILRB1 and LILRB2, but still showed similarities to homologous KIRs[87]. LILRA5 was found to have less α-helices, and a β-strand found to have replaced helices in the binding sites of its D1 domain, likely the reason why LILRA5 cannot bind HLA-I molecules; confirmed by the lack of binding seen with anti-LILRA5 antibodies to HLA-I-transfected cells by flow cytometry, or soluble LILRA5 to immobilised HLA-I molecules by Surface Plasmon Resonance (SPR)[87].

Cheng *et al* solved a 1.7 Å resolution crystal structure of LILRB4, another group 2 LILR. LILRB4 has only two Ig-like domains, and the D1 domain was found to be similar to other LILRs in the same family[92]. However the sequence similarity of its D2 domain was more similar to D4 of other LILRs[92]. β-strands were found to replace α-helixes in HLA-I binding sites in D1, that may explain the lack of HLA-I binding of LILRB4[92].

The crystal structures of LILRs in complex with three different types of ligands have been solved: LILRB1 in complex with HLA-A, LILRB1 in complex with UL18 and LILRB2 in complex with HLA-G[86, 93]. LILRB1 has been found to bind to HLA-A (an HLA-1 molecule) in a 1:1 binding ratio of receptor to ligand, between the D1/D2 domains of LILRB1 and the α3 and β2m domains of HLA-A, and this interaction occurs in *trans*[86]. A 2.5-Å resolution crystal structure of LILRB2 in complex with HLA-G was solved by Shiroishi *et al*. LILRB2 was found to bind to HLA-G through its α3 and β2m domains, similar to the structure of LILRB1 in complex with HLA-A[93]. However, whilst LILRB1 predominantly bound to the β2m domain of HLA-A, LILRB2 predominantly binds to the α3 domain of HLA-G in closer proximity, suggesting that LILRB1 and LILRB2, which both bind to HLA-G, bind differently to their ligands[93]. NMR confirmed the differences in HLA-G binding of the two receptors by expressing β2m as a ^{15}N-labeled protein and refolding the domain with or without the non-labelled heavy chain of HLA-I[93]. Finally, crystal structures of UL18 have previously been difficult to solve due to the viral protein being heavily glycosylated. Yang *et al* solved a 2.2-Å resolution crystal structure of LILRB1 in complex with a deglycosylated UL18[94]. The D1/D2 domains of LILRB1 displayed binding to the α3 and β2m domains of UL18 in a 1:1 ratio in *trans*[94].

Given the conserved regions between the group 1 LILRs, it is likely that other LILRs in the same group also bind to HLA-I molecules in the same way: in a 1:1 ratio, via the α3 and β2m in *trans*. The crystal structures of other LILRs have yet to be elucidated, but high sequence homology between the extracellular domains of these receptors suggests that the tertiary structures of these domains would be very similar to those determined for LILRA2, LILRA5, LILRB1, LILRB2 and LILRB4. So far only the D1/D2 domains of these receptors have been solved. However, in 2013, Nam *et al* solved the crystal structures for D3/D4 of LILRB1 and LILRB2[95]. As predicted these domains were similar in structure to D1/D2, with some changes to the number of β-strands in anti-parallel sheets. Whilst most of the strands were in two anti-parallel sheets, D3 for both receptors was found to have β-strands in 3 anti-parallel sheets. D4 differed between the two receptors with LILRB1 having β-strands in 5 and 3 anti-parallel sheets and LILRB2 having two β-strands in 4 anti-parallel sheets[95]. Although most of the LILR structures solved suggest HLA-I binding is static and independent of polymorphism in HLA-I, as these occur mainly in the α1 and α2 domains, studies have shown that LILR binding to HLA-I molecules is effected by polymorphism[96]. Therefore, Nam *et al* suggested an alternative binding model, where the D3/D4 domains are also involved in ligand binding, and could bind to the α1 and α2 domains of HLA-I molecules[95].

It should be noted that although the most characterised interaction of LILRs and their ligands is in *trans* (as described above), LILRs can bind in other ways. For example, LILRB2 has been found to bind to HLA-I molecules on mast cells and basophils in *cis*[97]. Similarly, on neutrophils, LILRA2 binds to soluble HLA-I in serum[76].

1.2.3.1.3 LILR Ligands

Activatory LILRs have been less studied, but it has been proposed that they bind to HLA-I molecules. LILRA1 has been found to bind to HLA-B27 and HLA-C free heavy chains, whilst LILRA2 and LILRA3 have been found to bind to soluble HLA-I[76, 96, 98]. LILRA3 also binds to HLA-C heavy chains[96]. The ligands for LILRA5 and LILRA6 are unknown[71].

Inhibitory LILRs, LILRB1 and LILRB2 both bind HLA-G, which has been shown to be involved in immune tolerance and escape[99]. HLA-G is a natural ligand for DC receptors and inhibits both activation and maturation of DCs, leading to the down-regulation of MHC-II molecules, thus decreasing their ability to present peptides to $CD4^+$ T cells[100]. HLA-G also decreases IL-2 and induces $CD4^+$ and $CD8^+$ T cells to produce IL-10, which promotes T cell anergy[100]. However, it remains unclear how this engagement affects LILR function[39]. LILRB1 fusion protein binds strongly to cell surface UL18, an MHC I homolog encoded by CMV, and this binding has been shown to have a 1000-fold higher affinity compared to binding to HLA-1 molecules[86, 88]. Binding to UL18 was tested using SPR, and soluble D1/D2 were found to bind strongly, whereas D3/D4 showed no binding. This suggested that the first two domains were responsible for binding to this ligand. Soluble D1 in particular showed the highest affinity for the ligand, suggesting D2 may contain residues that aid in binding, but that the key UL18 binding epitopes are found in D1. Binding of LILRB1 to UL18 has been shown to bind in a 1:1 ratio, and this interaction is believed to occur between the D1 domain of LILRB1 and UL18's α3 domain[88, 89]. LILRB2 D1/D2 fusion proteins have been found to bind to UL18 with a 3000 fold lower affinity than LILRB1, yet crystal structures of LILRB2 show it has similar D1 and D2 structures to LILRB1[86, 90]. However, differences found in the D1 domain of LILRB2, namely a shortened helix at resides 44-57, and alternative tyrosine 38 confirmation, both of which are believed to be important for LILRB1 binding to UL18, may suggest why LILRB2 binds this ligand with lower affinity[90]. Although the grouping for these LILRs suggests that all group 1 LILRs bind to HLA-I molecules whilst all group 2 do not, there has been some discrepancies seen. Zhang *et al* found that group 2 LILR, LILRB5 binds to HLA-B7 heavy chains, possibly due to its unique differences in its D1 and D2 domains,

which are different from other LILRs that do bind β2m-associated HLA-1 molecules[101]. Therefore, LILRB5 does not fit into group 2, as it potentially binds to HLA-1 molecules.

HLA-I molecules are by far the most characterised ligands that bind to the LILR family. However, these receptors have been shown to bind to other ligands also. A number of LILRs have been proposed to bind to bacteria and viruses. Nakayama *et al* showed that Staphylococcus aureus (*S. aureus*) bacteria bound to LILRB1 and LILRB3-transfected cells, suggesting these receptors may be involved in regulating innate immunity[102]. Given that *S. aureus* infection can cause septic arthritis, LILRs could be ideal targets for treating autoimmunity[102]. LILRs can also bind to viruses, for example, LILRB1 was shown to bind to dengue virus (DENV) and could be a potential target to treat the virus (see later)[103]. HIV-infected DCs express calcium-binding proteins S100A8 and S100A9, which have been found to interact with LILRB1[104]. NK cells expressing LILRB1 have been found to regulate HIV infection through an interaction between LILRB1 and its ligands S100A8 and S100A9[104]. LILRB2 has been found to bind CD1d tetramers, blocking CD1d from presenting lipid antigens to NKT cells[105]. Given the role of NKT cells in bacterial and viral infections, this supports the idea that LILRs are involved in anti-bacterial/viral responses[105].

LILRA4 is exclusively expressed on pDCs, and has been found to bind to bone marrow stromal cell antigen 2 (BST2)[106]. Although this LILR is activatory in structure, LILRA4 inhibits type 1 IFNs and pro-inflammatory cytokines, which are produced by pDCs through TLR7 and TLR9[106]. Therefore, LILRA4 controls excessive production of TLR7/9-induced type 1 IFNs that may lead to lymphopenia or autoimmunity[106]. LILRB2 has been found to bind to αβ oligomers in the brain via its D1 and D2 domains, increasing cofilin signalling - a feature of Alzheimer's disease (AD)[73]. LILRB2 has therefore been proposed to contribute to AD neuropathology, and is a potential therapeutic target in this disease[73]. Recently, LILRB3 and LILRA6 have been shown to bind necrotic glandular epithelial cells, and although the ligand they bind to on these cells in unclear, there was some evidence that the receptors may bind to cytokeratin 8 or cytokeratin 8-associated proteins on these cells[107]. LILRB2 has been found to bind to angiopoietin-like proteins (ANGPTLs), secreted glycoproteins that support expansion of HSCs and have a role in lipid metabolism, angiogenesis and inflammatory responses[108]. ANGPTL1, 2, 5 and 7 all bound to LILRB2^{+} human cord blood cells (enriched with HSCs), but LILRB2 had a higher affinity for ANGPTL2 and glutathione s-transferase (GST)-ANGPTL5[108]. It has been proposed that LILRB2 acts a sensor, able to prevent excessive activation and exhaustion of HSCs through binding to ANGPTLs that control HSC expansion[108]. Paired immunoglobulin-like receptors (PIRs) are found in mice and are

orthologs to human LILRs. However, unlike the many isoforms that humans possess, mice only have two isoforms: activatory receptor PIR-A, and inhibitory receptor PIR-B[109] (see later – *1.2.3.2*). Zheng *et al* showed that there was an increase in leukemic cell differentiation in PIR-B deficient mice and slower development of acute myeloid leukaemia (AML), suggesting that PIR-B inhibits leukemic differentiation and results in faster AML development. Therefore, given the homology between PIRs and LILRs, LILRB2 may also inhibit AML cell differentiation. LILRB3, and to a lower extent LILRB5-transfected cells were also found to bind to ANGPTL2 and GST-ANGPTL5 and may also play a role in inhibiting leukemic cell development[108].

A summary of the ligands for the family of LILRs is displayed below.

Table 1.5 Ligands of LILRs

LILR	Ligand
LILRA1	HLA-B27, HLA-C free heavy chains
LILRA2	Soluble HLA-I
LILRA3	HLA-C free heavy chains
LILRA4	BST2
LILRA5	Unknown
LILRA6	Unknown
LILRB1	HLA-I, UL18, CMV, DENV, *S. aureus**, S100A8, S100A9
LILRB2	HLA-I, CD1d, ANGPTL, αβ oligomers, myelin inhibitors
LILRB3	Cytokeratin 8 on necrotic glandular epithelial cells*, *S. aureus**
LILRB4	Unknown
LILRB5	HLA-B7 heavy chains

**unconfirmed ligand.*

1.2.3.1.4 LILR Signalling

LILRs influence innate and adaptive immune responses[66]. Activatory LILRs have a charged arginine residue that associates with the FcR γ-chain of FcεR, which has ITAMs that are involved in stimulating immune responses and signal transduction[110]. When these receptors are ligated, transient tyrosine phosphorylation occurs within these ITAM domains, thus creating a docking site for Syk family kinases such as Sky and Lyn, to be recruited downstream of the receptor, resulting in the induction of signalling activation pathways[111].

Inhibitory LILRs block activating signals by recruiting tyrosine phosphatases such as SHP-1 to its ITIM domains[64, 110]. Kinases are recruited to inhibitory LILR receptors, and these kinases phosphorylate tyrosine residues within the ITIM domains of the inhibitory LILR receptors, creating a docking site for SH2 phosphatases to be recruited to[112]. Other phosphatases can also interact with LILR ITIM domains, including SHP-2, SHIP-1 and SHIP-2[113]. However, not all of these phosphatases will interact with each inhibitory LILR. For example, Chang *et al* found that LILRB4 interacted with SHP-1 and SHIP-1 but showed no interactions with SHP-2 and SHIP-2; suggesting negative signalling by LILRB4 relies only on SHP-1 and/or SHIP-1[113]. Each inhibitory LILR has varying numbers of ITIM domains with varying amino acids in their conserved sequences[66, 112]. The number of ITIM domains and sequences of these domains for each inhibitory LILR receptor may affect signal amplification, *i.e.*, the more ITIMs present, the greater the level of inhibition of signalling. Alternatively, each ITIM domain could recruit different tyrosine phosphatases[112]. However, this is still understudied and remains to be clarified. NFκβ is a transcription factor involved in DC maturation and activation[114]. Upon LILRB1 ligation, NFκβ inhibitor ABIN1/TNIP1 is increased, suggesting that the inhibitory effect of LILRB1 on DCs may be regulated through the NFκβ pathway[114].

1.2.3.1.5 LILR Function

Activatory LILRs have been less studied in comparison to inhibitory LILRs. LILRA2 is expressed on eosinophils, and has been found to activate these cells, resulting in the release of cytotoxic granule proteins and pro-inflammatory cytokines such as IL-12[75]. LILRA2 is co-expressed with TLR4 and FcγRI on monocytes[115]. Cross-linking of LILRA2 on monocytes with an antibody results in secretion of pro-inflammatory cytokines such as IL-6, IL-8 and MIP-1α[115]. LILRA2 modulates LPS-induced monocyte activation, and inhibits IgG-dependent monocyte phagocytosis through down-regulation of TLR4 expression[115]. In a leprosy model LILRA2 was found to inhibit monocyte differentiation into DCs, as well as inhibiting antigen presentation; indicating that LILRA2 may regulate T cell responses to pathogens[116]. Therefore, LILRA2 may decrease self-reactive T cells that can result in autoimmunity[116]. LILRA4 has been found to inhibit pDC activation[117]. This has been proposed to be through binding to its ligand BST2, although this has been debated in the literature[71, 117]. LILRA5 and LILRA6 have been found to induce pro-inflammatory cytokine secretion, but their function, along with LILRA1 and LILRA3 are unknown[71].

When ligated, inhibitory LILRs prevent immune cells from functioning by causing down-regulation of cytokine/chemokine production, and they have also been found to inhibit the

antigen presenting ability of DCs, which influence T cell activity and are involved in self-tolerance[39, 118,113, 119, 120]. $CD8^+$ TS cells characterised by their $CD8^+CD28^-$ phenotype, interact with APCs that present HLA-I[121]. This interaction renders monocytes and DCs tolerogenic, subsequently leading to suppression of T cell responses[121]. This was demonstrated *in vitro* with T cell proliferation assays, which showed APCs exposed to TS cells were unable to drive $CD4^+$ T cell proliferation[121]. These tolerogenic APCs were found to up-regulate LILRB2 and LILRB4, and down-regulate co-stimulatory molecules such as CD86[121]. LILRB4 renders DCs tolerogenic, but these tolerogenic DCs (tDCs) can also be generated through treatment of IL-10, IFN-α, IFN-β, or vitamin D3 receptor agonists, all of which result in an up-regulation of LILRs[122, 123]. Chang *et al* found that LILRB4 acts through BCL6, which is expressed in T cells and inhibits transcription of genes that control $CD8^+$ T cells[122]. LILRB4 is expressed on APCs, and upon receptor cross-linking has also been reported to internalise, delivering its ligand into the cell for presentation to T cells, suggesting a role in antigen uptake and presentation[124]. Characterising the signalling pathways involved in LILR activation is still in its infancy and more work is necessary.

LILRs can therefore affect T cell function indirectly through APCs. However, LILRB1 has been found to be expressed on both $CD8^+$ and $CD4^+$ T cells, although other distinct subsets such as T_{regs} are yet to be elucidated[67, 125]. Mediated by HLA-1 ligands, LILRB1 has been shown to induce negative signals that resulted in inhibition of T cell killing, an increase in the activation threshold of $CD8^+$ T cells, and cross-linking of LILRB1 inhibited $CD4^+$ T cell proliferation[125]. LILRB1 has also been shown to compete with HLA-I molecules for binding to CD8; consequently regulating $CD8^+$ T cell activity[126]. Therefore, LILRB1 can affect T cell function directly.

Although to a much lower extent than on myeloid cells and B cells, LILRB1 is expressed on a subset of NK cells, and has been shown to aid in NK cell function[127]. NK cells have receptors that bind HLA-I on self-cells but destroy non-self that do not express HLA-I[128]. LILRB1 aids in recognising cells that down-regulate HLA-I[127]. However, this recognition is weak as NK cells expressing only LILRB1 and no other receptor provide a very low missing-self response (see earlier – *1.1.2.1*), therefore indicating this response relies on the presence of other HLA-I receptors e.g. KIRs[127, 129]. LILRB1 has been shown to down-regulate NK cell function, demonstrated through *in vitro* killing assays where anti-LILRB1 antibodies inhibited NK cell cytotoxicity[130]. However, LILRB1 function may be dependent on KIR signalling, as Kirwan *et al* showed that LILRB1/HLA-I signalling on NK cells, occurred in the presence of KIRs, but not in the presence of ITIM-deficient KIRs[127].

LILRB1 also inhibits calcium mobilisation on B cells and myelomonocytic cells[62]. Naji *et al* showed that HLA-G suppresses B cell proliferation and this is driven by an interaction between LILRB1 and HLA-G[131]. HLA-G does not induce apoptosis/necrosis but instead causes cell cycle arrest, by disturbing the mTOR-signalling pathway (commonly dysregulated in B cell disorders and activated tumours)[131]. This was supported by Ketroussi *et al* who showed that HLA-G caused cell cycle arrest of activated T cells and altered the mTOR pathway, mediated by SHP-2[132]. Naji *et al* further showed the LILRB1/HLA-G interaction plays an important role in B cell function[133]. They showed that this interaction regulates B cell responses through both T cell-dependent and independent responses, by inhibiting B cell proliferation and differentiation of B cells into antibody-secreting cells[133]. They demonstrated that upon ligation of HLA-G to LILRB1, IL-2, IFN-γ and chemokines are down-regulated, whilst IL-10 is increased, all through downstream signalling cascades involving SHP-1[133]. LILRB1 has also been shown to inhibit B cell trafficking. When treated with IL-10 and TGF-β1, fDCs and T_{FH} secrete HLA-G[133]. HLA-G binds to LILRB1 on the surface of germinal centre (GC) B cells via its α3 domain associated with a β2m domain and the LILRB1/HLA-G interaction results in a down-regulation of chemokine receptors CXCR4 and CXCR5, preventing chemotaxis to their ligands CXCL12 and CXCL13, respectively that are required for B cell migration to follicles[133]. Thus LILRB1/HLA-G interaction inhibits B cell trafficking. The role of LILRB1 in B cell function suggests its potential therapeutic role in treating B cell malignancies. Although LILRB1 has been well characterised, our understanding of the function of this family of receptors on myeloid cells as a whole is still fairly limited. Their exact mechanism of action and the way in which these receptors cause inhibition on different cell types has yet to be elucidated.

Inhibitory LILRs are also expressed and function on non-immune cells. They are all expressed on osteoclasts and play a role in bone homeostasis[79]. LILRB1, LILRB3 and LILRB4 were shown by Mori *et al* to play a role in regulating osteoclastogenesis through recruitment of SHP-1; suppressing osteoclasts *in vitro*[79]. Mori *et al* also demonstrated this down-regulation of osteoclastogenesis in a mouse model, with the LILRB mouse homolog PIR-B[79]. LILRB2 may play a role as a β-amyloid receptor that leads to cofilin signalling and could be responsible for memory loss and the development of Alzheimer's disease, as shown by Kim *et al* in a murine PIR-B model[73]. This suggests that regulating inhibitory LILRs may be therapeutic in a number of different diseases (see *1.3.4*).

The role LILRs play in disease can be studied using relevant animal models. However, few LILR mouse models exist. A T cell-specific LILRB1 transgenic (Tg) mouse model under a

CD2 promoter has been produced through microinjection of the construct into the pronuclei of fertilized oocytes of C57BL/6 mice[134]. LILRB1 was able to bind to murine MHC-I molecules in this model, therefore the function of this receptor *in vivo* could be elucidated[134]. LILRB1 expression showed a decrease in TCR-mediated T cell activation by targeting ZAP-70 and CD3ζ, and inhibition of $CD4^+$ T cell proliferation compared to wild-type mice[134]. A LILRB2 Tg mouse under DC-specific CD11c promoter, has been developed through the same procedure mentioned above[100]. In this model it was shown that upon treatment of DCs with HLA-G tetramers, the LILRB2/HLA-G interaction renders DCs tolerogenic and induces anergic $CD4^+$ T cells[100]. However, both these models have limitations. The LILRB1 Tg mouse model shows high expression on T cells and NK cells[100]. However, LILRB1 expression on these cells in humans has been found to be variable between donors or even absent[67]. A Tg model expressing LILRA1, LILRB1 and LILRB4 has also been developed[135]. However, the expression pattern was similar but not identical to that found in humans[135]. LILRA1 expression was not detected *in vivo*, but LILRB1 was found highly expressed on B cells as in humans, and NK cells[135]. High LILRB1 expression on NK cells has not been seen in humans[67, 135]. High LILRB4 expression was also found on B cells, which is not seen in humans[135]. Developing models with their endogenous promoters would be ideal in order to accurately mimic the receptor expression profiles.

Mouse models can only provide so much information given the differences between humans and mice, therefore studying the function of these receptors through human studies would be better. However, human studies have been limited. To study genes involved in activating innate immunity, Talwar *et al* mimicked sepsis syndrome by injecting healthy humans with intravenous endotoxin[136]. Blood samples were taken and then gene expression studied[136]. They found an increase in pro-inflammatory cytokines TNF-α, IL-1β, IL-6, IL-8, MCP-1, MIP-1α and –β, but also anti-inflammatory cytokine IL-10[136]. This increase occurred at 3 hours, but returned to baseline between 6-24 hours; and as endotoxin cleared after 30 minutes, these effects were likely the result of secondary mediators[136]. RNA levels of LILRA3, LILRB2, LILRB3 and LILRB4 were up-regulated in PBMC donors, compared to control PBMCs; whilst genes associated with T and B cell activation e.g. tumour necrosis factor receptor (TNFR) SF7, and cell lysis mediators such as perforin and granzyme were down-regulated compared to controls; with similar effects seen in whole blood samples[136]. An increase in pro-inflammatory cytokines and activatory receptor LILRA3 demonstrates an innate response to infection. However, an increase in anti-inflammatory IL-10 and inhibitory LILRs exhibits the importance of balancing activatory and inhibitory immune responses to prevent excessive inflammation and subsequent autoimmunity[136]. Smith *et al* showed that

inhibitory LILRB2, LILRB3 and LILRB4, as well as activatory LILRA3 and LILRA5, increased *in vivo* in response to neonatal sepsis[137]. This suggests that a balance between the activatory and inhibitory receptors is involved in controlling inflammatory responses. More human studies, and better animal models are warranted.

1.2.3.2 Paired Ig-like receptors (PIRs)

PIRs are orthologs of human LILRs, and like LILRs, PIRs recognise and bind MHC-I molecules[109]. Whilst a single gene encodes PIR-B, PIR-A is encoded by multiple genes[138]. These genes are found on the mouse chromosome 7, which is syntenic to the human chromosome that encodes human LILR receptors[138]. Human LILRs have up to four Ig-like domains that make up their extracellular domain, in contrast, mouse PIRs have six Ig-like domains (*Figure 1.9*)[138]. With the exception of LILRB1, expression of LILRs is restricted to monocytic cells, in comparison, PIRs are more uniformly expressed and are found on B cells, DCs, monocytes, macrophages, granulocytes and mast cells[39,138]. Inhibitory PIR-B has four ITIM domains in its cytoplasmic domain which are used to recruit phosphatases such as SHP-1 resulting in signal inhibition. In contrast, activatory receptor PIR-A has a short cytoplasmic domain and a polar transmembrane region that can interact with the γ-chain of the ITAM-bearing FcεR, resulting in activation[138, 139]. This was demonstrated by Maeda *et al* who showed that PIR-A activates signalling in mast cells when it associates with the ITAM-bearing FcR γ chain[139].

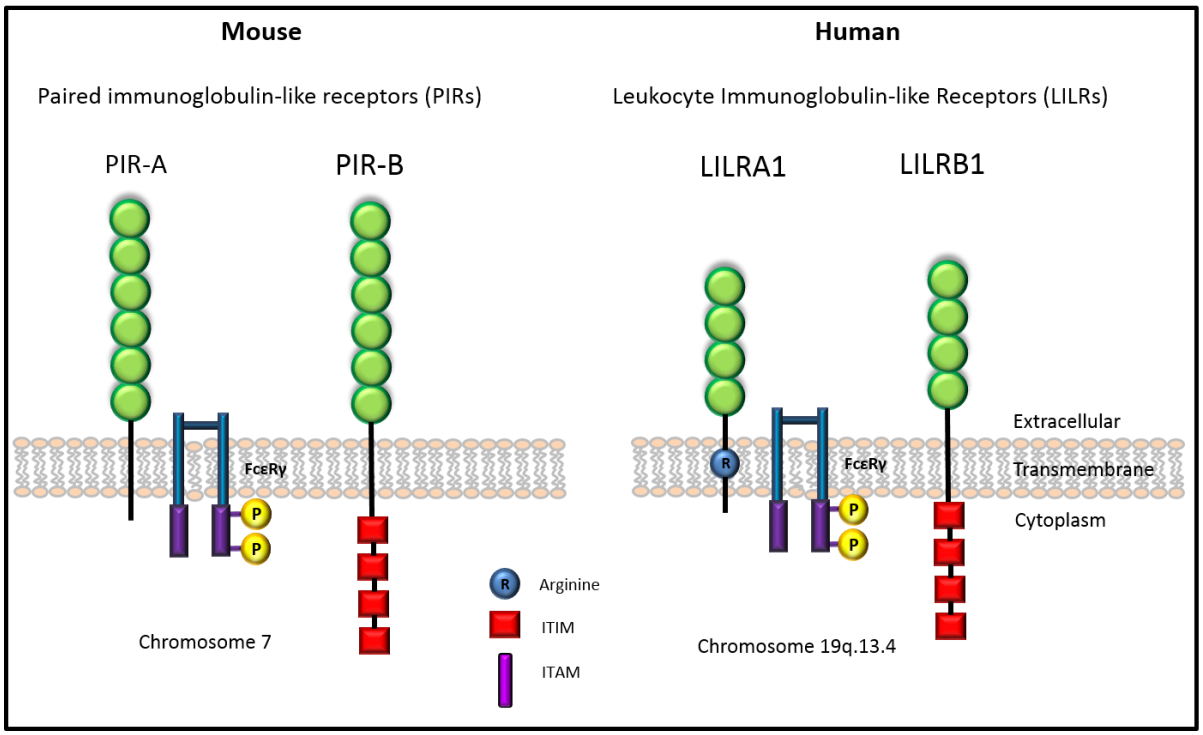

Figure 1.9 A comparison between mouse PIR receptors and human LILR receptors. PIRs and LILRs are orthologs and belong to the same superfamily of Ig-like cell surface receptors. They are found on syntenic chromosomes and both receptors have either an activating or inhibitory form. However, PIRs have only one of each activating or inhibitory receptor, whilst LILRs have six activating and five inhibitory receptors. Human LILRs have up to four Ig-like domains, whilst mouse PIRs have six. Inhibitory receptors block signalling through their ITIM domains. Activating receptors form activating receptor complexes through association with FcεR gamma chains containing ITAMs.

Whilst PIR-B has been shown to signal through its ITIMs in the same way as LILRs (see earlier), regulating immunity by binding in *trans* to HLA-I molecules, PIR-B can also modulate the activity of DCs through *cis* interactions[140]. DCs are important in the priming of CTLs that kill infected cells and PIR-B regulates such priming by blocking CD8 molecules from binding to MHC I[140]. PIR-B has also been shown to negatively influence integrin signalling in neutrophils and macrophages, which are important in linking the cytoskeleton to the external environment[141].

PIRs have also been implicated in various pathologies. PIRs regulate the differentiation of myeloid-derived suppressor cells (MDSCs) that aid in tumour progression[109]. Tumour-associated macrophages can display an M1-like pro-inflammatory phenotype, with increased induced nitrous oxide (iNOS) and TNF-α, or a wound healing M2-like phenotype with increased arginase 1 (ARG1) and IL-10[109]. IFN-γ and IL-4 stimulate MDSCs to produce iNOS, whilst IFN-γ and IL-13 induce ARG1 production[109]. Upon entry into tumours, MDSCs are believed to differentiate into TAMs, but the mechanisms behind this differentiation is unknown. Ma *et al*, showed that PIRs may be responsible for MDSC differentiation into

TAMs with an M2-like phenotype, which results in an increase in IL-10 production, induction of T_{regs} and decrease in T cell responses[109]. PIR-B deficient mice were found to display an M1-like phenotype, lose their ability to induce T_{regs} and supress T cell responses, resulting in a decrease in tumour growth[109]. A balance between activatory PIR-A and inhibitory PIR-B are therefore essential to control MDSC differentiation. Given that LILRB3 shares the highest sequence homology with PIR-B (see *Table 1.6* below), Ma *et al*, suggested that the human equivalent of PIR-B is LILRB3[109]. This implies that LILRB3 could be important in negatively regulating the function of MDSCs and the progression of tumours in humans, whilst also demonstrating that mouse models may be useful in studying this effect.

PIR-B has also been implicated in regulating pDCs, which upon viral infection induce type I IFNs and attack host DNA, leading to the development of SLE[142]. PIR-B dephosphorylates STAT1 and STAT2 causing down-regulation of TLR-mediated IFN-α[142]. PIR-B also influences the antigen presenting function of DCs and therefore T cell responses[65]. The receptor plays a role in the maturation of DCs, which when impaired causes an increase in T_H2 responses, and is therefore important for a balance between T_H1 and T_H2 responses[65].

As mentioned previously, LILRs bind to bacteria (see *1.2.3.1.3*). PIR-B is also exploited by bacteria to avoid immunological clearance. Nakayama *et al* showed that the bacteria *S. aureus* exploits PIR-B to promote infection[143]. TLRs recognise *S. aureus* and promote the production of pro-inflammatory cytokines IL-6 and TNF-α[143]. However, PIR-B can inhibit inflammation mediated by TLRs and *S. aureus* therefore enlists PIR-B to dampen inflammatory responses[143].

As with LILRs (see *1.2.3.1.3*), PIR-B has been found to be highly expressed on mouse HSCs, and found to bind to ANGPTL2, ANGPTL3 and GST-ANGPTL5, glycoproteins that support the expansion of HSCs[108]. PIR-B deficient mice showed an increase in AML differentiation but a decrease in HSC expansion. This suggests that PIR-B is involved in repopulation of HSCs and supports AML development through inhibition of leukemic cell differentiation[108].

PIR-B protein has been shown the have the high similarity to all the inhibitory LILRs, in particular to human LILRB3 protein (*Table 1.6*). The similarity between PIR-B and LILRB3 makes mice a good model to investigate the function of LILRB3 in health and disease.

Table 1.6 A comparison of homology between inhibitory LILRs and the inhibitory mouse PIR-B

Mouse	Human	Isoform	Homology (protein)
PIR-B	LILRB1	Isoform 1	49%
		Isoform 2	48%
		Isoform 3	48%
		Isoform 4	49%
	LILRB2	Isoform 1	47%
		Isoform 2	47%
	LILRB3	Isoform 1	54%
		Isoform 2	52%
		Isoform 3	54%
	LILRB4	Isoform 1	46%
		Isoform 2	46%
		Isoform 3	46%
	LILRB5	Isoform 1	49%
		Isoform 2	45%
		Isoform 3	49%

*Based on annotated full-length isoform sequences produced by alternative splicing in UNIPROT

1.2.3.3 Human Killer Ig-like Receptors (KIRs)

Another member of the IgLR superfamily of immune receptors are the human KIRs, which regulate NK cell development and activation[144]. Like LILR receptors KIRs are also found on chromosome 19q13.4[145]. KIRs are not found in mice, appearing only in primates[145]. Encoded by fourteen highly polymorphic genes, these receptors can be either activatory or inhibitory. As with LILRs and PIRs, inhibitory KIRs have long cytoplasmic domains with ITIMs that recruit phosphatases; whilst activating KIRs have short cytoplasmic domains and associate with ITAM-containing DAP12 – a signalling adapter protein[144]. KIR2DL4 is the exception to this rule, as this activatory receptor has a long cytoplasmic tail and does not interact with DAP12, but instead associates with the γ chain of FcεRI[144]. Different KIRs bind to different HLA-I ligands found on NK cells and some T cells[144, 145]. NK cells are involved in anti-viral responses and inhibitory KIRs have been implicated in providing protection against viruses such as HIV and Hepatitis C[146]. KIRs have also been found to be associated with malaria, mediating NK cell induction of pro-inflammatory cytokines, and in pregnancy, where NK cells are found in abundance, and a strong inhibitory signal but weak activatory signal is associated with pre-eclampsia[146]. The presence of KIRs and their HLA-I ligands have also resulted in autoimmune conditions such as psoriasis, where increased levels of activating KIR2DS1 and low levels of inhibitory KIR2DL1 were found to be associated with the development of psoriasis[146, 147]. NK cells are able to clear tumours, therefore KIRs play an important role in tumour clearance/progression[146]. Carrington *et al* showed that inhibitory KIRs are associated with lower disease severity in cervical cancer, whilst activating KIRs are

associated with increased severity[148]. Most of what is known about the effect of KIRs on tumours, however, involves tumours that are driven by viral infections[146].

1.2.3.4 Murine gp49 molecules

Although some suggest KIRs have no mouse orthologs, Wang and Yokoyama suggested murine gp49 molecules could be the mouse orthologs of human KIR receptors[145, 149]. These molecules inhibit NK cells upon stimulation, and are either activatory (gp49A) or inhibitory (gp49B)[149]. Unlike KIRs however, these molecules are only found on activated NK cells and their expression is not just restricted to NK cells alone, but macrophages and mast cells also[149]. They demonstrate no allelic polymorphism like other receptors in the same IgLR family[149]. Although some appear to be activatory, they have no charged residues in their transmembrane domain[149]. Murine gp49 molecules also show similarities to other IgLRs and could be orthologs of human LILRs (LILRA2 and LILRB1 are also found on NK cells)[149]. They also show homology to murine PIRs, but PIRs are not found on NK cells[149].

1.2.3.5 Signal induction receptor proteins (SIRPs)

Another IgLR family of receptors are SIRPs. There are at least fifteen SIRPs, which are also referred to as signal-regulatory proteins[150]. SIRPs are glycoproteins found on the cell surface of myeloid and neural cells in both humans and mice[65, 151]. Most of these proteins are inhibitory and regulate signalling by recruiting phosphatases such as SHP-1 and SHP-2 to their ITIM domains; with the exception of one SIRP that has a truncated cytoplasmic domain with no ITIMs, and signals activation through its association to the signalling molecule DAP12[151].

1.3 The immune system and disease

1.3.1 Cancer and the immune system

1.3.1.1 The biology of cancer

Cancer cells arise from the body's own cells, growing and dividing rapidly out of control. These immortal cells most commonly arise from epithelial cells – sheets of cells that cover cavity and channel walls[152]. The majority of these types of cancers or carcinomas can be grouped into one of two categories: squamous cell carcinomas (that arise from epithelial cells that form protective cell layers); or adenocarcinomas (arising from epithelial cells that secrete substances)[152]. Some cancers arise from non-epithelial cells that can be grouped into three types: sarcomas - these are tumours that arise from connective tissue made up of

mesenchymal cell types, such as fibroblasts, osteoblasts, adipocytes and myocytes; hematopoietic malignancies – arising from blood cells such as erythrocytes, plasma cells and lymphocytes that result in fluid leukaemias or solid lymphomas; and finally neuroectodermal tumours that arise from cells of the central and peripheral nervous system such as gliomas, glioblastomas, neuroblastomas, schwannomas, and medulloblastomas[152]. However, some cancers do not fall into any of these classifications, for example, melanomas, which appear to be neuroectodermal tumours as they arise from embryonic cells found in the neural crest, have no direct connection to the nervous system and instead develop from melanocytes[152].

1.3.1.2 The hallmarks of cancer

Once cancerous cells arise, there are six ways in which these tumours maintain their development: in what Hanahan and Weinberg referred to as "The Hallmarks of Cancer"[153]. The first "hallmark" is being able to continuously to proliferate. Cells are naturally in a feedback loop, whereby growth-promoting signals are constantly turned on and off to sustain homeostasis; defects in these negative feedback loops allow tumour cells to continue to proliferate and accumulate[153]. Alternatively, somatic mutations or down-regulation of proteins that make cells senescent can result in continuous proliferation of tumour cells[153]. The second hallmark is tumour cells being able to escape growth suppressors[153]. Tumour suppressor genes inhibit cell proliferation, defects in these genes allows tumour cells to continue proliferating. This along with impediment of contact inhibition and redirection of TGF-β from anti-proliferation pathways aids in tumour progression[153]. Cancer cells are often immortal, and therefore can circumvent cell death – this is the third hallmark[153]. Defects in genes involved in autophagy (cells 'self-eat') allow tumour cells to survive under conditions of stress and limited nutrition[153]. The fourth hallmark of cancer is being able to replicate constantly to achieve immortality[153]. By avoiding senescence, tumour cells go through repeated cycles of cell division[153]. To survive, tumour cells need access to a blood supply in order to have access to oxygen and nutrients as well as being able to remove waste products: this is hallmark five[153]. Tumour cells promote angiogenesis by up-regulation of angiogenic factors such as vascular endothelial growth factor-A (VEGF-A)[153]. Finally, hallmark six denotes that alterations in their shape and the way in which they attach to other cells and the extracellular matrix (ECM), allows tumour cells to metastasise and invade other tissues and organs[153].

Besides, these six well-characterised hallmarks, there are two "emerging hallmarks", that are still not fully understood: gene mutations that effect cellular metabolism; and tumour cells

being able to elude immune responses[153]. "Enabling characteristics" are also thought to play a role in tumour progression through genetic mutations, and inflammation resulting from infection that promotes tumour growth and survival[153].

1.3.1.3 The immune system and cancer

The immune system plays a pivotal role in the clearing of cancerous cells. Although, in 1909 Paul Erlich was accredited for being the first to suggest that the immune system could form protection from tumours, validating his theory was difficult at that time as little was known about the immune system[154]. Almost 20 years earlier, in 1891, William Coley discovered that cancer patients with bacterial infections showed signs of tumour regression[154]. Coley injected immunogenic bacterial toxins into advanced cancer patients and observed tumour regression[154]. As more became known about the way in which the immune system works and the discovery of tumour antigens, William Coley was regarded as the first to demonstrate experimentally that the immune system can indeed play a role in protection against tumours[154, 155, 156]. However, it was Burnett and Thomas who coined the term 'immunosurveillance' when they showed that lymphocytes were responsible for eliminating tumour cells[154]. Immunosurveillance or immunoediting as it is also referred to, is a theory that describes how the immune system successfully (but sometimes fails) to eliminate cancerous cells[155]. It is now accepted that the immune system can protect against viruses; eliminate pathogens promptly to ensure inflammatory environments (ideal for tumour progression) are not maintained; and eliminate tumours by recognising specific tumour antigens[155].

Immunoediting describes three distinct phases: elimination, equilibrium and escape[154, 155] (*Figure 1.10*). Normal healthy cells can become cancerous through genetic and environmental factors, such as carcinogens, radiation, chronic inflammation, inherited genetic predispositions or viral infections[155]. Intrinsic and extrinsic tumour suppression attempts to prevent transformation of these cells, and both the innate and adaptive responses play a role in the "elimination" phase[155]. These transformed cells can be recognised by the "danger signals" they emit, such as type I IFNs; damage-associated molecular pattern molecules (DAMPs) dying cancer cells or tissues release; or from stress ligands that bind to innate immune cells, such as MICA/B, which are expressed on tumour cells[155]. If immune responses successfully manage to eliminate transformed cells, tumour suppression is achieved[155]. However, some rare tumour variants may escape and subsequently enter the "equilibrium" phase[155]. Adaptive responses are responsible for keeping these variants in a tumour dormant phase, through IFN-γ, IL-12 and both $CD4^+$ and $CD8^+$ T cells, working to maintain equilibrium[155]. In spite of this,

some variant cells may "escape" due to their inability to be recognised by adaptive immune responses, which could be the result of tumour cells losing their antigens or acquiring defects in antigen processing and presentation[155]. Alternatively cells may enter the escape phase if these cells become insensitive to immune effector mechanisms or they exert an immunosuppressive state[155]. Consequently these poorly immunogenic and highly evasive cells can grow and tumour cells develop[155]. It is also possible that transformed cells can pass straight to the equilibrium or escape phase bypassing the elimination phase[155].

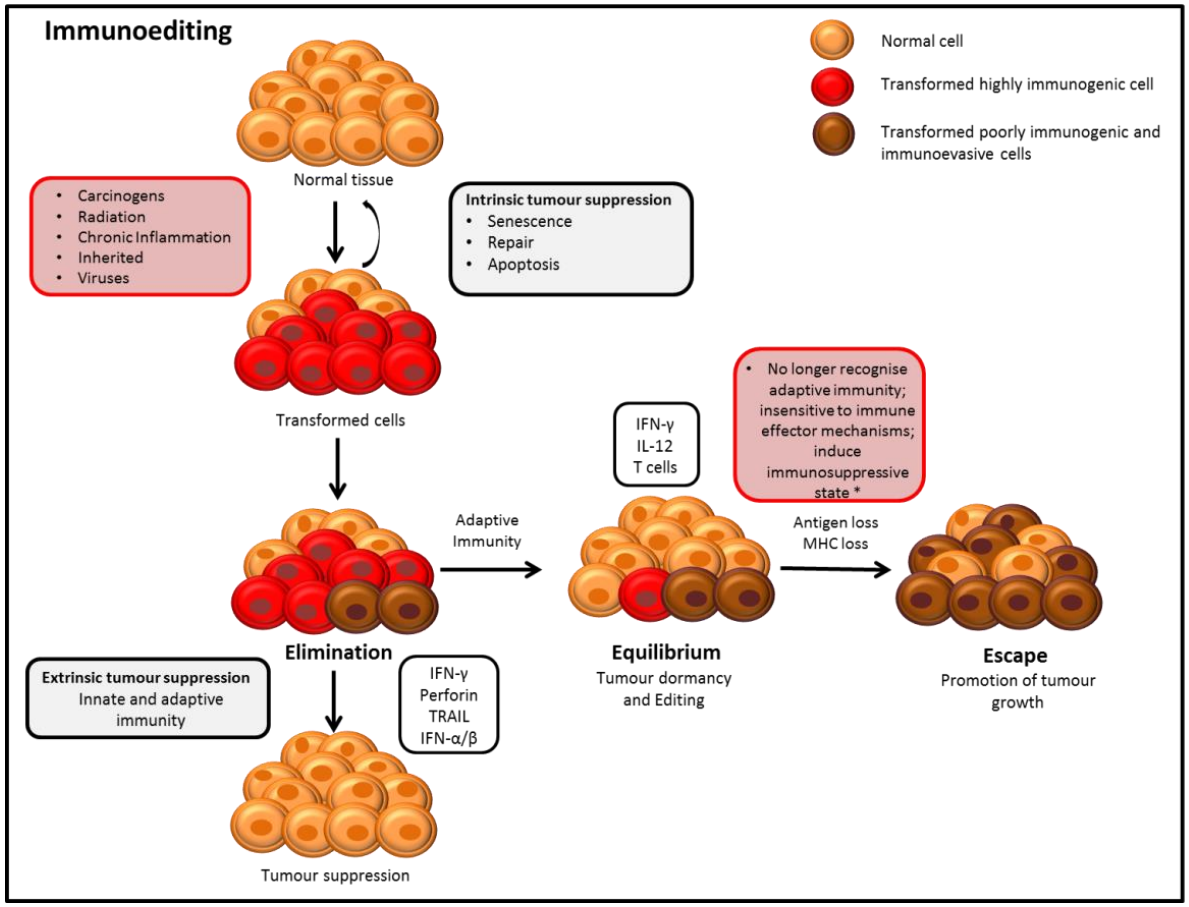

Figure 1.10 Immunoediting. Normal tissues can become cancerous when normal cells are transformed by genetic or environmental factors. Intrinsic tumour suppression methods try to prevent transformation of healthy cells. Both the innate and adaptive immune responses are also involved resulting in tumour suppression. However, one or more rare variants can escape this "elimination" phase and enter "equilibrium". Tumour dormancy is then maintained by adaptive immune responses controlled by IL-12, IFN-γ and T cells. Some variants can further breakout and enter the "escape" phase where they are allowed to grow and develop into tumours. Transformed cells can bypass the elimination phase and enter the equilibrium or escape phase directly. Figure adapted and sourced from Schreiber *et al* (2011) and Smyth *et al* (2006)[154, 155].

Although traditional therapies for treating cancers have involved surgery, chemo- and radio-therapy, as we learn and understand more about the immune system's role in cancer control, manipulation of the immune system could and has already lead to advances in cancer therapy through immunotherapy (see later).

1.3.2 Autoimmune Diseases

The immune system is very efficient at recognising foreign or "non-self" cells and eliminating them. However, sometimes, defects in adaptive immune responses result in the immune system recognising the bodies' own cells or "self" cells as foreign and destroying these cells leading to what is collectively referred to as autoimmune diseases[1]. The heterogeneity of pathology exhibited by this class of diseases makes them hard to classify, however, they can be categorised into two types: systemic; and organ-specific[1]. SLE is an example of a systemic autoimmune diseases, which is known to effect mainly women[157]. Self-peptides or autoantigens that lead to SLE are present on many different cells, and this is why systemic autoimmune diseases effect multiple organs and often become chronic[157]. In comparison, organ-specific autoimmunity is the result of autoantigens that are specific to a particular cell-type and therefore limited to only that organ[1]. In diseases such as multiple sclerosis (MS) self-reactive T cells cause pathogenesis[1, 158]. T cells that are specific for self-peptide: self-MHC complex cause inflammation by activating macrophages and damaging tissue[1]. Autoreactive T cells that target myelin antigens, cross the blood-brain-barrier in MS and mediate damage of neurons[158]. In both cases, the presence of these autoantigens causes more inflammation which eventually leads to chronic inflammation and production of more autoantigens[1]. Self-reactive B and T cells are usually removed by self-tolerance during development, however, low affinity cells are not destroyed and are therefore able to mature[1]. The mechanisms for understanding how autoimmunity progresses is still very much unknown.

Causes of autoimmunity can be genetic and/or environmental. One theory used to describe environmental contributions to autoimmunity is the "Hygiene Hypothesis", which theorises that the more 'clean' we become the less prone we are to infection but the more prone we are to developing autoimmune conditions[159]. Many theories as to how this happens have been proposed, including: down-regulation of T_H2 cells responsible for allergic responses and cytokines secretion for IgE production (however, most autoimmune diseases are in fact T_H1-mediated); these diseases could result from 'weak' binding antigens that are unable to compete with other 'stronger' binding antigens and are therefore ignored; suppressor T_{reg} cells lose their efficacy; or finally these diseases work through non-antigenic mechanisms to progress[159]. Genetic mutations or gene polymorphisms could alternatively be the cause of autoimmunity[159]. A single gene change can lead to pathogenesis or defects in cytokines: for example, down-regulation of TNF-α has been implicated in SLE; whilst overexpression has been implicated in inflammatory bowel disease (IBD)[1].

1.3.3 LILR receptors in Health and Disease

Inhibitory LILR receptors have been implicated in a number of different diseases. These receptors could therefore be ideal therapeutic targets.

1.3.3.1 LILRs and cancer

Inhibitory LILRs have been implicated in cancer progression. Velten *et al* found that when DCs were induced with the anti-inflammatory cytokine IL-10, there was an up regulation of inhibitory immune receptors, including inhibitory LILRs[123]. This suggests that inhibitory LILRs are present in an anti-inflammatory environment, and therefore potentially in diseases such as cancer.

Over expression of inhibitory LILRs is commonly found in many malignancies[39]. LILRB1 and LILRB4 have both been found to be up-regulated in human gastric cancer and the more the cancer differentiated, the higher the levels of LILRB1 and LILRB4 observed[160]. Increased levels of LILRB4 have also been found in AML patients[161]. As mentioned earlier, mouse studies have shown that PIR-B binds to ANGPTLs, is found to be highly expressed on HSCs and inhibits AML cell differentiation, resulting in AML development[108]. LILRB2 is also highly expressed on HSCs and has also been found to bind to ANGPTLs, therefore may play a role in AML development too[108]. *In silico* analysis of gene expression and overall AML survival in patients, showed that LILRB1, LILRB2, LILRB3 and LILRB4 were negatively correlated with AML survival, suggesting that these receptors promote AML progression[162].

Chronic lymphocytic leukaemia (CLL) results from malignant B cell accumulation in the bone marrow, peripheral blood and lymphoid tissues[163]. Normally, the only LILR found to be expressed on B cells is LILRB1[39]. However, Colovai *et al* found LILRB4 expression on neoplastic B cells in 23/47 CLL patients, whilst no expression was found in normal unaffected B cells from healthy donors[163]. LILRB4's presence and association with T cell anergy may promote tumour evasion in CLL[118, 163]. Notably increased expression of LILRB2 was also found in 6/11 LILRB4-expressing CLL patients[163]. Therefore, given the increase in inhibitory LILRs on tumours, co-ligation of inhibitory LILRs may amplify tumourigenesis. This immunosuppressive response may prove beneficial in autoimmune diseases/transplantation where dampening the immune response is ideal. However, in tumours this is detrimental[118]. Therefore, blocking inhibitory LILRs has the potential to be therapeutic in cancer treatment. LILRs are also expressed on T cell lymphomas, with LILRB1 found on

$CD56^+CD4^+$ and $CD8^+$ T cell lymphomas, as well as on infiltrating cells, suggesting LILRB1 may play a role in tumour progression[164].

HLA-G, the ligand for LILRB1, is also expressed on T cell lymphomas[164]. Therefore, the interaction between LILRs and their ligands may also contribute to tumour progression. HLA-G, has been found on infiltrating immune cells in breast cancer lesions[165]. A 2001 study by Lefebvre *et al* showed that HLA-G was up-regulated in 14/36 breast cancer lesions[165]. An increase in HLA-G correlated with a higher severity of breast carcinoma, suggesting tumour progression may be HLA-mediated. HLA-G was highest in lesions where there was greatest infiltration of immune cells, suggesting it may play a role in dampening inflammation[165]. Therefore binding of inhibitory LILRs (such as LILRB1) to their ligands, may block anti-tumour immune responses in neoplastic tissues, leading to tumour progression in cancer patients. Tumours that express HLA-G are associated with poor prognosis and are often resistant to immunotherapy. Targeting HLA-G and/or its receptors could be therapeutically advantageous as a result[166].

1.3.3.2 LILRs and infection

LILRs also play a role in infectious diseases – both bacterial and viral. The pathogen *Mycobacterium leprae* causes Leprosy - a bacterially infectious disease found to be associated with increased LILRA2, LILRB3 and LILRB5 (LILRA2 in particular showing greatest expression)[167]. As mentioned previously, LILRB1 and LILRB3-transfected cells were also found to bind to *s. aureus* (as described previously in *1.2.3.1.3*) indicating these receptors may play a role in pathogen recognition[102].

An association between some LILRs and viral infections has also been found. It has been suggested that viruses may escape immune attack by generating ligands that bind to LILRs, thereby blocking activation of lymphoid and myeloid cells[64]. Human CMV is a common virus that results after lung transplantation[168]. Berg *et al* found an increase in cells (NK and T cells) expressing LILRB1 in patients with CMV compared to those without, before the virus was even detectable[168]. LILRB1 has been found on $CD8^+$ memory T cells that are involved in memory inflation during CMV infection[68]. This suggests that LILRB1 could be a potential biomarker for CMV.

LILRB1 expression on NK and T cells were found to be increased in both viral human immunodeficiency virus (HIV) and long-term non-progressing HIV patients[169]. IL-10 inhibited T cell responses when produced by virally infected monocytes and was elevated in

HIV patients causing increased LILRB2 and LILRB4 expression that hindered the ability of monocytes to act as APCs[170].

As stated in *1.2.3.1.3*, LILRB1 has also been suggested to play a role in DENV infection. DENV is a life threatening virus for which no vaccines are currently available, in part due to the presence of sub-neutralising levels of antibody that actively promote viral infection[103]. In this scenario, interferon stimulated genes (ISGs) block viral replication in an antibody-dependent fashion, mediated by activatory FcγRs[103]. However, Chan *et al* proposed that under sub-neutralising levels of IgG, DENV is free to also bind to inhibitory LILRB1, which blocks the activatory FcγR pathway through dephosphorylation events, thus preventing ISG expression and allowing DENV to replicate[103]. Although LILRB1 has no effect on viral uptake, it aids in viral replication within the cell, and therefore blocking LILRB1 could be used in DENV therapy or vaccinations[103].

Therefore, drug treatments targeting these LILRs or their ligands may aid in treating infectious diseases.

1.3.3.3 LILRs and autoimmune diseases

RA is a chronic inflammatory synovial joint disease, caused by elevated levels of inflammatory cells. An imbalance between activating and inhibitory LILRs is believed to be associated with the development of autoimmune diseases such as RA[39]. In a study by Tedla *et al*, synovial tissue from RA patients was taken, and immunoreactive cells counted to determine LILR-positive cells[171]. As LILR expression is believed to be associated with RA through increasing cytokine production that results in elevated levels of inflammation, RA samples were compared to patients with osteoarthritis (OA) - which is not caused by inflammation – as well as control healthy samples[171]. Activatory LILRA2 and LILRA5 and inhibitory LILRB2 and LILRB3 were found to be significantly increased in the synovial tissue of 40 RA patients; whilst little to no LILR expression was found in OA or healthy samples[171]. LILRA5 was the strongest predictor of RA disease activity, as it was up-regulated in 100% (40/40) of patients[171]. Increased expression of LILRs correlated to an increase in the presence of inflammatory cells and in disease severity[171]. This supports claims that LILRs trigger cytokine production, which promotes inflammation and leads to RA progression[171]. The ratio of activating to inhibitory LILRs also affected disease severity. An increase in the ratio of activatory LILRA2 and LILRA5 in comparison to inhibitory LILRB2 and LILRB3 showed more inflammatory cells and increased disease severity[171]. In comparison, a higher ratio of inhibitory LILRB2 compared to activating LILRA2 and LILRA5 was found to be

associated with patient remission[171]. This suggests an imbalance between the activating and inhibitory LILRs can lead to disease progression[171]. Interestingly, LILRB1, the receptor most widely expressed on different cell types, was not found in RA patients[171]. Therefore, LILR expression patterns show diversity in different diseases. Further evidence of the involvement of LILRs in RA comes from Huynh *et al*, who found that after treatment with DMARD anti-rheumatic drugs, LILRs were down-regulated in the synovial tissue of RA patients[172].

LILRs have also been implicated in other autoimmune diseases. Decreased levels of LILRB1 have been associated with SLE, with PBMCs from SLE samples showing down-regulation in LILRB1, in particularly on B cells, however, treatment of DCs with IL-10 showed higher levels of LILRB1 expression on DCs compared to controls[39]. LILRB1 and its ligand HLA-G, which are normally not found in the central nervous system, have been found up-regulated on macrophages and microglial cells in MS lesions, and therefore may act as inhibitory regulators of neuroinflammation[173]. Soluble LILRA3 is also associated with MS, and believed to increase disease severity but not disease susceptibility[174].

1.3.3.4 LILRs and transplantation

Allograft transplantation involves the donation of cells, tissues or organs from one person to another. However, this process can often lead to the recipient's immune system rejecting the transplant either directly, or indirectly due to the presence of APCs that cause allograft rejection[175]. Transplant rejection occurs when the recipient's T cells recognise MHC alloantigens that are presented: either as intact molecules on donor APCs (direct rejection); or MHC alloantigens that have been processed and presented onto their own APCs (indirect rejection)[175]. When up-regulated on APCs such as DCs, inhibitory LILRs can suppress $CD4^+$ T cell activation[175]. These inhibitory LILRs are induced by alloantigen-specific TS cells commonly found circulating in transplant recipients; and upon interaction with their ligands can produce tolerance in donor APCs[100, 121]. Transplant patients that do not exhibit graft-host rejection were found to have increased LILRB4 and LILRB2 on their APCs. Chang demonstrated this by treating donor APCs with TS cells, and an increase in LILRB4 and LILRB2 was seen, suggesting the importance of these receptors in preventing transplant rejection[121]. Stallone *et al* also found that chronic exposure to the immunosuppressant Rapamycin, showed an increase in BDCA-2^+ cells (a marker of pDCs) but a down-regulation in BDCA-1^+ myeloid DCs, and an increase in LILRB4 and LILRB2. The increase in these inhibitory LILR receptors correlated strongly with a decrease in the co-stimulatory molecule CD40, and an increase in $CD4^+$ $CD25^+$ $Foxp3^+$ $CTLA4^+$ T_{regs} and $CD8^+$ $CD28^-$ TS cells[176].

Stallone also found a decrease in T_H1 responses (through down-regulation of the transcription factor T-bet) and an increase in T_H2 responses (down-regulation of GATA-3)[176]. This suggests that Rapamycin influences DC phenotypes and the increases in LILRB4 and LILRB2 could potentially promote transplant survival[176].

Although most LILR ligands are still unknown, LILRB1 and LILRB2 have been found to bind to HLA-I molecules[99]. Transplant patients have been found to have increased HLA-G and infiltrating mononuclear cells that express HLA-G in their grafted tissues; resulting in prolonged allograft survival[100, 176, 177]. Therefore both inhibitory LILRs and HLA-G are important in transplant success.

1.2.3.5 LILRs and pregnancy

HLA-G is only found on foetal trophoblast cells in healthy individuals[178]. To avoid allorecognition by maternal T cells, trophoblast cells found in the placenta do not express HLA molecules[179]. However, this makes the cells susceptible to NK cell lysis through missing self (mentioned earlier in *1.1.2.1*)[179]. They do however, express non-classical HLA-I molecules such as HLA-G[179]. Leukocytes taken from maternal placenta samples were found to express HLA-G and its receptor LILRB1[179]. LILRB1 likely detects HLA-G on trophoblastic cells, preventing NK cell-mediated lysis of these cells[179]. In the placenta, HLA-G/LILRB1 interaction renders DCs tolerogenic and inhibits T cell proliferation, indicating that LILRB1 and its ligand are modulating immunity in pregnancy[178].

1.3.3.6 LILRs and neurological diseases

LILRs have also been implicated in non-immune diseases. Kim *et al*, showed that deposition of high levels of β-amyloid oligomers that cause memory loss and the progression of AD, are mediated by the murine PIR-B receptor[73]. Although PIR-B has been described as a receptor only expressed on immune cells, studies have now shown the receptor is found on neurons also[73]. Kim *et al* found a direct interaction between PIR-B and β-amyloid oligomers but not to activatory PIR-A; and binding of β-amyloid oligomers to neurons decreased in PIR-B-deficient mice[73]. Conversely, to examine which human ortholog functionally related to PIR-B, β-amyloid oligomers were found to bind only to human LILRB2 but not LILRB1 or LILRB3[73]. This indicated that LILRB2 was the ortholog to PIR-B in this way, despite having the highest homology to LILRB3 (as mentioned previously in *Table 1.6*). LILRB2 was also detected in both healthy and AD human brain specimens, with no significant difference between the two, however, downstream signalling in AD samples were altered[73]. Full-length

and deletion mutants of both PIR-B and LILRB2 showed that both receptors bound to β-amyloid oligomers by their D1 and D2 domains (first two extracellular Ig-like domains)[73]. Therefore LILRB2 has been described as a β-amyloid receptor that plays a role in AD progression.

1.3.4 Mouse models to study disease

Mouse models provide the biological complexities involved in disease progression to be studied, which cannot be achieved through *in vitro* experiments. There are different types of mouse models available.

A widely used mouse model to study human malignancies are xenograft models. Xenografts are established by injecting tumour cells under the skin of mice, or into the organ from which the tumour cells originated, and then therapy can be administered and responses to therapy assessed[180]. To avoid tumour rejection, immunocompromised mice are used[180]. The use of primary human tissue, enables genetic complexities of human tumours to be encompassed, the model is quick to establish (matter of weeks), and multiple therapies can be tested on the same tumour biopsy[180]. However, the use of immunocompromised mice means that murine immune responses to the tumour are not impaired or absent, so the effect of immunity on therapy is not incorporated [180]. Nevertheless, successful therapies have been tested using xenograft models. The combinational therapy of Bortezomib (Velcade®) – the first proteasome inhibitor approved for the clinic, with chemotherapy drug Melphalen (Alkeran®) to treat multiple myeloma, was first tested in xenograft studies[181]. Approved antibody Herceptin was also tested on human breast cancer xenografts before being approved[182].

Another type of mouse model is Genetically Engineered Mice (GEM), which encompass genes mutated, deleted or overexpressed in mice[180]. This model allows specific human genetic defects to be studied in mice; and has advantages over xenograft models, as immunocompetent mice are utilised, therefore taking into considerations immune responses[180]. Unlike xenografts, however, GEM can take up to a year to establish, making them time-consuming to set up; and mouse tumours not primary human tissue is used, which may have significant differences, therefore may not necessarily be applicable to human disease[180]. Transgenic mice are created by transferring human genes into mouse models in order to study human development, diseases and disorders[183]. These mice models allow the influence of genes on cellular interactions to be studied in an *in vivo* model[183]. Tg mice are created through microinjections of DNA constructs with the desired transgene, into the nucleus of harvested donor zygotes[183]. These injected zygotes are then implanted into pseudo-

pregnant recipient mice and their offspring or "founder" mice are then screened for successful expression of the desired transgene[183].

Finally, humanised mice allow mice with human immune systems to be studied[184]. New born mice are given sub-lethal doses of irradiation before engraftment, and some strains are more sensitive to irradiation than others, especially if mice are unwell, and therefore only healthy mice can be used[185]. After irradiation mice are given human cells from umbilical cord blood[185]. These cells can be human PBMCs or HSCs[186, 187]. These models provide mice with a fully functioning human immune system, including functional T and B cells, therefore providing human adaptive responses[184]. However, this model also has its disadvantages. Umbilical cord blood is unsurprisingly hard to source, and experimental planning ensuring mice are available once cells are acquired is essential[185]. HLA-I/HLA-II selecting elements, important for driving T cell responses are not established, therefore, human cellular immunity is not completely replicated[185].

1.4 Immunotherapy

For diseases such as cancer, whose treatments have typically relied on surgery, and chemo/radiotherapy; new, more specific therapies are much needed to tackle the growing prevalence of these diseases. Immunotherapy aims to engage the immune system to be able to recognise and eliminate disease-causing target cells more efficiently, in the case of cancer for example, this involves re-educating our immune system to recognise cancer cells that undermine the immune system[1]. The advantage this type of therapy has over others - is that it utilises the body's own natural defences and therefore less side effects are likely.

1.4.1 Active Immunotherapy

Active immunotherapy involves stimulating the host's own intrinsic immune responses.

1.4.1.1 Vaccinations

Sanitation and vaccination have been responsible for a dramatic decline in the spread of infectious diseases[1]. Vaccination is a form of preventative therapy, allowing an attenuated version of an infectious agent to stimulate an immune response that leads to long-term immunity through establishing immune memory[188]. The success of vaccines was demonstrated with small pox in 1796, when Edward Jenner showed that vaccination of cowpox led to mild infection, followed by long-term protection against the deadly small pox[1, 188]. Small pox was eventually eradicated in 1977[188]. Vaccines use attenuated (live) or dead

infectious agents[1]. Attenuated vaccines are often more potent, however, killed vaccines prevent infection in immune suppressed individuals[1]. Vaccines have been successful in treating many infectious diseases including rabies, typhoid, measles, mumps, tetanus and many others[188]. A variety of vaccines exist: peptide or protein-based vaccines, DNA vaccines (although these have been found to be relatively weak), and recombinant or bacteria-based vaccines[188].

Much focus has been on exploiting DCs, in order to enhance APC function and therefore promoting activation of T cell responses[188]. Autologous DCs are taken from patients and loaded with tumour antigens *ex vivo*, before the patient is then re-immunised with the tumour-loaded DCs[189]. Although promising, to date, DC-based vaccines have had limited clinical success[189]. Alternatively, cytokines such as granulocyte-macrophage colony-stimulating factor (GM-CSF), IL-4, TNFs and IFN-γ have been used to promote DC maturation and activation[188].

Active immunotherapy has had success in treating infectious diseases, but this success has been limited in chronic diseases such as cancer[188]. However, as our recent understanding of viruses, idiotypes and tumour antigens has developed, hope for developing successful cancer vaccines has been restored. Some cancers are caused by certain viruses: for example, human papilloma virus (HPV) which leads to cervical cancer; Epstein-Barr virus (EBV) that can cause Burkitt lymphoma; human T cell lymphotrophic virus-1 that causes T cell leukaemia and lymphoma; and other viruses such as Hepatitis B and C that can cause liver cancer[188]. All of these viruses are being used or are being tested for use in vaccines. For example the HPV virus has been established as a preventative measure for cervical cancer[188]. A cohort of 1113 women aged 15-25 showed 91.6% efficacy with a vaccine against HPV-16 and HPV-18[190]. The vaccine showed success in incident and persistent cervical infections, and thus could reduce the risk of the development of cervical cancer[190].

Idiotypes are unique features found in the antigen-binding sites of an antibody[1]. Idiotype-directed vaccines have been used to treat B cell lymphomas[188]. After Levy *et al* had success in treating B cell lymphomas with an anti-idiotypic monoclonal antibody in 1982, using idiotypes of both GM-CSF and naked DNA was given to treat lymphomas[188, 191]. This resulted in remission of 8/11 patients who showed tumour clearance without the need for antibodies[191].

The discovery of tumour-associated antigens for use in vaccines has also advanced active cancer immunotherapy[188]. This includes screening circulating IgG in serum for tumour antigens, or using tumour-associated peptides in vaccines[188, 192]. The use of peptide vaccines

has had some success also. For example, in a phase II clinical trial, Spitler *et al* treated 48 high risk stage 3 or stage 4 melanoma patients with a GM-CSF vaccine, as an adjuvant therapy post-surgery, and found a 3-fold increase in survival with the GM-CSF vaccine[192].

1.4.1.2 Cytokines

Other active therapies also exist. Cytokines are secreted from cells and allow cross-talk between cells[188]. Examples of approved cytokine therapies are listed below in *Table 1.7*. Cytokines such as GM-CSF, IL-2, IL-12 and IL-15 have also been used in vaccines[188].

Table 1.7 Approved cytokine therapies

Cytokine	Therapeutic Use
TNF-α	RA, ankylosing spondylitis, psoriatic arthritis, crohn's disease, chronic plaque psoriasis, ulcerative colitis and psoriasis
IFN-γ	Osteopetrosis, Chronic granulomatous disease, ovarian cancer, idiopathic pulmonary fibrosis
IFN-α	HPV genital warts, west Nile virus, HIV, hairy cell leukaemia, malignant melanoma, follicular lymphoma, AIDs-related Kaposi sarcoma, condylomata acuminata, hepatitis B and hepatitis C
IFN-β	MS, chronic hepatitis B
IL-1Rα	RA, sepsis and osteoarthritis
IL-2	Metastatic renal cancer, malignant melanoma, NHL, renal transplantation, asthma, GvHD, MS, HIV, Psoriasis and ulcerative uveitis
IL-11	Chemotherapy-induced thrombocytopenia, Crohn's disease, RA, psoriasis, colitis
GM-CSF	Leukaemia, bone marrow/stem cell transplants and Crohn's disease

Table compiled from[188, 193]

IFN-β has been successfully used to treat autoimmune diseases such as MS[194]. IFN-β is a well-established cytokine therapy for the treatment of MS that blocks proteases involved in lymphocyte homing[194]. Type I IFNs have also been successful in treating viral infections and some cancers[194].

Although the high potency of cytokines makes them ideal therapeutics, their translational potential is still limited by their toxicity, due to the fact that cytokines have many different

effects on many different cell types, often in an unpredictable manner, and their effect is typically local not systemic[194]. This was demonstrated by the infamous TGN1412 trial, in which 6 volunteers were left with life threatening conditions after being administered the novel anti-CD28 monoclonal antibody and super agonist, which caused a rapid induction of pro-inflammatory cytokines in what was termed a "cytokine storm"[195].

1.4.2 Passive Immunotherapy

Passive immunotherapy involves driving host immunity with external components, to enhance host immunity.

1.4.2.1 Adoptive Cell Transfer

Adoptive cell transfer (ACT) involves the transference of highly reactive immune cells into a host. This form of passive immunotherapy has been used to treat cancer and autoimmunity.

In the case of cancer, autologous tumour infiltrating lymphocytes (TILs) have shown successful tumour regression in 50% of metastatic melanoma patients with manageable side effects[196]. For the treatment of melanoma, TILs that are isolated from a patient's own tumour mass are commonly grown *ex vivo* and selected for those that are tumour-specific and able to secrete IFN-γ in the presence of melanoma cells[196, 197]. These cells are then expanded in culture and transferred back into their host, along with IL-2[196, 197]. Low toxicity and the success of this treatment show its potential in treating melanoma. However, high costs of this patient-specific therapy is the drawback.

ACT has also been used in the treatment of autoimmune diseases. Autoimmunity is defined as the loss of self-tolerance[198]. T_{regs} are natural suppressor cells involved in maintaining tolerance by dampening immune responses[198]. These T_{regs} have good therapeutic potential in treating autoimmunity[198]. Pre-clinical data suggests that ACT of T_{regs} could be an ideal therapy to treat Type I diabetes, as a reduced numbers of T_{regs} has been found in these patients[198]. Freshly isolated T_{regs} could be expanded *ex vivo* and then transferred back into the host[198]. T_{reg} ACT therapy has also been proposed as a potential therapy in treating SLE and MS[198]. However, T_{reg} ACT therapy is still a long way from the clinic, as T_{regs} make up such a small percentage of human blood, and are not a homogenous population and therefore can readily revert back to conventional T cells[198].

1.4.2.2 Chimeric Antigen Receptors (CARs)

Given the drawbacks to ACT T cell therapy, being able to engineer these T cells to be more efficient at killing tumour cells is ideal[199]. Based on ACT therapy, another T cell therapy for treating cancers has been established. By removing T cells and modifying their properties to be more efficient at specifically targeting tumour cell markers, CARs can be used as a successful therapy in treating cancer patients[199]. CARs consist of an antibody fragment - usually a single chain variable fragment (scFv) that recognises tumour antigens linked to an activating signalling chain, most commonly CD3ζ, and co-stimulatory domains from molecules involved in T cell responses[199]. T cells are removed from patients, expanded *ex vivo* and transduced with the CAR, before then being transferred back in to the patient[199]. The scFv fragment targets tumour antigens, bypassing the need for antigen processing and presentation and therefore tackling the problem of TCR tolerance to tumour cells due to MHC down-regulation[199]. These engineered CAR-T cells can persist *in vivo*, however, many therapies have found high levels of toxicity in patients treated with these CARs due to "on-target off-organ reactivity" (whereby the CAR is antigen-specific, but is expressed on different tissues than the targeted tumour)[199]. Despite this, CAR-T cell therapy has shown promising success, as seen with CLL patients in remission for 2 year after receiving ACT with CD19-specific CAR-T cells[199]. Other studies with "second generation" CARs have also been successful. $CD19^+$ CARs with either a CD137 (4-1BB) or CD28 co-stimulation signalling domain have shown success in treating Acute Lymphoid Leukaemia (ALL) patients, or B-cell lymphoma and CLL patients respectively[200, 201].

1.4.2.3 Monoclonal Antibodies

Monoclonal antibodies or mAbs are proteins that are made up of light and heavy chains consisting of variable and constant regions (*Figure 1.11*) [1]. The light chains are either lambda (λ) or kappa (κ), although no functional difference has been found between the two, and these mAbs bind to their antigens through contact of their CDRs[1].

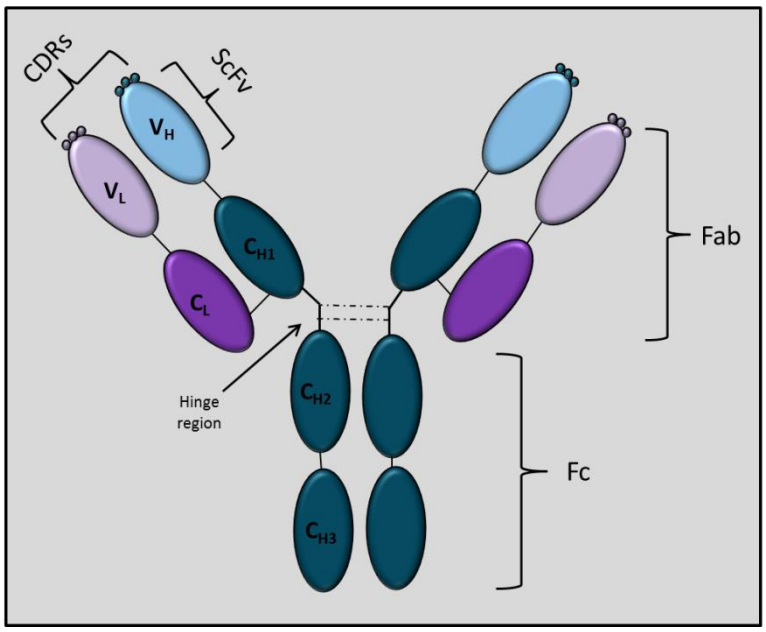

Figure 1.11 Structure of an IgG mAb. Antibodies are made of two heavy (blue) and two light (purple) chains; both of which are made up of variable (lighter in colour) and constant (darker in colour) regions. They have two Fab arms that make up the antigen binding region and the Fc tail that binds to effector cells and induces an immune response.

1.4.2.3.1 Generation of monoclonal antibodies

1.4.2.3.1.1 Hybridoma Technology

The majority of early studies on antibodies utilised myeloma cells[1]. Multiple myeloma is a cancer of plasma cells, and as antibodies are produced by plasma cells, myeloma was seen as an ideal model to study antibody biology[1]. These cells revealed that mAbs could be obtained from immortalised plasma cells, but their use as a model was limited due to their unknown antigen specificity[1]. However, in 1975, Köhler and Milstein described how antibodies of a single known specificity could be produced using hybridoma technology[202]. They showed that by fusing together immortalised murine myeloma cells with antigen immunised mouse spleen cells, hybrid cells that secreted specific antibodies against the immunised antigen were produced, and the cells were able to proliferate indefinitely[1, 202]. Hybrid cells or 'hybridomas' were selected using a drug that kills parental myeloma cells[1]. Hybridomas producing the desired specific antibodies can then be selectively grown[1]. Each fused cell produced derives from a single B cell, which produces a single specificity monoclonal antibody that is thus referred to as a mAb[1].

1.4.2.3.1.2 Phage Display Technology

Although phage display was first described in 1985 by George Smith to screen peptide libraries; it was McCafferty *et al* in 1990 that first used phage display to generate mAbs[203, 204].

Using polymerase chain reaction (PCR) variable (v) genes of Igs were amplified from hybridomas or B cells and cloned into expression vectors[203]. These v genes were displayed on bacteriophages and these phages specifically bound to a target antigen[203]. Soluble antibodies were produced by growing them in bacteria, and subsequently the secreted antibodies could be screened for antigen binding[203]. This was possible by reducing the mAb size to its Fab or scFv. The specific binding component of the mAb gene could then be expressed in bacteria and displayed on bacteriophages such as M13 filamentous phage, commonly used in phage display technology (*Figure 1.12*)[205].

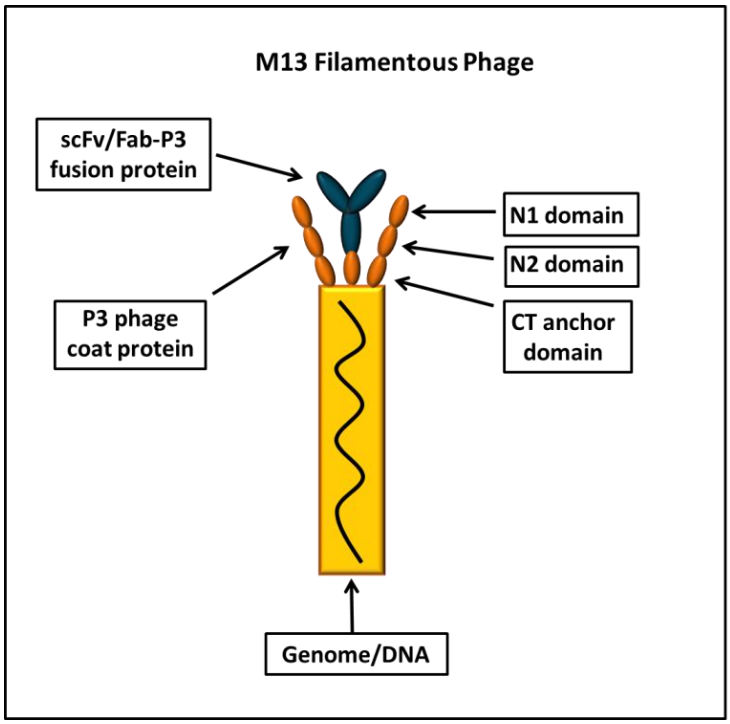

Figure 1.12 M13 Filamentous Phage is used to display antibody genes in phage display technology. The phage contains a single-stranded DNA genome and P3 phage coat protein made up of three domains: N1, N2 and CT anchor domain. The antibody gene is fused to this coat protein and binds to its specific antigen.

There are many different formats the antibody can be displayed in phage display. Fab or scFv genes, are the most common and both have their own pros and cons (*Table 1.8*)[205]. Fab libraries consist of the Fab or antibody binding domain, whilst scFv libraries are made up of the single chain variable fragments attached by a linker[205]. These libraries are derived from naïve B cells or immunised donors[205]. Synthetic libraries using synthetic variable genes and artificial CDRs are also available[205]. Other antibody fragments that can also be used include: Fv, which consists of the variable fragment, and bivalent antibody fragments termed diabodies[206].

Table 1.8 Comparison of Fab and scFv phage display library formats

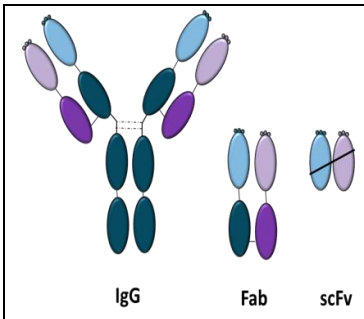	**Fab**	**ScFv**
	- More stable - Less Potential to dimerise - In addition to the V_H and V_L segments, they also have the constant regions (C_H and C_L)	- Less toxic on cells - Better yield and diversity - More popular choice as have higher avidity as they are displayed on phages at a higher frequency than Fab fragments

Information from Carmen and Jermutus[205].

Once the library has been constructed, during the selection or 'panning' stage, incubation of the target antigen with phages displaying the antibody library is carried out, unbound phages are washed away and phages bound specifically to the target are eluted[205]. Phagemids (plasmids containing the genes for both the antibody fragments and the phage coat protein) are utilised as the small vector size ensures efficient transformations in bacteria[205]. Helper phages are also utilised, which provide genes required for correct phage packaging[205].

The overall goal of phage display is to generate antibodies that are as diverse as possible, and there are many different ways to ensure this. Firstly, the way in which the target is displayed during the selections; this can be coated on plastic, biotinylated in solution and captured by streptavidin beads, displayed on the cell surface or in nitrocellulose after being separated by electrophoresis[205]. All of these methods have pros and cons: binding epitopes can be masked in each technique, the protein can be denatured, or as coating protein to plastic is non-covalent, smaller targets can become unbound; to avoid this, conjugating the protein e.g. to bovine serum albumin (BSA), ensures the protein stays bound[205]. Biotinylating the protein also eliminates the chance of the protein becoming unbound, as the interaction between biotin and streptavidin is so strong, it is almost covalent; this method also removes the chance of denaturation[205]. Although success has been gained from displaying the protein on cells, cells may also express other antigens on their surface, therefore introducing potential contaminates, although the blocking step performed after selections usually eliminates non-specific targets[205]. Different selection strategies can yield different types of mAbs, as shown by Lou *et al*, who screened a number of different antigens either by coating them to immunotubes (a typical method used) or to a 96-well plate[207]. Despite both methods utilising coated protein to plastic, different antigens produced varying amounts of mAbs with each method[207]. Therefore, to ensure maximum diversity of mAbs produced, exploiting more than one selection method is ideal. Secondly, the method of eluting phages can play a role in the success of the mAbs generated; methods include: exploiting pH, enzymatic cleavage, or the

use of a soluble antigen in competitive elution[205]. All of these techniques are dependent on the target and its properties[205]. Therefore, designing a selection strategy to produce specific and diverse mAbs is target-dependent.

Phage display technology may have pros and cons but the technology has allowed for fully human antibodies to be produced in a fast and automated way[205].

1.4.2.3.2 Monoclonal Antibodies in therapy

Given the specificity of mAbs and that phage display provides a high-throughput way of producing these antibodies, they have been used in therapy.

The production of mAbs by hybridoma technology earned Milstein and Köhler a Nobel Prize in 1984[208]. The first mAb to gain US Food and Drug Administration (FDA) approval was an anti-CD3 antibody known as Othoclone OKT3 (Janssen-Cilag) in 1986[208]. OKT3 is a mouse antibody used to treat acute transplant rejection, and targets the CD3-complex of the TCR[209, 210]. However, mouse antibodies proved to be less than ideal for human therapy[188]. Mouse antibodies can have adverse effects in humans due to their immunogenicity that results from the mouse proteins being recognised as foreign in humans: referred to as the human-anti-mouse-antibody (HAMA) response[2]. Mouse antibodies also have the disadvantage of having a short lifespan *in vivo*, and not being able to efficiently elicit human antibody-dependent effector mechanisms such as antibody-dependent cell cytotoxicity (ADCC), and therefore being inefficient at killing their targets[188]. In 1984, Morrison *et al* described how mouse-human or 'chimeric' antibodies could be produced through recombinant DNA techniques[211]. Variable regions of mouse antibody-producing myeloma cells were fused to human constant region genes[211]. Their aim was to reduce immunogenicity of mouse antibodies. Jones *et al* went one step further in 1986 when they first described humanised mAbs[212]. They replaced the majority of the mouse antibody with human antibody regions, with the exception of the CDRs that are responsible for antigen binding, to generate this new class of antibodies, in hopes that as these antibodies were more human, immunogenicity would decrease and the HAMA response would be avoided[212]. There are now many different forms of mAbs (*Figure 1.13*) and since OKT3, many other mAbs have been approved for therapies in cancer, autoimmunity and inflammatory diseases (see later)[213].

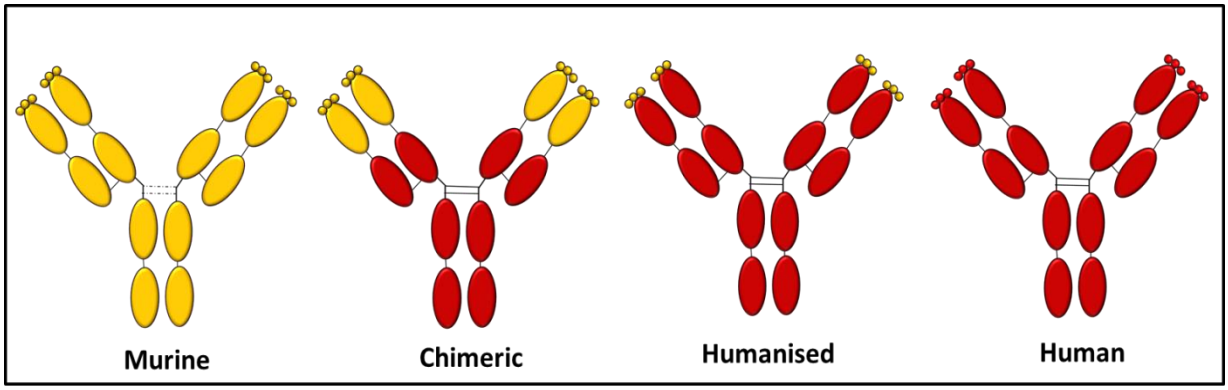

Figure 1.13 Types of monoclonal antibodies. Murine antibodies were the first monoclonal antibodies to be produced for therapeutic use by hybridoma technology. Due to the immunogenicity that resulted when injected into humans, chimeric antibodies were developed. Chimeric antibodies contain mouse variable regions fused onto human constant regions, therefore producing an antibody with the mouse Fc region replaces by a human Fc. Humanised antibodies came next, where the majority of the mouse antibody is replaced with human regions, except the CDRs, and these almost fully human antibodies have less immunogenicity. Fully human antibodies can now be produced using phage display technology. Yellow = mouse protein sequence, Red = human protein sequence.

In 1997, Rituximab, an anti-CD20 mAb was the first chimeric antibody to be FDA approved, whilst the anti-CD25 antibody Daclizumab was the first humanised antibody to gain FDA approval[208]. Thanks to the introduction of phage display by McCafferty *et al* to screen mAbs, in 2002 Adalimumab (a TNF-α specific antibody) was the first fully human antibody to be FDA approved[203, 214]. Antibodies produce high revenue, and the highest selling or "big 5" approved mAbs are listed below in *Table 1.9*

Table 1.9 "Big 5" approved monoclonal therapeutic antibodies

Target	Antibody Name	Other Names	Type of antibody	Production	Use In	Produced by	Date Approved
TNF-α	Infliximab	Remicade	Chimeric	Hybridoma Technology	Crohn's disease	Centocor/ Merck	1998
TNF-α	Adalimumab	Humira	Fully human	Phage Display	Rheumatoid arthritis	Trudex/ Abbott	2002
HER2	Trastuzumab	Herceptin	Humanised	Hybridoma Technology	Breast cancer	Genentech/ Roche	1998
VEGFA	Bevacizumab	Avastin	Humanised	Hybridoma Technology	Colorectal cancer	Genentech	2004
CD20	Rituximab	Rituxan/ Mabthera	Chimeric	Hybridoma Technology	Non-Hodgkin's lymphoma	Genentech/ Roche/ Biogen Idec	1997

Table describes the highest selling mAbs currently approved and the date of approval in the EU, their target, type of antibody, way in which they were produced and who produced them. *Table compiled from Leavy (2010) and Reichert (2015)*[47, 213].

Table 1.9 describes just some of the antibodies approved for therapy. Currently, there are at least 50 different antibodies approved or in review in the United States of America (USA) and European Union (EU)[47]. Most of these mAbs target cancer or autoimmune conditions[213].

1.4.2.3.3 Antibody-dependent mechanisms

Given the success of antibodies in immunotherapy, elucidating the mechanisms of action of these therapeutic mAbs will provide a better understanding into their success.

Antibodies mediate killing of antibody-opsonised cells through a number of different mechanisms: ADCC, complement-dependent cytotoxicity (CDC), antibody-dependent cell phagocytosis (ADCP) and potentially programmed cell death (PCD)[2]. A schematic of these mechanisms is displayed in *Figure 1.14* below.

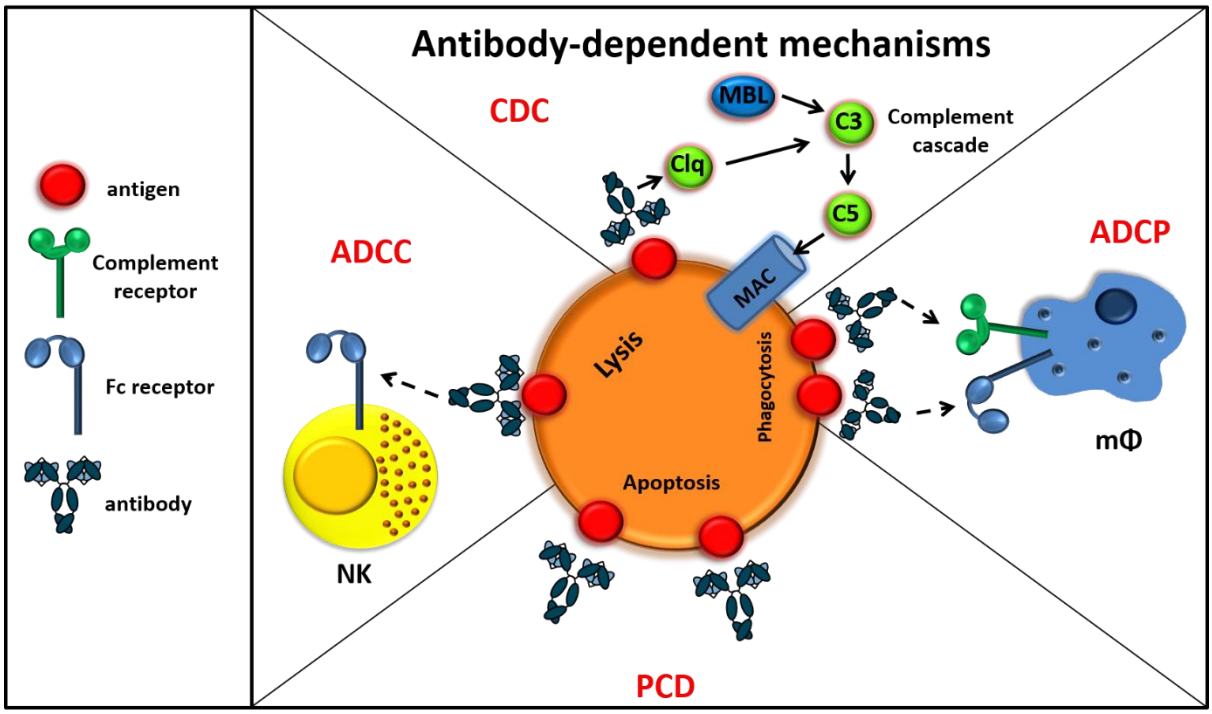

Figure 1.14 Antibody-dependent toxicity mechanisms. Antigen-antibody complexes are recognised by cytotoxic cells such as macrophages through their FcRs; these cells cause cell lysis of infected cells by ADCC through lytic enzymes, TNF and perforin. If these FcR-bearing cells are also phagocytic, such as macrophages and neutrophils, they can also cause ADCP, through digestive enzymes and ROS. CDC can also lead to cell lysis. Only the classical complement pathway is antibody-dependent and is triggered by antigen-antibody complexes, leading to the formation of the membrane attack complex (MAC), which causes cell death by disrupting osmotic stability of cells. PCD can also be antibody-induced through non-apoptotic pathways, this is dependent on actin, lysosomes and ROS. Figure adapted from Kasi *et al* (2012)[215].

1.4.2.3.3.1 ADCC

Certain immune cells can cause target cell death through ADCC, these include: NK cells, macrophages, monocytes, neutrophils and eosinophils[2]. When antibodies bind specifically to

their target antigens, cytotoxic cells such as these, recognise and bind these antigen-antibody complexes through FcγRs expressed on the cells, and mediate cell lysis through the release of lytic enzymes and TNF-α that kills infected cells[2].

NK cells have been found to primarily mediate ADCC, and are important for mAb therapy. *In vitro* experiments support this, and depletion of NK cells from PBMCs, has shown a decrease in ADCC and reduced efficacy of depletion of lymphoma cells by Rituximab, suggesting that Rituximab therapy may work through ADCC[216].

Antibody Fc interaction with FcγR is important for eliciting ADCC, and a number of therapeutic mAbs are believed to engage this mechanism, including Rituximab and Trastuzumab[217]. This is supported by studies in FcγR-deficient mice that showed almost no response to mAb therapies compared to wild type mice, indicating the importance of these receptors in this type of therapy[218]. FcγRIII is an IgG high affinity receptor found on NK cells, and may play a role in ADCC by mediating killing of antibody-opsonised cells in the blood[219]. This was demonstrated by Cartron *et al* who found that NHL patients with higher levels of FcγRIIIA showed better responses to Rituximab treatment, as they had a higher affinity for IgG1[219]. However, there is little evidence *in vivo* supporting the role of ADCC as a mechanism for Rituximab depletion. Mouse studies have shown that depletion of NK cells *in vivo* had no effect on Rituximab therapy[220].

1.4.2.3.3.2 ADCP

Another antibody-dependent mechanism that requires FcγR interaction is ADCP. FcγR-bearing cells that are also phagocytic i.e. macrophages and neutrophils can destroy antibody-opsonised cells through ADCP[2]. As with ADCC, antigen-antibody complexes are recognised by the FcγRs on these phagocytic cells, but unlike ADCC, which mediates cell lysis, opsonised cells are then destroyed through phagocytosis with the aid of digestive enzymes and ROS[2].

Uchida *et al* showed that ADCP was mediated through macrophages, by utilising anti-CD20 mAbs for B cell depletion[221]. They found that mice treated with clodronate, which rendered macrophages deficient, were unable to deplete B cells[221]. This has been further confirmed through advanced *in vivo* imaging. Montalvao *et al*, confirmed through intravital imaging that anti-CD20 mAbs depleted malignant B cells through ADCP[222]. B cell depletion was found to predominantly occur in the liver by kupffer cells (KCs)[222]. Gul *et al*, also confirmed through intravital microscopy that although KCs interacted with tumour cells, they were unable to

deplete them[223]. However, antibody-opsonised tumour cells were rapidly phagocytised and eliminated by KCs, demonstrating ADCP *in vivo*[223].

1.4.2.3.3.3 CDC

The complement system is made up of serum proteins including perforating glycoproteins that can lyse bacteria, viruses and infected cells.[2] Complement is also involved in triggering inflammation and immune tolerance[2]. There are three main complement pathways: the classical, alternative and lectin pathways[224]. The classical pathway is triggered by the C1 complex upon antigen-antibody binding (IgM, IgG1, IgG2, IgG3 and IgG4)[224]. C1q binds to Ig in close proximity, undergoing a conformational change that results in the activation of C1r and C1s[224]. C1s then cleave C2 and C4, resulting in activated C2a and C4b, which form C3 convertase, and enzyme that cleaves C3a and C3b, leading to the formation of C5 convertase and subsequently forming the membrane attack complex (MAC)[224]. The alternative pathway, is activated by spontaneous C3 cleavage, which does not require antigen stimulation, and is therefore part of the innate immunity[2, 224]. Finally, the lectin pathway, is also antibody-independent, and is triggered by mannose binding lectin (MBL), which binds to mannose residues on pathogens[2, 224]. Cleavage of C2 and C4 result in the formation of C3 convertase[224]. Consequently, following the formation of C3 convertase, all of the complement pathways result in the formation of the MAC, which allows ions to travel across membranes, causing osmotic stability of the cell to be disrupted and subsequent cell death[2].

An example of where therapeutic mAbs engage the complement system is demonstrated by Alemtuzumab (Campath-1H®) - an anti-CD52 mAb, previously approved for treating CLL, and now approved for treating MS[47]. One way in which it deletes antibody-opsonised cells is by eliciting the complement system[47, 218, 225]. CD52 is highly expressed on both normal and malignant T and B cells, and as demonstrated by Hu *et al*, Alemtuzumab can deplete $CD52^+$ tumours through CDC[225]. Studies have also shown that when immunocompromised mice were injected with different lymphoma cell lines, and treated with anti-CD20 mAbs, if they were also given cobra venom factor (CVF) to deplete complement, mAb therapy was hindered[226]. Knock-out mice lacking C1q, and important component of the classical complement pathway, also showed reduced Rituximab efficacy, suggesting the role of complement is important for this mAb therapy[220]. However, the importance of complement in anti-CD20 therapy is not seen with all anti-CD20 mAbs. This suggests that there are different types of anti-CD20 mAbs, and their mechanism of action differs; complement may be important for only some anti-CD20 therapies[226].

1.4.2.3.3.4 PCD

Cells are eliminated through PCD. An example of this is apoptosis, which is a programmed and regulated type of cell death that undergoes morphological changes, which are then engulfed through phagocytosis by macrophages[2]. However, there is now evidence that PCD can also be antibody-mediated.

Initial evidence for this mechanism comes from work described on the success of anti-idiotype mAbs that target the antibody binding sites. Vuist *et al* showed that treatment of NHL with these anti-idiotype mAbs resulted in remission of 68% of patients, and this therapy caused an induction of intracellular protein tyrosine phosphorylation, inducing intracellular signalling that led to PCD[227].

Different mAbs are capable of this to differing degrees. Chan *et al* showed that anti-CD20 mAbs were capable of eliciting caspase-independent PCD, and this was greater when molecules were translocated into lipid rafts, where signalling dominates[228]. PCD was further increased where there was greater homotypic cellular adhesion[228]. Ivanov *et al*, Honeychurch *et al* and Alduaij *et al* also showed that particular anti-CD20 mAbs can induce non-apoptotic PCD, assisted by actin and lysosomes that produce ROS[229, 230, 231]. In this scenario, homotypic cellular adhesion and actin relocalisation were believed to drive PCD[230]. This has powerful implications for immunotherapy, as this pathway is not dependent on effector cells[229]. Caspase modulation is believed to be one reason for chemotherapy resistance, given that these studies suggest that mAb-induced PCD can be caspase-independent has great implications for therapy[232]. However, there is little *in vivo* evidence for mAb depletion by PCD, suggesting it may not be a potent mechanism of action for mAbs[232].

1.4.2.3.3.5 Immunomodulation and signalling antibodies

All the mechanisms mentioned above are ways in which mAbs can directly target and kill tumour cells and pathogens. However, mAbs can also cross-link receptors at the cell surface, resulting in intracellular signalling[233]. This is known as immunomodulation, and mAbs can be either agonistic (enhance signalling) or antagonistic (suppress signalling). In cancer therapy, agonistic mAbs are designed to mimic ligands and increase signalling of co-stimulatory molecules leading to enhanced immune responses, whilst antagonistic antibodies are designed to block inhibitory receptor function causing dampened immune responses[234].

Examples of immunomodulatory antibodies include Ipilimumab (Yervoy®), a human IgG1 mAb targeting CTLA-4, approved in 2011 in both the USA and EU to treat metastatic

melanoma[47]. Ipilimumab blocks the inhibitory effect of the checkpoint blocker CTLA-4, preventing down-regulation of T cell responses[235]. Other antagonistic mAbs include anti-Programmed death 1 (PD-1) and anti- Programmed death 1 ligand (PDL-1), used to treat non–small-cell lung cancer (NSCLC), melanoma, or renal-cell cancer[236, 237]. Tumour cells express PDL-1 and interact with PD-1 receptor to avoid immune surveillance[238]. Antibodies against either PD-1 or PDL-1 have therefore been found to prevent this interaction, increasing T cell responses and aiding in tumour clearance[238].

Immunostimulatory antibodies such as anti-CD40 mAbs have also been reported[55]. CD40 is a member of the TNFR superfamily and is expressed on APCs such as B cells, macrophages and DCs[55]. When ligated CD40 activates APCs and induces adaptive immunity[55]. Proposed mechanisms of action of these mAbs in cancer therapy include: agonistic anti-CD40 mAbs activating APCs that result in increased T cell responses, activating macrophages that can clear tumours, or directly targeting CD40-expressing tumours, resulting in either PCD or cellular cytotoxicity[239]. So far, four anti-CD40 mAbs have been investigated in clinical trials, and the characteristics of these mAbs range from strong agonists to strong antagonists[239]. The reason for the differences in function are unclear, but have been proposed to be the result of FcγR interaction, as Fab antibodies are known to be unable to clear tumours, indicating the importance of mAb Fc: FcγR interaction[239]. Alternatively, mAb isotype has also been suggested to contribute the differences in function. I*n vivo* studies have shown that mouse (m) IgG1 but not mIgG2a can act as an immunostimulatory mAb[55, 234]. Other immunostimulatory mAbs include anti-CD27, -41BB, and -OX40[234].

Most immunomodulatory antibodies have so far targeted T cell surface receptors. However, research is underway into targets on other immune cells[238]. One such target is inhibitory KIRs found on NK cells that inhibit intracellular signalling, preventing NK cytotoxicity. Antibodies against these receptors, may aid in restoring NK cell-mediated cytotoxicity and tumour clearance[238]. Lirilumab is fully human mAb targeting inhibitory KIR2DL-1,-2 and -3, and is well-tolerated with low toxicity in a phase I clinical trial to treat AML[240].

1.4.2.3.4 Advances in antibody therapy

In order to enhance current mAb therapies, mAbs can be used in combination with chemotherapy, radiotherapy, vaccines, immunomodulators such as IL-2 and IFN-γ, or tyrosine kinase inhibitors that block intracellular signalling[218]. Alternative antibody formats, have also been proposed, for example, Bi-specific antibodies (BsAbs), which target two antigens, most commonly tumour antigens and cell surface markers found on effector cells[218].

However, high toxicity and their short half-lives have led to poor clinical success of these molecules[218]. Bi-specific T cell engager (BiTE) molecules, which target CD3 on the TCR and another target antigen are another novel alternative to generic mAb therapies for eliminating tumours[218]. Unlike BsAbs, BiTE molecules can activate T cell responses directly when engaged with tumours, making them more potent at tumour elimination[218, 241]. Blinatumomab (Blincyto®) is a BiTE used to treat Acute lymphoblastic leukaemia (ALL) approved in 2014 in the USA[47, 242]. The mAb targets both CD3 and CD19, allowing T cells to recognise malignant B cells[242].

Alternatives to fully human mAbs have also been approved or are waiting approval for therapy, in the form of Fabs[47]. One such example is Certulizumab pegol (Cimzia®), a pegylated Fab antibody fragment against TNF-α, approved for treating Crohn's Disease, and shown to have a prolonged half-life; with other Fabs also in review for approval[47, 243]. Choy *et al* found linking the Fab fragment to polyethylene glycol (PEG) made the therapy more tolerated in patients, as it disguises the drug from the hosts immune system[243].

Another way in which antibodies can be used therapeutically is by linking them to cytotoxic agents, collectively termed, Antibody-Drug Conjugates (ADCs). The first ADC that gained FDA approval in 2001, was Gemtuzumab ozogamicin (Mylotarg®), a humanised anti-CD33 mAb linked to a cytotoxic antibiotic Calicheamicin, used to treat AML[244]. AML cells express CD33, and given that anti-CD33 mAbs were reported to internalise, this feature was exploited to deliver toxic agents inside the tumour cells[244]. Although the ADC was later withdrawn, two other ADCs remain approved for therapy: Brentuximab vedotin (Adcetris®) and Trastuzumab emtansine (Kadcyla®)[47]. Brentuximab vedotin is a chimeric anti-CD30 conjugated to antimitotic agent monomethyl auristatin E (MMAE), which has anti-tumour activity by inducing apoptosis[245]. This drug is used to treat Hodgkin lymphoma (HL) and systemic anaplastic large cell lymphoma (sALCL)[47, 245]. Trastuzumab emtansine consists of the already approved humanised mAb Trastuzumab, which targets the HER2 receptor, conjugated to emtansine (DM1) a cytotoxic agent, used to treat breast cancer[47, 246].

Whilst the antibodies and effector mechanism described here are in the context of cancer therapies, antibody therapies are constantly developing and evolving. Antibodies previously approved for cancer treatment, are now approved for treating other diseases[47]. Therefore, characterising and studying the function of these mAbs for cancer therapy, will also aid in the treatment of various different diseases. As current therapies are modified and optimised, and knowledge about the importance of FcγR interactions with these antibodies is recognised, this type of therapy continues to revolutionise the treatment of cancer and other diseases.

AIMS AND HYPOTHESIS

The aim of this project was to characterise the expression and function of the inhibitory LILR receptor family on myeloid cells, and generate novel reagents to do this. This included generation of agonistic and antagonistic anti-LILRB1, LILRB2 and LILRB3 specific mAbs that could be tested in a number of different *in vitro* assays and then for therapeutic efficacy *in vivo*.

The aims of the project can be summarised as follows:

1. Generate a panel of specific mAbs able to bind to LILRB1, LILRB2 and LILRB3 receptors by phage display
2. Testing receptor expression on myeloid cells and characterising the antibodies
    - Confirming specificity and eliminating cross-reactivity against different activatory and inhibitory LILRs
    - Using flow cytometry to confirm expression on different immune cell types
    - Determining antibody affinity
    - Epitope mapping of mAbs
    - Testing tissue expression of LILR mAbs
3. Elucidating the function of these novel anti-LILRB-specific mAbs *in vitro*
    - Testing ability of antibodies to cross-link receptors and activate cells
    - Testing antibody agonism vs antagonism through ligand blocking assays
    - Macrophage phagocytosis and T cell proliferation assays to determine function on different cell types
    - Testing receptor internalisation
4. Deducing the therapeutic efficacy of these mAbs
    - Testing function of mAbs *in vivo*

2 MATERIALS AND METHODS

2.1 Cell culture

All cell culture media used were supplemented with 10% Foetal Calf Serum (FCS), 100 U/ml Penicillin-Streptomycin (PS) (Life Technologies) and Glutamine Pyruvate (GP) consisting of 2 mM Glutamine (Life Technologies) 1 mM Pyruvate (Life Technologies) unless otherwise stated. Conditions for individual cells were as detailed in *Table 2.1* below.

Table 2.1 Cell culture conditions

Cell Name	Cell Type	Species	Media	Supplement	Cell density	Extra Information
HEK293F	Cell line	Human	Freestyle 293F media (Life Technologies)	-	1-3x10^6 cells/ml	37°C, 8% CO_2, shaking at 130 rpm
HEK293F LILRB3 domain mutant transfectants*	Cell line	Human	Freestyle 293F media (Life Technologies)	-	1-3x10^6 cells/ml	37°C, 8% CO_2, shaking at 130 rpm
HEK293T	Cell line	Human	RPMI 1640	10% FCS, GP, PS	1x10^6 cells/ml	37°C, 5% CO_2
CHO-S	Cell line	Hamster	Freestyle CHO media (Life Technologies)	8 mM Glutamine	0.8-1x10^6 cells/ml	37°C, 8% CO_2, shaking at 140 rpm
Ramos	Cell line	Human	RPMI 1640	10% FCS, GP, PS	0.2-1x10^6 cells/ml	37°C, 5% CO_2
Ramos LILRB3 ITIM mutant transfectants†	Cell line	Human	RPMI 1640	10% FCS, GP, PS 1 mg/ml Geneticin	0.2-1x10^6 cells/ml	37°C, 5% CO_2
PBMCs/MDMs /MDDCs	Primary cells	Human	RPMI 1640	10% FCS, GP, PS	1x10^6 cells/ml	37°C, 5% CO_2
CLL	Primary cells	Human	RPMI 1640	10% FCS, GP, PS	1x10^6 cells/ml	37°C, 5% CO_2

*LILRB3 WT, LILRB3-3D, LILRB3-2D, LILRB3-1D-expressing HEK293F cells generated by transient transfection of HEK293F cells for surface expression (see 2.3.1.2).

†LILRB3 WT, truncated (t) LILRB3-3, tLILRB3-2, tLILRB3-1 and tLILRB3 (no ITIMs) - expressing Ramos cells were generated by nucleofection (see 2.3.1.4).

2.1.1 Clinical samples and ethics

Ethical approval for the use of clinical samples was obtained by the Southampton University Hospitals NHS Trust from the Southampton and South West Hampshire Research Ethics Committee. Informed consent was provided in accordance with the Declaration of Helsinki. Samples were released from the Human Tissue Authority licensed University of Southampton, Cancer Science Unit Tissue Bank as part of the LPD study LREC number 228/02/T

2.1.2 Human Peripheral Blood Mononuclear Cell (PBMC) Isolation and Purification

PBMC isolation was performed using a leukocyte blood cone (Blood Transfusion Services, Southampton General Hospital) or using blood from cancer patient samples (CLL cells provided by Dr Francesco Forconi, Southampton General Hospital). Blood was diluted in phosphate buffer saline (PBS), 2 mM ethylenediaminetetraacetic acid (EDTA), and 10% Foetal Calf Serum (FCS). The diluted blood was slowly layered onto lymphoprep (equal to the volume of blood). The samples were then centrifuged at room temperature for 20 minutes at 800xg with low deceleration. Then, the interphase layer for each sample (separating the blood and plasma) was removed; the interphase layer contained the PBMCs. The PBMCs were washed in PBS/serum mix and centrifuged at room temperature for 5 minutes at 300xg. The supernatant was carefully discarded and the cells washed three subsequent times or until the supernatant became clear.

2.1.3 Human monocyte-derived macrophages and dendritic cells

After PBMC isolation, to generate monocyte-derived macrophages (MDMs) or monocyte-derived DCs (MDDCs) from PBMCs, 1% human AB serum was added to the cells to aid in adherence and the cells were then plated at $2x10^7$ cells/well in a 6-well plate (Corning) and incubated at 37°C for 2 hours. Non-adherent cells were gently washed off (2-3 times) and discarded and 2ml fresh full-serum media was added to the cells, which were then left to incubate at 37°C overnight, 5% CO_2. The next day (day 1), 100 ng/ml human recombinant M-CSF or 50 ng/ml GM-CSF and 50 ng/ml IL-4 were added to each well to generate MDMs or MDDCs, respectively. On day 3 and 5/6, media and cytokines were replenished. Cells were then harvested day 7-8.

2.1.4 Monocyte isolation from PBMCs

PBMCs isolated from blood were cultured at high density at $1x10^7$ cells/ml in a 24-well plate (Corning) overnight at 37°C, 5% CO_2. Monocytes were isolated by negative selection using the Pan Monocyte Isolation Kit (Miltenyi Biotec) as per manufacturer's instructions. Cells were blocked with FcR Blocking Reagent (human IgG), incubated with a cocktail of biotin-conjugated antibodies against antigens on cells not expressed by human monocytes, then anti-biotin microbeads added to bind to these antibodies. The mixture was passed through an LS column (Miltenyi Biotec) and unlabelled monocytes passed through the column and collected. The cells were centrifuged for 5 minutes at 300xg and resuspended in fully-supplemented RPMI media, ready for use.

2.1.5 Bacterial cell culture

Bacterial cultures were grown by adding 5 µl transformed DNA or glycerol stock sample to 10 ml LB (Sigma) containing an appropriate antibiotic (50µg/mL kanamycin or 100µg/mL ampicillin). The culture was left to grow overnight at 37°C, shaking at 225 rpm. From these cultures small-scale plasmid purification could be performed. Alternatively, for larger scale plasmid purification, the 10 ml bacterial cultures were subsequently added to 100 ml LB (with appropriate antibiotic) and grown at 37°C overnight and shaking at 225 rpm.

2.1.6 Freezing down cells

Patient samples and cell lines were frozen down in freeze medium containing FCS with 10% DMSO. Cells were stored in liquid nitrogen until thawed for phenotyping or modulation assays.

For bacterial cell cultures, 10 ml bacterial cultures were centrifuged at 3000xg for 10 minutes. The bacterial pellet was resuspended in 1 ml LB with appropriate antibiotic and added to a cryovial containing 50-70% glycerol and stored at -20°C.

2.2 Molecular Biology

2.2.1 List of DNA constructs and primers used

Table 2.2 DNA constructs

Name	Vector	Use
LILRB1-hFc	SigPlg	Transfections - Generate protein (selection/screening)
LILRB2-hFc	SigPlg	Transfections - Generate protein (selection/screening)
LILRB3-hFc	SigPlg	Transfections - Generate protein (selection/screening)
LILRB1-FL	pHR-SIN	Generate target on cells (selection/screening)
LILRB2-FL	pHR-SIN	Generate target on cells (selection/screening)
LILRB3-FL	pHR-SIN	Generate target on cells (selection/screening/; generate transfectants)
LILRB4-FL	p3xFLAG-CMV9 (Sigma)	Generate target on cells (selection/screening)
LILRB3-1D	pcDNA3	Epitope mapping
LILRB3-2D	pcDNA3	Epitope mapping
LILRB3-3D	pcDNA3	Epitope mapping
tLILRB3	pcDNA3	Signalling/in vivo experiments
tLILRB3-1	pcDNA3	Signalling/in vivo experiments
t LILRB3-2	pcDNA3	Signalling/in vivo experiments
tLILRB3-3	pcDNA3	Signalling/in vivo experiments

Table 2.2 DNA constructs. hFc fusion protein and full length (FL) DNA constructs were provided by Dr Des Jones, University of Cambridge. All other constructs were generated by PCR. See appendix for vector maps.

Table 2.3 Primer sequences for generation of constructs

Primer Name	Sequence
Vector primers	
SigPlg F	ACTCACTATAGGGAGACCCA
SigPlg R	TGGGCATGTGTGAGGTTTGTC
pHR-SIN F	AAAGAGCTCACAACCCCTCA
pHR-SIN R	AATCCAGAGGTTGATTATCG
M13	CAGGAAACAGCTATGAC
Sp6	ATTTAGGTGACACTATAG
LILRB1 sequencing primers	
LILRB1-560R	GGA TCC GTG TAA TCC AGA GTG
LILRB1-755F	GGG AAT GTA ATC CTC CAG TGT
LILRB1-1415R	TGG TCA GAA GGA AAG TTT GCA
LILRB1-1455F	CAG GTG CTA CGG CTC ACA GAG
LILRB2 sequencing primers	
LILRB2-480R	TCA CAA GCT CTG GTC GTA TCC
LILRB2-675F	GGA AGG GTG ACC CTC CAG
LILRB2-1310R	CAT GAC TGA CAC AGC AGG GTC
LILRB2-1350F	GCT GAT GCC CCA CTC GGT CTA
LILRB3 sequencing primers:	
LILRB3 150R	GAC ACC AGA TGG TCA CGG GG
LILRB3-240R	TAT CTC CCC GCA TGG TGC T
LILRB3-330R	TGC ATA GTG CTG TGT CAT
LILRB3-500F	GAT ATC ACC ATT TTG TTC TG
LILRB3-1740	TTC CTG GAC ACA AAG GAC
LILRB3-855F	GCC AAC TTC ACC CTG GGC C
LILRB3-900	CTG GGC CCT GTT AGC CGC T
LILRB3-1200	TAC AGC TCC AAC CCC CAC CT
LILRB3-1300	TCA TGG TCT CAG GAC ACT
LILRB3-1660F	ACA CTC CAG TCG TAG GAG
LILRB3-1774R	CAG CCT CAG TGT CCA
LILRB3-1820	CTC CCA GGA TGT GAC CTA CG
LILRB4 sequencing primers	
LILRB4-ECDR	TTT GGG GAG GGG CCC TGC CTG
LILRB4-ECDF	CAG GCA GGG CCC CTC CCC AAA
LILRB4-500F	TGA GAT CAG AGC ACG GAG CTC
LILRB4-840R	CCT GTG TTT TCC CTG ACG CCA GTG TTG
LILRB4-778R	GTA CTG ATC GGG GTC TTG GTG
LILRB4-1150F	CTG GAC ACA AAG GAC AGA CAG
Generation of LILRB3 domain-mutants	
LILRB3-3D-TM-R	AAT CAA AAG CTC CAG GTA GTT CAG GGG GTC GCT GGG
LILRB3-3D-TM-F	CCC AGC GAC CCC CTG AAC TAC CTG GAG CTT TTG ATT
LILRB3-2D-TM-R	AAT CAA AAG CTC CAG GTA GGT CAG GAG GGA GGG CTT
LILRB3-2D-TM-F	AAG CCC TCC CTC CTG ACC TAC CTG GAG CTT TTG ATT
LILRB3-1D-TM-R	AAT CAA AAG CTC CAG GTA ATA GTG GCA GCG GTA
LILRB3-1D-TM-F	TAC CGC TGC CAC TAT TAC CTG GAG CTT TTG ATT
LILRB3-Cyt-R	GCG GCC TAG TGG ATG GCC
Generation of LILRB3 ITIM-mutants	
BamHI 30	GGG GAT CCG CCA CCA TGA CGC CCG CCC TCA
tLILRB3 (no ITIMs)	GCG GCC GCA TAT ATT CAC TGA CGT CGG AGG AGG AGG AA
tLILRB3-1 (1-ITIM)	GCG GCC GCT CAC ACA GCA GCA TAG AGG TT
tLILRB3-2 (2-ITIMS)	GCG GCC GCT CAC ACC GGG GCA TAC GTC AC
tLILRB3-3 (3-ITIMS)	GCG GCC GCT CAC AGC TGG GCC TAG GTC AC

Table 2.3 Primers sequences. F= forward, R = reverse, ECD = extracellular domain, TM = transmembrane domain, Cyt = cytoplasmic domain, D= domain, t = truncated, and numbers refer to position in the base pair sequence amplifying.

2.2.2 Polymerase Chain Reaction (PCR)

The following reaction mix was typically used for all PCR reactions.

Table 2.4 PCR Reaction Mix recipe/constituents

Reagent	Amount	Volume
DNA of interest	variable	1 µl
PFU buffer (with $MgCl_2$)	1x	2.5 µl
Primer Forward	100 ng	1 µl
Primer Reverse	100 ng	1 µl
dNTPs	0.2 mM	0.5 µl
PFU polymerase enzyme	1 U	1 µl
dH_2O	Made up to 25 µl	

LILRB3 domain mutants were generated by overlap PCR and LILRB3 ITIM mutants by truncation PCR. For the overlap PCR reaction two separate PCR reactions were performed. The first reaction was made up of 3-5 µl of gel extracted PCR product 1 and 3-5 µl gel extracted PCR product 2, along with dNTPs (Life Technologies), PFU 1x buffer (Promega) and PFU polymerase enzyme (Promega) as above in Table 2.4, made up to a total volume of 25 µl. The second PCR reaction mix was added to the 25 µl PCR reaction, and was as follows: 1 µl dNTPs, 2.5 µl 1x PFU buffer, 100 ng of both the forward and reverse primers, 1 µl PFU polymerase enzyme, and the reaction made up to 50 µl. For the truncation PCR, 5 ng DNA was amplified with the components detailed in Table 2.4. All primers were obtained through Life Technologies.

Using the PTC-200 Peltier Thermal Cycler (MJ Research), the PCR conditions typically used and performed were as follows.

Heated lid	-		
Hot start	95°C	5 minutes	
Denaturation	95°C	30 seconds	
Annealing	x°C*	1 minute	x cycles*
Elongation	72°C	3 minutes	
Final Elongation	72°C	10 minutes	
Hold at	4°C		

*The annealing temperature in the truncation PCR was 62°C and 30 cycles used. The PCR to test for the LILRB3 transgene in mouse tail lysate samples used an annealing temperature of 50°C and 28 cycles. To obtain PCR fragments for use in the overlap PCR the typical reaction mix and PCR reaction above was used and the PCR products were gel extracted for use in the overlap PCR. The overlap PCR used 15 cycles for PCR 1 and 20 cycles for PCR 2. The annealing temperature was dependent on the primers used and ranged between 62-64°C.

2.2.3 DNA Sequencing PCR

To determine the DNA sequence of a construct Sanger PCR sequencing was performed.

150-300 ng DNA was added to a sequencing reaction mix containing 2 µl Big Dye Terminator enzyme (AB Sciences), 1x sequencing buffer (AB Sciences), 10 ng sequencing primer (Invitrogen) and the reaction made up to 10 µl with dH_2O. The following sequencing reaction was performed using PTC-200 Peltier Thermal Cycler (MJ Research).

Heated lid			
Denaturation	96°C	10 seconds	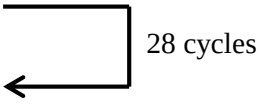
Annealing	50°C	5 seconds	
Elongation	60°C	4minutes	
Hold at	4°C		

28 cycles

The sequencing reaction was then precipitated by adding the 10 µl reaction to 1 µl 3M Sodium Acetate (NaAc) and 25 µl 100% Ethanol (EtOH). The reaction was incubated for 10 minutes on ice, after which time, the reaction was centrifuged at 14,500xg for 30 minutes at 4°C. The supernatant was removed, and the pellet washed in 125 µl 70% EtOH, then centrifuged for 5 minutes at 14,500xg at 4°C. The supernatant was removed and the pellet allowed to air dry for 15 minutes. 10 µl formamide was added to the pellet. Sanger short-chain termination sequencing was then performed in-house using 3130 XI Genetic Analyser (Applied BioSystems). Sequencing reactions were subsequently analysed using SeqMan Pro (DNAStar Lasergene 8).

2.2.4 Agarose gel electrophoresis

Ultra Pure™ Agarose (Life Technologies) was dissolved in 1x Tris Acetic EDTA (TAE) buffer (2 M Tris-base, 0.95 M glacial acetic acid and 50 mM EDTA (pH8) in dH_2O). The w/v was determined by the DNA fragment sizes used. DNA was visualised by adding 1 in 20,000 Gel Red™ (Biotium) to the mixture and allowed to set. 1x Orange DNA loading dye (Thermo Scientific) was then added to the DNA samples, which were then run alongside a DNA marker (O'Gene ruler 100 bp or 1 KB ladder; Thermo Scientific). Electrophoresis was carried out using in a horizontal electrophoresis system, kuroGEL tank (Jencons) containing 1x TAE buffer at 120 volts (V) using either the Power Pac 300 (Bio-Rad) or the PS 500 XT DC Power Supply (Hoefer Scientific). DNA bands were subsequently analysed using the Molecular Imager® Gel Doc™ XR Imaging System (Bio-Rad).

2.2.5 DNA gel extraction and purification

DNA bands were cut from agarose gels and the gel extracted DNA was purified using the QIAex®II gel extraction kit (Qiagen) as per manufacturer's instructions and stored at -20°C.

2.2.6 Restriction digests

Restriction digests were performed to confirm successful transformation and ligation reactions, as well as to cut DNA inserts out of plasmids for the purpose of ligating them into alternative plasmids.

Typical digest reactions consisted of 1 µg DNA plasmid, desired restriction enzyme(s) (Promega/New England BioLabs), 1x buffer corresponding to the enzyme used (Promega/ New England BioLabs), made up to 10 µl (single digest) or 20 µl (double digest) with deionised water (dH_2O). The digests were incubated for either 1 or 2 hours (for a single or double digest, respectively) at 37°C. Digests were subsequently analysed on an agarose gel, ligated into a new vector and transformed (*see 2.2.4, 7-8*).

2.2.7 DNA Ligation

2.2.7.1 Blunt-end ligation

Blunt end ligation was performed using the Zero Blunt® TOPO® PCR cloning kit (Life Technologies). 2 µl gel extracted DNA of interest was added to a reaction mix containing 0.5 µl TOPO vector and 0.5 µl salt solution. The reaction was incubated at room temperature for 30 minutes.

2.2.7.2 Sticky-end ligation

Digested and purified DNA insert and digested DNA vector were incubated together in a 3:1 ratio (insert to vector) along with 1 Unit (U) T4 Ligase enzyme (Promega/Life Technologies) and 1 x T4 ligase buffer (Promega/Life Technologies). The reaction was then incubated at 4°C or 16°C (for scFv antibody genes) overnight.

2.2.8 Heat-shock Transformation

For the majority of transformation reactions performed the chemically competent *Escherichia coli* (*E. coli*) cells used were JM109 cells (Promega). However, for blunt end ligations TOP10 *E. coli* cells (Life Technologies) were used respectively.

Plasmid DNA/ligation reaction mixes were mixed with chemically competent *E. coli* cells in a 1:10 ratio (DNA: cells). All DNA/cell mixtures were subsequently incubated on ice for 30 minutes. The reactions were then heat shocked for 45 seconds at 42°C, then transferred to ice for 2 minutes. 500 µl SOC medium (Life Technologies) was then added to the reaction, and incubated at 37°C for 1 hour shaking at 225 rpm. The DNA/cell mixtures were then plated out on LB/agar plates containing appropriate antibiotic (100 µg/ml ampicillin or 50 µg/ml kanamycin, Sigma).

Finally, plates were incubated overnight at 37°C to allow for bacterial growth. Individually transformed colonies were then hand-picked the following day and bacterial cultures grown for small-scale plasmid purification.

2.2.9 Plasmid Purification

2.2.9.1 Small –scale plasmid Purification

Small-scale plasmid purification was performed using the QIAprep Spin Miniprep Kit (Qiagen) as per manufacturer's instructions. Alkaline lysis was performed on bacteria cultures and then the lysate cleared by centrifugation. The plasmid DNA was then added to a QIA Spin column and the DNA bound, and impurities washed away. The pure DNA sample was subsequently eluted and stored at -20°C. DNA quantification was determined using the Nanodrop® Spectrophotometer ND-100 (LabTech International).

2.2.9.2 Large-scale plasmid purification

Large-scale plasmid purification was performed using the HiSpeed Plasmid Maxi Prep Kit (Qiagen) as per manufacturer's instructions. Alkaline lysis was performed on bacterial cultures. Lysed bacteria were then cleared by filtration. Low salt and pH provided ideal conditions that allowed the plasmid DNA to bind to a HiSpeed tip by anion exchange. Impurities were then washed away and the plasmid DNA was eluted. To concentrate and desalt the eluted DNA precipitation with isopropanol was carried out and the ultra-pure DNA collected using a Qiaprecipitator module provided and stored at -20°C. DNA quantification was determined using the Nanodrop® Spectrophotometer ND-100 (LabTech International).

2.3 Protein expression and analysis

2.3.1 Protein expression

2.3.1.1 Transient transfection of HEK293F cells for secreted proteins

Transient transfection in Human Embryonic Kidney (HEK) 293F cells was carried out to produce fusion protein for antibody generation. HEK293F cells were counted and the cell density determined. For a 500 ml transfection the desired cell density was $500x10^6$ cells. The cells were centrifuged at 400xg for 5 minutes. The supernatant was removed and the cells were resuspended in 25 ml 293F Freestyle media and placed in a 1L flask and incubated at 37°C, shaking at 130 rpm and 8% CO_2. 500 µg DNA was added to 10 ml 150 mM NaCl, and 0.3 mg polyethylenimine (PEI) added to 7.5 ml 150 mM NaCl. The DNA was then added to the PEI. The DNA/PEI mixture was subsequently added to the cells dropwise and incubated for 304 hours at 37°C, shaking at 130 rpm and 8% CO_2. Finally, 475 ml 293F Freestyle Media and 3.75 ml 0.5 M valproic acid were added to the cells and left for 7-10 days incubated at 37°C, shaking at 130 rpm and 8% CO_2.

The cells were subsequently harvested by centrifugation twice at 3000xg for 30 minutes, after which time the supernatant containing the secreted protein was filtered to avoid any contaminants.

2.3.1.2 Transient transfection of HEK293F cells for surface expression

Membrane-bound transfections in HEK293F cells by lipofection were carried out for use in epitope mapping studies. HEK293F cells were counted and their cell density determined. For a 10 ml transfection, 10 µg DNA was added to 330 µl Optimem I media; and 10 µl 293 fectin was added to 330 µl Optimem I media (Life Technologies). Both DNA and 293 fectin mixtures were incubated at room temperature for 5 minutes, then the DNA was added to the 293 fectin and incubated at room temperature for 15 minutes. During this time, for a 10 ml transfection the desired cell density was $10x10^6$ cells. The cells were centrifuged at 400xg for 5 minutes and then resuspended in 10 ml 293F Freestyle media. The DNA/293 fectin mixture was then added to the cells dropwise and incubated for 48 hours at 37°C, shaking at 130 rpm and 8% CO_2.

2.3.1.3 Transient transfection of suspension CHO-S cells for surface expression

Membrane-bound LILRB2, LILRB4, LILRB2 and LILRB3-transfections in Chinese hamster ovary-suspension (CHO-S) cells were carried out for use in phage display cell selections. CHO-S cells were counted and their cell density determined. For a 40 ml transfection, 40 µg DNA or phrGFP-II-I control plasmid was added to 750 µl OptiPro™ SFM media; and 50 µl FreeStyle™ MAX (Life Technologies) was added to 750 µl OptiPro™ SFM media (Life Technologies). The FreeStyle™ MAX mixture was added to the DNA mixture and incubated at room temperature for 20 minutes. The mixture was then added to cells dropwise. Desired expression level was reached after 72 hours post-transfection and the cells were frozen down.

2.3.1.4 Nucleofection of suspension Ramos cells for surface expression

To generate LILRB3 ITIM mutant-expressing cells, nucleofections were performed using the Amaxa® Cell Line Nucleofector® Kit V (Lonza), the Nucleofector® I Device (Lonza) and Amaxa optimised protocols provided by Lonza.

A 12-well plate was prepared by adding 1.5 ml fully supplemented RPMI media to each well used and pre-incubated at 37°C. $2x10^6$ Ramos cells were centrifuged at 90xg for 10 minutes at room temperature. The supernatant was completely removed and then 100 µl cell suspension (provided by the kit) was used to resuspend the cells. 2 µg DNA was added to the cell suspension, which was then transferred into a certified cuvette. The cuvette was inserted into the Nucleofector® Cuvette Holder and the programme 0-06 was selected and applied. The cells were then removed and transferred to the prepared 12-well plate (final volume 1.5 ml). The pmaxGFP® vector (provided in the kit) was used as a positive control at the same amount of DNA and cell density as other nucleofected cells in the same experiment.

To generate stable transfectants 1 mg/ml Geneticin (Life Technologies) was added to the nucleofected Ramos cells 48-hours post-nucleofection and the cells were sub-cloned by limiting dilution. Cells transfected with the positive control pmaxGFP® vector were screened for successful transfection by microscopy using the CKX41 Microscope (Olympus) and images acquired using Cell^B (Olympus). Cells were also screened by flow cytometry using an antibody against the transfected target. Propidium Iodide (PI) (Sigma) was used to screen for live cells (PI negative).

2.3.2 Protein Purification

Secreted protein was purified on a sepharose 4B Protein A column (generated in house). After purification, the protein was concentrated using a centrifugal filter (Millipore) and then sterile filtered and the concentration measured.

2.3.3 Biotinylation of protein

LILRB1-hFc, LULRB2-hFc, and LILRB3-hFc proteins were biotinylated for use in the phage selections. The proteins were initially in a Tris buffer containing 50mM TRIS-HCl (pH 7), 250 mM NaCl, 80 mM Glycine and 1 mM EDTA. However, before biotinylation could be performed, a buffer exchange to PBS was necessary as both Tris and Glycine can interfere with the biotinylation reaction. The buffer exchange was carried out using 150 µg of each protein using the 2 ml Zeba Desalt Spin Columns (Thermo Scientific), as per manufacturer´s instructions.

In a 5x molar excess, ChromaLink Biotin (SoluLink) was added to the protein solution and incubated at room temperature in the dark for 2 hours. To remove any excess biotin the material was buffer exchanged to PBS by centrifugation using a zeba desalt spin column (Thermo Scientific) according to the manufacturer´s instructions and then subsequently sterile filtered before being measured at A280 and A354.

To calculate the resultant ratio of protein to biotin, the following calculation was carried out:

1. Corrected absorbance (Ac): Ac = A280 – (A354 x 0.23)
2. Moles protein: $\left(\frac{(Ac\ /\ protein\ \text{'epsilon'}\ value) x\ (volume\ in\ ml)}{1000}\right)$/protein MW = moles protein
3. Moles biotin present: $(\frac{A354}{29000})$ x $(\frac{volume}{100})$ = moles biotin
4. Biotin/protein molecular substitution ratio (MSR): MSR = $\frac{eq.3}{eq.2}$

Biotinylation of antibodies for immunohistochemistry or immunofluorescence were performed using the Lightening-Link Rapid Biotin Conjugation Kit (Type A) (Innova Biosciences). 200 µg antibody was biotinylated following manufacturer's instructions: LL Rapid Modifier reagent was added to the antibody, which was then used to resuspend lyophilised Lightening Link Rapid mix and left to incubate at room temperature for 15 minutes. Subsequently, Rapid Quencher was added to the antibody and the biotinylated antibody stored at -20°C. Successful biotinylation was confirmed by electrophoresis.

2.3.4 Deglycosylation of protein

PNGase (Sigma, Promega) was made up to a concentration of 500 U/ml in MQ water. Then 0.05 U of PNGase/µg of IgG was added and incubated for ~20 hours at 37°C. Successful deglycosylation was confirmed by dodecyl sulfate polyacrylamide gel electrophoresis (SDS-PAGE), by running 5 µg IgG on a 4-12% Bis-Tris gel alongside wild-type IgG. The deglycosylated IgG should be smaller in size than the wild-type IgG.

2.3.5 Antibody labelling

2.3.5.1 Dialysis of antibodies

Using a 21G needle and 1ml syringe, antibodies were injected into a 0.5ml-3ml sized dialysis cassette. About 3ml of air was removed from the cassette, allowing the antibody solution to cover the entire membrane, increasing the surface area for dialysis. The cassette was then placed in a polystyrene float, and added to a beaker with the buffer the antibody was dialysed into PBS or bicarbonate buffer (see below) for A488 labelling. The beaker was left with a magnetic stirrer at 4°C for 1 hour. The buffer was changed twice at 1 hour intervals and then left in a cold room on a stirrer overnight.

2.3.5.2 APC labelling

Antibodies were labelled with APC using the "Phycolink Activated APC" kit (Europa Bioproducts cat#PZPJ25C) to label 1 mg (at a concentration of 1 mg/ml) of antibody with 1 vial of APC (1.5mg).

Antibodies were reduced with 20 mM DTT, at room temperature for 30 minutes. Buffer exchange was then carried out using a 2 ml Zeba™ desalting spin column (Thermo Scientific). Columns were first equilibrated with exchange buffer (50 mM MES, 2 mM EDTA, pH 6.0) by draining the column by centrifugation and adding 1.5 ml exchange buffer, then centrifuging at 1000xg for 3-4 minutes and the flow-through discarded. This was repeated twice. The reduced antibody was added to the column and centrifugation at 1000xg for 3-4 minutes performed, after which time the antibody was collected. Covalent conjugation was then performed by adding 1.5 mg of SMCC activated APC per mg of antibody, and incubated at room temperature for 1 hour, rotating in the dark. Unreacted free sulfhydryls on the antibody were blocked with the addition of 34 µg of N-ethylmaleimide (NEM) stock solution per mg of antibody, incubated at room temperature for 20 minutes, rotating in the dark. Excess NEM and exchange buffer was then removed, by performing a buffer exchange

to storage buffer (10 mM Tris-HCl, 150 mM NaCl, pH 8.2). A 2 ml Zeba™ desalting spin column (Thermo Scientific) was drained of its liquid by centrifugation at 1000xg for 2 minutes. 1 ml of storage buffer was added to the column and centrifugation was performed at 1000xg for 2 minutes and the flow-through discarded. This was repeated twice to equilibrate the column. The conjugate was centrifuged for ~30 seconds to pellet insoluble conjugate aggregates that may clog the column. The supernatant was removed and the labelled antibody conjugate added to the column and centrifuged at 1000xg for 2 minutes to collect the sample, which was then stored at 4°C in the dark.

2.3.5.3 A488 labelling

Using a 0.5ml-3ml sized dialysis cassette 2 mg/ml antibody was dialysed into bicarbonate buffer (90 mM $NaHCO_3$, 27 mM Na_2CO_3, pH 9.0). The A488 dye was resuspended at 10 mg/ml in DMSO. 200 µg of dye was added per antibody to be labelled, and incubated for 1 hour. Antibodies were then dialysed back into PBS.

The concentration of antibody was calculated by:

$$\frac{[A280 - (A494 \times 0.11)]}{1.45}$$

*Where 1.45 is the extinction coefficient of a human IgG1 antibody, A280 the absorbance of the antibody, A494 the absorbance of the A488 dye and 0.11 is a correction factor to account for absorption of the dye at 280 nm.

2.3.6 Cell staining

2.3.6.1 Direct staining of extracellular surface antigens

For direct staining of extracellular surface antigens, $1x10^6$ cells/tube were stained with conjugated staining antibody for 30 minutes at 4°C or 15 minutes at room temperature. Whole blood, PBMCs and primary patient cells were blocked with 0.2 mg/ml human IgG or with 2% human AB serum (Life Technology) for 10 minutes at 4°C prior to staining. Cells were then washed in FACS wash (PBS, 1% BSA, 10 mM NaN_3) and analysed by flow cytometry. Red Blood Cell (RBC) lysis buffer (AbDSerotec) was added to whole blood, PBMCs and primary patient cells for 10 minutes at room temperature or until clear, and then cells were washed in FACS wash before being analysed by flow cytometry.

2.3.6.2 Indirect staining of extracellular surface antigens

For indirect staining of extracellular surface antigens, $1x10^6$ cells/tube were stained with unconjugated staining antibody for 30 minutes (or 1 hour when staining phages) at 4°C. The cells were then washed twice in FACS wash, and then stained with a secondary conjugated antibody for 20 minutes (or 1 hour when staining phages) at 4°C, before being washed and analysed by flow cytometry. When staining phages, cells were washed and fixed with 4% paraformaldehyde solution (BioInvent, in-house) before being analysed by flow cytometry using the High-throughput Flow Cytometry (HTFC) Screening System (IntelliCyt).

To test if generated anti-LILR clones were binding to the same epitopes as commercial antibodies, cross-blocking assays were performed, whereby, PBMCs with 2% human AB serum (Life Technologies) for 10 minutes at 4°C. PBMCs were then stained with unconjugated anti-LILR clones as described above, followed by a conjugated secondary antibody, without a wash step between the two antibodies.

2.3.7 Flow cytometry

For all flow cytometry analysis the FACS Calibur (BD Bioscience) or the Canto (BD Bioscience) flow cytometers were used and data analysed using FCS Express 3 (De Novo Software) or FlowJo (LLC) for routine cell staining. Alternatively for screening of phages the HTFC Screening System (IntelliCyt) was used as per manufacturer's instructions.

2.3.8 Flourometric Microvolume Assay Technology (FMAT)

Flourometric Microvolume Assay Technology (FMAT) was performed in the primary screening of scFv clones using the BioInvent Robotic System for target-specificity. 4000 thawed suspension CHO cells, transiently transfected with LILRB1, LILRB2 or LILRB3 were added to 384-well plates at 40 µl/well (in cell culture medium). Then 10 µl *E. coli* expression supernatant containing scFv (from the "stock plate") were added, or control scFv-FITC8 (irrelevant scFv directed against a hapten, FITC8), followed by the addition of 0.2 µg/ml mouse-anti-His IgG (R&D Systems) and 0.1 µg/ml APC-conjugated goat-anti-mIgG (Jackson Labs). The plates were incubated for 10 hours at room temperature and then detected by the FMAT screening technology using the 8200 Cellular Detection System (Applied Biosytems).

2.3.9 Protein Electrophoresis (EP)

Electrophoresis was performed using the Serbia Hydrogel Protein (E) IC20 kit. 120 µl deionised water was added to the base of the carrier. A gel (hydragel 7 β1-β2; Sebia) was blotted with filter paper and gently placed at the base of the carrier. 8 µl of sample was then loaded to the applicator, and the sample was allowed to load onto the gel for 5 minutes. The gel was subsequently placed into an electrophoresis tank and electrophoresis performed for 22 minutes at 90V constant. The gel was then placed in a fixative solution for 15 minutes and then dried at ~90°C for 20 minutes (or until completely dry). Finally, the gel was stained with Amido Black dye for 4 minutes, and then destained 3 times for 2 minutes each time. The gel was blotted on blotting paper and dried.

2.3.10 Enzyme-linked immunosorbent assay (ELISA)

The binding target e.g. antibody, LILRB-hFc protein or streptavidin was coated in enzyme-linked immunosorbent assay (ELISA) coating buffer (0.1 M sodium carbonate, pH 9.5, Merck) in a 96 or 384-well plate, overnight at 4°C or at room temperature for 2 hours at 37°C. The following day plates were washed in ELISA wash buffer (PBS + 0.05% Tween20), and blocked in ELISA block buffer (3% BSA in PBS or 0.45% fish gelatine (Sigma) in ELISA wash buffer). Phages were then incubated for 3-4 hours at room temperature, E. coli expression supernatant containing scFv or a primary unconjugated antibody, were incubated for 1 hour at room temperature. Plates were once again washed in ELISA wash buffer and then incubated with a conjugated detection antibody for 1 hour at room temperature. Subsequently, plates were washed and a substrate was added for 10 or 30 minutes at room temperature, sulphuric acid added to stop the reaction, and then the plates were read using the E-max Micro Plate Reader using Soft-max (Molecular device) at both 490 nm and 650 nm in the phage ELISA, or 542 nm by the robotic ELISA system in the primary/secondary screening.

2.3.11 SDS-PAGE

To confirm LILRB1-hFc, LILRB2-hFc and LILRB3-hFc were of high enough quality for use in the selections of phage display, or to confirm anti-LILR antibody deglycosylation, 5 µg of each sample was denatured by incubating the samples at 70°C for 10 minutes with 4x lithium dodecyl sulfate (LDS) NuPAGE sample buffer (Life Technologies) or 95°C for 5 minutes with 4x Laemmli buffer (200 mM Tris Cl, (pH 6.8), 400 mM DTT, 8% SDS, 0.4% bromophenol blue, 40% glycerol) respectively. Samples were then centrifuged for 1 minute at

14,500xg. For LILR-hFc protein, the samples either had 25 mM DTT reducing agent (Life Technologies) added to them (i.e. reduced) or nothing added (non-reduced).

Samples were loaded and ran on a 4-12% Bis-Tris pre-cast gel (Life Technologies) in 3-(N-morpholino)-propanesulfonic acid (MOPS) running buffer (5mM MOPS, 70 mM SDS, 5 mM Tris, 1 mM EDTA) or commercially bought from Life Technologies, for 1 hour at 170 V or 200 V constant. Samples were run alongside the molecular weight marker SeeBlue Plus 2 (Life Technologies) as per manufacturer's instructions.

2.3.12 Size Exclusion Chromatography (SEC)

SEC analysis was carried out using the LC System: Dionex Ultimate 3000. The column Dionex MabPac SEC-1. 5 µm, 300Å. 4 x 300mm (Thermo Scientific) was used. The running buffers used were made up of 5 mM K_2HPO_4 and 0.4 M NaCl (pH 6.5). The flow was 0.3 ml/min and the running time 15 minutes. The molecular weight standards used were as follows: 1 mg/ml of Thyroglobulin (~660 kDa), human IgG1 (~150 kDa) and Ovalbumin (44 kDa), respectively, and 0.8 mg/ml Benzamidine (120 Da). SEC analysis was performed as per manufacturer's instructions.

2.3.13 Immunohistochemistry and immunofluorescence

Human tonsil tissue samples previously frozen in liquid nitrogen were obtained from the Histochemistry Research Unit (HRU), Southampton General Hospital,

2.3.13.1 Embedding human tissue

Embedding of frozen, non-fixed human tissue samples was accomplished using a water-based medium. Pre-frozen tissues were placed into aluminium foil moulds with the liquid embedding matrix OCT (Cell Path, Thermo Scientific), and frozen using isopentane on dry ice to form a hardened block. The tissue was then stored at -20°C for short-term storage.

2.3.13.2 Cutting human tissue sections with a cryostat

Fresh frozen human tonsil tissue was thawed, and tissue sections were cut to 10 µm using the cryostat microm HM 560 (CellPath, Thermo Scientific) set at -20°C. Cut sections were placed on Superfrost Plus, 25 x 75 x 1 mm slides (Thermo Scientific). The slides were left to dry overnight.

2.3.13.3 Immunohistochemistry (IHC)

IHC was performed using the ABC kit (Vector Labs) as per manufacturer's instructions.

Fresh tonsil samples embedded in OCT and cut to 10 μM sections were placed on slides to dry overnight. Tissue sections were fixed in 100% acetone at room temperature for 10 minutes, air dried and then a barrier pen (ImmEdge™ Pen, Vector Labs) was used to mark around the sections. In a "humidity chamber" sections were washed 3x with PBS-T (PBS + 0.05% Tween20). Peroxidase suppressor (Thermo Scientific) was added (15min, room temperature) to remove any endogenous peroxide produced by the tissue. The sections were washed 3x with PBS-T, blocked with 2.5% normal serum (diluted in PBS-T) from the same animal as the host species of 2° Ab used (or standard normal Goat Serum or BSA used if ABC kit used) for 30 min at room temperature. After excess serum was removed, sections were incubated with either a non-biotinylated primary antibody (for 1 hour, room temperature) or a biotinylated primary antibody (for 1.5 hours, room temperature). The sections were then washed 3x in PBS-T. For the non-biotinylated primary antibody a secondary biotinylated antibody was added for 30 minutes, room temperature and then sections washed 3x in PBS-T. A polymer-HRP or ABC-HRP was then added to sections treated with either a non-biotinylated or biotinylated primary antibody, respectively for 30 minutes, room temperature. After washing 3x in PBS-T, the chromogen Vector®NovaRed™ substrate was added to the sections (2-10 minutes, room temperature), and the sections washed once in PBS-T. Sections were counter-stained with haematoxylin for 30 seconds-1min, washed in tap water and then slides dehydrated in alcohol (twice in 90% ethanol, twice in 100% ethanol and then twice in histaclear). Finally sections were mounted in a non-aqueous mountant: Vectormount (Vector Labs). 20 mm x 40 mm coverslips were used and the slides left to dry overnight. The following day the slides were analysed using the CKX41 Microscope (Olympus) and images acquired using Cell^B (Olympus).

2.3.13.4 Immunofluorescence (IF)

IF was performed with biotinylated LILRB3 using the Tyramide Signal Amplification (TSA™) kit. 10 μm human tonsil sections were fixed in 100% acetone (10 minutes, room temperature), air dried, washed 3x in PBS, and incubated with a peroxidase inhibitor, then washed 3x in PBS again. 1% (10 mg/ml) TSA blocking solution (prepared by dissolving BSA in PBS provided in kit) was then added to sections and incubated for 30 minutes. After washing sections 3x in PBS, sections were incubated for 2 hours at room temperature with a 0.5-2 μg/ml biotinylated primary antibody. Sections were then washed 3x in PBS, and

incubated with streptavidin-HRP for 45 minutes at room temperature (HRP conjugate stock reconstituted in 200 µl PBS) and sections washed 3x in PBS. Amplification buffer was prepared by adding 30% hydrogen peroxide (H_2O_2) (component F) to amplification buffer (component E) to make a 0.0015% H_2O_2. Tyramide was prepared by dissolving tyramide (component A) in DMSO. The tyramide amplification solution was prepared by diluting the tyramide 1/100 in the amplification buffer. A488-labelled biotinylated tyramide was diluted 1/100 in tyramide amplification solution and sections stained with tyramide-A488 for 10 minutes at room temperature.

For IF performed with A488-conjugated anti-LILRB3 mAb, 10 µm human tonsil sections were fixed in 100% acetone (as above), blocked with 2.5% normal goat serum for 30 minutes at room temperature. Sections were incubated for 1 hour at room temperature with 2-10 µg/ml unconjugated commercial anti-LILRB3 mAb (R&D systems) or A488-labelled anti-LILRB3 mAb followed by 2 µg/ml rabbit anti-A488 secondary for 45 minutes at room temperature. Sections were washed in PBS and then incubated with 1/1000 either goat anti-mouse-A488 or goat anti-rabbit-A488, respectively.

For both the human tonsil sections stained with biotinylated LILRB3 or anti-LILRB3-A488 mAbs, the sections were washed 3x in PBS and then counterstained with DAPI and washed again 3x. The tissue sections were then mounted using Vectashield "hardset" mounting media (Vector Labs) and 20 mm x 40 mm coverslips added, leaving the slides to dry overnight in the dark. The following day the slides were analysed using the CKX41 Microscope (Olympus) and images acquired using Cell^B (Olympus).

2.3.14 Surface Plasmon Resonance (SPR) Analysis

SPR was performed with the Biacore T100 (GE Healthcare), to test protein to protein interaction as per manufacturer's instructions. LILRB3-hFc recombinant protein (the extracellular LILRB3 domain with a human Fc tag) was used as the ligand and immobilised onto a series S sensor chip (CM5, GE Healthcare) by amine coupling, and binding/immobilisation was tested by activation of the chip surface. Subsequently deactivation of the chip surface or regeneration was tested. Different antibodies or "analytes" were then flowed across the chip and the SPR measured. KD values were calculated from the' Univalent' model of 1:1 binding by Kd [1/s] / Ka [1/Ms], using the Biacore™ T100 Evaluation Software (GE Healthcare). All SPR assays were performed by Ian Mockridge, *University of Southampton*.

2.4 Antibody generation by phage display

Antibodies can be generated by phage display – an *in vitro* system in which antibody fragments are displayed on phages are screened against target proteins in selections or pannings. Phages bound to the target are eluted and unbound phages washed away.

2.4.1 Buffers used in pre-selection and selection

Table 2.5 Buffers used in pre-selection and selection

Reagent/Buffer	Use	Components	Concentration	Company
TPBSB (5%)	Selection blocking buffer	Tween 20	0.05%	Sigma
		Protease- free BSA	5%	Sigma-Aldrich
		Na-azide (NaN_3)	0.02%	BDH Biochemical
		D-PBS	1x	Invitrogen
TPBSB (3%)	Selection blocking buffer	Tween 20	0.05%	Sigma
		Protease- free BSA	3%	Sigma-Aldrich
		Na-azide (NaN_3)	0.02%	BDH Biochemical
		D-PBS	1x	Invitrogen
TPBS	Selection buffer	Tween 20	0.05%	Sigma
		Na-azide (NaN_3)	0.02%	BDH Biochemical
		D-PBS	1x	Invitrogen
PBSB (0.01%)	Used in both elution and amplification titration dilutions	Protease- free BSA	0.01%	Sigma-Aldrich
		D-PBS	1x	Invitrogen
Pre-selection 1 mix	Pre-selection mix for protein in solution	n-CoDeR® scFv	-	BioInvent (made in house)
		Protease- free BSA	20%	Sigma-Aldrich
		Tween 20	0.05%	Sigma
		D-PBS	1x	Invitrogen
Pre-selection 2 or 3 mix	Pre-selection mix for protein in solution	Amplified phages from previous panning	-	BioInvent (made in house)
		Protease- free BSA	3%	Sigma-Aldrich
		Tween 20	0.05%	Sigma
		Na-azide (NaN_3)	0.02%	BDH Biochemical
		D-PBS	1x	Invitrogen
Selection 3 mix	Selection mix for target on cells	Amplified phages from all three tracks of panning 2	-	BioInvent (made in house)
		FCS (heat inactivated)	10%	Invitrogen
		Complete, EDTA-free protease inhibitor cocktail	1x	Roche
		Na-azide (NaN_3)	0.02%	BDH Biochemical
		D-PBS	1x	Invitrogen

2.4.2. Pre-selection

Prior to each selection/panning round, depletion or pre-selection was performed, whereby the antibody library was incubated with a non-target. Pre-selection was performed in the same protein format as the selection (e.g., both in solution or both coated on plastic). No pre-selection was performed for cell selections.

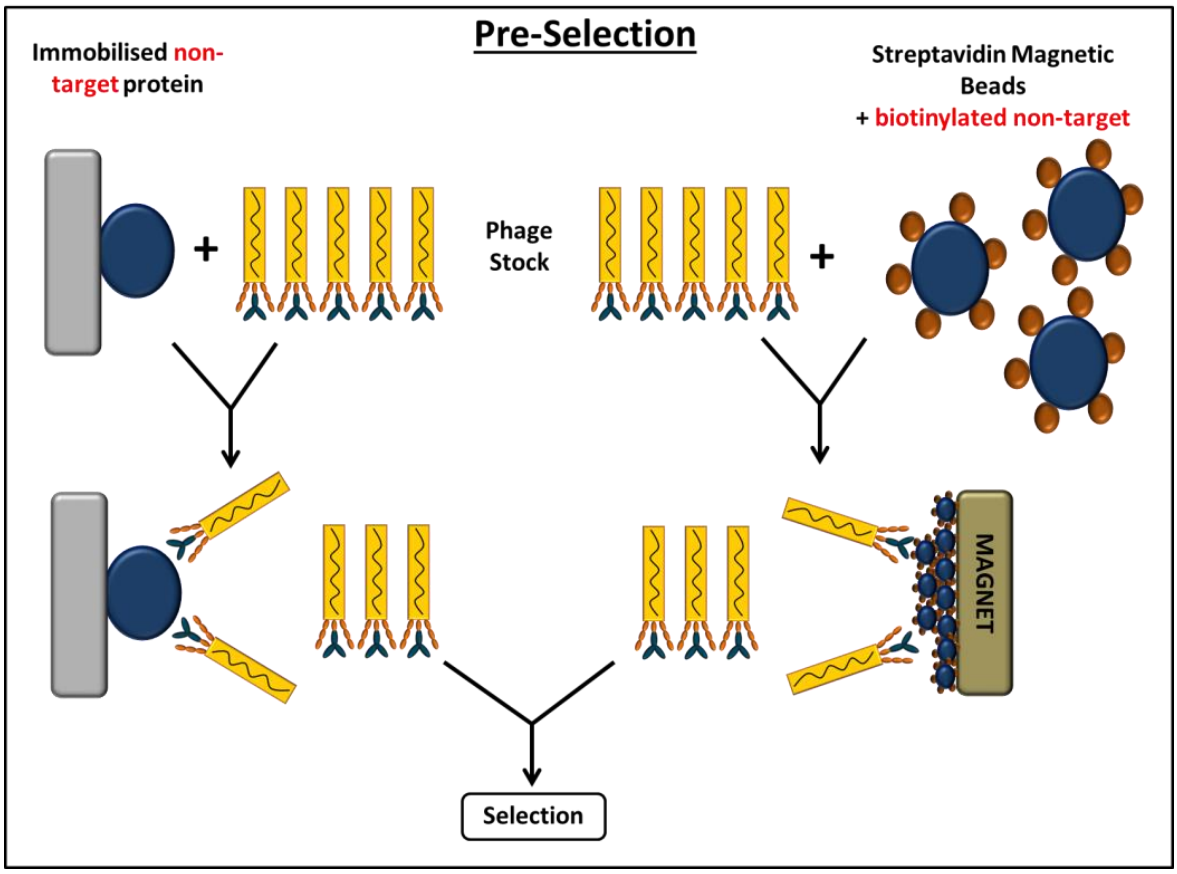

Figure 2.1 Pre-selection with non-target coated on plastic or biotinylated non-target pre-loaded onto magnetic beads. During the selections phage stocks were incubated with target antigen in a process referred to as positive panning. Before this, however, phage stocks were incubated with a non-target in a process known as negative panning to ensure target-specific antibody clones were not cross-reactive to other non-targets. When non-target antigen was coated on plastic Immunotubes and incubated with phage stocks, non-target binding phages bound to the non-target on plastic. The remaining unbound phages were taken into the selections or positive panning. Biotinylated non-target antigen, pre-loaded onto streptavidin magnetic beads were also incubated with phages. Non-target specific phages that bound to these beads, whilst unbound phages were taken into the subsequent positive panning round.

2.4.2.1 Pre-selection with non-target biotinylated in solution

For biotinylated protein selections, streptavidin magnetic Dynabeads® (Invitrogen) were washed in PBS prior to use to remove preservatives and then blocked in 3% TPBSB (see *Table 2.6*) before being resuspended in PBS. The biotinylated protein target was then added to

the beads for 1 hour with rotation at room temperature, after which time beads were washed twice in TPBSB (3%) to remove any unbound non-target antigen.

The pre-selection mix contained: either the n-CoDeR scFv library, amplified phages from selection 1 or amplified phages from selection 2 in the selection rounds 1, 2 and 3 respectively; 3% protease-free BSA; 0.05% Tween 20 (Sigma); 0.02% Na-azide and 1 x PBS). 10µg/ml additional streptavidin was also included in the pre-selection mix in selection 3, as a non-target, and incubated with the biotinylated non-target loaded on the magnetic beads. The pre-selection mix was added to the beads containing the biotinylated non-target and incubated at room temperature for 4 hours with rotation. After incubation, samples were centrifuged for 5 minutes at maximum speed and the supernatant was removed and transferred to a new Eppendorf tube, which was placed in a magnetic particle concentrator (MPC), before being transferred again to a new Eppendorf tube to rid all traces of the magnetic beads. The non-target specific phages would have bound to the beads, whilst those phages that did not recognise the non-target remained in the supernatant (referred to as the 'selection mix') and therefore were the phages of interest and taken through to the positive panning round (demonstrated through *Figure 2.1*).

2.4.2.2 Pre-selection with a non-target coated on plastic

For selections that included protein coated on plastic, "Immunotubes" (Nunc) were coated at room temperature for 1 hour and then at 4°C overnight with 10 µg/ml of the non-target protein diluted in ELISA coating buffer. The Immunotubes were then washed twice with 3 ml TPBS and blocked for 1 hour rotating at room temperature with TPBSB (5%). The blocked Immunotubes were then washed once with TPBSB (3%) and the pre-selection mix (as above) was added to the tubes and incubated for 4 hours rotating at room temperature. The pre-selection mix was then transferred to new Eppendorf tubes as non-target binding phages would have bound to the coated non-target in the Immunotube, leaving unbound and target-specific phages in the supernatant (*Figure 2.1*). This supernatant (containing unbound phages) was referred to as the 'selection mix' and was taken into the positive panning/selection stages.

2.4.2.3 Pre-selection with target expressed on cells

No pre-selection was carried out for the cell selections as they would only be in contact with protein and therefore it was unlikely that non-specific cell-binding phages were still in the phage pools eluted from the previous two rounds of panning.

2.4.3. Selection

After pre-selection, unbound phages were then incubated with the target protein. The protein target was either biotinylated in solution, coated on plastic or expressed on cells. A non-biotinylated non-target competitor was also used when the protein was biotinylated in solution.

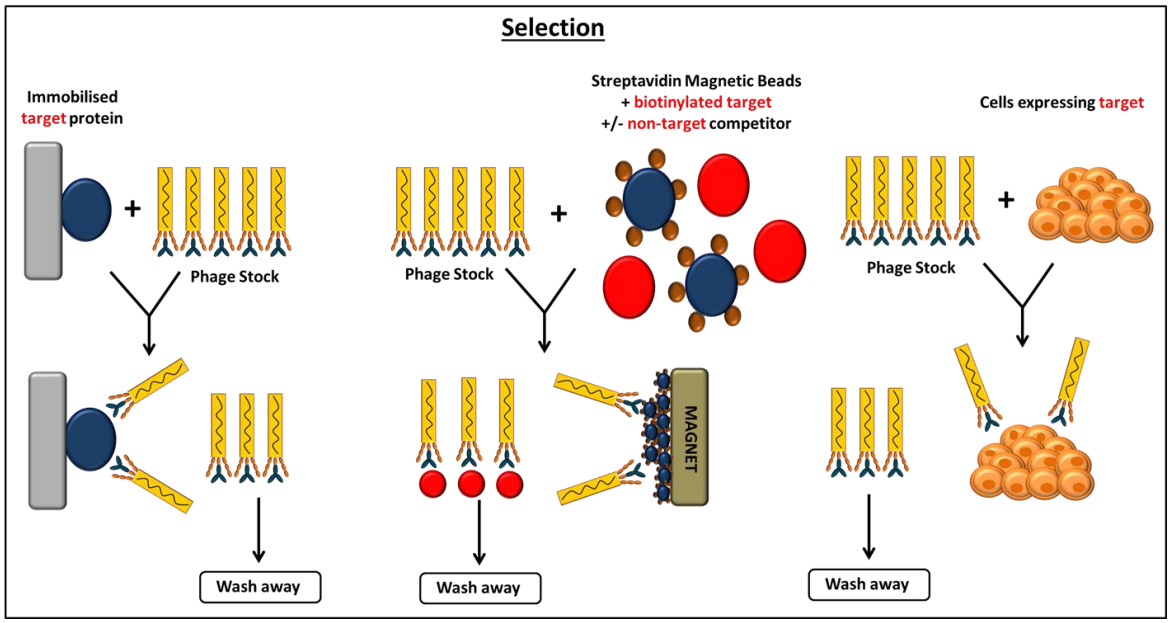

Figure 2.2 Selection with target coated on plastic, biotinylated target pre-loaded onto magnetic beads (with/without competition), or target expressed on cells. During the selections phage stocks taken from the pre-selection or previous selections were incubated with target antigen in a process referred to as positive panning. The target antigen was coated on plastic Immunotubes, biotinylated in solution (with or without a non-biotinylated, non-target competitor) or the target was expressed on cells. The target protein was incubated with phages from the pre-selection or from the previous selection round. Target-specific phages bound to the target (on plastic, on beads by introducing a magnet or on cells depending on the presentation of the target protein); and were taken through to the next selection round or screened after the final selection was completed. Unbound phages were washed away.

2.4.3.1 Selection with target biotinylated in solution (with or without competition)

The biotinylated target antigen (50 nM in selection 1; 20 nM in selection 2; and 5 nM in selection 3) was added to the "selection mix". When competition was included 500 nM in selection 1; 400 nM in selection 2; and 250 nM in selection 3 of a non-biotinylated competitor (10x surplus of the biotinylated target in selection 1, 20x surplus in selection 2 and 50x surplus in selection 3) was added to the selection mix. BSA in the buffer also served as a competitor. The samples were incubated at 4°C with rotation overnight.

After incubation with the biotinylated target antigen (and non-biotinylated non-target competitive antigen if competition was used) TPBSB blocked and washed Dynabeads®

(Invitrogen) were concentrated on an MPC and then re-suspended in the selection mixes and incubated at room temperature for 30 minutes; then additionally for an hour (in panning 1) or 30 minutes (in panning 2 and 3) at room temperature with rotation and placed on an MPC. The supernatant was then transferred to new Eppendorf tubes and stored at 4°C (for eventual use in the titrations). The Dynabeads® were subsequently washed by re-suspending them in 1 ml TPBSB (3%) rotating for 5 minutes at room temperature, then concentrating them again, discarding the supernatant and repeating the wash step twice. After being transferred to a new Eppendorf the beads were then washed three times in 1 ml TPBS and then three times in 1 ml PBS.

The phages were subsequently eluted with 0.5 mg/ml trypsin (Sigma) diluted in PBS. The beads were concentrated on an MPC and 400 µl trypsin was added to the beads and left to incubate for 30 minutes rotating at room temperature. The beads were concentrated and the eluted phages transferred to a new Eppendorf tube containing 40 µl Aprotinin (2 mg/ml) (Roche) to stop cleavage. The beads were washed in 200 µl PBS, which was thus pooled with the elution to ensure all traces of eluted phages were added and the elution was then stored at 4°C.

2.4.3.2 Selection with target protein coated on plastic

For selections where the target was coated on plastic, no competitor was used. Four etched polystyrene balls (diameter 1/8"; Polysciences) were placed in a 2 ml Eppendorf tube. 1 ml of the non-biotinylated protein target (diluted in coating buffer to 100 nM in both panning 1 and 2) was added to polystyrene balls and left to incubate for 1 hour at room temperature rotating; after which time they were stored at 4°C overnight.

The following day the polystyrene balls were washed twice with 1 ml TPBS and blocked in 1 ml TPBSB (5%) for 1 hour rotating at room temperature. The polystyrene balls were then washed once in 1 ml TPBSB (3%) and stored at 4°C until ready to use in the panning. The selection mix was then added to the washed and blocked polystyrene balls and the samples were incubated at 4°C with rotation overnight. The polystyrene balls were washed three times in 1 ml TPBSB (3%) rotating for 5 minutes at room temperature then discarding the supernatant. The polystyrene balls were then transferred to a 50 ml falcon tubes and washed three times in 10 ml PBS + 0.05% Tween20 and then three times in 10 ml PBS.

To elute the phages from the polystyrene balls, 0.5 mg/ml trypsin (Sigma) diluted in PBS was used. The balls were added to Eppendorf tubes containing 400 µl trypsin and left to incubate

for 30 minutes rotating at room temperature. The supernatant (eluted phages) was transferred to a new Eppendorf tube with 40 µl Aprotinin (2 mg/ml) to stop cleavage. The beads were washed in 200 µl PBS, which was thus pooled with the elution to ensure all traces of eluted phages were added. Finally, the elution was stored at 4°C.

2.4.3.3 Selection with target expressed on cells

For selections where the target were expressed on cells, LILRB1-, LILRB2 and LILRB3-transfected CHO-S cells were freeze-thawed and re-suspended in 15 ml D-PBS with 10% heat inactivated FCS (Invitrogen) + 0.02% NaN_3 (BDH Biochemical) in a 50 ml falcon tube. The samples were centrifuged for 10 minutes at 300xg and 4°C. After removing the supernatant, the cells were blocked in 10 ml PBS + 10% heat inactivated FCS and incubated on ice for 1 hour. After incubation the cells were counted.

Target LILR-transfected CHO-S cells (~$15x10^6$ cells/ml for each selection) were then centrifuged again at 300xg for 10 minutes at 4°C. After removing the supernatant the cells were resuspended in the selection mix and incubated at 4°C for 4 hours with slow agitation. The cells were then centrifuged at 300xg, for 8 minutes at 4°C and the supernatant containing the non-bound phages was removed.

To wash the cells and ensure all non-bound phages were discarded, 10 ml PBS with 10% FCS was added to the cells and centrifuged at 300xg for 8 minutes at 4°C. The supernatant was carefully aspirated and the target cells were resuspended in 10 ml PBS with 10% FCS and incubated on ice for 10 minutes. Once again the cells were centrifuged at 300xg for 8 minutes at 4°C and the supernatant carefully aspirated. Then cells were resuspended again, this time in 50 ml PBS with 10% FCS and centrifuged at 300xg for 8 minutes at 4°C. This was repeated twice. Finally, the cells were resuspended in 1 ml PBS (without FCS) and transferred to a new tube; the previous tube was washed with another 1 ml PBS and pooled with the cells. 8 ml PBS was added to the cells and mixed carefully, but thoroughly. The cells were then counted and centrifuged once more at 300xg, for 8 minutes at 4°C and the supernatant removed.

To elute phages from the cells, 400 µl of 1 mg/ml trypsin (Sigma) was added to the cells and incubated for 30 minutes at room temperature with slow agitation. To stop cleavage, 80 µl of 2 mg/ml Aprotinin was added and the mixture, transferred to an Eppendorf tube, and centrifuged at maximum speed for 10 minutes. The supernatant containing the eluted phages were transferred a new Eppendorf tube. The cell debris was washed once with 200 µl PBS

and centrifuged for 10 minutes at high speed before pooling the washings with the eluted phages. The elution was then stored at 4°C until further use.

2.4.4 Amplification of phages

HB101F' bacterial glycerol stock was used to inoculate and clean streak an agar plate containing 15 µg/ml tetracycline and 1% glucose. The plate was then incubated at 37°C overnight and then stored at 4°C until use in further inoculations.

10 ml LB containing 15 µg/ml tetracycline was inoculated with 100 µl of an overnight culture of HB101F' and incubated at 37°C, shaking at 200 rpm for 2.5-3 hours. Four cultures (panning 1) or two cultures (panning 2 and 3) per selection were inoculated and grown at 37°C and 200 rpm until the culture reached saturation. The E. coli culture was incubated for 10 minutes at 37°C, static, to allow for extension of the F-pili, and then the E. coli was infected with 4x 80 µl or 2x 160 µl eluted phage from panning 1 or panning 2/3 respectively, and incubated at 37°C and 50 rpm for 30 minutes. The tubes from the same selection were pooled, and centrifuged for 10 minutes at 2100xg at room temperature. The pellet was re-suspended in 1 ml of the supernatant (the rest was discarded) and spread on a large Q-tray (500 cm^2) LB Broth with agar (LA) plate containing 100 µg/ml ampicillin, 15 µg/ml tetracycline and 1% glucose. The plates were then left to incubate overnight at 30°C (or 37°C if the incubation was initiated later in the day).

The following day the bacteria were collected from the Q-tray plates by adding 10 ml LB with 100 µg/ml ampicillin and 15 µg/ml tetracycline per plate, then the bacteria scraped. Using a stripette, the bacterial suspension was collected into a clean falcon tube and the process repeated once again with another 10 ml fresh medium. The collected bacteria were then centrifuged at 2100xg for 10 minutes at room temperature.

To produce new phage stocks for the next round of panning, a calculated volume of 2-20 µl (calculated after an initial OD measurement of a 1000x times diluted sample) of the glycerol stock was added to 10 ml LB containing 100 µg/ml ampicillin and 15 µg/ml tetracycline (OD approx. 0.1). Two cultures per glycerol stock were grown at 37°C and 200 rpm until an OD600 = 0.5. Then $6x10^9$ pfu of R408 helper phage (Stratagen) per ml culture was added to the scFv-phage-elution inoculated cultures and incubated at 37°C, shaking at 50 rpm for 30 minutes. Isopropyl β-D-1-thiogalactopyranoside (IPTG) (ICN) – used to trigger scFv-PIII transcription through the lac promoter – was added at a concentration of 100 µM per 10 ml culture and the cultures were incubated at 25°C and 200 rpm overnight. The next day the

cultures were centrifuged for 10 minutes at 2100xg and room temperature, then the supernatant from the same selections were pooled and sterile filtered through a 0.2 µm filter. The phages were precipitated by adding ¼ volume of phage precipitation buffer containing 20 % polyethylene glycol (PEG6000) (BDH Biochemical) and 2.5 M NaCl (Merck), then centrifuged for 30 minutes at 4°C and 5000xg. The supernatant was discarded then the phage pellet resuspended in 1 ml D-PBS and left overnight at 4°C or with slow shaking at 37°C for 1 hour. The phage stock was then transferred to an Eppendorf tube and stored at 4°C.

2.2.5 Titration of phages

Amplified phage stocks were diluted in PBSB (PBS containing 0.01% BSA) in 10-fold dilutions. 100 µl of an overnight culture of HB101F' was inoculated into 10 ml LB with 15 µg/ml tetracycline, then left to grow at 37°C, 200rpm until the culture reached saturation. After which time the E. coli culture was incubated for 10 minutes at 37°C, static, to allow for extension of the F-pili. The culture (100 µl) was then added to a 96-well U-bottom plate, and 10 µl diluted phage stock added to it, then incubated at 37°C for 30 minutes. After incubation, the dilutions were plated (spread using glass beads) onto LB agar plates containing 100 µg/ml ampicillin, 15 µg/ml tetracycline and 1% glucose and incubated at 37°C overnight.

Dilutions performed to titrate eluted phages were 10^1, 10^2, 10^3, 10^4, 10^5 (depending on which panning the elution was taken from). For titrations of the amplified phage stocks, the dilutions used included 10^7, 10^8, 10^9. The concentration of phages was determined by calculating the number of ampicillin-resistant colony forming units (CFU) per ml, allowing for the volume added and the dilution factor used.

2.4.6 Conversion of phage-bound scFv to soluble scFv

2.4.6.1 Bacterial culture

The phage-bound antibody format is not compatible with the BioInvent screening system. Therefore, the phage clones were converted to a soluble antibody format. Glycerol stocks of *E. coli*, infected with the eluted phage pools from the final panning round, were inoculated into 10 ml LB with 100 µg/ml ampicillin, 15 µg/ml tetracycline and 0.1% glucose. The inoculated culture was then grown overnight at 37°C.

2.4.6.2 Phagemid purification

Phagemid DNA was isolated from overnight cultures using the QIAquick Miniprep kit (Qiagen) as per manufacturer's instructions.

2.4.6.3 Restriction digests

The scFv-encoding antibody genes were cut out from a pMIL phagemid vector using the restriction enzymes AvrII and SfiI and then ligated into a new vector, pKscFv-3xFH vector, cut with the same restriction enzymes. This new pKscFv-3xFH vector (made in house) expressed the soluble scFv gene with two C-terminus tags 3xFLAG and 6xHis in frame.

Phagemid plasmid DNA or pKscFv-3xFH vector (2 µg), 4 U AvrII (New England Biolabs), 1x NEB buffer2 (New England Biolabs) and Milli-Q (MQ) water made up to a total volume of 20 µl were incubated for 2 hours at 37°C. Then 1x NEB buffer 2 (New England Biolabs), 1x BSA (New England Biolabs), 20 U SfiI (New England Biolabs) and MQ water added to make a total volume of 30 µl was added. The digest was then incubated at 50°C for 2 hours.

2.4.6.4 Digested scFv plasmid purification

ScFv-encoding antibody genes were purified after being digested from their vectors using the QIAquick PCR purification Kit (Qiagen) as per manufacturer's instructions, and eluted in 50 µl MiliQ (MQ) water and stored at -20°C.

2.4.6.5 scFv DNA Ligation

To ligate the purified scFv-encoding antibody gene into the pKscFv.3xFH vector (made in house) 60 ng of the AvrII/SfiI digested pKscFv.3xFH vector, 240 ng AvrII/SfiI digested and purified DNA, 1x ligase buffer (Invitrogen), 1 U T4 DNA Ligase (Invitrogen) and MQ water to make the total volume up to 25 µl was incubated over night at 16°C.

2.4.6.6 Heat-shock Transformation

The ligation mix was then transformed into chemically competent TOP10 *E. coli* cells as described in *2.2.7* and grown on large Q-tray plates containing 20 µg/ml Kanamycin and 1% glucose overnight at 37°C. Each bacterial colony represented a single unique clone.

2.2.7 Colony picking

After eluted phages were converted to soluble scFv and transformed into TOP10 *E. coli* cells and grown on Q-tray plates, each colony formed on these Q-tray plates represents one scFv-clone cloned into the pKscFv.3xFH vector. These colonies were individually picked using the BioInvent robotic system (Genetics Q Bot). Once picked, these colonies were transferred to a 384-well "master plate" containing 60µl LB + 20 µg/ml kanamycin + 1% Glucose. The plate was then incubated overnight at 37°C.

2.2.8 Expression of purified scFv antibodies into E. coli

E. coli was induced to express soluble scFv molecules by the addition of IPTG. The scFv molecules that were produced, were secreted into the bacterial supernatant. The robotic system (CRS Expression System) was used to transfer 5 µl or 10 µl from the "master plate" to a new 384-well or 96-well "stock plate" containing 50 µl LB or 100 µl LB, with 20 µg/ml kanamycin, left shaking at 600 rpm or 130 rpm for 3.5 hours at 37°C in the primary and secondary screening of scFv antibodies, respectively. To induce scFv expression 12.5 µl of 2.5 mM IPTG was then added and the plate further incubated at 37°C for 10 hours for use in FMAT or ELISA (see *2.3.8* and *2.3.10*).

2.4.9 Sequencing of scFv

In a 96-well plate containing agar with Kanamycin and glucose (provided by GATC, Biotech), 5 µl of each scFv clone was inoculated. Clones were then sent for Sanger short-chain termination sequencing externally to GATC, Biotech. Analysis of the sequencing data to identify unique scFv antibody clones was carried out using the programme "Sequencing Net" (BioInvent). Using Microsoft Excel, each sequence was sorted firstly by its "status": failed sequencing data was "rejected" whilst good sequencing data was "accepted". Sequences were then sorted by identical sequences in their CDRs in the following order: CDRH3 (CDR heavy chain 3), CDRL3 (CDR light chain 3), CDRH2, CDRL2, CDRH1 and finally CDRL1. Sequences that were identical in all their CDRs were grouped together. Sequences were given an ID number (the same ID number was allocated to identical sequences). The number of different ID numbers indicated the number of identified unique clones.

All sequencing data is propriety, and as such was not included in the results of this thesis.

2.4.10 scFv antibody screening data analysis, "Cherry Picking" and "HIT Picking"

The computer programme "Spotfire" was used to analyse the data from the ELISA and FMAT primary and secondary screening. This programme presents data points two-dimensionally, allowing target-specific clones to be identified from those specific to, or cross-reactive with a non-target antigen. Spotfire identifies "active" clones that fulfil a specified criterion. The criteria in this case was to identify clones that were target-specific without being cross-reactive to non-targets, whilst also being greatly above the threshold of the FITC8 control used. Clones that fit this criteria were regarded as "active". Initially, cell-binding only

clones were chosen from the FMAT data, then using the ELISA data, cell-binders that were also found to bind to protein were chosen.

A list of active clones to be picked was then generated and compiled into an Excel spread sheet. This list was used to manually "cherry-pick" the desired clones from the 384-well "Master Plate" and transfer these "active" clones to a 96-well "Master Active" cultivation plate (containing 150 µl of LB media, 20 µg/ml Kanamycin and 1% glucose) and grown at 37°C overnight and shaking at 130 rpm.

Sequencing data received performed by GATC, Biotech, and analysed using "Sequencing Net" (BioInvent) was then imported into the "Spotfire" programme and used to confirm similar binding properties of identical clones (i.e. clones given the same sequence ID). Only one representative clone was kept, whilst the others were disregarded (the clone with the highest binding specificity to the target was preferentially chosen). The unique clones selected were referred to as "hits" and a "hit list" of clones to be picked was subsequently generated. This list was used to cherry pick the "hit" clones from 96-well Master Active plates and transfer these clones to a 96-well Master Hit Cultivation plate (containing 100 µl LB, 20 µg/ml kanamycin and 1% glucose) and grown at 37°C overnight and 130 rpm.

2.4.11 scFv glycerol stocks

To make glycerol stocks of scFv 10 ml bacterial cultures were centrifuged at 3000xg for 10 minutes. The bacterial pellet was resuspended in 1 ml LB with appropriate antibiotic and added to a cryovial containing 50-70% glycerol and stored at -20°C or -80°C for amplified phages.

To generate glycerol stocks of the unique antibody clones generated by phage display, 60 µl of each clone was added to a 96-well plate (Greiner) containing 30 µl 50% glycerol. The plates were stored at -80°C.

2.4.12 Conversion of scFv to IgG1

The scFv clone VH and VL domains were both amplified by PCR using primers designed to supply suitable enzyme restriction sites and complementary sequences. The amplified VH and VL fragments were then joined by overlap extension PCR, resulting in the two fragments in opposing directions and flanked by restriction enzyme sites compatible with the expression vector. The PCR-products from all the unique clones to be converted to IgG were then pooled together, purified and digested with restriction enzymes, before being inserted into an

expression vector containing the constant regions of both the heavy and light chains. To allow expression of both the VH and VL genes, the expression vector was digested with restriction enzymes and promoters and signal peptides were inserted between both the genes and transformed in to chemically competent *E. coli* TOP10 cells.

Finally, to retrieve each individual unique clone, DNA sequencing was performed with each individual transformant. Clones with vector constructs containing the expected VH and VL genes were mini prepped (small scale-DNA purification – *see 2.2.9*) and then transfected into HEK293-EBNA cells for protein expression.

2.5 Functional Assays

2.5.4 Macrophage phagocytosis

Human MDMs generated as described in *2.1.3*, were first harvested by incubating the cells in cold PBS for 15 minutes and adherent cells scraped. Cells were then centrifuged at 300xg for 5 minutes and resuspended in full-serum media at a desired concentration. The cells were then plated out into a 96-well flat-bottom plate at $1x10^5$ cells/well. To study the effect of anti-LILR antibodies on macrophage phagocytosis, MDMs were then treated with 10 µg/ml anti-LILR antibodies for 2 hours, then cells washed in media. Cultured Raji B cells or CLL cells were used as target cells, labelled with 5µM 5(6)-Carboxyfluorescein N-hydroxysuccinimidyl ester (CFSE) (Sigma) and opsonised with Rituximab (an anti-CD20 mAb) for 25 minutes at 4°C (opsonisation with Herceptin, an isotype control and non-opsonised MDMs were included as negative controls). MDMs and target cells were co-cultured for 1 hour at 37°C (in a 1:1 ratio of MDMs to Raji cells or 1:5 ratio with CLL cells). MDMs were then stained with 10 µg/ml CD16-APC (Biolegend) for 15 minutes at room temperature in the dark. Cells were washed, harvested and then analysed by flow cytometry.

To study if the LILRB3 antibody interferes with human macrophage FcγRs, 10 µg/ml protein G (Sigma) was incubated in a 96-well flat bottom plate (Corning) the night before the assay. MDMs were then harvested and plated with the protein-G coated plate, subsequently treated with anti-LILRB3 (R&D systems) and the assay performed as above. Alternatively, PNGase-treated (Promega) deglycosylated anti-LILRB1, -LILRB2 or -LILRB3 antibodies were used to treat macrophages.

To study the long-term effect of anti-LILRB3 treatment on human phagocytosis, MDMs were treated with anti-LILRB3 (R&D systems) 7 days prior to the assay. 1 µM R848 (a TLR7/8 agonist) was also added to stimulate macrophages the night before the assay was conducted.

2.5.6 T cell Proliferation

For DC-T cell co-culture assays, DCs were generated over 7 days as described in *2.1.3*. Two days prior to co-culture, either frozen autologous or allogeneic PBMCs were labelled with 2uM CFSE (Sigma), for 10 min at room temperature, quenched with FCS, and cultured at high density ($1x10^7$ cells/ml in 24-well plates) for ~48 hours. 24 hours before co-culture, DCs were treated with 10ug/ml anti-LILRB3 clone 222821 (R&D systems) or a relevant isotype control, 1ng/ml LPS, and 1µg/ml tetanus antigen (Sigma). Subsequently, T cells were isolated from high density cultured PBMCs, by negative selection with the EasySep™ Human T Cell Isolation Kit (StemCell Technologies). $1x10^4$ cells/well Tetanus and antibody-treated DCs were harvested and co-cultured with $1x10^5$ cells/well isolated T cells for 7-11 days.

For T cell proliferation assays where proliferation was antibody-driven, PBMCs were isolated as described previously (see *2.1.2*). 1-2 x 10^7 PBMCs were labelled with CSFE, and labelled with 2 µM CSFE at room temperature for 10 minutes. To quench the reaction, FCS was added for ~1 min then washed in PBS by centrifugation at 400xg twice. Cells were subsequently resuspended in serum-free CTL-Test™ media (Immunospot) and plated at $1x10^5$ cells/well in a 96-well round-bottom plate (Corning). Cells were then stimulated with 0.02 µg sub-optimal OKT3 (ATCC) – an anti-CD3 mAb and 5 µg/ml anti-CD28 (Biolegend) and 10 µg/ml anti-LILR antibodies. Plates were then incubated at 37°C for 4 days.

Finally in both assays, cells were stained with 5µg/ml anti-CD8-APC (Biolegend, clone SK1), harvested and CSFE dilution was measured by flow cytometry.

2.5.7 Receptor modulation

Receptor internalisation was measured using both indirectly-labelled antibodies and directly-labelled antibodies.

For indirectly-labelled antibodies, 1 $x10^6$ PBMCs were plated and monocytes allowed to adhere with 1% human AB serum (Sigma). Cells were incubated with 10 µg/ml wild type or deglycosylated anti-LILR antibodies or relevant isotype controls at 37°C for different time points. The cells were subsequently harvested on ice, washed and stained with an anti-human-PE secondary (Jackson Labs) for 25 minutes, 4°C. Cells were washed and then analysed by flow cytometry.

For directly-labelled antibodies, A488-quenching assays were performed on human monocytes, primary CLL cells, and LILRB3-FL (wild-type) or tLILRB3 (truncated no ITIMs)

transfected-Ramos cells. Monocytes were isolated using the pan-monocytes isolation kit (Miltenyi). Cells were plated at 1 x10^6 cells/well in either fully-supplemented RPMI media (10% FCS, 100 U/ml Penicillin-streptomycin, 2 mM Glutamine and 1 mM pyruvate), or fully-supplemented media with the addition of 15 mM azide (NaN_3) and 50 mM 2-Deoxy-D-glucose ($C_6H_{12}O_5$). Then 5 µg/ml A488-labelled anti-LILR antibodies or relevant isotype controls were incubated with the cells at 37°C for different time points. Cells were then harvested on ice into two separate FACS tubes (one for unquenched and one for quenched samples), washed and 25 µg/ml anti-A488 secondary added to the quenched samples for 25 minutes at 4°C. Cells were then washed and analysed by flow cytometry. Surface accessible antibody (%) was calculated as = [Unquenched (minus isotype) – Quenched (minus isotype)] /Unquenched (minus isotype).

2.5.8 Receptor trafficking

To measure cell trafficking, MDMs were grown on Poly-L-Lysine (PLL) (Sigma) coated 13 mm coverslips (VWR) at 37°C overnight. LILRB3 antibody clones A13 and A28 or the commercial anti-LILRB3 antibody were incubated with cells at various time points, alongside either 25 µg/ml transferrin (15 minutes, 37°C) or 60 nM lysosomal tracker (1 hour, 37°C). Cells were then fixed in 4% paraformaldehyde (PFA), washed in PBS and mounted in non-hardset mountant with DAPI (Vectashield). Images were collected with a Leica SP5 CLSM Confocal Microscope using a 100x (NA1.4) Plan-Apochromatic objective and pinhole of 1 Airy disc (LAS-AF software, Version2, Leica). Images were then processed in Photoshop. Co-localisation was assessed in ImageJ.

2.6 In vivo experiments

2.6.1 Animal husbandry

All animals were bred and maintained in an approved facility, and all experiments performed were in accordance with the UK Home Office guidelines as states in the Animal (Scientific Procedures) Act 1986, under the personal licence 30/2964. All procedures used were mild in severity.

SCID and NOD SCID mice were purchased from Charles River and subsequently bred in house. Human FcγRIIB Tg x mouse FcγRIIB -/- (hFcγRIIB Tg) and mouse FcγRIIB -/- (mFcγRIIB -/-) mice were as described previously[52].

2.6.1 CLL Xenografts

CLL cells were established in either NOD SCID or human FcγRIIB Tg NOD SCID mice by injecting fresh CLL patient blood samples into the mice by intravenous injection (i.v.) as described by Roghanian *et al*[52]. Fresh blood samples from high counter CLL patients were kindly provided by Dr Francesco Forconi, Southampton General Hospital. The samples were first verified by the Tissue Bank, Southampton General Hospital for confirmation of patient consent for use in animal studies. Once confirmation was given the samples were processed as with healthy human blood samples (*see 2.1.2*). Mice were irradiated with 1 Gy, 2-5 hours prior to CLL cell injection. CLL patient PBMCs were reconstituted at $5x10^8$ cells/ml in autologous serum, then $1x10^8$ cells (in a 200 µl volume) were injected intravenously into the tail of each mouse. Mice were then treated with 50 or 100 µg anti-LILR mAb on day 3 and 6 (after splenic engraftment). Mice were terminated on day 9, and blood, bone marrow, spleen and liver harvested from each mouse, after which their cells were analysed by flow cytometry.

2.6.2 Ramos *in vivo* experiments

Wild-type LILRB3 or truncated (no ITIMs) LILRB3$^+$ transfected Ramos cells were injected into either SCID, mouse FcγRIIB knockout (KO) NOD SCID or human FcγRIIB Tg NOD SCID mice to establish tumour engraftment. Cells were injected intravenously (i.v.) or intraperitoneally (i.p.) into the tail at $1x10^6$ cells in 200 µl volume of sterile PBS. Mice were either left untreated to assess survival and growth dynamics of the cells, or the mice were treated 7 days post-injection of cells with 100 µg anti-LILRB3 or Rituximab, and in some cases given a second 100 µg dose 14 days post-injection of cells. Once mice began to display terminal symptoms, they were culled and survival measured as days survived. For some mice, blood samples and/or tumour samples (post-mortem) were taken and assessed by flow cytometry for presence of Ramos cells and LILRB3$^+$ transfected protein cell surface expression.

3 GENERATION OF ANTIBODIES DIRECTED TO LILRB1, LILRB2 AND LILRB3

3.1 Introduction

The LILR family are a group of immune regulatory receptors expressed on myeloid cells. The inhibitory LILR receptors in particular, are interesting, due to their ability to regulate immune responses and their implications in different health and disease pathways[66]. LILRB1 and LILRB2 have been widely studied, and hold potential therapeutic value as targets in immunotherapy. However, LILRB3, although less studied, could also be therapeutic. Unlike, LILRB1 and LILRB2, the crystal structure of LILRB3 is unknown, and although there is some evidence that LILRB3 binds to bacteria, ANGPTLs or a ligand found on necrotic glandular epithelial cells, further validation is needed[102, 107, 108]. LILRB3 expression is restricted to myeloid cells, unlike LILRB1, which has been reported to be expressed on lymphocytes also. This restricted expression potentially makes LILRB3 an attractive therapeutic target.

Agonistic antibodies against LILRB3 would stimulate the LILRB3 receptor; initiating inhibitory signalling pathways through its ITIM domains. Therefore, therapeutic anti-LILRB3 antibodies that are agonistic could be useful in treating autoimmune diseases, where the immune system is overactive, and inhibition of signalling is required. Alternatively antagonistic antibodies against LILRB3 could block receptor signalling. This could be useful for treating cancer, where immune responses are important in driving inflammatory responses that help to fight cancerous cells. Typically tumour cells suppress immune responses, therefore preventing inhibitory signals from LILRB3 may lead to cancer immunity. Alternatively, direct targeting antibodies against LILRB3-expressing malignant cells could be used to deplete the cells.

Therefore, developing anti-LILRB3 agonistic/antagonistic antibodies, or direct targeting antibodies could have a great therapeutic advantage. Current the majority of commercially available LILRB3 antibodies are cross-reactive with other LILR receptors, or they fail to recognise all LILRB3 variants (personal communication with Dr Des Jones, *University of Cambridge*). LILRB3 is highly polymorphic, possibly due to selective pressure, with at least 13 different variants reported, it is possible that current commercial antibodies against the receptor do not recognise all LILRB3 alleles found in the general population[77]. Generating antibodies that display either agonistic or antagonistic properties as well as antibodies that are

specific, will help elucidate the expression and function of the LILRB3 receptor, as well as provide new antibody-based therapeutics.

Thus the aim of this project was to generate antagonistic and/or agonistic antibodies against the LILRB3 receptor, which could have therapeutic efficacy in the treatment of cancer and/or autoimmune diseases respectively. By furthering our understanding of homologous receptors LILRB1 and LILRB2, which have already been characterised, this will further aid in deducing the function of LILRB3. This chapter focuses on the antibody generation against these receptors.

3.2 Results

3.2.1 Generation of reagents for antibody production

After unsuccessful attempts to generate LILRB3 antibodies by hybridoma technology both internally (University of Southampton) and commercially (Abmart, China) (data not shown), we sought to develop antibodies by phage display technology, in collaboration with BioInvent International AB (Sweden). It was decided to generate anti-LILRB1 and -LILRB2 antibodies also, to characterise the inhibitory receptor family, given what is already known about these two receptors. An overview of the antibody generation process is displayed below (*Figure 3.1*).

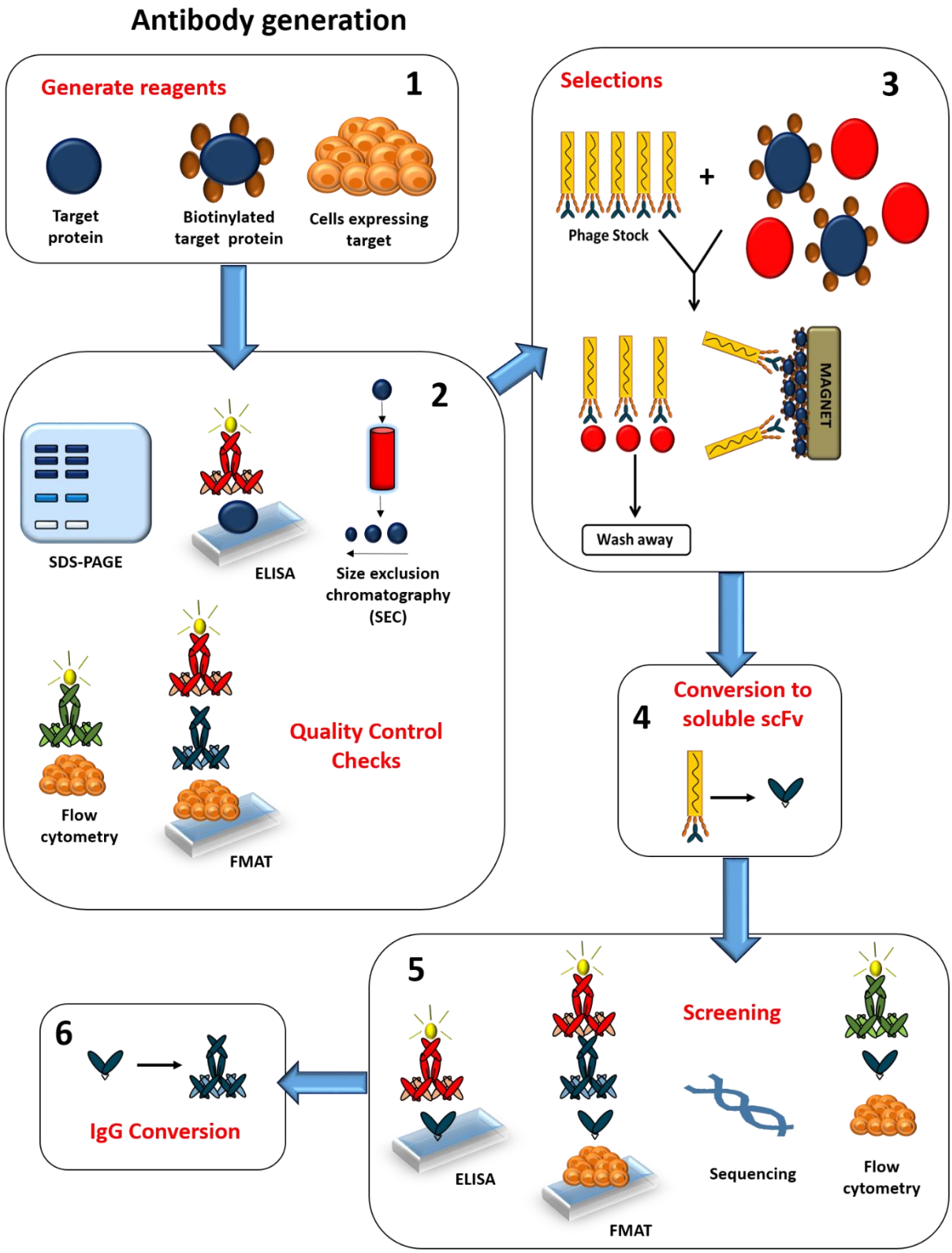

Figure 3.1 Schematic of antibody generation. Reagents were first generated (1) and tested for their compatibility to the phage display technology (2). Selections against generated target proteins were then carried out using a scFv library (3). After conversion of selected target-specific scFv to a soluble format (4), scFvs were screened (5) and target-specific scFv converted to IgGs (6).

3.2.1.1 Target protein generation

To generate antibodies against the inhibitory receptors, phage display technology was utilised. Phage display allows fully-human antibodies to be generated, ideal for potential therapeutics, eliminating cross-reactivity and unwanted immune responses. Phage display allows many different ways to display the target protein, and therefore a range of different strategies were chosen to guarantee successful target-specific antibodies were generated.

The first step was to generate the target proteins for use in phage display selections. Soluble proteins and protein expressed on cells were generated.

LILRB1-hFc, LILRB2-hFc, and LILRB3-hFc DNA constructs (in a SigPlg vector) consisted of the extracellular domain of each target antigen tagged with a human Fc. To generate target protein for both the selection and screening, the fusion protein DNA constructs were transfected into suspension HEK 293F cells, and cultured over 10 days. The supernatant containing the secreted protein was then filtered to remove any contaminants and purified using a Protein-A column. After purification the proteins were also biotinylated for use in the selections. The full length/wild-type (WT) LILRB1, LILRB2 and LILRB3 DNA constructs (in the vector pHR-SIN) were used in transient transfections of suspension CHO (CHO-S) cells for use in both the selections and screening, as CHO-S cells are more compatible with the selection process in comparison to HEK cells. LILRB4-FL in a p3xFlag CMV9 vector (Sigma) was also provided by Dr Des Jones and used to produce cells expressing the target for use in the secondary screening. Transfected cells were analysed after 72 hours for LILR expression by flow cytometry analysis using commercial antibodies specific to each LILR target. The transfected cells were then frozen down and thawed when needed in either the selection or screening. All these reagents were then tested for their quality and compatibility to the selection and screening methods used, through various different techniques. All DNA constructs were produced and provided by Dr Des Jones, *University of Cambridge*.

3.2.1.2 Target protein analysis by SDS-PAGE

Protein samples were run on an SDS-PAGE gel (*Figure 3.2*) to confirm the expected molecular weight of the target proteins, their quality and structure (i.e. if the proteins are in a monomeric or dimeric form) and degradation of the proteins. The quality of the protein used in the selections will affect the quality of the antibodies generated, as misfolded or degraded proteins may prevent isolation of the most relevant antibodies. LILRB1, LILRB2 and

LILRB3 proteins were run under non-reducing or reducing conditions respectively, in that order (lanes 1-6). Representative figures of two gels is displayed below.

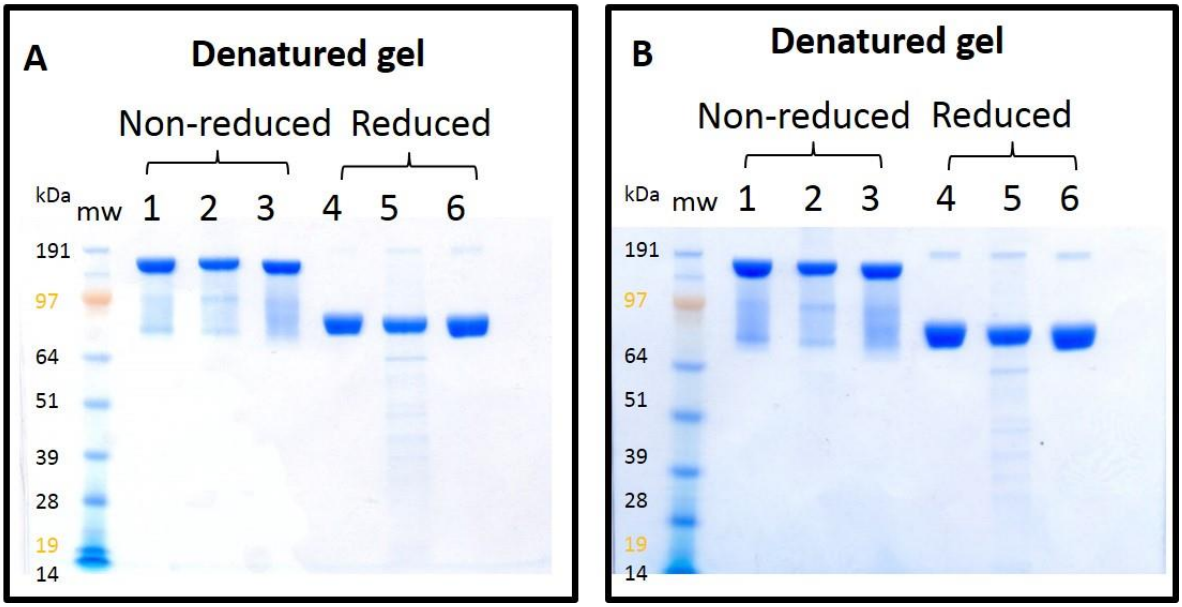

Figure 3.2 SDS-PAGE gel analysis to test quality of protein targets for selection and screening. All samples, both reduced (with 25mM DTT reducing agent; Invitrogen) and non-reduced, were denatured at 70°C for 10 minutes, run using MOPS running buffer (Invitrogen) on a NuPAGE 4-12% Bis-Tris gel (Invitrogen) for 1 hour at 170V constant, then stained with Simply Blue Safe Stain (Invitrogen). The first lane of each gel shows the molecular weight (mw) marker: SeeBlue Plus 2 (Invitrogen); followed by LILRB1-hFc (1), LILRB2-hFc (2) and LILRB3-hFc (3) in the next three lanes without the addition of a reducing agent, and then with 25mM DTT in the next three lanes (4-6 respectively). Gel A was ran first, and gel B ran the next day to confirm the results found in the first gel (n=2).

All three LILRB Fc-tagged proteins had an expected monomeric molecular weight of ~75 kDa. Samples without a reducing agent (LILRB1-3 in lanes 1-3, respectively), showed a band under the 190 kDa marker (~150 kDa), whilst the reduced samples (LILRB1-3 in lanes 4-6, respectively) showed the proteins below the 97 kDa marker (~75 kDa). These results were expected and indicate that in lanes 4-6 the proteins are in their monomeric form, as the LILRBs have a predicted extracellular molecular weight of ~50 kDa, whilst the human Fc tag is predicted at ~25 kDa. Therefore, lanes 1-3, where no reducing agent was added, are likely to represent their dimeric forms. Therefore the bands observed in both gel A and the repeat gel B coincide with the expected molecular weights of the LILRB proteins. Besides small amounts of additional bands the samples appeared to be 'clean', and therefore relatively pure protein samples. However, LILRB2-hFc and LILRB3-hFc (lanes 2 and 3) showed what appeared to be precipitation in their wells (data not shown). When repeated the next day after being frozen and thawed once, the results were the same (gel B – lanes 2 and 3). Precipitation could be seen predominately for non-reduced LILRB2-hFc. However, this did not heavily

effect the purity of the protein, and therefore did not make the protein insufficient for use in the selections and screening.

3.2.1.3 Size exclusion chromatography (SEC) analysis to test protein aggregation

To further confirm the purity of the protein samples, SEC was performed. This allowed for verification that all the proteins samples (LILRB1, LILRB2 and LILRB3) were not aggregated, as aggregation can affect protein confirmation and result in potential binding sites being hidden, thus affecting the selection process.

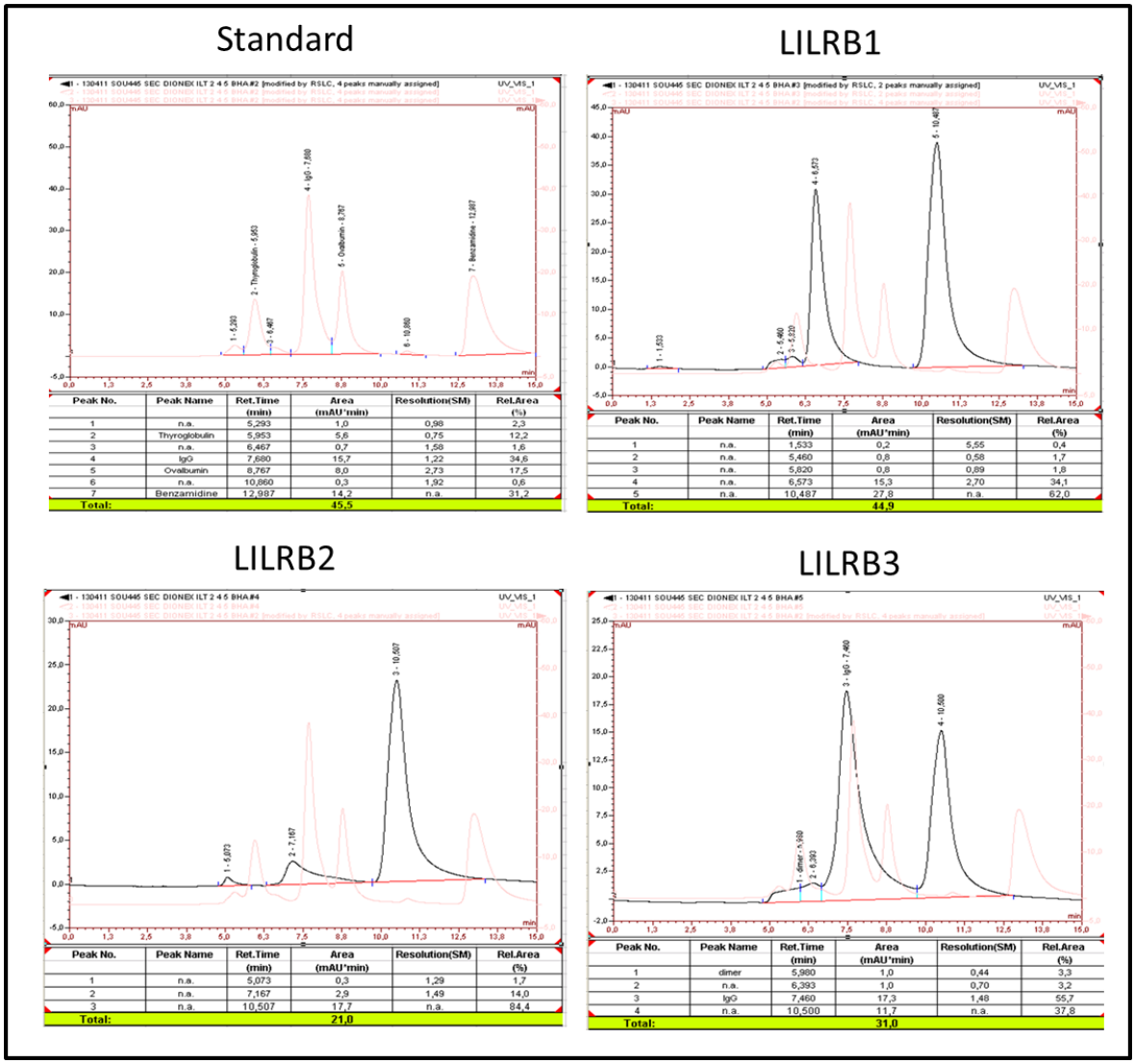

Peak No.	Peak Name	Ret.Time (min)	Area (mAU*min)	Resolution(SM)	Rel.Area (%)
1	n.a.	5,293	1,0	0,98	2,3
2	Thyroglobulin	5,953	5,6	0,75	12,2
3	n.a.	6,467	0,7	1,58	1,6
4	IgG	7,680	15,7	1,22	34,6
5	Ovalbumin	8,767	8,0	2,73	17,5
6	n.a.	10,860	0,3	1,92	0,6
7	Benzamidine	12,987	14,2	n.a.	31,2
Total:			45,5		

Peak No.	Peak Name	Ret.Time (min)	Area (mAU*min)	Resolution(SM)	Rel.Area (%)
1	n.a.	1,533	0,2	5,55	0,4
2	n.a.	5,460	0,8	0,58	1,7
3	n.a.	5,820	0,8	0,89	1,8
4	n.a.	6,573	15,3	2,70	34,1
5	n.a.	10,487	27,8	n.a.	62,0
Total:			44,9		

Peak No.	Peak Name	Ret.Time (min)	Area (mAU*min)	Resolution(SM)	Rel.Area (%)
1	n.a.	5,073	0,3	1,29	1,7
2	n.a.	7,167	2,9	1,49	14,0
3	n.a.	10,507	17,7	n.a.	84,4
Total:			21,0		

Peak No.	Peak Name	Ret.Time (min)	Area (mAU*min)	Resolution(SM)	Rel.Area (%)
1	dimer	5,980	1,0	0,44	3,3
2	n.a.	6,393	1,0	0,70	3,2
3	IgG	7,460	17,3	1,48	55,7
4	n.a.	10,500	11,7	n.a.	37,8
Total:			31,0		

Figure 3.3 SEC Analysis of LILRB1-hFc, LILRB2-hFc and LILRB3-hFc to test for protein aggregation. 20 µl LILRB1, LILRB2 and LILRB3-hFc protein (~1-2 mg/ml) was injected into an LC column, along with 10 µl molecular weight standards. The molecular weight standards used included: 1mg/ml of Thyroglobulin (~660 kDa), human IgG1 (~150 kDa) and Ovalbumin (44 kDa), respectively, and 0.8mg/ml Benzamidine (120 Da). The LC System: Dionex Ultimate 3000 (MC-39) with SN 1273 Dionex MabPac SEC-1.5 µM, 300Å, 4x 300mm column (Thermo Scientific) was used.

Figure 3.3 shows that three major peaks were identified: the first peak occurred ~5 minutes after sample injection, the second ~6.5-7.5 minutes; and a third ~10.5 minutes. The first peak likely represented tetramers or possibly small amounts of larger aggregates. Observing aggregation was consistent with the results seen in the SDS-PAGE analysis (*Figure 3.2*), where some of the material had a large molecular weight (precipitated material) and was unable to leave the wells and enter into the gel. The second peak is likely to be the LILR-hFc protein, as this correlated with the elution of the IgG standard (eluted at ~7.5 minutes). Therefore, the third peak eluted ~10.5 minutes may have been an artefact (a salt peak resulting from the sample formulation buffer: 50 mM TRIS-HCl pH 7, 250 mM NaCl, 80 mM Glycine and 1 mM EDTA). To determine if this was the case, the SEC analysis was repeated (*data not shown*). 20 µl sample, this time undiluted, was injected through the column. The data showed a relative decrease seen in the peak ~10.5 minutes, when undiluted in the second SEC analysis, suggesting it was indeed an artefact caused by the formation buffer.

Therefore, the peak at ~6.5-7.5 minutes corresponded to the protein fraction. Taking into account the SDS-PAGE data (*see Figure 3.2*) this peak most likely represented the LILRB-hFc proteins in their dimeric form (~150 kDa), as this peak corresponded to the IgG standard peak. The smaller peaks that were eluted earlier where also more pronounced with the undiluted samples and thus likely represented tetramers or possibly larger aggregates. Although some aggregation was observed, the SEC analysis clearly showed that the protein was present and of an expected size. Taken together both the SDS-PAGE and SEC data supported that the LILR-hFc proteins were of acceptable purity and quality for use in phage display selections.

3.2.1.4 ELISA analysis to test the compatibility of the protein targets with the selection/screening methods

After confirming the size and purity of the target proteins, an ELISA was carried out on the LILR proteins before the selection and screening to confirm firstly, that proteins effectively coated to a plastic surface, secondly that the human Fc tag was exposed and therefore able to be detected by an anti-Fc antibody, thirdly that the biotinylated proteins were able to bind to streptavidin (as this was necessary in the selections), and finally (and most importantly) that the LILR proteins were still exposing functional epitopes after biotinylation or coating to a plastic surface, and therefore still recognised by their specific LILR antibodies.

This was carried out by detection of the different LILR antigens (either biotinylated or non-biotinylated) with their specific LILR antibodies or an anti-hFc antibody to detect their Fc tag. The schematic below shows the different ELISA approaches carried out *(Figure 3.4*).

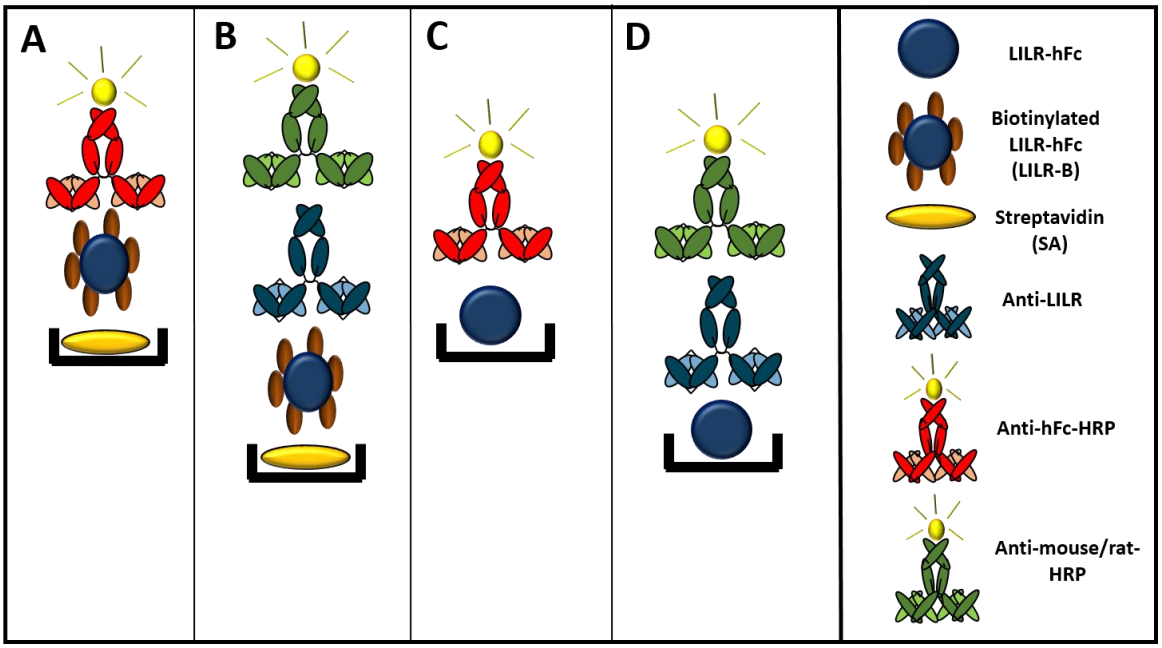

3.4 Schematic of ELISA to test protein compatibility with selection and screening methods. Four different ELISAs were performed: Biotinylated LILR-hFc (LILR-B) protein binding to coated streptavidin, and being detected either by a HRP-conjugated anti-hFc, or by a specific LILR antibody, followed by HRP-conjugated secondary. Alternatively, non-biotinylated target LILRs were detected in the same way.

The respective graphs illustrating the results for each approach are shown in *Figure 3.5* below.

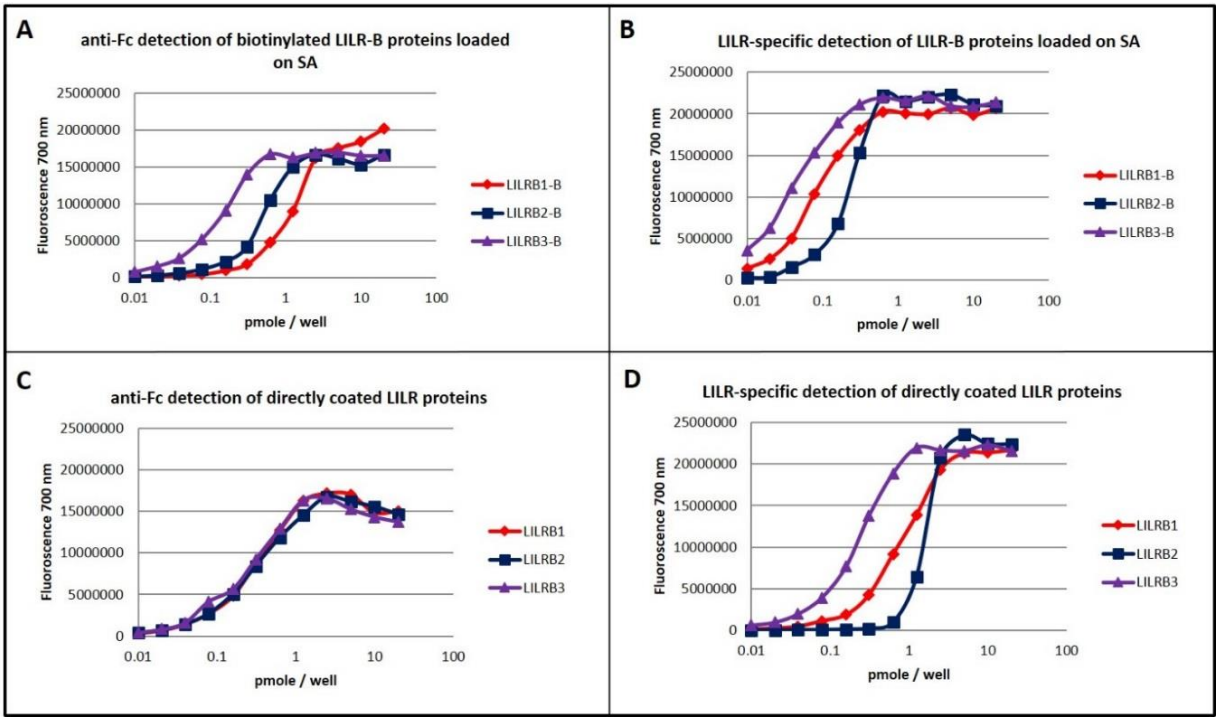

Figure 3.5 ELISA pre-test to confirm compatibility of protein targets for selections and screening. LILRB1, LILRB2 and LILRB3 were diluted two-fold in coating buffer and coated to a 96-well ELISA plate at 4°C overnight. For the biotinylated protein samples, streptavidin (SA) was coated overnight and a two-fold dilution of the target antigens incubated with streptavidin the following day. The plate was then blocked in PBS 0.45% fish-gelatine (Sigma) and then either 1 µg/ml of their specific LILR antibodies mouse-anti human LILRB1 (BioLegend) rat anti- human LILRB2 (BioLegend) mouse anti-hLILRB3 (R&D Systems), or donkey Fab'2 hFc-HRP (Jackson Laboratories) (diluted 1 in 10,000) was used for detection, at room temperature for 1 hour. Plates were then washed, and donkey-anti-mouse-HRP for LILRB1 and LILRB3 or donkey-anti-rat-HRP for LILRB2 (diluted 1 in 5,000) secondary antibodies added where LILR-specific antibodies were used, for 1 hour at room temperature. The plates were washed and SuperSignal ELISA Pico Maximum Sensitivity Substrate (Pierce) was added and left for 10 minutes at room temperature before the plate was read at 700 nm using Victor2V, Wallac (Perkin Elmer).

All the biotinylated proteins could successfully be detected by both their human Fc tag and by their respective specific LILR antibodies in a dose-dependent manner (*Figure 3.5 A and B*). This indicated that the biotinylated proteins were able to bind to streptavidin and that antibody epitope binding sites were still exposed after biotinylation, as was their Fc-tag. The non-biotinylated targets coated to a plate (*Figure 3.5 C and D*) were also detected by both an anti-hFc antibody and by their specific LILR antibodies, suggesting that the LILR proteins coated well to a plastic surface and their antibody binding sites were available for detection. This suggested that it was likely that the antigens could also be coated on plastic polystyrene beads during the selections. It also demonstrated that both the proteins and their hFc-tags were functionally folded and well exposed.

In summary, the ELISA showed the LILR proteins were able to coat plastic surfaces and that biotinylation, or coating the target proteins to a plastic surface, did not interfere with the

overall protein structure or binding sites. Therefore, these proteins were compatible with the selection and screening strategies.

3.2.1.5 Identifying the compatibility of biotinylation of target proteins for selection/screening methods by the "Pull Down" experiment

Although, the ELISA confirmed that the biotinylated target proteins were able to bind to streptavidin that had been coated on a plastic surface, the next step was to identify if the same proteins could bind to streptavidin-coated beads. The "pull-down" method was used to verify this.

Ratios of biotin to protein were as follows for each protein target: LILRB1 2.8, LILRB2 3.1 and LILRB3 3.1. During the selections, biotinylated target antigens would be captured by magnetic streptavidin beads. The aim of the "Pull down" experiment was to test if biotinylated target antigens could successfully and efficiently bind to these beads. Biotinylated protein samples were run on an SDS-PAGE gel (reference sample), then the proteins were captured by streptavidin beads, and the remaining supernatant also run on a gel (to test if any protein did not bind to the beads). Finally, the beads were boiled to remove the biotinylated proteins, and samples were also run on a gel (as by boiling, and removing proteins from the beads demonstrated that the biotinylated proteins must have been attached on the beads in the first place). The three different samples for LILRB1 were run in lanes 1-3, LILRB2 in lanes 4-6 and LILRB3 lanes 7-9, see *Figure 3.6*. Lane 10 was a control sample (boiled beads that did not come into contact with biotinylated protein).

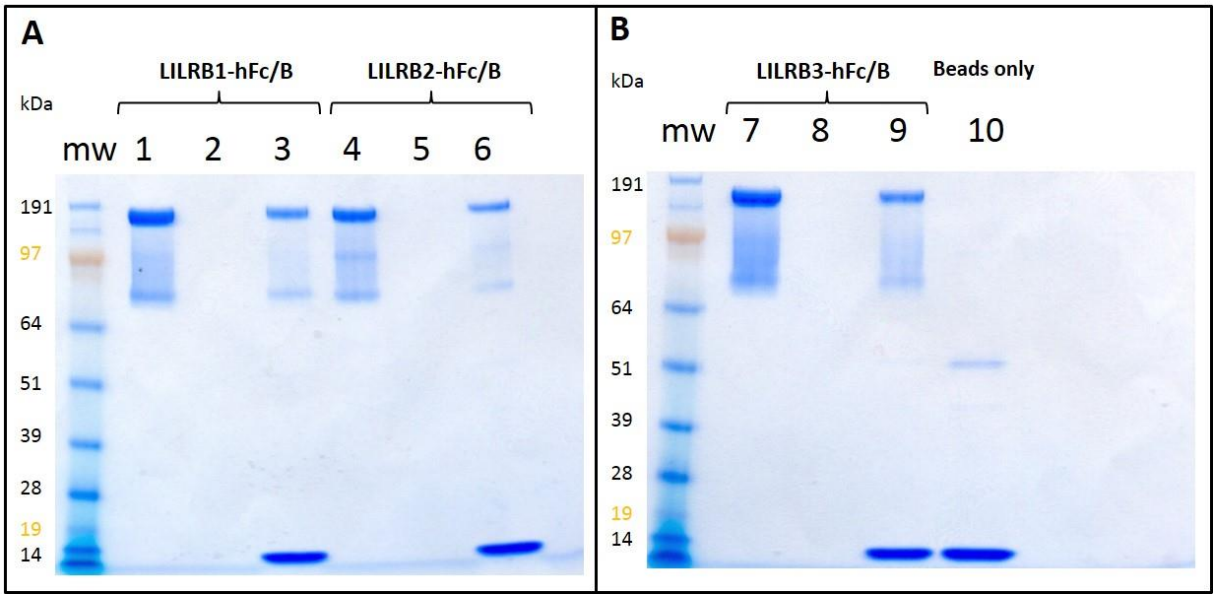

Figure 3.6 Testing the efficiency of biotinylated proteins binding to magnetic streptavidin beads. In Gel A, biotinylated LILRB1 (samples 1-3) and biotinylated LILRB2 (samples 4-6) are represented; and in Gel B biotinylated LILRB3 (samples 7-9). 5µg LILRB1-, LILRB2- and LILRB3-hFc biotinylated proteins were run on a gel (samples 1, 4 and 7 respectively) as a reference sample. Then proteins were captured by magnetic streptavidin beads and the supernatant that remained after drawing the beads to a magnet, were also run on the gel (samples, 2, 5 and 8 respectively). The beads were then boiled at 70°C for 10 minutes, to remove the protein, which was subsequently run on the gel (samples 3, 6 and 9 respectively). Boiled beads not incubated with any biotinylated protein sample were also run as a control (sample 10). A molecular weight (mw) marker: SeeBlue Plus 2 (Invitrogen) was included in both gels and all samples were run under non-reducing conditions, on a NuPAGE 4-12% Bis-Tris gel (Invitrogen) for 1 hour at 170V constant, then stained with Simply Blue Safe Stain (Invitrogen).

All three biotinylated targets, LILRB1 (samples 1-3), LILRB2 (samples 4-6) and LILRB3 (samples 7-9), displayed similar results (*Figure 3.6*). Three different samples for each target were run on an SDS-PAGE gel under non-reducing conditions. The first sample for each target (samples 1, 4 and 7 representing LILRB1, LILRB2 and LILRB3, respectively) is a reference sample and corresponds to the biotinylated protein before being added to the Streptavidin beads. The band observed seemed to show little or no difference in appearance and size (~150 kDa) to that observed for the non-biotinylated proteins seen previously by SDS-PAGE (*Figure 3.2*). This indicates that biotinylation of the proteins did not affect the overall size and structure. Then the biotinylated protein was added to the magnetic streptavidin beads, and a magnet used to collect the sample. The remaining supernatant was run on the gel (samples 2, 5 and 8). No bands were observed for these samples, suggesting that the majority, if not all, of the biotinylated protein successfully bound to the beads. The beads were then boiled to remove the biotinylated protein and the samples run on the gel (samples 3, 6 and 9). A band could be seen in all of these samples, suggesting that after denaturation, the biotinylated proteins were successfully recovered from the streptavidin beads. However, it was observed that the bands seen in these samples were fainter when

compared to that seen in the reference samples for each target. This suggests that although most of the protein was removed, some protein remained on the beads. This is most likely due to the strong covalent bonds between streptavidin and biotin. Boiled beads (not incubated with any biotinylated protein) were also ran on their own as a control (sample 10) and a very faint band (~51 kDa) could be seen (not found in other samples). This band likely represent streptavidin protein, which is ~52 kDa. A smaller, but sharper band was also seen (~14 kDa), and also appeared in the samples for all targets that represented the protein that had been removed from the beads (samples 3, 6 and 9). This suggests that this band represents something found on the beads themselves.

In conclusion, this experiment demonstrates that the biotinylated LILRB1, LILRB2 and LILRB3 proteins can successfully bind well to streptavidin beads and therefore are compatible with the methods used in the selections.

3.2.1.6 Flow cytometry and FMAT analysis shows successful transient transfection of LILRs on CHO-S cells

After confirming that the target proteins were compatible with the selection and screening methods used, next the target-transfected cells were assessed. During the selections, the use of cells that expose the target proteins in their natural environment is ideal, to ensure antibodies produced can bind to cells. Therefore, LILR-expressing CHO-S cells were generated through a 72-hour transient transfection of LILRB1, LILRB2, LILRB3 and LILRB4 in CHO-S cells. These cells were chosen based on their compatibility with the selection process, and the transfections were analysed by both FMAT and flow cytometry.

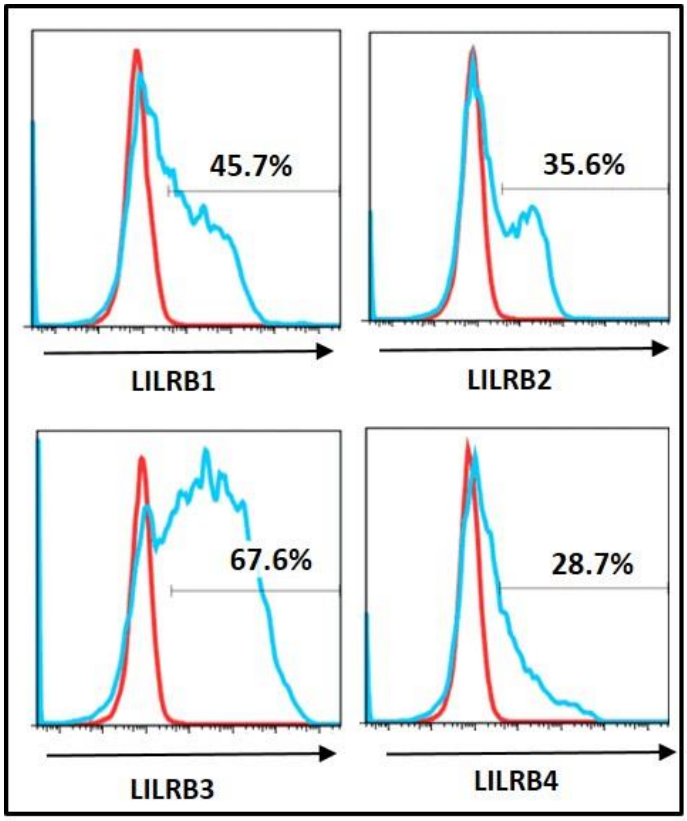

Figure 3.7 Expression of LILRB1, LILRB2, LILRB3 and LILRB4 protein transiently transfected into suspension CHO cells. Commercial anti-LILRB1 (clone GHI/75, Biolegend), LILRB2 (clone 42D1, Biolegend), LILRB3 (clone 222821, R&D systems) and LILRB4 (clone ZM4.1, Biolegend) antibodies (all in blue) or respective isotype controls (red) were incubated at 10 µg/ml with $1x10^5$ cells at room temperature for 1 hour. Expression of LILR-transfected cells was tested by flow cytometry analysis using the HTFC Screening System (IntelliCyt). %LILR-positive gated cells are displayed on histograms and represented by marker. The y-axis represents cell count and the x-axis mean fluorescence intensity (MFI).

Flow cytometry analysis determined that LILRB3 showed the highest expression on CHO-S cells (67.6%) whilst LILRB1 (45.7%), LILRB2 (35.6%) and LILRB4 (28.7%) showed less expression (*Figure 3.7*). It was decided to not use LILRB4 in the selections as expression was very low and thus not compatible with cell selections (no protein selections could be performed in the absence of purified LILRB4 protein). However, the LILRB1-, LILRB2- and LILRB3-transfected cells were of sufficient expression for use in the selections.

LILR-expressing CHO-S cells were also analysed by FMAT to demonstrate if expression levels were adequate enough for detection by the FMAT technology (used in the screening), and therefore determine the compatibility of these cells in the screening process.

FMAT is a fluorescent cell-based antibody binding approach, allowing expression levels of proteins on cells to be detected with fluorescently-labelled antibodies. These antibodies allow detection and quantification of protein expression. This technology is ideal for testing many antibody clones generated from phage display, as it is reliable, reproducible, specific and

high-throughput. Unlike flow cytometry the technique allows a homogenous assay to be performed, where cells and fluorescent antibodies are added at the same time, as unbound fluorophore is ignored, and therefore avoiding high background signals. Most importantly, the native protein conformation is being detected, unlike with an ELISA for example, where antibodies are not binding to cell surface proteins in their native form[247].

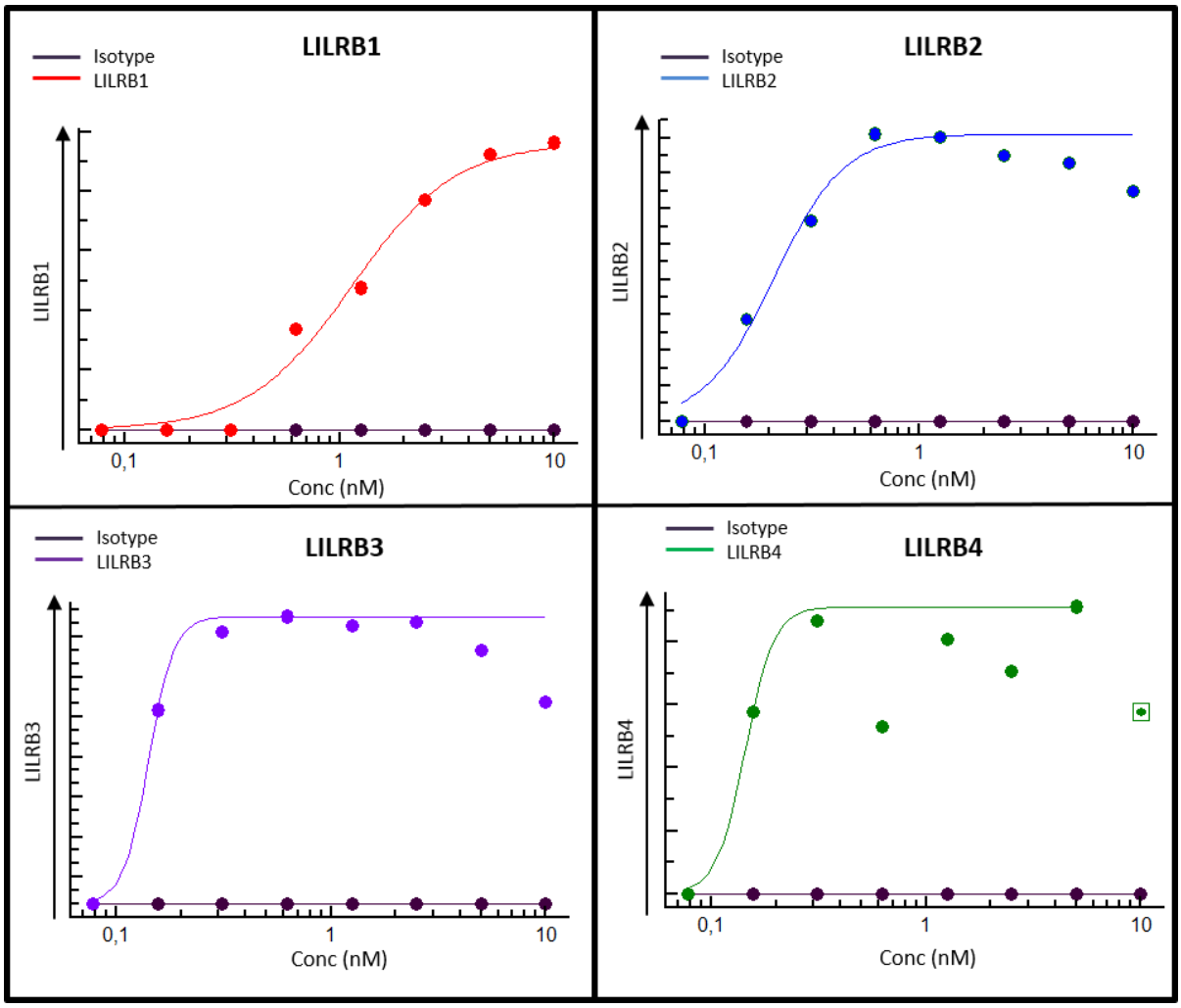

Figure 3.8 FMAT analysis to confirm compatibility of LILR-transfected cells with the FMAT technology. $1x10^5$ LILR-expressing CHO-S cells were incubated with varying concentrations of their specific LILR antibodies, anti-LILRB1 (Biolegend), LILRB2 (Biolegend), LILRB3 (R&D systems) and LILRB4 (Biolegend) or isotype controls for 10 hours at room temperature then analysed using the FMAT 8200 Cellular Detection System (Applied Biosystems). Mean fluorescent intensity (MFI) is displayed as the y-axis with concentration (nM) as the x-axis. LILRB1 staining shown in red, LILRB2 in blue, LILRB3 in purple, LILRB4 in green and isotype controls in dark purple.

The FMAT data showed that expression could be detected for all four LILR-expressing CHO-S cells in a dose-dependent manner (*Figure 3.8*). LILRB2, LILRB3 and LILRB4 reached saturation at lower concentrations (by 0.5 nM all saturated) compared to LILRB1, which only began to saturate at ~10 nM, suggesting the LILRB1 antibody binds to cells slower at lower concentrations or has a lower affinity. However, all antibodies were able to bind and detect

target cells. Therefore, LILRB expression on target cells was sufficient to be detected by FMAT, and thus the transfected cells were compatible with using the FMAT technology in the screening.

In summary, all the quality control checks carried out on the reagents to be used in both the selections and screening indicated that these reagents were of good enough quality and were compatible for use in the antibody generation methods to be used.

3.2.2 Antibody selections: generating LILRB1, LILRB2 and LILRB3-specific scFv clones

3.2.2.1 Designing and implementing selection strategy for phage display

The phage display *in vitro* system was highly stringent and the high-throughput and flexible nature of the technology allowed antibodies to be generated against three different targets: LILRB1, LILRB2 and LILRB3.

Antibody fragment libraries are used in phage display to generate antibodies. The first step before performing the phage display was to design the format of each selection. As human antibodies were desired, a human antibody library was chosen. BioInvent have two different human antibody libraries: n-CoDeR Fab-lambda and n-CoDeR scFv. These libraries consist of together ~20 billion fully human antibody fragments with low immunogenicity[248]. The scFv library was chosen, as scFvs often result in a better yield and diversity of antibodies. This is likely due to the fact they express better in bacteria, are less toxic on cells and their small sizes results in them being displayed better on phages, therefore providing them with a higher avidity[205].

A typical selection/panning cycle includes incubation of the phage antibody particles with the antigen before washing away unbound phage particles and eluting the bound phages for amplification in *E. coli*. A complete selection strategy typically includes three such cycles, and may involve a pre-selection or depletion step, to eliminate cross-reactive clones to a non-target. To guarantee successful antibody generation, and in case one strategy failed, three different strategies of displaying the target protein were chosen, i.e., two protein-selection strategies and one cell-selection strategy. The schematic below (*Figure 3.9*) represents the different selection strategies that were utilised during the selection process, detailing how the target was displayed in various ways.

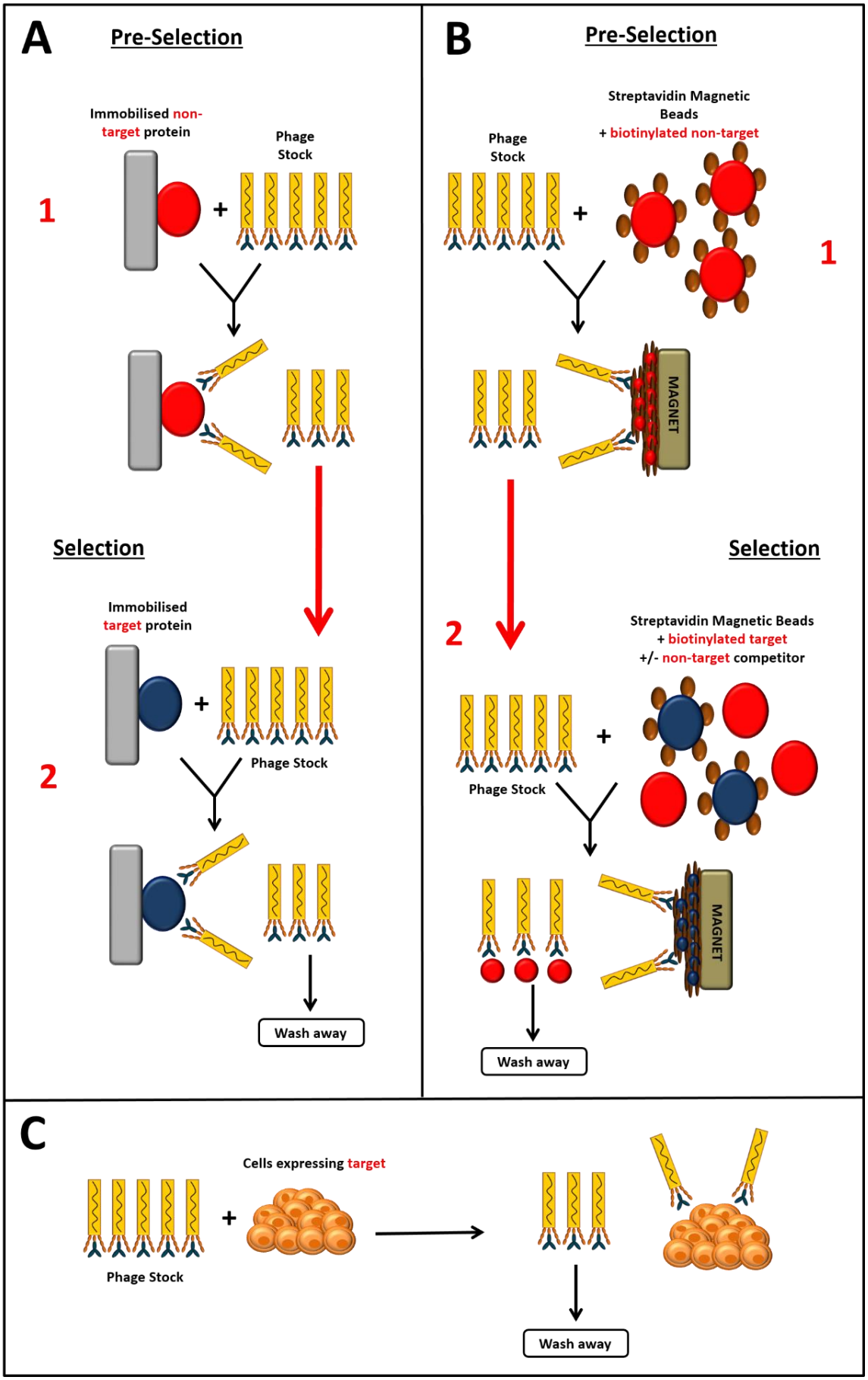
A
Pre-Selection
Immobilised non-target protein
Phage Stock
1
Selection
Immobilised target protein
2
Phage Stock
Wash away
B
Pre-Selection
Streptavidin Magnetic Beads
+ biotinylated non-target
Phage Stock
1
MAGNET
Selection
2
Streptavidin Magnetic Beads
+ biotinylated target
+/- non-target competitor
Phage Stock
MAGNET
Wash away
C
Cells expressing target
Phage Stock
Wash away

Figure 3.9 Different selection strategies were chosen to isolate scFv clones. A) Selection using polystyrene beads. During the pre-selection, an immobilised non-target protein (red) was incubated with the scFv library and unbound phages taken through to the selection. Immobilised target protein (blue) was then incubated with the phages from the pre-selection, and unbound phages washed away. **B) Selection using streptavidin-Dynabeads.** Biotinylated non-target (red) in solution was incubated with the scFv library in the pre-selection and captured by streptavidin magnetic beads, whilst unbound phages taken through to the selection. Biotinylated target protein (blue) was then incubated with the phages from the pre-selection, with or without a non-biotinylated homologous competitor. Phages were captured by streptavidin magnetic beads, and unbound phages washed away. **C) Selection using cells.** No separate pre-selection step used. Phages were incubated with target-expressing CHO-S cells and unbound phages washed away.

Figure 3.9 represents the different strategies that were performed. For the protein selection strategies the phages were either incubated with biotinylated target protein in solution, or incubated with target protein coated to a plastic surface. The protein selections were performed in two stages: pre-selection (negative selection/depletion) and the selection itself (positive selection).

For selection strategies involving protein coated on plastic, the pre-selection involved a non-target protein being coated to plastic tubes (Immunotubes), which were incubated with the scFv phage library. Any phages that did not bind to the coated non-target were taken forward into the selection (*Figure 3.9A1*). This process was then repeated with the target protein coated on polystyrene beads, this time incubated with phages from the pre-selection, and unbound phages discarded (*Figure 3.9A2*).

For selection strategies involving biotinylated protein in solution, in the pre-selection a biotinylated non-target attached to streptavidin-dynabeads, were incubated with the scFv library then captured on a magnet, whilst unbound phages were taken into the selection (*Figure 3.9B1*). This was then repeated with a biotinylated target in solution, which was incubated with the scFv phage library taken from the pre-selection, captured by streptavidin magnetic beads, and unbound phages this time discarded (*Figure 3.9B2*). This strategy was also performed in parallel, but with "competition" during the selection process. Competition involves the use of a non-target (having structural similarities and/or carrying the same tag as the target) in excess. Both competition and pre-selection aim to increase the proportion of target specific phages. Pre-selection ensures non-target specificity is eliminated whilst, a non-target competitor in excess ensures that any shared binding epitopes between the non-target and target are eliminated. In a final round of selection, for some selection strategies, phages were incubated with target-expressing CHO-S cells, without any pre-selection step, and unbound phages were discarded (*Figure 3.9C*).

After completion of each selection-round, eluted phages were amplified in bacteria and titrated to determine concentrations before the following selection-round, to indicate the quantity of enriched phages after each selection. With each round of selection the yield (phage out / phage in) increased (data not shown). This was expected, as the proportion of target-specific phages should increase for each selection round.

A summary of the different selection strategies utilised for all three targets is given below in *Figure 3.10*.

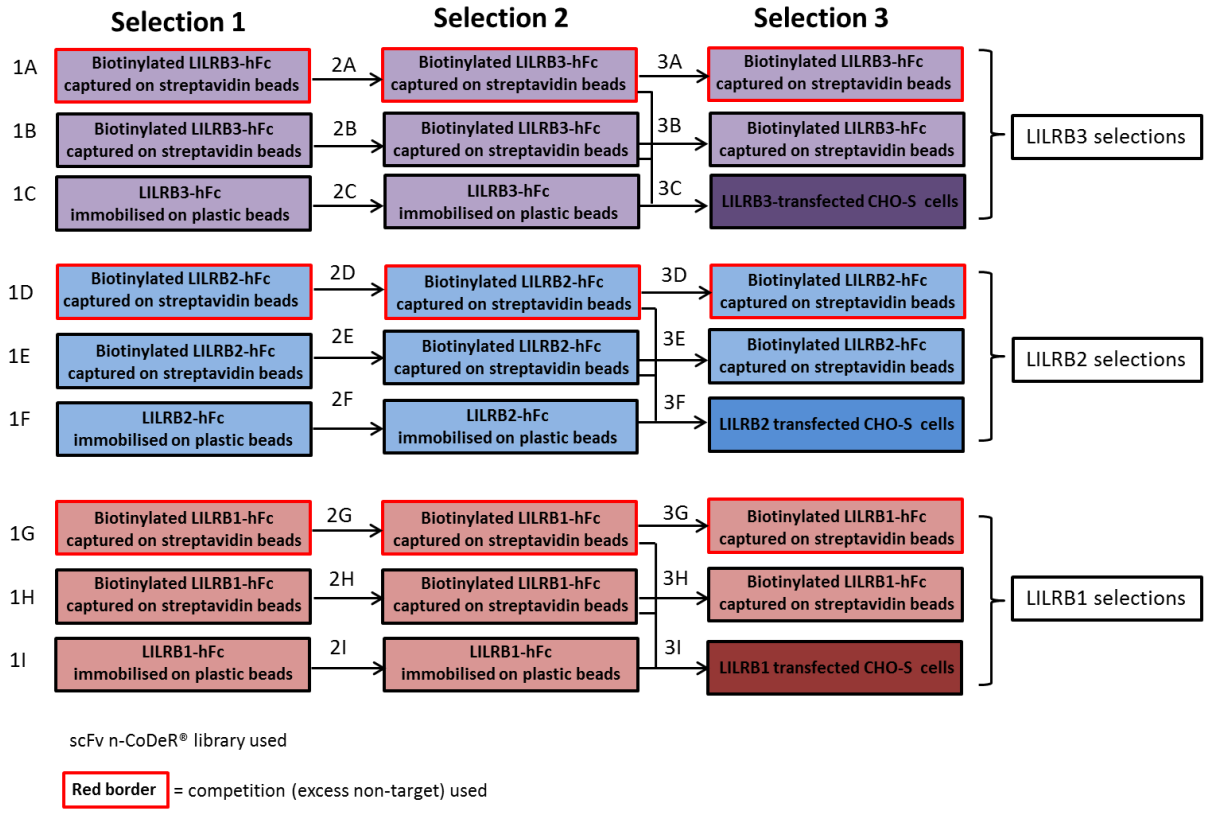

Figure 3.10 Selection strategies for generating LILRB3, LILRB2 and LILRB1-specific antibodies by phage display. To generate LILR-specific antibodies to LILRB3, LILRB2 and LILRB1 (in order of priority), 3 selections were performed. In each selection, for each target protein, different selection techniques were used. In selection 1, strategy 1 (A, D and G) biotinylated target captured on streptavidin magnetic beads with competition was used. This was repeated in selections 2 and 3. In strategy 2 (B, E and H) for each target, biotinylated target captured on streptavidin magnetic beads, this time without competition was utilised for all three selections. In selection 1 of the third and final strategy (C, F and I) for each target, the protein target was immobilised by coating it to plastic polystyrene beads, this was repeated in selection 2. In selection 3 however, the third strategy utilised cells expressing the target, and phages from all three tracks in selection 2 were pooled for use in selection 3 for each target. LILRB1 was used as a non-target and as a competitor for both LILRB2 and LILRB3 throughout the selections, whilst LILRB2 was used as a non-target and competitor for LILRB1. 50 nM biotinylated non-target was used in the pre-selection for strategies where biotinylated protein was used (A, B, D, E, G and H). 10 µg/ml non-target was used for strategies where coated protein was used (C, F and I). No pre-selection was required for the cell strategies (3C, 3F and 3I).

Each box in each column in *Figure 3.10* represents one round of selection, and each box a different strategy, detailing how the target was displayed in the selections and which target that was used. The selections were performed in two stages: pre-selection and the selection itself, which could include 'competition' (represented by a red border). The three different strategies chosen included: the protein target biotinylated and in solution with the use of a non-target competitor antigen in excess (strategies A, D and G), the protein target biotinylated and in solution without competition (tracks B, E and H), and the protein target coated on plastic (strategies C, F and I). Where the target protein was coated on plastic, this applied only in the first two selections rounds, followed by (in the third selection) the target antigens expressed on cells. For each target, in this third selection round, eluted and amplified phages from all three strategies from selection 2 were pooled and used in selection 3 (strategies 3C, 3F and 3I). Introducing cells in the last selection was ideal, to select for 'real' binding epitopes, as the target protein on cells was in its natural protein conformation, and therefore less likely for epitope binding sites being hidden. Also, the likelihood of developing antibodies that cross-react to cells is reduced by utilising cells in the final selection, as by this stage most clones selected for are target-specific.

These strategies were chosen based on previous successful selections performed at BioInvent. Using different strategies increased the probability of finding antibodies against different epitopes. Ensuring specificity and reducing cross-reactivity was a priority, and the use of pre-selection and competition ensured this. Where biotinylated protein was used, decreasing concentrations of the target protein in selections 1, 2 and 3 (50 nM, 20 nM and 5 nM respectively), provided a selection pressure that favoured high affinity binding phages to be selected for.

In order to deduce which LILR protein would be used as a non-target for each receptor, sequence homology was evaluated. To highlight amino acid similarities the sequences of LILRB1, LILRB2 and LILRB3 were aligned, and sequence identity and an evolutionary tree evaluated, using the programme CLUSTALO in UNIPROT. See *Figure 3.11* below for analysis.

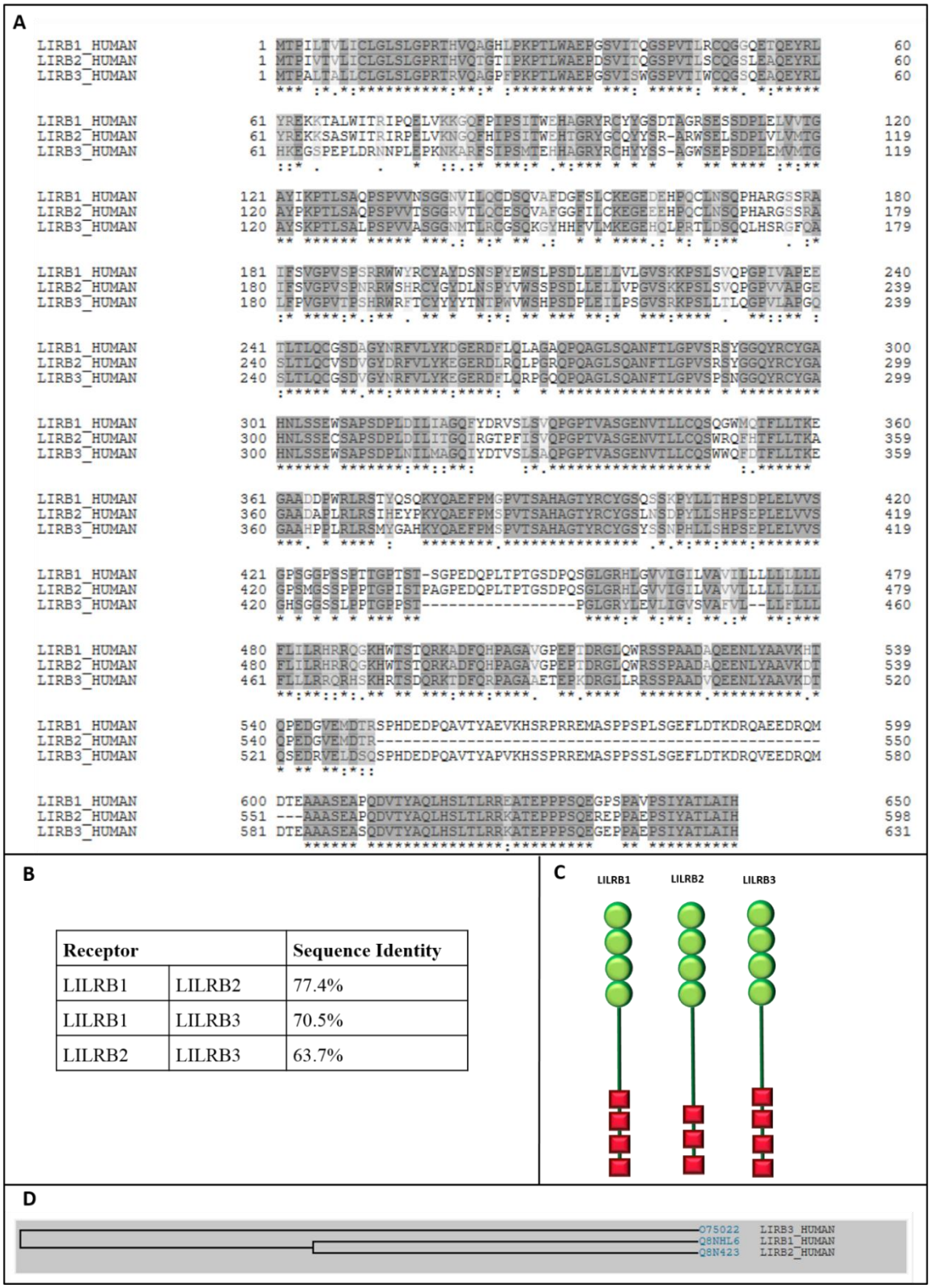

Receptor		Sequence Identity
LILRB1	LILRB2	77.4%
LILRB1	LILRB3	70.5%
LILRB2	LILRB3	63.7%

Figure 3.11 Protein homology between inhibitory LILR receptors. A) LILR sequence alignment. Alignment of LILRB1, LILRB2 and LILRB3 protein. Shaded in grey is the similar amino acids. Stars (*) indicated positions with a single fully conserved residue in all three receptor sequences, dots (.) indicated conservation between groups of weakly similar properties and hyphens (-) indicated conservation between groups of strongly similar properties. **B) LILRB1, LILRB2 and LILRB3 sequence identity. C) Schematic of LILRB1, LILRB2 and LILRB3 receptors. D) Phylogenetic Tree.** Alignment, sequence identity and phylogenetic tree were performed using the programme CLUSTALO in UNIPROT.

Aligning LILRB1, LILRB2 and LILRB3 protein sequences shows all three receptors have high sequence homology (as indicated by the amino acids shaded in grey – *Figure 3.11A*). *Figure 3.11B* shows LILRB1 and LILRB2 had the highest homology (77.4%), whilst LILRB2 and LILRB3 had the lowest (63.7%). The schematic in *Figure 3.11C* shows that the three receptors have a similar structure – with four extracellular Ig-like domains, and 3-4 intracellular ITIMs. The phylogenetic tree (*Figure 3.11D*) shows LILRB1 and LILRB2 are more closely related in terms of evolution, compared to LILRB3. This data suggests that LILRB1 and LILRB2 are more homologous to each other than LILRB3.

Based on this, the non-targets were picked accordingly: LILRB1 was used as a non-target and as a competitor for both LILRB2 and LILRB3 throughout the selections, whilst LILRB2 was used as a non-target and competitor for LILRB1. LILRB1 and LILRB2 were used as non-targets for each other as they have the highest similarity in terms of homology (77.4% based on annotated UNIPROT sequences –*Figure 3.11*) and therefore pre-selection is important to eliminate cross-reactivity. LILRB1 was used as a non-target for LILRB3 as there was higher sequence homology compared to LILRB2 and LILRB3.

3.2.2.2 Screening of phages after selections by ELISA

After each round of selection, the eluted phages were screened by ELISA to confirm specificity, before moving into the next round of selection. TAR (target), NOT (non-target) or non-target streptavidin (NOT-Strep) were coated onto a plate overnight at 4°C. The next day phages from each selection (diluted two-fold) were incubated with the protein and then detected using an anti-M13 HRP-conjugated antibody, followed by OPD substrate. The plates were then read at 490 and 650 nm. LILRB1 was used as a non-target for both LILRB2 and LILRB3. LILRB2 was used as a non-target for LILRB1. Below is a schematic of the phage ELISA performed (*Figure 3.12*)

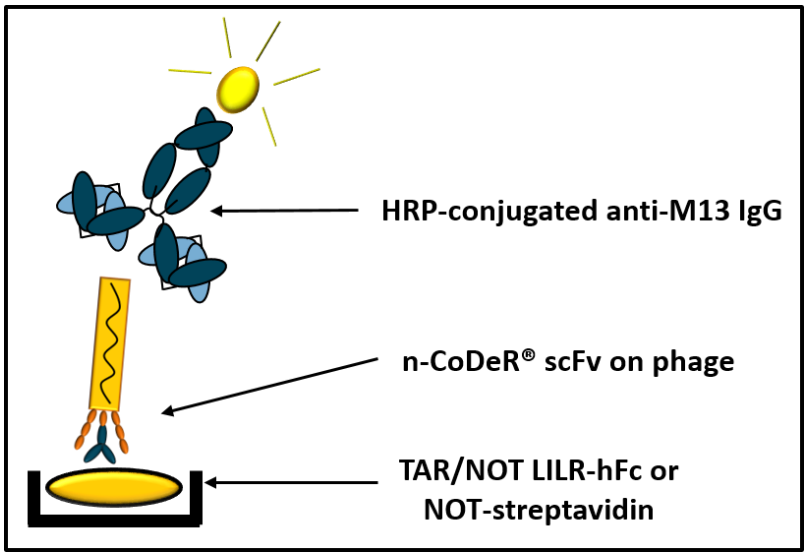

Figure 3.12 Schematic of phage ELISA performed after selections. After each selection scFv-phage pools were screened against target (TAR) or non-target (NOT) LILR-hFc protein or non-target streptavidin. Bound phages were detected with an anti-M13-HRP antibody and OPD substrate. Absorbance was measured at 490 and 650 nm.

The phage ELISA was carried out to evaluate the phage-pool eluted and amplified after selection 2. Phages from selection 1 were also evaluated to compare enrichment of target-specific phages. Another phage ELISA was performed on the eluted and amplified phages after the final round of selection (selection 3). All selection strategies used for the different targets were included (*Figure 3.13*).

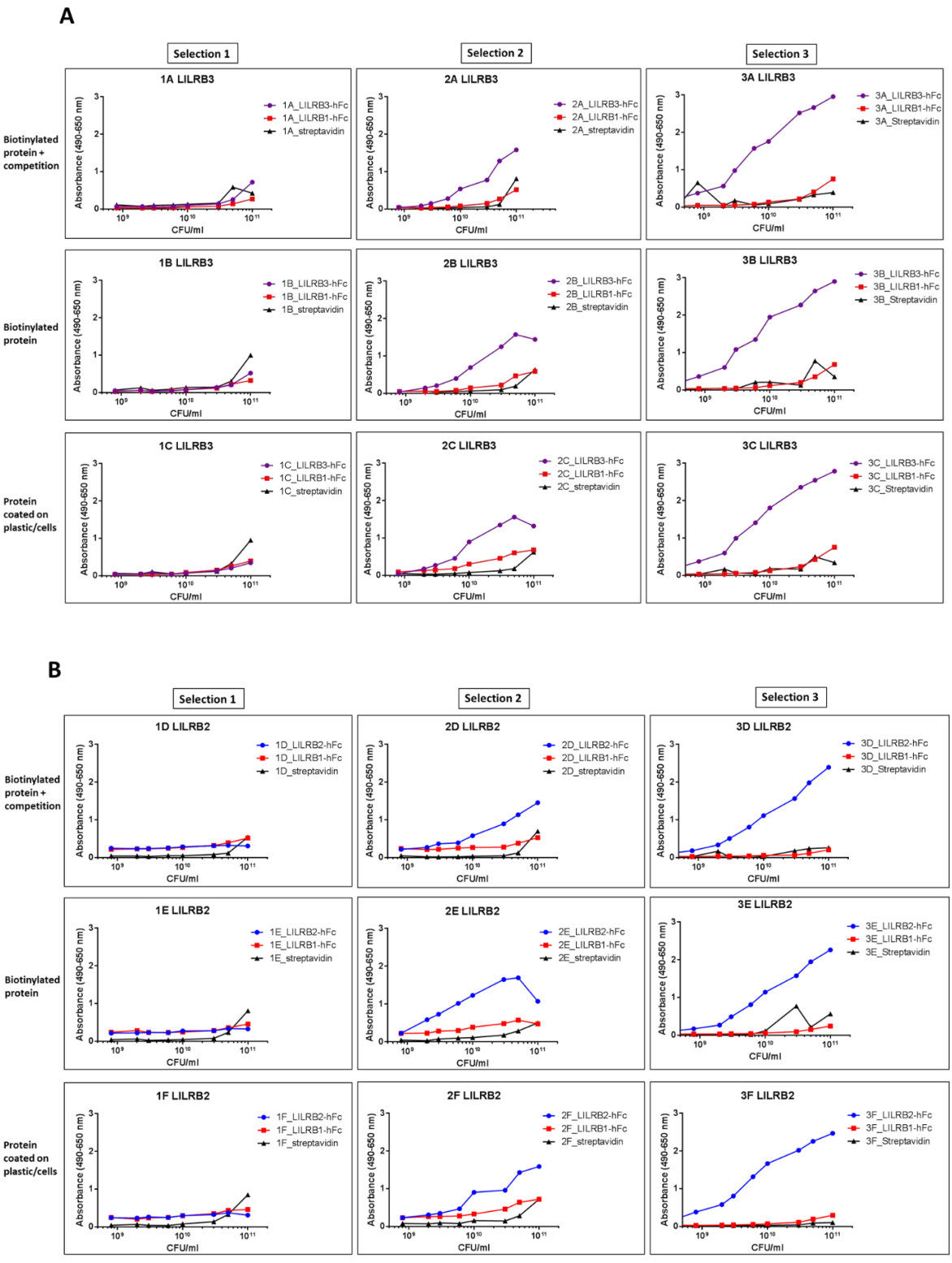
A
Selection 1
Selection 2
Selection 3
Biotinylated protein + competition
Biotinylated protein
Protein coated on plastic/cells
1A LILRB3
1A_LILRB3-hFc
1A_LILRB1-hFc
1A_streptavidin
2A LILRB3
2A_LILRB3-hFc
2A_LILRB1-hFc
2A_streptavidin
3A LILRB3
3A_LILRB3-hFc
3A_LILRB1-hFc
3A_Streptavidin
1B LILRB3
1B_LILRB3-hFc
1B_LILRB1-hFc
1B_streptavidin
2B LILRB3
2B_LILRB3-hFc
2B_LILRB1-hFc
2B_streptavidin
3B LILRB3
3B_LILRB3-hFc
3B_LILRB1-hFc
3B_Streptavidin
1C LILRB3
1C_LILRB3-hFc
1C_LILRB1-hFc
1C_streptavidin
2C LILRB3
2C_LILRB3-hFc
2C_LILRB1-hFc
2C_streptavidin
3C LILRB3
3C_LILRB3-hFc
3C_LILRB1-hFc
3C_Streptavidin
Absorbance (490-650 nm)
CFU/ml
B
Selection 1
Selection 2
Selection 3
Biotinylated protein + competition
Biotinylated protein
Protein coated on plastic/cells
1D LILRB2
1D_LILRB2-hFc
1D_LILRB1-hFc
1D_streptavidin
2D LILRB2
2D_LILRB2-hFc
2D_LILRB1-hFc
2D_streptavidin
3D LILRB2
3D_LILRB2-hFc
3D_LILRB1-hFc
3D_Streptavidin
1E LILRB2
1E_LILRB2-hFc
1E_LILRB1-hFc
1E_streptavidin
2E LILRB2
2E_LILRB2-hFc
2E_LILRB1-hFc
2E_streptavidin
3E LILRB2
3E_LILRB2-hFc
3E_LILRB1-hFc
3E_Streptavidin
1F LILRB2
1F_LILRB2-hFc
1F_LILRB1-hFc
1F_streptavidin
2F LILRB2
2F_LILRB2-hFc
2F_LILRB1-hFc
2F_streptavidin
3F LILRB2
3F_LILRB2-hFc
3F_LILRB1-hFc
3F_Streptavidin
Absorbance (490-650 nm)
CFU/ml

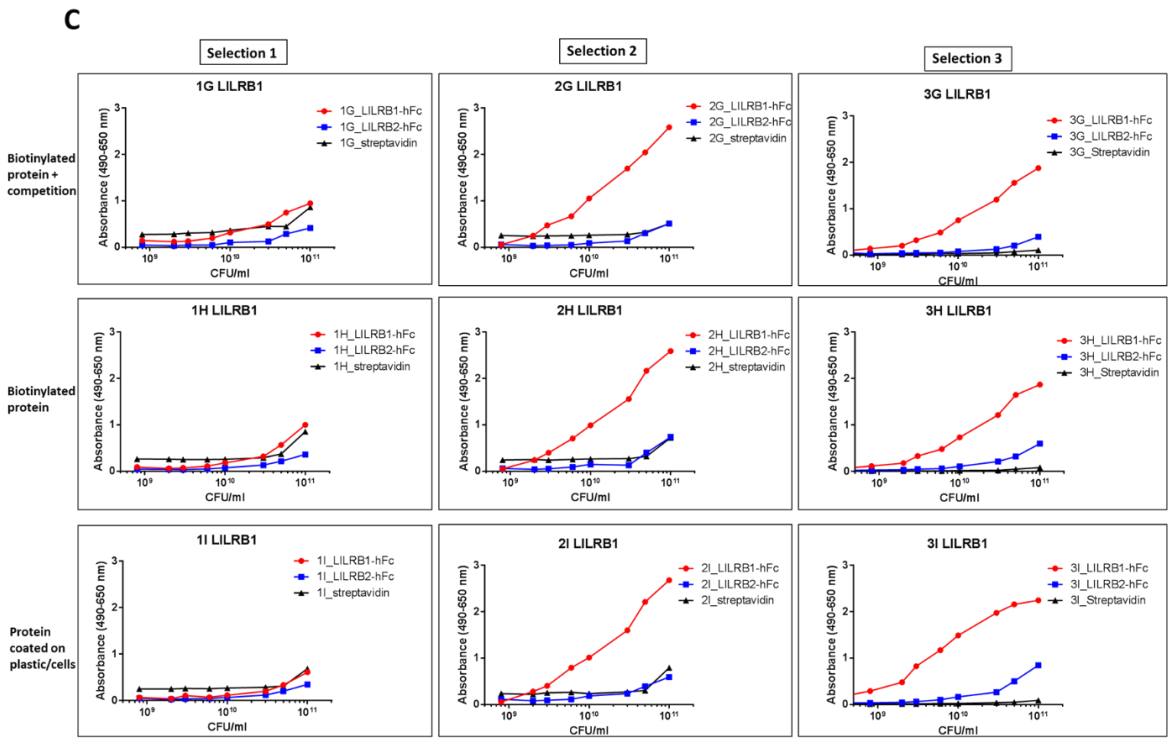

Figure 3.13 Assessing phage specificity by ELISA after each selection. Target (TAR) protein and non-target (NOT) protein or streptavidin, were coated at 1 pmole/well (protein) and 1.7 pmole/well (streptavidin), in a 96-well ELISA plate overnight at 4°C. LILRB1 was used as a NOT for both LILRB2 and LILRB3, whilst LILRB2 was used as a NOT for LILRB1. Plates were washed 3 x with ELISA wash buffer (PBS + 0.05% Tween20) using the SkanWasher SkanSTACKER (SKATRON model 12201) then blocked with 3% BSA PBS for 30 minutes at room temperature (RT), before being washed again in ELISA wash buffer. Phages from all three selection rounds were serially diluted (two-fold) from $1x10^{11}$ CFU/ml in ELISA wash buffer and then incubated for 3-4 hours at RT. The ELISA plate was then washed and mouse anti-M13-HRP (Fisher Scientific) added for 1 hour at RT. After washing, OPD substrate solution (Sigma) was added for 10 minutes at RT. The reaction was stopped with 1M HCl. Finally, the plates were read in an E-max Micro Plate Reader using Soft-max (Molecular device) set at: Endpoint Assay; and dual wavelength 490 nm and 650 nm. **A)** LILRB3 selection phages tested **B)** LILRB2 selection phages tested and **C)** LILRB1 selection phages tested.

The ELISA data (*Figure 3.13*) showed that enrichment of target-binding phages was seen for all targets (LILRB1, LILRB2 and LILRB3). All targets showed enrichment after selection 2, when compared to phages screened from selection 1, as the increase in signal on each curve demonstrated an increase in target-specific phages between the two selections. This suggests that an increase in target-specific phages occurred during the second selection when compared to the first. After selection 2, all targets also showed some enrichment for phages that were specific to streptavidin in the strategies that used biotinylated protein captured on streptavidin magnetic beads (A, B, D, E, G and H). To reduce this cross-reactivity with streptavidin, it was included as a non-target in the pre-selection step of the third selection round. The additional streptavidin was separately coated on plastic tubes ('Immunotubes') at a concentration of 10µg/ml in coating buffer and the pre-selection mix was incubated with the biotinylated non-target loaded on magnetic beads and placed in the coated Immunotubes.

Enrichment of target-specific phages was even greater for LILRB2 and LILRB3-specific phages after selection 3 (*Figure 3.13 A and B*), showing an increase in target-specific phages with every selection performed. However, phage pools from the LILRB1 selection strategies (*Figure 3.13 C*) did not display the same increase after selection 3. No apparent difference between selection 2 and selection 3 was seen, suggesting no enrichment of LILRB1-binding phages during the third selection. This implies that the final round of selection (3G, 3H and 3I) failed. The reason for this is unknown but could be due to technical errors, in the phages added from the previous selection or concentration of target/non-target being used. After selection 3, the phage ELISA indicated that enrichment for streptavidin had successfully been reduced (as seen for all strategies).

Notably, the ELISA curves for all targets in all three selections did not display the 'typical' sigmoidal shape graph. This is in accordance with the fact that a pool of binding phage/antibodies all with different affinities against the target antigen were present.

3.2.2.3 Screening of selected phages by flow cytometry

After each selection scFvs were also screened by flow cytometry to assess enrichment of target-specificity. Whilst the ELISA allowed for specificity to be assessed by a protein-based technique, flow cytometry assessed specificity by a cell-based technique. These two techniques ensure that scFvs are selected for based on not just their specificity, but a range of different binding epitopes are selected for, as protein confirmation is different in the two techniques. The flow cytometry analysis performed is outlined in *Figure 3.14A* and the data from selection 3 is summarised below in *Figure 3.14B.* As detectable enrichment by flow cytometry is unlikely after just one round of selection (based on previous selections performed at BioInvent that showed little to no enrichment), the eluted phages were only screened after selections 2 (data not shown) and 3 to confirm specificity before moving into the next round of selection. LILRB3 strategies are represented in histograms A-C, LILRB2 in D-F and LILRB1 in G-H for the three different strategies utilised.

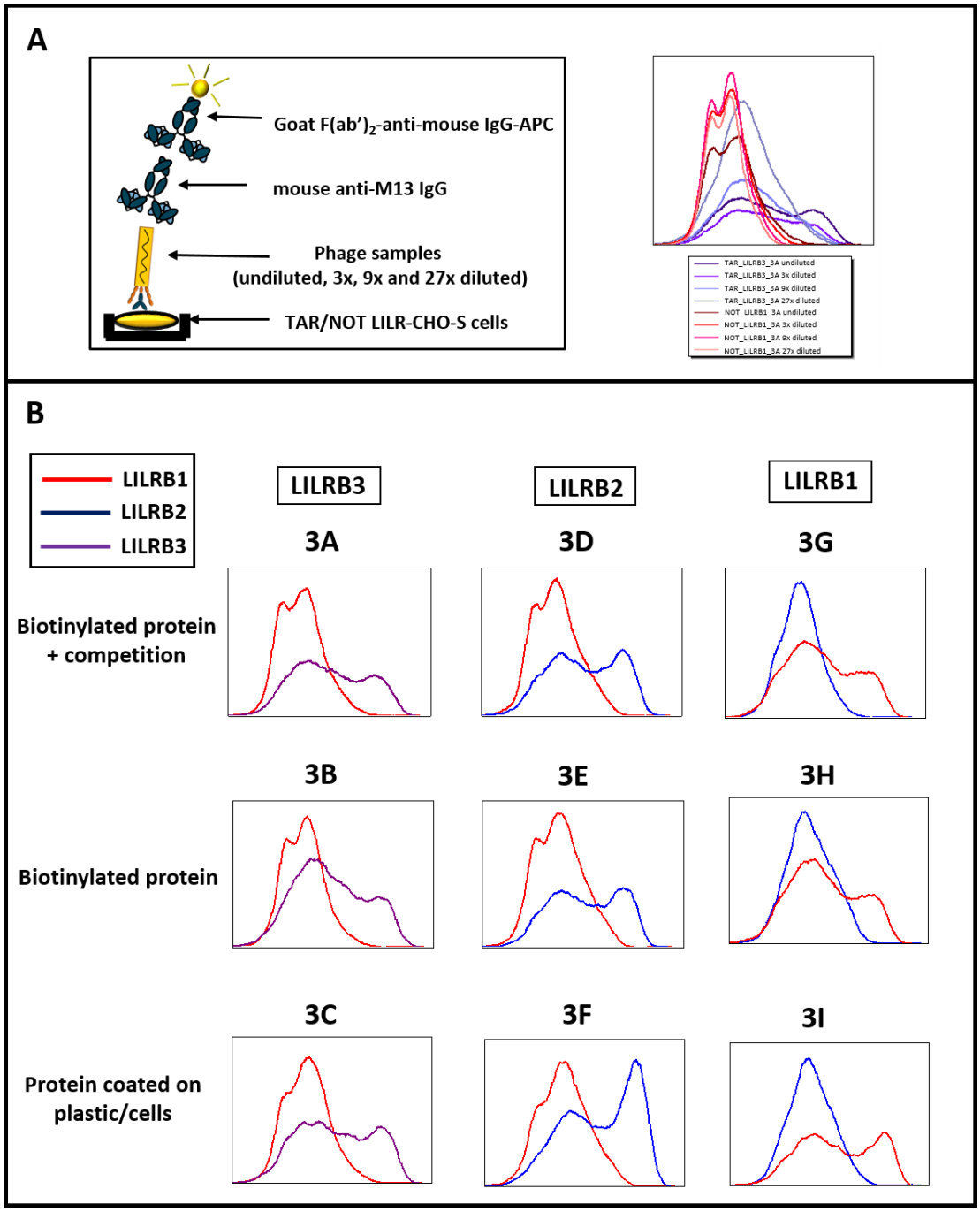

Figure 3.14 Phage specificity assessed by flow cytometry. A) Schematic of flow cytometry assay to analyse enriched phages after selection. Phages (undiluted, 3x, 9x and 27x diluted) were screened against target (TAR) or non-target (NOT)-expressing CHO-S cells, then detected with a mouse anti-M13 antibody and anti-mouse-APC secondary. Representative histogram showing all dilutions of non-target and target included. **B) Evaluation of phage specificity after selection 3 by flow cytometry.** TAR-LILR or NOT-LILR transiently transfected CHO-S cells were blocked for 10 minutes on ice with 0.2 mg/ml human IgG and seeded at $1x10^5$ cells/well. The cells were then incubated with undiluted, 3x, 9x or 27x diluted phage samples (amplified pools) for 1 hour at 4°C, then washed in FACS buffer. Subsequently, the cells were incubated for 1 hour at 4°C, with 10 µg/ml mouse anti-M13 IgG (GE Healthcare). After the cells were washed, this was followed by a 1 hour incubation at 4°C with 5 µg/ml goat-F(ab')2-anti-Mouse IgG-APC (Jackson Labs). Plates were washed and the cells fixed in 4% paraformaldehyde (BioInvent, made in house) for 10 minutes, at 4°C, then analysed by flow cytometry using the High-throughput Flow Cytometry (HTFC) Screening System (IntelliCyt). The letter A-I relates to the strategies used in each selection and the numbers relates to the selections they were used in. LILRB3 (purple) strategies are represented in A-C, LILRB2 (blue) in D-F and LILRB1 (red) in G-H. Only undiluted samples are represented here.

Figure 3.14A demonstrates how the flow cytometry assay was performed, and an example histogram shows the different dilutions for both the non-target and target, demonstrating a clear shift right in the target samples when compared to the non-target samples. *Figure 3.14B* shows only the undiluted samples for both the target and non-targets in each selection strategy. Phages from the nCoDer library before selections showed no binding to the LILR-transfected cells (data not shown). Binding increased after selection 2 (data not shown) and again after selection 3 (*Figure 3.14B*).

The undiluted samples for either the target or non-target samples only are displayed in each histogram, for each strategy in selection 3 (*Figure 3.14B*). LILRB1-transfected CHO-S cells (represented in red) were used as non-target cells for both LILRB2 cells (blue) and LILRB3-specific phages (purple), whilst LILRB2-transfected CHO-S cells were used as non-targets for LILRB1-specific phages. The histograms show a clear shift to the right in phages incubated with their target-specific transfected CHO-S cells compared to the non-target transfected cells. The undiluted targets show the greatest shift right compared to those diluted, respectively (representative histogram in *Figure 3.14A*, data not shown for other samples), indicating specificity in a dose-dependent manner. The selection strategy that utilized cells in the third round of selection (3C, 3F and 3I) shows an even greater shift compared to strategies where the target was biotinylated and in solution throughout the selections. This is expected as these phages have already seen cells during the final round of selection, and therefore this increases the likelihood of generating target-specific cell-binding phages.

In summary, all targets showed target-specific enrichment of phages. Therefore, the scFv antibodies expressed on these phages were converted to a soluble antibody format through plasmid purification, digesting the scFv-encoding antibody gene from its pMIL phagemid vector and ligating it into a new pKscFv-3xFH vector with two C-terminus tags (3xFLAG and 6xHis), and transforming the vector into Top10 *E. coli* cells to produce more DNA. Each colony grown represented one unique scFv clone.

3.2.3 Screening soluble scFv clones for LILRB1, LILRB2 and LILRB3-specificity

The soluble scFv antibody clones were then screened to verify specificity and to identify unique clones. BioInvent have a high-throughput robotic screening method, which is capable of screening for scFv-target complexes, and can be cell- or protein-based using FMAT and/or ELISA, respectively.

3.2.3.1 Primary screening

The primary screening was performed in a 384-well plate format. The screening strategy, and the number of clones (plates) used in both FMAT and ELISA are displayed in table 3.1 below.

Table 3.1 Primary Screening Strategy

Selection	FMAT Screening		ELISA Screening		#plates (FMAT:384)	#plates (ELISA:384)
	TAR	NOT	TAR	NOT		
3A	CHO-S/LILRB3	CHO-S/LILRB1/2	LILRB3-hFc	LILRB1-hFc	1	4
3B	CHO-S/LILRB3	CHO-S/LILRB1/2	LILRB3-hFc	LILRB1-hFc	1	4
3C	CHO-S/LILRB3	CHO-S/LILRB1/2	LILRB3-hFc	LILRB1-hFc	6	-
3D	CHO-S/LILRB2	CHO-S/LILRB1	LILRB2-hFc	LILRB1-hFc	-	2
3E	CHO-S/LILRB2	CHO-S/LILRB1	LILRB2-hFc	LILRB1-hFc	-	2
3F	CHO-S/LILRB2	CHO-S/LILRB1	LILRB2-hFc	LILRB1-hFc	3	2
3G	CHO-S/LILRB1	CHO-S/LILRB2	LILRB1-hFc	LILRB2-hFc	-	2
3H	CHO-S/LILRB1	CHO-S/LILRB2	LILRB1-hFc	LILRB2-hFc	-	2
3I	CHO-S/LILRB1	CHO-S/LILRB2	LILRB1-hFc	LILRB2-hFc	3	2
				Total	**14**	**20**

Table 3.1 Primary screening strategy for both FMAT and ELISA. Target cells/protein (TAR) and non-target cells/protein (NOT) are shown for scFvs taken from each different selection strategy (A to I) in selection 3. A summary of the total number of plates chosen for both FMAT and ELISA is given, or where no plates were chosen (-).

In the primary screening, emphasis was placed on LILRB3, as this was the most important target; 16 plates were chosen for both FMAT and ELISA compared to 9 plates each for LILRB1 and LILRB2 (*Table 3.1*). For FMAT, screening was carried out on clones that originated from selection strategies where cells were used for all three targets (3C, 3F and 3I) but also from the protein tracks used for LILRB3 (3A and 3B). In comparison, the protein selection strategies (3A, 3B, 3D, 3E, 3G and 3H) were screened by ELISA, again putting more emphasis on LILRB3, but this time also including the cell-selection strategies used for LILRB2 and LILRB1 (3F and 3I). For each target-transfected cell (in the FMAT) or protein target (in the ELISA), the same non-target transfected cell/protein that was used during the selections, was also used in the screening. However, in the FMAT screening, as LILRB1-transfected CHO-S cells were limited, a mixture of LILRB1 and LILRB2 expressing cells were used as non-targets for LILRB3.

The primary screening FMAT and ELISA were both performed by the BioInvent robotic system. The results were analysed by Spotfire software and data from the scFv clones

displayed graphically with the fluorescence of the target plotted against its non-target as indicated in the schematic below (*Figure 3.15).*

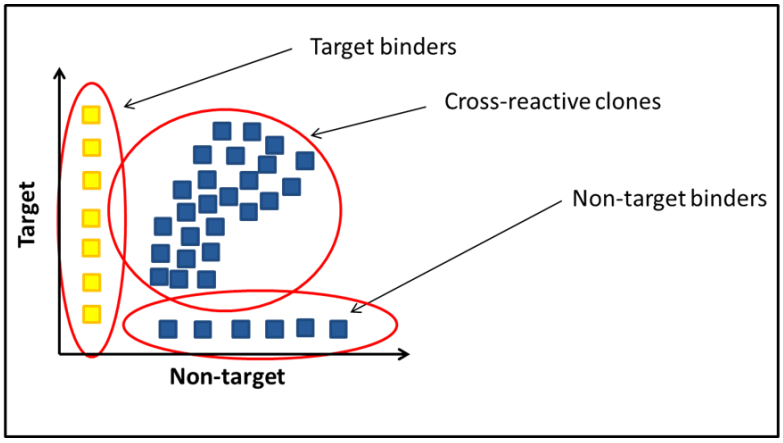

Figure 3.15 Schematic illustrating Spotfire analysis. scFv clones were analysed in the primary screening by FMAT and ELISA. Both were performed using the BioInvent robotic system. The results were analysed and displayed graphically using Spotfire, displaying the target clones plotted against its non-target. Each blue square represented an individual scFv antibody clone. Clones that were chosen, due to their high specificity for their target antigen and lack of cross-reactivity to non-targets were displayed in yellow. These yellow clones were "cherry picked" (chosen) and taken into the next round of screening.

3.2.3.1.1 Primary screening FMAT technology to test specificity of LILR scFv clones

Prior to the FMAT screening, transfected CHO-S cells (that had previously been frozen) were re-analysed to confirm LILR expression by flow cytometry (data not shown). Analysis showed that the expression levels were comparable to those seen before for each of the different LILR-expressing CHO-S cells (*Figure 3.7*). This indicated that expression is maintained after freeze-thawing the cell samples.

After confirming that the LILR-transfected cells were still expressing LILR, FMAT was performed to confirm specificity of the scFv clones. LILR-expressing CHO-S cells, the soluble scFv clones, anti-His detection antibody and secondary APC-conjugated antibody were all incubated in a homogenous assay for 10 hours, before being screened by FMAT and the results analysed by Spotfire. A schematic of the FMAT analysis is displayed in *Figure 3.16* and the results in *Figure 3.17.*

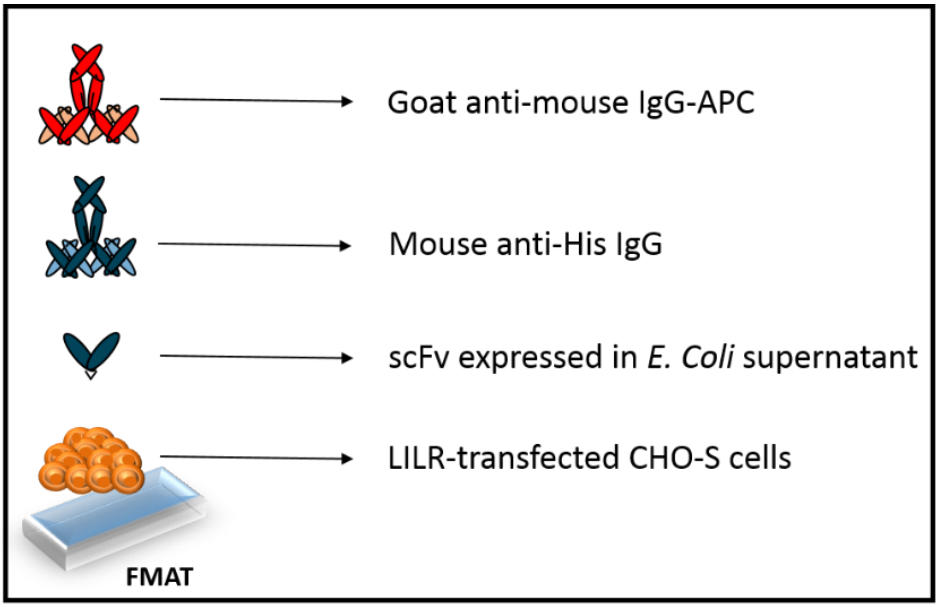

Figure 3.16 Schematic of primary screening FMAT analysis. In a 384-well plate, target or non-target LILR-expressing CHO-S cells were incubated with scFv clones expressed in *E. Coli* supernatant, an anti-His detection antibody and a secondary APC-conjugated antibody, in a homogenous assay for 10 hours at room temperature, then fluorescence analysed by FMAT.

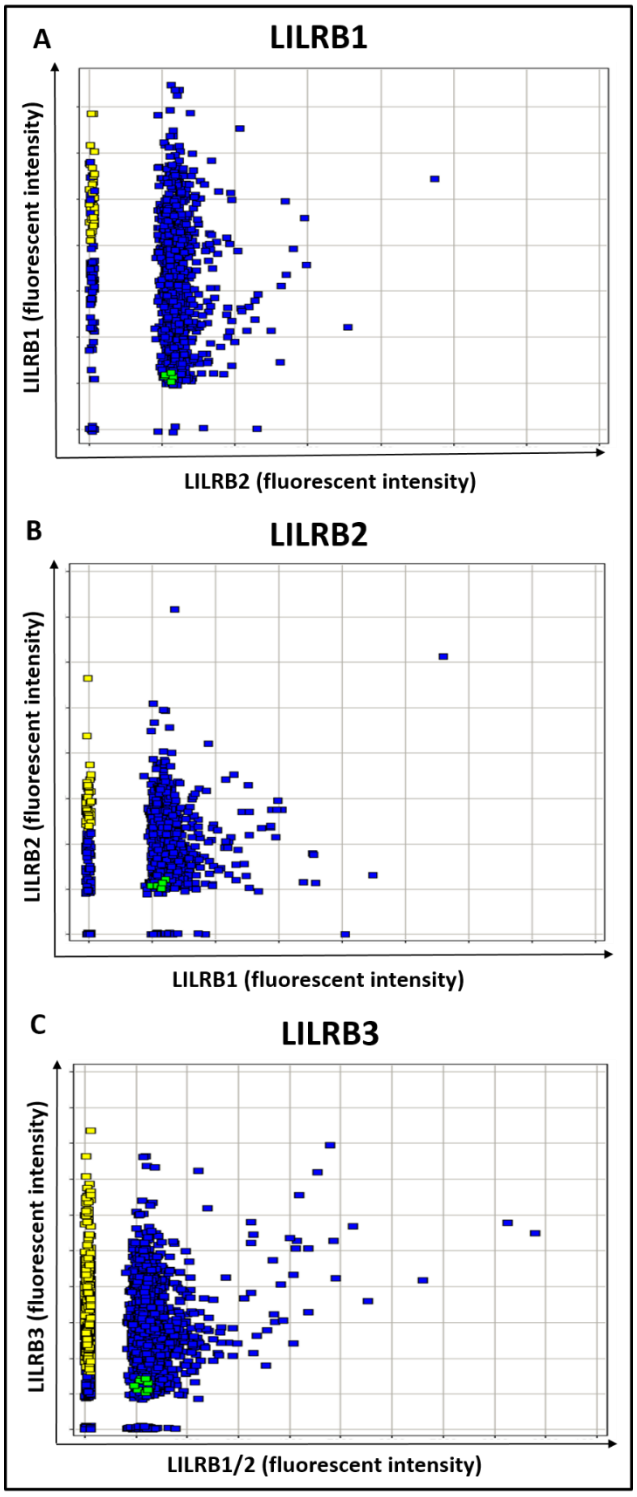

Figure 3.17 Evaluation of LILRB3, LILRB2 and LILRB1-specific clones in primary screening by FMAT. 4x10^3 LILR-transfected CHO-S cells expressing either the target (TAR) LILR or non-target (NOT) LILR were dispensed into a 384-well plate. 10 µl of E. coli expression supernatant containing scFv from individual clones from the different selection strategies were added to the cells, along with 0.2 µg/ml mouse-anti-His IgG (to detect the scFvs) and 0.1 µg/ml of the secondary antibody APC-conjugated goat-anti-mouse IgG. The samples were incubated for 10 hours at room temperature before being analysed by FMAT. The results were analysed using Spotfire and plotted target fluorescence (y-axis) against non-target fluorescence (x-axis). Each clone is represented by a blue square. A scFv-FITC8 control was also included (green). Active (target-specific) scFv clones are in yellow and these were 'cherry picked' (chosen based on their high specificity and lack of cross-reactivity). **A.** LILRB1 was compared to its non-target LILRB2. **B**. LILRB2 was compared to its non-target LILRB1. **C.** LILRB3 was compared to its non-target LILRB1.

In total, 3072 (eight plates) LILRB3 clones were analysed by FMAT, from which 525 'active' (specific) clones were identified (above background – based on isotype control) resulting in 123 'cherry picked' (chosen/selected) clones, based on their specificity and lack of cross-reactivity to their non-target. 1152 (3 plates) LILRB2 clones were analysed by FMAT, from which 80 active clones were identified resulting in 48 cherry picked clones. 1152 LILRB1 clones were analysed by FMAT, from which 101 active clones were identified resulting in 48 cherry picked clones. This is summarised in *Table 3.2* below.

Table 3.2 Summary of clones chosen from FMAT primary screening

Target	Selection Strategy	No. of clones tested	Active clones	'Chery Picked' clones
TAR_LILRB3	3A	384	262	35
TAR_LILRB3	3B	384	46	11
TAR_LILRB3	3C	2304	217	77
TAR_LILRB2	3F	1152	80	48
TAR_LILRB1	3I	1152	101	48

Table 3.2 Clones chosen after primary screening FMAT. For each target and each selection strategy a set number of clones was tested. Active (specific) clones were chosen based on the isotype control and then clones were 'cherry picked', based on their specificity and lack of cross-reactivity, for the secondary screening.

3.2.3.1.2 Primary screening ELISA to test specificity of LILR scFv clones

To further confirm specificity of the soluble scFv clones an ELISA was performed using the BioInvent ELISA robotic system. Each target was coated overnight at 4°C, before being incubated with the scFv clones, which were detected using an anti-FLAG-AP antibody and CDPStar Emerald II substrate. A schematic of the ELISA is outlined in *Figure 3.18* and the data analysed by Spotfire in *Figure 3.19.*

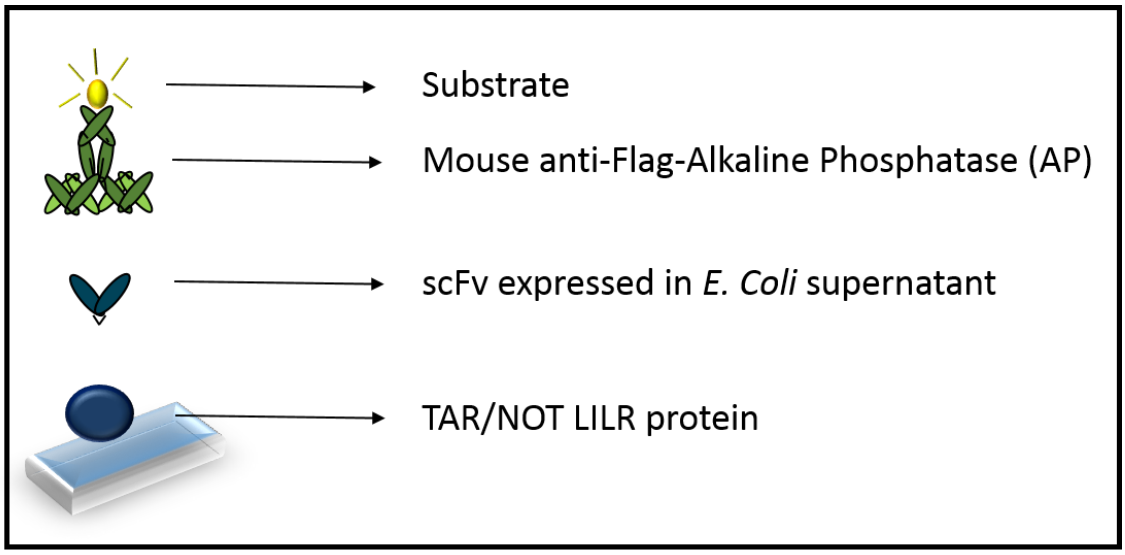

Figure 3.18 Schematic detailing the primary screening ELISA. TAR or NOT protein was coated in a 384-well plate overnight at 4°C, then incubated with the scFv clones, and detected using an anti-FLAG-AP antibody and CDPStar Emerald II substrate (Tropix).

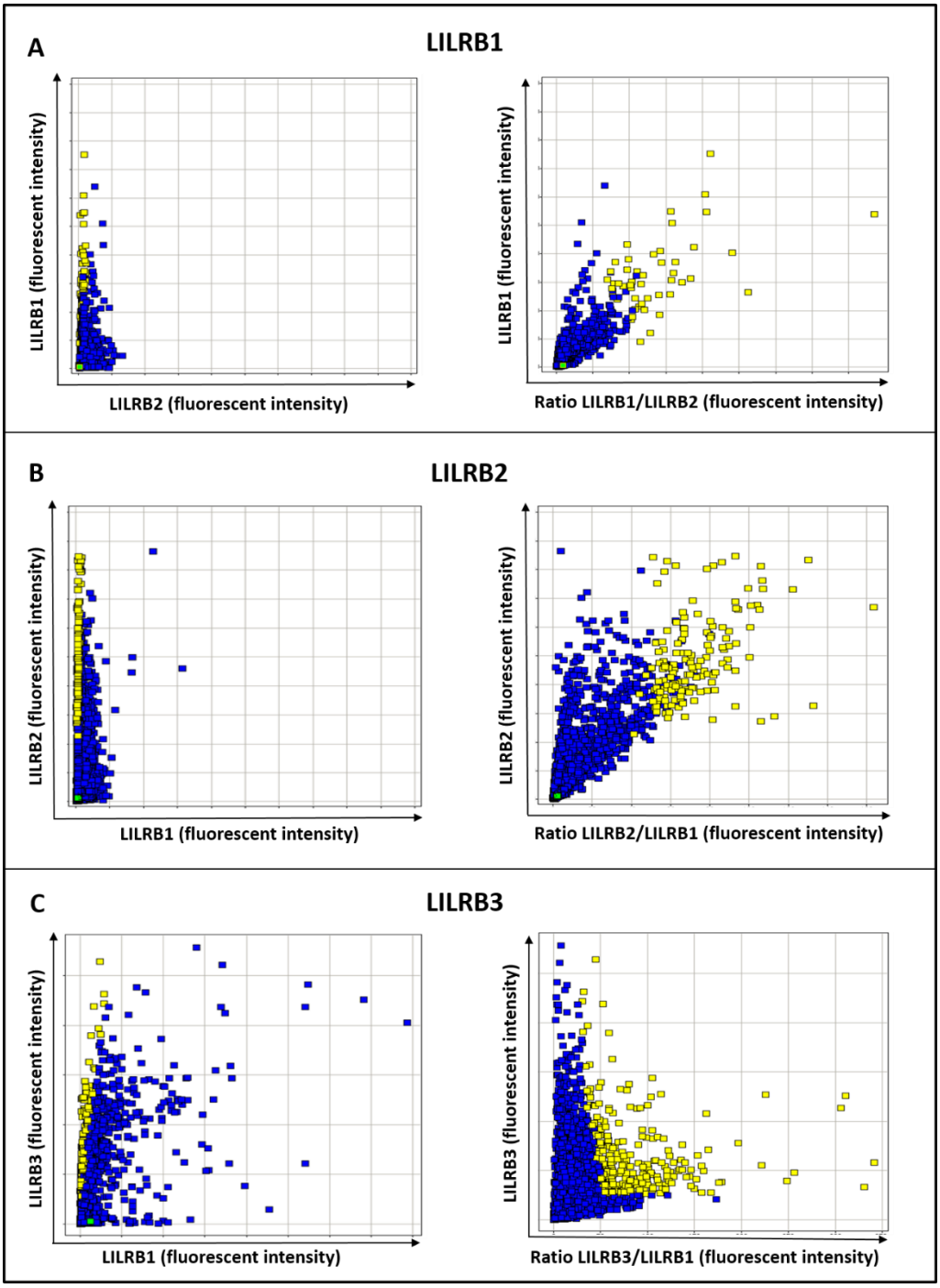

Figure 3.19 Evaluation of LILRB3, LILRB2 and LILRB1-specific clones by primary screening ELISA. 0.5 pmole of protein target (TAR) antigen or non-target (NOT) antigen were coated in a 384-well plate overnight at 4°C. The following day, 10 µL E. coli expression supernatant containing scFv was added for 1 hour at room temperature. Plates were washed and incubated with 50 µl mouse-anti-FLAG-AP antibody for 1 hour at room temperature, washed, CDPStar Emerald II luminescent substrate (Tropix) added for 30 minutes at room temperature, and luminescence read at 700 nM by the robotic ELISA system. Spotfire was used to analyse the data obtained and the target luminescence (y-axis) was plotted against its non-target luminescence (x-axis) graphically. The target (y-axis) was also plotted against a ratio of target/non-target (x axis). Clones in yellow represent active clones identified, and then 'cherry picked' (chosen based on their specificity and TAR/NOT ratio). A scFv-FITC8 control was included (green). **A)** LILRB3 was compared to its non-target LILRB1 and also to a ratio of target versus non-target. **B)** LILRB2 was compared to its non-target LILRB1 and also to a ratio of target versus non-target. **C)** LILRB1 was compared to its non-target LILRB2 and also to a ratio of target versus non-target.

In total, 3072 LILRB3 clones were analysed by ELISA, from which 1023 'active' (specific) clones were identified resulting in 261 'cherry picked' (chosen/selected) clones. 2304 LILRB2 clones were analysed by FMAT, from which 470 active clones were identified resulting in 144 'cherry picked' clones. 2304 LILRB1 clones were analysed by ELISA, from which 133 active clones were identified resulting in 48 'cherry picked' clones. This is summarised below (*Table 3.3*).

Table 3.3 Summary of clones chosen from ELISA primary screening

Target	Selection Strategy	No. of clones tested	Active clones	'Cherry picked' clones
TAR_LILRB3	3A	1536	450	94
TAR_LILRB3	3B	1536	573	167
TAR_LILRB2	3D	768	128	31
TAR_LILRB2	3E	768	145	34
TAR_LILRB2	3F	768	197	79
TAR_LILRB1	3G	768	56	14
TAR_LILRB1	3H	768	35	16
TAR_LILRB1	3I	768	42	18

Table 3.3 Clones chosen after primary screening ELISA. For each target and each selection strategy a set number of clones was tested. Active (specific) clones were chosen based on the isotype control and then clones were 'cherry picked', based on their specificity and lack of cross-reactivity, for the secondary screening.

Taking into account chosen clones from both the FMAT and ELISA screening, a total of 672 clones i.e. 7x96-well plates (384 LILRB3 clones, 192 LILRB2 clones and 96 LILRB1 clones) were cherry-picked for sequencing and re-screening again by FMAT and ELISA.

3.2.3.2 Secondary screening

The 672 scFv clones picked during the primary screening were then analysed again by FMAT and ELISA in the secondary screening (data not shown) to further reduce the number of clones. No recombinant LILRB4 protein was available for screening by ELISA as generating this protein is difficult due to poor transfection efficiency. However, LILRB4-transfected CHO-S cells were included in the secondary FMAT analysis on this occasion as a further non-target for all three targets (LILRB1, LILRB2 and LILRB3). For both the FMAT and ELISA less clones were taken forward into the secondary screening, thus narrowing down the target-specific clones.

LILRB1, LILRB2 and LILRB3-specific scFv clones that were identified and chosen in the primary screening were also sequenced commercially by GATC Biotech. The sequencing data was analysed using Sequencing Net (in house BioInvent programme) and imported into the Spotfire programme. From the sequencing data, unique clones were identified by their unique CDR sequence (data not shown). Clones with the same CDR sequence were given the same sequence identity and only one representative clone chosen - referred to as a "HIT" clone. These HIT clones were then further reduced in the secondary screening data, where unique cross-reactive clones were eliminated by FMAT and ELISA.

A total of 398 unique clones were identified through the secondary screening and sequencing data (216 unique LILRB3 clones, 111 unique LILRB2 clones and 71 unique LILRB1 clones). These clones were 'cherry picked' based on their ability to bind to the target specifically and not cross-react to non-targets.

The clones were then screened against PBMCs and again by LILR-CHO-S transfected cells, this time by flow cytometry, in a third round of screening, to further reduce the number of clones before IgG-conversion.

3.2.3.3 Tertiary screening

LILR receptors are found predominately on myeloid cells. Before performing the tertiary screen, phenotyping of myeloid cells (monocytes and granulocytes) and B cells was performed using commercially available LILRB1, LILRB2 and LILRB3 antibodies to deduce the expression profile of these receptors.

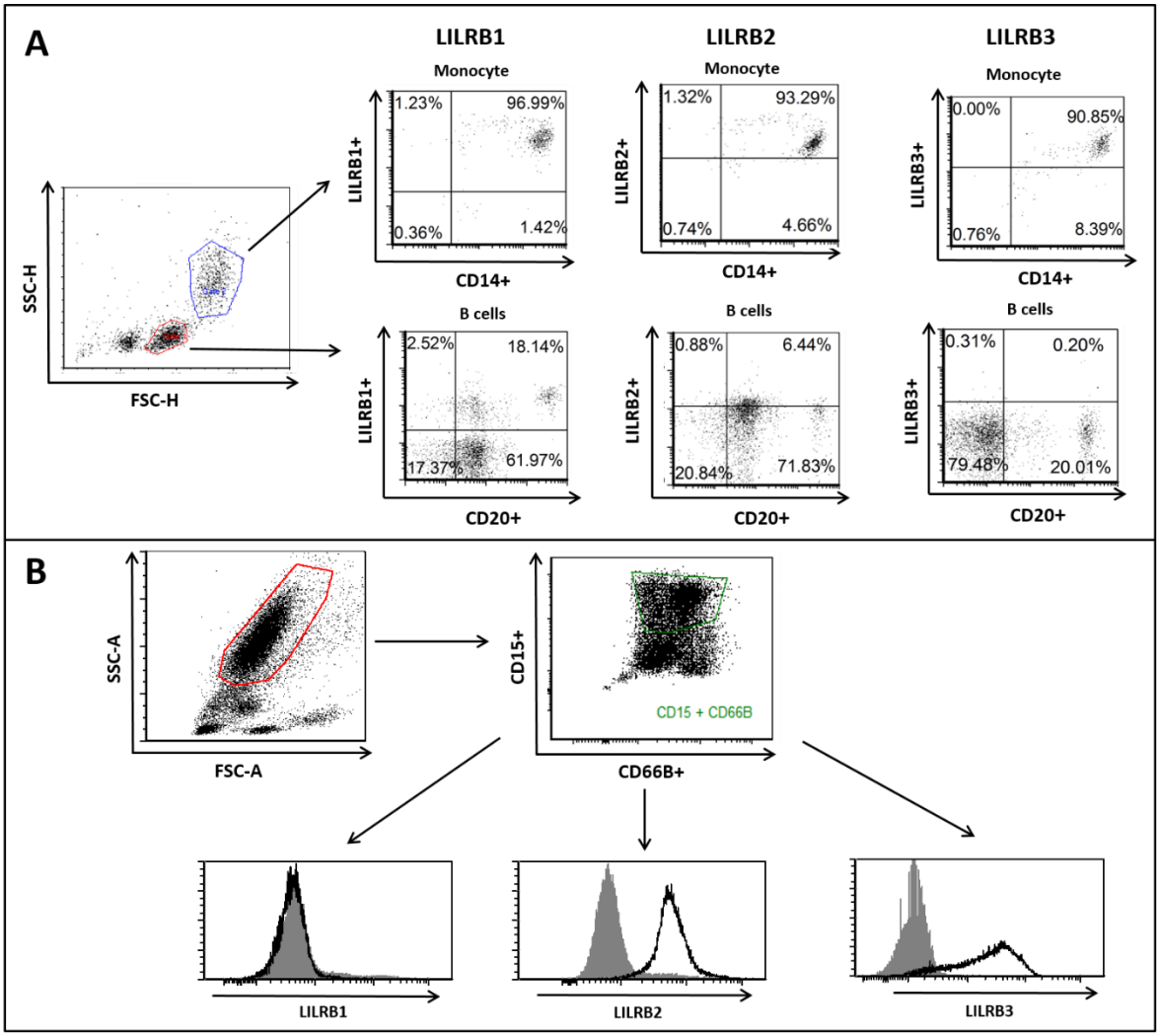

Figure 3.20 LILRB expression on myeloid cells and B cells. LILRB1, LILRB2 and LILRB3 staining was assessed on monocytes (CD14+), B cells (CD20+), and neutrophils (CD15+ CD66B+). **A) Staining of monocytes and B cells.** To stain monocytes and B cells PBMCs were blocked with human AB serum (2%) for 10 minutes, and then stained with LILRB1-PE (Beckam Coulter), LILRB2-PE (eBioscience) or LILRB3-APC (R&D systems) and either an anti-CD14-APC or PE (eBioscience) or anti- CD20-A488 or APC (Rituximab, in house) antibody for 30 minutes at 4℃, before being washed in RBC lysis buffer and FACS wash and then analysed by flow cytometry. **B) Staining of neutrophils.** To stain neutrophils, 100 µl whole blood was blocked with human AB serum (2%) for 10 minutes on ice, and then double-stained with either 5 µl/test LILRB1-PE (Beckam Coulter), LILRB2-PE (eBioscience) or LILRB3-APC (R&D systems), and neutrophil markers CD15-Pacific Blue (Biolegend) and CD66B-FITC (Biolegend) for 30 minutes at 4℃. Stained cells were then washed twice, first in 10% RBC lysis buffer (Serotec) and then FACS wash, and then analysed by flow cytometry. Histograms are representative plots of three experiments.

Phenotyping cells with commercially available antibodies revealed that LILRB3 was found to be expressed on myeloid cells including monocytes and neutrophils, but not lymphocytes such as B cells, as the literature suggests (*Figure 3.20*)[249]. Comparatively, both LILRB1 and LILRB2 showed expression on monocytes, but only LILRB1 showed expression on B cells, as expected. However, although no LILRB1 expression was found on neutrophils, LILRB2 was found to be expressed on these cells, which was unexpected (based on the literature) and could be due to poor antibody specificity of the commercially available antibody[39].

In conclusion, phenotyping different cells types with commercially available antibodies showed that LILRB1, LILRB2 and LILRB3 expression is predominately found on myeloid cells, namely monocytes, however, these antibodies may cross-react to other LILRs.

To further reduce the number of clones for IgG conversion, and to analyse each clone's ability to bind to 'real' cells by flow cytometry, a tertiary screening was performed. This would ensure that antibody clones that were able to bind to natural conformational epitopes found on primary cells (not just overexpressed transfected cells) were selected for.

Each unique scFv clone was tested for binding to PBMCs gated on monocytes (from two donors), as previous phenotyping (*Figure 3.20*) showed that all three LILR receptors are highly expressed on these cells. Target-specific LILR-transfected CHO-S cells were also included as a positive control. The scFv clones were detected by an anti-His-AF647 antibody and analysed using the high-throughput flow cytometer (HTFC).

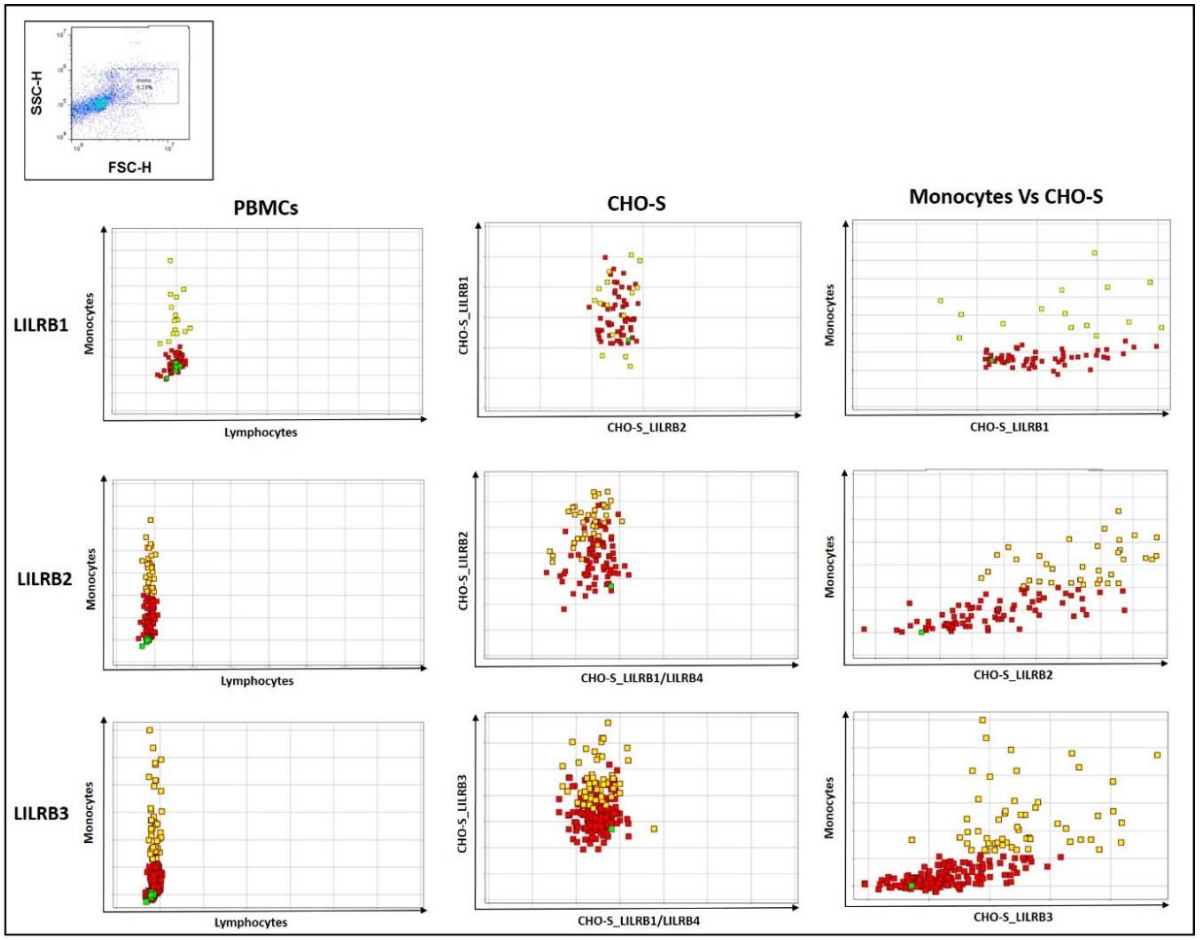

Figure 3.21 Evaluation of LILRB1, LILRB2 and LILRB3-specific clones by tertiary screening FACS analysis. PBMCs were blocked with human IgG at 4°C for 10 minutes. 25 µl scFv supernatant was added to a 96-well plate, and incubated with $0.5x10^6$ blocked PBMCs or LILR-transfected CHO-S cells for 1 hour, 4°C. The cells were washed and 1 µg/ml deglycosylated anti-His-AF647 was incubated with the cells for 1 hour, 4°C. The cells were washed again and analysed using the HTFC screening system (Intellicyte). LILRB1 and LILRB4-transfected CHO-S cells were used as non-targets for LILRB2 and LILRB3 whilst LILRB2-transfected CHO-S cells were used as non-targets for LILRB1. Antibody clones were also tested against gated monocytes from two different PBMC donors. The clones were then compared against both monocytes and target transfected CHO-S cells. Clones were graphically displayed in Spotfire, represented by red squares. Clones that were chosen are highlighted in yellow, and the anti-FITC isotype control in green.

Clones were chosen based on their ability to bind to monocytes, as well as their target, but not their non-target LILR-transfected CHO-S cells. Clones that were picked are displayed in yellow (in *Figure 3.21*). One LILRB3 scFv clone that bound to monocytes appeared to bind to non-target CHO-S cells, possibly LILRB4-transfected cells (as these were not included in the original selections). However, the majority of scFv clones chosen that bound to monocytes were also able to specifically bind to their target-specific CHO-S cells.

After completing the tertiary screening, 101 clones were chosen and converted to a full IgG format. However, 6 clones were not compatible with the BioInvent standard IgG conversion method, due to the presence of current restriction cleavage sites in the CDR´s. This left 95

clones to be converted, of which 89 were successfully converted (46 LILRB3, 32 LILRB2 and 11 LILRB1 clones).

The number of clones produced throughout the antibody generation process are displayed below in Table 3.4.

Table 3.4 Summary of unique clones produced

Target	Number of clones after:					
	Selections	Screening			IgG conversion	Successfully converted
		Primary	Secondary	Tertiary		
LILRB3	6144	384	216	54	51	46
LILRB2	3456	192	111	36	33	32
LILRB1	3456	96	71	11	11	11
Total	**13,056**	**672**	**398**	**101**	**95**	**89**

Table 3.4 Number of scFv clones throughout antibody generation. Table shows the number of scFv clones at the start of each stage for all three targets: LILRB1-3, and the total number of clones that were chosen.

In conclusion 89 antibody clones were successfully generated and converted to IgG: 46 LILRB3, 32 LILRB2 and 11 LILRB1 clones. These clones specifically bound to target, but not non-target cells and/or protein, and displayed unique CDR sequences.

3.3 Discussion

The aim of this chapter was to generate antibodies against LILRB1, LILRB2 and LILRB3 by phage display technology. Reagents for this process were successfully generated and their quality and compatibility with the phage display techniques were confirmed. After these quality control checks, the reagents were used in the selections and screening showed that LILRB1-, LILRB2- and LILRB3-specific scFv antibodies were generated.

Both the ELISA and flow cytometry analysis of the phages, performed after each round of the selections showed successful enrichment of target-specific phages.

Despite the atypical ELISA curves (that were not the “typical” sigmoidal shape – likely due to the pool of binding phage/antibodies with different affinities against each target antigen) the ELISA data showed target-specific enrichment. LILRB1 clones showed enrichment between selection 1 and 2, but there did not appear to be any further enrichment between selection 2 and 3; suggesting selection 3 failed for this target. This was later supported by the fact that a

reduced number of unique clones were found for LILRB1 compared to LILRB2 and LILRB3. The reason for this failure is unclear, but could have been due to technical errors. A fourth selection could have been performed to increase the number of target-specific binding clones identified in the screening. However, there is a possibility the diversity of the clones may have reduced if a fourth selection was carried out, as high-binding clones would be preferentially selected for. Instead, repeating selection 3 in this instance would have been a more ideal solution to ensure diversity of the clones was maintained. Generally, the more selection rounds that are used in the selections, the greater the likelihood of selecting for the same high affinity binding phages each time, thus reducing the amount of variability and diversity of unique clones in the phage pool. Therefore, three selection rounds is a good compromise between enriching for target-specific binders whilst maintaining the diversity of the unique clones identified, and avoiding selecting for the same single clone.

It should be noted that although ELISA analysis of the phages for LILRB1 indicated that all LILRB1 strategies in selection 3 failed (3G, 3H and 3I), flow cytometry analysis of the phages showed otherwise, as target-specific enrichment for all targets and all strategies used for each target was observed (*Figure 3.14*). Flow cytometry analysis thereby suggested that the LILRB1 selections did not fail; in particularly, regarding the third strategy of the LILRB1 selections (3I), which involved the target on cells. As the target on cells, displayed the receptor in its 'natural' format, cell-binding epitopes could have been more exposed and therefore more favourable, causing clones that preferentially bind to cells rather than soluble protein to be selected. This could explain why the flow cytometry data after selection 3, suggested anti-LILRB1 enrichment, whilst the ELISA data did not.

In summary, despite a lack of enrichment for LILRB1 from the ELISA data, the flow cytometry data showed some enrichment. Therefore, combining both the phage ELISA and flow cytometry analysis, successful enrichment of target-specific scFv clones for all three LILR targets was achieved.

Both the ELISA and FMAT primary screening data indicated that LILRB3 and LILRB2 selections had been successful and many target-specific "active" clones were identified. As with the phage ELISA data, the primary screening ELISA data also resulted in less LILRB1 "active" clones identified compared to the LILRB2 and LILRB3 clones (*Table 3.3*). However, as with the phage flow cytometry data, the FMAT data did show an enrichment in clones produced (*Figure 3.17*). Despite the same number of clones being screened (1152 clones) in the cell selection strategies for LILRB1 (3I) and LILRB2 (3F) the FMAT screening data shows that more LILRB1 clones (101 active clones) were identified compared to LILRB2

clones (80 active clones) (*Table 3.2*). This reinforces the phage flow cytometry analysis (*Figure 3.14*) that indicated the LILRB1 cell selection strategy was successful, and that cell-binding LILRB1 clones were likely favoured compared to soluble LILRB1-binding clones. Thus, more LILRB1 clones from strategy 3I were taken forward through to the secondary screening.

The tertiary screening identified that whilst there were many clones that bound specifically to target-specific transfected CHO-S cells, as well as monocytes, there were still some clones that appeared to be either non-specific or non-cell binding. As clones were screened against both a protein-based (ELISA) and cell-based (FMAT) technique, it is not surprising that some clones did not appear to be cell binding.

A total of 101 unique clones were identified for all three targets after three screening rounds – a large number of clones that still included many non-specific clones. The number of unique and specific clones found by phage display is governed by many different factors. Firstly, the number of unique clones identified depends on the target antigen used. For example: the size of the protein, the proportion of exposed protein epitopes and the quality and purity of the antigen all affect the number of unique clones that will be found. Another factor is the presence of "immunogenic" epitopes i.e., epitopes that antibodies are more likely to bind to because they are more exposed compared to other epitopes. Therefore, the greater number of these epitopes found in LILRs, the greater the amount of unique clones identified. LILRs are believed to be heavily glycosylated. Heavily glycosylated proteins have less protein surface/epitopes for phages to bind too. This suggests that the expected number of unique clones identified should be low. On the contrary, LILRs have large extracellular domains that provide a large surface area for binding, therefore promoting the number of unique clones that can be identified.

Secondly, the number of unique clones identified can depend on the type and the number of different strategies used in the selections. The three strategies used in this project were chosen based on previous successful selections at BioInvent. The selection strategies used could have been more complex, e.g. other species could have been included in the selections as non-targets – such as, cynomologous (monkey) or mouse, which have receptors baring high sequence homology with the human LILRs. This would have further reduced the number of unique clones, but ensured the antibodies generated did not cross-react with other species. This would be ideal for *in vivo* studies, such as testing these human antibodies in LILR Tg mice, which would allow the antibody effects seen to be attributed to a response between the

human LILRs and their antibodies, and not due to cross-reactivity with mouse PIRs for example.

Thirdly, the concentration of antigen used in the selections can also influence the number of unique clones identified. A higher concentration of target antigen will result in the selection of low affinity binding clones, whilst lower antigen concentrations (especially in later selection rounds) will decrease the diversity of unique clones and favour high affinity antibody clones. For biotinylated protein targets in solution, the concentration was reduced as more selections were completed, to promote selection of high affinity binding clones.

The method of screening chosen and the criteria set for the clones to be 'cherry picked' also influences the number of unique clones that will be retrieved. In this screening campaign two different screening techniques (protein and cell-based) were used that allowed clones to be picked with different binding properties, increasing the diversity of the clones selected.

Finally, the diversity of the clones may also be influenced by the amplification of the clones in bacteria. Some clones may have an advantage during the amplification in bacteria, creating biases for selection. If this occurs the overall repertoire of clones that are eluted may decrease due to a few "dominating" clones being present after amplification (as there are more copies of these clones and therefore a larger amplification degree for these). The dominating clones overpower the rest in the next selection even though they may have the same affinity as other less dominating clones.

In this chapter, the selections and screening methods used were chosen based on the properties of the target antigen, and previous successful antibody generation at BioInvent. These techniques are comparable with other techniques used. Utilising more than one selection strategy ensures genetic diversity of the antibodies produced, as previously shown by Lou *et al*, who found that using different methods to screen against the same antigens, produced different numbers of antibodies, indicating that more than one method is required to ensure all types of diversities are selected for[207]. A scFv library was used, although Fabs dimerise less than scFvs, scFvs are less toxic on cells (therefore increasing the yield and diversity of clones produced), and despite success with both libraries, scFv libraries are more common[205]. The first scFv library produced from peripheral blood lymphocytes (PBLs) was made up of more than 10^7 clones, within 5 years this had increased to more than 10^{10} clones[205]. BioInvent's scFv library has 10^9 clones, therefore making it a large library, increasing the diversity and larger number of possible unique clones[248]. The library is made up of human B cells from many donors, with CDR recombination by overlap extension PCR

creating the diversity[248]. The target antigen determined how the selections were performed. BioInvent have reported that two selection rounds can often be sufficient for some targets, and increasing the number of selections can result in a reduction in variability. However, three selections have been found to be optimal (personal communication with BioInvent). Analysing target enrichment by flow cytometry and ELISA allowed target enrichment to be identified, and whether another selection round was needed. Introducing a different antigen format can counteract "selection-related" binding phages. For example, the target protein was immobilised in the third selection strategy for the first two selections, then in selection three, the target was displayed on cells. This prevented phage binders with a bias for a particular strategy being enriched. Through previous selections, BioInvent have found they yield better clones when using biotinylated proteins with streptavidin magnetic beads (personal communication with BioInvent). This is likely due to the strong bonds between biotin and streptavidin. However, running more than one selection strategy is important to ensure successful enrichment.

Since the introduction of phage display libraries in 1985 for screening peptide fragments, and then later antibody fragments in 1990, the size and diversity of these libraries has continued to grow[203, 250]. However, these libraries are restricted by the fact they rely on amplification in bacterial cells[205]. New libraries, such as ribosomal libraries, first described by Mattheakis in 1994, where target proteins bind to mRNA instead of antibody fragments displayed on phages, are therefore a possible alternative[251]. These libraries do not require amplification in bacterial cells, therefore selections are not limited by the transformation efficiency in these cells, and larger libraries of up 10^{14} clones are possible, thus providing more diversity[252].

In conclusion, the selections may not have been vigorous enough and more selection pressures could have been needed to really narrow down the number of specific and unique clones obtained. On the other hand, the selection strategies chosen provide a compromise between acquiring as many unique clones as possible, whilst maintaining the diversity of the clones discovered. Unique clones were identified against the desired targets, therefore the selections were a success in this instance.

4 CHARACTERISING PANELS OF ANTIBODIES DIRECTED TO LILRB1, LILRB2 OR LILRB3

4.1 Introduction

Antibodies against LILRB1, LILRB2 and LILRB3 inhibitory immune receptors were generated by proprietary phage display technology, in collaboration with BioInvent International AB, Sweden. These antibody clones were produced using a scFv library. After initial screening of the clones produced, a total of 89 clones were produced to a fully human IgG format: 46 LILRB3, 32 LILRB2 and 11 LILRB1 clones.

In this chapter, characterisation of the generated antibodies was performed. These antibody clones were characterised and tested *in vitro* to re-confirm their target specificity, as well as their lack of cross-reactivity to the homologous mouse PIR-B receptor, binding affinity, mapping their epitope binding sites and their tissue expression. Different antibodies against the same target were found to bind to different domains of the receptor and have different binding affinities.

Characterisation of these antibodies will help elucidate LILR function, and whether these clones hold agonistic or antagonistic potential. This in turn will indicate their use in therapy.

4.2 Results

4.2.1 Antibody specificity reconfirmed against transfected cell lines

4.2.1.1 Confirming specificity against LILRB1-, LILRB2- and LILRB3-transfected HEK 293T cells

Firstly, the antibodies generated as IgG were re-tested for specificity to their target receptor; testing each clone for binding to LILRB1, LILRB2 or LILRB3-HEK 293T stably transfected cells. A selection of the results are shown in *Figure 4.1*, and a summary table of the specificity against all 89 generated clones is displayed in *Table 4.1*.

Figure 4.1 shows binding specificity of representative LILR antibodies against LILRB1/2/3-transfected HEK 293T cells. Clones were named accordingly: A represents LILRB3 clones, B LILRB2 clones and C LILRB1 clones, followed by a specific number allocated to each clone.

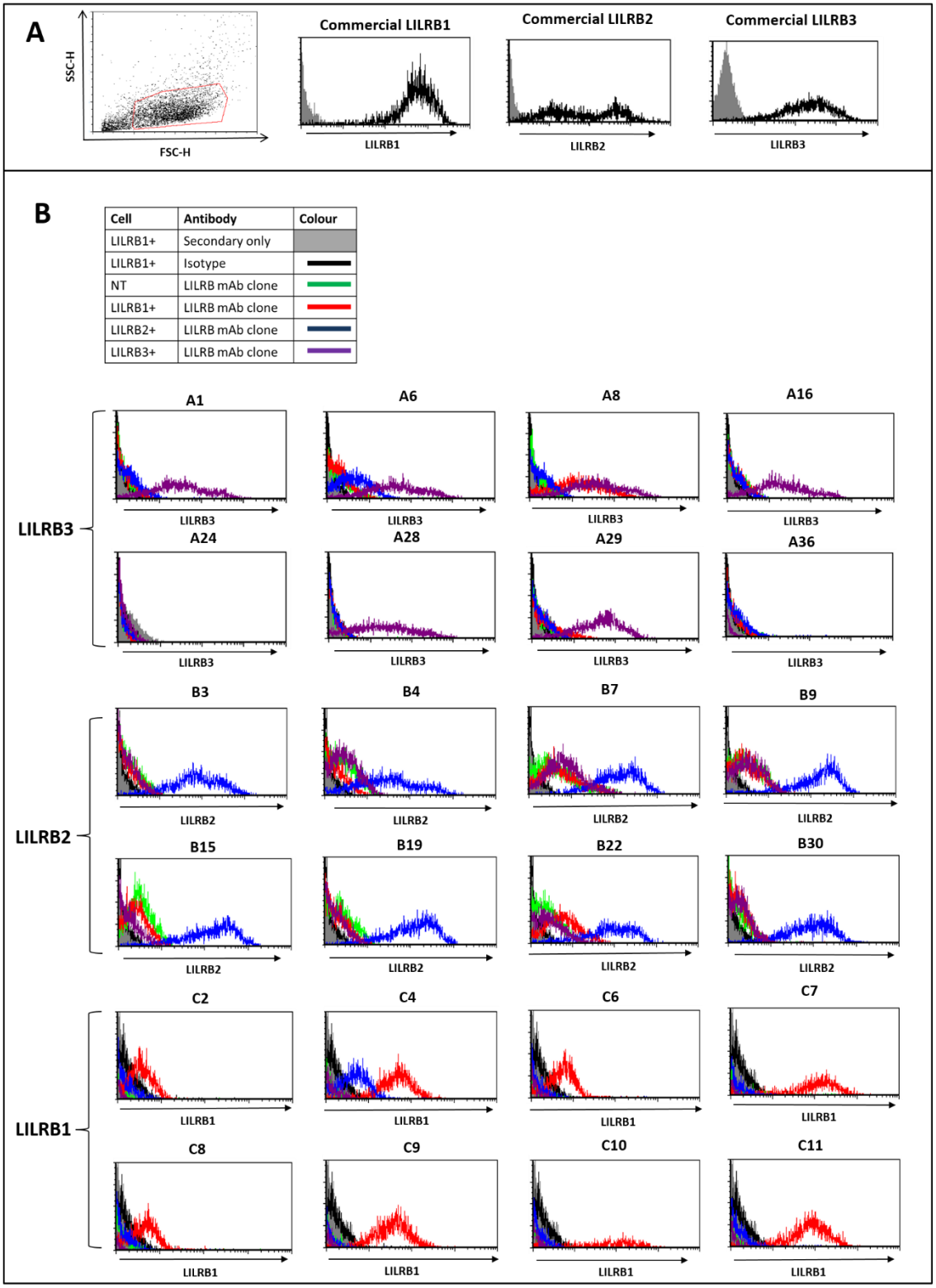

Figure 4.1 Specificity of LILRB1, LILRB2, LILRB3 clones. Converted IgG clones were tested to reconfirm specificity against LILRB1, LILRB2 and LILRB3-transfected HEK293T cells. 1x10^5 non-transfected (NT)-, LILRB1-, LILRB2- and LILRB3-transfected HEK293T cells were stained with commercial anti-LILRB1 (eBioscience), -LILRB2 (eBioscience), -LILRB3 (R&D Systems) in **A)** or 10 µg/ml anti-LILRB1, -LILRB2 and -LILRB3 generated IgG antibody clones (BioInvent) or relevant isotype controls in **B)**, for 30 minutes at 4℃, and washed twice. Cells were then stained with a secondary anti-human hFc PE-conjugated antibody (Jackson Labs) for 20 minutes at 4℃ and measured by flow cytometry. **A)** Gating strategy and commercial antibody staining (black) compared to isotype (grey) **B)** Generated LILRB3, LILRB2 and LILRB1 clones tested.

Table 4.1 Re-confirming antibody specificity against LILR-transfected HEK 293T cells

Target	Clone	HEK 293T		Target	Clone	HEK 293T	
		Specific?	Cross-reactive			Specific?	Cross-reactive
LILRB3	A1	Yes	-	LILRB3	A46	Yes	-
LILRB3	A2	Yes	-	LILRB2	B1	Yes	-
LILRB3	A3	Yes	-	LILRB2	B2	Yes	-
LILRB3	A4	Yes	-	LILRB2	B3	Yes	-
LILRB3	A5	Yes	-	LILRB2	B4	No	B1, B3, NT cells
LILRB3	A6	No	B2	LILRB2	B5	No	B3, NT cells
LILRB3	A7	Yes	-	LILRB2	B6	No	B1, B3, NT cells
LILRB3	A8	No	B1	LILRB2	B7	No	B1, B3, NT cells
LILRB3	A9	Yes	-	LILRB2	B8	Yes	-
LILRB3	A10	Yes	-	LILRB2	B9	No	B1, B3, NT cells
LILRB3	A11	Yes	-	LILRB2	B10	Yes	-
LILRB3	A12	Yes	-	LILRB2	B11	Yes	-
LILRB3	A13	Yes	-	LILRB2	B12	Yes	-
LILRB3	A14	Yes	-	LILRB2	B13	Yes	-
LILRB3	A15	Yes	-	LILRB2	B14	Yes	-
LILRB3	A16	Yes	-	LILRB2	B15	Yes	-
LILRB3	A17	No	B1, B2, NT cells	LILRB2	B16	Yes	-
LILRB3	A18	Yes	-	LILRB2	B17	Yes	-
LILRB3	A19	Yes	-	LILRB2	B18	No	B3, NT cells
LILRB3	A20	Yes	-	LILRB2	B19	Yes	-
LILRB3	A21	Yes	-	LILRB2	B20	Yes	-
LILRB3	A22	Yes	-	LILRB2	B21	Yes	-
LILRB3	A23	Yes	-	LILRB2	B22	No	B1, B3, NT cells
LILRB3	A24	No	No staining	LILRB2	B23	Yes	-
LILRB3	A25	N o	B1, B2, NT cells	LILRB2	B24	Yes	-
LILRB3	A26	Yes	-	LILRB2	B25	Yes	-
LILRB3	A27	Yes	-	LILRB2	B26	Yes	-
LILRB3	A28	Yes	-	LILRB2	B27	Yes	-
LILRB3	A29	Yes	-	LILRB2	B28	No	B1, B3
LILRB3	A30	Yes	-	LILRB2	B29	Yes	-
LILRB3	A31	Yes	-	LILRB2	B30	Yes	-
LILRB3	A32	Yes	-	LILRB2	B31	Yes	-
LILRB3	A33	Yes	-	LILRB2	B32	Yes	-
LILRB3	A34	Yes	-	LILRB1	C1	Yes	-
LILRB3	A35	Yes	-	LILRB1	C2	Yes	Low staining
LILRB3	A36	No	No staining	LILRB1	C3	Yes	-
LILRB3	A37	Yes	-	LILRB1	C4	No	B1
LILRB3	A38	Yes	-	LILRB1	C5	Yes	-
LILRB3	A39	Yes	-	LILRB1	C6	Yes	Low staining
LILRB3	A40	Yes	-	LILRB1	C7	Yes	-
LILRB3	A41	Yes	-	LILRB1	C8	Yes	Low staining
LILRB3	A42	Yes	-	LILRB1	C9	Yes	-
LILRB3	A43	Yes	-	LILRB1	C10	Yes	-
LILRB3	A44	Yes	-	LILRB1	C11	Yes	-
LILRB3	A45	No	B1, B2, NT cells				

Table 4.1 IgG specificity re-confirmed by flow cytometry. 10 μg/ml antibody stained LILR-transfected HEK 293T. LILRB1 clones given nomenclature C, LILRB2 clones B and LILRB3 clones A, followed by an allocated number. (-) indicated no cross-reactivity, whilst NT, B1, B2 and B3 represent cross-reactivity to non-transfected, LILRB1, LILRB2 and LILRB3-transfected cells respectively.

Table 4.1 shows that the majority of the antibodies produced were found to be specific, as expected, as these clones were chosen based on their lack of cross-reactivity. Examples of specific clones include LILRB3 clones A1, A16, A28 and A29; LILRB2 clones B3, B15, B19 and B30; and LILRB1 clones C7, C9, C10 and C11 shown in *Figure 4.1*.

Both *Figure 4.1* and *Table 4.1* show that only 5 LILRB3 clones were found to be non-specific (A6, A8, A17, A25 and A45), and two appeared to have no staining (A24 and A36). However, A17, A25 and A45 were found to also bind to non-transfected HEK293T cells, indicating they may be 'sticky', binding to the cells themselves, rather than cross-reactive. Only 8 LILRB2 clones were cross-reactive (B4, B5, B6, B7, B9, B18, B22 and B28 – see appendix for full list of characterisation), however, although these clones appeared to bind to either LILRB1 or LILRB3-transfected 293T cells, all of these clones also showed binding to the non-transfected cells (as seen with B4, B7, B9 and B22 in *Figure 4.1*). This indicates that these clones may have been binding to something on the cells themselves, or just very "sticky". All of the LILRB1 clones were found to be specific (*appendix*), except one clone, C4, which showed binding to LILRB2-transfected cells (shown in *Figure 4.1*). Three clones showed very low binding to the LILRB1-transfected 293T cells (C2, C6, and C8), suggesting these clones are of low affinity.

Therefore, 39/46 LILRB3, 24/32 LILRB2, and 10/11 LILRB1 clones, were found to be target-specific.

4.2.1.2 Confirming specificity against LILR-2B4 transfected reporter cells

After re-confirming specificity against transfected cells, to confirm these findings but also to screen against a larger repertoire of related receptors, the generated LILR clones were then screened against a panel of LILR activatory and inhibitory receptors. During both the selection and screening process of antibody generation, the clones were produced using only other inhibitory LILR receptors as non-targets, and therefore lack of cross-reactivity to other receptors could not be presumed. 2B4 reporter cells were transfected with a whole panel of LILR receptors containing the extracellular domain of the different LILRs, and intracellular CD3 to produce signalling. Each antibody clone was tested against 8 different LILR receptors (LILRA1, LILRA2, LILRA5, LILRB1, LILRB2, LILRB3, LILRB4 and LILRB5), and control non-transfected 2B4 cells. Representative clones are displayed below in *Figure 4.2*.

Figure 4.2 Confirming specificity of LILRB1, LILRB2, LILRB3 clones with 2B4 reporter cells. 10 µg/ml of the generated anti-LILRB1, LILRB2 and LILRB3 antibodies were incubated with LILR-A1, -A2, -A5, -B1, -B2, -B3, -B4 and -B5 2B4 reporter cells or non-transfected 2B4 cells (2B4) at 37°C, 5% CO_2, overnight. The following day, the cells were washed and stained with a secondary α-human PE antibody (Jackson Labs) at 4°C, for 45 min. The cells were washed and samples analysed for binding by flow cytometry. These assays were performed by Dr Des Jones, *University of Cambridge*.

16/46 anti-LILRB3 clones were found to be specific (*see appendix for all clones*) and one clone showed no staining (A24), which was shown previously when tested against 293T cells (*Figure 4.1*). As seen previously all of the LILRB3 clones displayed here appeared to be specific, except A13 which showed staining on LILRA5- and LILRB5-transfected cells, both of which were not screened against previously (*Figure 4.2*). A35 also showed some cross-reactivity to LILRB1- and LILRB2-transfected cells (as well as other LILRs), which was not seen previously (Table *4.1*). However, A35 also appeared to bind to non-transfected 2B4 cells, indicating that this clone may not be cross-reactive to other receptors, but instead was binding to something expressed on the parental cells themselves (*Figure 4.2*).

All of the LILRB2 clones shown here appeared be binding to the LILRB3-transfected cells, indicating they are cross-reactive to the LILRB3 receptor, however, due to the high expression of LILRB3 (confirmed with an antibody against the HA tag – *Figure 4.2*), it could be that the antibodies are just 'sticking' to these overexpressed cells. This is further supported by initial screening, where the same clones were screened against LILRB3-transfected HEK 293T cells, but showed no cross-reactivity to LILRB3 (*Figure 4.1*).

As seen with the LILRB2 clones, LILRB1 clones C9 and C10 also showed some cross-reactivity to LILRB3. Again, this could have been the result of the high expression of LILRB3 on the 2B4 cells. LILRB1 clone C7, and C9 both showed cross-reactivity to activatory LILRA1.

Therefore, all the clones represented above generally lack cross-reactivity to other inhibitory LILR receptors - most of the binding seen may likely be due to binding of the mAbs to the transfected cells themselves, or overexpression of the LILRs on the transfected cells resulting in a high background. Instead, the only cross-reactivity seen in these clones appears to be against activatory LILR receptors. Activatory LILR receptors were not including in either the selection or screening process of the antibody generation, and this could have resulted in the co-selection of cross-reactive clones. Notably, LILRA3, LILRA4 and LILRA6 were not represented in this panel due to poor transfection efficiency (data not shown) and therefore cross-reactivity to these receptors cannot be ruled out. LILRA6 in particular has a very high homology to LILRB3, and the two receptors are almost identical extracellularly (the receptors have >95 % identity), therefore it is likely that the LILRB3 clones may bind to this activatory LILR receptor also[78].

4.2 Summary table of antibody specificity

Target	Clone	Specificity			
		HEK 293T		2B4 reporter cells	
		Specific?	Cross-reactivity	Specific?	Cross-reactivity
LILRB3	A1	Yes	-	Yes	-
LILRB3	A13	Yes	-	No	A5, B5
LILRB3	A16	Yes	-	Yes	-
LILRB3	A20	Yes	-	Yes	-
LILRB3	A28	Yes	-	Yes	-
LILRB3	A29	Yes	-	Yes	-
LILRB3	A35	Yes	-	No	A5, B1, B2, B4, B5, cells
LILRB2	B3	Yes	-	Yes	B3
LILRB2	B15	Yes	-	Yes	B3
LILRB2	B19	Yes	-	Yes	B3
LILRB2	B30	Yes	-	Yes	B3
LILRB1	C7	Yes	-	No	A1
LILRB1	C9	Yes	-	No	A1, B3
LILRB1	C10	Yes	-	No	B3

Table 4.2 Re-confirming antibody-specificity by screening against transfected cell lines. Cross-reactivity against LILR receptors was tested by screening antibodies against LILR-transfected HEK 293T or 2B4 cell lines. "Clones" refer to antibody clone names, whilst cross-reactivity refers to antibodies that stained LILR-transfected cell lines (LILR-A1, -A2, -A5, -B1, -B2, -B3, -B4 and -B5), non-transfected cells referred to as "cells" or if clones stained only target-specific cells (-).

Table 4.2 summarises the data from both *Figure 4.1* and *4.2* showing antibody-specificity against both HEK 293T-transfected cells and the 2B4-transfected reporter cells. The majority of the LILRB3 clones represented above were specific, except A13 which cross-reacted with LILRA5 and LILRB5. A35 displayed some stickiness to the 2B4 cells. This could explain the staining seen on various other LILR-transfected cells for this clone, and therefore A35 is likely to be specific.

All the LILRB2 clones showed binding to the LILRB3-transfected 2B4 cells but this was not seen in the original screening against LILRB3-transfected HEK 293T cells, suggesting that the overexpression of LILRB3 on the 2B4 reporter cells could account for the high background staining.

Finally, although the LILRB1 clones appeared to be specific against the HEK 293T cells, they showed some cross-reactivity to the LILRB3-transfected 2B4 cells, which could again be accounted for by the high expression of LILRB3 on these cells. However, the clones C7 and C9 showed some staining of LILRA1-transfected 2B4 cells. It is likely that this is real, as the generated clones were picked for their target specificity to their inhibitory LILR targets, but activatory LILRs were not accounted for during the generation process.

In summary, all the clones represented above were re-confirmed to specifically recognise their inhibitory LILR target antigens, however, some of these clones may cross-react with activatory LILR receptors.

4.2.1.1 Testing cross-reactivity of generated anti-human LILRB1/2/3 antibodies with mouse PIR-B

After confirming that target-specific and non-cross reactive clones were generated against human LILRs, the antibody clones that were found to be specific to their human targets were then tested for cross-reactivity to the mouse homolog PIR-B. Blocking of PIR-B was tested by firstly incubating wild-type mouse blood with the human anti-LILRB clones, then the PIR-B conjugated secondary antibody. In theory, blocking of PIR-B expression implicated that the human LILRB clones were binding to the same epitopes as the PIR-B antibody.

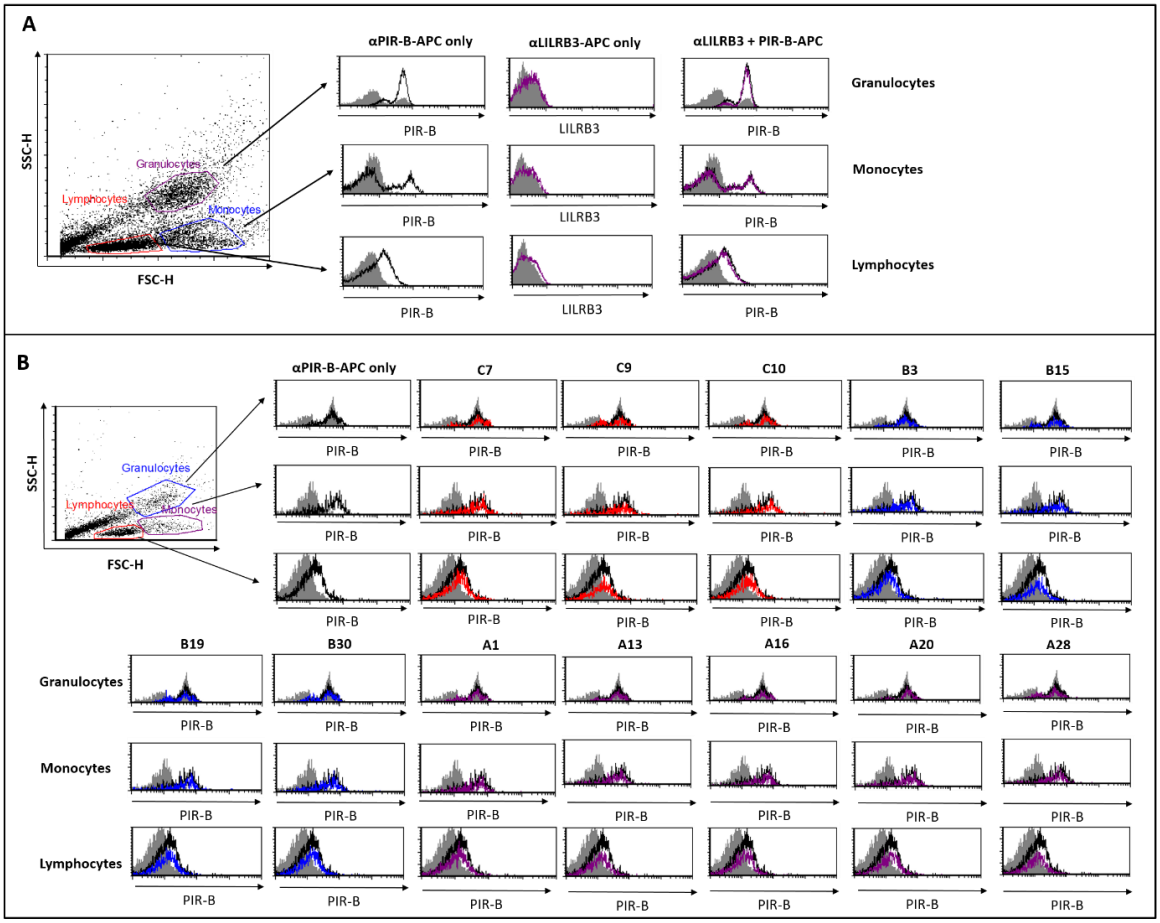

Figure 4.3 Testing cross-reactivity of generated anti-human antibody clones to the homologous mouse PIR-B receptor. Wild-type C57BL/6 mouse blood was stained with 10 µg/ml LILRB1, LILRB2 and LILRB3 clones for 30 minutes, 4 °C, and then PIR-B-APC (R&D systems) was added for 25 minutes, 4°C, cells washed twice and then analysed by flow cytometry. LILRB1 clones are represented in red, LILRB2 clones in blue, LILRB3 in purple, PIR-B in black and isotype control in grey, gated on granulocytes, monocytes or lymphocytes. Representative data of n = 3. PIR-B and commercial clone 222821 (R&D systems) were tested by single and double staining in A) and double staining of PIR-B and generated anti-LILR clones tested in B).

The commercial anti-LILRB3 antibody (clone 222821, R&D Systems) showed no binding to mouse blood, and was unable to block PIR-B staining (*Figure 4.3A*), implicating that the antibody does not cross-react with mouse PIR-B. Similar results were seen for all other tested LILRB clones (Figure 4.3B), which also did not block PIR-B staining. In summary, the clones represented here do not cross-react with mouse PIR-B.

4.2.2 LILR expression on healthy donors

After confirming LILR antibody clones showed no cross-reactivity to mouse PIR-B and were target-specific when screened against LILR-transfected cell lines, binding to normal human blood cells was assessed. To do this, representative antibodies for LILRB1, LILRB2 and LILRB3 were selected based on their specificity and lack of cross-reactivity to other LILR receptors and PIR-B. These antibodies were then allophycocyanin (APC)-labelled and used to stain various human blood cell types. Cells were stained with APC-labelled clones C7 (LILRB1), B3 (LILRB2) and A16 (LILRB3).

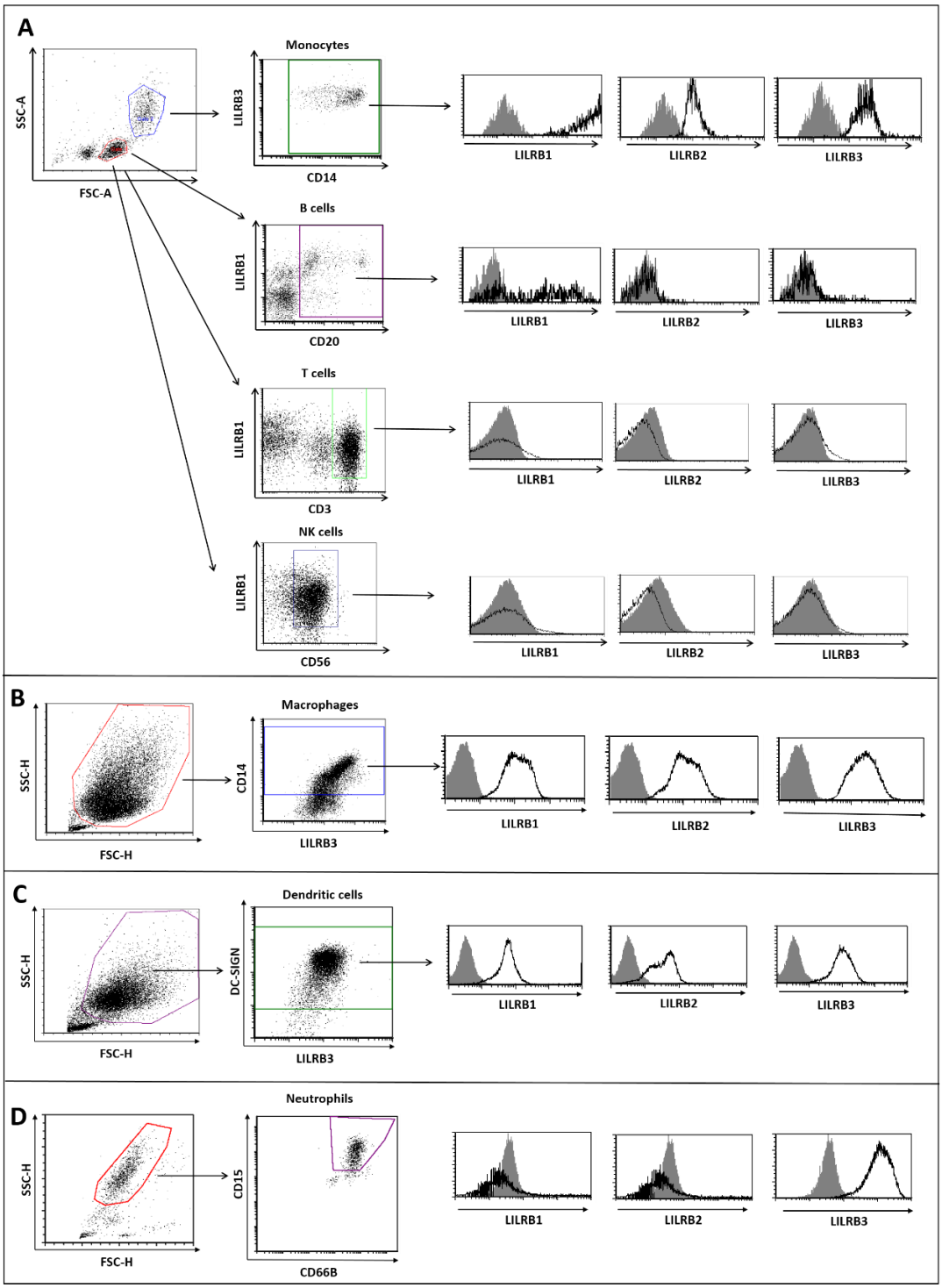

Figure 4.4 LILRB expression assessed on myeloid and lymphoid cells. All cells were blocked with 2% human AB serum for 10 minutes and then stained with either APC-labelled A16 (LILRB3), B3 (LILRB2), C7 (LILRB1) or hIgG1 isotype (BioInvent) alongside the following cell surface markers: **A) Staining of PBMCs**. PBMCs were stained with anti-CD14-PE (eBioscience), anti- CD20-A488 (Rituximab, in house), anti-CD3-PE-Cy7 (Biolegend) or anti-CD56-APC-Cy7 (Biolegend). **B) Staining of monocyte-derived macrophages (MDMs).** MDMs were stained with anti-CD14 (eBioscience). **C) Staining of monocyte-derived dendritic cells (MDDCs).** MDDCs were stained with DC-SIGN. **D) Staining of neutrophils**. 100 µl whole blood was blocked with human AB serum (2%) for 10 minutes on ice, and then stained with neutrophil markers CD15-Pacific Blue (Biolegend) and CD66B-FITC (Biolegend). All cells were stained for 30 minutes at 4℃ and then were washed twice, first in 10% RBC lysis buffer (Serotec) and then FACS wash, before being analysed by flow cytometry. Histograms are representative plots of one-nine donors.

PBMCs were isolated from blood cones and monocytes, B cells, T cells and NK cells identified. Neutrophils were stained from whole blood. MDM and MDDCs were both differentiated from monocytes by M-CSF or IL-4 and GM-CSF, respectively. Different cell types were identified by different cell markers. Monocytes and macrophages (MDMs) were classed as $CD14^+$, B cells as $CD20^+$, T cells as $CD3^+$, NK cells as $CD56^+$, MDDCs as DC-$SIGN^+$, and neutrophils as both $CD15^+$ $CD66B^+$.

Figure 4.4 shows that the anti-LILRB1 clone C7 stained monocytes, B cells, MDMs, MDDCs, but not T cells, NK cells or neutrophils. LILRB1 staining was highest on monocytes, followed by B cells (n = 9). Equal staining was seen on MDMs and MDDCs. Little or no staining was seen on T cells, NK cells or neutrophils. The literature states that LILRB1 has been found to be expressed on both T cells and NK cells, although admittedly this expression is variable from clear expression to negligible, however, low expression was seen in these experiments (n = 6)[67]. This could be the result of the antibody used in these assays being target-specific and less cross-reactive to other LILR receptors, compared to those commercially available. The anti-LILRB2 clone B3, stained monocytes equally to MDMs. This expression was higher than the staining seen on MDDCs. No staining was seen on B cells, T cells, NK cells or neutrophils. The anti-LILRB3 clone A16, showed the highest staining on MDMs and neutrophils. Staining was also seen on monocytes, which was equal to that seen on MDDCs. No staining was seen on B cells, T cells and NK cells.

In summary, LILRB1, LILRB2 and LILRB3 staining was the highest on myeloid cells, namely monocytes, MDMs, MDDCs and in the case of LILRB3, neutrophils. With the exception of LILRB1, no staining was seen on B cells, and none of the antibodies stained T cells or NK cells. This suggests that these receptors are predominantly found on myeloid cells and not lymphoid cells, although LILRB1 is also found on B cells. The assay also showed that the generated antibody clones were able to bind specifically to ‘real’ cells and not just cell lines.

4.2.3 Determining antibody affinity by SPR

After binding to normal human blood subsets was confirmed, the antibodies were further characterised by studying their affinity or binding strength, and the kinetics of these interactions (on/off rates), was measured by SPR using Biacore™ T100 (GE Healthcare). LILRB3-hFc recombinant protein (the extracellular LILRB3 domain with a human Fc tag) was used as the ligand and immobilised onto a gold-coated glass sensor chip. Each anti-LILRB3 antibody or “analyte” was then flowed across the chip at various concentrations (5

fold dilutions from 100 nM to 0.16 nM) for 700 seconds, after which time buffer was added to dissociate the analyte from the chip. All SPR assays were performed by Ian Mockridge, *University of Southampton*.

Representative LILRB3 antibodies are shown in *Figure 4.5* below. Clone 222821 (R&D systems) was also included as a control. LILRB1 and LILRB2 clones were not tested in this incidence due to lack of available fusion proteins as a result of poor transfection efficiency.

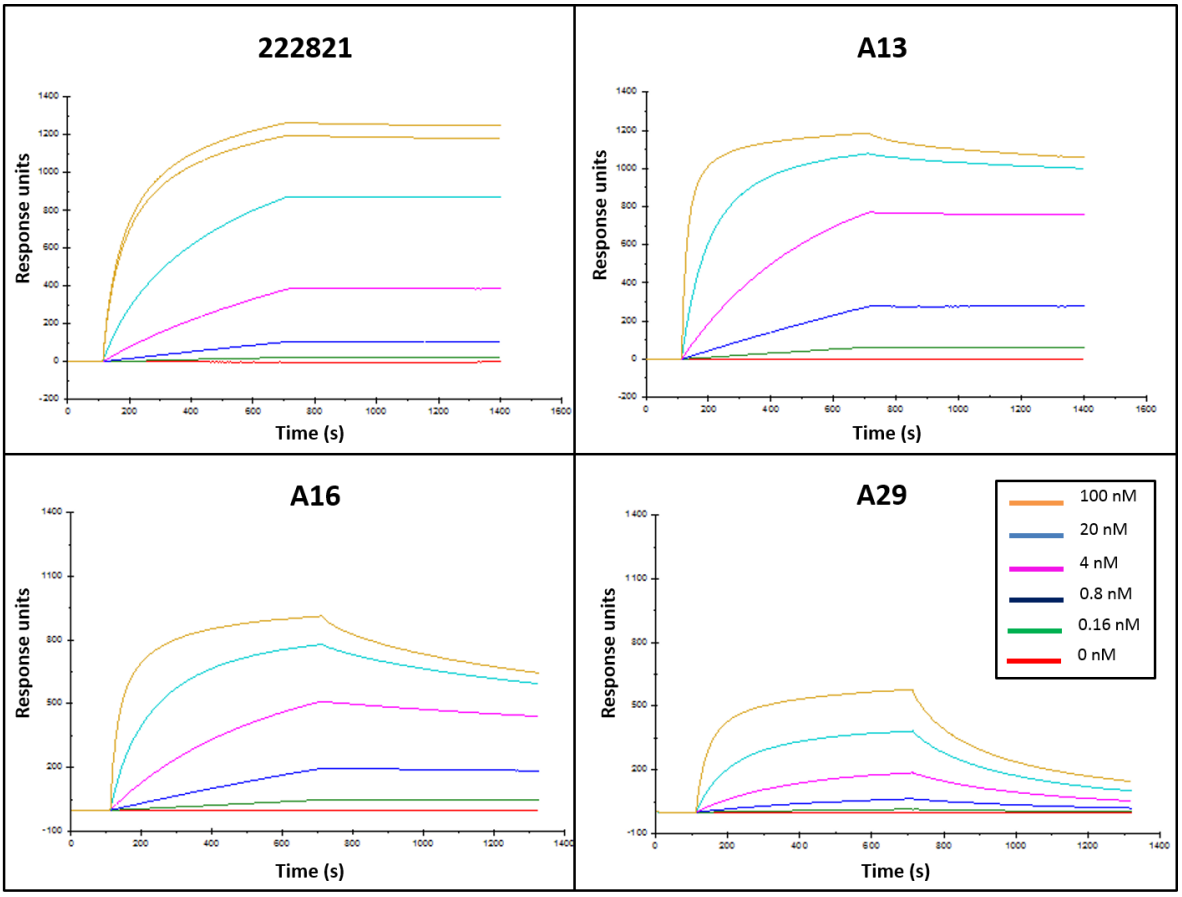

Figure 4.5 Antibody affinity tested by surface plasmon resonance (SPR). LILRB3-hFc recombinant protein was used as the ligand and coated on a series S sensor chip (CM5, GE Healthcare). Generated antibody clones (BioInvent) or anti-LILRB3 clone 222821 (R&D Systems) was then passed across the chip at various concentrations (5 fold dilutions from 100 nM to 0.16 nM) until 700 seconds, when buffer was then passed across. SPR was measured using Biacore™ T100 (GE Healthcare), and displayed as sensorgrams. Representative sensorgrams displayed. All SPR assays were performed by Ian Mockridge, *University of Southampton*.

Four representative sensorgrams depicting the SPR data for three representative anti-LILRB3 clones and the commercial as a control were studied *(Figure 4.5)*. The sensorgrams showed that binding was concentration dependent, the higher the concentration of analyte or mAb used, the higher the response units, or binding that was seen. They also showed that the mAbs were specific, as they were able to bind to the LILRB3-hFc ligand.

The antibodies were flown across the chip for 700 seconds. When the antibodies associated with the chip, this was referred to as the 'on' rate. The 'on' rates were similar for all the mAbs illustrated (*Figure 4.5*). Each mAb had a fast 'on' rate, as the available binding sites on the ligand were taken up by the mAb. As the antibody/analyte was passed across the chip with the immobilised LILRB3-hFc ligand, plenty of ligand binding sites were available. The SPR response is initially fast for all the antibodies shown and this is likely the result of the abundance of ligand binding sites available. However, the mAbs differed in 'off' rate, or dissociation of the mAb after no more mAb was flown over the chip at ~700 seconds. *Figure 4.5* showed mAbs that represented a slow (A13), medium (A16) and quick (A29) off rate. Whilst clone 222821 and A13 both appeared to be approaching equilibrium before 700 seconds, A16, and to a greater extent A29 still appeared to be increasing in response units. This suggests that these two clones had not yet reached equilibrium. After withdrawing the analyte/mAb the curve remained consistently flat for clone 222821, and A13 although displaying a slight dip at ~700 seconds, also remained consistently flat. This suggests both these clones have slow off rates. A16 however, showed a more pronounced dip, and A29 showed a steep decline in the curve after 700 seconds. This suggests that A29 had a very fast off rate, whilst A16 is medium comparatively to the other clones.

In conclusion, A13 appeared to have a slow 'off' rate, similar to the commercial clone 222821, suggesting both of these mAbs are of high affinity. A16 had a medium binding affinity, but A29 had a low affinity, demonstrated by its fast 'off' rate.

The sensorgram data was then fitted to a mathematical model. Although, a model such as the bivalent model (given that antibodies are bivalent) would have been more representative, this model did not provide a good fit with the data. Once one antibody Fab arm binds, the other binds more easily, resulting in the Bivalent model producing two very dissimilar K_D values. Therefore, the univalent model was used instead. Although the analyte was not univalent, the 1:1 binding model was the model that best fit. Although this model did not provide absolute affinity, it did provide an overall affinity.

The association ('on') and dissociation ('off') rates (ka & kd, respectively), and the dissociation equilibrium constant (KD) for a few representative anti-LILRB3 antibodies are displayed in *Table 4.3*. The KD values were calculated using the ratio of the dissociation to association (kd/ka).

4.3 Summary table of Biacore data

mAb	Association (ka)	Dissociation (kd)	Affinity (K_D)
221821	$1.178x10^{5}$	$1.924x10^{-6}$	$1.63x10^{-11}$
A13	$5.450x10^{5}$	$1.167x10^{-4}$	$2.14\ x10^{-10}$
A16	$5.174x10^{5}$	$4.222x10^{-4}$	$8.16\ x10^{-10}$
A29	$2.048x10^{5}$	$2.258x10^{-3}$	$1.10x10^{-8}$

Table 4.3 Antibody affinity of different anti-LILRB3 clones assessed by SPR. K_D values (nM) were calculated from the 1:1 binding model by Kd [1/s] / Ka [1/Ms], using Biacore™ T100 Evaluation Software (GE Healthcare).

Table 4.3 shows that the 'on' rate or association for each antibody was similar (all ~10^5), however they differed in 'off' rates. A29 had a higher dissociation value ($2.258x10^{-3}$) and therefore faster 'off' rate, whilst A13 and A16 had similar values (~10^4), and commercial clone 222821 had the smallest dissociation value and therefore slowest 'off' rate ($1.924x10^{-6}$). This coincides with the sensorgram data, which shows that all the clones represented in *Figure 4.5* have similar 'on' rates but vary in their 'off' rates.

Generally a K_D value around 10^{-9} was considered a high affinity binding antibody, and a K_D of 10^{-12} a very high affinity binding antibody (*Biacore handbook, GE healthcare*). From the K_D values above in *table 4.3*, these values suggested that all the antibodies tested had high binding affinities. A29, however, had the lowest K_D ($1.10x10^{-8}$), which agrees with the fast off rate seen (*Figure 4.5*). The antibody with the highest K_D was the commercial clone 222821 ($1.63x10^{-11}$), followed by A13 then A16. This coincided with the sensorgrams depicting the 'on' and 'off' rates, as A29, which had both a quick 'on' and 'off' rate also had the lowest K_D value and therefore the lowest affinity.

It should be noted that fitting data to a mathematical model does not prove its interaction. It is possible that results may fit more than one mathematical model. Models are picked on 'best fit'. Whilst these K_D values are not absolute affinities, they do provide an estimate of the affinity of these clones.

4.2.4 Determining shared antibody epitope binding sites by cross-blocking with commercial antibodies

To further characterise the LILR antibodies and map if the generated antibody clones bound to the same or similar epitopes as commercially available antibodies, cross-blocking assays were performed. Initially LILR antibodies were tested to see if they bound to the same site as the commercially available antibodies. In these assays the unlabelled LILR clones were first added to cells, followed by the addition of the fluorescently-labelled commercial antibody. Representative clones are shown in *Figure 4.6*.

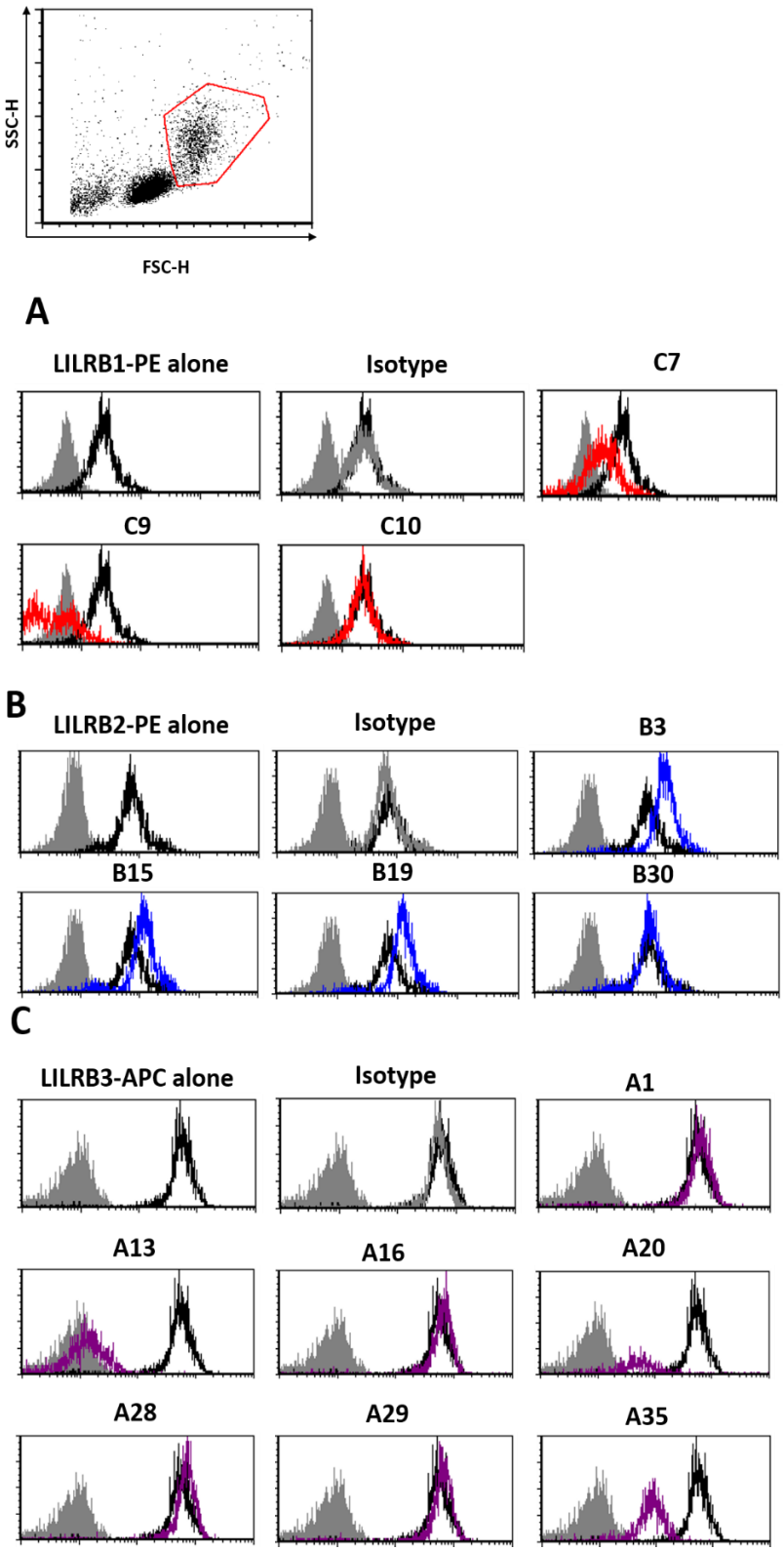

Target	Block
LILRB3	
A1	No
A13	Yes
A16	No
A20	Yes
A28	No
A29	No
A35	Yes
LILRB2	
B3	No
B15	No
B19	No
B30	No
LILRB1	
C7	Partially
C9	Yes
C10	No

Figure 4.6 Cross-blocking commercial antibodies with generated antibody clones to identify shared binding sites. $1x10^6$ PBMCs were blocked with 2% human AB serum (Life Technologies) for 10 minutes, 4°C. Cells were then stained with 10 µg/ml unconjugated antibody clones (A – LILRB1, B – LILRB2, C – LILRB3 clones) for 30 minutes at 4°C. The cells were subsequently stained with their respective directly-conjugated commercial LILR antibodies for 20 minutes at 4°C (no wash step), and analysed by flow cytometry, gating on the monocyte population. The PIR-B isotype is shown in grey, commercial antibody in black, LILRB1 clones in red, LILRB2 clones in blue, LILRB3 clones in purple and hIgG1 isotype in dark grey. Table summarises histogram data. n=1.

Figure 4.6 showed that the LILRB1 clone C10 did not block the commercial antibody from binding, suggesting it binds to an alternative binding site. In contrast, clone C9 did block binding, and C7 partially blocked binding. All LILRB2 clones shown here did not block the commercial antibody from binding. LILRB3 clones A1, A16, A28 and A29 did not block the commercial antibody, whilst A13, A20 and A35 were all able to block binding. This demonstrates the variability in epitope binding of clones produced by phage display.

3/7 LILRB1 (A13, A20 and A35), no LILRB2 and 2/3 LILRB3 (C7 and C9) clones were able to block their respective commercial antibodies, suggesting that they bind to similar or the same epitopes. LILRB1 clone C11, LILRB2 clones B3, B15, B19 and B30 and LILRB3 clones A1, A16, A28 and A29 are likely to bind to alternative epitope binding sites as they were unable to block commercial antibody staining. Overall, 6/11, 30/36 and 20/46 anti-LILRB1, -LILRB2 and –LILRB2 clones did not show cross-blocking of their commercial antibody (*see appendix*), suggesting they bind to novel binding epitopes.

It should be noted that this data is best interpreted taking into account the Biacore results. For example, A35 (a partial blocker), had a faster 'off' rate than the commercial antibody. This could explain why it is only a partial blocker, it cannot completely block the commercial antibody because it binds with less affinity and therefore comes 'off' too quickly, no longer occupying epitopes and therefore potentially allowing the commercial antibody to bind. A29 (a non-blocker), had a quick 'on' and 'off' rate, making it difficult to interpret the data, as its inability to block the commercial antibody could be due to the fact it comes off the chip too quickly, allowing the commercial antibody to bind. However, overall, the 'on/off' rates were reasonably slow, indicating the changes in the ability to block the commercial antibody seen in this assay, are likely due to epitope binding.

4.2.5 Antibody epitope mapping to LILRB3 IgG-like extracellular domains

To characterise LILRB3 antibody epitope mapping more precisely, IgG-like extracellular LILRB3 domain mutant DNA constructs were generated. These constructs had one domain (1D), two (2D), three (3D) or all four LILRB3 extracellular IgG-like domains (wild-type or WT). These DNA constructs were transfected into HEK 293F cells and staining of each anti-LILRB3 clone was tested against each of the domain constructs, to identify which domain each clone bound to. Representative anti-LILRB3 clones are shown in *Figure 4.7*.

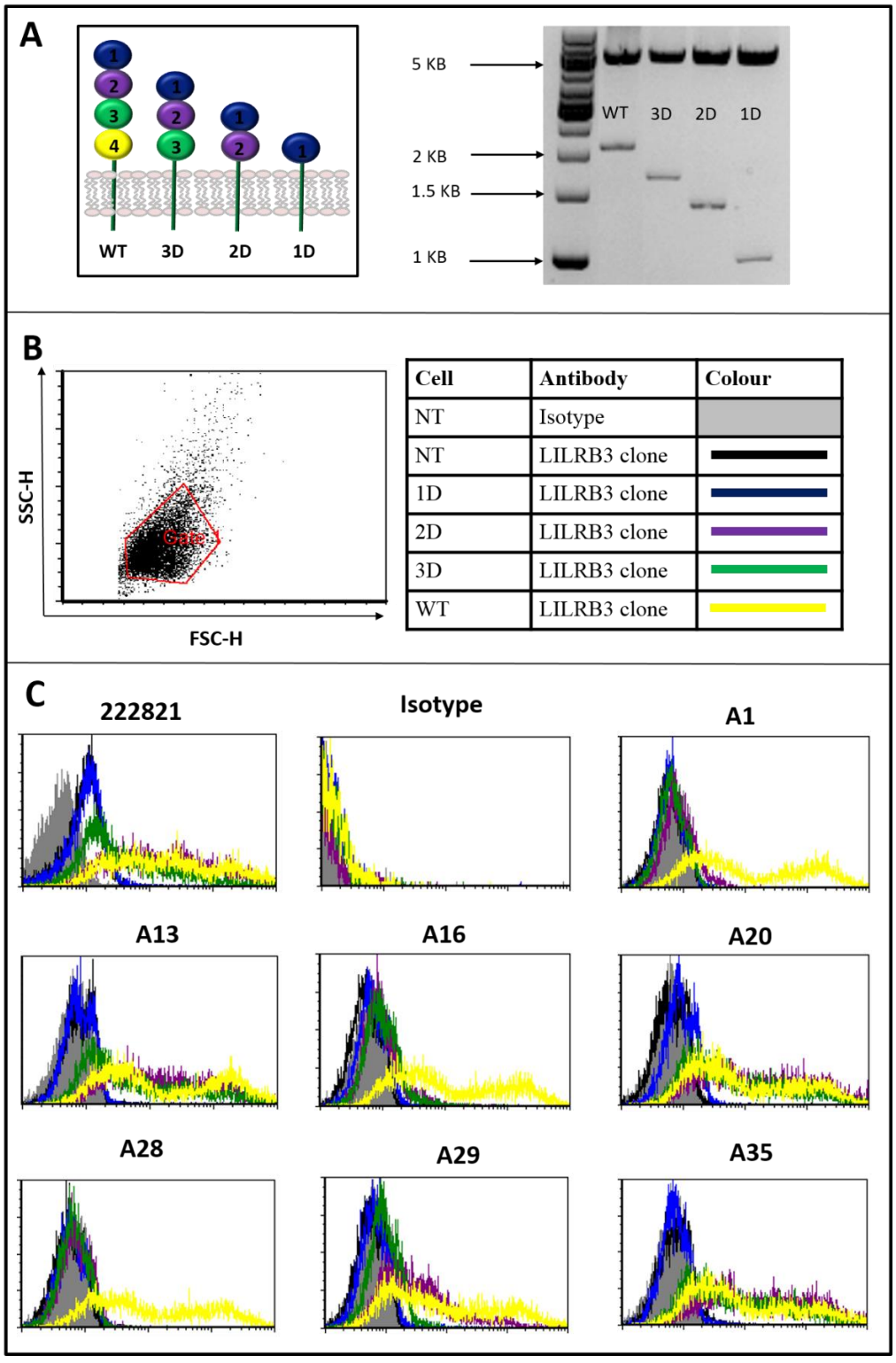

Figure 4.7 Assessing epitope mapping domains of LILRB3 antibodies against extracellular domain construct transfections. HEK293F cells were transfected (by lipofection) with either a wildtype-LILRB3, 3-domain (D), 2D or 1D-LILRB3 construct. After 48 hours transfected cells were stained with different commercial anti-LILRB3 clone 222821 (R&D systems) or generated anti-LILRB3 clones for 25 minutes, 4°C, washed twice and then stained with an anti-human-PE secondary (Jackson Labs) for 20 minutes, 4°C, washed then analysed by flow cytometry using the FACS Calibur. **A)** Schematic of domain constructs generated and restriction digest of each insert from its vector (pcDNA3). LILRB3 (WT), ILT5-3D (3D), ILT5-2D (2D) and ILT5-1D (1D). **B)** Flow cytometry gating strategy and key colour schematic of histograms. **C)** Example histograms of anti-LILRB3 clone 222821 (R&D Systems) or generated clones tested. Representative of n=3.

Figure 4.7A shows that LILRB3 domain constructs were successfully generated, and the DNA gel shows the different sizes of each insert: LILRB3 (WT) ~1.9 KB, LILRB3-3D (3D) ~1.8 KB, LILRB3-2D (2D) ~1.2 KB, LILRB3-1D (1D) ~0.9 KB, and pcDNA3 ~5.4 KB. *Figure 4.7C* shows that like clone 222821 (commercial antibody, R&D systems), A13, A20 and A35 bound to the WT, 3D and 2D-transfected cells, suggesting they bind to domain 2. Alternatively, A1, A16, A28 and A29 bound to only the WT-transfected cells suggesting they bind to domain 4. This data supports earlier blocking experiments (*Figure 4.6*) as clone 222821 binds to the second domain, and the same antibodies that were shown to block clone 222821 were also found to bind to the second domain.

Below is a schematic showing a summary of all the anti-LILRB3 clones and the domains they bind to.

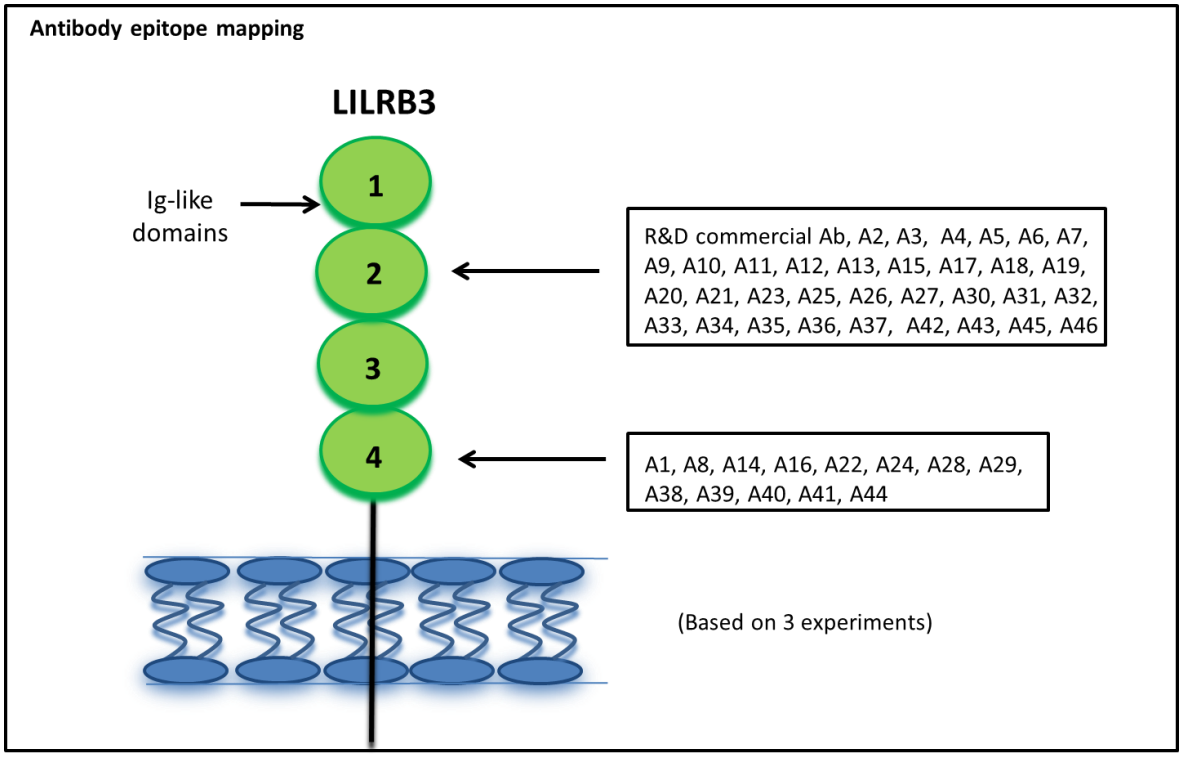

Figure 4.8 Schematic of extracellular Ig-like domain binding of each anti-LILRB3 antibody. The LILRB3 receptor has four extracellular Ig-like domains. The schematic shows which domain each generated anti-LILRB3 antibody binds to, based on epitope mapping experiments highlighted in *Figure 4.7*. Clone 222821 (R&D Systems) is included as a control. Schematic represents three independent experiments.

From the schematic above (*Figure 4.8*), it is clear that all the clones produced bound to domains 2 or 4. The majority of clones bound to domain 2. This could be owing to domains 2 and 4 being the only exposed domains, due to protein folding, rendering domains 1 and 3 to be concealed. Alternatively, there could have been conformational bias towards epitopes in

these domains resulting from the selections performed during the phage display. The protein format during the selections may have favoured binding to epitopes in these domains.

A summary of all the antibody characterisation performed in this chapter is summarised in *Table 4.4.*

Table 4.4 Summary table of LILR antibody characterisation

Target	Clone	Specific		PIR-B cross-reactivity	Affinity (K_D)	Block commercial	Domain binding
		293T	2B4				
LILRB1	A1	Yes	Yes	No	1.760×10^{-9}	No	4D
LILRB1	A13	Yes	No	No	2.352×10^{-9}	Yes	2D
LILRB1	A16	Yes	Yes	No	3.429×10^{-9}	No	4D
LILRB1	A20	Yes	Yes	No	1.229×10^{-8}	Yes	2D
LILRB1	A28	Yes	Yes	No	7.421×10^{-9}	No	4D
LILRB1	A29	Yes	Yes	No	1.278×10^{-8}	No	4D
LILRB1	A35	Yes	Yes?	No	3.463×10^{-9}	Yes	2D
LILRB2	B3	Yes	Yes?	No	-	No	-
LILRB2	B15	Yes	Yes?	No	-	No	-
LILRB2	B19	Yes	Yes?	No	-	No	-
LILRB2	B30	Yes	Yes?	No	-	No	-
LILRB1	C7	Yes	No	No	-	Partially	-
LILRB1	C9	Yes	No	No	-	Yes	-
LILRB1	C10	Yes	No	No	-	No	-

Table 4.4 Antibody characterisation. Generated antibody clones were characterised and tested *in vitro* to re-confirm their target specificity, as well as their lack of cross-reactivity to other LILR receptors and the homologous mouse PIR-B receptor. Antibody binding affinity by SPR and mapping their epitope binding sites was also assessed. (-) indicates untested characterisation.

Table 4.4 shows that specific anti-LILRB1, -LILRB2 and -LILRB3 clones were generated, and the majority showed no cross-reactivity to other LILR receptors or the homologous mouse PIR-B receptor. The anti-LILRB3 clones all bound with high affinity, although some clones appeared to have faster 'off' rates than others. Although some antibodies appeared to share binding epitopes with the commercial antibody, antibodies with different epitope binding capabilities were revealed. This indicates that novel antibodies have been generated.

4.2.6 Tissue expression of generated antibody clones

Ideally, the generated antibody clones will be used *in vivo* in various therapeutic settings. The tissue expression of these clones is therefore important. Although the literature suggests that LILRs are restricted to immune cells, little data is available to validate this as microarray data

is scarce. Recent studies have indicated that LILRB2 is involved in the progression of Alzheimer's disease, present on αβ amyloid oligomers and neural cells[73]. LILRs have also been shown to be important in bone formation[79]. This indicates expression of LILRs on brain cells, as well as other immune cells in the body, which could result in off-target effects if the clones were used as therapeutic agents. Immunofluorescence and immunohistochemistry were therefore carried out to confirm tissue staining of the clones.

4.2.6.1 Studying LILRB3 expression by IHC

To study LILRB3 expression in human tissue, IHC was performed. Specific anti-LILRB3 antibodies (A16 and A28) were firstly biotinylated, and biotinylation confirmed by electrophoresis. Biotinylated anti-LILRB3 antibodies were then used to stain human tonsil sections.

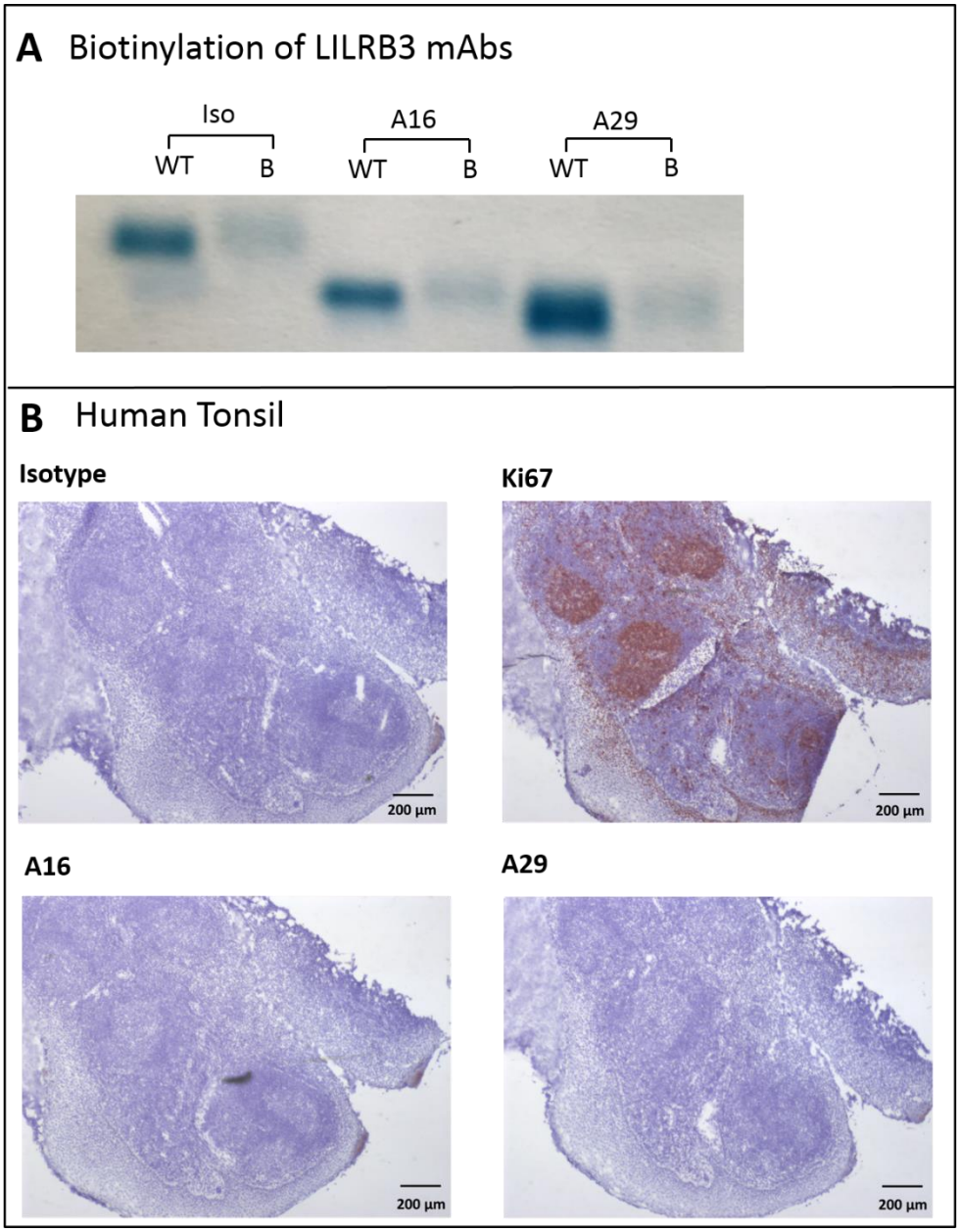

Figure 4.9 LILRB3 mAb staining of human tissue. A) Biotinylation of LILRB3 mAbs. Biotinylation of antibodies was performed using the Lightening-Link Rapid Biotin Conjugation Kit (Type A) (Innova Biosciences) as per manufacturer's instructions. Biotinylation was confirmed by electrophoresis and Amido Black dye staining. Electrophoresis performed on wild-type (WT) and biotinylated (B) antibodies run side-by-side. **B) Assessing biotinylated anti-LILRB3 mAb staining by Immunohistochemistry (IHC).** 10 µm fresh frozen human tonsil samples were cut using the cryostat microm HM 560 (CellPath, Thermo Scientific). Sections were fixed in 100% Acetone, at room temperature for 10 minutes, washed in PBS 0.05% Tween, and incubated with a peroxidase suppressor (Sigma) at room temperature for 15 minutes, before washing sections again. Sections were blocked in 2.5% normal goat serum for 30 minutes at room temperature and incubated with 2 µg/ml biotinylated anti-LILRB3 antibodies A16 and A29, an isotype control or positive control (rabbit anti-human Ki67) for 1 hour at room temperature. A biotinylated goat anti-rabbit secondary antibody was added to the samples stained with Ki67 for 45 minutes at room temperature. After washing sections in PBS-Tween, an ABC-HRP secondary (Vector Labs) was added for 30 minutes at room temperature, sections washed again and NovaRed Chromagen substrate added for 10 minutes at room temperature. After a final wash in PBS, sections were counterstained with haematoxylin and slides mounted with a hardset mountant (Vector Labs). Images taken using the CKX41 microscope (Olympus) and visualised with the Cell^B (Olympus) software. Images were acquired at 4x magnification and 100 seconds exposure.

Figure 4.9A shows the biotinylated (B) antibodies displayed (faint) bands, similar in weight to the wild type antibodies. Adding biotin to the antibody should have produced a band slightly higher than the wild type antibodies. Although, very faint, there is a minimal increase in size in the biotinylated antibodies, and therefore this indicated successful biotinylation. The kit does not provide information on how many biotin molecules are added per antibody. Therefore, it could be that only a few molecules are added, and therefore this would not dramatically increase the molecular weight.

When the substrate was added to the peroxidase secondary brown staining was seen, whilst blue staining was seen with nucleic stain haematoxylin. *Figure 4.9B* shows that all four antibodies (negative and positive controls and the anti-LILRB3 clones), all showed successful haematoxylin staining, represented by the blue staining seen. However, only the positive Ki67 control showed brown staining. No brown staining was seen with the biotinylated anti-LILRB3 clones A16 and A29 or the negative isotype control. This suggests that no LILRB3 is present in the tonsil tissue or that the antibody staining with these clones was not successful.

It is likely that the lack of staining that was seen, was the result of poor or unsuccessful biotinylation of the anti-LILRB3 antibodies, however electrophoresis showed a very slight increase in molecular weight. Therefore, poor signal amplification could also have been the cause of the lack of staining.

4.2.6.2 Studying LILRB3 expression by IF

Given the lack of IHC staining seen with the biotinylated anti-LILRB3 mAbs, believed to be due to poor signal amplification, immunofluorescence (IF) was performed with tyramide to increase signal amplification. Human tonsils were once again stained with biotinylated anti-LILRB3 mAbs, but this time a streptavidin-HRP antibody followed by A488-conjugated tyramide (which recognised the HRP), was also added.

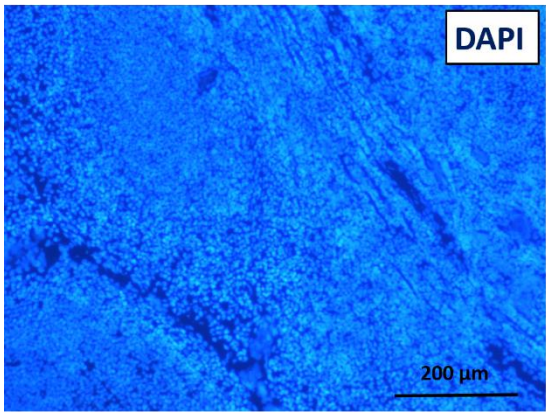
DAPI
200 µm

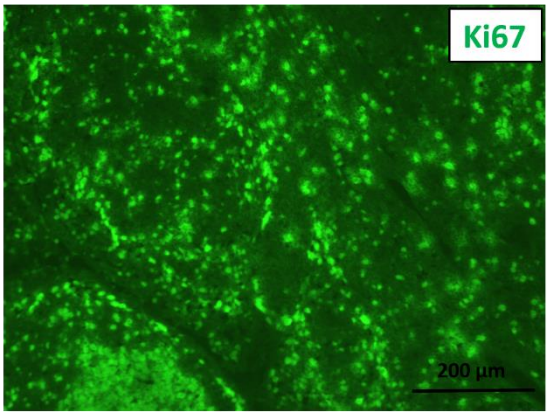
Ki67
200 µm

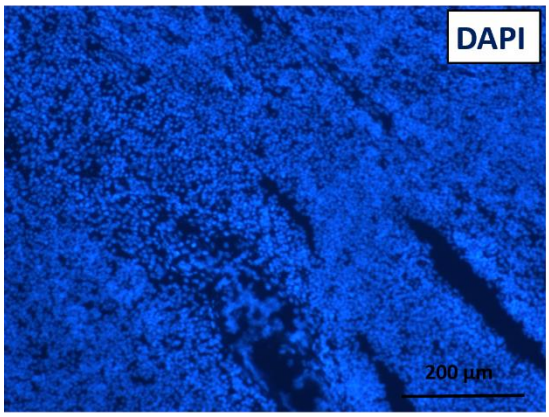
DAPI
200 µm

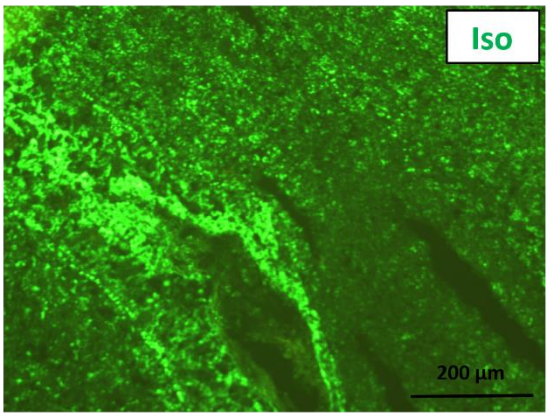
Iso
200 µm

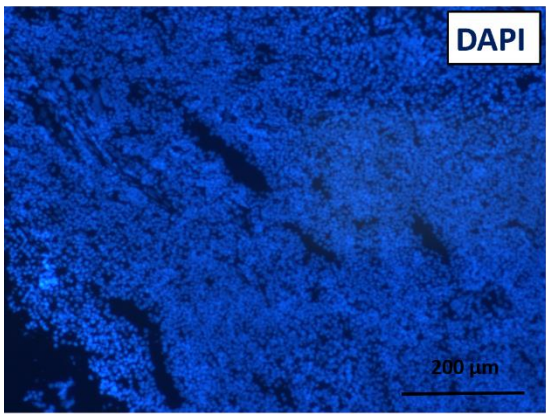
DAPI
200 µm

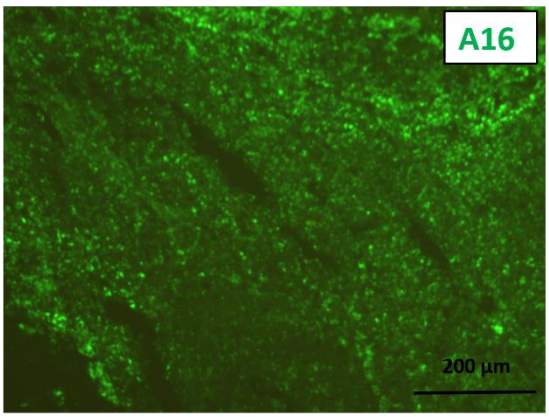
A16
200 µm

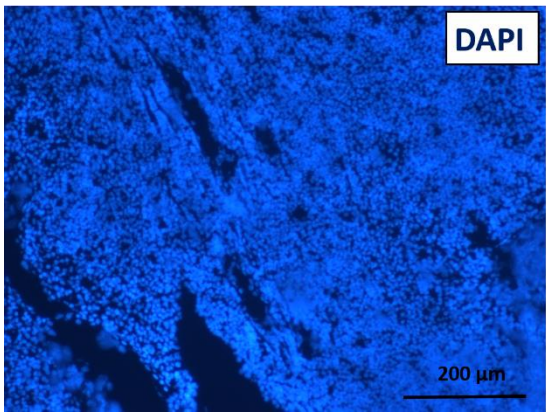
DAPI
200 µm

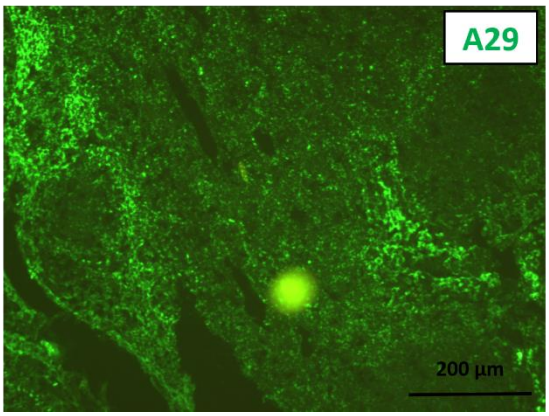
A29
200 µm

Figure 4.10 Assessing biotinylated anti-LILRB3 mAb staining by Immunofluorescence (IF) with tyramide signal amplification. 10 µm fresh frozen human tonsil samples were cut using the cryostat microm HM 560 (CellPath, Thermo Scientific). Sections were fixed in 100% Acetone, at room temperature for 10 minutes, washed in PBS 0.05% Tween, and incubated with a peroxidase suppressor (Sigma) at room temperature for 15 minutes, before washing sections again. Sections were blocked with TNB block buffer for 30 minutes at room temperature and incubated with 2 µg/ml biotinylated anti-LILRB3 antibodies, an isotype control or positive control (rabbit anti-human Ki67) for 1 hour at room temperature. A biotinylated goat anti-rabbit secondary antibody was added to the samples stained with Ki67 for 45 minutes at room temperature. After washing sections in PBS-Tween, Streptavidin-HRP was then added for 45 minutes at room temperature, sections washed again and A488-conjugated tyramide added for 10 minutes at room temperature. After a final wash in PBS, sections were counterstained with DAPI and slides mounted with a hardset mountant (Vector Labs). Images taken using the CKX41 microscope (Olympus) and visualised with the Cell^B (Olympus) software; 10x magnification and 200 milliseconds exposure (DAPI) or 10 seconds (A488).

Round cells were identified by nuclear stain DAPI. The tissue was intact. When stained with two different specific anti-LILRB3 mAbs, A16 and A29 staining was seen, and this was comparable with the staining seen with the positive control Ki67 (*Figure 4.10*). However, there was a lot of background staining seen with the negative (isotype) control. This suggests that although the tyramide was able to amplify the signal, and staining with the anti-LILRB3 mAbs was now observed, high background was also amplified. Given the similarity between the negative control and anti-LILRB3 staining, it unlikely that this is real staining, and the majority can be accounted for by background, likely due to the use of human antibodies on human tissue.

The biotinylated antibodies showed poor staining when used alone with a HRP-conjugated secondary (*Figure 4.9*). However, signal amplification, in the form of A488-conjugated tyramide, increased the background staining seen with these antibodies, likely due to the use of human antibodies to stain human tissue. Therefore, directly labelled antibodies were utilised instead, to try and decrease background. However, given the poor staining previously seen with the biotinylated antibodies, signal amplification was applied with the addition of a goat-anti-mouse-A488 conjugated antibody, followed by a rabbit anti-A488 secondary.

Staining of fresh frozen human tonsil samples with representative clone, A16 is shown in *Figure 4.11* below. Clone 222821 (R&D Systems) was included as a positive control.

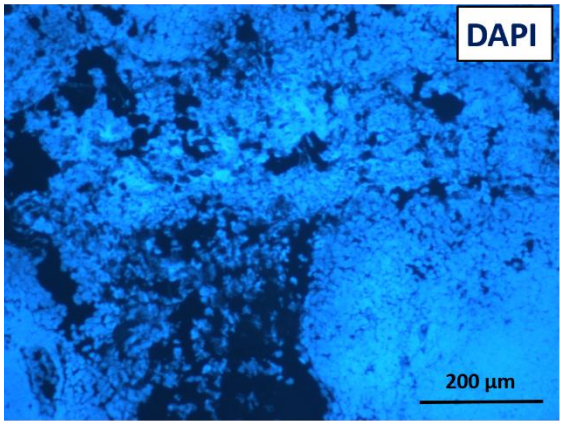
DAPI
200 µm

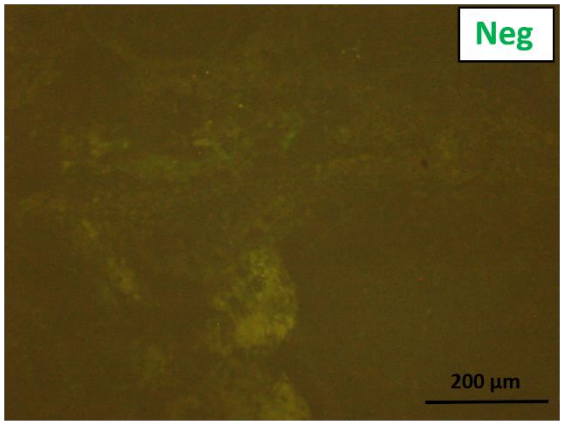
Neg
200 µm

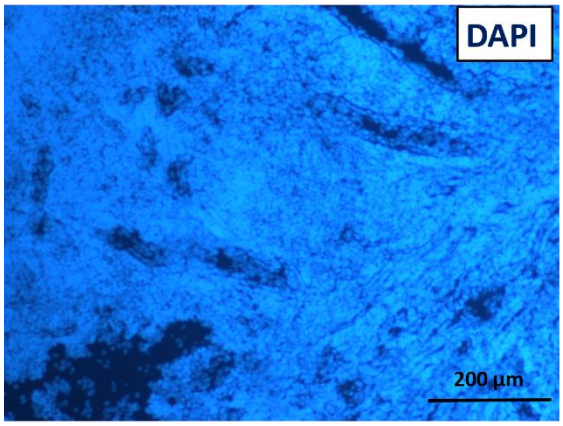
DAPI
200 µm

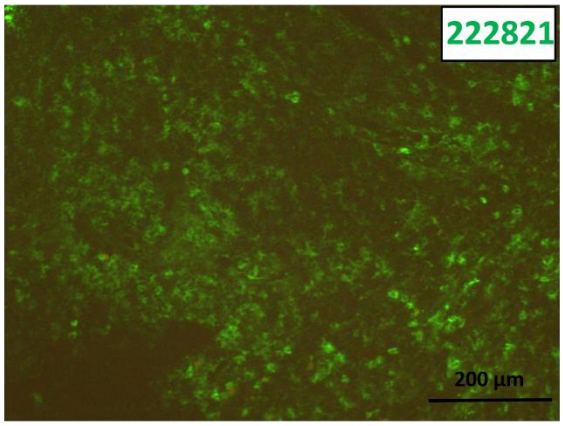
222821
200 µm

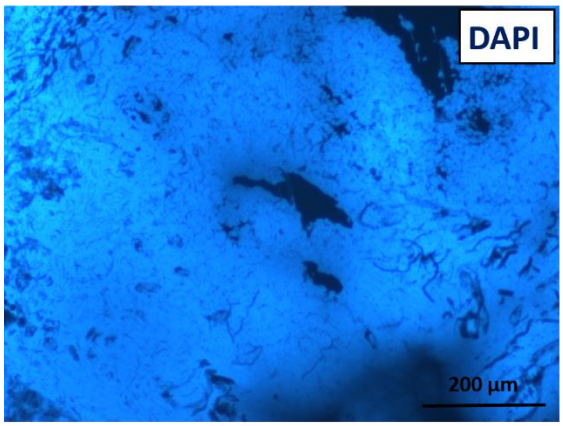
DAPI
200 µm

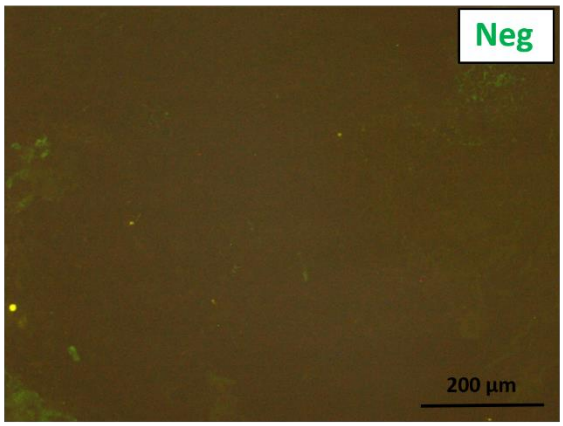
Neg
200 µm

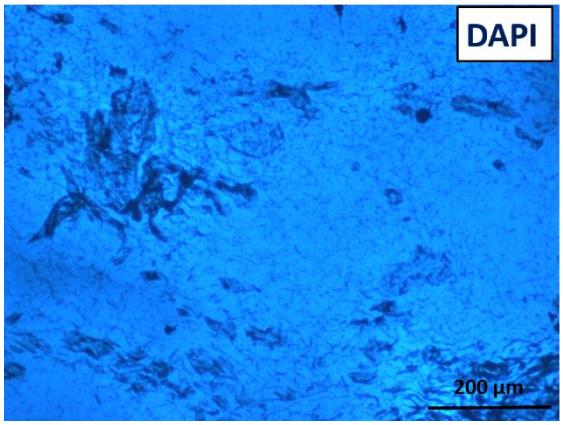
DAPI
200 µm

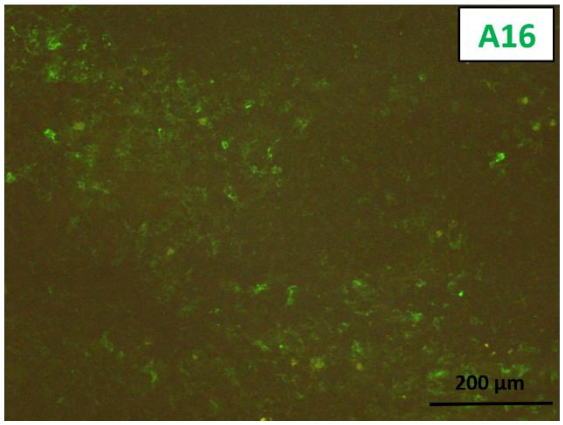
A16
200 µm

Figure 4.11 Immunofluorescence showing LILRB3 expression in human tonsils. Fresh frozen human tonsil samples (HRU, Southampton General Hospital) were embedded in OCT (CellPath) and 10 μm sections cut with the cryostat microm HM 560 (CellPath, Thermo Scientific). Tissue was fixed in acetone for 10 minutes at room temperature (RT), blocked in 2.5% normal goat serum, and 10 μg/ml either a A488-labelled commercial anti-LILRB3 clone 222821 (R&D systems) or generated anti-LILRB3 clone A16 (BioInvent) were used to stain tissue for 1 hour, RT. The tissue was then washed in PBS, and stained with a goat-anti-mouse-A488 conjugated antibody for the commercial antibody, or firstly a rabbit anti-A488 secondary for 45 minutes, RT, before being washed and stained with a goat-anti-rabbit-A488 antibody for 45 minutes, RT for tissue stained with representative clone A16-A488. Both samples were then counter-stained with nuclear stain DAPI, mounted and analysed by fluorescent microscopy using the CKX41 microscope (Olympus). Cell^B (Olympus) was used to capture and analyse images; 10x magnification and 200 milliseconds exposure (DAPI) or 1 second (A488).

Round cells were seen throughout the tissue, these are likely to be monocytes (although co-staining with a monocyte marker would need to be performed to confirm this). Representative anti-LILRB3 clone A16, showed staining of human tonsil tissue by IF. However, this staining appeared to be less than the staining observed with clone 222821 (R&D Systems). Ideally time permitting other human tissue samples would be tested, both healthy tissue and tumour tissue to study the expression profile of these clones.

In conclusion, IHC staining of human tonsil samples showed that biotinylated anti-LILRB3 mAbs required signal amplification to display staining. However, signal amplification with tyramide increased the high background, likely due to the use of human antibodies used to stain human tissue. IF staining provided a much cleaner staining, with lower background, but signal amplification was still needed. This staining was lower than that seen with commercial clone 222821. Therefore, anti-LILRB3 staining still requires optimisation. However, the generated antibodies are specific and can be used to stain human tissue. Co-staining with other cell surface markers, and in other tissues, will illustrate LILRB3 expression in different tissues.

4.3 Discussion

Due to the limitations of current commercial LILR antibodies lacking specificity, the aim of this project was to generate novel specific antibodies that could be used to study expression and function of LILRB3 and other inhibitory LILRs that may also have therapeutic potential.

Firstly antibodies were screened against LILR-transfected cell lines to re-confirm target specificity and lack of cross-reactivity to other LILR receptors. 39/46 LILRB3, 24/32 LILRB2, and 10/11 LILRB1 clones, were potentially specific, showing the least amount of cross-reactivity to other LILR receptors. The majority of the clones were therefore specific, which was expected as they had been chosen during the selections and screening for target-specificity. However, when the generated antibodies were tested against a larger panel of LILR receptors for cross-reactivity (assays performed by Des Jones, *University of Cambridge*), only 16/46 anti-LILRB3 clones were found to be specific (see appendix), and one LILRB3 clone showed no staining (A24) against either LILRB3-transfected HEK 293T cells (*Figure 4.1*) or LILRB3-transfected 2B4 cells (*Figure 4.2*). All the LILRB2 clones appeared to show some binding to the LILRB3-transfected cells (*Figure 4.2B*). This could be that all the clones are cross-reactive to LILRB3 receptor, however, due to the high expression of LILRB3 (confirmed with an antibody against the HA tag – *Figure 4.2C*), it could be that the antibodies are just 'sticking' to these overexpressed transfected cells, which may not be comparable to endogenous physiologically expression. Initial screening against LILRB3-transfected HEK 293T cells, showed no cross-reactivity of these clones to LILRB3 (*Figure 4.1*). Therefore, clones that showed binding to LILRB3 only could be LILRB2-specific (see appendix), including six clones that showed no cross-reactivity to LILRB3-transfected HEK 293T cells (B3, B8, B15, B19, B33 and B30). As seen with the LILRB2 clones, all the LILRB1 clones showed some cross-reactivity to LILRB3 (*Figure 4.2C*). Again, this could have been the result of the high expression of LILRB3 on the 2B4 cells. By sorting all the transfectants to get similar levels of expression, this could be avoided. The LILRB1 clone, C10, was the only antibody clone that showed cross-reactivity only to LILRB3 alone. C7, C8 and C9 showed minimal cross-reactivity to LILRA1, as well as LILRB3.Therefore these 4 LILRB1 clones showed the least cross-reactivity with other LILR receptors. C6 also showed cross-reactivity to only LILRB3, however the antibody clone showed very low staining to LILRB1-transfected 2B4 cells, suggesting it has a poor affinity.

In summary, 16/46 LILRB3-clones were found to be specific, 6/32 LILRB2 and 2/11 LILRB1 clones were potentially specific (with the exception of their staining to LILRB3-transfected

cells). This is lower than expected due to the various screening methods used to select for specific clones. However, this screening only included the inhibitory LILRs, and many of these clones were found to cross-react with activatory LILRs.

LILRB1 was chosen as a non-target for LILRB2 in the selections and *vice versa,* due to their high similarity (77.4% extracellularly, *Figure 3.11),* in an attempt to avoid cross-reactivity. LILRB1 was chosen as a non-target for LILRB3. Extracellularly, LILRB1 and LILRB2 are both homologous to LILRB3 with 63.7 and 70.5% protein sequence identity, respectively (*Figure 3.11*). Typically when homology is under ~60% it is less likely there will be cross-reactivity (based on communication with BioInvent). Therefore ideally both LILRB1 and LILRB2 should have been utilised as non-targets for LILRB3 in the pre-selection. However, LILRB1 was chosen based on the lack of availability of the LILRB2 protein.

Notably, mAbs were not screened for cross-reactivity to cells expressing LILRA3, LILRA4 and LILRA6, due to poor transfection efficiency (data not shown). Therefore cross-reactivity to these receptors cannot be ruled out. LILRA6 is an activatory receptor with very high similarity to LILRB3 (68% protein homology based on UNIPROT sequences), particularly in their extracellular domains (>95%)[78]. It is thought that gene duplication and deletions resulted in exchange of genes between the extracellular domains of LILRB3 and LILRA6, making them so similar[253]. Due to this high similarity, generating LILRB3-specific antibodies that do not cross-react with LILRA6 is very difficult. Producing recombinant LILRA6 protein is also difficult. Therefore, despite LILRA6 being an ideal non-target for LILRB3, it could not be included in the selection process. Therefore, there is a high chance that LILRB3 antibodies generated in this way may be cross-reactive with LILRA6. Dual antibody specificity against both LILRA6 and LILRB3 could result in inconclusive results *in vitro* or *in vivo* as both receptors are co-expressed on the same cells[64]. LILRB3 expression however, is thought to be higher on monocytes than LILRA6, as qPCR analysis has shown lower level of LILRA6 transcripts compared with LILRB3 transcripts on cells[253]. A greater level of LILRB3 could mean that despite generating dual-specificity antibodies, binding to LILRB3 may be preferential, due to its higher expression. However, the expression levels of both receptors may alter in disease states or even upon antibody stimulation in healthy donors, once receptors are activated. Transcripts are not necessarily translated into protein and therefore qPCR studies although indicative of protein expression, may not entirely reflect real expression. Generating anti-LILRA6 specific antibodies would divulge the expression pattern of the receptor. Ideally including all the activatory and inhibitory LILR receptors as non-

targets would have been attractive, but some receptors have poor transfection efficiencies, making it hard to generate soluble protein or stably transfected target cells.

Although, all the clones tested showed no binding to mouse leukocytes or blocking of the mouse PIR-B receptor, PIR-A was not tested. There are currently no commercially available antibodies generated against PIR-A alone (they all bind both PIR-A/B or PIR-B alone). This could be due to difficulty in raising antibodies against this receptor. For this reason, cross-reactivity to PIR-A cannot be eliminated.

After re-confirming antibody specificity, the clones were further characterised by assessing affinity by SPR (using Biacore). All the LILRB3 antibodies had high K_D values, indicating they were all high affinity binding clones. However, although they all appeared to have fast 'on' rates, SPR analysis showed the 'off' rates of individual clones differed. Some clones showed poor binding to transfected cells. Whilst this could have been the result of experimental error (antibody not added to cells), some clones, such as A24 and C6 showed low staining against both the LILRB3 and LILRB1-transfected HEK 293T and 2B4 cells, respectively. This suggested that A24 and C6 were both low affinity binding clones. Unfortunately, there was not enough antibody to confirm this by SPR (Biacore) for clone A24 (due to poor transfection efficiency of IgG in HEK-EBNA cells), and LILRB1 and LILRB2 clones were not tested on the Biacore (due to no protein availability because of poor transfection efficiency). Other clones, A36, C2 and C8 that also showed low staining to their target-specific transfected cells, could have been the result of experimental error, as low staining was only seen against transfected 293T cells, but a significant shift was seen in the histograms displaying the staining of these clones against their target-specific 2B4-transfected cells (*Figure 4.2*). A36 was found to have a K_D of 1.781 $x10^{-10}$ by Biacore (see appendix), which is high. Affinity can have an effect on antibody effector function, as antibodies need to bind to their target to cause an effect. If they have very fast 'off' rates, they may not have enough time to be able to initiate an effect. However, one caveat of using amine coupling in SPR analysis, is the ligand may bind to the chip in any format, therefore certain epitopes may be hidden, preventing mAb binding.

Antibody epitope mapping was also assessed. All the LILRB3 antibodies generated bound to domains two and four. This could have been due to these domains have better exposed epitopes, or a bias in the phage display selection process that skewed the chances of binding in these domains. The majority of the LILRB3 clones produced were found to bind to the second extracellular domains of LILRB3. This correlates with protein sequence alignments of

all the inhibitory LILRs (*Figure 4.12 below*), which shows that LILRB3 domain two has the most unique binding sites when aligned with other LILRBs.

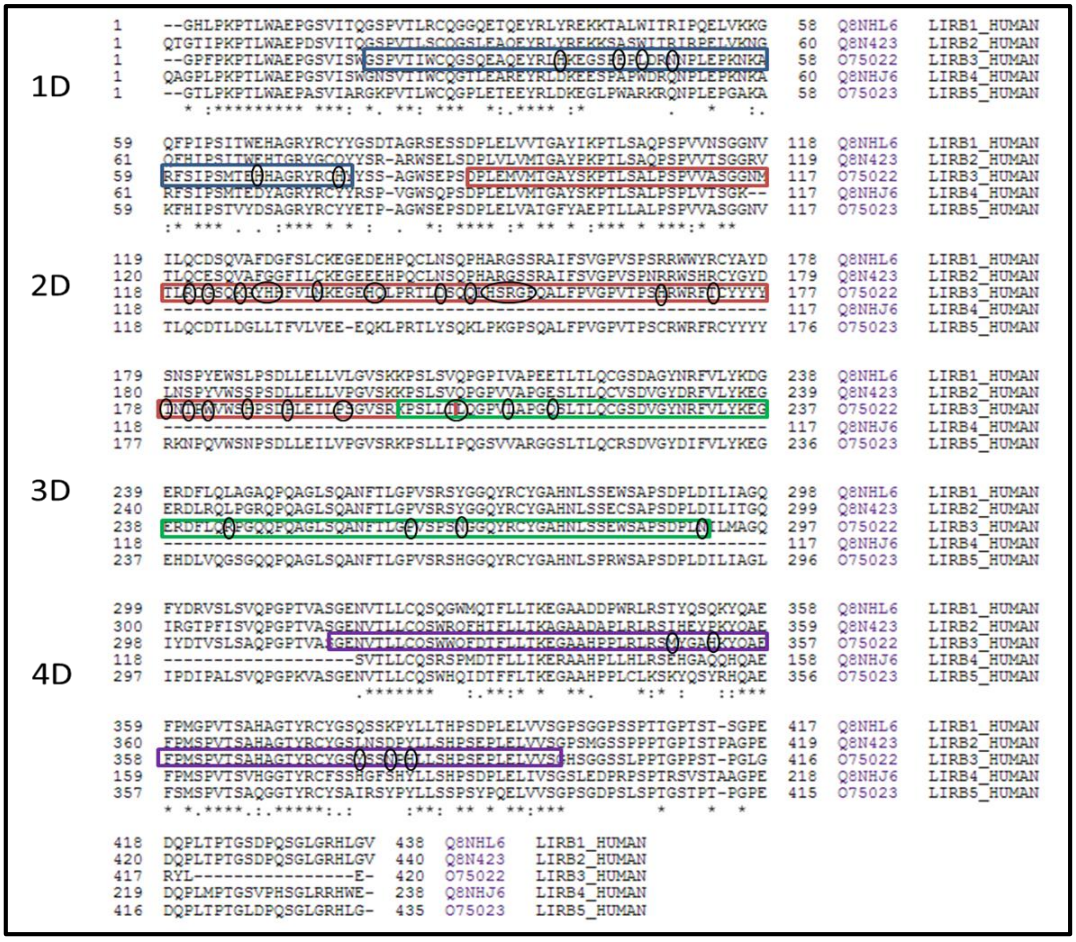

Figure 4.12 Alignment of the extracellular domains of the inhibitory LILRB receptor family. The extracellular domain of each inhibitory receptor was aligned: LILRB1, LILRB2 LILRB3, LILRB4 and LILRB5. Aligning each inhibitory LILR receptor revealed unique protein sites in LILRB3 compared to other LILR receptors. Domains are highlighted by different colours (domain 1 –blue, domain 2 – red, domain 3 – green and domain 4 – purple) and unique sites circled in black. The majority of the unique sites found in LILRB3 are located in domain 2. Sequences obtained and alignment generated in UNIPROT.

The alignment shows that the second Ig-like extracellular domain of LILRB3 contains the most unique sites, therefore, it is logical that LILRB3-specific antibodies generated that were not cross-reactive with other inhibitory LILRs would bind to this domain. Alternatively, 2D may contain epitopes that are more/better exposed, therefore generated antibodies maybe more likely to bind to these sites. Another observation was that although 20/46 anti-LILRB3 mAbs were found to not cross-block the 2D-binding commercial mAb, suggesting they bind to an alternative domain, 13/46 mAbs were found to bind to domain 4. This implies that 7 anti-LILR3 mAbs although unable to cross-block the commercial clone, were still binding to the same domain (2D). This suggest that not only were novel antibodies produced, binding to alternative epitopes in Ig-like domains, but also novel epitopes within the same domain.

Notably, in all three experiments (data not shown), no antibody including the commercial, were able to bind to the 1D-expressing cells. However, given the lack of a positive control, there is no way of knowing if these antibodies did in fact not bind to the first domain or if this transfection was unsuccessful. Adding a tag to the first domain (1D) construct, and screening for this tag post-transfection would reveal if the 1D transfection resulted in successful surface expression, and if any of the antibodies do bind to this domain. Adding a tag to all the domain constructs would also allow general expression levels of all constructs to be studied. Low expression of one construct could result in weak or no antibody binding, and it is possible this was the case for the 1D-transfected cells.

Crystal structures of LILRB1 and LILRB2 show that their ligand binding epitopes are in the first two Ig-like domains, and as these are the most exposed on the cell surface this would appear logical[86, 88]. This agrees with the data shown in this chapter that suggests that the majority of the antibodies bind to domain two (*Figure 4.7*). Although binding to domain one was undetermined, it could be that LILRB3 (whose crystal structure has yet to be determined) may have different binding epitopes to other inhibitory LILRs. Also, generating the domain mutants may have altered the structural conformation of these Ig-like domains, and misfolding may have led to certain epitopes being hidden or no longer exposed for the antibodies to bind. Each construct was designed based on UNIPROT annotations that suggested where one domain ended and the next one began. However, many of these annotated domains overlapped, therefore the constructs generated will also overlap in sequence. Irrespective of these potential caveats, the experiments did provide a good estimate of where these antibody clones could be binding. This agreed with the antibody cross-blocking assays, as the same antibodies that were able to block the commercial antibody were also found to bind to the second domain.

Although, these experiments were able to determine domain binding, fine epitope mapping should be performed, in order to identify different antibody-binding epitopes within the same domain. Utilising chimeric LILRB3-Fc fusion molecules, Jones *et al*, identified different amino acid ligand binding residues within domain 1, 3 and 4. Similar experiments could be performed[107]. Alternately, phage display peptide libraries could be used to for refined epitope mapping, screening each antibody clone against small peptide fragments in the different domains[254].

Biotinylation of the anti-LILRB3 antibody clones A16 and A29 was carried out and immunohistochemistry (IHC) performed. However, no staining was seen (*Figure 4.9B*). Electrophoresis showed that the antibody clones had increased in mass slightly, indicating

successful biotinylation (*Figure 4.9A*). However, the bands were faint for the biotinylated antibodies (more antibody should have been loaded on the gel), and therefore it is difficult to assess this increase in size. The lack of staining could therefore have been due to poor biotinylation or lack of signal amplification. The molecular mass of biotin is 0.244 kDa[255]. However, the kit does not provide information on how many molecules of biotin are added the antibody. It could be that the antibodies were labelled with only a few biotin molecules, therefore the molecular weight would not be greatly increased, making it hard to identify a difference in molecular weight changes between the biotinylated and wild-type samples. To confirm successful biotinylation using avidin-fluorescein conjugates e.g. streptavidin with a GFP tag; and then assessing fluorescence by UV-transillumination, would have been a clearer method of deducing biotinylation, as high sensitivity and the strong interaction between streptavidin and biotin would pick up even just a few biotin molecules. Alternatively, if the binding regions (CDRs) of the antibodies were blocked by the biotin, this would render them unable to stain the tissue samples. Therefore, the lack of antibody staining could have been the result of lack of compatibility between the clones and the biotinylation method, due to blocked CDR binding regions in the clones.

To eliminate the possibility of lack of signal amplification being the cause for the lack of staining seen by IHC, IF was performed using a tyramide amplification kit. High background was seen however, and even the negative control showed staining. This suggested that signal amplification by this method was not ideal, as even the background signal was amplified (*Figure 4.10*). High background staining was also likely caused by human IgG clones being used on human tissue.

Instead, A488-conjugated anti-LILRB3 antibodies were used to stain the tissue sections, with a rabbit anti-A488 secondary and then an A488-conjugated goat-anti-rabbit antibody. This provided signal amplification, without having to use biotinylated anti-LILRB3 antibodies. Staining was seen with the anti-LILRB3 clone A16, although this was weak, as was staining for the commercial 222821 clone (*Figure 4.11*). This suggests successful staining, and the presence of LILRB3 in these tonsil sections, but poor signal amplification, and these mAbs may not be compatible with IHC/IF. Other tissue samples will need to be stained to elucidate the tissue expression pattern of LILRB3. Co-staining with a monocyte marker, for example, would also have confirmed this staining was not non-specific, as LILRB3 is expressed on these cells.

There is little information on LILRs in mRNA and microarray databases of previous work studying tissue expression of these receptors. However, of the data that is available, the literature suggests that these receptors are restricted to immune cells (*Figure 4.13*).

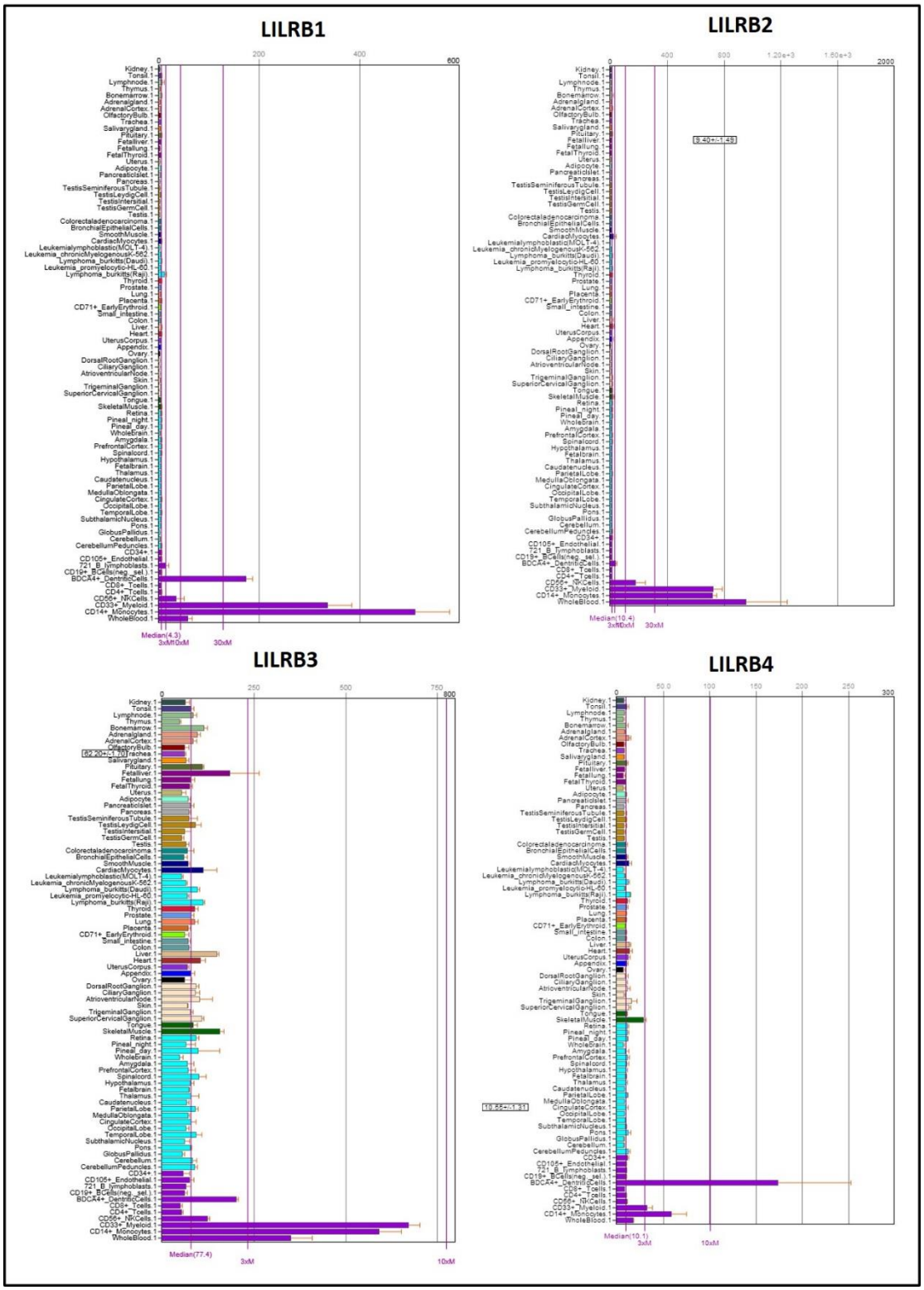

Figure 4.13 Tissue expression of inhibitory LILRs shows expression is restricted to immune cells. Data taken from http://biogps.org/#goto=genereport&id=11025, 10288, 11025 and 11006. Microarray data showing LILRB1, LILRB2, LILRB3 and LILRB4 expression in different human cell types.

The data in *Figure 4.12* shows that all four inhibitory receptors are predominantly found on DCs, $CD33^+$ myeloid cells, and $CD14^+$ monocytes. Expression on DCs and monocytes were confirmed in this chapter (*Figure 4.4*). Therefore, the phenotyping performed with these antibodies confirms the expression profiles previously seen with other groups. No LILR expression was observed in non-immune cells. This will need to be further confirmed by staining various different human tissue samples by IF as performed in *Figure 4.11*.

5 ASSESSING THE FUNCTION OF ANTI-LILRB1, LILRB2 AND LILRB3 ANTIBODIES *IN VITRO*

5.1 Introduction

In the previous chapters, a series of anti-LILRB1, LILRB2 and LILRB3 antibodies were generated and their specificity verified. In this chapter, their functions were assessed in a selection of *in vitro* assays. Antibodies are capable of eliciting functions in various ways including ADCC, ADCP, CDC and PCD described in detail previously (see Chapter 1 section 1.4.2.3.3). ADCC involves cytotoxic cells, such as NK cells binding to antibody-immune complexes; prompting cell lysis; ADCP comprises of phagocytic cells such as macrophages engulfing antibody-opsonised cells; CDC employs the complement cascade to initiate cellular cytotoxicity and antibodies can instigate cell necrosis by inducing PCD[217, 221, 225, 229].

Anti-CD20 antibody Rituximab has successfully been used to treat NHL since its approval in 1997[208]. This antibody is thought to work by eliciting ADCC through engagement of inhibitory receptor FcγRIIB[217]. Anti-CD20 antibodies have also been proposed to work through ADCP, as macrophages have been shown to be important for B cell depletion[221]. Alemtuzumab (Campath-1H®), an anti-CD52 antibody, has been shown to deplete tumours by CDC[225]. Finally, anti-CD20 GA101, has been shown to act by triggering PCD[229]. Therefore, different antibodies have been shown to bring about therapy in different ways.

Accordingly, various functional tests were performed to assess the therapeutic potential of the antibodies. These included testing the ability of the generated antibodies to activate or block the relevant receptor in the presence or absence of the physiological ligand (where known), and their effect on effector cells, by studying antibody effect on macrophage phagocytosis and T cell proliferation, all of which assess agonistic/antagonistic antibody potential. The ability of antibodies to cause receptor internalisation was also studied as this will influence drug delivery, important if these antibodies are to be used therapeutically, possibly as ADCs.

5.2 Results

5.2.1 Assessing the ability of LILR antibodies to activate cells

5.2.1.1 Cell activation by LILR antibodies in the absence of ligand

To assess whether the antibody clones could bind to cells and activate intracellular signalling in these cells, in the absence of any ligand, LILRB1, LILRB2 and LILRB3-transfected 2B4

reporter cells were generated. These reporter cells consisted of the extracellular domains of the relevant LILR receptors, fused to the CD3 ζ cytoplasmic domain. Nuclear Factor of Activated T cells (NFAT) proteins are responsible for regulating T cell development and function[256]. These reporter cells were able to stimulate GFP protein expression under the NFAT promoter, through the activatory CD3 intracellular domain. See *Figure 4.1* below for a schematic of how these reporter cells induce GFP expression.

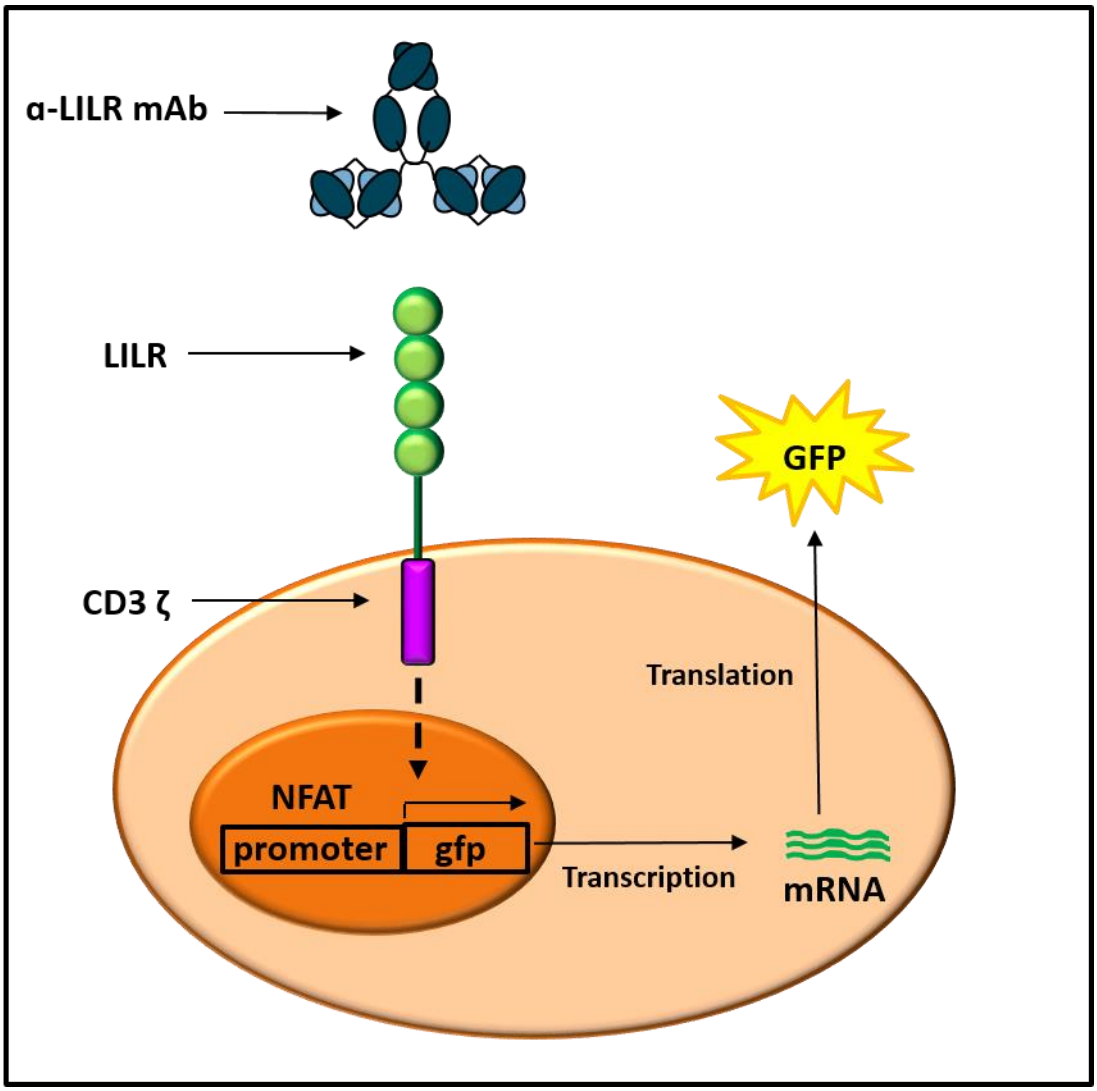

Figure 5.1 GFP reporter assay. 2B4 cells transfected with the extracellular domain of 3 different LILR receptors (LILRB1, LILRB2 and LILRB3), and the CD3 ζ cytoplasmic domain was activated by either an endogenous ligand (if known) or a target-specific antibody that is able to cause sufficient receptor cross-linking. This extracellular stimuli causes activation of an intracellular signalling cascade, where the transcription factor NFAT binds to its promoter and induces transcription of the reporter *gfp* gene to mRNA. This is then translated into GFP protein, which is released extracellularly and measurable by flow cytometry. The reporter cells were a gift from Dr Lewis Lanier, UCSF, San Francisco, California, USA, and transfected by Dr Des Jones, University of Cambridge.

Figure 5.1 shows that GFP expression was the result of CD3 intracellular signalling. This signalling is caused by receptor-ligand interaction. However, when no ligand is present,

antibodies against the receptor can cause sufficient cross-linking by binding to their receptor and activating cell signalling. Therefore, GFP expression was a measure of cellular activation. Cross-linking is defined as the ability of numerous antibody molecules coming together on the cell surface, and together are able to stimulate their receptor and result in cellular activation in the absence of a ligand.

The LILR-transfected 2B4 reporter cells were stained with the various anti-LILRB1, LILRB2 and LILRB3 antibodies overnight at 37°C, and then a PE-labelled secondary for 45 minutes at 4°C. Receptor binding was assessed by flow cytometry through fluorescence of the secondary antibody and cellular activation measured by GFP expression. The double positive (PE^+ GFP^+) cell populations were taken as the population of cells able to bind and activate cells i.e. elicit sufficient receptor cross-linking leading to GFP expression. Antibodies that were able to produce this double positive population were defined as agonists, as they were able to stimulate cellular activation in the absence of a ligand. Antibodies that were unable to induce these double populations were defined as non-agonists, potentially being antagonists (blocking cellular activation) or antibodies that are non-immunomodulatory (unable to cause a cellular response). Alternatively, they could be weak agonists, unable to reach the threshold of activation. The results are displayed in *Figure 5.2* below.

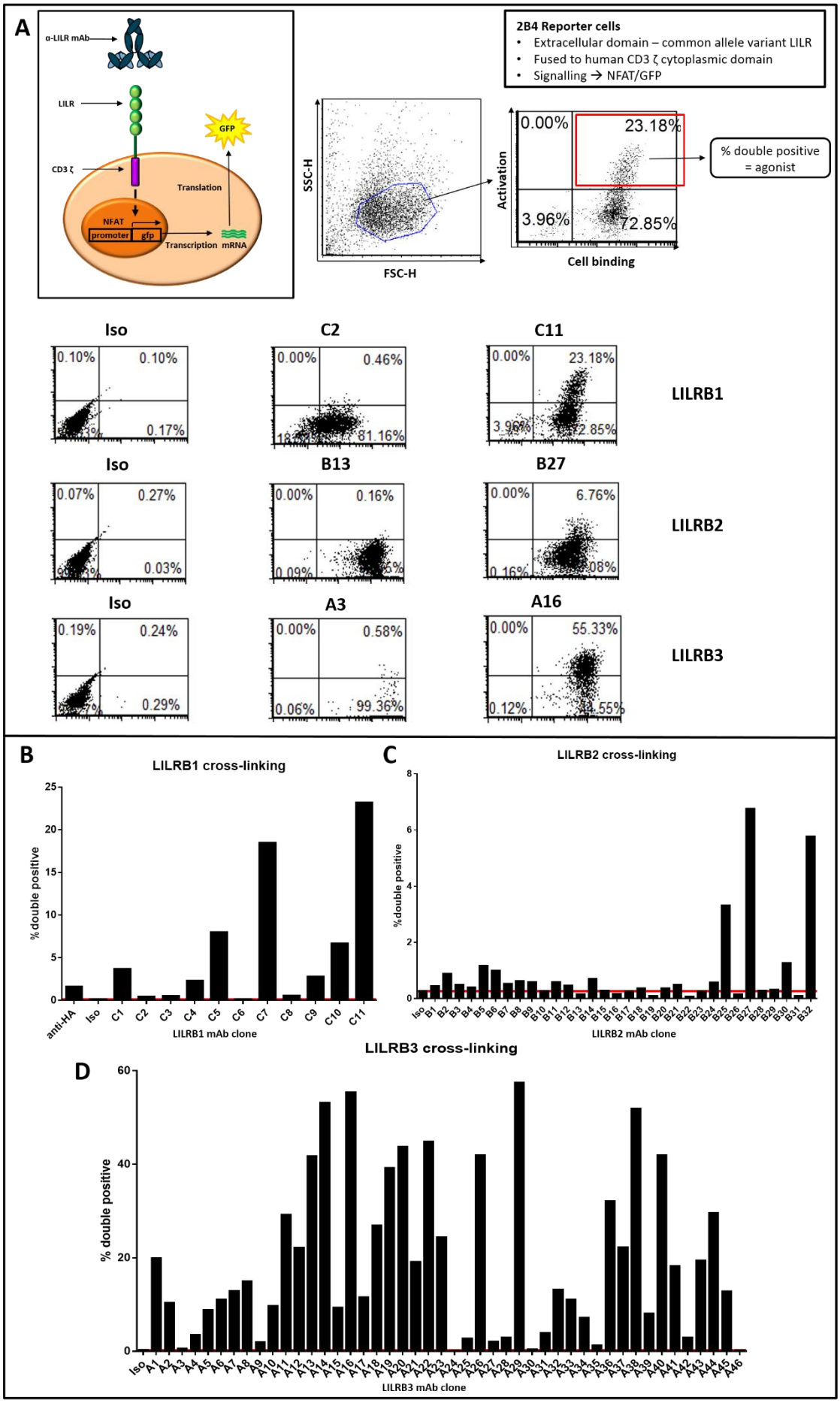
A
α-LILR mAb
LILR
CD3 ζ
GFP
Translation
NFAT
promoter
gfp
Transcription
mRNA
2B4 Reporter cells
Extracellular domain – common allele variant LILR
Fused to human CD3 ζ cytoplasmic domain
Signalling → NFAT/GFP
SSC-H
FSC-H
Activation
Cell binding
0.00%
23.18%
3.96%
72.85%
% double positive = agonist
Iso
C2
C11
LILRB1
0.10%
0.10%
0.17%
0.00%
0.46%
81.16%
0.00%
23.18%
3.96%
72.85%
Iso
B13
B27
LILRB2
0.07%
0.27%
0.03%
0.00%
0.16%
0.00%
6.76%
Iso
A3
A16
LILRB3
0.19%
0.24%
0.29%
0.00%
0.58%
99.36%
0.00%
55.33%
0.12%
B
LILRB1 cross-linking
% double positive
anti-HA
Iso
C1
C2
C3
C4
C5
C6
C7
C8
C9
C10
C11
LILRB1 mAb clone
C
LILRB2 cross-linking
% double positive
LILRB2 mAb clone
LILRB3 cross-linking
D
% double positive
LILRB3 mAb clone

Figure 5.2 Assessing antibody receptor cross-linking and cellular activation. 2B4 reporter cells were transfected with the extracellular domain of LILRB1, LILRB2 and LILRB3, fused with the human CD3 ζ cytoplasmic domain, and capable of GFP signalling under the NFAT promoter. 10 μg/ml generated anti-LILRB1, LILRB2 and LILRB3 antibodies were incubated with their respective reporter cell lines over night at 37°C, 5% CO_2. The following day the cells were stained with a secondary anti-human PE antibody (Jackson Labs) for 45 minutes at 4°C. Antibody cell staining (FL-2) and GFP activation (FL-1) were subsequently assessed by flow cytometry. The double positive (PE^+ GFP^+) cell populations were taken as agonistic antibodies able to bind and cause cellular activation. A schematic of the assay performed, the gating strategy used and example plots analysed in FCS express, are displayed in **A)**. Results represented graphically (GraphPad) for each antibody against their target LILR-transfected 2B4 cells in **B)** LILRB1 clones, **C)** LILRB2 clones and **D)** LILRB3 clones. A human IgG1 isotype control was taken as baseline (represented by solid red line on graph). These assays were performed by Dr Des Jones, *University of Cambridge*.

Figure 5.2A shows that some antibodies were able to bind to their receptor, but were unable to cause GFP expression: LILRB1 clone C2 (0.46% double positive cells), LILRB2 clone B13 (0.16%), and LILRB3 clone A3 (0.58%) all were able to bind but no GFP expression resulted. These clones were defined as non-agonists and may potentially be antagonistic (blocking cellular activation) or weak agonists unable to cause an immune response due to poor affinity. In comparison, some clones were able to both bind to their receptor and cause GFP expression (PE^+GFP^+ double positive), including LILRB1 clone C11 (23.18%), LILRB2 clone B27 (6.76%) and LILRB3 clone A16 (55.33%). These clones were defined as agonists.

Out of the 11 LILRB1 clones, 7 were found to cross-link the receptor sufficiently to drive GFP expression (above isotype/anti-HA controls): C1, C4, C5, C7, C9, C10 and C11 (*Figure 5.2B*). The majority of LILRB2 clones however, were unable to induce GFP expression, with the exception of 4 clones; B25, B27, B30 and B32, which showed a slight increase above the isotype control (~0.5-6% increase) (*Figure 5.2C*). However, this increase was minimal and therefore, these antibodies are very weak agonists. In comparison, almost all of the LILRB3 clones were able to cross-link their receptor sufficiently to cause GFP expression, although 10 clones; A3, A9, A25, A27, A28, A30, A31, A35, A42 and A45, showed very low GFP expression, and are likely to be weak agonists. A24 did not show agonistic potential at all, and was under the isotype control baseline. This clone was therefore a non-agonist.

This data indicated that a proportion of antibody clones were able to bind to cells and result in GFP expression. These antibodies therefore are likely to function as agonistic antibodies that stimulate receptor activation. In contrast, those antibodies unable to cause sufficient receptor cross-linking and GFP expression are weak or non-agonistic.

In summary, 7 LILRB1, 4 LILRB2 and 35 LILRB3 antibody clones showed clear agonistic potential and caused cellular activation in the absence of a ligand.

5.2.1.2 Blocking cell activation by generated antibodies in the presence of a ligand

Whilst some antibodies were able to activate cells (inducing GFP) without the presence of a ligand, others could not cause GFP expression. Those antibodies that did not cross-link their receptor sufficiently to cause GFP expression, may have needed the presence of a ligand to cause activation. To deduce this, antibodies that did not cross-link were therefore tested, to see if they could cause activation in the presence of a ligand. Accordingly, LILRB1 and LILRB2-transfected 2B4 reporter cells were stained with the various anti-LILRB1 and LILRB2 antibodies respectively, and co-cultured with 721.221 cells transfected with their ligand HLA-G. The ligand for LILRB3 is unknown and therefore blocking activation in the presence of its ligand could not be assessed. The reporter cells used in these assays (*Figure 5.3* below) functioned in the same as before (*see Figure 5.1*), this time in the presence of a ligand. Activation was measured by GFP expression as before.

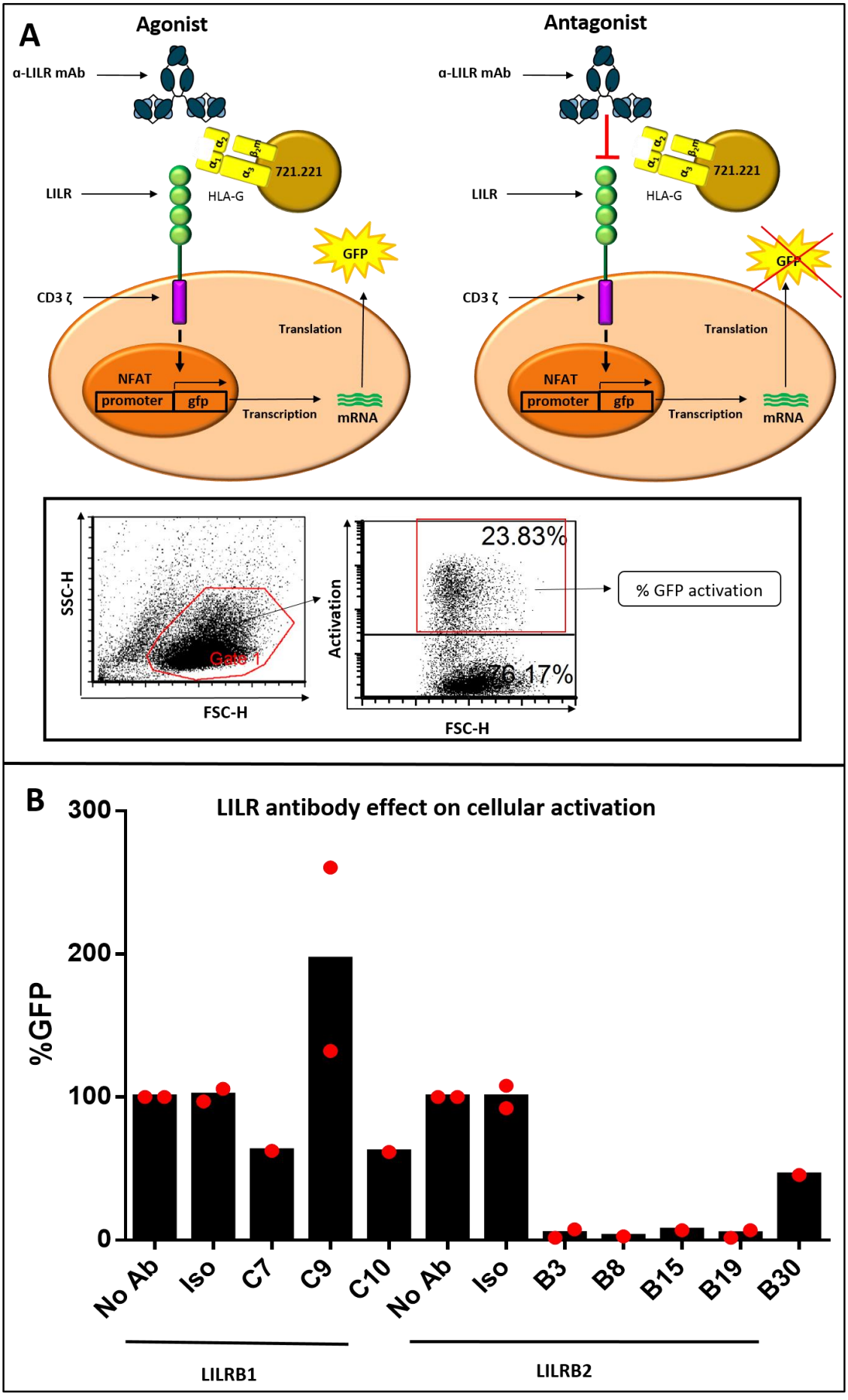
A
Agonist
Antagonist
α-LILR mAb
LILR
HLA-G
721.221
GFP
CD3 ζ
Translation
NFAT
promoter
gfp
Transcription
mRNA
SSC-H
FSC-H
Gate 1
Activation
23.83%
76.17%
% GFP activation
B
LILR antibody effect on cellular activation
%GFP
300
200
100
0
No Ab
Iso
C7
C9
C10
No Ab
Iso
B3
B8
B15
B19
B30
LILRB1
LILRB2

Figure 5.3 Assessing the effect of anti-LILRB1 and -LILRB2 antibodies on ligand-induced cellular activation. A) Schematic of the assays performed and gating strategy. LILRB1 and LILRB2 2B4 Reporter cells were co-cultured with a Lymphoblastoid cell line (LCL) 721.221 cells transfected with HLA-G, resulting in GFP expression. LILRB1 or LILRB2 antibodies were incubated with the co-culture to assess receptor agonism or antagonism. Antibodies able to enhance GFP expression were defined as agonists, whilst those that blocked GFP expression, antagonists. **B) LILR antibody effect on ligand-induced cellular activation.** LILRB1- or LILRB2-transfected 2B4 reporter cells, were treated with either no antibody (no Ab), 10 µg/ml anti-LILRB1, LILRB2 or an isotype antibody, and incubated with HLA-G-transfected 721.221 cells, at 37°C, 5% CO_2, overnight. GFP activation was then measured by flow cytometry. Summary of two independent experiments are given here. These assays were performed by Dr Des Jones, *University of Cambridge*. Data normalised to no Ab control as 100%.

Figure 5.3A shows the way in which the assay was performed and the gating strategy used. Co-culturing LILRB1 or LILRB2-transfected 2B4 reporter cells with HLA-G-transfected cells resulted in GFP expression. Antibodies able to enhance this GFP expression were termed agonists, whilst antibodies that blocked this GFP expression were defined as antagonists.

GFP expression was measured as an output of cellular activation. No GFP activation was seen when LILRB1- or LILRB2-transfected 2B4 cells were incubated with 721.221 cells deficient in HLA-G (data not shown). However, the presence of HLA-G (in the absence of antibody) resulted in GFP expression (*Figure 5.2B*). This shows that LILRB1 and LILRB2 are binding to their ligand HLA-G and causing GFP activation, not a ligand found on the 721.221 cells themselves. When the co-culture of cells expressing LILRB1 or LILRB2 and HLA-G were incubated with anti-LILRB1 or LILRB2 antibodies GFP expression was found to either be enhanced or reduced, indicating these antibodies were agonist or antagonists respectively.

LILRB1 clones, C7, C9 and C10, and LILRB2 clones B3, B8, B15, B19 and B30 were tested in this assay, as they caused little or no cross-linking (*Figure 5.2*). LILRB1 clone C9 showed enhanced GFP expression (~100% increase in GFP activation compared to isotype). This suggests this clone is an agonist, although this clone showed no ability to cross-link in previous assays (*Figure 5.1*). This could be due to the antibody clone being unable to cross-link enough to reach an activation threshold able to cause cellular activation, but in the presence of a ligand it can, therefore, the agonistic potential of the clone is ligand-dependent. LILRB1 clones C7, C10 and LILRB2 clones B3, B8, B15, B19 and B30 all blocked GFP activation, suggesting they are antagonistic antibodies. This agrees with their lack of ability to cross-link (although C7 showed some ability to cross-link). B30 is a poorer blocker (activation drops from 100% with isotype to ~45% with B30) compared to the other LILRB2 clones that almost completely block activation. Although B30 was unable to initiate cross-linking, this clone did show a slightly higher ability to cause a little cellular activation when

compared to B3, B15 and B19, and this could be why it only partially blocks, as it is a weakly antagonistic antibody.

In summary, all five LILRB2 clones blocked GFP expression and therefore receptor activation, and LILRB2 clones C7 and C10 also showed blocking of activation, indicating these antibodies are antagonists and capable of blocking HLA-G binding. However, C9 enhanced GFP expression and receptor activation, and therefore is an agonist.

5.2.2 T-cell Proliferation

Having established the agonistic or antagonistic properties of these antibodies on transfected cell lines expressing their receptors, their ability to either stimulate or block receptor signalling on primary cells was then assessed.

T cells are important immune cells in both cancer and autoimmunity. APCs regulate T cell responses through processing and presenting antigens to these cells. APCs such as DCs express LILRs[249]. Finding ways in which to manipulate T cell proliferation is therefore important for therapy. To assess the ability of the anti-LILR antibodies to manipulate T cell proliferation, a series of different T cell assays were attempted.

5.2.2.1 DC-based assays

Firstly, to assess the effect of the anti-LILR antibodies on T cell proliferation, a DC/T cell co-culture was established. MDDCs were generated from PBMCs using IL-4 and GM-CSF over 7 days. The cells were then treated with/without LPS (data not shown) to activate the cells, and with/without tetanus antigen to drive re-call responses, and as a result T cell proliferation. PBMCs from the same donor used to generate the MDDCs (autologous), or from a different donor (allogeneic) were labelled with CFSE, and T cells were isolated using a negative pan-T cell isolation kit (Stem Cell Technologies). LPS/tetanus-treated MDDCs were then co-cultured with CFSE-labelled autologous or allogeneic T cells. CFSE dilution was then used to measure T cell proliferation after 7-11 days by flow cytometry. However, stimulating T cell proliferation in this manner was unsuccessful, as no clear CFSE dilution was observed. Example histograms are displayed below (*Figure 5.4*) from one MDDC donor co-cultured with allogeneic T cells.

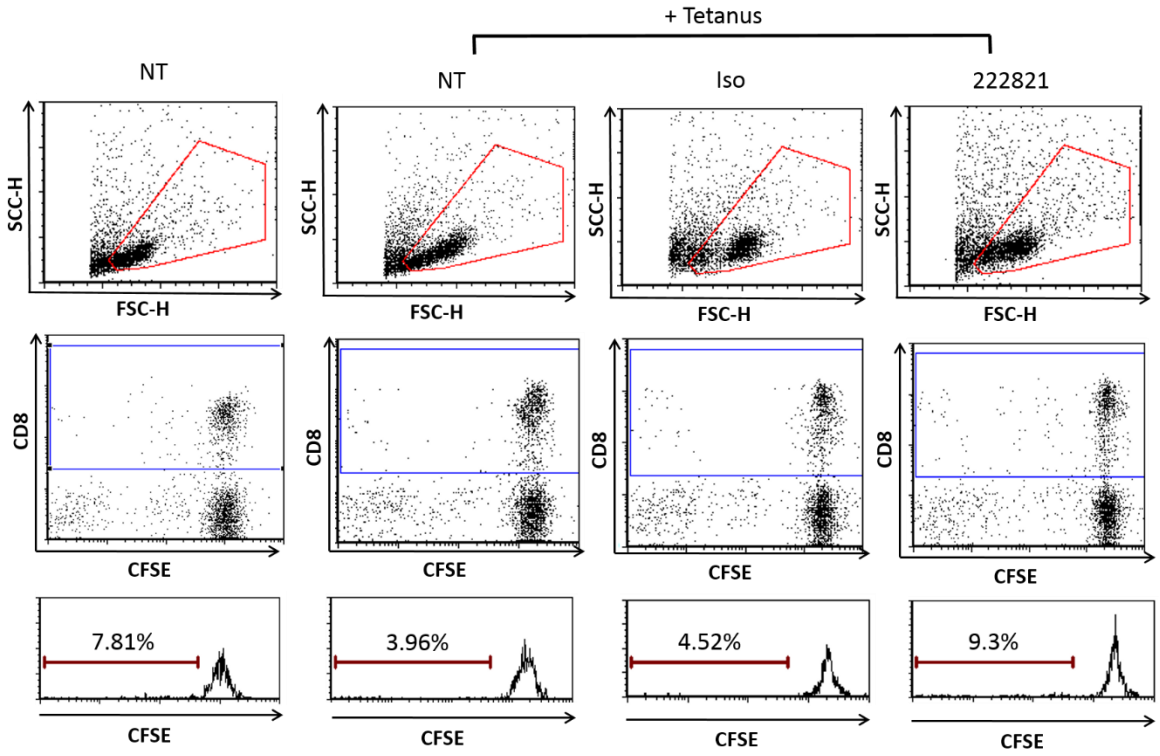

Figure 5.4 DC-T cell co-culture. MDDCs were generated over 7 days as described in methods section 2.5.2. 48 hours before co-culture frozen allogeneic PBMCs were CSFE-labelled for 10 min at room temperature, then quenched with FCS. Cells were then cultured at high density ($1x10^7$ cells/ml). 24 hours before co-culture, MDDCs were incubated with 10ug/ml anti-LILRB3 clone 222821 (R&D systems), or a relevant isotype control, +/- 1ug/ml tetanus antigen (Sigma). T cells were isolated from CFSE-labelled PBMCs, by negative selection with the EasySep™ Human T Cell Isolation Kit (StemCell Technologies). $1x10^4$ cells/well MDDCs were then harvested and co-cultured with $1x10^5$ cells/well isolated CFSE-labelled T cells for 11 days. Subsequently, cells were stained with 5µg/ml anti-CD8-APC (Biolegend), harvested and CSFE dilution (as a measure of T cell proliferation) was measured by flow cytometry.

Figure 5.4 shows one representative assay, where MDDCs were co-cultured with allogeneic T cells. In the absence of antigen (Tetanus), no CFSE dilution was observed and therefore no T cell proliferation. However, even when MDDCs were treated with antigen, no CFSE dilution was observed. This was also the case when antigen-treated MDDCs were incubated with anti-LILRB3 or an isotype control. Activating MDDCs with LPS also did not drive T cell proliferation (data not shown). The assay was repeated with autologous T cells (data not shown) and similar results were obtained. In all cases, cells appeared to be large and granular (based on SSC vs FSC profiles), with no signs of CFSE dilution, rather a high and low CFSE cell population. This indicated that cells were dying, and any CFSE reduction was likely due to cell death, rather than cell division.

Therefore, it was concluded that recall responses with the donors tested, were not obtained and no proliferation could be generated. Further optimisation of the assay was needed.

5.2.2.2 PBMC-based assays

Given the difficulty of generating T cell proliferation with the DC-T cell co-culture experiments, a T cell proliferation assay mediated by antibody-driven CD3/CD28 stimulation was instead performed. PBMCs were CFSE labelled and T cell proliferation induced with soluble anti-CD3 and anti-CD28 stimulation.

To first establish the assay, the cells were cultured for 4 days with a positive control: commercial anti-LILRB3 clone 222821 (R&D Systems) – a known agonist; and a relevant negative (isotype) control. Wild-type and deglycosylated (PNGase-treated) antibodies were compared. Deglycosylation was confirmed by comparing molecular weights of wild-type versus deglycosylated antibodies by SDS-PAGE. Light microscopy images were taken of the cells after 4 days, and proliferation was measured as CFSE dilution by flow cytometry, gating on CD8+ T cells.

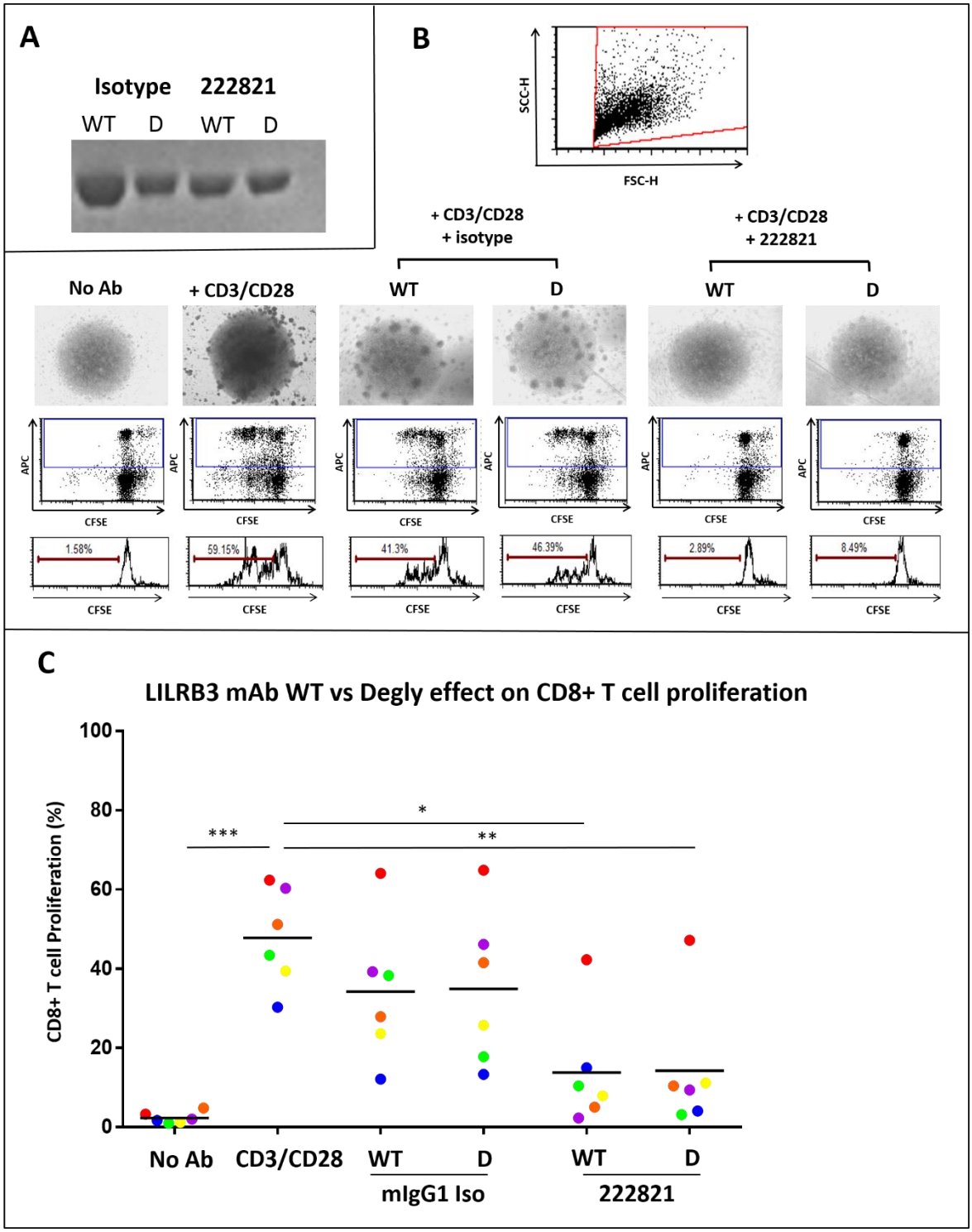
A
Isotype
222821
WT
D
WT
D
B
SCC-H
FSC-H
+ CD3/CD28
+ isotype
+ CD3/CD28
+ 222821
No Ab
+ CD3/CD28
WT
D
WT
D
APC
CFSE
1.58%
59.15%
41.3%
46.39%
2.89%
8.49%
C
LILRB3 mAb WT vs Degly effect on CD8+ T cell proliferation
CD8+ T cell Proliferation (%)
100
80
60
40
20
0
***
*
**
No Ab
CD3/CD28
WT
D
WT
D
mIgG1 Iso
222821

Figure 5.5 Assessing the effect of anti-LILRB3 wild-type vs deglycosylated antibody on T cell proliferation. A) Confirmation of deglycosylation by SDS-PAGE. 5 µg wild-type (WT) or PNGase-treated (Promega)/deglycosylated (D) anti-LILRB3 clone 222821 (R&D systems) or relevant isotype were denatured in 4x Laemmli buffer for 95°C for 5 minutes. Samples were then run on a NuPAGE 4-12% Bis-Tris pre-cast gel (Life Technologies) in MOPS running buffer for 1 hour at 200 V constant, and visualised with the Molecular Imager® Gel Doc™ XR Imaging System (Bio-Rad). **B) Assessing T cell Proliferation.** Proliferation assays were then performed. PBMCs were isolated by lymphoprep and labelled with 2 µM CFSE (Sigma) for 15 minutes at room temperature. $1x10^6$ cells were plated and stimulated with 0.02 µg/ml anti-CD3 (clone OKT3, in-house) and 5 µg/ml anti-CD28 (Biolegend). Cells were also treated with 10 µg/ml wild-type (WT) or PNGase (Promega) treated deglycosylated (D) anti-LILRB3 (R&D systems) or relevant isotype control (in house) and incubated at 37°C for 4 days. Light microscopy images were taken on day 4 using the CKX41 microscope (Olympus) and visualised with the Cell^B (Olympus) software. **C) Comparing the effect of WT and D anti-LILRB3 treatment on proliferating T cells.** Proliferation was performed as described above in B). Cells were then stained with 5 µg/ml anti-CD8-APC (Biolegend) for 15 minutes at room temperature, harvested and analysed by flow cytometry. Flow cytometry was used to assess CFSE dilution of gated $CD8^+$ cells and %CFSE dilution taken as a measurement of proliferation. Graphs and statistics performed in Graphpad. One-way ANOVA was performed comparing each treatment to CD3/CD28 treated only, n= 6 different donors (in different colours), and mean represented by solid line, ($p < 0.05$ *, $p < 0.005$ **, $p < 0.0005$ ***).

Although, subtle, there was a slight difference in molecular weight when comparing WT versus D clone 222821 or its isotype control, suggesting successful deglycosylation (*Figure 5.5A*).

Anti-CD3 and anti-CD28 stimulation were successfully able to drive $CD8^+$ T cell proliferation as evidence by CFSE dilution, representing cell division (*Figure 5.5B*). $CD4^+$ T cell proliferation was not shown in this instance due to poor CD4 antibody staining (data not shown). *Figure 5.5B* shows one sample (from duplicate results) from one representative donor. Microscopy images showed cells aggregate in one large cluster when not stimulated with any antibody and no CFSE dilution was observed by flow cytometry (1.58%). However, upon anti-CD3 and -CD28 stimulation, these cells began to divide and clump, demonstrated by the budding cell clusters around the larger mass and 59.15% CFSE dilution observed by flow cytometry. Treatment of antibody-driven proliferating cells with an irrelevant isotype control, showed similar cell clusters as the anti-CD3 and -CD28 stimulated cells, suggesting the isotype does not inhibit proliferation. Treatment of antibody-driven proliferating cells with clone 222821 however, showed no budding cell clusters, similar to the image of the no antibody treated control, suggesting that this clone inhibits cells proliferation. When comparing the WT and D isotype control-treated samples, similar results were seen by microscopy and flow cytometry (41.3% compared to 46.39% respectively). Both WT and D anti-LILRB3 treated sample also show similar results by microscopy and flow cytometry (2.89% compared to 8.49%, respectively). Although there was slightly more inhibition with 222821 WT compared to 222821 D.

Figure 5.5C shows a summary of combined proliferation assays taken from 6 donors. Clone 222821 blocked proliferation and this was statistically significant. The isotype control appeared to show some inhibition for both the WT and D antibody (~20% decrease). However, when compared to the anti-CD3/CD28 control neither of the isotype samples were significantly different. Treatment with anti-LILRB3 WT and D however, was significantly different compared to the anti-CD3/CD28 control (~40% inhibition).

There was no significant difference between the WT and D samples for both the isotype and anti-LILRB3 treated cells. However, when comparing each individual donor, there did appear to be a difference between some WT and D samples. This indicated that antibody Fc-interaction could be having a slight effect on the assay, causing a greater decrease/increase in proliferation. For this reason, in all future T cell proliferation assays, only deglycosylated antibodies were used.

To assess the inter-donor variability and reproducibility of these findings, the assay was repeated with two different deglycosylated commercial anti-LILRB3 clones, one that is a known agonist (222821) and another that is a known antagonist (TRX585).

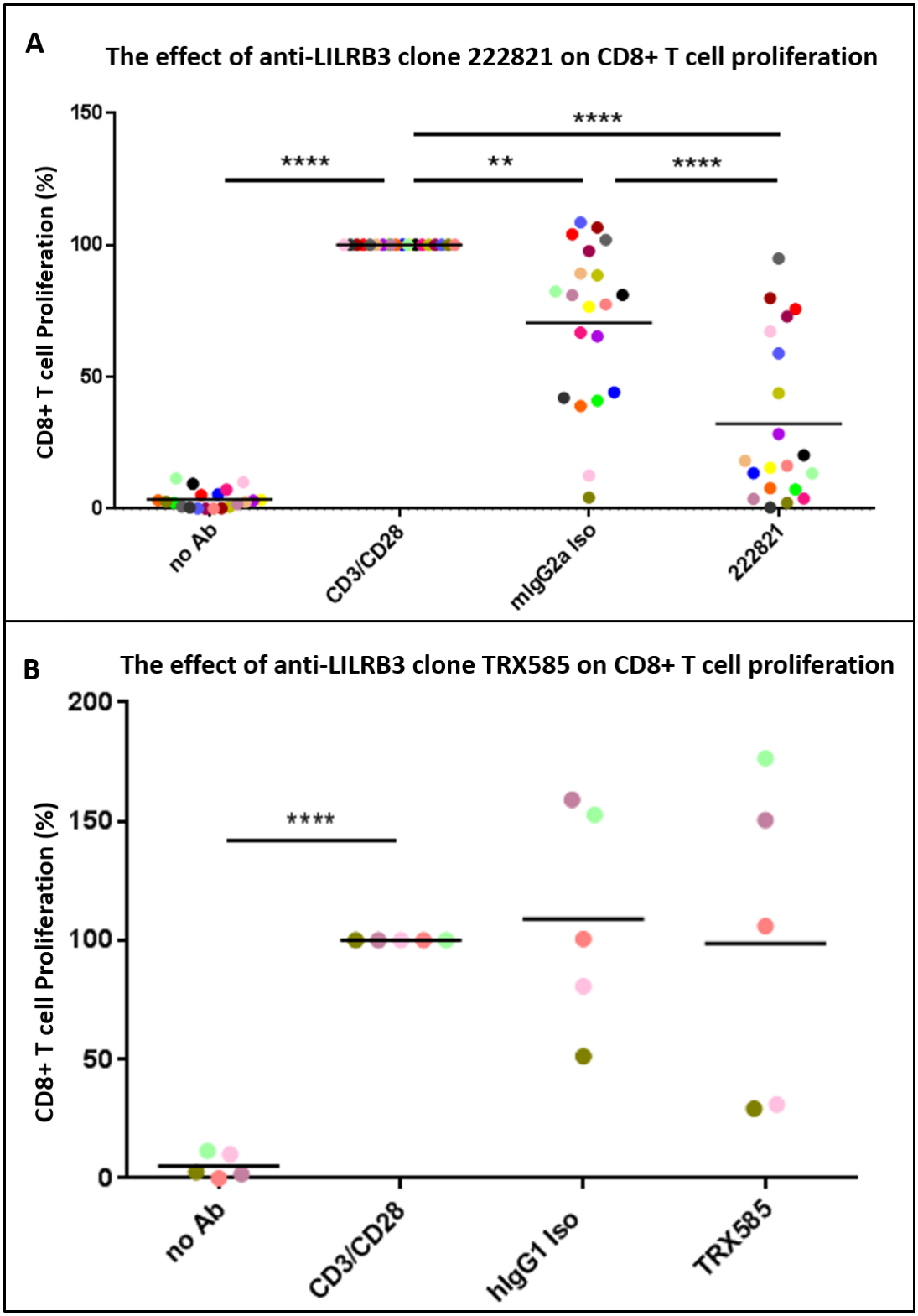

Figure 5.6 The effect of deglycosylated commercial anti-LILRB3 mAbs on T cell proliferation. PBMCs were isolated by lymphoprep and labelled with 2 µM CFSE (Sigma) for 15 minutes at room temperature. $1x10^6$ cells were plated and stimulated with 0.02 µg/ml OKT3 (in-house) and 5 µg/ml anti-CD28 (Biolegend). Cells were also treated with 10 µg/ml anti-LILRB3 or isotype control and incubated at 37°C for 4 days. Cells were then stained with 5 µg/ml anti-CD8-APC (Biolegend) for 15 minutes at room temperature, harvested and analysed by flow cytometry. **A)** Clone 222821 (R&D systems) n= 20 (donors in different colours) **B)** clone TRX585 (Tolerx Inc) n= 5 (donors in different colours). One-way ANOVA performed,), data normalised to CD3/CD28-treated only samples, mean represented by solid line ($p < 0.05$ *, $p < 0.005$ **, $p < 0.0005$ ***, $p < 0.00005$ ****).

As previously (*Figure 5.5*), no antibody treatment resulted in no T cell proliferation, demonstrated by no CFSE dilution. However, treatment with anti-CD3/CD28 showed proliferation (normalised to 100% in *Figure 5.6). Figure 5.6A* shows that treating the cells with both anti-CD3/CD28 and the commercial anti-LILRB3 antibody clone 222821 however, resulted in a reduction in CFSE dilution and therefore inhibition of T cell proliferation. When comparing 20 different donors, clone 222821 showed clear inhibition of T cell proliferation compared to its isotype control (75% compared to 25% inhibition). In comparison, another previously developed clone TRX585 shows no significant difference in T cell proliferation (*Figure 5.6B*). TRX585 is a commercial antibody (Tolerx Inc) shown previously to stimulate T cell proliferation in a mixed lymphocyte reaction (MLR)[257]. However, here the antibody showed no significant difference on T cell proliferation. Though there was a lot of donor variability, and some donors did appear to enhance proliferation (*Figure 5.6B*). As only five donors for this antibody treatment were performed, more donors were needed to validate these findings. In summary, known agonist clone 222821 inhibited T cell proliferation whilst known antagonist TRX585 showed no difference in this instance, likely due to a small sample size.

As inhibition of T cell proliferation was observed with the commercial anti-LILRB3 antibody, various deglycosylated LILRB1, LILRB2 and LILRB3 clones were tested in the same way. PBMCs were treated with anti-CD3 and anti-CD28 as previously (*Figure 5.5*). Cells were then treated with different anti-LILRB1, -LILRB2 and -LILRB3 antibodies and CFSE dilution measured after 4 days. Representative clones are shown in *Figure 5.7*.

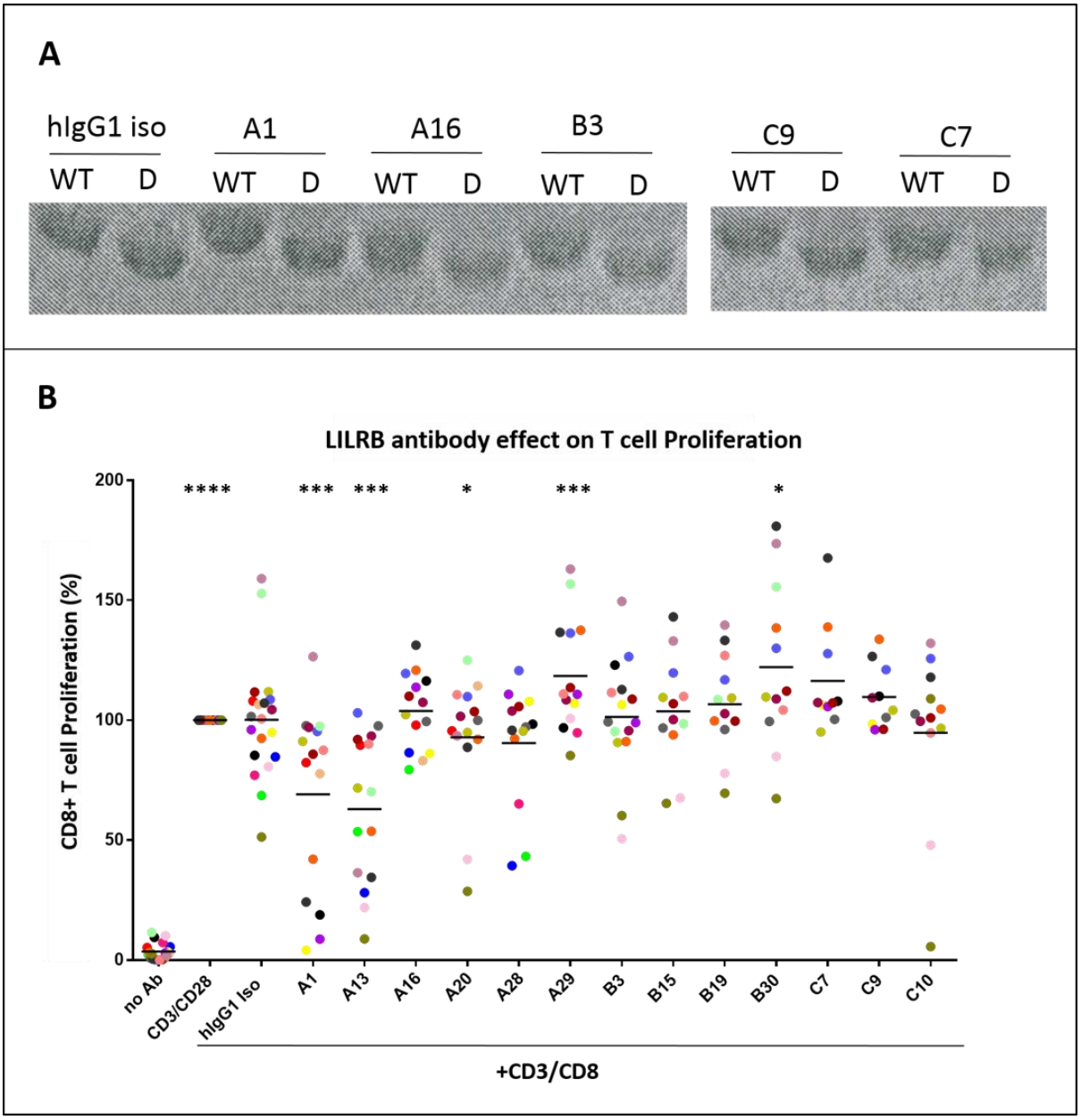

Figure 5.7 The effect of various anti-LILR antibodies on T cell proliferation. A) Confirmation of anti-LILR deglycosylation by SDS-PAGE. 5 µg wild-type (WT) or PNGase-treated (Promega)/deglycosylated (D) anti-LILR antibodies or relevant isotype were denatured in 4x Laemmli buffer for 95°C for 5 minutes, and samples run on a NuPAGE 4-12% Bis-Tris pre-cast gel (Life Technologies) in MOPS running buffer for 1 hour at 200 V constant. Samples were visualised with the Molecular Imager® Gel Doc™ XR Imaging System (Bio-Rad). Example anti-LILRB3 clones A1 and A16, anti-LILRB2 clone B3 and anti-LILRB1 clones C7 and C9 are displayed here. **B) The effect on anti-LILRs on T cell proliferation.** PBMCs were isolated by lymphoprep and labelled with 2 µM CFSE (Sigma) for 15 minutes at room temperature. $1x10^6$ cells were plated and stimulated with 0.02 µg/ml OKT3 (in-house) and 5 µg/ml anti-CD28 (Biolegend). Cells were then treated with 10 µg/ml deglycosylated with PNGase (Promega) anti-LILRB1, LILRB2 and LILRB3 clones (BioInvent), commercial anti-LILRB3 (Tolerx Inc) or a hIgG1 isotype control (BioInvent) and incubated at 37°C for 4 days. Cells were then stained with 5 µg/ml anti-CD8-APC (Biolegend) for 15 minutes at room temperature, harvested and analysed by flow cytometry. n= 5-20 independent donors (represented in different colours) and data is normalised to CD3/CD28-treated only samples. Mean represented by solid line. Two-tailed paired T-test was performed and stars represent level of significant difference compared to isotype control ($p < 0.05$ *, $p < 0.005$ **, $p < 0.0005$ ***).

Successful deglycosylation was observed by a decrease observed in molecular mass of deglycosylated antibodies compared to their wild-type counterparts (*Figure 5.7A*).

Figure 5.7B shows that LILRB3 clones A1, A13 and A20 all significantly decreased proliferation (mean decrease to ~70, 60 and 90% proliferation compared to CD3/CD28 control), whilst clone A29 significantly increased proliferation (to ~120% mean proliferation). Only the LILRB2 clone B30 had a significant increase on T cell proliferation (to ~125%) whilst none of the LILRB1 clones show a significant difference in T cell proliferation. This suggests that most of the LILRB3 clones are agonistic antibodies, which drive LILRB3 inhibition, thus causing a decrease in T cell proliferation. However, one clone A29 appears to be antagonistic and can increase proliferation. B30 also appears to be antagonistic.

Table 5.1 below summarises the p values and subsequent significant differences between the different LILRB1, LILRB2 and LILRB3 clones tested in *Figure 5.7*, compared to their isotype control.

Table 5.1 Significant differences of LILRB antibody treatment compared to isotype control on $CD8^+$ T cell proliferation

Comparison	Donors	P value	Significant?	
No Ab vs CD3/CD28	20	<0.0001	Y	****
hIgG1 iso vs CD3/CD28	20	0.9730	N	
hIgG1 iso vs TRX585	5	0.4566	N	
hIgG1 iso vs A1	15	0.0001	Y	***
hIgG1 iso vs A13	15	0.0004	Y	***
hIgG1 iso vs A16	14	0.2524	N	
hIgG1 iso vs A20	14	0.0224	Y	*
hIgG1 iso vs A28	13	0.2926	N	
hIgG1 iso vs A29	14	0.0003	Y	***
hIgG1 iso vs B3	15	0.6636	N	
hIgG1 iso vs B15	12	0.6343	N	
hIgG1 iso vs B19	12	0.9756	N	
hIgG1 iso vs B30	12	0.0415	Y	*
hIgG1 iso vs C7	10	0.0746	N	
hIgG1 iso vs C9	10	0.1517	N	
hIgG1 iso vs C10	12	0.0758	N	

Two-tailed T-test performed comparing isotype control to each antibody treatment in GraphPad ($p < 0.05$ *, $p < 0.005$ **, $p < 0.0005$ *** $p < 0.00005$ ****)

A1, A13 and A20 as seen in *Table 5.1* significantly decrease proliferation whilst A29 and B30 significantly increase proliferation.

As only LILRB1 has been reported to be expressed on T cells, it is unlikely that this effect is a direct effect, but likely indirect through APCs[67]. It has already been previously reported that LILRBs may act on DCs, rendering them tolerogenic and decreasing T cell proliferation[120]. LILRs are expressed on DCs (*see Chapter 4 Figure 4.4*) and therefore, these antibodies are potentially targeting the DCs in this assay, which in turn are effecting the T cells. Alternatively, other myeloid cells expressing LILRs may be involved such as monocytes or macrophages. Macrophages are phagocytic cells but are also able to act as APCs. As described in *Chapter 1.1.2.1*, M1 macrophages are pro-inflammatory and are especially good at presenting antigen to T cells, inducing T_H1 responses[4]. These macrophages are able to regulate T cell responses and can inhibit T cell proliferation [258].

5.2.3 Macrophage phagocytosis assays

After establishing that anti-LILRB clones could affect T cell proliferation indirectly, possibly through APCs, the direct effect that these clones can have on effector cells was studied. LILRBs are highly expressed on macrophages, therefore to further characterise the function of these receptors on myeloid cells, the effect of these antibody clones on macrophage phagocytosis was studied.

Human MDMs were generated from monocytes isolated from PBMCs and cultured with recombinant human M-CSF every other day for a period of 7 days. MDMs were stained with anti-LILRB3-APC (R&D systems) (*Figure 5.8A*), to confirm LILRB3 expression on these cells. Uniform expression of LILRB3 was seen, and a representative donor is displayed in *Figure 5.8A*. Having established LILRB3 expression, MDMs were plated and then pre-treated with anti-LILRB3 for 2 hours before being co-cultured with anti-CD20 (Rituximab)-opsonised B cells. The percentage of phagocytosis was measured as: the percentage of double-positive cells (MDMs + B cells) divided by the total number of MDMs, multiplied by 100 (*Figure 5.8B*). Then the percentage of phagocytosis was plotted for the various different treatments.

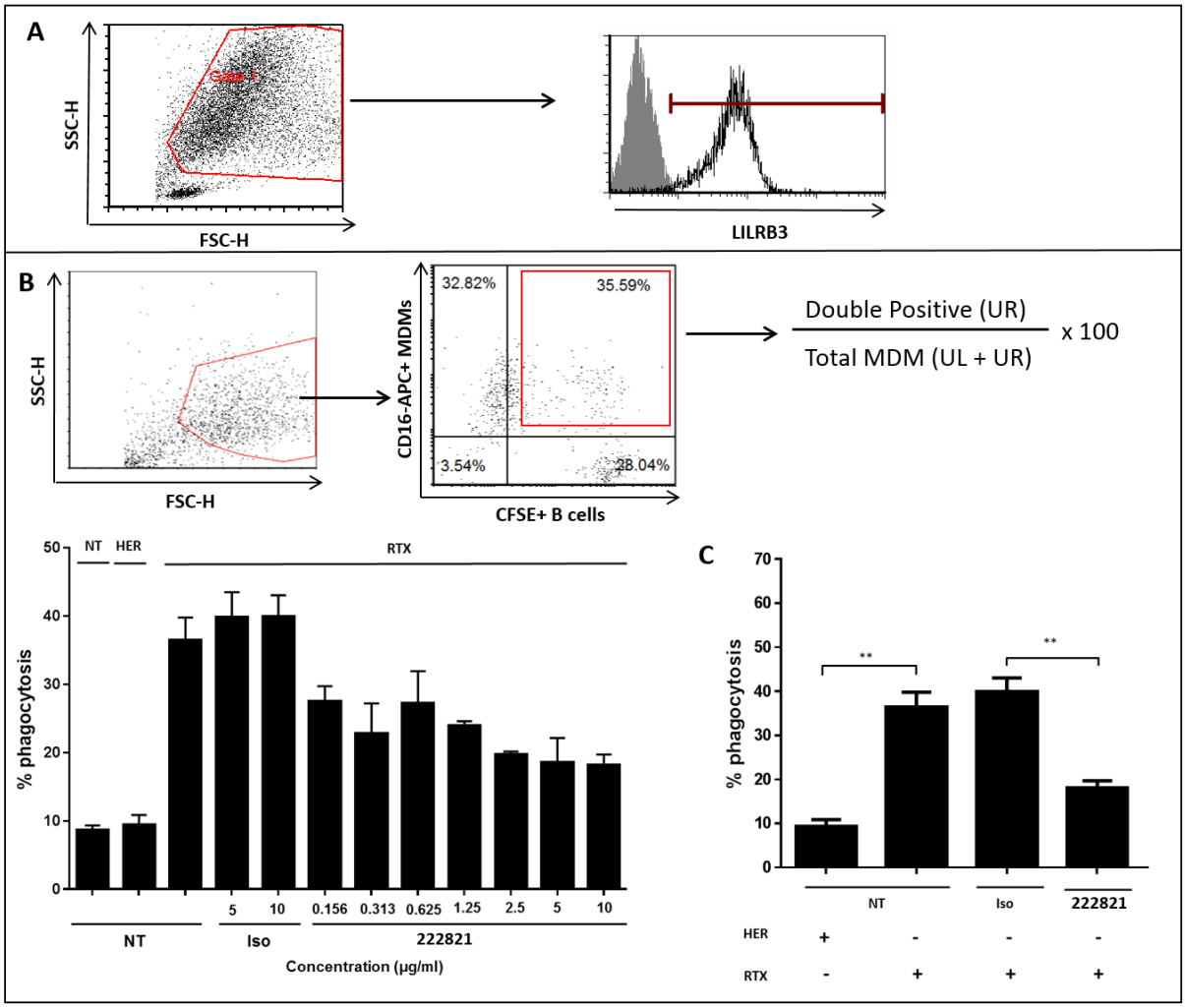

Figure 5.8 Assessing the effect of anti-LILRB3 on macrophage phagocytosis. A) Day 8 human MDMs were stained with anti-LILRB3-APC (R&D systems) for 25 minutes, 4°C, washed with FACS wash and analysed by flow cytometry. **B)** MDMs were pre-treated with anti-LILRB3 clone 222821 (R&D systems) or TA99 isotype control (in house) at various concentrations for 2 hours in culture at 37°C. Raji B cells were labelled with 5 µM CFSE (Sigma) for 15 minutes at room temperature. Opsonisation of B cells was carried out by adding 10µg/ml Rituximab (RTX) (in house) or 10µg/ml control isotype antibody Herceptin (HER) (in house), for 25 minutes at 4°C. MDMs were then co-cultured with opsonised Raji B cells in a 1:1 ratio ($1x10^5$ cells) for 1 hour at 37°C. MDMs were then stained with 10µg/ml CD16-APC (Biolegend), for 15 minutes at room temperature and analysed by flow cytometry. The percentage of phagocytosis was measured as: the percentage of double-positive cells (MDMs + B cells) divided by the total number of MDMs, multiplied by 100. All treatments were carried out in triplicate. Error bars represent standard deviation. **C)** Paired T test was performed on the data. Displayed here are MDMs treated with 10 µg/ml Iso (TA99) or anti-LILRB3 clone 222821, co-cultured with 10 µg/ml RTX-opsonised B cells; or control MDMs with no antibody treatment, or opsonised with 10 µg/ml HER. Non-treated MDMS with RTX-opsonised B cells vs Non-treated MDMS with HER-opsonised B cells: p = 0.0042. TA99 vs LILRB3: p = 0.0033. (n=1 donor, performed in triplicates).

MDMs expressed LILRB3 (*Figure 5.8A*). Macrophage phagocytosis required macrophages to be co-cultured with anti-CD20 opsonised B cells, as B cells opsonised by an isotype or non-opsonised B cells, resulted in low levels of phagocytosis (*Figure 5.8B*). The percentage of phagocytosis (double positive cells) decreased with increasing concentration of 222821 in a dose-dependent manner (*Figure 5.8B*). *Figure 5.8C* shows a summary of the data. ~40%

phagocytosis seen with Rituximab (RTX)-opsonised B cells co-cultured with isotype-treated MDMs, is decreased to ~20% when MDMs are treated with 222821, and this difference is statistically significant (p = 0.0033). Therefore, the commercial antibody clone 222821 has an agonistic effect on the LILRB3 receptor, augmenting the inhibitory nature of the receptor with respect to ADCP.

Antibody efficacy can be altered by interaction with Fc receptors, as seen by the important role of FcγRIIB in anti-CD20 therapy[52, 217]. To eliminate antibody-Fc receptor interaction as the potential cause of the inhibition seen in *Figure 5.9* macrophage phagocytosis was performed again, this time first coating the plate with Protein-G (binds to antibody Fc), therefore immobilising the antibody and preventing anti-LILRB3 antibody-Fc-interaction with FcγRs on the cell surface of macrophages. Long-term treatment of anti-LILRB3 (over 7 days) was also studied.

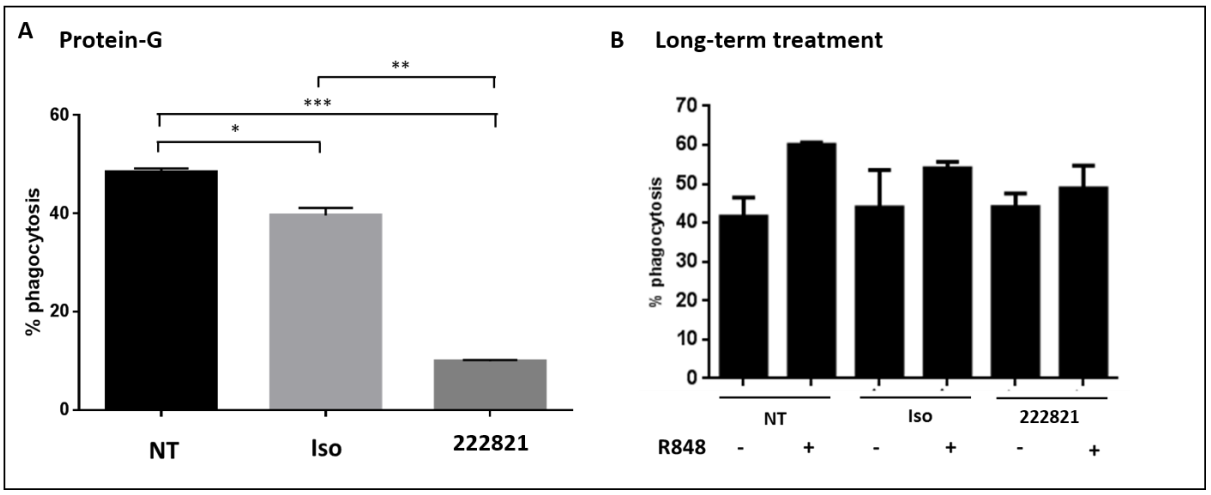

Figure 5.9 Assessing the effect of anti-LILRB3 on macrophage phagocytosis without interfering with macrophage Fc receptors and long-term antibody treatment. A). LILRB3 inhibition is not Fc-dependent. Human MDMs were plated at $1x10^5$ cells/well and allowed to adhere. MDMs were subsequently treated with anti-LILRB3 at various concentrations (5 fold dilutions from 5 µg/ml to 0.008 µg/ml). The LILRB3-treated MDMs were co-cultured with 5 µM CFSE-labelled (Sigma) 2 µg/ml Rituximab (RTX)-opsonised Raji B cells in a 1:1 ratio for 1 hour at 37°C and MDMs stained with 10µg/ml CD16-APC (Biolegend), for 15 minutes at room temperature, then analysed by flow cytometry. In a spate assay, a 96-well plate was coated with 10 µg/ml Protein-G (PrG) overnight, and then MDMs were plated at $1x10^5$ cells/well and treated with 5 µg/ml anti-LILRB3 clone 222821 (R&D systems) or an isotype control (WR17, in house), before being co-cultured with Rituximab-opsonised B cells for 1 hour at 37°C and then analysed by flow cytometry. Paired T test was performed on data from the protein-G assay. NT vs Iso: p=0.0048. Iso vs LILRB3: p= 0.0011. NT vs LILRB: p=0.0002 (n=1). **B) Long-term anti-LILRB3 treatment has no effect on MDM phagocytosis**. Human MDMs were treated with 5 µg/ml anti-LILRB3 clone 222821 or isotype (WR17), 7 days prior to the assay. The MDMs were either stimulated with 1 µM R848 or were left unstimulated. After 7 days, MDMs were co-cultured with 5 µM CFSE-labelled Raji B cells, opsonised with 2 µg/ml Rituximab. MDMs were stained with 10µg/ml CD16-APC (Biolegend), for 15 minutes at room temperature. Paired T-test was performed, but no significant difference was found between any of the treatment groups. NT + R848 vs Iso + R848: p = 0.3795. NT + R848 vs LILRB3+ R848: p= 0.2532. Iso + R848 vs LILRB3 + R848: p= 0.1622 (n=1).

222821 (as previously seen in *Figure 5.8*) inhibited phagocytosis in a dose-dependent manner. The addition of Protein-G had no effect on phagocytosis as seen with the non-treated (NT) samples (*Figure 5.9A*). However, treatment with Protein-G trapped 222821 showed that the anti-LILRB3 antibody was still able to inhibit phagocytosis (10% phagocytosis with 222821 compared to 40% phagocytosis with isotype). This inhibition was statistically significant ($p = 0.0011$). This indicated that the inhibition of phagocytosis seen by anti-LILRB3 is not Fc-mediated, which agrees with the T cell proliferation data (*Figure 5.5*) that showed that deglycosylated versus WT anti-LILRB3 antibody showed no significant difference in inhibition of T cell proliferation. However, this inhibition appeared to be greater in the presence of Protein-G (80% inhibition from 50 to 10% compared to 43% inhibition from 35% to 20%). This could be the result of Protein-G affecting the way in which the antibody is presented to its receptor on the macrophages or the result of donor variability. Protein G may also be crosslinking the anti-LILRB3-bound antibodies, resulting in greater inhibitory downstream signalling. Notably, the isotype control inhibits phagocytosis slightly as well: ~40% phagocytosis compared to ~50% non-treated MDMs (*Figure 5.8A*). It could be that the presence of an antibody, regardless of specificity causes a minor inhibition in phagocytosis.

Long-term treatment of 222821 was also studied, to elucidate if long-term stimulation results in a prolonged inhibitory effect, or a transient one (e.g. if the receptor is internalised and then degraded, or recycled back to the surface, as short-term antibody stimulation may have no lasting effects). To study the effect of long-treatment of anti-LILRB3, MDMs were treated for 7 days with the anti-LILRB3 antibody. Although, short-term treatment (2 hours) of anti-LILRB3 was enough to see inhibition of macrophage phagocytosis, long-term treatment (7 days) did not appear to have a substantial effect with or without macrophage stimulation with TLR7/8 agonist R848 (*Figure 5.9B*). The % phagocytosis was similar (~40% without stimulation and ~50-60% with R848 stimulation) for non-treated, isotype-treated and 222821-treated macrophages. This suggested that treatment with anti-LILRB3 had no long-term effect on macrophage phagocytosis. This could be the result of receptor internalisation, making no available receptor present for the antibody to bind at the time of the assay. If the receptor is recycled back to the surface, a more extensive study of phagocytosis at different time points over a week could indicate this, and identify if inhibition of phagocytosis fluctuates with internalisation. A week may be too long to see internalisation and shorter intervals may be ideal.

These data suggests that the commercial antibody 222821 is an agonist that has a functional effect on effecter cells such as macrophages, and therefore being able to generate both

agonistic and antagonistic antibodies against LILRB3 could be both novel and therapeutically advantageous.

Therefore, the assay was repeated, with various anti-LILRB1, LILRB2 and LILRB3 clones and two different commercial anti-LILRB3 antibodies (R&D systems, Tolerx Inc). See *Figure 5.10* below.

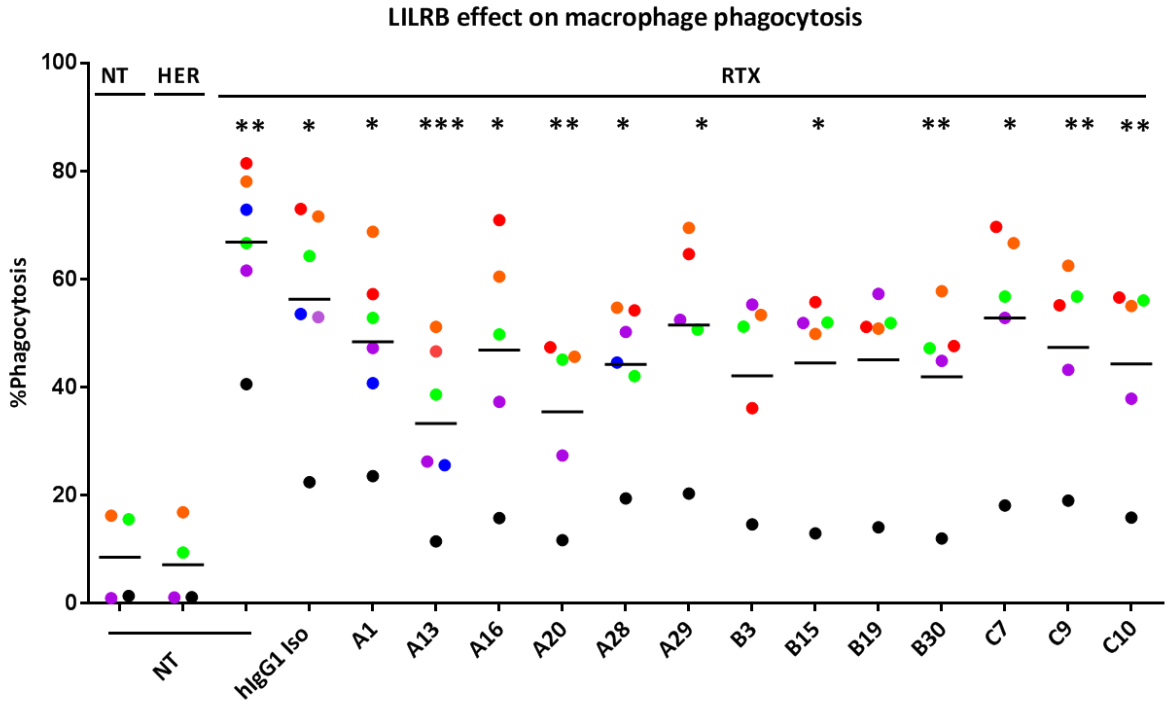

Figure 5.10 Assessing the effect of various anti-LILRB antibodies on macrophage phagocytosis. $1x10^5$ day 7-8 human monocyte-derived macrophages (MDMs) were treated with 10µg/ml PNGase deglycosylated (Promega) anti-LILRB1, LILRB2 and LILRB3 clones (BioInvent), commercial anti-LILRB3 clones TRX585 or 222821 (Tolerx Inc or R&D systems respectively) or relevant isotype controls hIgG1 anti-FITC (BioInvent) and mIgG2a 18B12 (in house) for 2 hours, 37°C. CLL cells were labelled with 5 µM CFSE (Sigma) and opsonised with 10µg/ml anti-CD20 (Rituximab, in house) or isotype control Herceptin (in house) for 25 minutes, 4°C. MDMs were then washed and co-cultured with the same donor of opsonised CLL cells (CLL 657C) in a 1:5 ratio for 1 hour at 37°C. MDMs were stained with 10µg/ml CD16-APC (Biolegend), for 15 minutes at room temperature. Cells were washed, harvested and analysed by flow cytometry. The percentage of phagocytosis was measured as the percentage of double-positive cells ($CD16\text{-}APC^+$ MDMs + $CFSE^+$CLL cells) divided by the total number of MDMs, multiplied by 100. Different MDM donors are represented in different colours (n=4-6) but the same donor of CLL cells (CLL 657C) was used each time. Each donor represents an average of triplicates, mean represented by solid line. Two-tailed paired T-test was performed and stars represent level of significant difference compared to isotype control ($p < 0.05$ *, $p < 0.005$ **, $p < 0.0005$ ***).

Figure 5.10 shows that the two commercial anti-LILRB3 clones significantly inhibited macrophage phagocytosis. All the LILRB3 clones showed some inhibition of macrophage phagocytosis and this was statistically significant (with the exception of A29). The LILRB2 clones B15 and B30 also showed significant decreases in phagocytosis alongside the LILRB1 clones C7, C9 and C10. Overall none of the clones appeared to increase phagocytosis. The

level of inhibition was dependent on the level of phagocytosis i.e. the less phagocytosis observed with a particular donor (for example, donor in black in *Figure 5.10*), the less inhibition with the different anti-LILR clones was also observed. This suggests that all the clones are acting as agonists in this assay, and the level of agonism is dependent on the level of phagocytosis.

The p values and significant difference for each treatment are displayed in Table 5.2 below.

Table 5.2 Significant differences of LILRB antibody treatment compared to isotype control on macrophage phagocytosis

Comparison	Donors	P value	Significant?	
NT non-ops vs HER-ops	4	0.4464	N	
NT non-ops vs RTX-ops	4	0.0020	Y	**
RTX-ops vs hIgG1 iso	6	0.0121	Y	*
hIgG1 iso vs TRX585	5	0.0057	Y	**
hIgG1 iso vs A1	6	0.0307	Y	*
hIgG1 iso vs A13	6	0.0003	Y	***
hIgG1 iso vs A16	5	0.0166	Y	*
hIgG1 iso vs A20	5	0.0019	Y	**
hIgG1 iso vs A28	6	0.0165	Y	*
hIgG1 iso vs A29	5	0.0968	N	
hIgG1 iso vs B3	5	0.0860	N	
hIgG1 iso vs B15	5	0.0246	Y	*
hIgG1 iso vs B19	5	0.0680	N	
hIgG1 iso vs B30	5	0.0077	Y	**
hIgG1 iso vs C7	5	0.0280	Y	*
hIgG1 iso vs C9	5	0.0157	Y	*
hIgG1 iso vs C10	5	0.0043	Y	**
mIgG1 iso vs LILRB3	5	0.0028	Y	**

Two-tailed T-test performed comparing isotype control to each antibody treatment in GraphPad. ($p < 0.05$ *, $p < 0.005$ **, $p < 0.0005$ ***) n = 4-6.

In summary all the LILR antibody clones tested inhibited macrophage phagocytosis, at different levels, and therefore they all are likely to be agonists in this setting, as they stimulate LILRB inhibitory signalling.

5.2.4 Receptor Internalisation

5.2.4.1 Indirect antibody staining to assess LILRB3 receptor internalisation

After establishing the effect different LILR antibodies had on receptor function, their therapeutic potential was considered. Antibody internalisation can dampen antibody therapy, as shown previously by Beers *et al*, who demonstrated a reduction in the efficacy of anti-

CD20 therapy, Rituximab, which was dampened by receptor modulation[259]. Receptors on the cell surface can be internalised when activated by their ligand. This can aid in a negative feedback loop, so that inhibitory receptors such as LILRB3 are not constantly turned on. Receptors can be recycled back to the surface or degraded in the lysosomes. Therefore, assessing the effect of different LILR antibodies on receptor internalisation is important.

To do this, commercial anti-LILRB3 clone 222821 was incubated with human monocytes over three hours and then using a secondary anti-human-PE antibody, cell surface antibody was detected.

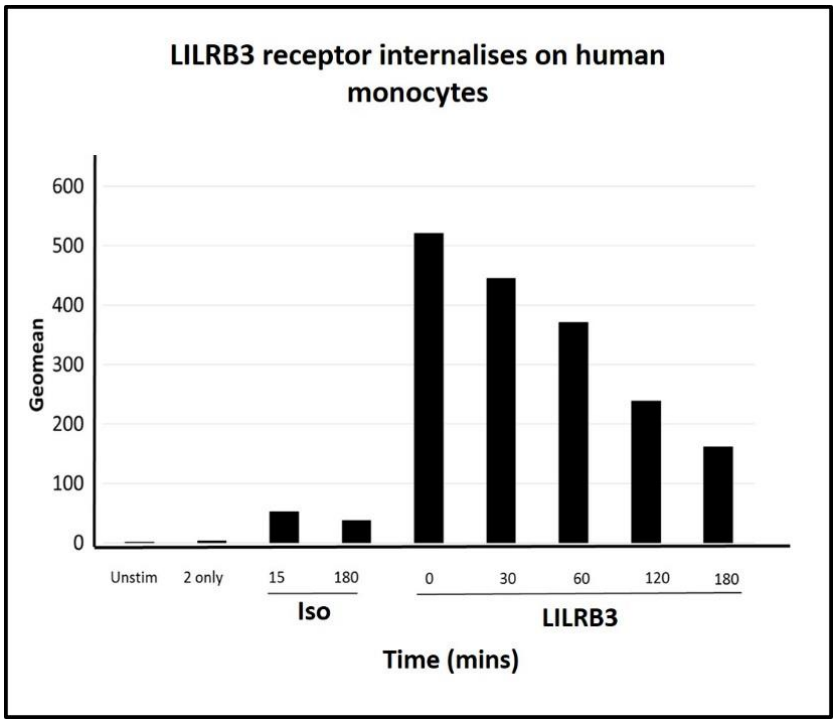

Figure 5.11 The effect of anti-LILRB3 on LILRB3 internalisation on human monocytes. PBMCs were isolated by lymphoprep. $1x10^6$ cells/well were plated in a 24-well plate o/n and monocytes allowed to adhere. Non-adherent cells washed off the next day and cells were incubated with 10ug/ml commercial LILRB3 antibody (R&D systems) or an isotype control at different time points for up to 3 hours at 37°C. Then cells were harvested and washed and an anti-human PE secondary added for 30 minutes, 4°C (Jackson Lab). Cells were washed and analysed by flow cytometry, measuring the geomean (mean fluorescence). One donor is represented here (n=3).

Figure 5.11 shows that LILRB3 internalises very quickly. Over a 3 hour time period, detection of the receptor on the cell surface dramatically declined (geomean of over 500 at time 0 compared to just under 200 at 3 hours).

Indirect staining of anti-LILRB3 demonstrated reduced cell surface expression of LILRB3 over time. Indirect staining allows signal amplification and therefore higher sensitivity. However, a qualitative way to study the effect of individual antibodies can be performed by direct staining in a quenching assay.

5.2.4.2 Direct antibody staining to assess LILRB receptor internalisation

Therefore, to assess LILRB internalisation with direct antibody staining, a quenching assay was performed. In this assay cells were incubated with A488-labelled commercial clone 222821, over a period of 6 hours. After which time, samples from each time point were harvested and either unquenched (no secondary added) or cell surface expression was quenched with an anti-A488 secondary. This allowed surface accessible antibody to be calculated. Cells were also analysed by fluorescent and confocal microscopy (*Figure 5.12*).

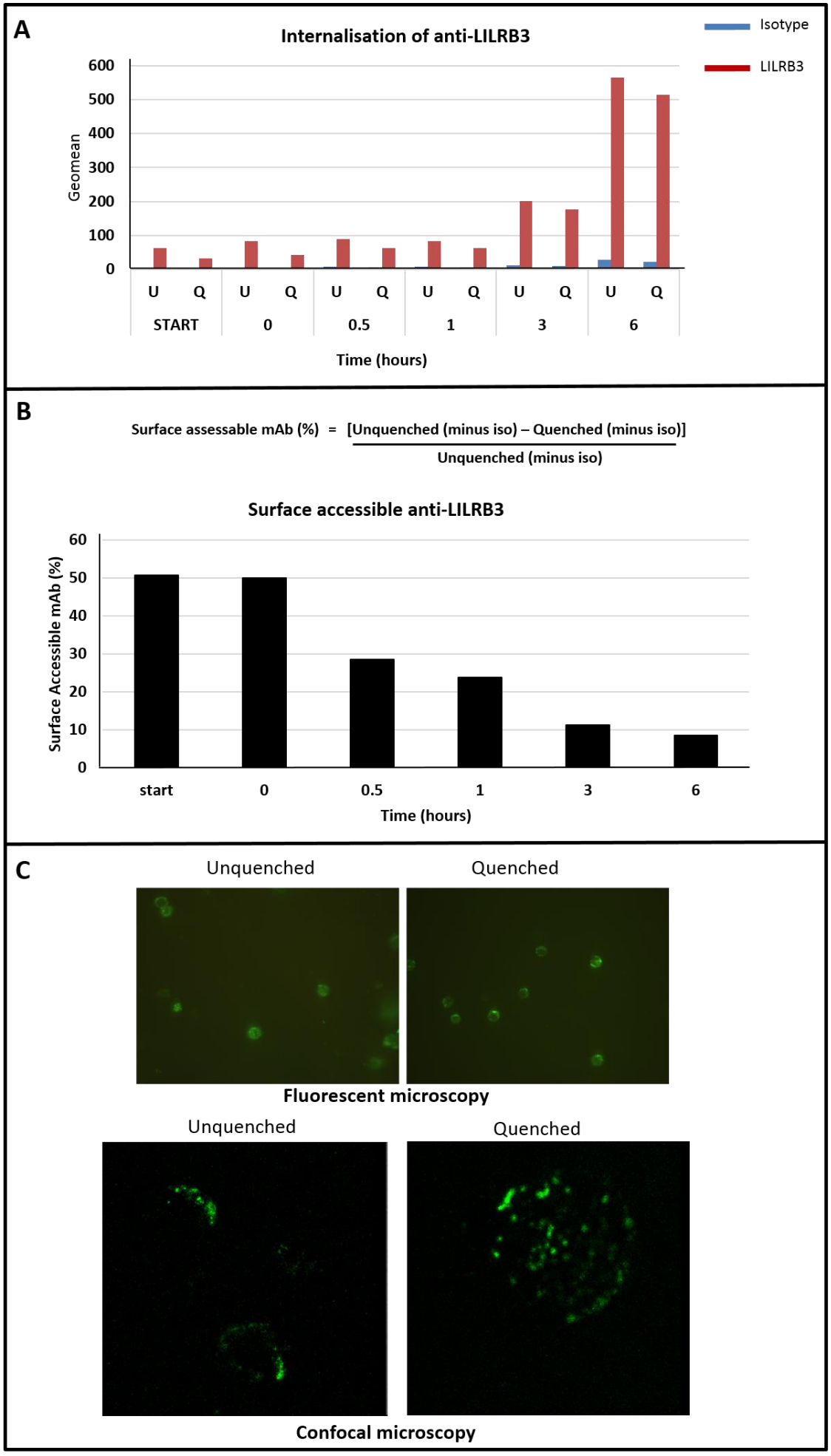
A
Internalisation of anti-LILRB3
Isotype
LILRB3
Geomean
600
500
400
300
200
100
0
U Q U Q U Q U Q U Q U Q
START 0 0.5 1 3 6
Time (hours)
B
Surface assessable mAb (%) = [Unquenched (minus iso) – Quenched (minus iso)] / Unquenched (minus iso)
Surface accessible anti-LILRB3
Surface Accessible mAb (%)
60
50
40
30
20
10
0
start 0 0.5 1 3 6
Time (hours)
C
Unquenched
Quenched
Fluorescent microscopy
Unquenched
Quenched
Confocal microscopy

Figure 5.12 Assessing the effect of anti-LILRB3 on cell surface LILRB3 over time. **A)** An A488-quenching assay was performed. $1x10^6$ isolated monocytes were incubated with 5 ug/ml directly labelled A488 commercial anti-LILRB3 clone 222821 (R&D systems) over six hours. Then cells were washed (unquenched) or washed and stained with an anti-A488 secondary (quenched) and washed again. One donor is represented here. **B)** Surface accessible antibody was calculated for the same donor by subtracting the geometric MFI of the quenched samples from the unquenched, and dividing by the unquenched, removing the background (isotype) each time. **C)** Internalisation was analysed by fluorescent and confocal microscopy at time 0'.

The secondary anti-A488 antibody quenched cell surface fluorescence, therefore the MFI detected in the quenched samples represented intracellular fluorescence only. Consequently, a higher MFI in the unquenched samples compared to the quenched samples, indicated cell surface fluorescence; whilst similar MFIs between the quenched and unquenched samples indicated no cell surface fluorescence and therefore intracellular fluorescence only.

The quenching assays in *Figure 5.12* revealed that LILRB3 quenched samples displayed a lower geometric MFI than the unquenched samples at the start of the assay (*Figure 5.12A*). However, the MFI for the quenched samples increased and became more similar to the unquenched samples over time. This indicated that LILRB3 was present at the cell surface (and therefore able to be quenched by the secondary antibody), but over time internalised into the cell, rendering it unable to be quenched. Notably, the MFI accumulated over time (very high by six hours compared to at the start). This indicated that LILRB3 builds up over time within the cell (*Figure 5.12A*).

Surface accessible antibody was plotted over time. At the start of the assay only 50% of accessible antibody was detectable (*figure 5.12B*). – implying that even at the time 0', internalisation has happened. By six hours less than 10% of the antibody is present at the cell surface, suggesting internalisation (*Figure 5.12B*). Both fluorescent and confocal microscopy confirm this, as the images show LILRB3 staining both outside and inside the cell in the unquenched samples, however, only staining inside the cells can be seen in the quenched samples (*Figure 5.12C*).

To validate these findings the assay was repeated with different anti-LILRB1, -LILRB2 and -LILRB3 clones with several donors, to see how different clones effected receptor internalisation, and how this compared to the commercial LILRB3 antibody (*Figure 5.13* below).

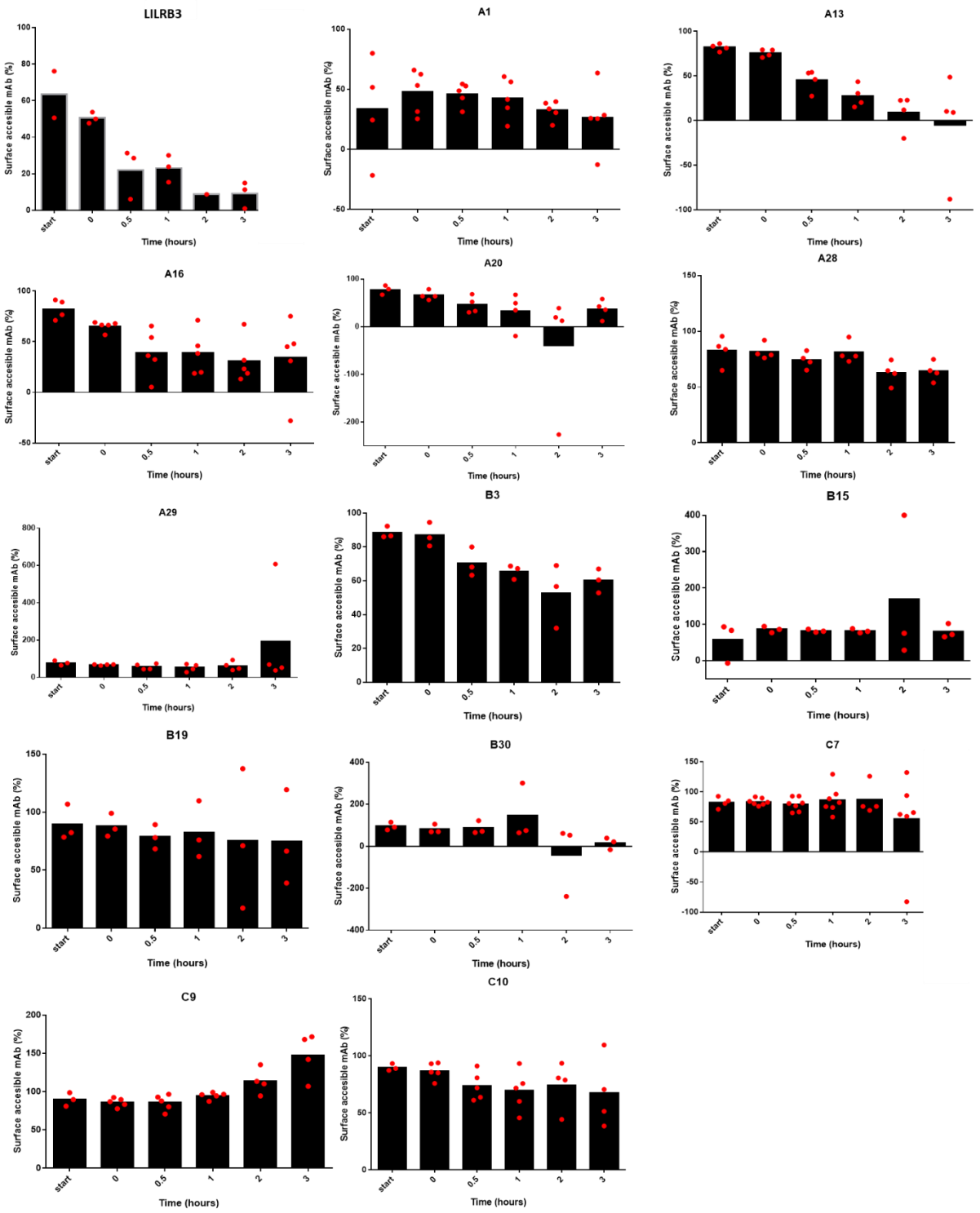

Figure 5.13 Assessing the effect of different anti-LILR antibodies on LILR internalisation over time. $1x10^6$ isolated monocytes were incubated with 5 µg/ml directly labelled A488 anti-LILRB1 (C), -LILRB2 (B), LILRB3 (A) clones (BioInvent) and the commercial anti-LILRB3 antibody (R&D systems) over three hours. The cells were washed (unquenched) or washed and stained with an anti-A488 secondary (quenched) and washed again and surface accessible antibody and plotted graphically. n = 3-7.

Donor variability was observed in all cases. All three LILRB1 clones maintained their level of surface accessible antibody, indicating they did not internalise. Although by 3 hours C7 showed reduced surface level antibody, suggesting that this clone may cause internalisation, but over longer durations. Only one anti-LILRB2 clone - B3 - showed slow internalisation (accessible antibody reduced from ~90% to 60% over three hours). The other LILRB2 clones, B15, B19 and B30 maintained surface accessible antibody over time. Four anti-LILRB3 clones (A1, A20, A28 and A29) showed no internalisation (as they maintained their level of surface accessible antibody). However, two clones A13 and A16 showed a decline in surface accessible antibody over time. For A13 this was quick (75% to 0% in 3 hours), and for A16 this was slower (75% to 40% in 3 hours). The commercial antibody also showed quick internalisation (~60% to 10% by 3 hours). Therefore different antibody clones were able to induce internalisation at different rates.

As monocytes are phagocytic cells, it is possible that they are taking up cell debris, and the assay was measuring endocytosis of this cell debris rather than receptor internalisation. To confirm that LILRB3 is indeed internalising, the quenching assay was repeated, this time with or without 15 mM azide (NaN_3) and 50 mM 2-Deoxy-D-glucose ($C_6H_{12}O_5$). Endocytosis is an energy-dependent process that requires ATP. Azide inhibits ATP synthase, whilst 2-Deoxy-D-glucose inhibits glycolysis, which produces ATP[260, 261]. Therefore both of these reagents prevent endocytosis and any internalisation observed will therefore be receptor internalisation only. A13 (which internalised quickly) and A28 (which did not internalise) were chosen as representative clones.

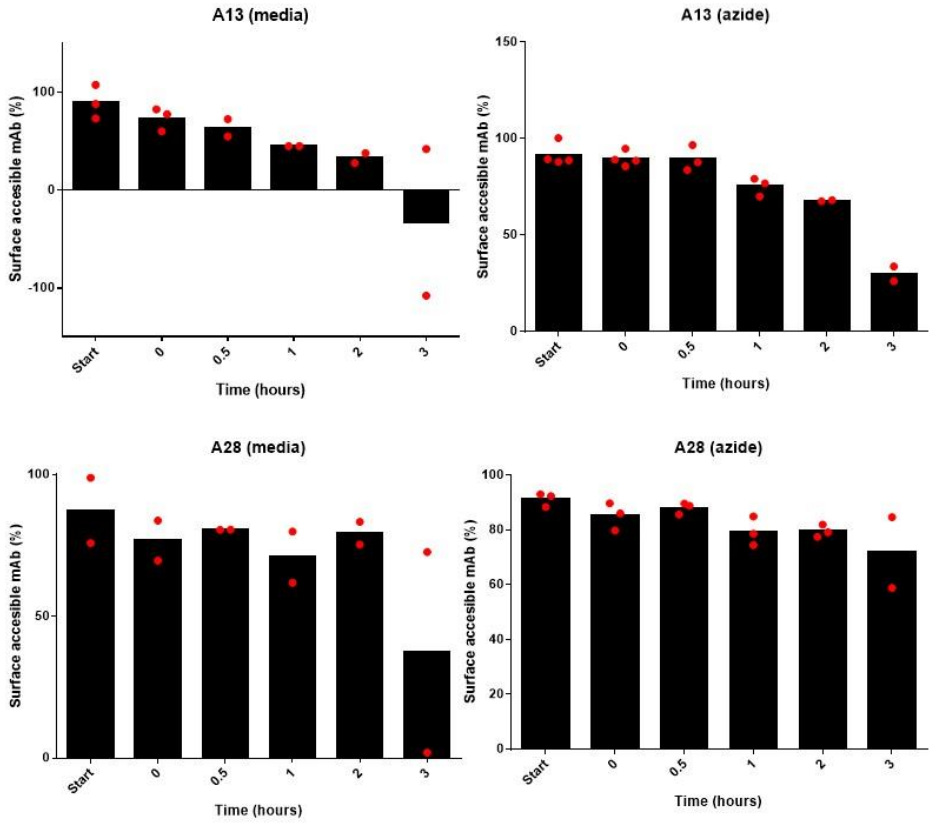

Figure 5.14 Confirming LILRB3 internalisation on monocytes. 1x10^6 isolated monocytes in media or in media treated with 15 mM azide and 50 mM 2-Deoxy-D-glucose were incubated with 5 ug/ml directly labelled A488 anti-LILRB3 clones A13 and A28 (BioInvent) over three hours. The cells were washed (unquenched) or washed and stained with an anti-A488 secondary (quenched) and washed again and surface accessible antibody and plotted graphically. The background was removed. n=2-4 donors.

Figure 5.14 shows that A13 was still able to induce internalisation in the presence of azide and 2-Deoxy-D-glucose. In media, surface accessible antibody dropped from ~90% to 0% but in the presence of azide and 2-Deoxy-D-glucose a drop from ~90% to 30% was seen. Although this was less than the drop seen in media, suggesting that some internalisation seen in media was the result of cell debris taken in by endocytosis, the majority was the result of receptor internalisation. A28 showed slower internalisation compared to A13 ~80% to 40% in media, but ~90% to 70% in azide and 2-Deoxy-D-glucose. The effect seen with both endocytosis inhibitors appeared to only take effect after 30 minutes, as surface accessibly antibody is maintained up to 0.5 hours for both A13 and A28. After this time, a slight decrease at 1 hour, then 2 hours and a more pronounced decrease by 3 hours ensued for both A13 and A28. However, as seen in media, the decrease in antibody for A28 was minimal in comparison to A13, which showed much faster internalisation. This suggested that receptor internalisation seen in the first ~30 minutes was likely the uptake of cell debris by endocytosis, and receptor internalisation is likely occurring after this time. It should be noted

that there was donor variability as seen previously, and more donors would have generated a more robust sample size. This suggested that the results were consistent with results seen previously (*Figure 5.13*) and indicated that different antibody clones can cause quick receptor internalisation or slow/prevent modulation.

5.2.4.3 LILRB3 receptor cell trafficking

After establishing that LILRB3 internalises, and different antibodies cause the receptor to internalise at different rates, the next step was to determine if LILRB3 receptor internalisation results in the receptor being degraded in the lysosomes or recycled back by transferrin receptors. This was assessed by confocal microscopy. MDMs were grown on Poly-L-Lysine (PLL)-coated coverslips overnight and then incubated with APC labelled anti-LILRB3 clones A13 (that caused fast internalisation) and A28 (slow internalisation), at various time points (0 to 3 hours). The cells were then also stained with either A488-labelled transferrin, or with A488-labelled lysosomal tracker, and co-localisation was assessed by confocal microscopy. The distance between the APC and A488 dyes in any given cell was calculated in Image J. These two markers were chosen as they reflected two different fates for internalised proteins. Transferrin collects iron and then binds to its receptor on the cell surface, which results in internalisation of transferrin into the cells by endocytosis. The transferrin receptor releases iron inside the cell and recycles back to the cell surface to collect more iron[262]. If LILRB3 co-localised with transferrin, it would indicate that it was internalised and recycled back in the same way. The lysosome is a cell membrane organelle involved in degradation of proteins inside the cell[263]. These proteins are degraded by hydrolytic enzymes that work at low pH (acidic). The LysoTracker probes (Molecular Probes, Thermo Scientific) are fluorescent acidotropic probes for labelling and tracing acidic organelles in live cells, and therefore are able to track lysosomes. Deducing if LILRB3 co-localises with the LysoTracker would indicate that the receptor was internalised and degraded inside the cell.

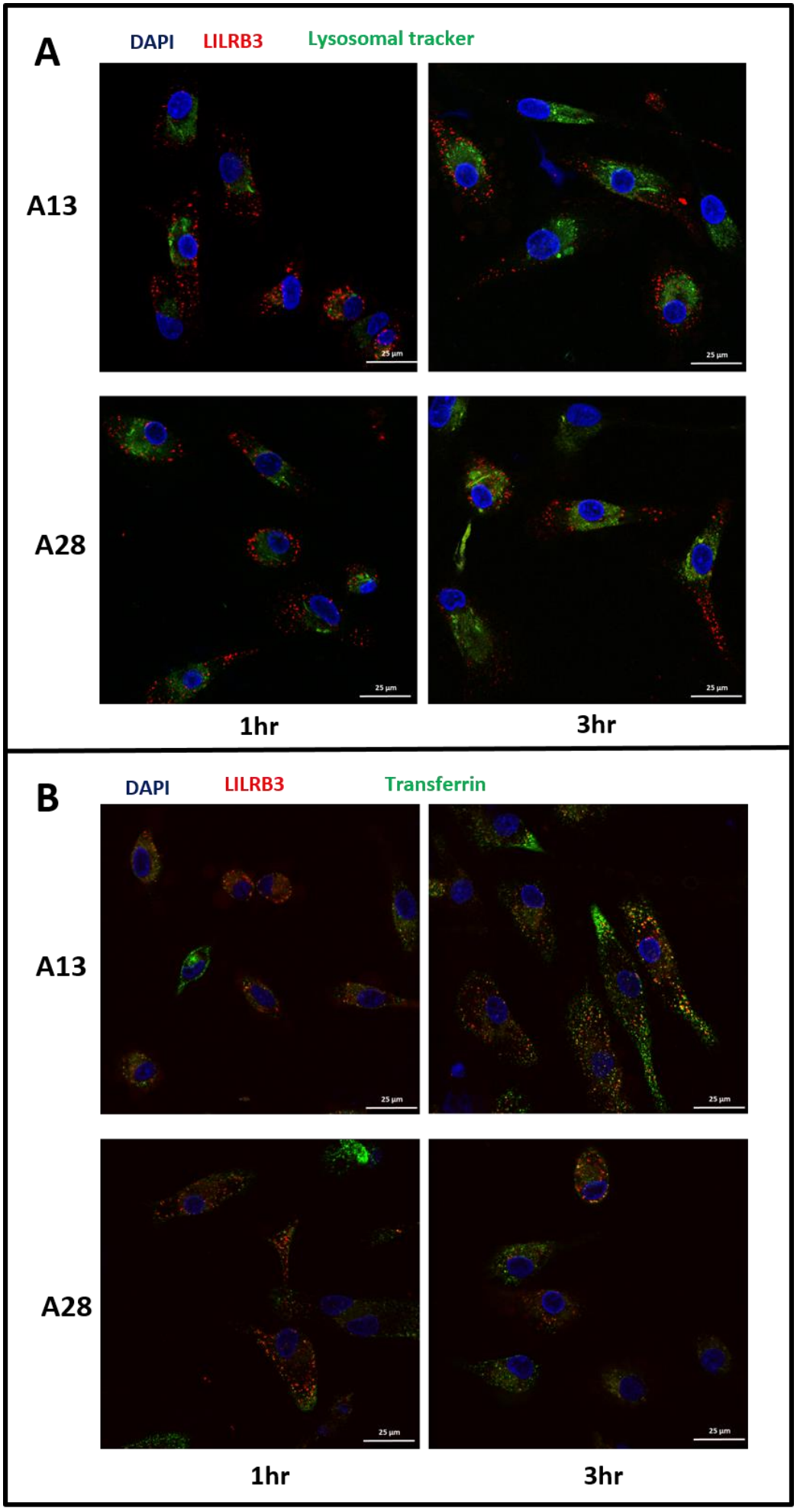
A
DAPI
LILRB3
Lysosomal tracker
A13
A28
1hr
3hr
B
DAPI
LILRB3
Transferrin
A13
A28
1hr
3hr

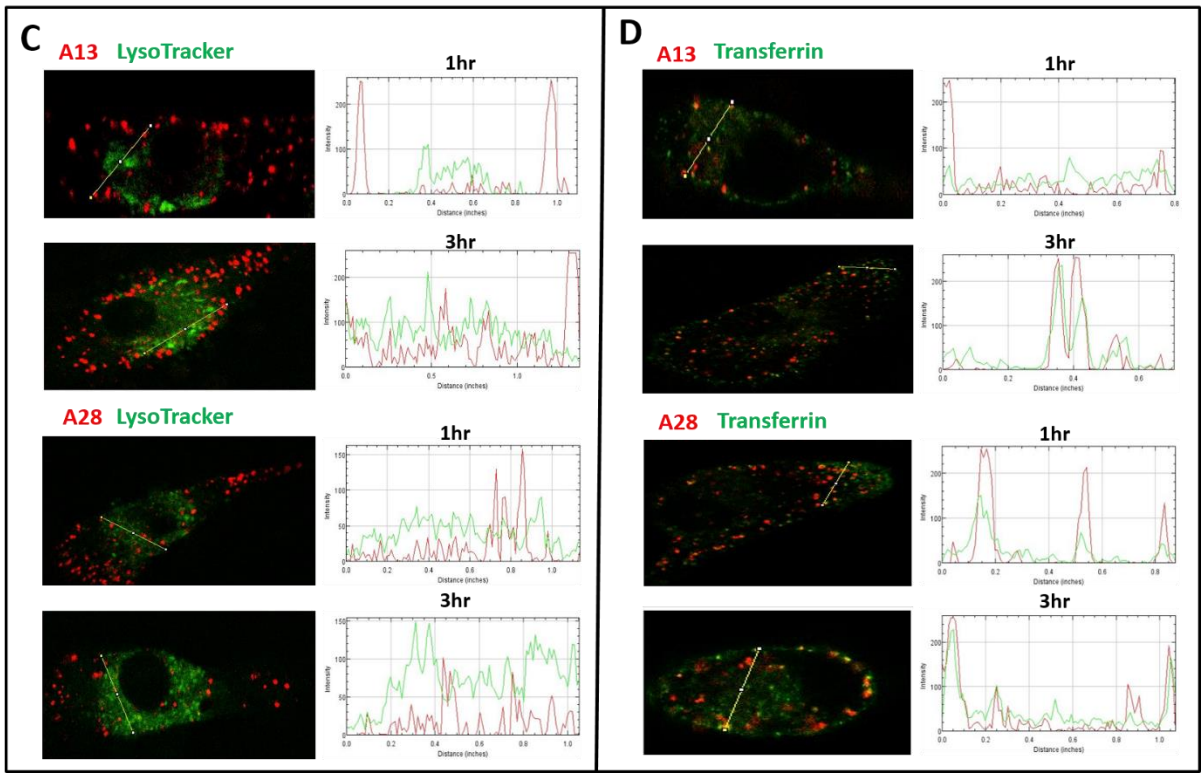

Figure 5.15 Assessing LILRB3 cell trafficking by confocal microscopy. MDMs were grown on PLL-coated coverslips over night at 37°C. The following day cells were staining with 10 µg/ml APC-labelled LILRB3 clones A13 and A16 for 1 and 3 hours at 37°C. Cells were co-stained with either 25 µg/ml A488-labelled transferrin (Molecular Probes) for 15 minutes at 37°C or 60 nM A488-labelled LysoTracker (Molecular probes) for 1 hour at 37°C. Cells were then fixed in 4% paraformaldehyde (PFA) at 4°C for 10 minutes, then washed in PBS and mounted in non-hardset mountant with DAPI (Vectashield), allowed to dry overnight. Images were collected with a Leica SP5 CLSM confocal microscope using a 100x (NA1.4) Plan-Apochromatic objective and pinhole of 1 Airy disc (LAS-AF software, Version2, Leica). **A/B** cells were imaged using Photoshop. **C/D**. Focusing on one cell, co-localisation was determined in Image J by calculating the distance between APC and A488 staining.

Figure 5.15A/B shows successful LILRB3 and either transferrin or LysoTracker staining on MDMs. Both LILRB3 clones showed weaker staining, in comparison to the transferrin and lysosomal tracker staining. Unfortunately, staining at time 0 minutes with the anti-LILRB3 clones was not achieved, as the clones were unable to stain for 30 minutes at 4°C (data not shown), and therefore a baseline expression could not be determined by confocal microscopy. This could be that the antibodies were unable to bind at a detectable level for microscopy for this length of time and temperature (even though staining in this way is detectable by flow cytometry – data not shown). Fixing the cells first and then staining at room temperature could be an alternative option. Regardless, punctate LILRB3 staining was observed at both 1 and 3 hours, and this appeared to be inside the cells (*Figure 5.15A/B*). This suggested that LILRB3 does internalise into the cell, as previously seen by flow cytometry. Transferrin staining is also more punctate (*Figure 5.15B*), whilst the LysoTracker staining is more spread within the cell (*Figure 5.15A*).

Where cells were stained with both LILRB3 (red) and either LysoTracker or transferrin (green) they appear yellow (*Figure 5.15C/D*). Yellow staining can be seen in cells stained with both LILRB3 and transferrin (*Figure 5.15D*) suggesting co-localisation. Analysis in Image J showed that the distance between A488 staining and APC staining was more spread with the LysoTracker, but the distance was much closer, and almost aligned in places with the transferrin for both clones at both 1 and 3 hours (*Figure 5.15C/D*). This indicated that LILRB3 staining co-localised with the transferrin staining, thus the LILRB3 receptor internalises and is recycled back to the surface, not degraded in the lysosomes. The time it takes the receptor to be recycled back has yet to be determined. It could happen very quickly (shorter time points to be studied) or much more slowly (longer time points studied).

In conclusion, LILRB3 is internalised, and different antibody clones elicit different rates of internalisation, for example A13 causes fast internalisation on monocytes, whilst A28 causes slow internalisation. This internalisation occurs in the presence of endocytosis inhibitors azide and 2-Deoxy-D-Glucose, suggesting this internalisation is not the result of cell debris taken up by endocytosis. It is likely that the LILRB3 receptor once internalised is recycled back to the cell surface, in a constant loop.

To summarise, in this chapter the function of a variety of specific antibodies generated were studied. Some antibodies demonstrated an ability to agonise receptor signalling by binding to their target receptor and inducing intracellular signalling, in the absence or presence of a ligand. Other antibody clones were shown to be unable to induce intracellular signalling in the absence of a ligand, suggesting they were non-agonists. These clones then showed an ability to either enhance or inhibit cellular activation in the presence of a ligand, indicating their ability to act as agonists or antagonists respectively. The capability of these antibodies to either agonise or antagonise signalling was further demonstrated by studying the effect of these clones on different cell types, by studying T cell proliferation and macrophage phagocytosis. Antibodies were found to either inhibit or enhance these processes *in vitro*. Finally, studying LILRB3 receptor internalisation showed that different anti-LILRB3 clones were able to cause different rates of receptor internalisation, and this receptor internalisation was likely co-localising with transferrin, suggesting that LILRB3 is recycled back to the cell surface.

All data in this chapter is summarised in Table 5.3 below.

Table 5.3 Summary data of functional effect of LILRB antibodies

Target	Clone	Cross-link	GFP	Proliferation	Phagocytosis	Internalise
LILRB3	R&D	N/A	N/A	↓↓↓ (****)	↓↓↓ (**)	Yes
	TRX	N/A	N/A	↓	↓↓ (**)	N/A
	A1	Yes	N/A	↓↓↓ (***)	↓ (*)	No
	A13	Yes	N/A	↓↓↓ (***)	↓↓↓ (***)	Yes
	A16	Yes	N/A	ND	↓↓ (*)	Yes
	A20	Yes	N/A	↓ (*)	↓↓↓ (**)	No
	A28	No	N/A	↓	↓↓ (*)	No
	A29	Yes	N/A	↑↑↑ (***)	↓	No
LILRB2	B3	No	↓	ND	↓↓	Yes
	B15	No	↓	ND	↓↓(*)	No
	B19	No	↓	↑	↓↓	No
	B30	No	↓	↑↑↑ (*)	↓↓ (**)	No
LILRB1	C7	Yes	↓	↑↑	↓ (*)	Yes
	C9	No	↑	↑↑	↓↓ (*)	No
	C10	Yes	↓	↓	↓↓ (**)	No

Table shows representative clones. Symbols and abbreviations represent: Enhanced (↑ <10%, ↑↑ 10-20%, ↑↑↑ >20% compared to isotype) Blocked (↓ <10%, ↓↓ 10-20%, ↓↓↓ >20% compared to isotype) or no difference (ND). Two-tailed T-test performed comparing isotype control to each antibody treatment. ($p < 0.05$ *, $p < 0.005$ **, $p < 0.0005$ ***, $p < 0.00005$ ****). N/A = not tested.

The table summarises the functional data in this chapter. A range of different antibody characteristics are illustrated here. Some clones showed an agonistic effect on receptor activation in both the ligand-blocking assays and on effector functions, whilst other antibodies were antagonistic. For full list of all antibodies tested see appendix.

5.3 Discussion

This chapter describes assays carried out *in vitro* to assess the functional properties of the specific anti-LILR antibodies generated. The antibodies were assessed for their ability to bind to their receptor and activate intracellular signalling causing GFP expression, in the absence of a ligand by eliciting sufficient receptor cross-linking or in the presence of a ligand. The antibodies were also assessed for their effector function indirectly on T cell proliferation, or directly on macrophage phagocytosis. Finally, the antibodies were assessed for their ability to internalise.

Whilst most LILRB3 clones were found to elicit sufficient receptor cross-linking leading to GFP expression and therefore suggesting they were acting as agonists, the majority of LILRB1 and LILRB2 clones did not, suggesting they were non-agonists. The GFP reporter assays showed that the majority of LILRB1 and LILRB2 clones were antagonists with only one LILRB1 clone, C9 able to act as an agonist. However, cellular activation could have been influenced by the mode in which ligand binding occurred. LILRB1$^+$ 2B4 cells showed less activation (GFP expression) compared to LILRB2$^+$ 2B4 cells when co-cultured with HLA-G$^+$ 721.221 cells, despite the expression levels of these reporter cells being similar (see chapter 4 *Figure 4.2* for anti-HA flow cytometry profiles). LILRB1 and LILRB2 both bind to HLA-G with a high affinity, and although the most characterised ligand binding for LILRs is HLA-G in *trans*, LILRs can bind to their ligands in other ways[39]. For example, LILRA2 binds soluble HLA-I in serum, whilst LILRB2 binds cell-surface HLA-I in *cis*[76, 97]. It could be that the format of the ligand also influenced activation, as cell-surface expression of HLA-G may have different binding epitopes available when compared to soluble HLA-G. LILRB2 therefore, may be better at binding to its ligand HLA-G when expressed on the cell surface, whilst LILRB1 might bind better to soluble HLA-G. LILRB1 binds to HLA-G multimers with higher affinity compared to binding of HLA-G monomers. Cell surface HLA-G may not bind to LILRB1 with high enough affinity to cause activation[264]. The LILRB1$^+$ cells were less healthy than the LILRB2$^+$ cells at the time of the assay (based on communication with Dr Des Jones, *University of Cambridge*), and this is likely what influenced their activation rate. It should also be noted that the LILR transfected-2B4 and HLA-G-transfected 721.22 cell co-culture assay is an artificial system, where both receptor and ligand are over-expressed on cell lines. Therefore, the ability of antibodies to agonise or antagonise their receptor on 'real' cells maybe different and more or less pronounced than seen in these assays. This could explain why agonistic/antagonistic antibodies in these assays, do not appear to have the same effect in functional assays. For example, B3 which appears to be an antagonist in the GFP blocking assays, as it blocks GFP expression, was unable to block macrophage phagocytosis.

Therefore, the function of these antibodies on 'real' cells was also studied. Although in chapter 4, no staining on T cells was observed with the LILRB1-specific antibodies generated, previous studies have suggested that LILRB1 is the only LILR receptor found on T cells, and therefore anti-LILRB1 clones are the only antibodies that may have a direct effect on T cell proliferation[67]. The other clones are likely having an effect on their receptors found on APCs such as DCs. The effect of LILRs on DCs has been shown previously, whereby activation of the receptors are thought to render DCs tolerogenic, subsequently inhibiting T cell proliferation by preventing antigen presentation[120]. To confirm this DC-T cell co-culture

assays were attempted, where recall responses were driven by treating MDDCs with Tetanus. However, as seen in *Figure 5.4* driving T cell proliferation in this way was not possible. Instead, it appeared that cells were losing CFSE as they were dying, rather than as they divided. It is possible that donors used were poor responders to tetanus, or not previously vaccinated to the antigen (as donors were anonymously acquired from the Southampton General Hospital blood donation service). Another alternative is that in assays where allogenic T cells were utilised, the donors were not HLA-matched, as no HLA-typing was performed. Therefore, these assays required further optimisation. As a result, assays were performed where T cell proliferation was subsequently driven through anti-CD3/CD28 antibodies. As PBMCs were used in these assays, a mixed population, including APCs such as DCs were present. To therefore determine if the effect of LILRs on APCs indirectly effects T cell proliferation, individually removing cell-types, or culturing isolated T cells with either DCs or monocytes expressing LILRs, and studying T cell proliferation should be done. However, preliminary experiments culturing anti-LILR clones with isolated T cells showed no effect on T cell proliferation (data not shown), suggesting that the antibodies are not working directly on the T cells, but through effector cells.

Given that it appeared LILRBs were functioning through effector cells, the function of effector cells expressing LILRBs were studied through macrophage phagocytosis assays. The effect of each antibody on macrophage phagocytosis was studied using M0 macrophages (i.e. macrophages that had not been skewed in any way). M1/M1-like (classically activated) macrophages are pro-inflammatory, whilst M2/M2-like (alternatively activated) macrophages are anti-inflammatory[4]. Studying the effect of these antibodies on different types of macrophages would be ideal, as LILRs are often upregulated in anti-inflammatory environments, therefore are likely to be up-regulated on M2-like macrophages, resulting in a greater antibody effect on these cells compared to cells that are not skewed[123].

The purpose of this chapter was to define the generated anti-LILR antibodies as agonists or antagonists for their receptor, and examine their functional ability to manipulate immune cell behaviour. LILRB3 clone A1, showed a cross-linking ability and significantly decreased both T cell proliferation and macrophage phagocytosis, all indicating it was a strong agonist. However, deducing if each antibody clone was either an agonist or antagonist was not always clear-cut. LILRB1 clone C9 did not cross-link, but enhanced GFP expression in the HLA-G blocking assays, indicating it was an agonist. However, the clone enhanced T cell proliferation (showing antagonistic properties) but significantly decreased macrophage phagocytosis implying it was an agonist. These disparities may have been the result of

different signalling thresholds on different cell types. For example, lower signalling thresholds on macrophages compared to effector cells that drive T cell proliferation, may have allowed clone C9 to elicit a sufficient response. In the absence of a ligand, LILRB2 clone B3, was unable to cause sufficient receptor cross-linking and GFP expression, indicative of cellular activation, and therefore did not demonstrate characteristics of an agonist. This was reaffirmed in the HLA-G blocking assays, where clone B3 showed blocking of GFP expression, indicating it was an antagonist. However, although B3 showed little effect on T cell proliferation, it was able to block macrophage phagocytosis, indicating the clone was able to stimulate LILRB2 inhibitory signalling and therefore is likely to be an agonist, contradicting what was seen in the blocking assays. The ligand blocking assays give an indication of whether antibodies are agonist or antagonists. The effector function of these antibodies on both T cell proliferation and macrophage phagocytosis, however, may be influenced by activation thresholds. It could be that clones like B3 which appeared to be antagonists, blocking GFP expression, are unable to reach the activation thresholds required to block the inhibitory LILRB2 receptor on macrophages and DCs. Therefore, inhibition of proliferation and/or phagocytosis is not achieved. In the T cell proliferation assay other cells are present, this could also influence the activation threshold, for example by activatory receptors expressed on other cells, counteracting the inhibitory signalling. Therefore, eliminating these other cell types would be ideal. Most of the anti-LILRB3 antibodies appeared to function as agonists, based on their ability to either elicit sufficient cross-linking in the absence of a ligand, or blocking cell function such as T cell proliferation and/or macrophage phagocytosis. It could be that most exposed antibody epitope binding sites result in agonism. The antibody generation process, e.g. the format of the target proteins, may have only exposed certain binding sites that preferentially cause receptor stimulation. It may therefore be harder or unlikely to generate antagonist anti-LILR antibodies based on the antibody generation methods used. However, the commercial antibody (R&D systems) is a known agonist (personal communication with Dr Des Jones) and this antibody was produced by hybridoma technology, perhaps suggesting that the receptor itself has preferential binding sites that cause receptor stimulation, rather than this being a result of the way in which the antibodies were made. In chapter 4, epitope binding studies showed that all the LILRB3 antibodies generated mapped to the second and fourth IgG-like domains. It could be that these domains promote receptor stimulation, and binding sites correlate to function.

After establishing effector function of these antibodies, and deducing their capabilities to either agonise or antagonise receptor signalling, internalisation was assessed. If these antibodies were potentially therapeutic, studying internalisation was important. Antibody

internalisation is important for antibody therapy in two ways: firstly internalisation could serve as a positive effect to boost a drug delivery mechanism by allowing ADCs to be delivered into the cell, such as Gemtuzumab ozogamicin, previously used to treat acute AML; secondly internalisation could have a negative effect, as the receptor can be lost from the cell surface, preventing immunomodulating antibodies from being able to bind and act on their receptors at the cell surface, or reducing the ability of antibodies to trigger target cell deletion, as shown with Rituximab following internalisation[244, 259]. LILR clones were found to modulate at different rates. LILRB3 clone A13 for example caused fast receptor internalisation, whilst A16 showed slower internalisation and A28 showed little to no internalisation. This internalisation could affect therapy as the receptor will no longer be present on the cell surface for the antibody to bind, or affect antibody half-life (as the antibody will be taken into the cell during receptor internalisation). Cell trafficking assays in this chapter indicated the receptor is likely recycled back to the cell surface rather than degraded in lysosomes (*Figure 5.15*). However, not all cells in the tissue were found to co-stain with both LILRB3 and transferrin, suggesting not all cells internalise the LILRB3 receptor. This is likely due to variations of cells in their cell cycle. Not all cells will be at the same stage in their cycle, resulting in variation. LILRB4 is expressed on APCs and has been reported to internalise upon receptor cross-linking, delivering its ligand into the cell for presentation to T cells[124]. Other inhibitory LILRs may also do this. Notably, both A13 and A28 showed similar levels of co-staining with transferrin, indicating that they internalised at similar rates, which contradicted what was seen earlier with the quenching assays. However, although some co-staining was seen, this was not in every cell present, and therefore the cell trafficking assay requires further validation.

In summary novel antibodies with a range of different functional characteristics have been generated. These antibodies may therefore be useful in different types of therapy. For example, agonistic antibodies that stimulate the inhibitory LILRs may be used to treat autoimmune conditions, whilst antagonistic antibodies may be used to treat malignancies. The mechanisms underlying the function of therapeutic antibodies has been poorly understood. The mechanisms in which these anti-LILRs function has yet to be deduced. Although the ability of these antibodies to affect macrophage phagocytosis suggests ADCP may be one way in which these antibodies function. Human studies assessing the function of anti-CD20 antibodies for example, thus far have focused on analysing patient blood samples, and as the blood accounts for less than 2% of B cells outside of the bone marrow, this suggests that such studies are grossly underestimating underlying mechanisms[221]. Studying patients undergoing immunotherapy to study these mechanisms has been understandably difficult. Therefore,

testing these antibodies in a model system to assess the function and therapeutic efficacy *in vivo* is essential.

6 ASSESSING THE THERAPEUTIC POTENTIAL OF ANTI-LILRB1, LILRB2 AND LILRB3-GENERATED ANTIBODIES

6.1 Introduction

In previous chapters (3-5), it was shown that antibodies against LILRB1, LILRB2 and LILRB3 were successfully generated, each with a range of different characteristics. The specificity of antibodies were confirmed, lacking cross-re activity to other LILRs in the same family, or the homologous mouse receptor PIR-B. The generated antibodies were able to not only stain transfected cell lines, but primary cells also, when tested against various human blood cell types, and human tissue samples. Different clones were found to have different binding affinities, and whilst the majority of the anti-LILRB3 clones were shown to bind to the second IgG-like domain of the receptor, some clones also bound to domain four, showing variation in epitope binding sites for the different antibodies. Furthermore, characterisation *in vitro*, showed that both agonistic and antagonistic antibodies had been generated, when tested in ligand blocking assays, and when studying the effect of different antibody clones on different effector cell function. Finally, the antibodies appeared to internalise at different rates on monocytes, suggesting that they may have different therapeutic applications, for example fast internalising antibodies would serve as good antibody drug conjugates. Comparatively, slow internalising antibodies would allow immunomodulatory antibodies to act on their target at the cell surface. This extensive characterisation provided important information about the possible activities of the different antibody clones generated, as well as indications as to how they may perform *in vivo*. This chapter focuses on whether these antibodies had anti-cancer *in vivo* activity.

Almost 50 different therapeutic antibodies have already been approved, or are under review for approval in the USA and EU[47]. Understanding the mechanism of action of mAbs is important for improving current therapies and discovering more potential therapeutic targets. Effector cells are crucial players in mediating antibody therapy, and in the past, this was generally believed to be through mechanisms such as ADCC. However, we now know that antibodies may work through other mechanisms, such as immunomodulation[233]. This involves the antibody acting a substitute ligand, binding to its receptor and either stimulating (agonising) or blocking (antagonising) receptor signalling[265]. In Chapter 5, the effect of the generated specific LILR antibodies on effector cells, such as macrophages, and indirect effect on T cells was shown. Effector cells such as macrophages are important for antibody therapy[221]. In these assays, it was shown that the generated antibodies could act as

immunomodulating antibodies – able to either agonise/antagonise their receptor on myeloid cells. The aim of this chapter is to deduce if these antibodies can also directly target tumour cells *in vivo*.

Although LILRB1 and LILRB2 *in vivo* models have been developed, there are currently no mouse models developed to study LILRB3 and no Tg mice is currently available[100, 134]. Therefore, establishing a LILRB3 *in vivo* model would not only be novel, but allow the therapeutic function of the generated anti-LILRB3 antibodies to be studied. In the absence of a Tg mouse model, as the generated anti-human LILR antibodies did not cross-react with mouse PIRs (see Chapter 4, *Figure 4.3*), they could not be used to assess function *in vivo*. Therefore, establishing other models using primary human cancer cells and human cell lines was warranted.

6.2 Results

Previous studies have demonstrated LILR receptors are up-regulated on both the tumour cells themselves and their surrounding immune infiltrate, and LILRs have been implicated in cancers such as CLL and AML[161, 163]. In chapter 4 (*Figure 4.4*) staining different cell types with the generated anti-LILRB1, LILRB2 and LILRB3 antibodies, showed that only LILRB1 is expressed on B cells. However, both LILRB2 and LILRB4 have been found to be up-regulated on malignant B cells in CLL patients[163]. Therefore, phenotyping primary cancer cells was performed to establish whether they express different LILRs, which may then serve as targets for antibody immunotherapy.

6.2.1 Phenotyping primary cancer cells

6.2.1.1 Assessing cell populations in healthy vs CLL donors

To confirm previous findings, and study expression of the inhibitory LILRs, CLL samples were phenotyped with the specific anti-LILR antibodies characterised in this thesis. Before studying LILR expression, the proportion of different blood cell populations in both healthy verses CLL donors was compared. The number of cells in each blood population was calculated as a percentage of the total number of live cells (as determined from FSC/SSC) and represented graphically (*Figure 6.1*).

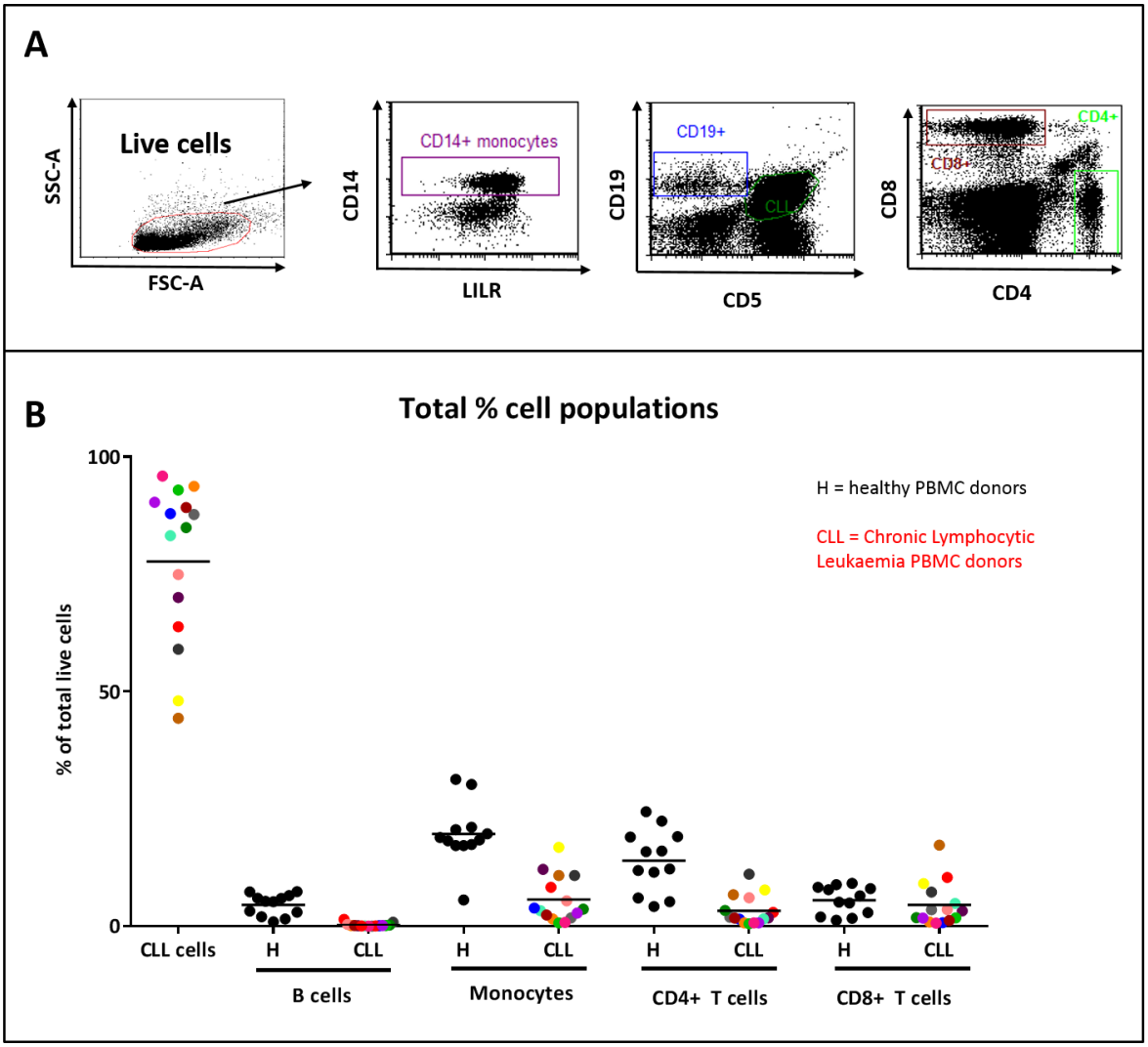

Figure 6.1 Comparison of blood populations in healthy versus CLL donors. The number of cells for different blood populations was calculated as a percentage of the total number of live cells. Cell populations were identified and stained with the following markers: CD14-Amcyan (BD Horizon), CD19-Pacific Blue (Biolegend), both CD19-Pacific Blue and CD5-FITC (Biolegend), CD8-APC-Cy7 (Biolegend), and CD4-PE-Cy7 (BD Biolegend), to identify monocytes, B cells, CLL cells, $CD8^+$ T cells and $CD4^+$ T cells respectively. 12 Healthy (H) (black) and 15 CLL (different colours) frozen and thawed PBMCs were compared. The gating strategy with an example CLL donor is shown in **A)** and the distribution of different blood populations of healthy versus CLL donors as a percentage of total live cells in **B)**. Data analysed using FlowJo software. Mean indicated by straight line.

Different cell populations were identified by the cell surface markers detailed above in *Figure 6.1A*. *Figure 6.1B* showed that whilst healthy donors showed a distribution of different blood populations, CLL samples were predominantly tumour (defined by $CD19^+$ $CD5^+$ profile). Mean values for healthy donors were ~5% B cells, ~20% monocytes, ~13% $CD4^+$ T cells and ~5% $CD8^+$ T cells. In comparison, for the CLL donors, ~80% were CLL cells ($CD19^+$ $CD5^+$), with almost no B cells ($CD19^+$ $CD5^-$) present, ~5% monocytes, ~3% $CD4^+$ T cells and ~5% $CD8^+$ T cells. The majority of CLL donors ranged from medium to high levels of $CD19^+$ $CD5^+$ cells.

6.2.1.2 Inhibitory LILR expression on CLL cells

Once the different blood populations were defined, LILR expression on both healthy and CLL donors were assessed and compared. Frozen healthy donor or CLL PBMCs were stained with representative specific anti-LILRB1, -LILRB2 and -LILRB3 antibodies, and also a commercial anti-LILRB4 antibody, then analysed by flow cytometry. As the numbers of $CD4^+$ and $CD8^+$ T cells was low (typically accounting for less than 5% of the CLL population – *Figure 6.1B*), reliable data was unattainable, due to low cell counts. Therefore, only the monocyte and CLL or healthy B cell populations were assessed.

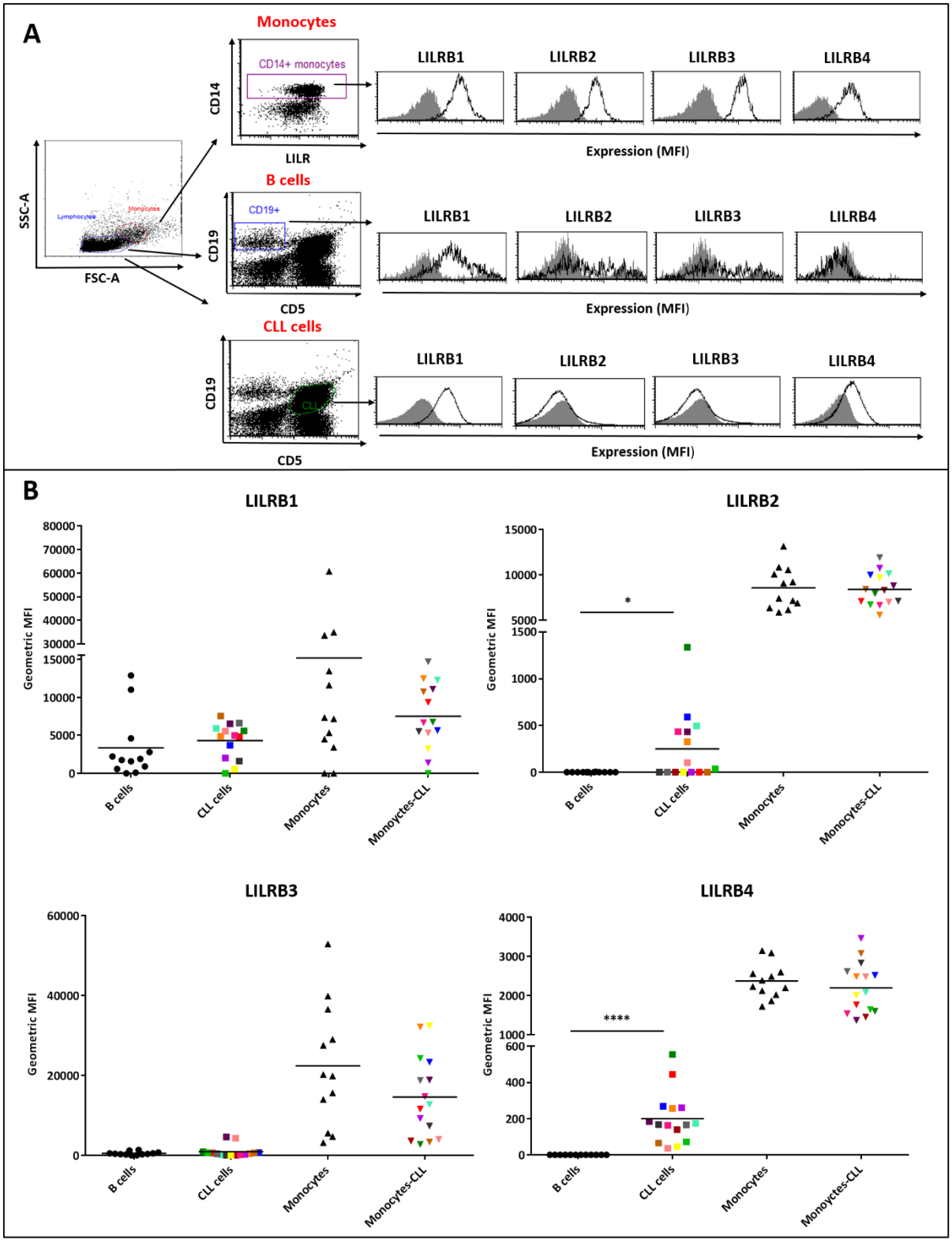

Figure 6.2 LILR expression on CLL cells. Frozen CLL or healthy PBMC samples were thawed and stained with representative anti-LILRB1, -LILRB2, and -LILRB3-APC antibodies (BioInvent), an anti-LILRB4 antibody (BD Pharmingen™) or relevant isotype controls. LILR antibodies were co-stained with CD14-Amcyan (BD Horizon), CD19-Pacific Blue (Biolegend) and CD5-FITC (Biolegend), then analysed by flow cytometry. Gating strategy with one example CLL donor is displayed in **A)** and summary of 12 healthy (black) donors and 15 CLL (different colours) donors in **B).** Data analysed using FlowJo software. Two-tailed paired T test was performed where stars represent p values as follows: $p < 0.05$ *, $p < 0.005$ **, $p < 0.0005$ *** and $p < 0.00005$ ****.

Figure 6.2A showed inhibitory LILR expression of one representative CLL donor, which showed all the inhibitory LILR antibodies stained $CD14^+$ monocytes, and expression was at similar levels. Only anti-LILRB1 stained B cells, although expression was low, as was the cell count of $CD19^+$ $CD5^-$ B cells, indicating, the number of healthy B cells in this sample was low. Both LILRB1 and to a lesser extent LILRB4, were found on $CD19^+$ $CD5^+$ CLL cells.

Twelve healthy and fifteen CLL frozen donors were phenotyped and summarised in *Figure 6.2B*. LILRB1 was found to be expressed both on B cells from healthy donors ($CD19^+$ $CD5^-$) and CLL cells ($CD19^+$ $CD5^+$) as expected, on average at a similar level. LILRB1 was also found to be expressed on both healthy and CLL monocytes, and this expression was higher than that found on B cells. However, expression was more variable on healthy donor monocytes (ranging from low to high expression) compared to on CLL monocytes. The average geometric MFI was decreased on CLL donors compared to healthy controls, suggesting that LILRB1 expression was down-regulated on monocytes in CLL donors.

LILRB2 was not found on B cells from healthy donors as expected. However, although the majority did not, a few CLL donors did express LILRB2. This suggested that in some cases, although LILRB2 was typically not found on healthy B cells, it could be up-regulated on malignant B cells, and this was statistically significant ($p = 0.0288$). LILRB2 was highly expressed on monocytes in both healthy and CLL donors. The average MFI was similar for both healthy and CLL donors, indicating that LILRB2 expression was consistent on monocytes in both healthy and malignant microenvironments.

LILRB3 was not expressed on B cells from healthy donors as expected. Although a few CLL donors expressed LILRB3, the majority did not. Both healthy and CLL monocytes were found to express LILRB3 and as with LILRB1 this was very variable (ranging from low to high expression). The average MFI of LILRB3 expression was decreased on CLL monocytes compared to healthy monocytes.

LILRB4 was not expressed on B cells from healthy donors as expected. However, the majority of donors analysed showed some LILRB4 expression on CLL cells, suggesting that LILRB4 was up-regulated on malignant B cells, and this was statistically significant ($p < 0.0001$). LILRB4 was found to be highly expressed on both healthy and CLL monocytes, at a similar degree.

In summary the LILRBs were expressed on monocytes from healthy donors, and LILRB1 on B cells from healthy donors. Whilst LILRB2 and LILRB4 remained consistently expressed on monocytes from both conditions, LILRB1 and LILRB3 expression on monocytes was down-

regulated on CLL donors, indicating that these receptors were down-regulated on monocytes during malignancy, possibly as LILRBs on these phagocytic cells may internalise with substances such as exosomes released from malignant cells. Only LILRB2 and LILRB4 were consistently expressed on malignant B cells, but a few CLL donors did show up-regulation of both LILRB2 and LILRB3 as well. This suggested that whilst LILRB1 and LILRB4 expression were commonly found on malignant B cells in CLL donors, other inhibitory LILRs may also be up-regulated. It was difficult to identify if tumour burden correlated to LILR expression, as all the CLL donors assessed here had medium to high tumour burden (~50-100% of cells were $CD19^+$ $CD5^+$ population). Therefore, a more varied sample size that included CLL samples with a lower tumour burden is warranted to clarify if LILR expression correlated to tumour burden.

6.2.1.3 Studying other Inhibitory receptor expression on CLL cells

The up-regulation of LILRBs on CLL donor PBMC samples indicated an increase in inhibitory cell surface markers on CLL cells. To test if this was a general trend, other inhibitory cell surface markers were also assessed. The cell surface markers assessed included: FcγRIIB, HLA-G, Programmed Cell Death-1 (PD-1), and its ligand PD-L1, T cell Immunoglobulin Mucin-3 (TIM-3), Lymphocyte Activation Gene-3 (LAG-3) and Cytotoxic T Lymphocyte Antigen-4 (CTLA-4).

FcγRIIB is an inhibitory FcγR expressed predominantly on B cells and shown to effect antibody cancer therapy[52, 217]. HLA-G, a non-classical HLA-I molecule, is a ligand for LILRB1 and LILRB2[99]. Studies have shown that expression of HLA-G is up-regulated in various tumours[131, 133, 166]. CD22 is an inhibitory B cell receptor, and its expression is restricted to B cells[266]. During infection or malignancies, naive T cells become effector T cells, but if chronic infection or exposure to antigen persists, these effector T cells become overworked or 'exhausted'[267]. Signs of this exhaustion can be characterised through 'exhaustion markers', found on the cell surface of T cells. PD-1, TIM-3, LAG-3 and CTLA-4 are all inhibitory receptors and T cell markers of exhaustion. Although individual expression of any one of these markers is not indicative of exhaustion, expression of multiple markers is[267]. Since its discovery on activated T and NK cells in 1990, LAG-3 has been found up-regulated in CLL and identified as a potential prognostic marker for the disease, as studies show high expression of the receptor correlates with a decrease in treatment-free survival[268, 269].

Therefore, the aim was to study expression levels of LILR ligands, and inhibitory receptors that may correlate with LILR expression.

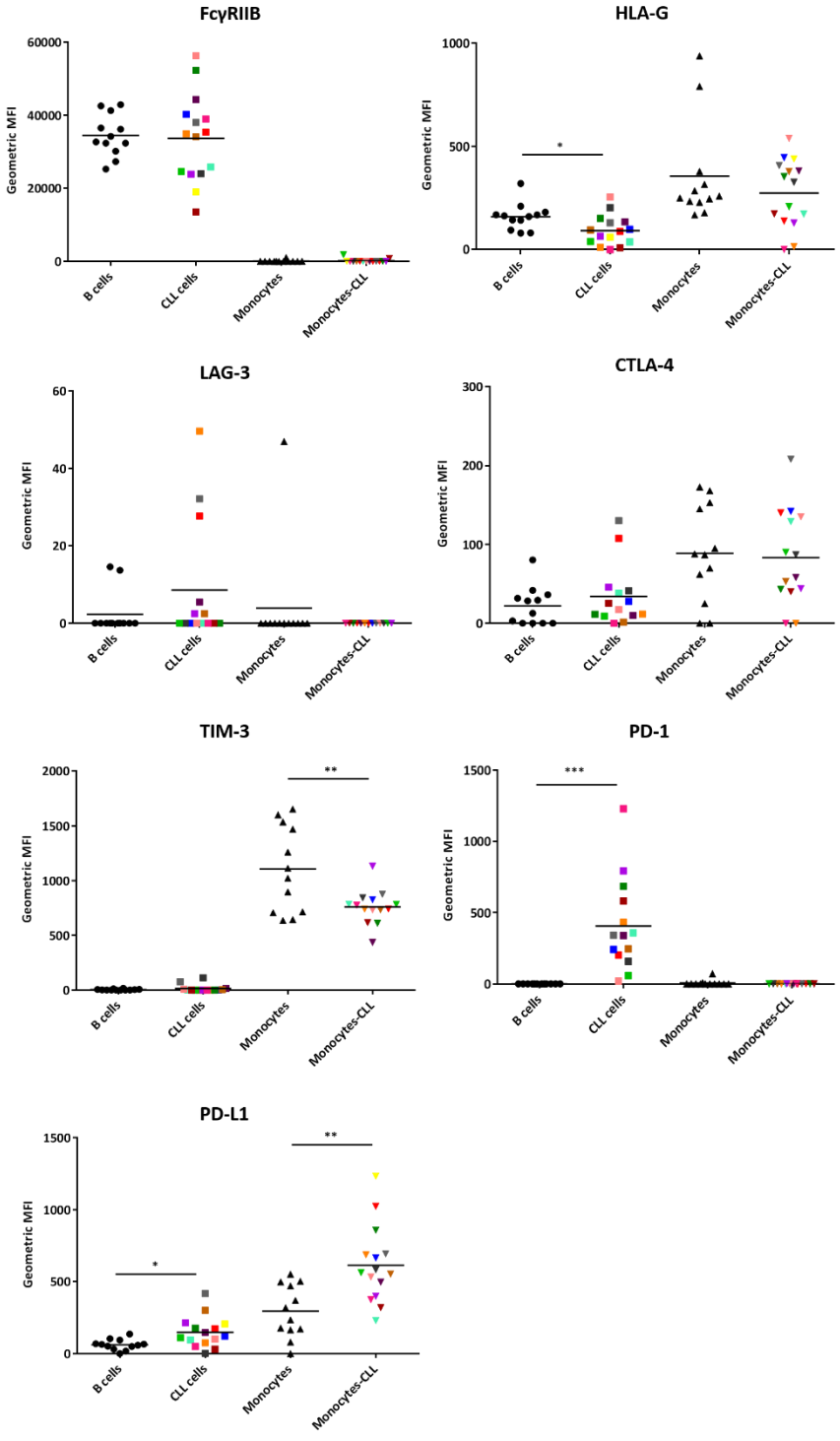

Figure 6.3 FcγR and exhaustion marker expression on CLL cells. 1x10^6 Healthy (H) PBMCs or CLL donors were blocked for 10 minutes at 4°C with 2% human AB serum and then stained for with the following antibodies: FcγRIIB-APC (BioInvent), LAG-3-PE (eBioscience) CTLA-4-PE (Biolegend), HLA-G-PE (Biolegend), TIM-3-PE (Biolegend), PD-1-PE (Biolegend), PD-L1-PE (Biolegend), and their relevant isotype controls for 30 minutes at 4°C. Surface expression was assessed with the FACS Canto (BD Bioscience). Data was analysed using FlowJo. N= 12 healthy and 15 CLL donors. Two-tailed paired T test was performed where stars represent p values as follows: $p < 0.05$ *, $p < 0.005$ **, $p < 0.0005$ *** and $p < 0.00005$ ****.

Figure 6.3 showed that both healthy and malignant B cells showed similar levels of expression of FcγRIIB, but no expression on monocytes in either setting. The non-classical HLA-I molecule, HLA-G was found to be expressed on B cells from healthy donors and the MFI decreased on CLL cells, this was statistically significant ($p = 0.0192$). HLA-G was expressed to a greater extent on monocytes from healthy donors. From CLL donors, the MFI slightly decreased on monocytes, compared to healthy donors. Therefore, HLA-G expression appeared to decrease on these two cell types.

T cell exhaustion markers, LAG-3, TIM-3 and PD-1, were not found to be expressed on B cells from healthy donors, and only TIM-3 was found on monocytes from healthy donors. There was some expression of LAG-3 on CLL cells, for a few donors, but for the majority of donors, LAG-3 was not found on either B cells or monocytes in either healthy or malignant samples. PD-1 expression was found on CLL cells, suggesting that although this marker is absent on healthy cells, malignant B cells up-regulated PD-1 and this was statistically significant ($p = 0.0002$). TIM-3 was found on monocytes but not B cells from healthy donors. Although TIM-3 is predominantly a T cell marker, previous studies have reported its expression on DCs and low levels on monocytes[270]. CLL monocytes also expressed TIM-3, although to a lower extent than healthy cells, suggesting this marker is significantly down-regulated on monocytes during malignancy ($p = 0.0056$). T_{reg} and activated T cell checkpoint blocker CTLA-4 was found to be expressed on both B cells from healthy donor and CLL donor samples at similar levels. Higher expression of CTLA-4 was found on monocytes from both healthy and CLL donor samples, at similar levels. Low expression of PD-1 ligand PD-L1 was found on B cells from healthy donors, and higher expression on monocytes from healthy donors. In CLL samples, expression of both of these markers increased significantly ($p = 0.0139$ and $p = 0.0016$, respectively).

In conclusion, these data suggested that overall inhibitory cell surface markers are up-regulated on tumours and down-regulated on cells circulating the tumour. This could be due to tumour cells having increased expression of inhibitory receptors to dampen immune response, resulting in tumour evasion. However, monocytes may down-regulate inhibitory receptors, such as LILRBs (*Figure 6.2*) possibly due to internalisation of exosomes released by tumours, thus promoting tumour regression. As before (*Figure 6.2*) it was difficult to correlate inhibitory receptor expression to tumour burden, given the high percentage of $CD19^+$ $CD5^+$ tumour cells.

6.2.2 The effect of anti-LILRB1 in CLL therapy

Given that LILRB1 was highly expressed on CLL cells, the effect of anti-LILRB1 antibodies were tested *in vivo*. A CLL xenograft model was chosen, as this model had been previously optimised in the lab, and access to fresh CLL blood was possible.

6.2.2.1 Assessing anti-LILR therapy in immunocompromised mice with human or mouse FcγRIIB

To conduct these experiments a Severe Combined Immunodeficiency (SCID) Non-obese Diabetic (NOD), mouse model was chosen. SCID mice lack T and B lymphocytes, whilst NOD mice have impaired NK cells[271, 272]. Therefore, SCID NOD mice have compromised innate and adaptive immunity; increasing the chance of tumour engraftment, as the host immune system cannot reject the foreign cells. To further facilitate engraftment, the mice were first irradiated with a low dose of ionising radiation. The inhibitory receptor FcγRIIB (CD32B) has been shown to hinder anti-CD20 therapy, therefore as human IgG1 antibodies were used for treatment in these experiments, mice with the mouse FcγRIIB gene knocked out, and replaced with human FcγRIIB were also utilised in some of these experiments[52, 217].

Once irradiated, tumour cells were administered intravenously (i.v.) allowing rapid engraftment. Antibody was given intraperitoneal (i.p.), 3 days later. A schematic of the experiment is displayed in *Figure 6.4* below.

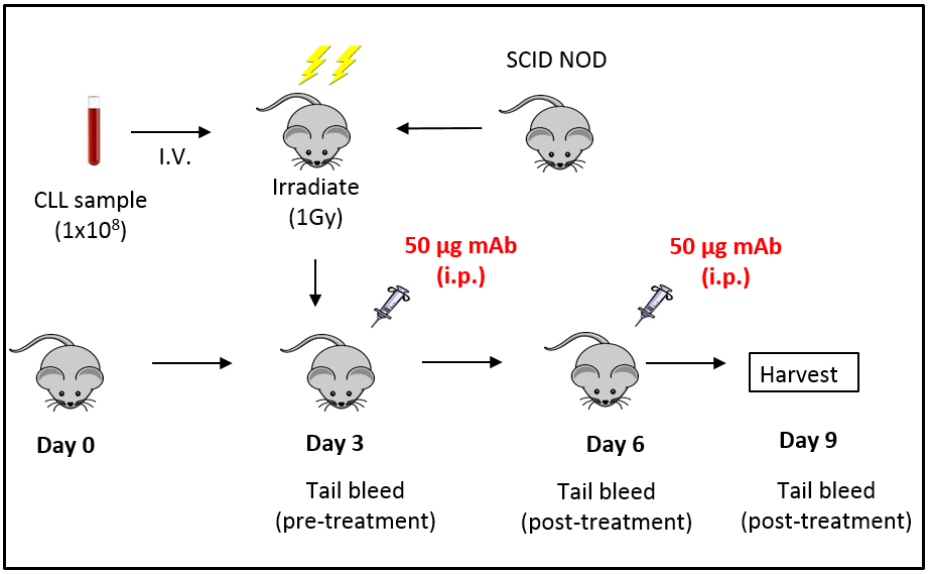

Figure 6.4 Schematic of CLL xenograft experiment. Mice were irradiated with 1Gy for 2-5 hours, then $1x10^8$ isolated PBMCs from fresh CLL blood in autologous serum was injected into irradiated mice. Tumour cells were left to engraft for 3 days, then mice were treated with 2mg/kg of anti-LILR monoclonal antibody (mAb), i.e., ~ 50 µg mAb/mouse, on day 3 and day 6 (and bled on both days). Mice were culled on day 9, and blood, bone marrow and spleen harvested for analysis.

As LILRB1 was found to be highly expressed on malignant CLL cells, anti-LILRB1 therapy was tested. Based on the HLA-G blocking assays performed in Chapter 4 (*Figure 5.2*), where C7 blocked signalling (an antagonist) and C9 enhanced signalling (an agonist), these two different anti-LILRB1 antibodies were tested in this model.

Prior to the initiation of the experiment, the CLL sample was first examined for its cellular composition ($CD19^+$ $CD5^+$ CLL cells), inhibitory LILR expression profile, and sensitivity to antibody modulation. CLL cells were first phenotyped for LILR expression and then an A488 quenching assay was performed to assess antibody internalisation.

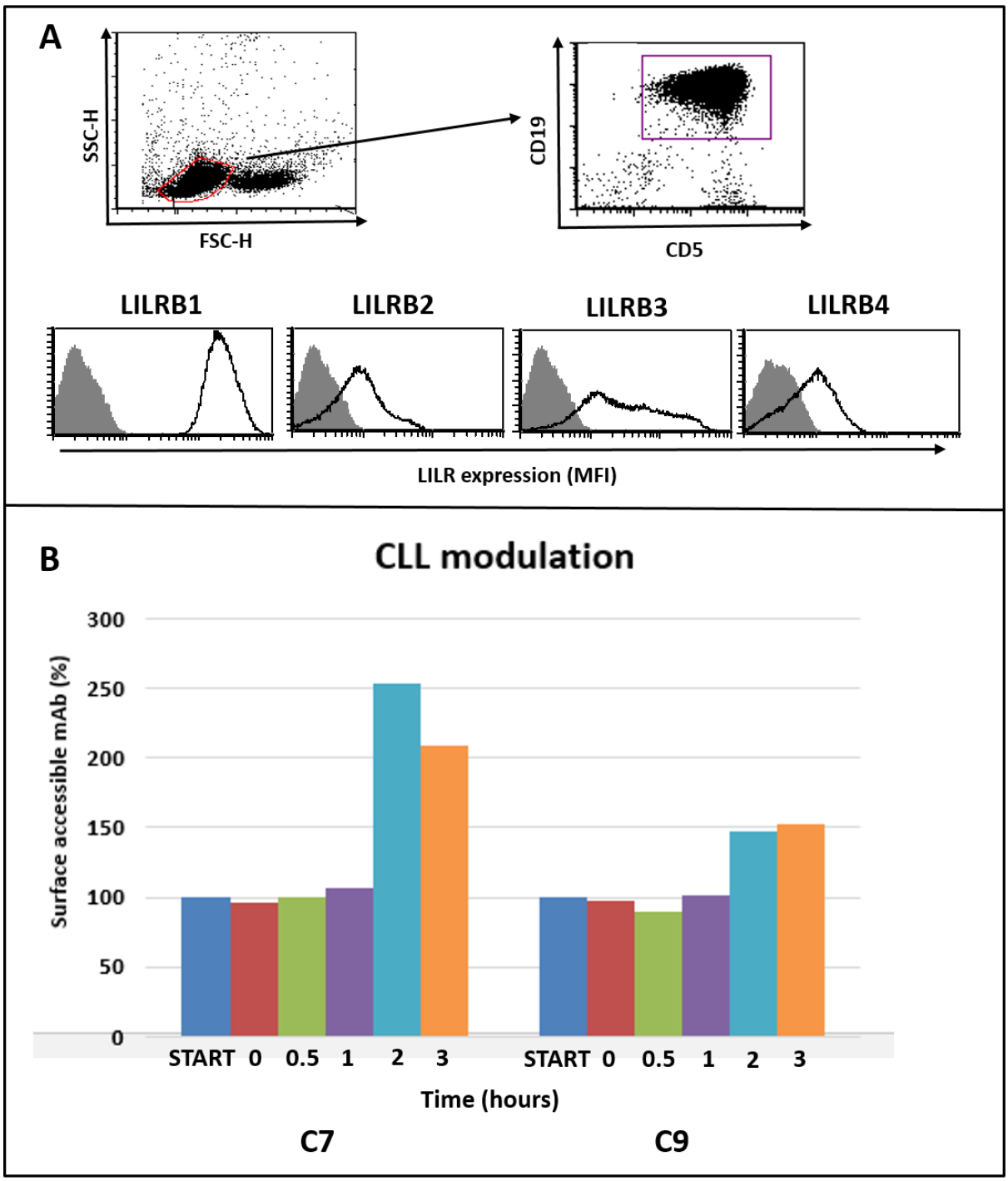

Figure 6.5 Assessing LILR expression and antibody modulation on CLL575. A) LILR expression on fresh CLL cells. CLL sample CLL575 was utilised here. CLL cells were co- stained with CD19-PE (Biolegend) and CD5-FITC (Biolegend) and 10 µg/ml either anti-LILRB1, -LILRB2, -LILRB3 (BioInvent), anti-LILRB4 (Biolegend) or relevant isotype controls for 30 minutes at 4°C, before being analysed by flow cytometry. **B) Effect of anti-LILRB1 antibodies on receptor modulation.** A488 quenching assay was performed. $1x10^6$ CLL cells were incubated with 5 µg/ml directly labelled A488 anti-LILRB1 clones (BioInvent) or an isotype control over three hours at 37°C. Cells were washed (unquenched) or washed and stained with an anti-A488 secondary (quenched) and washed again. Surface accessible antibody was measured by subtracting the geometric MFI of the quenched samples from the unquenched, and dividing by the unquenched, removing the background (isotype) each time.

Figure 6.5A showed that the majority of the lymphocyte cell population were $CD19^+$ $CD5^+$, characteristic of CLL cells. LILRB1 and LILRB3 were both highly expressed on the CLL sample used in this xenograft experiment. LILRB1 expression was more homogenous and all cells were positive for the receptor. Comparably, LILRB3 had a more heterogeneous expression with both low, and high expressing cells. Both LILRB2 and LILRB4 were expressed to a lower, but similar extent.

Figure 6.5B showed that both C7 and C9 showed no receptor internalisation on CLL cells. Surface accessibly antibody was consistent between 0 and 1 hour, and then accumulated between 2 and 3 hours. This showed that the LILRB1 receptor remained at the cell surface and did not internalise on CLL cells, but did accumulate over time. Previously, C7 showed slow internalisation on monocytes (*Chapter 4, Figure 5.11*). However, on CLL cells this was not the case. This indicated that the receptor would still be accessible on the cell surface for the antibody to bind to, allowing antibody therapy to take place.

This CLL donor was then injected into SCID NOD mice to establish a xenograft model (as described in *Figure 6.4*). Two different anti-LILRB1 antibodies C7 and C9, were used to treat the tumours. Given that high LILRB3 staining was also observed for this CLL sample (*Figure 6.5B*), an anti-LILRB3 antibody was also included (A1 – which displayed agonistic properties in the *in vitro* assays performed in Chapter 4). Tumour levels in the blood were measured by assessing human CD45 (hCD45) expression in the blood by flow cytometry. On day 9, spleen and bone marrow samples were also harvested and hCD45 expression assessed in these tissues also.

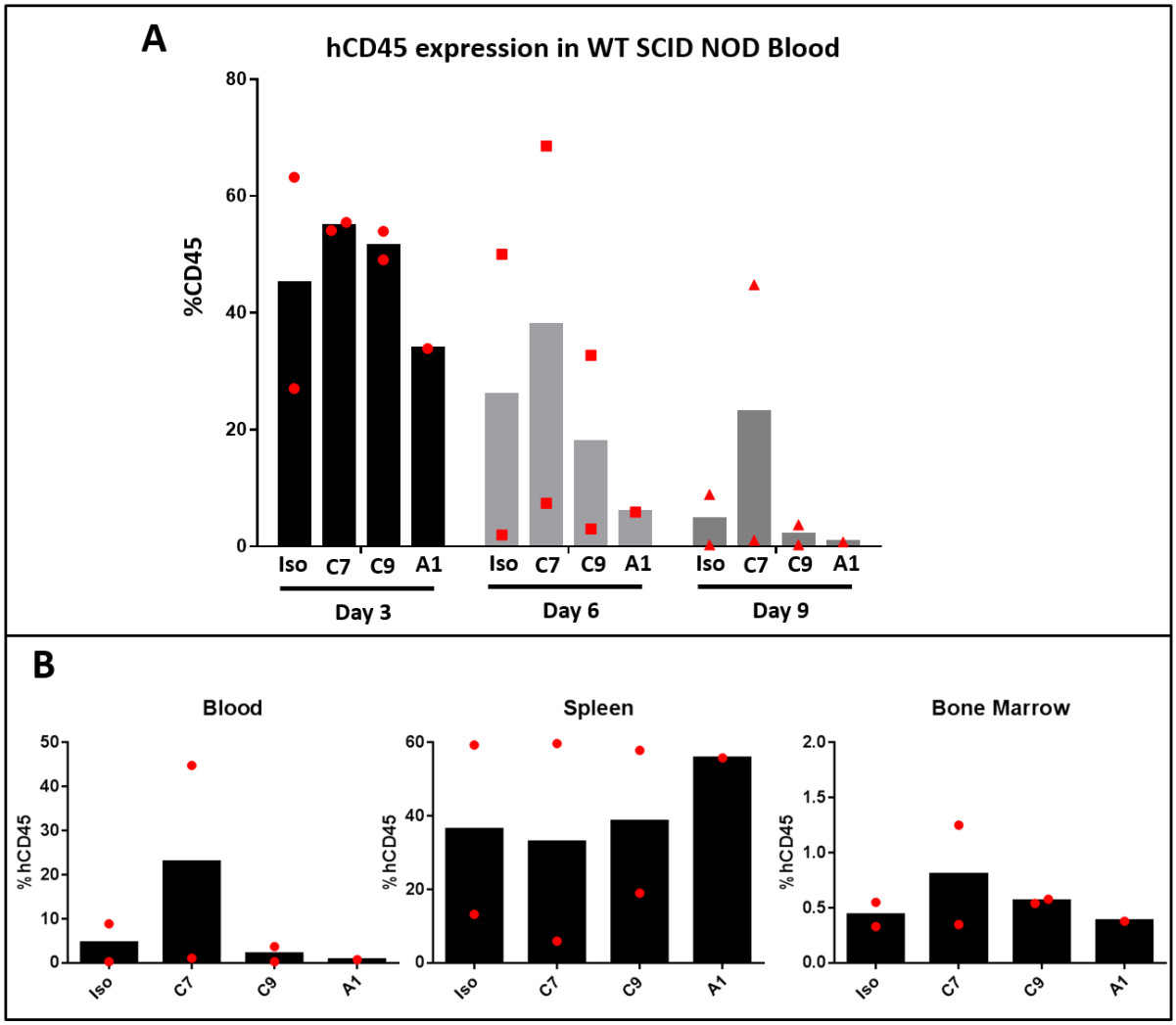

Figure 6.6 Effect of anti-LILR antibodies on CLL tumour growth in SCID NOD mice. Mice, irradiated with 1Gy for 2-5 hours, were injected with $1x10^8$ isolated PBMCs from fresh CLL blood in autologous. Mice were treated with 50 µg mAb/mouse, on day 3 and day 6, then culled on day 9, and blood, bone marrow and spleen harvested for analysis. % positive human CD45 expression was monitored over time to test tumour expression. Treatment groups were as follows: anti-LILRB1 antibodies C7, and C9, anti-LILRB3 clone A1 or isotype (Iso) control. N=1-2 mice/group. In **A)** hCD45 expression assessed in blood on day 3, 6 and 9 for different treatment groups and in **B)** Day 9 hCD45 expression compared in blood, spleen and bone marrow.

Tumour levels were monitored by screening for hCD45 expression. Tumour engraftment was measured on day 3 (before antibody therapy) and different levels of engraftment were observed in the SCID NOD mice, ranging from an average of 35-55% (*Figure 6.6A*). After initial treatment (day 6), hCD45 expression decreased to ~30%, 40%, ~20% and 5% in the isotype, C7, C9 and A1-treated groups, respectively. This further decreased after a second dose of antibody treatment (Day 9) to ~5% for isotype-treated, 25% for C7-treated, and almost nothing for both C9 and A1-treated mice, respectively. C7 therefore had the highest amount of hCD45 in the blood by day 9, suggesting C7 was less efficient at depleting CLL cells compared to C9 and A1. Although, it should be noted that two mice were treated with C7, one showed very high levels of hCD45 in the blood by day 9, whilst the other showed

very low levels. Therefore, this variation between the mice in this treatment group skewed the average, and a larger sample size was needed. Also, as the isotype control-treated group also showed depletion in the blood, it could have been that the tumour cells were homing elsewhere.

Analysis of hCD45 expression in the spleen and bone marrow supported this idea, as although levels of hCD45 were decreasing in the blood, high levels appeared in the spleen (between 35-60% in all groups), but very little in the bone marrow (*Figure 6.6B*). This indicated that the tumour cells were leaving the blood and migrating to the spleen, a common feature of leukemic cells. As hCD45 expression was so high in the spleen across all treatment groups, this suggested that cells were not depleted with the anti-LILR therapy once they had entered the spleen.

In summary, together this data indicated that certain LILR antibodies were able to delete leukemic cells in the blood but not within the tumour microenvironment of the spleen.

Given that studies have shown that FcγRIIB can impact anti-CD20 antibody therapy, the same CLL donor was also injected into human FcγRIIB Tg SCID NOD mice (human gene overexpressed, but mouse FcγRIIB is absent)[52, 217].

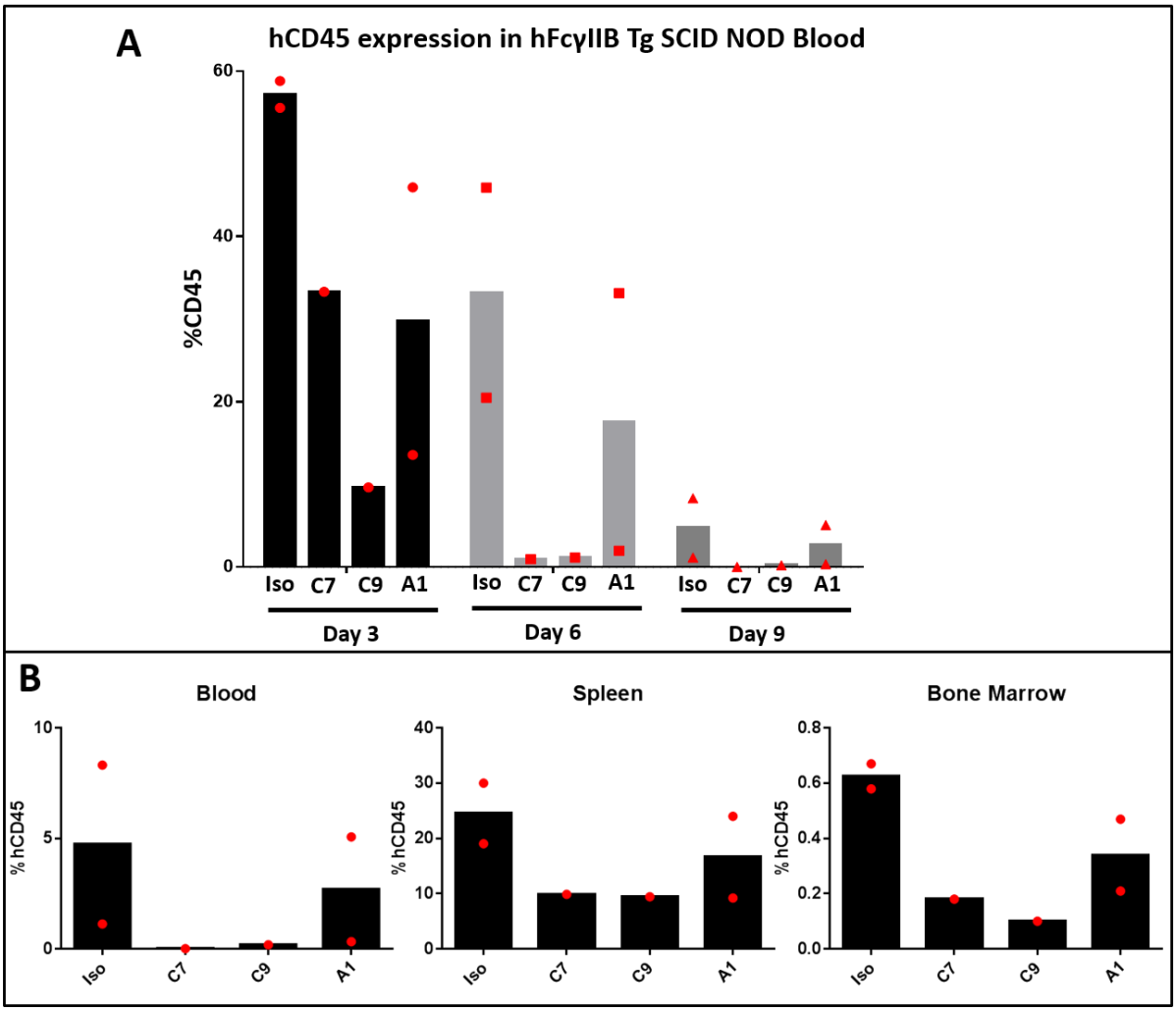

Figure 6.7 Effect of anti-LILR antibodies on CLL tumour growth in hFcγRIIB Tg SCID NOD mice. Experiment performed as described in *Figure 6.6*, but in hFcγRIIB Tg SCID NOD mice. N=1-2 mice/group. In **A)** hCD45 expression assessed in blood on day 3, 6 and 9 for different treatment groups and in **B)** Day 9 hCD45 expression compared in blood, spleen and bone marrow.

In these mice, similar results were observed to those seen in the SCID NOD mice (in *Figure 6.6*). *Figure 6.7A* shows that tumour engraftment (day 3) was achieved but varied between groups, and as before hCD45 levels in the blood decreased between days 3-9. The levels of hCD45 decreased at a much faster rate in the C7 and C9-treated groups, compared to the isotype and A1-treated groups. This suggested that C7 and C9 were more efficient at depleting the leukemic cells in this model.

Comparison of the blood, spleen and bone marrow on day 9 showed that high levels of hCD45 were seen in the spleen for all groups, but more so in the isotype and A1-treated groups (*Figure 6.7B*). Although, comparisons between different treatment groups is difficult due to the varying levels of tumour engraftment, nevertheless, both C7 and C9 appeared to achieve more potent deletion of tumour cells from the blood and spleen compared to their isotype control and A1.

In summary, these data indicated that for this donor, CLL cells depleted better in the hFcγRIIB Tg mice, and unlike in the SCID NOD mice, C7 and C9 were able to deplete tumour cells in the spleen as well as the blood. This suggested that the presence of FcγRIIB aids in tumour elimination, not just in the blood but in the tumour microenvironment of the spleen also. However, given the difference in engraftment efficiency and small sample size, this requires further validation.

6.2.2.2 Assessing anti-LILR therapy in immunocompromised mice with or without human FcγRIIB

Given the promising results seen in previous experiments, a second CLL donor was utilised in a second batch of experiments. This time, given the lack of toxicity, the amount of antibody treatment was increased to 100 μg to try and increase tumour depletion. The number of mice used per group was also increased to provide more conclusive findings.

As previously, the CLL sample was first phenotyped for inhibitory LILR expression and antibody modulation assessed.

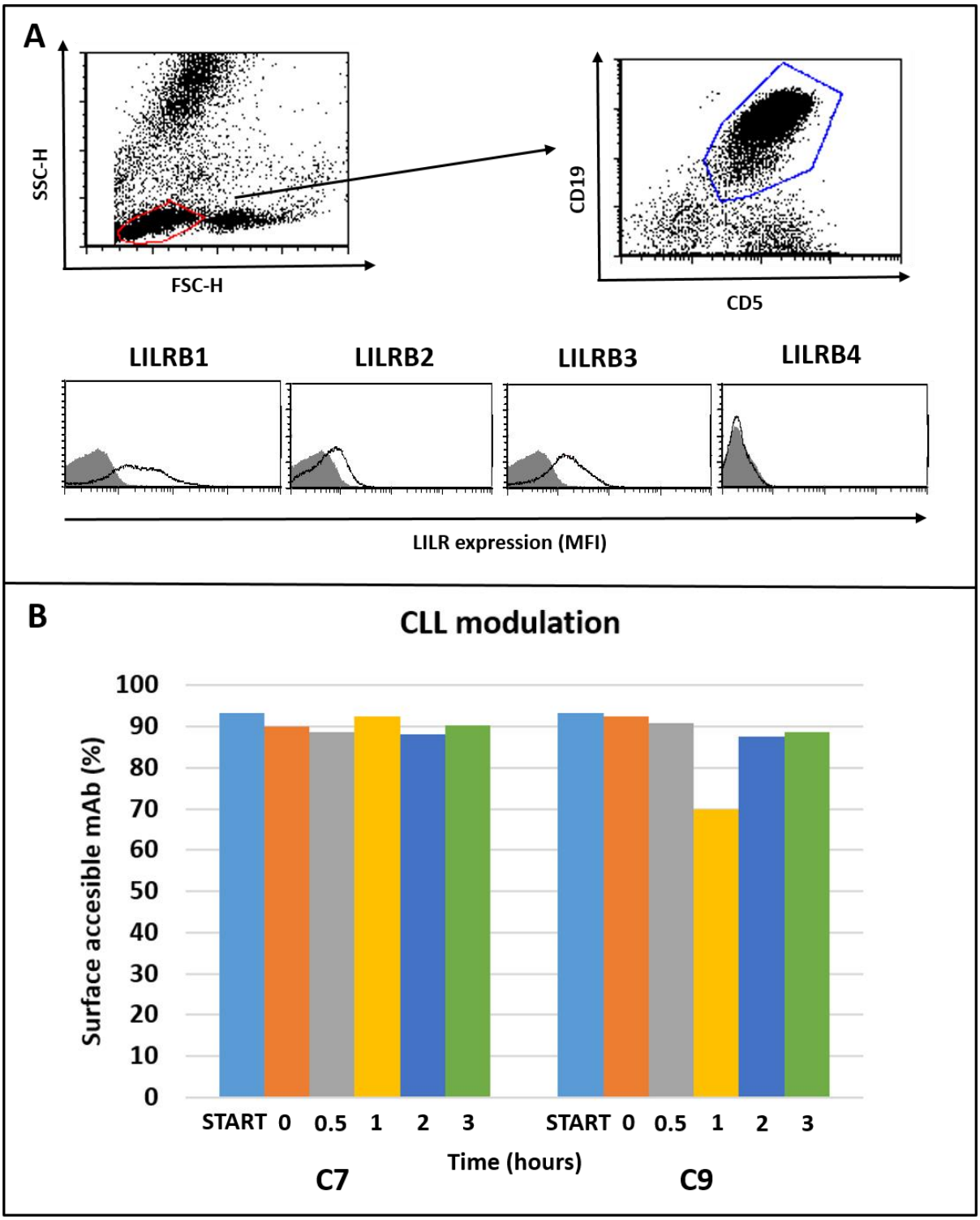

Figure 6.8 Assessing LILR expression and antibody modulation on CLL391. A) LILR expression on fresh CLL cells. CLL sample CLL391 was utilised here. CLL cells were co- stained with CD19-PE (Biolegend) and CD5-FITC (Biolegend) and 10 µg/ml either anti-LILRB1, -LILRB2, -LILRB3 (BioInvent), anti-LILRB4 (Biolegend) or relevant isotype controls for 30 minutes at 4°C, before being analysed by flow cytometry. **B) Effect of anti-LILRB1 antibodies on receptor modulation.** A488 quenching assay was performed as described in *Figure 6.5*.

As with the previous sample used, *Figure 6.8A* shows that the majority of the lymphocyte cell population were $CD19^{+}$ $CD5^{+}$, characteristic of CLL cells. LILRB1 and LILRB3 were both expressed on the CLL sample used in this xenograft experiment. This time however, LILRB1

expression was higher and more heterogeneous with both low and high expressing cells, whilst LILRB3 had a lower more homogenous expression of high expressing cells. LILRB2 was expressed to a much lower extent, and no LILRB4 expression was found on this donor.

Figure 6.8B showed that both C7 and C9 showed no receptor internalisation on CLL cells. For C7, surface accessibly antibody was consistent across the 3 hours, maintaining around ~90% of the antibody at the cell surface. C9 showed similar levels of antibody (~90%) with the exception of a drop to ~70% at 1 hour. This may have been receptor internalisation and fast recycling back to the surface by 2 hours, or more likely due to experimental error, as this was not seen with previous donor (*Figure 6.5B*).

In conclusion, LILRB1 was expressed the highest on this donor and remained at the cell surface and did not internalise on CLL cells.

As the expression level of LILRB3 was lower with this CLL donor (*Figure 6.8A*), mice were treated with only anti-LILRB1 antibodies. Given that the anti-LILRB antibodies appeared to deplete CLL cells more efficiently in the presence of the human FcγRIIB gene (hFcγRIIB Tg SCID NOD mice), compared to mice with the mouse FcγRIIB gene (SCID NOD), mFcγRIIB KO mice were used as a model instead of the SCID NOD mice. The aim of this experiment was therefore to deduce if the presence of FcγRIIB was hindering antibody therapy, therefore allowing a comparison of mice with or without FcγRIIB, and how this may impact antibody therapy. With the exception of the changes mentioned above, the experiment was performed as described in *Figure 6.4*.

Firstly, anti-LILR therapy with two different anti-LILRB1 antibodies C7 and C9, were used to treat tumours in mFcγRIIB KO mice. Tumour levels were measured by assessing hCD45 expression in the blood by flow cytometry and then on day 9, hCD45 expression was compared in the blood, spleen and bone marrow.

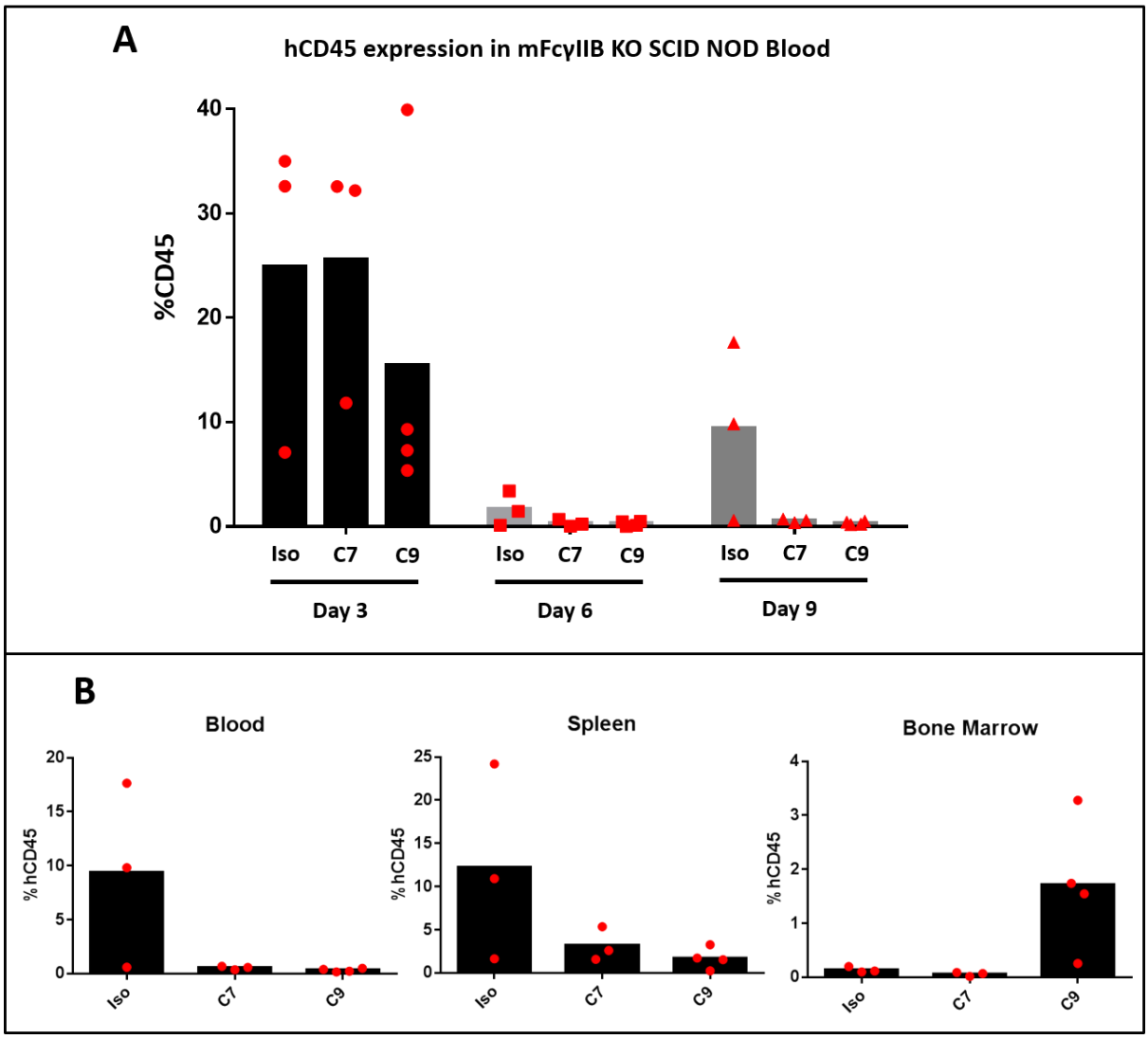

Figure 6.9 Effect of anti-LILR antibodies on CLL tumour growth in mFcγRIIB KO SCID NOD mice. Mice, irradiated with 1Gy for 2-5 hours, were injected with $1x10^8$ isolated PBMCs from fresh CLL blood in autologous. Mice were treated with 100 µg mAb/mouse, on day 3 and day 6, then culled on day 9, and blood, bone marrow and spleen harvested for analysis. % positive human CD45 expression was monitored over time to test tumour expression. Treatment groups were as follows: anti-LILRB1 antibodies C7 or C9, or isotype (Iso) control. N=3-4 mice/group. In **A)** hCD45 expression assessed in blood on day 3, 6 and 9 for different treatment groups and in **B)** Day 9 hCD45 expression compared in blood, spleen and bone marrow.

Figure 6.9A showed that although engraftment levels (day 3) were better matched in this experiment with the mFcγRIIB KO mice, engraftment within treatment groups was still variable. A decrease in hCD45 in the blood was seen as before, ~25% to <5% and then increasing again to 10% for the isotype-treated mice on day 3, 6 and 9 respectively; ~25% on day 3 to almost 0% on day 6 through to 9 in the C7-treated group; and ~15% on day 3 to almost 0% by day 6 through to 9. This suggested that with C7 and C9, CLL cells are almost completely depleted after just one dose of antibody, as almost no hCD45 expression was observed on day 6 for both groups. Comparatively, although the levels of hCD45 decrease by

day 6 for the isotype-treated mice, this then increases again on day 9. This could have been due to tumour relapse.

As seen previously, tumours appeared to migrate to the spleen as hCD45 expression was seen on day 9 here, but very little was observed in the bone marrow (*Figure 6.9B*). Only the isotype-treated group still had hCD45 expression in the blood by day 9. This supported the idea that both C7 and C9 were able to deplete tumour cells from the blood, compared to the isotype, which showed CLL cells were still present in the blood and migrated to the spleen by day 9. *Figure 6.9B* shows that as seen with the hFcγRIIB Tg mice (*Figure 6.7B*), the level of hCD45 in the spleen was reduced in the C7 and C9-treasted groups, suggesting these antibodies were able to deplete tumour cells not just in the blood but in the spleen also, or that they deplete CLL cells in the blood preventing homing to the spleen. Given that anti-LILRB1 mAbs were able to deplete CLL cells in the mFcγRIIB KO, it suggests that FcγRIIB was not required for therapy.

After assessing anti-LILRB1 therapy in mFcγRIIB KO mice, to confirm findings seen previously with hFcγRIIB Tg mice (*Figure 6.7B*), and to compare anti-LILRB1 therapy in the absence or presence of FcγRIIB, the experiment was repeated with the same CLL donor in hFcγRIIB Tg SCID NOD mice. As before, CLL tumours were treated with C7 and C9 or a relevant isotype, this time in hFcγRIIB Tg mice. Tumour levels were again measured by assessing hCD45 expression in the blood by flow cytometry and then on day 9, hCD45 expression compared in the blood, spleen and bone marrow.

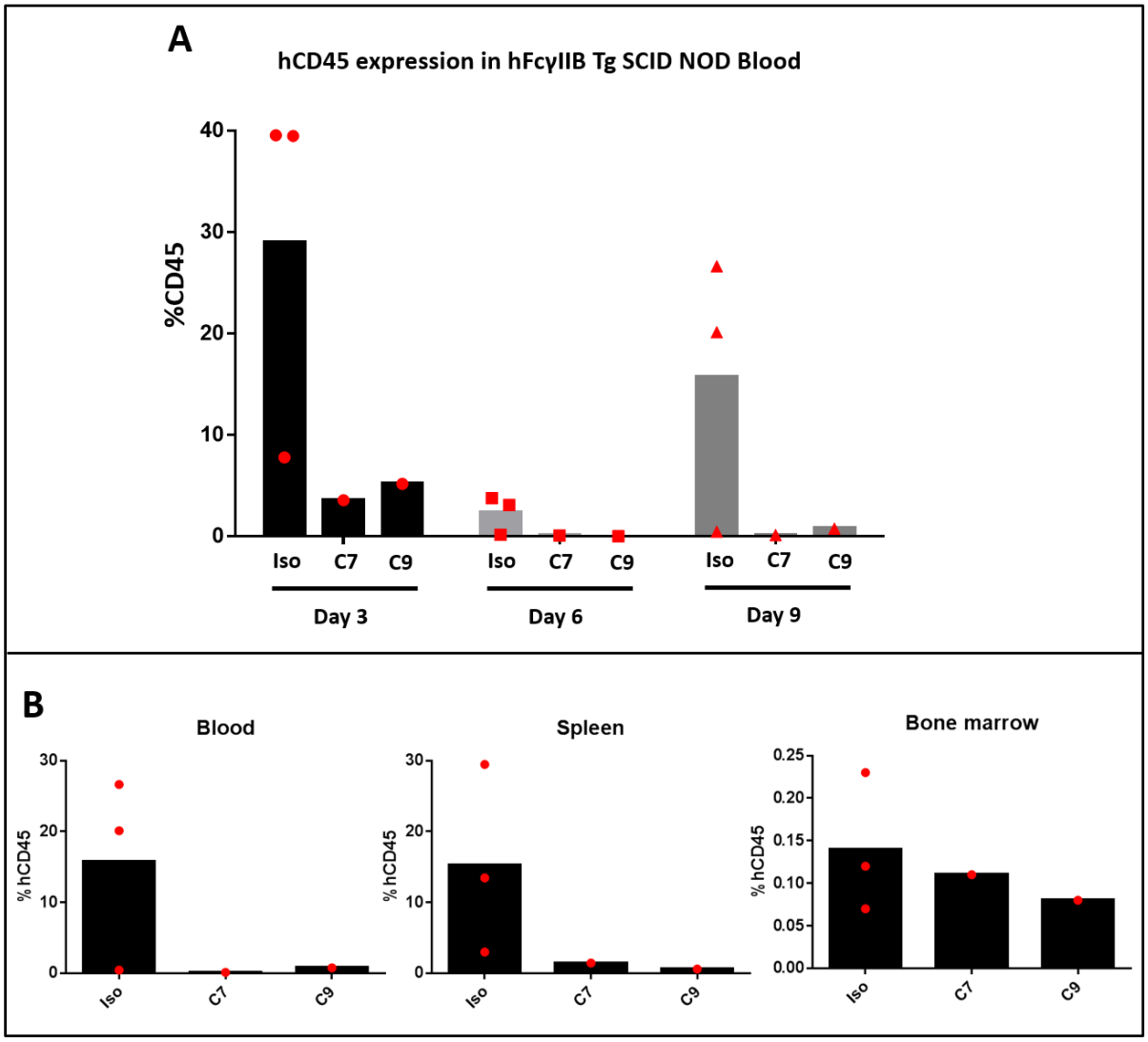

Figure 6.10 Effect of anti-LILR antibodies on CLL tumour growth in hFcγRIIB Tg SCID NOD mice. Experiment was performed as previously described in *Figure 6.9* this time in hFcγRIIB Tg SCID NOD mice. N=1-3 mice/group. In **A)** hCD45 expression assessed in blood on day 3, 6 and 9 for different treatment groups and in **B)** Day 9 hCD45 expression compared in blood, spleen and bone marrow.

In the hFcγRIIB Tg mice (*Figure 6.10*) similar results were observed. Engraftment once again was variable in the different mice, and treatment groups, but the level of hCD45% did decrease from day 3 to day 9 (*Figure 6.10A*). The isotype-treated group showed a decrease from ~30% to <5% then an increase to ~15% on day 3, 6 and 9, respectively. This suggested that CLL cells were depleted or migrated elsewhere by day 6, but then appeared to accumulate again in the blood by day 9 in this treatment group. Both the C7 and C9-treated groups showed a decrease from ~5% on day 3 to almost nothing by day 6 through to 9.

Figure 6.10B showed that hCD45 expression for the isotype-treated group migrated to the spleen, but very little expression was seen in the C7 and C9-treated groups. This indicated that both C7 and C9 were able to deplete the tumour cells, either before they had a chance to

migrate to the spleen, or were able to deplete the cells in the spleen as well. Very little tumour was seen for any group in the bone marrow, suggesting CLL cells do not migrate here.

In summary, in the hFcγRIIB Tg mice anti-LILRB1 antibodies C7 and C9 were both able to deplete leukemic cells. Given that cells did not engraft very well in this experiment (only two mice showed decent levels of engraftment – in the isotype-treated group of ~40% hCD45), deducing anything conclusive from this experiment was difficult.

6.2.2.3 Assessing anti-LILR therapy in immunocompromised mice in the absence of FcγRIIB

Finally, to confirm previous findings, the experiment was repeated again with a third donor. However this time, no hFcγRIIB Tg mice were available, therefore only mFcγRIIB KO mice were utilised.

As previously, before carrying out the xenograft experiment, LILR expression was assessed. Given the lower LILRB1 expression, modulation could not be studied (*Figure 6.11* below).

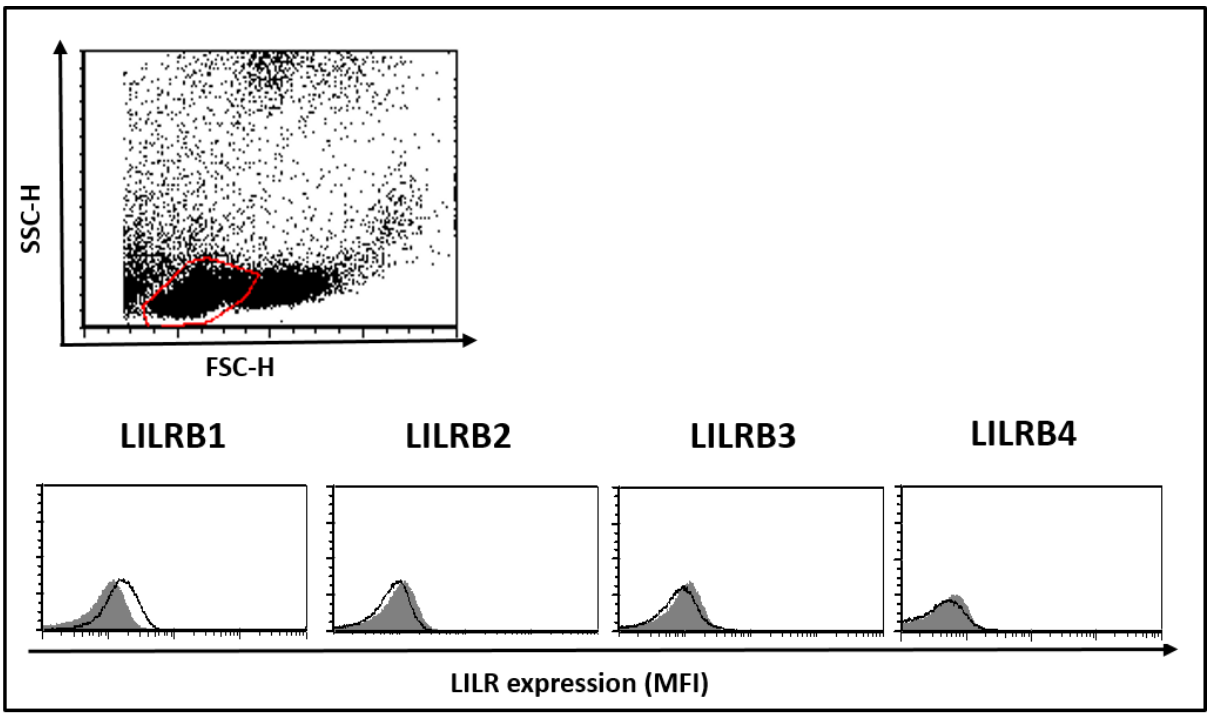

Figure 6.11 Assessing LILR expression on CLL donor CLL629. CLL sample CLL629 was utilised here. CLL cells were co- stained with CD19-PE (Biolegend) and CD5-FITC (Biolegend) and 10 µg/ml either anti-LILRB1, -LILRB2, -LILRB3 (BioInvent), anti-LILRB4 (Biolegend) or relevant isotype controls for 30 minutes at 4°C, before being analysed by flow cytometry.

The donor used in this xenograft experiment showed much lower LILRB1 expression and no expression of LILRB2, LILRB3 or LILRB4 (*Figure 6.11*). Once again, this highlighted the

variability in LILR expression on CLL tumours. Given the low expression of LILRB1, antibody modulation could not be studied. However, although low, as there was some LILRB1 expression, the xenograft experiment was performed.

In this experiment, tumour engraftment was measured (on day 3) before assigning mice to different treatment groups, to match the different levels of engraftment as best as possible. The experiment was performed as previously described in *Figure 6.4* with 100 µg antibody treatment, and tumour levels in the blood, spleen, and bone marrow were assessed by hCD45 expression. The liver was also assessed for hCD45 expression to study if tumour cells migrated here from the blood. Given the availability of more mice this time, treatment with anti-LILRB1 clone C10 was also included.

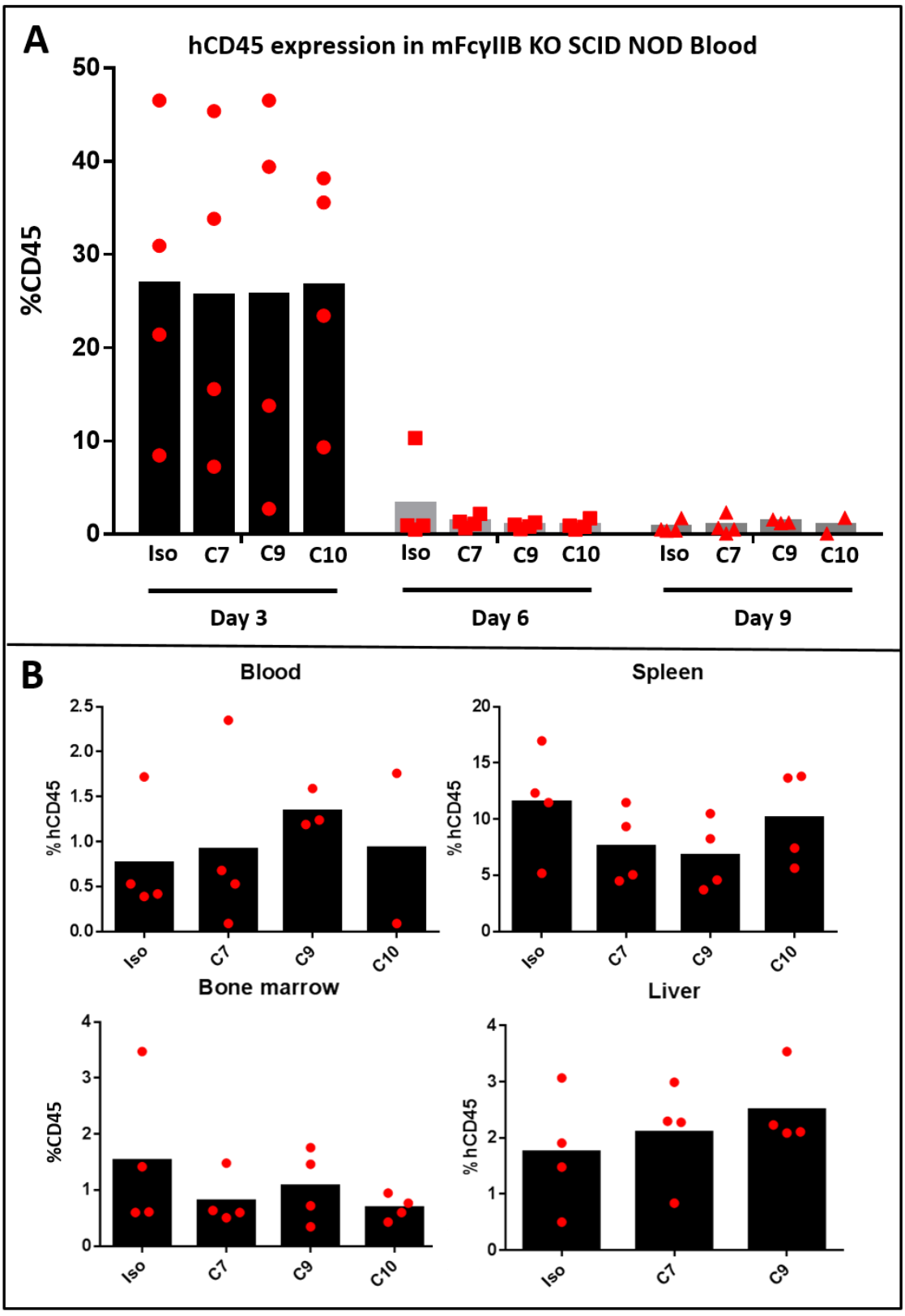

Figure 6.12 The effect of anti-LILR antibody therapy on CLL tumour growth. A) Effect of anti-LILR mAbs in CLL xenografts in mFcγRIIB KO SCID NOD mice. Mice, irradiated with 1Gy (~40ly) for 2-5 hours, were injected with $1x10^8$ isolated PBMCs from fresh CLL blood in autologous. Mice were treated with 100 µg mAb/mouse, on day 3 and day 6, then culled on day 9, and blood, bone marrow, spleen and liver harvested for analysis. % positive human CD45 expression was monitored over time to test tumour expression. Treatment groups were as follows: anti-LILRB1 antibodies C7, C9, C10, and isotype (Iso) control. N=4 mice/group In **A)** hCD45 expression assessed in blood on day 3, 6 and 9 for different treatment groups and in **B)** Day 9 hCD45 expression compared in blood, spleen, bone marrow and liver.

Tumour engraftment was matched in this experiment between the different treatment groups and an average of ~25% hCD45 in all groups on day 3 was observed. However, variability within treatments groups was still observed, showing how heterogeneous engraftment can be (*Figure 6.12*). *Figure 6.12A* showed that in the mFcγRIIB KO mice, hCD45 expression decreased in the blood to ~5% isotype-treated group and <5% in all other treatment groups by day 6 through to 9. This suggested that less tumour was present in the blood on day 9 in the groups treated with anti-LILRB1 antibodies, compared to the isotype where cells may have migrated elsewhere. *Figure 6.12B* showed that by day 9, ~12% hCD45 was found in the spleen for the isotype-treated group, compared to 8% in the C7 and C9-treated groups and ~10% in the C10-treated group. This suggests that both C7 and C9 deplete slightly better than C10.

Figure 6.12B showed that very little hCD45 expression was observed in the blood, bone marrow and liver on day 9 (on average ~2.5% or less for all groups). However, some hCD45 expression was observed in the spleen, suggesting as seen in previous experiments, the tumour migrated to the spleen. Less hCD45 was seen in the C7 and C9-treated groups (~7%) compared to the isotype or C10-treated groups (~10%). Suggesting that both C7 and C9 may be better at depleting cells than C10, however, this difference is minimal, and the levels of hCD45 are similar in all groups.

In summary, although hCD45 expression decreased from day 3 to 9, suggesting that the human tumour cells were cleared from the blood and/or migrated to the spleen; the extent of deletion for this CLL donor was much less than seen previously, as demonstrated by the similar levels of hCD45 in all treatment groups in the spleen. This may have been the result of the low expression levels of LILRB1 seen on this donor (*Figure 6.11*). High LILRB1 expression may be necessary for successful antibody therapy.

A summary of hCD45 expression in the spleen (day 9) for all the xenograft experiments performed in the different mouse models utilised in this chapter is given below in *Figure 6.13*.

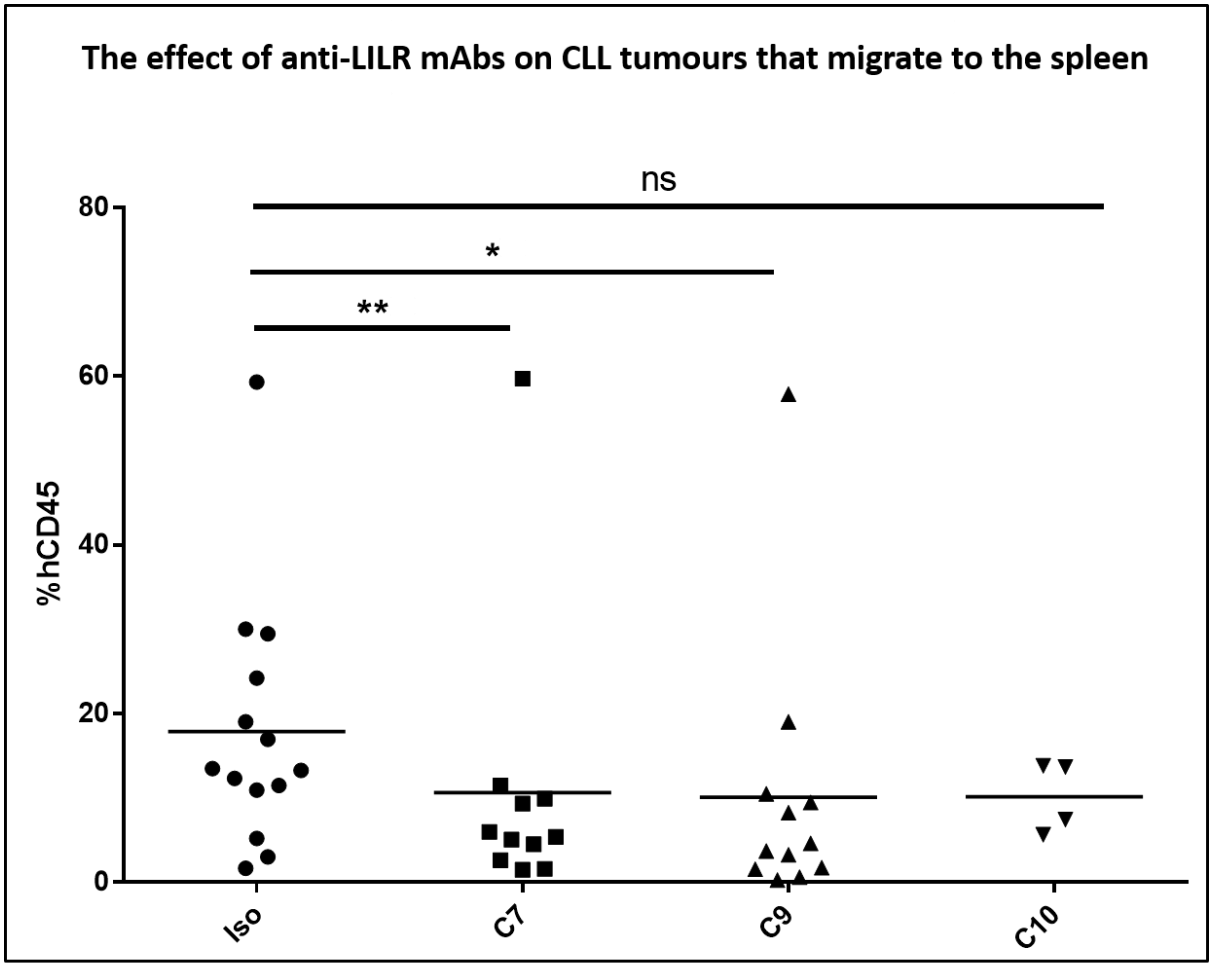

Figure 6.13 Effect of anti-LILR antibodies on CLL cells in the spleen. hCD45 expression was assessed by flow cytometry on day 9 harvested spleens from xenograft experiments described in *Figure 6.4*. Paired T test was performed: Iso vs C7 p = 0.0035, Iso vs C9 p = 0.0084 and Iso vs C10 not significant (n.s). (p < 0.05 *, p < 0.005 **, p < 0.0005 ***). N = 4-14 mice/group.

Figure 6.13 showed that hCD45 expression decreased by ~50% in all three anti-LILRB1 treatment groups (~10% C7, C9 and C10-treated compared to ~20% isotype-treated). Although only C7 and C9 appeared to be statistically significant, the lower number of mice per group in the C10-treatment group is likely the cause of this. This suggested that the anti-LILRB1 clones were able to deplete the tumour cells. However, it is difficult to infer data from these experiments due to small sample sizes, variation in levels of engraftment, and the expression of LILRB1 on these tumour cells, which may have dampened the therapeutic efficacy of the antibodies. In order to study tumour depletion high levels of engraftment are necessary, and therefore aggressive tumour samples are ideal. Given the unpredictable and rare acquisition of these samples, (as availability depends on available consenting patients with high tumour counts), it was not possible to ensure this. Also, given the heterogeneous expression levels of LILRB1 on different CLL donors, antibody therapy varied with donors,

as it was likely that the higher expression of LILRB1 resulted in better therapy with the different anti-LILRB1 clones.

In conclusion, in previous chapters (see chapter 5), the generated anti-LILR antibodies were shown to be immunomodulatory, able to agonise or antagonise their inhibitory receptors on effector cells, and therefore inhibit or stimulate immune responses, respectively. In this chapter (*Figures 6.5-6.13*), the generated antibodies show some ability to act as direct targeting antibodies, working to delete tumour cells themselves. However, given the variability in expression levels on CLL tumours and engraftment levels in these experiments, a model system with overexpressed, stable LILR expression would be more ideal, to study the effect of these antibodies on tumour therapy.

6.2.3 The effect of anti-LILRB3 on LILRB3 ITIM mutant tumour cells

Given the higher expression of LILRB1 on CLL cells, the anti-LILRB1 antibodies could be tested in the xenograft model. However, the lower expression of LILRB3 made this difficult to implement. Therefore, to test if the anti-LILRB3 clones could also act as direct targeting antibodies an alternative model was required. However, although preliminary studies show LILRB3 expression on AML tumours (data not shown), this expression was variable between donors and an optimised *in vivo* model was unavailable, due to lack of access to primary AML cells. Given the heterogeneity of using primary cells, a LILR Tg mouse model would have allowed an ideal way of studying antibody therapeutic efficacy, as this would provide stable endogenous receptor expression. However, although a LILRB3 Tg construct was generated (data not shown), the generation of the Tg mouse has yet to be completed. Therefore, an alternative *in vivo* model was established.

6.2.3.1 Generation of LILRB3 ITIM mutants

LILRB3 has four ITIMs in its intracellular domain. Although phosphatase recruitment to the ITIMs of LILRBs has been shown, little research has been conducted on whether certain phosphatases are recruited to certain ITIM domains[64, 110, 112, 113]. Given that LILRB3 has four ITIMs, it could be that different phosphatases are recruited to different ITIMs, or that the more ITIMs present, the more signal amplification that results, if all these ITIMs are indeed required for signalling.

Therefore, to test the effect of the presence of these ITIMs, LILRB3 ITIM mutants were generated by PCR (see materials and methods for details). These constructs were then transfected into Ramos cells (a B cell lymphoma cell line) and stable transfectants created

through sub-cloning and cell sorting. Although a myeloid cell line would have been a more ideal choice as LILRB3 expression is restricted to myeloid cells, transfecting various myeloid cell-lines to generate stable transfectants was unsuccessful (data not shown). Ramos cells were chosen based on previous experiments in the lab that show these cells engraft well *in vivo* and these cells have successfully been transfected with other receptors, allowing *in vivo* study.

Five constructs were generated: LILRB3 wild type (WT), LILRB3 with 3 ITIM domains (tLILRB3-3), 2 ITIM domains (tLILRB3-2), 1 ITIM domain (tLILRB3-1) and no ITIM domains (tLILRB3). See *Figure 6.9* below for schematic of LILRB3 ITIM constructs generated and expression levels of the stable transfections.

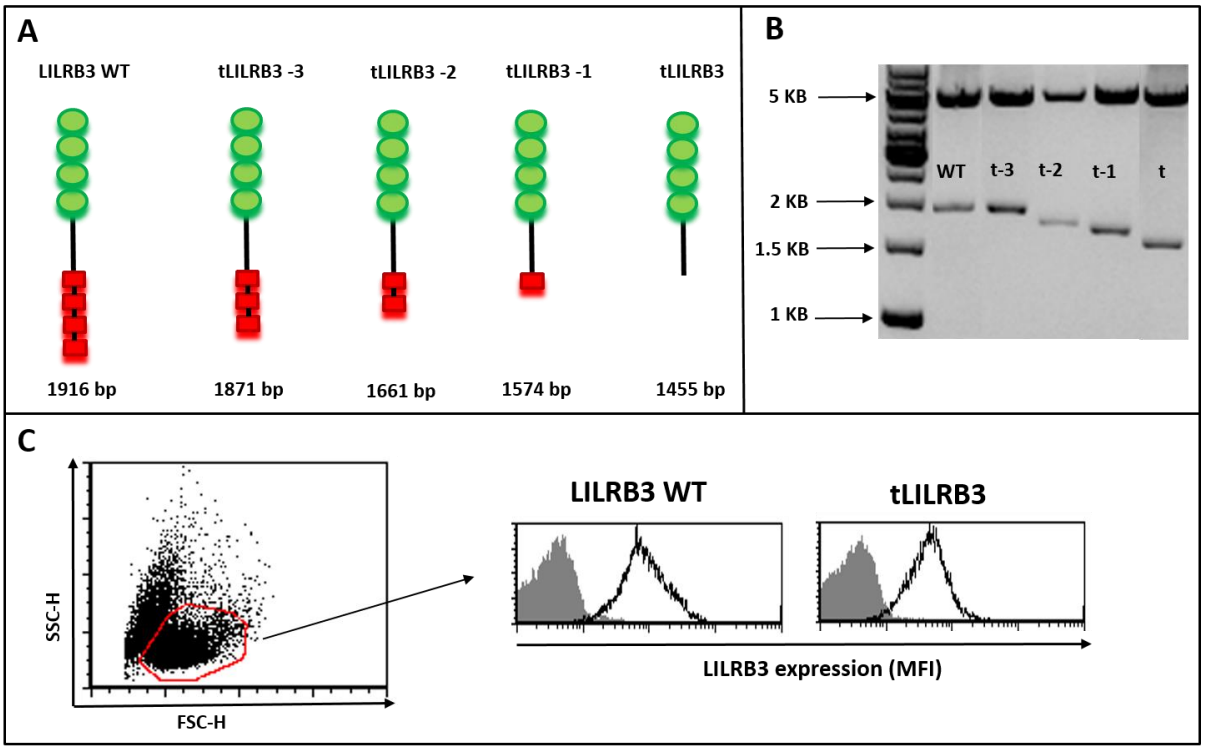

Figure 6.14 LILRB3 ITIMs were generated and overexpressed on stably transfected cells. **A) Schematic of LILRB3 ITIM mutant constructs generated by PCR.** Five constructs were generated: LILRB3 wild type (WT), LILRB3 with 3 ITIM domains (tLILRB3-3), LILRB3 with 2 ITIM domains (tLILRB3-2), LILRB3 with 1 ITIM domain (tLILRB3-1) and LILRB3 with no ITIM domains (tLILRB3). **B) DNA gel shows constructs vary in size.** LILRB3 WT (WT), tLILRB3-3 (t-3), tLILRB3-2 (t-2), tLILRB3-1 (t-1) and tLILRB3 (t) in pcDNA3 were digested with 10 U each BamHI and NotI (Promega) for 2hours at 37°C. Constructs separated by size by electrophoresis on a 0.7% agarose gel at 120 V for 45 minutes, and visualised with Gel Red™ (Biotium). **C) Transfection efficiency of stable transfections.** Expression levels assessed by staining with LILRB3-APC (BioInvent) or relevant isotype controls, for 30 minutes at 4°C, and analysed by flow cytometry. Representative stable transfections of LILRB3 WT and tLILRB3 are shown here.

LILRB3 ITIM mutant constructs were successfully generated (*Figure 6.14A*) and identified by their different molecular weights: LILRB3 WT at ~2 KB, tLILRB3-3 at ~1.9 KB,

tLILRB3-2 at ~1.7 KB, tLILRB3-1 at ~1.6 KB and tLILRB3 at ~1.5 KB (*Figure 6.14B*). The pcDNA3 vector ran at ~5.4 KB. These constructs were stably transfected into Ramos cells, and after sub-cloning and cell sorting, similar levels of expression for these constructs were generated and confirmed by flow cytometry (*Figure 6.14C*).

6.2.3.2 Establishing LILRB3 ITIM mutant expressing-tumour engraftment in vivo

After generating Ramos cells stably-transfected with LILRB3 ITIM mutants, these cells were injected into mice to establish tumours, and to test anti-LILRB3 therapy. To first explore the extreme phenotypes of having four ITIMs or none at all, only LILRB3 WT and tLILRB3 stably transfected cells were utilised in these experiments.

Firstly, engraftment of these two different tumour cell-lines was established in immunocompromised SCID mice and survival assessed. The aim of the experiment was to assess if transfected Ramos cells expressing either LILRB3 WT or tLILRB3, could firstly form tumours and secondly form these tumours with similar growth dynamics *in vivo*. SCID mice were chosen due to their immunocompromised nature, therefore increasing the probability of the foreign human cells not being rejected by the mouse host. Tumour cells were injected i.v. When mice reached the expected endpoint (hind-leg paralysis) these mice were culled.

From previous experiments performed in the lab, it is known that Ramos cells do not migrate to the places normal B cells would i.e. spleen, lymph nodes. This is likely because they are a cell line, and due to their immortal nature and prolonged culturing have likely acquired many mutations that have distorted their homing properties. These cells instead have been found to migrate to the spine; attacking the peripheral nervous system (PNS)[273]. Although this is rarely seen in humans, a few cases of spinal injury as a result of Burkitt's Lymphoma have been reported[274]. Hind-leg paralysis was a sign of this occurring, and mice were culled once they began displaying signs of spinal pathology i.e. hind-leg paralysis. A schematic of the experiment and the survival of the mice in this experiment are reported in *Figure 6.15* below.

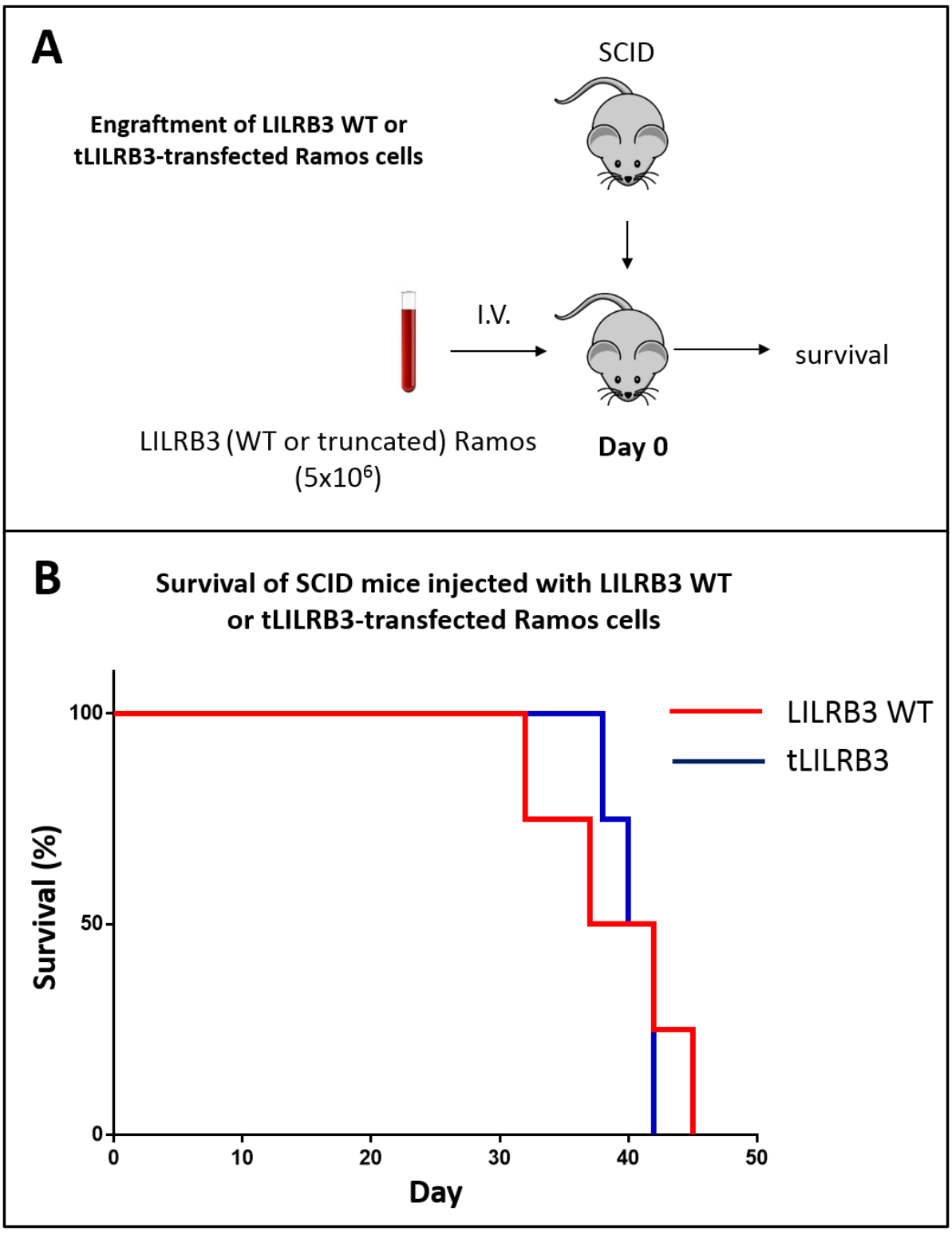

Figure 6.15 Establishing LILRB3 ITIM mutant-transfected Ramos cell tumour engraftment in SCID mice. $5x10^6$ cells (in 200 µl sterile PBS) - either LILRB3 wild type (WT) or truncated with no LILRB3 (tLILRB3) were injected i.v. into four female SCID mice per group respectively and survival assessed at a given endpoint of signs of hind-leg paralysis. A schematic of the experiment is given in **A)** and in **B)** Survival was analysed in GraphPad. Getran-Breslow-Wilcoxon Test was performed where stars represent p values as follows: $p < 0.05$ *, $p < 0.005$ **, $p < 0.0005$ *** and $p < 0.00005$ ****.

Figure 6.15 shows that both tumours were able to engraft successfully and all mice were culled around the same time – between 42 and 45 days; with median survival of 39.5 and 41 for the WT and truncated cells, respectively. No significant difference was found between the two cell types. This indicated that both tumour cell-lines expressing LILRB3 WT and tLILRB3 formed tumours at the same rate, and these tumours were equally aggressive. Therefore, ITIM signalling is unlikely to play a role in tumour engraftment or the aggressive nature of the tumour.

6.2.3.3 The effect of LILRB3 intracellular signalling in anti-LILRB3 therapy

After establishing that both tumour cell-lines expressing LILRB3 WT and tLILRB3 were able to engraft in SCID mice, and comparable engraftment was seen with both, a larger experiment was performed; this time the tumours were treated with anti-LILRB3 antibodies.

Both anti-LILRB3 clones A13 and A28 were highlighted as clones that were able to induce receptor modulation quickly or not at all, respectively on human monocytes (Chapter 5, *Figure 5.11-12*). As discussed previously in Chapter 5, receptor internalisation is important for antibody therapy. This can be positive, as it can aid in drug delivery when a toxic agent is conjugated to the antibody, or negatively by preventing immunomodulatory antibodies from being available to act on their receptor at the cell surface. Therefore, before testing these antibodies *in vivo*, their ability to modulate the receptor on LILRB3 WT or tLILRB3-transfected Ramos cells was assessed. An A488-quenching assay was performed as described previously (Chapter 5, *Figure 5.10*) and surface accessible antibody assessed.

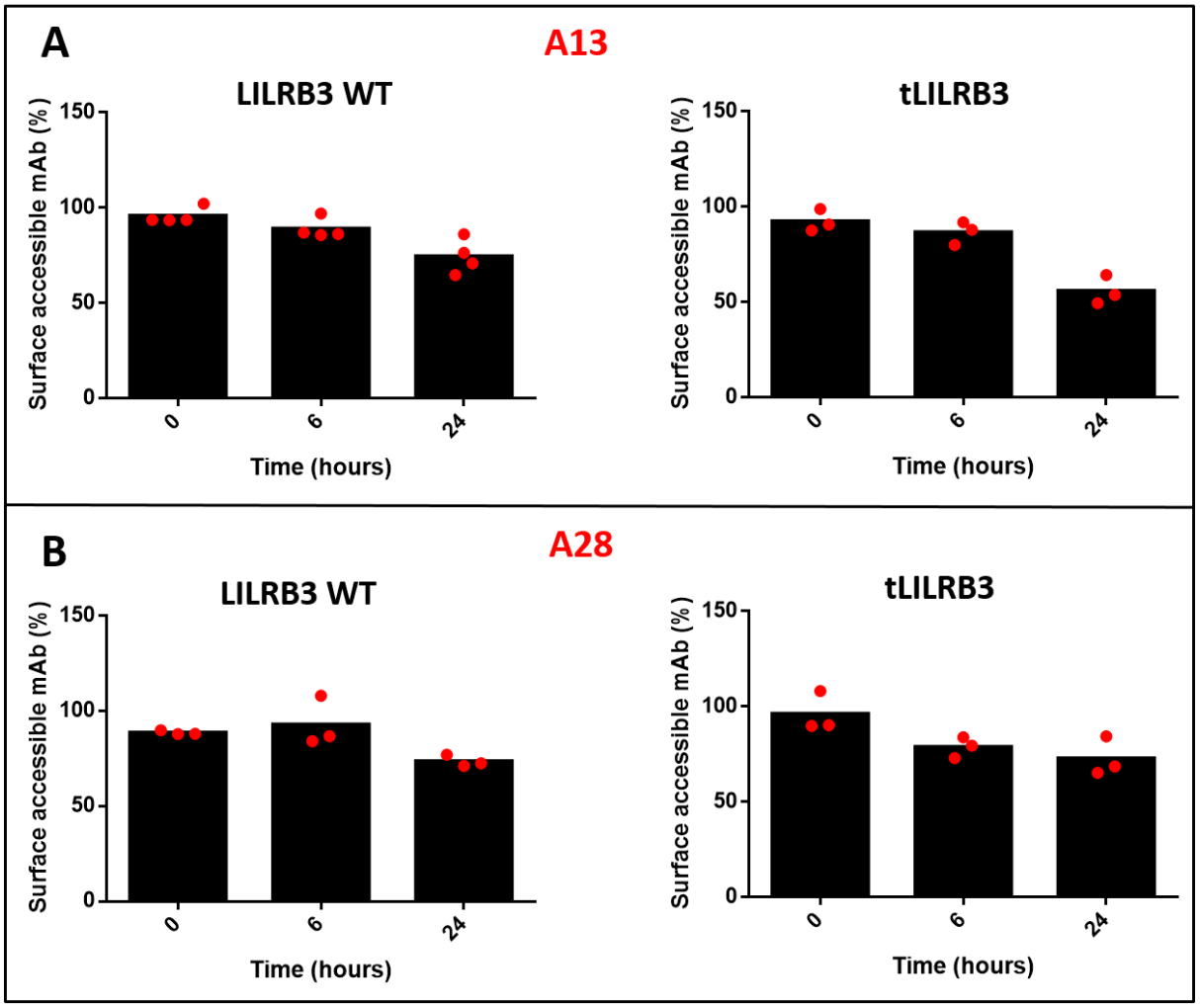

Figure 6.16 Assessing receptor modulation of anti-lILRB3 antibodies on LILRB3 WT- or tLILRB3-transfected cells. $1x10^6$ LILRB3 WT- or tLILRB3-transfected cells were incubated with 5 µg/ml A488-conjugated anti-LILRB3 clones A13, A28 or a relevant isotype control at 0, 6 and 24 hours. Quenched cells were then washed and stained with 25 µg/ml secondary anti-A488 antibody for 25 minutes at 4°C. Surface accessible antibody was then assessed by the following equation: [unquenched (minus isotype) – quenched (minus isotype)]/ unquenched (minus isotype).

A13 was previously shown to promote fast internalisation of its receptor on human monocytes (Chapter 5 *Figure 5.11-12*). *Figure 6.16A* showed that incubation of LILRB3 WT-expressing Ramos cells with A13 resulted in very slow internalisation. At 0 hours an average mean of 96% surface assessable antibody was present, this reduced to 89% by 6 hours and 75% by 24 hours. Comparatively, incubating A13 with tLILRB3-expressing cells resulted in an average mean of 92%, 87% and 56% at 0, 6 and 24 hours respectively. This suggested that internalisation on tLILRB3-expressing cells was much quicker than on the LILRB3 WT cells. The presence of the intracellular signalling domains may therefore have reduced internalisation on these cells. When incubated with human monocytes, A28 did not show any internalisation (Chapter 5 *Figure 5.11-12*). *Figure 6.16B* shows that incubation of A28 with either LILRB3 WT- or tLILRB3-expressing cells resulted in very slow internalisation. An

average mean of 89% or 96% at time 0 reduced to 74% or 73% after 24 hours with either the LILRB3 WT- or tLILRB3 expressing cells, respectively.

Assessing the ability of these antibodies to result in receptor internalisation indicated that although there appeared to be some receptor internalisation (with A13 on tLILRB3-expressing cells), this was slow and the majority of the receptor was still available at the cell surface after 24 hours. Therefore, the lack of internalisation and the presence of LILRB3 at the cell surface, suggested depletion of LILRB3-expressing tumour cells with anti-LILRB3 antibodies should be attainable. The antibodies were therefore tested *in vivo* to assess their ability to directly target and deplete the tumour cells overexpressing these various LILRB3 signalling receptors. Immunocompromised mice were used to ensure successful engraftment of the human cell lines. As before, with the CLL xenograft experiments, mFcγRIIB KO and hFcγRIIB Tg SCID NOD mouse models were compared. As previously (*Figure 6.15*), mice were injected i.v. with either LILRB3 WT or tLILRB3-expressing Ramos cells, and survival assessed. This time however, mice were treated 7 days after injection of tumours, with 100 µg of either anti-LILRB3 clone A13, A28 or a relevant isotype control. As only one dose was administered, antibodies were given i.v. to follow the route of cells given. A schematic of the experiment is displayed below in *Figure 6.17* below.

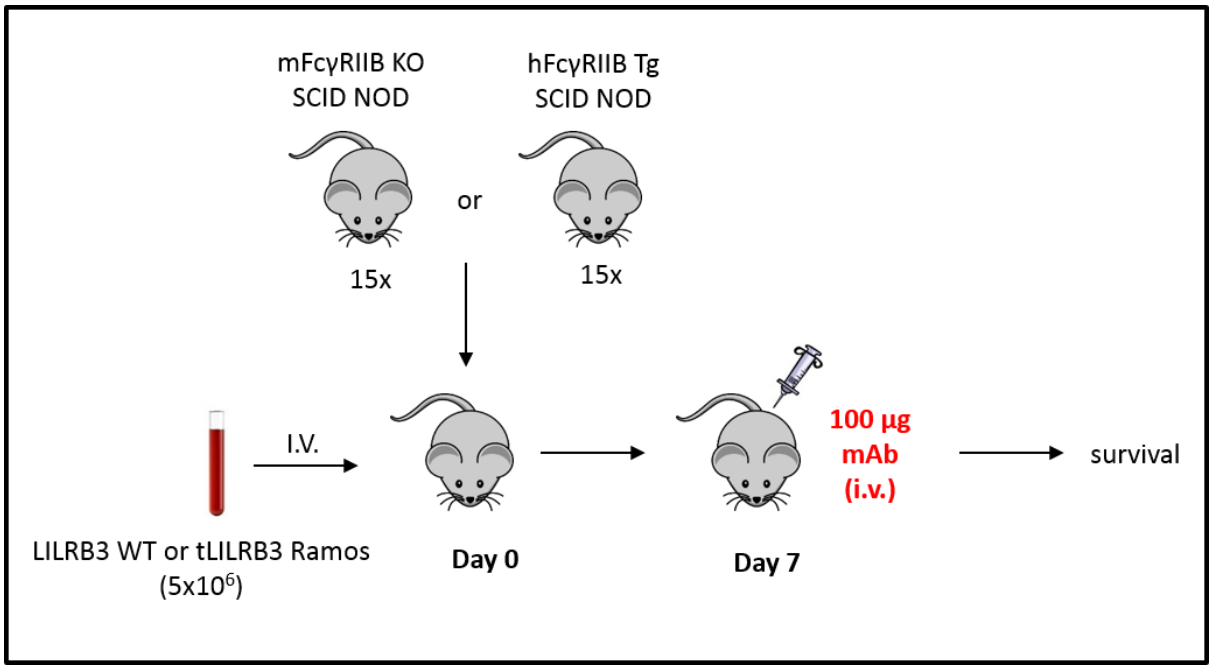

Figure 6.17 Effect of anti-LILRB3 on tumours expressing LILRB3 WT or tLILRB3 with or without FcγRIIB. $5x10^6$ (in 200 µl sterile PBS) LILRB3 WT or tLILRB3-expressing Ramos cells were given i.v. to either mFcγRIIB KO or hFcγRIIB Tg SCID NOD mice. Mice were then treated with 100 µg anti-LILRB3 clones (A13 and A28) or an isotype control i.v. 7 days post-injection. Survival was measured, as days mice survived post-injection.15 mFcγRIIB KO were injected with LILRB3 WT and 15 with tLILRB3. 15 hFcγRIIB Tg SCID NOD mice were injected with LILRB3 WT and 16 with tLILRB3. In each of the 4 groups, 5-6 mice were treated with A13, A28 or an isotype.

The schematic above (*Figure 6.17*) shows that groups of 15-16 mice were established: LILRB3 WT-expressing cells injected into mFcγRIIB KO mice, LILRB3 WT-expressing cells injected into hFcγRIIB Tg mice, tLILRB3-expressing cells injected into mFcγRIIB KO mice, and tLILRB3-expressing cells injected into hFcγRIIB Tg mice. In each group, 5-6 mice were treated with 100 µg of either A13, A28 or a relevant isotype.

Survival was assessed for all the mice in each group and recorded. See *Figure 6.18* below.

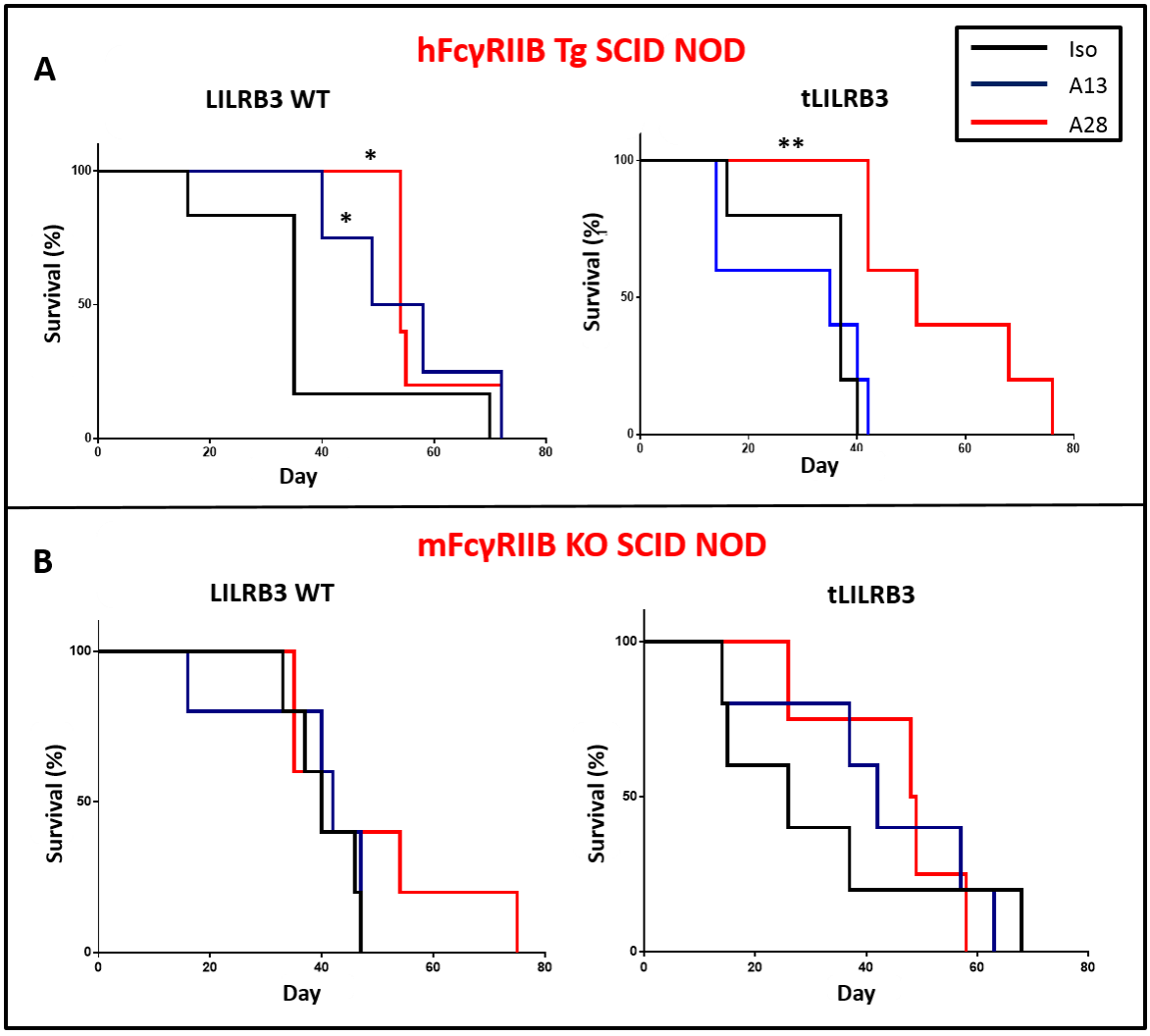

Figure 6.18 The effect of anti-LILRB3 antibodies on depleting LILRB3 WT or tLILRB3-expressing tumour cells. The experiment was performed as described above in *Figure 6.17* in either hFcγRIIB Tg or mFcγRIIB KO SCID NOD mice. Survival was analysed in GraphPad. N = 15-16 mice/group and 4-5 mice/treatment. Getran-Breslow-Wilcoxon test performed where stars represent p values as follows: $p < 0.05$ *, $p < 0.005$ **, $p < 0.0005$ *** and $p < 0.00005$ ****.

The table below summarises the statistical testes performed on the results from *Figure 6.18*.

Table 6.1 Median survival and statistical significance of LILRB3 WT vs tLILRB3 tumour cell lines.

Model	Cells	Median			P value	
		Iso	A13	A28	Iso vs A13	Iso vs A28
hFcγRIIB Tg	LILRB3-WT	35	53.5	54	0.0495 *	0.0348 *
hFcγRIIB Tg	tLILRB3	37	35	51	0.6695	0.0039 **
mFcγRIIB KO	LILRB3-WT	40	42	42	0.6750	0.6041
mFcγRIIB KO	tLILRB3	26	42	48.5	0.4637	0.2751

Table 6.1 Median survival and statistical significance of the effect of anti-LILRB3 antibodies on depleting LILRB3 WT or tLILRB3-expressing tumour cells. Median values and Getran-Breslow-Wilcoxon test performed. Tests performed in GraphPad. Stars represent p values as follows: $p < 0.05$ *, $p < 0.005$ **, $p < 0.0005$ *** and $p < 0.00005$ ****.

Figure 6.18A shows that hFcγRIIB Tg SCID NOD mice administered with both the LILRB3 WT and tLILRB3-expressing tumour cells, succumbed to their disease by day 20, and all mice were culled before day 80. Mice given LILRB3 WT-expressing tumour cells and treated with A13 or A28 survived longer than those treated with the isotype, as demonstrated by their median survival of 53.5 and 54 compared to 35 days, respectively. This difference was statistically significant (*Table 6.1*). Therefore, despite overall similar endpoints across all treatment groups (all culled by ~day 75) both anti-LILRB3 antibodies increased survival in this model. Comparatively, in the mice given tLILRB3-expressing tumour cells, A28 had a much clearer advantage over A13. Mice treated with an isotype or A13 were all culled by ~day 40, similar to what was seen with mice not treated at all in SCID mice previously (*Figure 6.15*). Comparatively, mice treated with A28 were able to survive for just under 80 days (*Figure 6.18A*). Median survival for A28-treated mice was 51 days compared with 35 days when A13-treated or 37 days with the isotype control, and this difference with A28 was statistical significant (*Table 6.1*). The modulation data showed that although internalisation was slow for both A13 and A28 on the LILRB3 WT cells, A13 internalised faster on the tLILRB3 cells (*Figure 6.16*). This could therefore explain why A13 performed in a similar manner to A28 in the LILRB3 WT model, but with the tLILRB3 cells, A28 was able to deplete the tumour cells much better, as the antibody (unlike A13) is retained at the cell surface for longer.

In the mFcγRIIB KO model A28 was able to deplete LILRB3 WT tumour cells, as mice treated with this antibody survived up to just under ~80 days, and this was greater than those treated with an isotype or A13, which were all gone before ~day 50. However, median survival data showed that A28 and A13 performed similarly, as they both had median survival

of 42 days (*Table 6.1*) compared to 40 with the isotype. This was not statistically significant, and this was a minimal increase in survival when compared to the control. In comparison, both A13 and A28 appeared to increase survival of mice given tLILRB3-expressing tumours (*Figure 6.18*). *Table 6.1* shows that the median survival was increased for both A13 and A28, with medians of 42 and 48.5 days, respectively compared to 26 days in the isotype-treated mice. This suggested that although this was not statistically significant, both anti-LILRB3 clones were able to deplete tumours, A28 increased survival greater than A13, and was therefore better at depleting the tLILRB3-expressing tumours.

In conclusion, both LILRB3 antibodies A13 and A28 appeared to deplete tumour cells at differing levels in the different models. However, A28 appeared to deplete tumour cells better than A13 in all cases. In particular, A28 depleted tLILRB3-expressing tumour cells better, possibly due to faster internalisation seen with A13 on these cells. Results were statistically significant in the hFcγRIIB Tg model, suggesting that FcγRIIB may aid in therapy. However, FcγRIIB is not crucial to depletion of tumours in these models, as anti-LILRB3 clones were able to demonstrate some depletion in the mFcγRIIB KO model also.

6.2.3.4 Confirming anti-LILRB3 mAb depletion of LILRB3 WT-expressing tumour cells

Given the fragility of the SCID NOD mice, the experiments were subsequently performed in SCID mice. Although immunocompromised, these mice were less so than SCID NOD mice, and are known to be more robust, with less model and age-related problems. Unfortunately no mFcγRIIB KO or hFcγRIIB Tg SCID mice were available and so wild-type SCID mice were utilised.

Firstly, expression of both LILRB3 and CD20 were assessed on the Ramos cells. Ramos cells express CD20, and Rituximab is an approved anti-CD20 therapy able to deplete lymphoma cells. Therefore, Rituximab was utilised as a positive control. *Figure 6.20A* shows that transfected Ramos cells express both LILRB3 and CD20, but the expression of CD20 was much higher on these cells. Having established expression levels, SCID mice were given LILRB3 WT-expressing Ramos cells i.v., and treated with 100 µg antibodies i.v.7 days later. The mice were given a repeat dose i.p. on day 14. Survival was then assessed. A schematic of the experiment is given below in *Figure 6.19.*

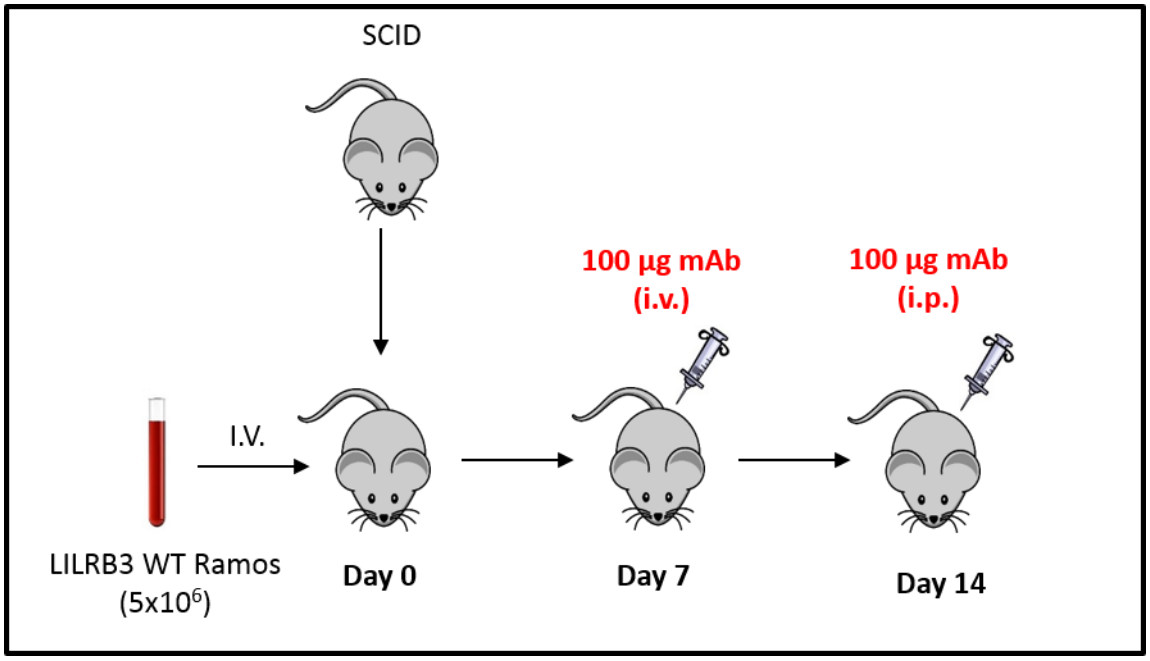

Figure 6.19 Effect of anti-LILRB3 antibodies on LILRB3 WT-expressing tumours. $5x10^6$ (in 200 µl sterile PBS) LILRB3 WT-expressing Ramos cells were given i.v. to 34 SCID mice. Mice were then treated with 100 µg anti-LILRB3 clones (A13 and A28), an isotype control, or positive control anti-CD20 Rituximab i.v. 7 days post-injection of cells. A second dose of antibody was given at day 14 i.p. Survival was measured, as day's mice survived post-injection.

Two different anti-LILRB3 antibodies, one that caused fast receptor internalisation on human monocytes (A13) and one that caused no internalisation (A28), were tested to see if they could deplete LILRB3-WT expressing tumour cells *in vivo*, alongside an isotype (negative control), or an anti-CD20 antibody Rituximab (positive control). Phenotyping Ramos transfectants for LILRB3 and CD20, and the survival data are displayed in *Figure 6.20* below.

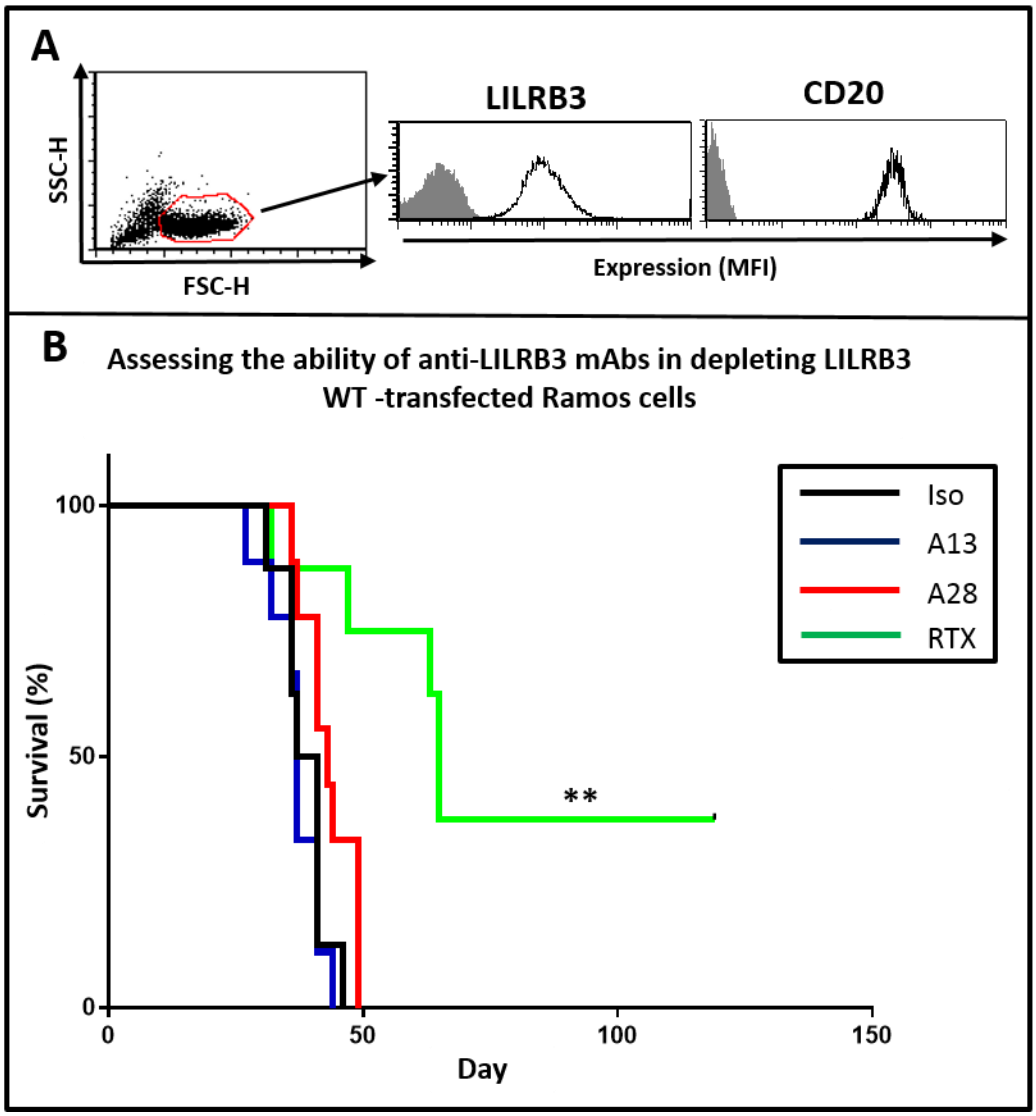

Figure 6.20 Assessing the effect of anti-LILRB3 mAbs on depleting LILRB3 WT-expressing tumour cells. A) Comparing CD20 and LILRB3 expression on transfected Ramos cells. LILRB3 WT-transfected Ramos cells were stained with anti-LILRB3-APC (BioInvent) or anti-CD20 Rituximab (RTX)-A488 or relevant isotype (iso) controls for 30 minutes at 4°C, and analysed by flow cytometry. B) Assessing LILRB3 antibody therapy *in vivo*. Experiment was performed as described previously in *Figure 6.19*. n =34 mice, 8-9 mice/treatment group. Getran-Breslow-Wilcoxon test performed where stars represent p values as follows: $p < 0.05$ *, $p < 0.005$ **, $p < 0.0005$ *** and $p < 0.00005$ ****.

The table below summarises the statistical tests performed on the results from *Figure 6.20*.

Table 6.2 Median survival and statistical significance of LILRB3 WT vs tLILRB3 tumour cell lines.

Model	Cells	Median				P value		
		Iso	A13	A28	RTX	Iso vs A13	Iso vs A28	Iso vs RTX
SCID	LILRB3-WT	39	37	43	65	0.6611	0.0660	0.0052 **

Table 6.2 Median survival and statistical significance comparing the effect of anti-LILRB3 mAbs and anti-CD20 Rituximab on depleting LILRB3 WT-expressing tumour cells. Median values and Getran-Breslow-Wilcoxon test performed. Tests performed in GraphPad. Stars represent p values as follows: $p < 0.05$ *, $p < 0.005$ **, $p < 0.0005$ *** and $p < 0.00005$ ****. Antibodies compared: Isotype (Iso), anti-LILRB3 clones A13 and A28, and anti-CD20 Rituximab (RTX).

Figure 6.20B showed that both anti-LILRB3 clones in this experiment displayed similar levels of survival, with no particular antibody showing any advantage. Nonetheless, although not statistically significant, A28 did appear to outperform A13 in extending survival, as median survival with A28 was 43 days compared to 37 days with A13. Rituximab, however, showed a much greater ability to deplete the Ramos cells, as mice in this group survived past 100 days, with a median survival of 65 days, which was statistically significant when compared to the isotype control. This suggested that Rituximab was a much better at depleting the cells, possibly because CD20 is a better target than LILRB3 to deplete Ramos cells.

In summary, the experiments performed here with the transfected Ramos cells, showed that both anti-LILRB3 mAbs A13 and A28 were able to deplete LILRB3-expressing Ramos cells. However, A28 showed a higher ability to delete these cells, by extending survival of mice treated with the Ramos tumours; suggesting A28 is a better therapeutic antibody in this situation. However, both anti-LILRB3 clones did not outperform Rituximab, an antibody already approved to treat lymphomas, and therefore LILRB3 is unlikely a better target than CD20, at least in the context of depleting antibodies.

6.3 Discussion

In this chapter, studying the ability of anti-LILRB antibodies to deplete tumour cells was evaluated. Primary CLL tumour cells were phenotyped for LILRBs as well as other inhibitory receptors. Studying the ability of anti-LILRB1 antibodies to deplete tumour cells *in vivo*, in CLL xenograft models was then assessed. Whilst some depletion was seen in this model, due to the variation in engraftment, transfected Ramos cells overexpressing signalling variants of LILRB3 were injected into mice to establish a LILRB3 *in vivo* model instead, and anti-LILRB3 antibodies tested. A28 showed better survival rates in these models compared to A13.

Firstly, primary tumour samples were assessed by studying the expression of LILRBs on CLL cells. LILRB expression has already been reported in the literature[163]. The findings in this chapter supported previous reports, with LILRB1 and LILRB4 predominantly found to be up-regulated on CLL cells, and a few donors also expressing LILRB2 and LILRB3 (*Figure 6.2*). This implies that co-ligation of these receptors may promote tumour growth and LILR expression may correlate with the aggressiveness of the tumour. This has previously been observed by Zhang *et al*, who found that increased differentiation of human gastric cancers correlated with higher expression of LILRB1 and LILRB4[160]. All the CLL donors assessed in

this chapter had medium to high tumour burden (defined by their $CD19^+$ $CD5^+$ population). However, less $CD19^+$ $CD5^+$ cells may show reduced levels of inhibitory LILRs. Screening donors with a lower tumour burden would validate this theory, and could indicate that the expression of these LILRBs could act as biomarkers for tumour severity or aggressiveness. However, without assessing a varying level of low to high tumour burden, this cannot be confirmed.

Expression of other cell surface receptors and their ligands were also assessed. FcγRIIB on B cells remained unchanged compared to healthy donors. T cell exhaustion markers LAG-3, PD-1 and TIM-3 were all absent from healthy B cells. This was expected, as although there were not enough T cells present in the CLL samples assessed here, studies have shown that these markers are expressed predominantly on activated T cells[267]. However, these markers were upregulated on CLL cells. TIM-3, although absent from tumours, was found on upregulated on healthy monocytes, possibly due to effector cells working to enhance inflammatory responses against tumours. CTLA-4 remained unchanged in either setting, whilst PD-L1 was up-regulated on both malignant B cells and monocytes in CLL samples.

In summary, overall inhibitory receptors are up-regulated on tumours, possibly to prevent inflammatory responses against the tumour, promoting T cell exhaustion, and aiding in tumour survival. However, inhibitory receptors are downregulated on circulating monocytes, possibly due to effecter cells preventing immune suppression, subsequently enhancing inflammation and avoiding tumour progression. Downregulation of LILRBs on monocytes in CLL samples may be the result of receptor internalisation. Both healthy and diseased cells can release extracellular vesicles for example, exosomes that allow communication with other cells[275]. In the case of tumours, exosomes result in increased proliferation and tumour invasiveness of other cancer cells, and can be taken up by effector cells[275]. It is possible that LILRBs expressed on monocytes may recognise exosomes released by malignant cells, and internalise them through endocytosis.

After confirming LILRB1 expression on CLL cells, xenograft models were established to study the therapeutic efficacy of anti-LILRB1 antibodies. LILRB1 clones C7 and C9 were utilised in these experiments. C7 showed an ability to cause internalisation on monocytes after 3 hours but C9 retained surface accessible antibody expression over the 3 hours (see *Chapter 5 Figure 5.13*). Given that receptor modulation can affect antibody therapy, comparing an antibody that showed signs of slow receptor internalisation (C7) to one that did not internalise (C9), would further deduce the ideal antibody characteristics for optimal therapy[259]. However,

where tested, no internalisation was observed with either clone on CLL cells (*Figure 6.5 and 6.8*), possibly due to the tumour microenvironment preventing internalisation.

In all the experiments performed, regardless of the mouse model used, CLL cells (measured by $hCD45^+$ cells) gradually decreased in the blood over 9 days. However, hCD45 expression was seen in the spleen, suggesting that the tumour cells migrated here from the blood (*Figures 6.6-7, 6.9-10 and 6.12*). Low hCD45 expression was observed in the bone marrow or liver (*Figure 6.12*). The level of $hCD45^+$ in the spleen in the mFcγRIIB KO mice (*Figure 6.9B*) was greatly reduced compared to in the SCID NOD mice (*Figure 6.6B*), suggesting that the antibodies are able to clear the tumour cells not just in the blood but also in the spleen, in the absence of mFcγRIIB. This suggested that in the absence of mFcγRIIB, the anti-LILRB1 antibodies were able to delete tumour cells better, and therefore mFcγRIIB may have hindered therapy. However, the anti-LILRB1 antibodies were also able to clear tumours in the spleen in the hFcγRIIB Tg mice (*Figure 6.7B*). Therefore, in this situation the presence of hFcγRIIB may have aided anti-LILR therapy. These contradicting results may imply that the ability of the antibodies to clear tumours was independent of FcγRIIB, and in fact tumour-dependent, if one tumour was more aggressive than the other. The two different CLL donors used in these experiments expressed differing levels of LILRs, and this may have influenced antibody therapy instead. Overall, combining all the models used, the anti-LILRB1 clones did appear to show an ability to deplete tumours in the spleen (*Figure 6.13*). However, given the variability in LILRB1 expression and CLL engraftment, reproducibility was difficult. Choosing aggressive CLL tumours that were able to engraft well but also express high levels of LILRB1 was not feasible, due to the rarity of acquiring fresh CLL samples on a regular basis. The limiting amount of CLL cells, but high number of cells required for engraftment, also meant the number of mice per group was very small, thus making it difficult to assess validity due to a reduction in experimental power.

Therefore, an alternative *in vivo* model was established. Expression of LILRBs has been reported on AML cells[161, 162]. However, there are no established AML models in our lab, due to lack of access to primary AML tissue. For this reason, and based on the difficulties in establishing engraftment with primary CLL cells, an alternative *in vivo* model was established[161, 162].

LILRB3-transfected Ramos cells were utilised as an alternative *in vivo* model. Either wild-type or truncated (no ITIM signalling capability) LILRB3-expressing transfectants were produced, with similar expression levels (*Figure 6.14*) and similar engraftment levels *in vivo* (*Figure 6.15*). LILRB3 clones A13 and A28 were chosen to test anti-LILRB3 therapy in this

model, as these clones internalised quickly or not at all on human monocytes, respectively. However, on the Ramos cells, there was some internalisation observed with A28, and this was similar on both LILRB3 WT- and tLILRB3-transfected Ramos cells. This was demonstrated by a slow decrease in surface assessable antibody over 24 hours. It could be that if left for 24 hours, this may have been observed on human monocytes also, although some of this internalisation may have been the result of endocytosis of dying cells, given the prolonged time points. Incubating the cells with an agent that prevents endocytosis, such as sodium azide, then studying receptor modulation would assess this. In comparison, A13, which resulted in fast internalisation on human monocytes, showed slow internalisation on LILRB3 WT-transfected Ramos cells, however, on tLILRB3-transfected cells, internalisation appeared to be accelerated. This suggested, that at least in the case of A13, the intracellular signalling domains aided in preventing quick receptor internalisation. In their absence, with A13, LILRB3 internalised faster on these cells. Although A13 was able to cause fast receptor internalisation on primary monocytes but not the LILRB3 WT cell lines, these transfected cells overexpress the LILRB3 receptor, therefore providing the antibody with more receptor molecules on the cell surface that are able to internalise. It could be that the increased level of expression requires a higher threshold of activation in order for internalisation to be induced. This could explain why A13 did not internalise as quickly on these cells.

After assessing receptor modulation, the ability of A13 and A28 to deplete tumours cells in different models *in vivo* were tested. In the hFcγRIIB Tg SCID NOD model, although A28 showed a slight advantage, A13 and A28 depleted LILRB3 WT-expressing cells to a similar degree, however, A28 was able to deplete tLILRB3-expressing tumours better (*Figure 6.18A*). This was likely due to the faster internalisation of the A13 antibody on these tLILRB3 cells (*Figure 6.16*). It could be that ITIM domains aid in preventing internalisation, and in the absence of the intracellular signalling domains, internalisation can occur. Alternatively, the differences in therapeutic efficacy of these two clones may have been due to their antibody characteristics. As discussed in Chapter 4, different anti-LILRB3 clones were found to bind to different extracellular Ig-like domains, with A13 binding to the second domain and A28 the fourth. This difference in epitope mapping, could also influence function, and could be why A28 is better at depleting tumour cells than A13. Comparatively, in the mFcγRIIB KO model, both antibodies depleted LILRB3-WT and tLILRB3-expressing cells to a similar level, demonstrated by their similar median survival rates (~42-49 days in all cases – see *Table 6.1*). However, A28 performed slightly better with the tLILRB3-expressing cells (*Figure 6.18B*). Given that A28 was able to deplete tumour cells in both the mFcγRIIB KO and hFcγRIIB Tg

models, it suggests that the presence of hFcγRIIB did not influence tumour depletion. However, it is important to note that cell lines may not be physiologically relevant.

SCID NOD mice were extremely immunocompromised, lacking B and T cells, and having impaired NK cell function. They were therefore, prone to a shorter life span, and greater risk of age-related problems. This was observed with several of the mice in these experiments, with many mice dying due to age-related, rather than tumour-related problems. Instead of spinal injury, most mice were culled for inflamed or blocked guts, encephalitis or breathing problems. Based on previous work in the lab, and previous experiments with the Ramos cells *in vivo*, it is known that these problems are age-related. Therefore, it was difficult to deduce how well the anti-LILRB3 antibodies were able to deplete cells in these models, as survival may have been influenced by other factors unrelated to the tumours. As a result of the age-related problems seen in the SCID NOD mice, the experiment was repeated in SCID mice, due to their more robust nature. Given the lack of mice and tLILRB3 cells available, only LILRB3-WT mice were utilised in these experiments. Both A13 and A28 showed some improvement in survival compared to their isotype control, and this was more pronounced with A28. Median survival with both anti-LILRB3 clones were similar in the SCID model compared to the mFcγRIIB KO and hFcγRIIB Tg SCID NOD models, previously used. A28 appeared to outperform A13 in all the models used. Therefore, this suggested that the FcγRIIB did not aid in survival, or anti-LILRB3 antibody therapy in these models. However, neither anti-LILRB3 clones performed better than Rituximab (*Figure 6.20B*). Rituximab showed better tumour depletion than the anti-LILRB3 antibodies, despite previous reports stating that the antibody is prone to causing receptor internalisation, which leads to a reduced efficacy in therapy[259]. However, this did not prevent the antibody from successfully depleting Ramos cells in these experiments. Therefore, receptor internalisation cannot be the only reason that A28 performed better than A13 in these experiments, and A28 may be better at depleting tumour cells. Expression levels may have influenced therapy, as CD20 was shown to express much higher on the Ramos cells than LILRB3 (*Figure 6.20A*). Therefore, more CD20 molecules were available for the antibody to bind to, compared to LILRB3.

In conclusion, the LILRB3-transfected Ramos cells allowed the effect of anti-LILRB3 antibodies in an *in vivo* model, with a consistent level of LILRB3 expression to be studied. Overall, A28 appeared to show better efficacy for depleting LILRB3-expressing tumour cells compared to A13, possibly due to the ability of A13 to cause receptor internalisation. However, the level of LILRB3 expression was markedly lower than that of CD20 on these

Ramos cells, and therefore the anti-LILRB3 antibodies showed a much lower capability at depleting these cells, compared to anti-CD20 antibody Rituximab.

In summary, in both the primary CLL and Ramos xenograft *in vivo* models, anti-LILRB1 and -LILRB3 clones showed limited ability to deplete tumour cells. This could have been due to low receptor expression levels, or in the case of the Ramos model, lack of endogenous expression, as Ramos cells are a B cell line, and LILRB3 is a myeloid receptor. Although, LILRB3-trasnfected Ramos cells allowed anti-LILRB3 clones to be tested for their therapeutic efficacy, the overexpressed cell line provided an artificial tumour model for study, which may not be comparable to primary cells. Both models showed that FcγRIIB may play a role in anti-LILR therapy, and LILRB3 signalling may also influence therapy, as tLILRB3 showed receptor internalisation with clone A13. Therefore, the presence of the ITIM domains, may influence immunomodulatory antibody therapy also, as agonistic antibodies that stimulate the receptor will activate intracellular ITIM signalling.

Overall, the data in this chapter demonstrated that anti-LILRB antibodies are able to deplete tumour cells *in vivo*, however, this depletion is minimal and showed reduced efficacy when compared to current therapies. Therefore, the antibodies may serve better as immunomodulatory antibodies, as work described in Chapter 5 showed these antibodies may influence effector cell function. If expression levels of LILRB3 influenced the therapeutic efficacy of anti-LILRB3 antibodies, then it is important to note that these tumour cells are overexpressed cell lines, and therefore are not representative of LILRB3 expression on primary cells. LILRB3 expression varies on different immune cells, as previously shown in Chapter 4 (*Figure 4.4*), LILRB3 expression was highest on macrophages and neutrophils, followed by monocytes and DCs, with no expression on lymphocytes. Therefore, LILRB3 expression is restricted to myeloid cells, a myeloid tumour would therefore have been more representative. If the anti-LILRB3 antibodies are better at targeting effector cells, rather than depleting tumours, as this data would suggest, then these antibodies may work better when targeting macrophages and neutrophils for example in the tumour microenvironment rather than the tumour itself.

Better experimental models would have been ideal. Preferably, using primary tumour cells that express LILRB3 would have been more appropriate as they would represent endogenous LILRB3 expression. Preliminary work in the lab showed that AML cells may express LILRB3 (data not shown) and previous studies suggest inhibitory LILRs are up-regulated on AML cells[161, 162]. Therefore, establishing AML xenograft models and optimising these in the lab could be performed. However, expression on primary cells can be heterogeneous and

variable between donors. Alternatively, another *in vivo* model that could have been utilised was generating a LILRB3 Tg model. A T-cell specific LILRB1 Tg model under a CD3 promoter, and a DC-specific LILRB2 Tg model under a CD11c promoter have both been developed, but no LILRB3 models[100, 134]. Although a LILRB3 Tg construct was generated during this project (data not shown), successful embryo implantation has yet to be accomplished. A human LILRB3 Tg model under a human LILRB3 promoter, would allow endogenous LILRB3 expression to be established, and antibody therapy could then be tested. This would more likely represent real LILRB3 expression. However, even in this system, the lack of other human proteins that may play a role in aiding anti-LILRB3 therapy will not be present. Therefore, humanised mouse models may be the best solution. This would allow human anti-LILR antibody therapy to be tested in a mouse with a human immune system, established by engrafting human PBMCs or HSCs into immunocompromised mice[186, 187]. Humanised mouse models have T and B cells, providing functional human adaptive immune responses[184]. This would be the closest and most accurate way to measure antibody efficacy.

Finally, the focus in this chapter has been on testing anti-LILR antibody therapy in treating cancer, but LILRs have also been implicated in autoimmunity e.g. RA[171]. Therefore, it would be advantageous to study the effect of these antibodies in a model of autoimmunity also. Many approved antibodies previously used in cancer therapy are now being used in other diseases, such as Campath, therefore these anti-LILR antibodies may have dual potential if both agonistic and antagonistic antibodies are found to be therapeutic[47].

7 DISCUSSION

In this thesis, novel antibodies against LILRB1, LILRB2 and LILRB3 were generated, characterised, and their function and therapeutic efficacy investigated. LILRs are a family of receptors, predominantly expressed on myeloid cells, known to regulate immune responses[39]. Inhibitory LILRB1 and LILRB2 have been extensively characterised. All four extracellular domains of these two receptors have been crystallised and binding to their HLA-I ligands studied[39, 88, 90, 97, 276]. Their signalling and function has also been characterised[66, 112]. However, other LILRs in the same family, have been less studied. Although LILRB1 and LILRB2 expression in different diseases makes them attractive therapeutic targets, they are ubiquitously expressed on many different cells; LILRB3 however, is an inhibitory LILR with a more restricted expression profile, making it a more attractive therapeutic target[39]. The crystal structure of LILRB3 is yet to be elucidated, and despite some evidence of binding to bacteria, ANGPTLs or cytokeratin on necrotic glandular epithelial cells, no clear ligand has been found[102, 107, 108]. However, LILRB3 has been implicated in both cancer and autoimmunity, with increased expression on AML cells and in the synovial tissue of RA patients[162, 171]. However, LILRB3 is very polymorphic in nature with at least 13 different variants described[77]. As a result current commercial antibodies against LILRB3 may not recognise all LILRB3 alleles. Furthermore, given the relatively high homology between different LILRs, the existing reagents may not be specific. Studying the expression of this family of receptors, requires highly specific reagents which in turn may help elucidate their function. The aim of this thesis was therefore, to generate antibodies against three of the inhibitory LILRs: LILRB1, LILRB2 and LILRB3, characterise these antibodies in terms of functional effects and then test their therapeutic efficacy.

Many pre-existing anti-LILR antibodies were generated by hybridoma technology, including the two previously defined anti-LILRB3 antibodies used in this thesis: clone 222821 (R&D systems) and TRX585 (Tolerx Inc.). In contrast the novel antibodies produced and described in this thesis were generated by phage display. Phage display has many advantages over other antibody generation techniques, including the use of an *in vitro* system, bypassing the need for animals, and allowing many different target protein formats to be utilised, whilst eliminating non-targets in a negative selection step[205]. A scFv library was utilised, as they are thought to provide more diversity and higher yields of clones compared to Fab libraries[205]. Phage display libraries are typically made up of 10^6-10^{11} clones, and even smaller libraries of 10^7 clones have been reported to generate successful high affinity antibodies[206]. The library used to generate antibodies in this thesis was made up of ~$1x10^9$ clones, providing a vast

amount of antigens that could be targeted[248]. The BioInvent nCoDeR antibody library is different from traditional phage display libraries, as it was generated using CDR shuffling technology[277]. CDRs were recombined in a specific framework by PCR and shuffled to give different combinations[277]. This allowed different antibody genes to be present in one antibody fragment, and increased the phage library size, creating new binding specificities and affinities, whilst also increasing genetic diversity[277]. Therefore the antibodies generated in this way should be more diverse than if traditional libraries were used. The selection strategy chosen can yield different characteristics of antibodies generated[207]. Different selection strategies were utilised in this thesis, which increased the diversity of the clones produced. Therefore, the antibodies generated here are likely to be novel, with higher binding affinities and specificities than if only one selection strategy was used. Antibodies with binding affinities between 10^8-10^{11} were generated (see later).

After generating these antibodies, the different clones were then characterised. Firstly, specificity was reconfirmed and cross-reactivity to other LILRs was tested. Current commercial antibodies are cross-reactive to other LILRs (based on personal communication with Dr Des Jones, *University of Cambridge*). When screened against each other: 42/46 LILRB3, 25/32 LILRB2, and 10/11 LILRB1 clones, were found to be target-specific. However, when screened against a larger repertoire of LILRs, 16 LILRB3 clones were found to be specific. Although the majority of LILRB2 and LILRB1 clones showed some binding to LILRB3-transfected cells, this was likely due to the high expression of LILRB3 on these cells compared to other LILR-transfectants. Therefore, novel and target-specific LILRB antibodies were generated. However, the antibodies were not screened against LILRA3, LILRA4 and LILRA6-transfected cells, due to poor transfection efficiencies, and it is possible that they cross-react with these receptors. LILRA6 in particular has high sequence homology to LILRB3 (>95 % identity extracellularly), and therefore it is possible that the anti-LILRB3 antibodies cross-react with this receptor[78]. If LILRA6 recombinant protein had been available at the time of generation, it could have been included as a non-target in the selection process. It should also be noted that antibodies against LILRB3 were generated using recombinant LILRB3 protein based on the sequence of the most common variant found in humans (construct provided by Des Jones, *University of Cambridge*). Due to the highly polymorphic disposition of LILRB3, it is possible that the anti-LILRB3 clones generated will not bind to all variants of LILRB3, or even that LILRB3 may be absent in some individuals, as was found with soluble LILRA3[70, 77, 80]. Thus if the anti-LILRB3 antibodies are were to be used therapeutically, their use would be limited to only those with this variant. However, phenotyping of primary cells from various different donors (n = 12) has to date failed to

identify a single individual who did not stain with these anti-LILRB3 antibodies, suggesting that they bind to most if not all variants, and no reports of variations in expression of LILRB3 in different populations has been reported.

As well as lacking cross-reactivity to the majority of other LILRs, the generated clones lacked cross reactivity to mouse PIR-B (Chapter 4, *Figure 4.3*). Although there are LILRB1 and LILRB2 Tg mouse models, no LILRB3 model has been generated[100, 134]. Whilst lack of cross-reactivity to PIR-B reinforces the human specificity of the anti-LILR antibodies, cross-reactivity to homologous mouse PIR-B would have allowed the therapeutic efficacy of the antibodies to be studied *in vivo*, as targeting the effect these antibodies had on mouse PIR-B could indicate their effect on their human counterparts. PIR-B expression however, is more ubiquitously expressed on immune subsets in comparison to LILRB3, therefore, targeting PIR-B may not be completely representative of LILRB3.

After testing specificity of the antibodies against other LILRs in the same family, their binding to healthy primary cells was tested. LILRB1, LILRB2 and LILRB3 staining was found on monocytes, macrophages and DCs; with only LILRB2 staining on B cells, and only LILRB3 staining on neutrophils (Chapter 4, *Figure 4.4*). This coincided with previous studies that LILRs are predominately found on myeloid cells[39, 74]. No staining was seen on T cells or NK cells. Although there are some reports of LILRB1 expression on T cells and NK cell subsets, staining has been reported to be very low or absent in some individuals, and varies between donors[67]. Therefore, the expression profile of these antibodies agreed with previous reports. The anti-LILRB3 clones were also tested for binding to fresh frozen human tissue samples (Chapter 4, *Figures 4.9-4.11*). Although when biotinylated the antibodies showed poor staining by IHC, they were able to stain tissue by IF when fluorescently conjugated, indicating that poor biotinylation of clones may have been the reason for their lack of staining by IHC. The antibodies could be used in IF to test different healthy and tumour tissue samples, to see the expression profile of LILRB3 in these tissues, as well as ensuring no off-target effects in unwanted tissues will result if these antibodies are used therapeutically.

All the antibodies were able to bind to LILR-transfected cell lines and primary cells, suggesting that they had a high enough affinity for their receptors on these cells. After showing that these antibodies were able to bind to different cell subsets and tissues, their binding affinity was also determined by SPR analysis. The data reported in chapter 4, showed that the commercial anti-LILRB3 clone 222821 had a slower off rate than the anti-LILRB3 clones generated in this thesis, and a dissociation constant (K_D) of $1.63x10^{-11}$. Comparatively, examples of generated clones shown in *Figure 4.5* and *Table 4.3* had K_D values between 10^{8}-

10^{11}, suggesting they had faster off rates than the commercial clone. However, all these K_D values signify high affinity binding, representing nM and pM affinities. Therefore, phage display was able to produce high affinity antibodies.

Anti-LILRB3 antibodies were found to bind to either the second or fourth Ig-like domains of LILRB3. Given that the commercial clone 222821 bound to the second domain, this suggests that the generated antibodies binding to domain four, are binding to novel epitopes. Also, seven anti-LILRB3 clones were found to bind to the same domain as the commercial (2D) but novel epitopes within the domain (as they did not cross-block the commercial mAb). Why no clones binding to domains one or three were observed it not clear. It is possible that the selection strategies performed during antibody generation favoured certain antibody binding sites, as they may have been more exposed. It could also be the way in which the LILRB3 domain mutants were generated, as conformational changes occurred that destroyed or masked certain binding sites, or the LILRB3 protein was mis-folded in some way as constructs were generated through annotated UNIPROT sequences where domains overlapped. Or finally, it could be that 1D and 3D do not have immunogenic epitopes, or at least none more favourable than those found in 2D or 4D.

Although it is unknown if epitope mapping and function are correlated, this could suggest that novel binding sites will also result in novel functional antibody properties. Most reports have suggested that the ligand binding sites of both LILRB1 and LILRB2 are in their first two Ig-like domains, which bind to HLA-I molecules through their α3 and β2m in *trans*[86, 93, 94]. However, Nam *et al* suggested that the third and fourth domains may also play an important role in ligand binding via the α1 and α2 domains of HLA-I molecules[276]. Therefore, generating antibodies against all the different extracellular domains could be important to elucidate the role each domain plays in ligand binding.

The functional ability of the generated antibodies was also tested, through studying the effect of anti-LILR antibodies on T cell proliferation and macrophage phagocytosis. The effect of inhibitory LILRB1 on T cell proliferation has been studied previously, through ligation with either an anti-LILRB1 antibody or hCMV-UL18-Fc ligand[120]. The inhibitory effect on T cell proliferation was described as being the result of LILRB1 modulating DCs[120]. In the assays performed in Chapter 6, T cell proliferation was studied using PBMCs. Data shown in chapter 5, showed that some of the anti-LILR antibodies were able to inhibit or enhance CFSE dilution and therefore T cell proliferation. Separating different cell populations could help deduce if APCs are responsible for the effect seen on T cell responses, by culturing isolated anti-CD3 stimulated T cells with individual cell types treated with anti-LILR antibodies, e.g.

isolated T cells co-cultured with LILR-treated isolated DCs, monocytes or B cells, that can act as APCs. The role of LILRs on APCs leading to inhibition of T cell responses has been well documented[113, 118, 119, 120]. Although there have been reports on the role of LILRB1 on B cell responses also, the role of LILRs on other effector cells has been less studied[131, 132, 133]. Data in chapter 5 showed that all the antibodies tested inhibited macrophage phagocytosis. Therefore, the data in this thesis on the role of LILRs on macrophage phagocytosis is novel. Ma *et al* showed that PIR-B may regulate the differentiation of MDSCs to M2-like TAMs in the tumour microenvironment, and suggested that homologous LILRB3 may also play this role in humans, although this has not been confirmed[109]. Therefore, more work on the role of other effector cells is warranted, to fully understand the function of LILRBs in immunity.

Clone 222821 is a mIgG2a shown in this thesis to be agonistic for LILRB3, stimulating its inhibitory function and blocking T cell proliferation and macrophage phagocytosis. TRX585 was originally a mIgG1, however, in the assays reported in this thesis, a hIgG1 was used, to enable comparisons to be made with the hIgG1 antibodies that were generated by phage display. TRX585 has been shown to be an antagonist for LILRB3, in this manner enhancing T cell proliferation, and pro-inflammatory TNF-α cytokine release (US patent US2013/0030156 A1). The antibodies generated in this thesis also showed signs of both agonistic and antagonistic properties on receptor cell function. Therefore, these antibodies may function as immunomodulatory therapeutic antibodies. The different techniques of antibody generation could have led to different types of antibody function. As shown by Rossant *et al*, who generated antibodies against chemokine receptor CXCR2 by both immunisation in mice and phage display technology[278]. They found antibodies produced by hybridomas were agonistic, whilst antibodies produced by phage display were antagonistic; the different antibodies were also found to bind different epitope binding sites[278]. These differences could be the result of different epitopes being exposed during the generation process. However, the commercial clone 222821 generated by hybridoma (R&D systems website) had agonistic properties in assays described in this thesis, comparatively although overall TRX585 showed inhibition of T cell proliferation, some donors showed an increase, which coincides with the description of the antibody as an antagonist in its patent[257]. More donors would need to be assessed to validate these findings. Antibodies generated in this thesis by phage display showed different functional properties also, with some showing clear inhibition of effector function, and others having no effect or enhancing immune responses (chapter 5). Therefore, the same antibody generation technology yielded antibodies with different functional properties, indicating the way in which antibodies are generated may not favour certain characteristics, but rather that the epitopes targeted may elicit differential functions. One possible reason for the difference

in function could have been due to cross-linking. Some antibodies may have been able to elicit sufficient cross-linking of their target receptor on effector cells, whilst others may not. For example, although data in chapter 5 *Figure 5.2* showed that almost all anti-LILRB3 clones showed an ability to elicit sufficient cross-linking that resulted in cellular activation on reporter cells, however, on 'real' cells this may not be the case, possibly as a result of higher activation thresholds on these cells. It could also be that they are binding to their receptor with different affinities. Although SPR analysis showed all the anti-LILRB3 clones generated are high affinity antibodies, SPR was performed with LILRB3-hFc as a ligand, which may have had different epitopes exposed when coated to a chip, in comparison to the LILRB3 receptor on effector cells. As LILRB3 is expressed highly on macrophages (see chapter 4 *Figure 4.4*), more LILRB3 molecules would be present also. On real cells, the anti-LILRB3 antibodies may be blocking endogenous ligands also, further effecting cellular function.

Another functional characteristic that was tested was the ability of these antibodies to induce receptor internalisation. The results revealed that some anti-LILRB3 clones were able to cause rapid internalisation, whilst others did not induce internalisation (Chapter 5, *Figure 5.12*). Antibody internalisation is a characteristic that has already been shown to effect therapy. For example, studies have shown that Rituximab internalises, and this reduces its therapeutic efficacy[259]. Exploiting the ability of anti-LILR mAbs to internalise however, could be beneficial in therapies such as ADCs, which consist of internalising antibodies linked to drugs that can deliver cytotoxic signals into the cell. The first ADC, Gemtuzumab ozogamicin has now been withdrawn from the market[47]. However, there are still two ADCs approved for therapy: Brentuximab vedotin (Adcetris®) to treat HL and sALCL; and Trastuzumab emtansine used to treat breast cancer[245, 246]. Conjugating anti-LILR clones that showed receptor internalisation to cytotoxic agents, could therefore be an effective cancer treatment.

LILRB1 is the only LILR to be expressed on normal B cells, but LILRB4 has also been reported to be expressed on malignant CLL B cells[39, 163]. Phenotyping CLL cells in Chapter 6 *Figure 6.2*, showed that LILRB1, LILRB2, LILRB4 and in some cases LILRB3 were also expressed on these malignant cells. This suggests that LILRB expression is not just restricted to cells surrounding tumour cells, but also the tumour cells themselves. Increased LILRB expression on CLL cells may correlate with disease severity, as the tumour may exploit these receptors to supress T cell responses against the tumour through down-regulation of cytokine/chemokine production. Increased expression of LILRB4 on AML samples has been found[161]. LILRB1, LILRB2 and LILRB3 have also been predicted to aid in AML progression[162]. LILRB1 and LILRB4 have been found up-regulated in gastric cancer[160].

Therefore, increased expression of LILRBs may be a common feature in many malignancies, and phenotyping other cancer cell types would be informative

Given LILR expression on tumours, these antibodies were tested for their ability to directly target tumour cells. Whilst the anti-LILR antibodies did show some depletion of tumours in both the CLL and Ramos transfectant xenograft models, this depletion was relatively ineffective, especially in comparison to current anti-CD20 therapy Rituximab (Chapter 6). Antibody efficacy could have been affected by LILRB expression levels in both the CLL and Ramos models, as LILRB expression was low or lower than CD20, respectively. If LILRB expression was to effect anti-LILR therapy, this would suggest that using these antibodies for direct targeting would only be useful in patients with high LILRB expression. CD20 expression is variable on different lymphomas, and there have been reports speculating that lower expression may result in reduced therapeutic efficacy of Rituximab, and so enhancing expression may enhance therapy, however, this has not been proven[279].

To study therapeutic efficacy, xenografts models using either LILRB3-transfected cell lines or primary tumour cells were utilised in immunocompromised mice. However, these models have their limitations. Xenografts with cell lines don't necessarily represent real human cells and may therefore not be clinically relevant; however, using primary human tissue provides real human cells with all their genetic complexities to be studied[180]. However, these so-called primary cell models are also limited in that primary tissue can be difficult to source, and immunocompromised mice are utilised, which lack some or all functional immune cells, therefore immune responses to tumours are diminished[180]. Tg models are therefore potentially more advantageous and allow human genes and receptors to be studied, without the need for immunocompromised mice[183]. A LILRB1 Tg model under a CD3 promoter, providing LILRB1 T cell-specific expression, and a DC-specific LILRB2 Tg model under a CD11c promoter have both been developed[100, 134]. However, no LILRB3 mouse models have currently been developed, so the models described in Chapter 6 are novel. Testing human antibodies in Tg mouse models results in studying mouse immune responses to therapy, therefore a better alternative would be to use humanised mouse models, in which a fully functioning human immune systems can be established, allowing human cell immune responses to human therapies[184]. However, these models depend on obtaining human stem cells, for example from human umbilical cord samples, which are difficult to source, and HLA selecting elements are not encompassed in the developed immunity[185].

In summary, this thesis describes the generation of novel anti-LILRB1, LILRB2 and LILRB3 clones, that were specific, bind to novel binding sites with high affinity, are able to induce

receptor internalisation, and display agonistic/antagonistic properties against effecter cell function. These characteristics have helped further our understanding of the LILRB family of receptors. Using these anti-LILRBs as ADCs is a possibility, given the ability of some clones to induce internalisation. However, given that these LILRs are expressed not just on tumours but on many different healthy myeloid cells, this could result in high levels of toxicity. Xenograft experiments with primary CLL cells and Ramos transfectants showed a potential (albeit limited) ability of the antibodies to deplete tumour cells directly. However, these antibodies did show they could enhance or inhibit immune responses on effector cells, through T cell proliferation and macrophage phagocytosis assays. Therefore, these antibodies are likely to be most efficiently used as immunomodulatory therapy, rather than ADCs or as direct targeting antibodies. The work carried out in this thesis explores the therapeutic ability of these clones in cancer therapies, however given that LILRs are up-regulated in autoimmune conditions such as RA and SLE, therapeutic efficacy of these antibodies in autoimmune models should also be tested[39, 171]. LILR activatory to inhibitory ratio has been shown to be important for maintaining tolerance, as higher expression of inhibitory LILRB2 compared to activatory LILRA2 and LILRA5 was found to be associated with patient remission in RA patients[171]. Therefore, antibodies generated against inhibitory LILRB1, LILRB2 or LILRB3, which showed agonistic receptor function in this thesis, may enhance inhibitory immune responses in RA patients, and possibly aid in preventing disease progression.

8 APPENDICES

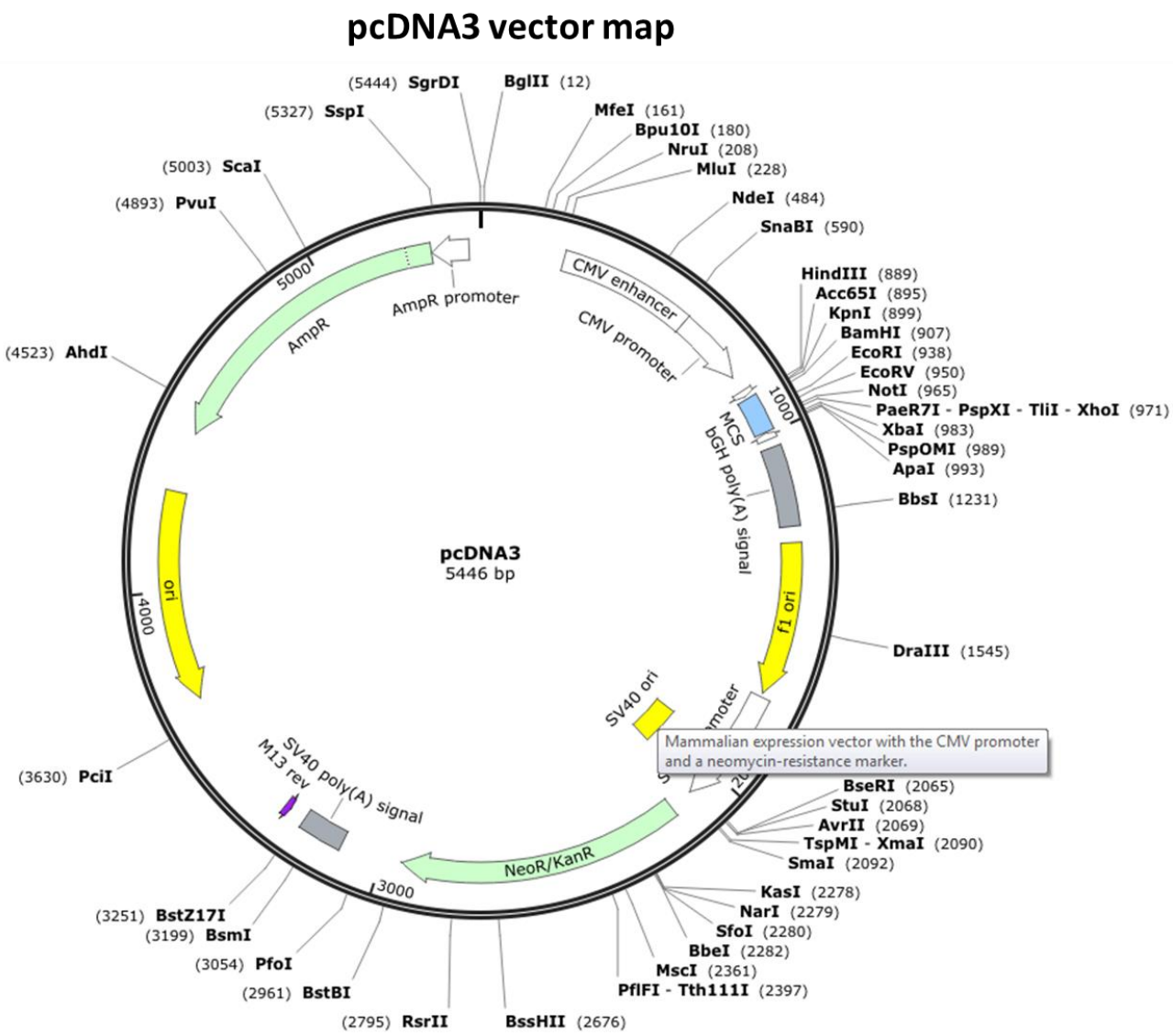

SigPlg vector map

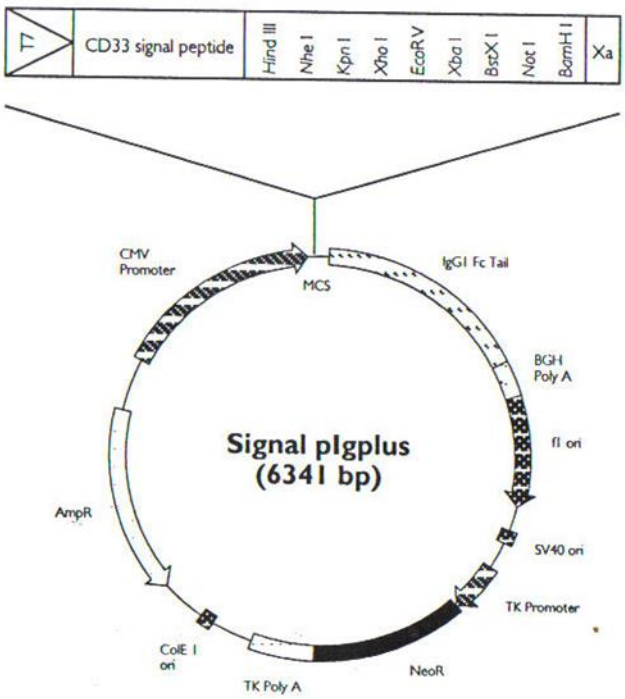

Functional site listings

CMV Promoter	5612-6244	Amp^R	5246-4386
IgG_1 Fc tail	91-789	T7 Promoter	6245-6261
BGH Poly A	826-1118	MCS	1-62
f1 ori	1119-1545	Factor Xa site	64-75
SV40 ori	1641-1729	ColE1 ori	3613-4195
TK Promoter	1761-2005	CD33 signal sequence	6288-6341
Neo^R	2014-2808		
TK Poly A	2813-3183		

pHR-SIN vector map

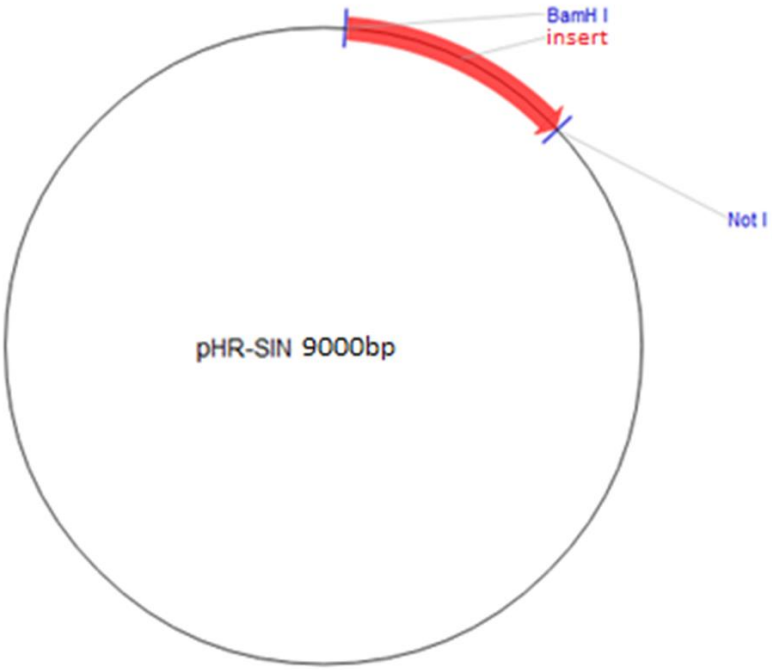

3xFLAG (sigma) vector map

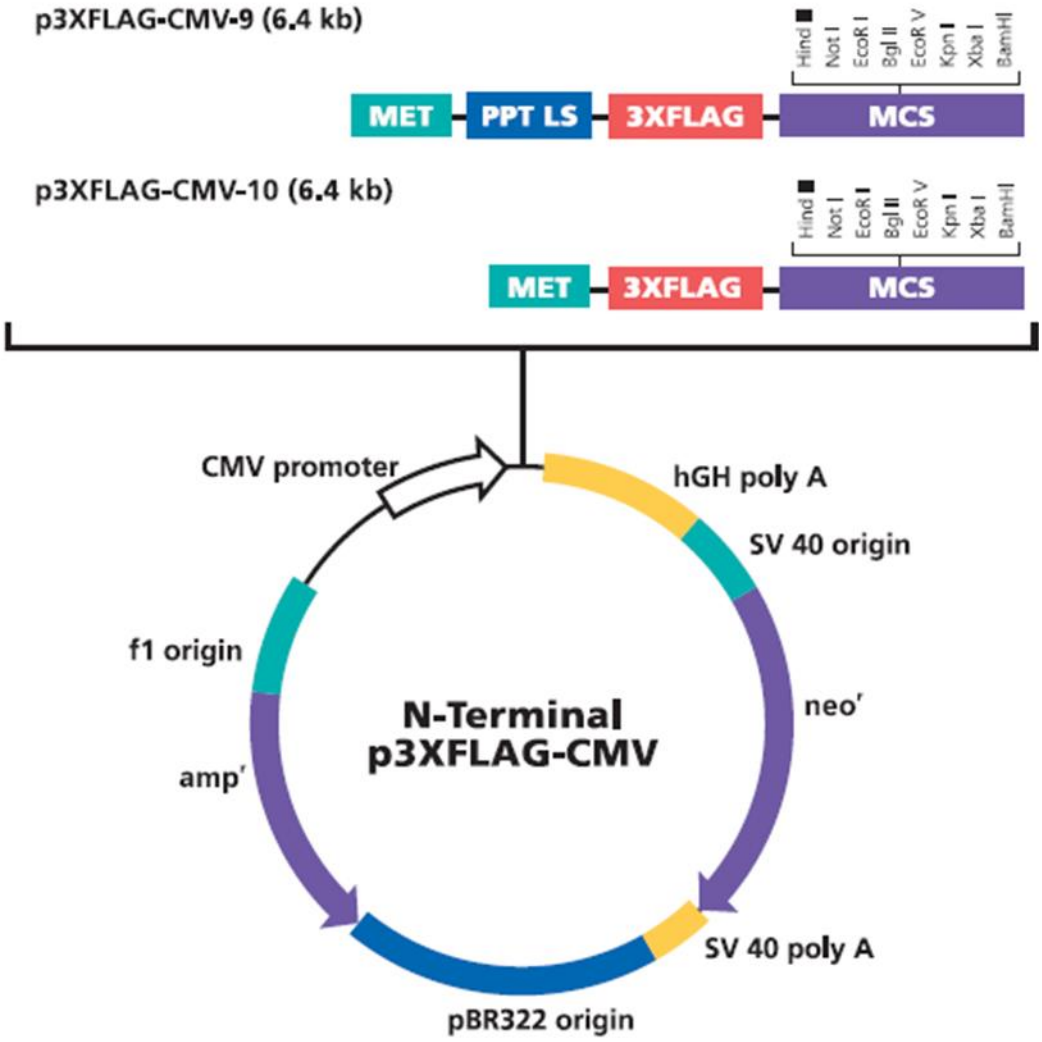

Multiple Cloning Site

(p3XFLAG-CMV-9* and p3XFLAG-CMV-10)

	3XFLAG Peptide Sequence														
Met*	Asp	Tyr	Lys	Asp	His	Asp	Gly	Asp	Tyr	Lys	Asp	His	Asp	Ile	
ATG	GAC	TAC	AAA	GAC	CAT	GAC	GGT	GAT	TAT	AAA	GAT	CAT	GAC	ATC	
TAC	CTG	ATG	TTT	CTG	GTA	CTG	CCA	CTA	ATA	TTT	CTA	GTA	CTG	TAG	

3XFLAG Peptide Sequence							
Asp	Tys	Lys	Asp	Asp	Asp	Asp	Lys
GAT	TAC	AAG	GAT	GAC	GAT	GAC	AAG
CTA	ATG	TTC	CTA	CTG	CTA	CTG	TTC

Not I: GCG GCC GCG
EcoR I: AAT TCA
TCG ATA
TTA AGT AGC TAT
GAA CGC CGG CGC
Hind III

Bgl II: GAT CTG
EcoR V: ATA TCG
Kpn I: GTA CCA
Xba I: TCT AGA
Bam HI: GGA TCC
CGG GTG
CTA GAC TAT AGC CAT GGT CAG CTG AGA TCT CCT AGG CCC CAC

*For pFLAG-CMV-9, the Met-preprotrypsin leader sequence (PPT LS) precedes the FLAG coding sequence.

Table 8.1 Summary of LILR antibody characterisation

Clone	Specific?		Block Ab?	Domain	K_D	X-link?	Functional			Intern.
	HEK 293T	2B4					GFP	MØ	Prolif	
LILRB3 clones										
222821	Yes	No	N/A	2D	$1.63x10^{-11}$	N/A	N/A	↓	↓	Yes
TRX585	N/A	N/A	N/A	N/A	N/A	N/A	N/A	↓	↓	N/A
A1	Yes	Yes	No	4D	$3.73\ x10^{-10}$	Yes	N/A	↓	↓	No
A2	Yes	No	Partially	2D	$3.14\ x10^{-10}$	Yes	N/A	N/A	↓	N/A
A3	Yes	No	Partially	2D	$1.10\ x10^{-8}$	No	N/A	N/A	↓	N/A
A4	Yes	No	Partially	2D	N/A	Yes	N/A	N/A	↓	N/A
A5	Yes	No	Partially	2D	$1.16\ x10^{-9}$	Yes	N/A	N/A	↓	N/A
A6	No	No	Partially	2D	N/A	Yes	N/A	N/A	↓	N/A
A7	Yes	No	Partially	2D	$1.01\ x10^{-9}$	Yes	N/A	N/A	↓	N/A
A8	No	No	No	4D	$7.92\ x10^{-10}$	Yes	N/A	N/A	↓	N/A
A9	Yes	No	Partially	2D	$3.44\ x10^{-10}$	No	N/A	N/A	↓	N/A
A10	Yes	No	Partially	2D	$7.01\ x10^{-10}$	Yes	N/A	N/A	↓	N/A
A11	Yes	No	Partially	2D	$2.23\ x10^{-10}$	Yes	N/A	N/A	↓	N/A
A12	Yes	Yes	Partially	2D	$5.29\ x10^{-10}$	Yes	N/A	N/A	↓	N/A
A13	Yes	No	Yes	2D	$2.14\ x10^{-10}$	Yes	N/A	↓	↓	Yes
A14	Yes	Yes	No	4D	$2.92\ x10^{-10}$	Yes	N/A	N/A	↓	N/A
A15	Yes	No	No	2D	$5.37\ x10^{-10}$	Yes	N/A	N/A	↓	N/A
A16	Yes	Yes	No	4D	$8.16\ x10^{-10}$	Yes	N/A	↓	↑	Yes
A17	No	No	Partially	2D	$5.46\ x10^{-11}$	Yes	N/A	N/A	↓	N/A
A18	Yes	No	No	2D	$1.86\ x10^{-10}$	Yes	N/A	N/A	↓	N/A
A19	Yes	No	No	2D	$4.31\ x10^{-10}$	Yes	N/A	N/A	↓	N/A
A20	Yes	Yes	Partially	2D	$9.61\ x10^{-10}$	Yes	N/A	N/A	↓	No
A21	Yes	Yes	No	2D	$1.55\ x10^{-9}$	Yes	N/A	N/A	↓	N/A
A22	Yes	Yes	No	4D	$3.84\ x10^{-9}$	Yes	N/A	N/A	↓	N/A
A23	Yes	No	Partially	2D	$1.99\ x10^{-10}$	Yes	N/A	N/A	↓	N/A
A24	No	No	No	4D	N/A	No	N/A	N/A	↓	N/A
A25	No	No	Partially	2D	$4.68\ x10^{-10}$	No	N/A	N/A	↓	N/A
A26	Yes	No	Partially	2D	$1.79\ x10^{-9}$	Yes	N/A	N/A	↑	N/A
A27	Yes	No	Partially	2D	$3.19\ x10^{-12}$	No	N/A	N/A	↓	N/A
A28	Yes	Yes	No	4D	$6.87\ x10^{-10}$	No	N/A	↓	↓	No
A29	Yes	Yes	No	4D	$1.10\ x10^{-8}$	Yes	N/A	↓	↑	No
A30	Yes	No	Yes	2D	$4.07\ x10^{-11}$	No	N/A	N/A	↑	N/A
A31	Yes	Yes	No	2D	$3.71\ x10^{-10}$	No	N/A	N/A	↓	N/A
A32	Yes	No	Partially	2D	$3.95\ x10^{-10}$	Yes	N/A	N/A	↓	N/A
A33	Yes	No	Partially	2D	$4.07\ x10^{-10}$	Yes	N/A	N/A	↓	N/A
A34	Yes	No	Partially	2D	$5.61\ x10^{-10}$	Yes	N/A	N/A	↑	N/A
A35	Yes	No	Partially	2D	$2.75\ x10^{-12}$	No	N/A	N/A	↓	N/A
A36	No	No	Partially	2D	$1.78\ x10^{-10}$	Yes	N/A	N/A	↓	N/A
A37	Yes	No	Partially	2D	$5.22\ x10^{-10}$	Yes	N/A	N/A	↓	N/A
A38	Yes	Yes	No	4D	$1.37\ x10^{-9}$	Yes	N/A	N/A	↑	N/A
A39	Yes	Yes	No	4D	$1.24\ x10^{-10}$	Yes	N/A	N/A	↓	N/A
A40	Yes	No	No	4D	$2.01\ x10^{-9}$	Yes	N/A	N/A	↑	N/A
A41	Yes	Yes	No	4D	$3.25\ x10^{-9}$	Yes	N/A	N/A	↑	N/A
A42	Yes	No	Partially	2D	N/A	No	N/A	N/A	↓	N/A
A43	Yes	Yes	No	2D	$3.05\ x10^{-10}$	Yes	N/A	N/A	↓	N/A
A44	Yes	Yes	No	4D	$1.55\ x10^{-9}$	Yes	N/A	N/A	↑	N/A
A45	No	Yes	No	2D	$1.68\ x10^{-8}$	No	N/A	N/A	↓	N/A
A46	Yes	No	Partially	2D	$5.05\ x10^{-12}$	Yes	N/A	N/A	↑	N/A
LILRB2 clones										
B1	Yes	No	No	N/A	N/A	No	N/A	N/A	N/A	N/A

B2	Yes	No	No	N/A	N/A	No	N/A	N/A	N/A	N/A
B3	Yes	Yes	No	N/A	N/A	No	↓	↓	NC	Yes
B4	No	No	No	N/A	N/A	No	N/A	N/A	N/A	N/A
B5	No	No	No	N/A	N/A	No	N/A	N/A	N/A	N/A
B6	No	No	No	N/A	N/A	No	N/A	N/A	N/A	N/A
B7	No	No	No	N/A	N/A	No	N/A	N/A	N/A	N/A
B8	Yes	Yes	No	N/A	N/A	No	↓	N/A	N/A	N/A
B9	No	No	Partially	N/A	N/A	No	N/A	N/A	N/A	N/A
B10	Yes	No	No	N/A	N/A	No	N/A	N/A	N/A	N/A
B11	Yes	No	No	N/A	N/A	No	N/A	N/A	N/A	N/A
B12	Yes	No	No	N/A	N/A	No	N/A	N/A	N/A	N/A
B13	Yes	No	No	N/A	N/A	No	N/A	N/A	N/A	N/A
B14	Yes	No	No	N/A	N/A	No	N/A	N/A	N/A	N/A
B15	Yes	Yes	No	N/A	N/A	No	↓	↓	NC	No
B16	Yes	No	No	N/A	N/A	No	N/A	N/A	N/A	N/A
B17	Yes	No	No	N/A	N/A	No	N/A	N/A	N/A	N/A
B18	No	No	No	N/A	N/A	No	N/A	N/A	N/A	N/A
B19	Yes	Yes	No	N/A	N/A	No	↓	↓	↑	No
B20	Yes	No	No	N/A	N/A	No	N/A	N/A	N/A	N/A
B21	Yes	No	No	N/A	N/A	No	N/A	N/A	N/A	N/A
B22	No	No	No	N/A	N/A	No	N/A	N/A	N/A	N/A
B23	Yes	Yes	No	N/A	N/A	No	N/A	N/A	N/A	N/A
B24	Yes	No	No	N/A	N/A	No	N/A	N/A	N/A	N/A
B25	Yes	No	No	N/A	N/A	Yes	N/A	N/A	N/A	N/A
B26	Yes	No	No	N/A	N/A	No	N/A	N/A	N/A	N/A
B27	Yes	No	No	N/A	N/A	Yes	N/A	N/A	N/A	N/A
B28	No	No	Partially	N/A	N/A	No	N/A	N/A	N/A	N/A
B29	Yes	No	No	N/A	N/A	No	N/A	N/A	N/A	N/A
B30	Yes	Yes	No	N/A	N/A	Yes	↓	↓	↑	No
B31	Yes	No	No	N/A	N/A	No	N/A	N/A	N/A	N/A
B32	Yes	No	No	N/A	N/A	Yes	N/A	N/A	N/A	N/A
LILRB1 clones										
C1	Yes	No	Partially	N/A	N/A	Yes	N/A	N/A	N/A	N/A
C2	Yes	No	No	N/A	N/A	No	N/A	N/A	N/A	N/A
C3	Yes	No	Yes	N/A	N/A	No	N/A	N/A	N/A	N/A
C4	No	No	No	N/A	N/A	Yes	N/A	N/A	N/A	N/A
C5	Yes	No	No	N/A	N/A	Yes	N/A	N/A	N/A	N/A
C6	Yes	Yes	No	N/A	N/A	No	N/A	N/A	N/A	N/A
C7	Yes	No	Partially	N/A	N/A	Yes	↓	↓	↑	No
C8	Yes	No	No	N/A	N/A	No	N/A	N/A	N/A	N/A
C9	Yes	No	Yes	N/A	N/A	Yes	↑	↓	↑	No
C10	Yes	Yes	No	N/A	N/A	Yes	↓	↓	↓	No
C11	Yes	No	Yes	N/A	N/A	Yes	N/A	N/A	N/A	N/A

Table 8.1 Summary of LILR antibody characterisation. Summary of specificity against HEK293T or 2B4-transfected cells, epitope mapping studied, affinity and functional properties. See key below for details and abbreviations.

Key:
Specificity HEK293T = antibodies tested against LILRB1, LILRB2 and LILRB3-transfected HEK293T cells
Specificity 2B4 = antibodies tested against non-transfected or LILR-A1, -A2, -A5, -B1, -B2, -B3, -B4 and -B5 2B4 reporter cells
Block Ab = block commercial antibody
Domain = antibody binding to extracellular Ig-like domain
K_D = dissociation constant calculated by SPR
cross (x)-link = agonist (able to both bind to receptor on cell and cause cellular activation)
block GFP = block HLA-G ligand binding resulting in no intracellular signalling and GFP expression
block mØ = block macrophage phagocytosis
block prolif = block T cell proliferation
Intern. = antibody induces receptor internalisation
N/A = not applicable/not tested
NC = no change
↑ = increase
↓ = decrease

REFERENCES

1. Murphy, K., Travers, P. & Walport, M. *Janeway's Immunobiology*, 7 edn. Garland Science, Taylor & Francis Group, LLC: New York, 2008.

2. Kindt, T.J., Goldsby, R.A. & Osborne, B., A. *Kuby Immunology*, 6th edn. W.H. Freeman and Company New York, 2007.

3. Ehrlich, P. Beiträge zur Kenntniss der Anilinfärbungen und ihrer Verwendung in der mikroskopischen Technik. *Archiv für mikroskopische Anatomie* **13**, 263-277 (1877).

4. Biswas, S.K. & Mantovani, A. Macrophage plasticity and interaction with lymphocyte subsets: cancer as a paradigm. *Nat Immunol* **11**, 889-896 (2010).

5. Mantovani, A., Sica, A. & Locati, M. Macrophage polarization comes of age. *Immunity* **23**, 344-346 (2005).

6. Mantovani, A. *et al.* The chemokine system in diverse forms of macrophage activation and polarization. *Trends in immunology* **25**, 677-686 (2004).

7. Collin, M., McGovern, N. & Haniffa, M. Human dendritic cell subsets. *Immunology* **140**, 22-30 (2013).

8. Banchereau, J. *et al.* Immunobiology of dendritic cells. *Annual review of immunology* **18**, 767-811 (2000).

9. Ban, Y.L., Kong, B.H., Qu, X., Yang, Q.F. & Ma, Y.Y. BDCA-1+, BDCA-2+ and BDCA-3+ dendritic cells in early human pregnancy decidua. *Clinical and experimental immunology* **151**, 399-406 (2008).

10. Demedts, I.K., Bracke, K.R., Maes, T., Joos, G.F. & Brusselle, G.G. Different roles for human lung dendritic cell subsets in pulmonary immune defense mechanisms. *American journal of respiratory cell and molecular biology* **35**, 387-393 (2006).

11. Tversky, J.R. *et al.* Human blood dendritic cells from allergic subjects have impaired capacity to produce interferon-alpha via toll-like receptor 9. *Clinical and Experimental Allergy* **38**, 781-788 (2008).

12. van Nierop, K. & de Groot, C. Human follicular dendritic cells: function, origin and development. *Seminars in immunology* **14**, 251-257 (2002).

13. Kumar, V. & McNerney, M.E. A new self: MHC-class-I-independent natural-killer-cell self-tolerance. *Nature reviews. Immunology* **5**, 363-374 (2005).

14. Edwards, J.C. & Cambridge, G. B-cell targeting in rheumatoid arthritis and other autoimmune diseases. *Nature reviews. Immunology* **6**, 394-403 (2006).

15. Pieper, K., Grimbacher, B. & Eibel, H. B-cell biology and development. *The Journal of allergy and clinical immunology* **131**, 959-971 (2013).

16. Clark, M.R., Mandal, M., Ochiai, K. & Singh, H. Orchestrating B cell lymphopoiesis through interplay of IL-7 receptor and pre-B cell receptor signalling. *Nature reviews. Immunology* **14**, 69-80 (2014).

17. Bruce Alberts, A.J., Julian Lewis, Martin Raff, Keith Roberts, and Peter Walter. The Generation of Antibody Diversity. *Molecular Biology of the Cell, 4th edition*, 4th edn. Garland Science: New York, 2002.

18. Mongini, P.K.A., Blessinger, C., Posnett, D.N. & Rudich, S.M. Membrane Igd and Membrane Igm Differ in Capacity to Transduce Inhibitory Signals within the Same Human B-Cell Clonal Populations. *J Immunol* **143**, 1565-1574 (1989).

19. Lutz, C. *et al.* IgD can largely substitute for loss of IgM function in B cells. *Nature* **393**, 797-801 (1998).

20. Matza, D. *et al.* Invariant chain induces B cell maturation in a process that is independent of its chaperonic activity. *Proceedings of the National Academy of Sciences of the United States of America* **99**, 3018-3023 (2002).

21. Blom, B. & Spits, H. Development of human lymphoid cells. *Annual review of immunology* **24**, 287-320 (2006).

22. Teng, G. & Papavasiliou, F.N. Immunoglobulin somatic hypermutation. *Annual review of genetics* **41**, 107-120 (2007).

23. Malek, A. Role of IgG antibodies in association with placental function and immunologic diseases in human pregnancy. *Expert review of clinical immunology* **9**, 235-249 (2013).

24. Geisberger, R., Lamers, M. & Achatz, G. The riddle of the dual expression of IgM and IgD. *Immunology* **118**, 429-437 (2006).

25. Starr, T.K., Jameson, S.C. & Hogquist, K.A. Positive and negative selection of T cells. *Annual review of immunology* **21**, 139-176 (2003).

26. Germain, R.N. T-cell development and the CD4-CD8 lineage decision. *Nature reviews. Immunology* **2**, 309-322 (2002).

27. Engel, I. & Murre, C. The function of E- and Id proteins in lymphocyte development. *Nature reviews. Immunology* **1**, 193-199 (2001).

28. Jelley-Gibbs, D.M., Strutt, T.M., McKinstry, K.K. & Swain, S.L. Influencing the fates of CD4 T cells on the path to memory: lessons from influenza. *Immunology and cell biology* **86**, 343-352 (2008).

29. Zou, W. & Restifo, N.P. T(H)17 cells in tumour immunity and immunotherapy. *Nature reviews. Immunology* **10**, 248-256 (2010).

30. Russ, B.E., Prier, J.E., Rao, S. & Turner, S.J. T cell immunity as a tool for studying epigenetic regulation of cellular differentiation. *Frontiers in genetics* **4**, 218 (2013).

31. Eyerich, S. *et al.* Th22 cells represent a distinct human T cell subset involved in epidermal immunity and remodeling. *J Clin Invest* **119**, 3573-3585 (2009).

32. Gerlach, K. *et al.* TH9 cells that express the transcription factor PU.1 drive T cell-mediated colitis via IL-9 receptor signaling in intestinal epithelial cells. *Nat Immunol* **15**, 676-686 (2014).

33. O'Shea, J.J. & Paul, W.E. Mechanisms underlying lineage commitment and plasticity of helper CD4+ T cells. *Science* **327**, 1098-1102 (2010).

34. Crotty, S. Follicular helper CD4 T cells (TFH). *Annual review of immunology* **29**, 621-663 (2011).

35. Duhen, T., Geiger, R., Jarrossay, D., Lanzavecchia, A. & Sallusto, F. Production of interleukin 22 but not interleukin 17 by a subset of human skin-homing memory T cells. *Nat Immunol* **10**, 857-863 (2009).

36. Neefjes, J., Jongsma, M.L., Paul, P. & Bakke, O. Towards a systems understanding of MHC class I and MHC class II antigen presentation. *Nature reviews. Immunology* **11**, 823-836 (2011).

37. Borrego, F. *et al.* Structure and function of major histocompatibility complex (MHC) class I specific receptors expressed on human natural killer (NK) cells. *Molecular immunology* **38**, 637-660 (2002).

38. Lanier, L.L. NK cell recognition. *Annual review of immunology* **23**, 225-274 (2005).

39. Anderson, K.J. & Allen, R.L. Regulation of T-cell immunity by leucocyte immunoglobulin-like receptors: innate immune receptors for self on antigen-presenting cells. *Immunology* **127**, 8-17 (2009).

40. Braud, V.M., Allan, D.S. & McMichael, A.J. Functions of nonclassical MHC and non-MHC-encoded class I molecules. *Current opinion in immunology* **11**, 100-108 (1999).

41. Alfonso, C. & Karlsson, L. Nonclassical MHC class II molecules. *Annual review of immunology* **18**, 113-142 (2000).

42. Joffre, O.P., Segura, E., Savina, A. & Amigorena, S. Cross-presentation by dendritic cells. *Nature reviews. Immunology* **12**, 557-569 (2012).

43. Bevan, M.J. Cross-priming for a secondary cytotoxic response to minor H antigens with H-2 congenic cells which do not cross-react in the cytotoxic assay. *The Journal of experimental medicine* **143**, 1283-1288 (1976).

44. Barrow, A.D. & Trowsdale, J. You say ITAM and I say ITIM, let's call the whole thing off: the ambiguity of immunoreceptor signalling. *Eur J Immunol* **36**, 1646-1653 (2006).

45. Nimmerjahn, F. & Ravetch, J.V. Fc-receptors as regulators of immunity. *Advances in Immunology, Vol 96* **96**, 179-204 (2007).

46. Pleass, R.J. & Woof, J.M. Fc receptors and immunity to parasites. *Trends in parasitology* **17**, 545-551 (2001).

47. Reichert, J.M. Antibodies to watch in 2015. *Mabs-Austin* **7**, 1-8 (2015).

48. Nimmerjahn, F. & Ravetch, J.V. Fcgamma receptors as regulators of immune responses. *Nature reviews. Immunology* **8**, 34-47 (2008).

49. Jonsson, F. & Daeron, M. Mast cells and company. *Frontiers in immunology* **3**, 16 (2012).

50. Hargreaves, C.E. *et al.* Fcgamma receptors: genetic variation, function, and disease. *Immunological reviews* **268**, 6-24 (2015).

51. Smith, K.G. & Clatworthy, M.R. FcgammaRIIB in autoimmunity and infection: evolutionary and therapeutic implications. *Nature reviews. Immunology* **10**, 328-343 (2010).

52. Roghanian, A. *et al.* Antagonistic human FcgammaRIIB (CD32B) antibodies have anti-tumor activity and overcome resistance to antibody therapy in vivo. *Cancer cell* **27**, 473-488 (2015).

53. Lee, C.S. *et al.* Expression of the inhibitory Fc gamma receptor IIB (FCGR2B, CD32B) on follicular lymphoma cells lowers the response rate to rituximab monotherapy (SAKK 35/98). *Br J Haematol* **168**, 145-148 (2015).

54. Lim, S.H. *et al.* Fc gamma receptor IIb on target B cells promotes rituximab internalization and reduces clinical efficacy. *Blood* **118**, 2530-2540 (2011).

55. White, A.L. *et al.* Interaction with FcgammaRIIB is critical for the agonistic activity of anti-CD40 monoclonal antibody. *J Immunol* **187**, 1754-1763 (2011).

56. Dahal, L.N., Roghanian, A., Beers, S.A. & Cragg, M.S. FcgammaR requirements leading to successful immunotherapy. *Immunological reviews* **268**, 104-122 (2015).

57. Bosques, C.J. & Manning, A.M. Fc-gamma receptors: Attractive targets for autoimmune drug discovery searching for intelligent therapeutic designs. *Autoimmun Rev* (2016).

58. Bruhns, P. Properties of mouse and human IgG receptors and their contribution to disease models. *Blood* **119**, 5640-5649 (2012).

59. Vidarsson, G. *et al.* FcRn: an IgG receptor on phagocytes with a novel role in phagocytosis. *Blood* **108**, 3573-3579 (2006).

60. Kaetzel, C.S., Robinson, J.K., Chintalacharuvu, K.R., Vaerman, J.P. & Lamm, M.E. The polymeric immunoglobulin receptor (secretory component) mediates transport of immune complexes across epithelial cells: a local defense function for IgA. *Proceedings of the National Academy of Sciences of the United States of America* **88**, 8796-8800 (1991).

61. Yoo, E.M., Trinh, K.R., Lim, H., Wims, L.A. & Morrison, S.L. Characterization of IgA and IgM binding and internalization by surface-expressed human Fcalpha/mu receptor. *Molecular immunology* **48**, 1818-1826 (2011).

62. Colonna, M. *et al.* A common inhibitory receptor for major histocompatibility complex class I molecules on human lymphoid and myelomonocytic cells. *The Journal of experimental medicine* **186**, 1809-1818 (1997).

63. Borges, L., Hsu, M.L., Fanger, N., Kubin, M. & Cosman, D. A family of human lymphoid and myeloid Ig-like receptors, some of which bind to MHC class I molecules. *J Immunol* **159**, 5192-5196 (1997).

64. Colonna, M., Nakajima, H., Navarro, F. & Lopez-Botet, M. A novel family of Ig-like receptors for HLA class I molecules that modulate function of lymphoid and myeloid cells. *J Leukocyte Biol* **66**, 375-381 (1999).

65. Ujike, A. *et al.* Impaired dendritic cell maturation and increased T(H)2 responses in PIR-B-/- mice. *Nat Immunol* **3**, 542-548 (2002).

66. Brown, D., Trowsdale, J. & Allen, R. The LILR family: modulators of innate and adaptive immune pathways in health and disease. *Tissue Antigens* **64**, 215-225 (2004).

67. Cosman, D. *et al.* A novel immunoglobulin superfamily receptor for cellular and viral MHC class I molecules. *Immunity* **7**, 273-282 (1997).

68. Northfield, J., Lucas, M., Jones, H., Young, N.T. & Klenerman, P. Does memory improve with age? CD85j (ILT-2/LIR-1) expression on CD8 T cells correlates with 'memory inflation' in human cytomegalovirus infection. *Immunology and cell biology* **83**, 182-188 (2005).

69. Davidson, C.L., Li, N.L. & Burshtyn, D.N. LILRB1 polymorphism and surface phenotypes of natural killer cells. *Hum Immunol* **71**, 942-949 (2010).

70. Hirayasu, K. *et al.* Evidence for natural selection on leukocyte immunoglobulin-like receptors for HLA class I in Northeast Asians. *Am J Hum Genet* **82**, 1075-1083 (2008).

71. Hirayasu, K. & Arase, H. Functional and genetic diversity of leukocyte immunoglobulin-like receptor and implication for disease associations. *J Hum Genet* **60**, 703-708 (2015).

72. Jensen, M.A. *et al.* Functional genetic polymorphisms in ILT3 are associated with decreased surface expression on dendritic cells and increased serum cytokines in lupus patients. *Ann Rheum Dis* **72**, 596-601 (2013).

73. Kim, T. *et al.* Human LilrB2 is a beta-amyloid receptor and its murine homolog PirB regulates synaptic plasticity in an Alzheimer's model. *Science* **341**, 1399-1404 (2013).

74. Borges, L., Kubin, M. & Kuhlman, T. LIR9, an immunoglobulin-superfamily-activating receptor, is expressed as a transmembrane and as a secreted molecule. *Blood* **101**, 1484-1486 (2003).

75. Tedla, N. *et al.* Activation of human eosinophils through leukocyte immunoglobulin-like receptor 7. *Proceedings of the National Academy of Sciences of the United States of America* **100**, 1174-1179 (2003).

76. Ottonello, L. *et al.* Nonleukoreduced red blood cell transfusion induces a sustained inhibition of neutrophil chemotaxis by stimulating in vivo production of transforming growth factor-beta1 by neutrophils: role of the immunoglobulinlike transcript 1, sFasL, and sHLA-I. *Transfusion* **47**, 1395-1404 (2007).

77. Bashirova, A.A. *et al.* Diversity of the human LILRB3/A6 locus encoding a myeloid inhibitory and activating receptor pair. *Immunogenetics* **66**, 1-8 (2014).

78. Lopez-Alvarez, M.R., Jones, D.C., Jiang, W., Traherne, J.A. & Trowsdale, J. Copy number and nucleotide variation of the LILR family of myelomonocytic cell activating and inhibitory receptors. *Immunogenetics* **66**, 73-83 (2014).

79. Mori, Y. *et al.* Inhibitory immunoglobulin-like receptors LILRB and PIR-B negatively regulate osteoclast development. *J Immunol* **181**, 4742-4751 (2008).

80. Torkar, M. *et al.* Arrangement of the ILT gene cluster: a common null allele of the ILT6 gene results from a 6.7-kbp deletion. *Eur J Immunol* **30**, 3655-3662 (2000).

81. Jones, D.C. *et al.* Alternative mRNA splicing creates transcripts encoding soluble proteins from most LILR genes. *Eur J Immunol* **39**, 3195-3206 (2009).

82. Vlad, G., Liu, Z.R., Zhang, Q.Y., Cortesini, R. & Suciu-Foca, N. Immunosuppressive activity of recombinant ILT3. *Int Immunopharmacol* **6**, 1889-1894 (2006).

83. Suciu-Foca, N. *et al.* Soluble Ig-like transcript 3 inhibits tumor allograft rejection in humanized SCID mice and T cell responses in cancer patients. *J Immunol* **178**, 7432-7441 (2007).

84. Low, H.Z. *et al.* Association of the LILRA3 deletion with B-NHL and functional characterization of the immunostimulatory molecule. *PloS one* **8**, e81360 (2013).

85. An, H. *et al.* Soluble LILRA3, a potential natural antiinflammatory protein, is increased in patients with rheumatoid arthritis and is tightly regulated by interleukin 10, tumor necrosis factor-alpha, and interferon-gamma. *J Rheumatol* **37**, 1596-1606 (2010).

86. Willcox, B.E., Thomas, L.M. & Bjorkman, P.J. Crystal structure of HLA-A2 bound to LIR-1, a host and viral major histocompatibility complex receptor. *Nat Immunol* **4**, 913-919 (2003).

87. Shiroishi, M. *et al.* Crystal structure of the human monocyte-activating receptor, "Group 2" leukocyte Ig-like receptor A5 (LILRA5/LIR9/ILT11). *J Biol Chem* **281**, 19536-19544 (2006).

88. Chapman, T.L., Heikema, A.P. & Bjorkman, P.J. The inhibitory receptor LIR-1 uses a common binding interaction to recognize class I MHC molecules and the viral homolog UL18. *Immunity* **11**, 603-613 (1999).

89. Chapman, T.L., Heikema, A.P., West, A.P., Jr. & Bjorkman, P.J. Crystal structure and ligand binding properties of the D1D2 region of the inhibitory receptor LIR-1 (ILT2). *Immunity* **13**, 727-736 (2000).

90. Willcox, B.E. *et al.* Crystal structure of LIR-2 (ILT4) at 1.8 A: differences from LIR-1 (ILT2) in regions implicated in the binding of the Human Cytomegalovirus class I MHC homolog UL18. *BMC structural biology* **2**, 6 (2002).

91. Chen, Y. *et al.* Crystal structure of myeloid cell activating receptor leukocyte Ig-like receptor A2 (LILRA2/ILT1/LIR-7) domain swapped dimer: molecular basis for its non-binding to MHC complexes. *J Mol Biol* **386**, 841-853 (2009).

92. Cheng, H. *et al.* Crystal structure of leukocyte Ig-like receptor LILRB4 (ILT3/LIR-5/CD85k): a myeloid inhibitory receptor involved in immune tolerance. *J Biol Chem* **286**, 18013-18025 (2011).

93. Shiroishi, M. *et al.* Structural basis for recognition of the nonclassical MHC molecule HLA-G by the leukocyte Ig-like receptor B2 (LILRB2/LIR2/ILT4/CD85d). *Proceedings of the National Academy of Sciences of the United States of America* **103**, 16412-16417 (2006).

94. Yang, Z. & Bjorkman, P.J. Structure of UL18, a peptide-binding viral MHC mimic, bound to a host inhibitory receptor. *Proceedings of the National Academy of Sciences of the United States of America* **105**, 10095-10100 (2008).

95. Nam, G. *et al.* Crystal structures of the two membrane-proximal Ig-like domains (D3D4) of LILRB1/B2: alternative models for their involvement in peptide-HLA binding. *Protein Cell* **4**, 761-770 (2013).

96. Jones, D.C. *et al.* HLA class I allelic sequence and conformation regulate leukocyte Ig-like receptor binding. *J Immunol* **186**, 2990-2997 (2011).

97. Masuda, A., Nakamura, A., Maeda, T., Sakamoto, Y. & Takai, T. Cis binding between inhibitory receptors and MHC class I can regulate mast cell activation. *Journal of Experimental Medicine* **204**, 907-920 (2007).

98. Allen, R.L., Raine, T., Haude, A., Trowsdale, J. & Wilson, M.J. Leukocyte receptor complex-encoded immunomodulatory receptors show differing specificity for alternative HLA-B27 structures. *J Immunol* **167**, 5543-5547 (2001).

99. LeMaoult, J., Zafaranloo, K., Le Danff, C. & Carosella, E.D. HLA-G up-regulates ILT2, ILT3, ILT4, and KIR2DL4 in antigen presenting cells, NK cells, and T cells. *Faseb J* **19**, 662-664 (2005).

100. Ristich, V., Liang, S.Y., Zhang, W., Wu, J. & Horuzsko, A. Tolerization of dendritic cells by HLA-G. *Eur J Immunol* **35**, 1133-1142 (2005).

101. Zhang, Z. *et al.* The Leukocyte Immunoglobulin-Like Receptor Family Member LILRB5 Binds to HLA-Class I Heavy Chains. *PloS one* **10**, e0129063 (2015).

102. Nakayama, M. *et al.* Paired Ig-like receptors bind to bacteria and shape TLR-mediated cytokine production. *J Immunol* **178**, 4250-4259 (2007).

103. Chan, K.R. *et al.* Leukocyte immunoglobulin-like receptor B1 is critical for antibody-dependent dengue. *Proceedings of the National Academy of Sciences of the United States of America* **111**, 2722-2727 (2014).

104. Arnold, V. *et al.* S100A9 protein is a novel ligand for the CD85j receptor and its interaction is implicated in the control of HIV-1 replication by NK cells. *Retrovirology* **10** (2013).

105. Li, D. *et al.* Ig-like transcript 4 inhibits lipid antigen presentation through direct CD1d interaction. *J Immunol* **182**, 1033-1040 (2009).

106. Cao, W. *et al.* Regulation of TLR7/9 responses in plasmacytoid dendritic cells by BST2 and ILT7 receptor interaction. *The Journal of experimental medicine* **206**, 1603-1614 (2009).

107. Jones, D.C. *et al.* Allele-specific recognition by LILRB3 and LILRA6 of a cytokeratin 8-associated ligand on necrotic glandular epithelial cells. *Oncotarget* **7**, 15618-15631 (2016).

108. Zheng, J. *et al.* Inhibitory receptors bind ANGPTLs and support blood stem cells and leukaemia development. *Nature* **485**, 656-660 (2012).

109. Ma, G. *et al.* Paired Immunoglobin-like Receptor-B Regulates the Suppressive Function and Fate of Myeloid-Derived Suppressor Cells. *Immunity* **34**, 385-395 (2011).

110. Sloane, D.E. *et al.* Leukocyte immunoglobulin-like receptors: novel innate receptors for human basophil activation and inhibition. *Blood* **104**, 2832-2839 (2004).

111. Isakov, N. Immunoreceptor tyrosine-based activation motif (ITAM), a unique module linking antigen and Fc receptors to their signaling cascades. *J Leukocyte Biol* **61**, 6-16 (1997).

112. Borges, L. & Cosman, D. LIRs/ILTs/MIRs, inhibitory and stimulatory Ig-superfamily receptors expressed in myeloid and lymphoid cells. *Cytokine Growth F R* **11**, 209-217 (2000).

113. Chang, C.C. *et al.* Ig-Like Transcript 3 Regulates Expression of Proinflammatory Cytokines and Migration of Activated T Cells. *J Immunol* **182**, 5208-5216 (2009).

114. Khanolkar, R.C. *et al.* Leukocyte Ig-Like receptor B1 restrains dendritic cell function through increased expression of the NF-kappaB regulator ABIN1/TNIP1. *J Leukoc Biol* **100**, 737-746 (2016).

115. Lu, H.K. *et al.* LILRA2 Selectively Modulates LPS-Mediated Cytokine Production and Inhibits Phagocytosis by Monocytes. *PloS one* **7**, e233478 (2012).

116. Lee, D.J. *et al.* LILRA2 activation inhibits dendritic cell differentiation and antigen presentation to T cells. *J Immunol* **179**, 8128-8136 (2007).

117. Tavano, B. *et al.* Ig-like transcript 7, but not bone marrow stromal cell antigen 2 (also known as HM1.24, tetherin, or CD317), modulates plasmacytoid dendritic cell function in primary human blood leukocytes. *J Immunol* **190**, 2622-2630 (2013).

118. Kim-Schulze, S. *et al.* Recombinant Ig-like transcript 3-Fc modulates T cell responses via induction of th anergy and differentiation of CD8(+) T suppressor cells. *J Immunol* **176**, 2790-2798 (2006).

119. Tenca, C. *et al.* CD85j (leukocyte Ig-like receptor-1/Ig-like transcript 2) inhibits human osteoclast-associated receptor-mediated activation of human dendritic cells. *J Immunol* **174**, 6757-6763 (2005).

120. Young, N.T. *et al.* The inhibitory receptor LILRB1 modulates the differentiation and regulatory potential of human dendritic cells. *Blood* **111**, 3090-3096 (2008).

121. Chang, C.C. *et al.* Tolerization of dendritic cells by T(S) cells: the crucial role of inhibitory receptors ILT3 and ILT4. *Nat Immunol* **3**, 237-243 (2002).

122. Chang, C.C. *et al.* BCL6 Is Required for Differentiation of Ig-Like Transcript 3-Fc-Induced CD8(+) T Suppressor Cells. *J Immunol* **185**, 5714-5722 (2010).

123. Velten, F.W., Duperrier, K., Bohlender, J., Metharom, P. & Goerdt, S. A gene signature of inhibitory MHC receptors identifies a BDCA3(+) subset of IL-10-induced dendritic cells with reduced allostimulatory capacity in vitro. *Eur J Immunol* **34**, 2800-2811 (2004).

124. Cella, M. *et al.* A novel inhibitory receptor (ILT3) expressed on monocytes, macrophages, and dendritic cells involved in antigen processing. *The Journal of experimental medicine* **185**, 1743-1751 (1997).

125. Saverino, D. *et al.* The CD85/LIR-1/ILT2 inhibitory receptor is expressed by all human T lymphocytes and down-regulates their functions. *J Immunol* **165**, 3742-3755 (2000).

126. Shiroishi, M. *et al.* Human inhibitory receptors Ig-like transcript 2 (ILT2) and ILT4 compete with CD8 for MHC class I binding and bind preferentially to HLA-G. *Proceedings of the National Academy of Sciences of the United States of America* **100**, 8856-8861 (2003).

127. Kirwan, S.E. & Burshtyn, D.N. Killer cell Ig-like receptor-dependent signaling by Ig-like transcript 2 (ILT2/CD85j/LILRB1/LIR-1). *J Immunol* **175**, 5006-5015 (2005).

128. Karre, K. Natural killer cell recognition of missing self. *Nat Immunol* **9**, 477-480 (2008).

129. Yawata, M. *et al.* MHC class I-specific inhibitory receptors and their ligands structure diverse human NK-cell repertoires toward a balance of missing self-response. *Blood* **112**, 2369-2380 (2008).

130. Vitale, M. *et al.* The leukocyte Ig-like receptor (LIR)-1 for the cytomegalovirus UL18 protein displays a broad specificity for different HLA class I alleles: analysis of LID-1(+) NK cell clones. *Int Immunol* **11**, 29-35 (1999).

131. Naji, A., Menier, C., Maki, G., Carosella, E.D. & Rouas-Freiss, N. Neoplastic B-cell growth is impaired by HLA-G/ILT2 interaction. *Leukemia* **26**, 1889-1892 (2012).

132. Ketroussi, F. *et al.* Lymphocyte Cell-Cycle Inhibition by HLA-G Is Mediated by Phosphatase SHP-2 and Acts on the mTOR Pathway. *PloS one* **6**, e22776 (2011).

133. Naji, A. *et al.* Binding of HLA-G to ITIM-bearing Ig-like transcript 2 receptor suppresses B cell responses. *J Immunol* **192**, 1536-1546 (2014).

134. Liang, S.Y., Zhang, W. & Horuzsko, A. Human ILT2 receptor associates with murine MHC class I molecules in vivo and impairs T cell function. *Eur J Immunol* **36**, 2457-2471 (2006).

135. Belkin, D. *et al.* Killer cell Ig-like receptor and leukocyte Ig-like receptor transgenic mice exhibit tissue- and cell-specific transgene expression. *J Immunol* **171**, 3056-3063 (2003).

136. Talwar, S. *et al.* Gene expression profiles of peripheral blood leukocytes after endotoxin challenge in humans. *Physiological genomics* **25**, 203-215 (2006).

137. Smith, C.L. *et al.* Identification of a human neonatal immune-metabolic network associated with bacterial infection. *Nat Commun* **5**, 4649 (2014).

138. Chen, C.C., Hurez, V., Brockenbrough, J.S., Kubagawa, H. & Cooper, M.D. Paternal monoallelic expression of the paired immunoglobulin-like receptors PIR-A and PIR-B. *Proceedings of the National Academy of Sciences of the United States of America* **96**, 6868-6872 (1999).

139. Maeda, A., Kurosaki, M. & Kurosaki, T. Paired immunoglobulin-like receptor (PIR)-A is involved in activating mast cells through its association with Fc receptor gamma chain. *The Journal of experimental medicine* **188**, 991-995 (1998).

140. Endo, S., Sakamoto, Y., Kobayashi, E., Nakamura, A. & Takai, T. Regulation of cytotoxic T lymphocyte triggering by PIR-B on dendritic cells. *Proceedings of the National Academy of Sciences of the United States of America* **105**, 14515-14520 (2008).

141. Pereira, S., Zhang, H., Takai, T. & Lowell, C.A. The inhibitory receptor PIR-B negatively regulates neutrophil and macrophage integrin signaling. *J Immunol* **173**, 5757-5765 (2004).

142. Mitsuhashi, Y. *et al.* Regulation of plasmacytoid dendritic cell responses by PIR-B. *Blood* **120**, 3256-3259 (2012).

143. Nakayama, M. *et al.* Inhibitory receptor paired Ig-like receptor B is exploited by Staphylococcus aureus for virulence. *J Immunol* **189**, 5903-5911 (2012).

144. Campbell, K.S. & Purdy, A.K. Structure/function of human killer cell immunoglobulin-like receptors: lessons from polymorphisms, evolution, crystal structures and mutations. *Immunology* **132**, 315-325 (2011).

145. Moretta, L. & Moretta, A. Killer immunoglobulin-like receptors. *Current opinion in immunology* **16**, 626-633 (2004).

146. Khakoo, S.I. & Carrington, M. KIR and disease: a model system or system of models? *Immunological reviews* **214**, 186-201 (2006).

147. Suzuki, Y. *et al.* Genetic polymorphisms of killer cell immunoglobulin-like receptors are associated with susceptibility to psoriasis vulgaris. *The Journal of investigative dermatology* **122**, 1133-1136 (2004).

148. Carrington, M. *et al.* Hierarchy of resistance to cervical neoplasia mediated by combinations of killer immunoglobulin-like receptor and human leukocyte antigen loci. *The Journal of experimental medicine* **201**, 1069-1075 (2005).

149. Wang, L.L. & Yokoyama, W.M. Regulated expression of non-polymorphic gp49 molecules on mouse natural killer cells. In: Cooper, M.D., Takai, T. & Ravetch, J.V. (eds). *Activating and Inhibitory Immunoglobulin-Like Receptors*. Springer: Japan, 2001, pp 25-29.

150. Kharitonenkov, A. *et al.* A family of proteins that inhibit signalling through tyrosine kinase receptors. *Nature* **386**, 181-186 (1997).

151. Dietrich, J., Cella, M., Seiffert, M., Buhring, H.J. & Colonna, M. Cutting edge: signal-regulatory protein beta 1 is a DAP12-associated activating receptor expressed in myeloid cells. *J Immunol* **164**, 9-12 (2000).

152. Weinberg, R.A. *The Biology of Cancer*. Garland Science, Taylor & Francis Group: New York, 2007.

153. Hanahan, D. & Weinberg, R.A. Hallmarks of cancer: the next generation. *Cell* **144**, 646-674 (2011).

154. Smyth, M.J., Dunn, G.P. & Schreiber, R.D. Cancer immunosurveillance and immunoediting: the roles of immunity in suppressing tumor development and shaping tumor immunogenicity. *Advances in immunology* **90**, 1-50 (2006).

155. Schreiber, R.D., Old, L.J. & Smyth, M.J. Cancer Immunoediting: Integrating Immunity's Roles in Cancer Suppression and Promotion. *Science* **331**, 1565-1570 (2011).

156. Coley, W.B. The Classic - the Treatment of Malignant-Tumors by Repeated Inoculations of Erysipelas - with a Report of 10 Original Cases. *Clin Orthop Relat R*, 3-11 (1991).

157. Rosen, A. & Casciola-Rosen, L. Autoantigens in systemic autoimmunity: critical partner in pathogenesis. *Journal of internal medicine* **265**, 625-631 (2009).

158. Fletcher, J.M., Lalor, S.J., Sweeney, C.M., Tubridy, N. & Mills, K.H. T cells in multiple sclerosis and experimental autoimmune encephalomyelitis. *Clinical and experimental immunology* **162**, 1-11 (2010).

159. Okada, H., Kuhn, C., Feillet, H. & Bach, J.F. The 'hygiene hypothesis' for autoimmune and allergic diseases: an update. *Clinical and experimental immunology* **160**, 1-9 (2010).

160. Zhang, Y. *et al.* Expression of immunoglobulin-like transcript (ILT)2 and ILT3 in human gastric cancer and its clinical significance. *Molecular medicine reports* **5**, 910-916 (2012).

161. Dobrowolska, H. *et al.* Expression of immune inhibitory receptor ILT3 in acute myeloid leukemia with monocytic differentiation. *Cytometry. Part B, Clinical cytometry* **84**, 21-29 (2013).

162. Kang, X.L. *et al.* The ITIM-containing receptor LAIR1 is essential for acute myeloid leukaemia development. *Nat Cell Biol* **17**, 665-U286 (2015).

163. Colovai, A.I. *et al.* Expression of inhibitory receptor ILT3 on neoplastic B cells is associated with lymphoid tissue involvement in chronic lymphocytic leukemia. *Cytom Part B-Clin Cy* **72B**, 354-362 (2007).

164. Urosevic, M., Kamarashev, J., Burg, G. & Dummer, R. Primary cutaneous CD8(+) and CD56(+) T-cell lymphomas express HLA-G and killer-cell inhibitory ligand, ILT2. *Blood* **103**, 1796-1798 (2004).

165. Lefebvre, S. *et al.* Specific activation of the non-classical class I histocompatibility HLA-G antigen and expression of the ILT2 inhibitory receptor in human breast cancer. *J Pathol* **196**, 266-274 (2002).

166. Loumagne, L. *et al.* In vivo evidence that secretion of HLA-G by immunogenic tumor cells allows their evasion from immunosurveillance. *Int J Cancer* **135**, 2107-2117 (2014).

167. Bleharski, J.R. *et al.* Use of genetic profiling in leprosy to discriminate clinical forms of the disease. *Science* **301**, 1527-1530 (2003).

168. Berg, L. *et al.* LIR-1 expression on lymphocytes, and cytomegalovirus disease in lung-transplant recipients. *Lancet* **361**, 1099-1101 (2003).

169. O'Connor, G.M., Holmes, A., Mulcahy, F. & Gardiner, C.M. Natural Killer cells from long-term non-progressor HIV patients are characterized by altered phenotype and function. *Clin Immunol* **124**, 277-283 (2007).

170. Vlad, G. *et al.* Interleukin-10 induces the upregulation of the inhibitory receptor ILT4 in monocytes from HIV positive individuals. *Hum Immunol* **64**, 483-489 (2003).

171. Tedla, N. *et al.* Expression of activating and inhibitory leukocyte immunoglobulin-like receptors in rheumatoid synovium: correlations to disease activity. *Tissue Antigens* **77**, 305-316 (2011).

172. Huynh, O.A. *et al.* Down-regulation of leucocyte immunoglobulin-like receptor expression in the synovium of rheumatoid arthritis patients after treatment with disease-modifying anti-rheumatic drugs. *Rheumatology* **46**, 742-751 (2007).

173. Wiendl, H. *et al.* Expression of the immune-tolerogenic major histocompatibility molecule HLA-G in multiple sclerosis: implications for CNS immunity. *Brain* **128**, 2689-2704 (2005).

174. An, H.Y. *et al.* Serum Leukocyte Immunoglobulin-Like Receptor A3 (LILRA3) Is Increased in Patients with Multiple Sclerosis and Is a Strong Independent Indicator of Disease Severity; 6.7kbp LILRA3 Gene Deletion Is Not Associated with Diseases Susceptibility. *PloS one* **11** (2016).

175. Cortesini, R. & Suciu-Foca, N. ILT3+ ILT4+ tolerogenic endothelial cells in transplantation. *Transplantation* **82**, S30-32 (2006).

176. Stallone, G. *et al.* Rapamycin induces ILT3(high)ILT4(high) dendritic cells promoting a new immunoregulatory pathway. *Kidney international* **85**, 888-897 (2014).

177. Naji, A., Durrbach, A., Carosella, E.D. & Rouas-Freiss, N. Soluble HLA-G and HLA-G1 expressing antigen-presenting cells inhibit T-cell alloproliferation through ILT-2/ILT-4/FasL-mediated pathways. *Hum Immunol* **68**, 233-239 (2007).

178. Apps, R., Gardner, L., Sharkey, A.M., Holmes, N. & Moffett, A. A homodimeric complex of HLA-G on normal trophoblast cells modulates antigen-presenting cells via LILRB1. *Eur J Immunol* **37**, 1924-1937 (2007).

179. Ponte, M. *et al.* Inhibitory receptors sensing HLA-G1 molecules in pregnancy: decidua-associated natural killer cells express LIR-1 and CD94/NKG2A and acquire p49, an HLA-G1-specific receptor. *Proceedings of the National Academy of Sciences of the United States of America* **96**, 5674-5679 (1999).

180. Richmond, A. & Su, Y. Mouse xenograft models vs GEM models for human cancer therapeutics. *Dis Model Mech* **1**, 78-82 (2008).

181. Mateos, M.V. *et al.* Bortezomib plus melphalan and prednisone in elderly untreated patients with multiple myeloma: results of a multicenter phase 1/2 study. *Blood* **108**, 2165-2172 (2006).

182. Baselga, J., Norton, L., Albanell, J., Kim, Y.M. & Mendelsohn, J. Recombinant humanized anti-HER2 antibody (Herceptin) enhances the antitumor activity of paclitaxel and doxorubicin against HER2/neu overexpressing human breast cancer xenografts. *Cancer research* **58**, 2825-2831 (1998).

183. Cho, A., Haruyama, N. & Kulkarni, A.B. Generation of transgenic mice. *Current protocols in cell biology / editorial board, Juan S. Bonifacino ... [et al.]* **Chapter 19**, Unit 19 11 (2009).

184. Brehm, M.A., Shultz, L.D. & Greiner, D.L. Humanized mouse models to study human diseases. *Curr Opin Endocrinol Diabetes Obes* **17**, 120-125 (2010).

185. Bernard, D., Peakman, M. & Hayday, A.C. Establishing humanized mice using stem cells: maximizing the potential. *Clinical and experimental immunology* **152**, 406-414 (2008).

186. Mosier, D.E., Gulizia, R.J., Baird, S.M. & Wilson, D.B. Transfer of a functional human immune system to mice with severe combined immunodeficiency. *Nature* **335**, 256-259 (1988).

187. Lapidot, T. *et al.* Cytokine stimulation of multilineage hematopoiesis from immature human cells engrafted in SCID mice. *Science* **255**, 1137-1141 (1992).

188. Waldmann, T.A. Immunotherapy: past, present and future. *Nature medicine* **9**, 269-277 (2003).

189. Gilboa, E. DC-based cancer vaccines. *J Clin Invest* **117**, 1195-1203 (2007).

190. Harper, D.M. *et al.* Efficacy of a bivalent L1 virus-like particle vaccine in prevention of infection with human papillomavirus types 16 and 18 in young women: a randomised controlled trial. *Lancet* **364**, 1757-1765 (2004).

191. Bendandi, M. *et al.* Complete molecular remissions induced by patient-specific vaccination plus granulocyte-monocyte colony-stimulating factor against lymphoma. *Nature medicine* **5**, 1171-1177 (1999).

192. Spitler, L.E. *et al.* Adjuvant therapy of stage III and IV malignant melanoma using granulocyte-macrophage colony-stimulating factor. *Journal of clinical oncology : official journal of the American Society of Clinical Oncology* **18**, 1614-1621 (2000).

193. Cutler, A. & Brombacher, F. Cytokine therapy. *Annals of the New York Academy of Sciences* **1056**, 16-29 (2005).

194. Feldmann, M. & Steinman, L. Design of effective immunotherapy for human autoimmunity. *Nature* **435**, 612-619 (2005).

195. Suntharalingam, G. *et al.* Cytokine storm in a phase 1 trial of the anti-CD28 monoclonal antibody TGN1412. *New Engl J Med* **355**, 1018-1028 (2006).

196. Besser, M.J. *et al.* Clinical responses in a phase II study using adoptive transfer of short-term cultured tumor infiltration lymphocytes in metastatic melanoma patients. *Clinical cancer research : an official journal of the American Association for Cancer Research* **16**, 2646-2655 (2010).

197. Dudley, M.E. & Rosenberg, S.A. Adoptive-cell-transfer therapy for the treatment of patients with cancer. *Nature reviews. Cancer* **3**, 666-675 (2003).

198. Riley, J.L., June, C.H. & Blazar, B.R. Human T regulatory cell therapy: take a billion or so and call me in the morning. *Immunity* **30**, 656-665 (2009).

199. Barrett, D.M., Singh, N., Porter, D.L., Grupp, S.A. & June, C.H. Chimeric antigen receptor therapy for cancer. *Annual review of medicine* **65**, 333-347 (2014).

200. Grupp, S.A. *et al.* Chimeric antigen receptor-modified T cells for acute lymphoid leukemia. *The New England journal of medicine* **368**, 1509-1518 (2013).

201. Kochenderfer, J.N. *et al.* B-cell depletion and remissions of malignancy along with cytokine-associated toxicity in a clinical trial of anti-CD19 chimeric-antigen-receptor-transduced T cells. *Blood* **119**, 2709-2720 (2012).

202. Kohler, G. & Milstein, C. Continuous cultures of fused cells secreting antibody of predefined specificity. *Nature* **256**, 495-497 (1975).

203. McCafferty, J., Griffiths, A.D., Winter, G. & Chiswell, D.J. Phage antibodies: filamentous phage displaying antibody variable domains. *Nature* **348**, 552-554 (1990).

204. Smith, G.P. Filamentous Fusion Phage - Novel Expression Vectors That Display Cloned Antigens on the Virion Surface. *Science* **228**, 1315-1317 (1985).

205. Carmen, S. & Jermutus, L. Concepts in antibody phage display. *Briefings in functional genomics & proteomics* **1**, 189-203 (2002).

206. Bazan, J., Calkosinski, I. & Gamian, A. Phage display--a powerful technique for immunotherapy: 1. Introduction and potential of therapeutic applications. *Hum Vaccin Immunother* **8**, 1817-1828 (2012).

207. Lou, J. *et al.* Antibodies in haystacks: how selection strategy influences the outcome of selection from molecular diversity libraries. *Journal of immunological methods* **253**, 233-242 (2001).

208. Beck, A., Wurch, T., Bailly, C. & Corvaia, N. Strategies and challenges for the next generation of therapeutic antibodies. *Nature reviews. Immunology* **10**, 345-352 (2010).

209. Goldstein, G. *et al.* OKT3 monoclonal antibody reversal of acute renal allograft rejection unresponsive to conventional immunosuppressive treatments. *Progress in clinical and biological research* **224**, 239-249 (1986).

210. Sgro, C. Side-effects of a monoclonal antibody, muromonab CD3/orthoclone OKT3: bibliographic review. *Toxicology* **105**, 23-29 (1995).

211. Morrison, S.L., Johnson, M.J., Herzenberg, L.A. & Oi, V.T. Chimeric human antibody molecules: mouse antigen-binding domains with human constant region domains. *Proceedings of the National Academy of Sciences of the United States of America* **81**, 6851-6855 (1984).

212. Jones, P.T., Dear, P.H., Foote, J., Neuberger, M.S. & Winter, G. Replacing the complementarity-determining regions in a human antibody with those from a mouse. *Nature* **321**, 522-525 (1986).

213. Leavy, O. Therapeutic antibodies: past, present and future. *Nature reviews. Immunology* **10**, 297 (2010).

214. Lorenz, H.M. Technology evaluation: Adalimumab, Abbott Laboratories. *Curr Opin Mol Ther* **4**, 185-190 (2002).

215. Kasi, P.M., Tawbi, H.A., Oddis, C.V. & Kulkarni, H.S. Clinical review: Serious adverse events associated with the use of rituximab - a critical care perspective. *Critical care* **16**, 231 (2012).

216. Beum, P.V., Lindorfer, M.A. & Taylor, R.P. Within peripheral blood mononuclear cells, antibody-dependent cellular cytotoxicity of rituximab-opsonized Daudi cells is promoted by NK cells and inhibited by monocytes due to shaving. *J Immunol* **181**, 2916-2924 (2008).

217. Clynes, R.A., Towers, T.L., Presta, L.G. & Ravetch, J.V. Inhibitory Fc receptors modulate in vivo cytotoxicity against tumor targets. *Nature medicine* **6**, 443-446 (2000).

218. Weiner, L.M., Surana, R. & Wang, S. Monoclonal antibodies: versatile platforms for cancer immunotherapy. *Nature reviews. Immunology* **10**, 317-327 (2010).

219. Cartron, G. *et al.* Therapeutic activity of humanized anti-CD20 monoclonal antibody and polymorphism in IgG Fc receptor FcgammaRIIIa gene. *Blood* **99**, 754-758 (2002).

220. Di Gaetano, N. *et al.* Complement activation determines the therapeutic activity of rituximab in vivo. *J Immunol* **171**, 1581-1587 (2003).

221. Uchida, J. *et al.* The innate mononuclear phagocyte network depletes B lymphocytes through Fc receptor-dependent mechanisms during anti-CD20 antibody immunotherapy. *The Journal of experimental medicine* **199**, 1659-1669 (2004).

222. Montalvao, F. *et al.* The mechanism of anti-CD20-mediated B cell depletion revealed by intravital imaging. *J Clin Invest* **123**, 5098-5103 (2013).

223. Gul, N. *et al.* Macrophages eliminate circulating tumor cells after monoclonal antibody therapy. *J Clin Invest* **124**, 812-823 (2014).

224. Holers, V.M. Complement and Its Receptors: New Insights into Human Disease. *Annual Review of Immunology, Vol 32* **32**, 433-459 (2014).

225. Hu, Y. *et al.* Investigation of the mechanism of action of alemtuzumab in a human CD52 transgenic mouse model. *Immunology* **128**, 260-270 (2009).

226. Cragg, M.S. & Glennie, M.J. Antibody specificity controls in vivo effector mechanisms of anti-CD20 reagents. *Blood* **103**, 2738-2743 (2004).

227. Vuist, W.M., Levy, R. & Maloney, D.G. Lymphoma regression induced by monoclonal anti-idiotypic antibodies correlates with their ability to induce Ig signal transduction and is not prevented by tumor expression of high levels of bcl-2 protein. *Blood* **83**, 899-906 (1994).

228. Chan, H.T. *et al.* CD20-induced lymphoma cell death is independent of both caspases and its redistribution into triton X-100 insoluble membrane rafts. *Cancer research* **63**, 5480-5489 (2003).

229. Honeychurch, J. *et al.* Antibody-induced nonapoptotic cell death in human lymphoma and leukemia cells is mediated through a novel reactive oxygen species-dependent pathway. *Blood* **119**, 3523-3533 (2012).

230. Ivanov, A. *et al.* Monoclonal antibodies directed to CD20 and HLA-DR can elicit homotypic adhesion followed by lysosome-mediated cell death in human lymphoma and leukemia cells. *J Clin Invest* **119**, 2143-2159 (2009).

231. Alduaij, W. *et al.* Novel type II anti-CD20 monoclonal antibody (GA101) evokes homotypic adhesion and actin-dependent, lysosome-mediated cell death in B-cell malignancies. *Blood* **117**, 4519-4529 (2011).

232. Oldham, R.J., Cleary, K. L. S. & Cragg, M. S. CD20 and Its Antibodies: Past, Present, and Future. *Forum on Immunopathological Diseases and Therapeutics* **5**, 7-23 (2014).

233. Cragg, M.S., French, R.R. & Glennie, M.J. Signaling antibodies in cancer therapy. *Current opinion in immunology* **11**, 541-547 (1999).

234. White, A.L. *et al.* Fcgamma receptor dependency of agonistic CD40 antibody in lymphoma therapy can be overcome through antibody multimerization. *J Immunol* **193**, 1828-1835 (2014).

235. Hodi, F.S. *et al.* Improved survival with ipilimumab in patients with metastatic melanoma. *The New England journal of medicine* **363**, 711-723 (2010).

236. Topalian, S.L. *et al.* Safety, activity, and immune correlates of anti-PD-1 antibody in cancer. *The New England journal of medicine* **366**, 2443-2454 (2012).

237. Brahmer, J.R. *et al.* Safety and activity of anti-PD-L1 antibody in patients with advanced cancer. *The New England journal of medicine* **366**, 2455-2465 (2012).

238. Page, D.B., Postow, M.A., Callahan, M.K., Allison, J.P. & Wolchok, J.D. Immune modulation in cancer with antibodies. *Annual review of medicine* **65**, 185-202 (2014).

239. Vonderheide, R.H. & Glennie, M.J. Agonistic CD40 antibodies and cancer therapy. *Clinical cancer research : an official journal of the American Association for Cancer Research* **19**, 1035-1043 (2013).

240. Vey, N. *et al.* A phase 1 trial of the anti-inhibitory KIR mAb IPH2101 for AML in complete remission. *Blood* **120**, 4317-4323 (2012).

241. Weiner, L.M., Murray, J.C. & Shuptrine, C.W. Antibody-based immunotherapy of cancer. *Cell* **148**, 1081-1084 (2012).

242. Molhoj, M. *et al.* CD19/CD3-bispecific antibody of the BiTE class is far superior to tandem diabody with respect to redirected tumor cell lysis. *Molecular immunology* **44**, 1935-1943 (2007).

243. Choy, E.H.S. *et al.* Efficacy of a novel PEGylated humanized anti-TNF fragment (CDP870) in patients with rheumatoid arthritis: a phase II double-blinded, randomized, dose-escalating trial. *Rheumatology* **41**, 1133-1137 (2002).

244. Bross, P.F. *et al.* Approval summary: Gemtuzumab ozogamicin in relapsed acute myeloid leukemia. *Clinical Cancer Research* **7**, 1490-1496 (2001).

245. Francisco, J.A. *et al.* cAC10-vcMMAE, an anti-CD30-monomethyl auristatin E conjugate with potent and selective antitumor activity. *Blood* **102**, 1458-1465 (2003).

246. Niculescu-Duvaz, I. Trastuzumab emtansine, an antibody-drug conjugate for the treatment of HER2+metastatic breast cancer. *Curr Opin Mol Ther* **12**, 350-360 (2010).

247. Lee, R., Tran, M., Nocerini, M. & Liang, M. A high-throughput hybridoma selection method using fluorometric microvolume assay technology. *J Biomol Screen* **13**, 210-217 (2008).

248. Soderlind, E. *et al.* Recombining germline-derived CDR sequences for creating diverse single-framework antibody libraries. *Nature biotechnology* **18**, 852-856 (2000).

249. Hudson, L.E. & Allen, R.L. Leukocyte Ig-Like Receptors - A Model for MHC Class I Disease Associations. *Frontiers in immunology* **7**, 281 (2016).

250. Smith, G.P. Filamentous fusion phage: novel expression vectors that display cloned antigens on the virion surface. *Science* **228**, 1315-1317 (1985).

251. Mattheakis, L.C., Bhatt, R.R. & Dower, W.J. An in-Vitro Polysome Display System for Identifying Ligands from Very Large Peptide Libraries. *Proceedings of the National Academy of Sciences of the United States of America* **91**, 9022-9026 (1994).

252. Amstutz, P., Forrer, P., Zahnd, C. & Pluckthun, A. In vitro display technologies: novel developments and applications. *Curr Opin Biotech* **12**, 400-405 (2001).

253. Bashirova, A., Apps, R., Vince, N., Yu, X. & Carringotn, M. Genetic polymorphism in the human LILRB3/LILRA6 locus. *J Immunol* **188** (2012).

254. Bottger, V. & Bottger, A. Epitope Mapping Using Phage Display Peptide Libraries. *Epitope Mapping Protocols, Second Edition* **524**, 181-201 (2009).

255. Swann, M.J., Peel, L.L., Carrington, S. & Freeman, N.J. Dual-polarization interferometry: an analytical technique to measure changes in protein structure in real time, to determine the stoichiometry of binding events, and to differentiate between specific and nonspecific interactions. *Anal Biochem* **329**, 190-198 (2004).

256. Macian, F. NFAT proteins: Key regulators of T-cell development and function. *Nature Reviews Immunology* **5**, 472-484 (2005).

257. Apostolou, I., Guild, J., Vaickus, L. & Rosenzweig, M. Immunoregulatory properties of TRX585, a novel monoclonal antibody specific for immunoglobulin-like transcript 5. *Journal of Clinical Oncology* **28** (2010).

258. Raveney, B.J., Copland, D.A., Calder, C.J., Dick, A.D. & Nicholson, L.B. TNFR1 signalling is a critical checkpoint for developing macrophages that control of T-cell proliferation. *Immunology* **131**, 340-349 (2010).

259. Beers, S.A. *et al.* Antigenic modulation limits the efficacy of anti-CD20 antibodies: implications for antibody selection. *Blood* **115**, 5191-5201 (2010).

260. Vasilyeva, E.A., Minkov, I.B., Fitin, A.F. & Vinogradov, A.D. Kinetic mechanism of mitochondrial adenosine triphosphatase. Inhibition by azide and activation by sulphite. *Biochem J* **202**, 15-23 (1982).

261. Giammarioli, A.M. *et al.* Differential effects of the glycolysis inhibitor 2-deoxy-D-glucose on the activity of pro-apoptotic agents in metastatic melanoma cells, and induction of a cytoprotective autophagic response. *Int J Cancer* **131**, E337-347 (2012).

262. Maxfield, F.R. & McGraw, T.E. Endocytic recycling. *Nat Rev Mol Cell Biol* **5**, 121-132 (2004).

263. Bainton, D.F. The discovery of lysosomes. *J Cell Biol* **91**, 66s-76s (1981).

264. Carosella, E.D., Moreau, P., Lemaoult, J. & Rouas-Freiss, N. HLA-G: from biology to clinical benefits. *Trends in immunology* **29**, 125-132 (2008).

265. Vitetta, E.S. & Uhr, J.W. Monoclonal-Antibodies as Agonists - an Expanded Role for Their Use in Cancer-Therapy. *Cancer research* **54**, 5301-5309 (1994).

266. Tedder, T.F., Tuscano, J., Sato, S. & Kehrl, J.H. CD22, a B lymphocyte-specific adhesion molecule that regulates antigen receptor signaling. *Annual review of immunology* **15**, 481-504 (1997).

267. Wherry, E.J. & Kurachi, M. Molecular and cellular insights into T cell exhaustion. *Nature Reviews Immunology* **15**, 486-499 (2015).

268. Kotaskova, J. *et al.* High Expression of Lymphocyte-Activation Gene 3 (LAG3) in Chronic Lymphocytic Leukemia Cells Is Associated with Unmutated Immunoglobulin Variable Heavy Chain Region (IGHV) Gene and Reduced Treatment-Free Survival. *J Mol Diagn* **12**, 328-334 (2010).

269. Triebel, F. *et al.* Lag-3, a Novel Lymphocyte-Activation Gene Closely Related to Cd4. *Journal of Experimental Medicine* **171**, 1393-1405 (1990).

270. Anderson, A.C. *et al.* Promotion of tissue inflammation by the immune receptor Tim-3 expressed on innate immune cells. *Science* **318**, 1141-1143 (2007).

271. Bosma, G.C., Custer, R.P. & Bosma, M.J. A severe combined immunodeficiency mutation in the mouse. *Nature* **301**, 527-530 (1983).

272. Shultz, L.D. *et al.* Multiple defects in innate and adaptive immunologic function in NOD/LtSz-scid mice. *J Immunol* **154**, 180-191 (1995).

273. Gurtsevitch, V.E., Turusov, V.S. & Lenoir, G.M. Metastatic capacity of Burkitt's lymphoma cell lines in nude mice. *Exp Toxicol Pathol* **44**, 375-380 (1992).

274. Malani, A.K., Gupta, C., Weigand, R.T., Gupta, V. & Rangineni, G. Spinal Burkitt's lymphoma in adults. *Clin Lymphoma Myeloma* **6**, 333-336 (2006).

275. Zaborowski, M.P., Balaj, L., Breakefield, X.O. & Lai, C.P. Extracellular Vesicles: Composition, Biological Relevance, and Methods of Study. *Bioscience* **65**, 783-797 (2015).

276. Nam, G. *et al.* Crystal structures of the two membrane-proximal Ig-like domains (D3D4) of LILRB1/B2: alternative models for their involvement in peptide-HLA binding. *Protein Cell* **4**, 761-770 (2013).

277. Jirholt, P., Ohlin, M., Borrebaeck, C.A. & Soderlind, E. Exploiting sequence space: shuffling in vivo formed complementarity determining regions into a master framework. *Gene* **215**, 471-476 (1998).

278. Rossant, C.J. *et al.* Phage display and hybridoma generation of antibodies to human CXCR2 yields antibodies with distinct mechanisms and epitopes. *Mabs-Austin* **6**, 1425-1438 (2014).

279. McLaughlin, P. *et al.* Rituximab chimeric anti-CD20 monoclonal antibody therapy for relapsed indolent lymphoma: half of patients respond to a four-dose treatment program. *Journal of clinical oncology : official journal of the American Society of Clinical Oncology* **16**, 2825-2833 (1998).